WAVE CLIMATE AND COASTAL CHANGE IN SOUTHEAST AUSTRALIA

Thomas Robert Cranfield Mortlock

Faculty of Science and Engineering

Department of Environmental Sciences

This thesis is presented for the degree of Doctor of Philosophy

20th November 2015

TABLE OF CONTENTS

THESIS ABSTRACT

Wave-driven currents are the principle mechanism for sand transport on the southeast Australian inner continental shelf and surf zone. An understanding of changes to wave climate is thus imperative for projecting and managing coastal change in the coming century. Two important climate change signatures for southeast Australia are tropical expansion and the changing behaviour of El Niño Southern Oscillation (ENSO). Results suggest that tropical expansion will lead to longer periods of more easterly modal wave conditions along the southeast Australia shelf (SEAS) than at present, punctuated by less frequent but higher magnitude storm events from the east to north-east. This will lead to more (less) cross- (along-) shore sediment transport. Parabolic bay-beaches in the lee of southern headlands are most vulnerable to these changes. On longer timescales, changes to wave-induced cross-shelf transport with tropical expansion may facilitate coastal evolution with sea-level rise.

There is considerable uncertainty in the prediction of future ENSO behaviour, and the coastal response to different central Pacific (CP) versus eastern Pacific (EP) flavours of ENSO is thus far unknown. Results show that CP ENSO produces significantly different wave climates to EP ENSO along the SEAS, by the modulation of trade-wind wave generation. Results also show that a) the shoreline response to ENSO in a headland-bay beach is more complex than the existing paradigm that (anti-) clockwise rotation occurs during El Niño (La Niña), and b) coastal change between ENSO phases cannot be inferred from shifts in the deepwater wave climate, as previously assumed. Morphodynamic modelling indicates that CP ENSO leads to higher coastal vulnerability than EP ENSO during an El Niño/La Niña cycle. A new link between surf zone morphology and the shoreline equilibrium profile of headland-bay beaches has also been made, which allows the Parabolic Bay Shape Equation to be applied to real-world wave conditions with a greater level of objectivity.

STATEMENT OF CANDIDATURE

I certify that the work in this thesis entitled “**Wave Climate and Coastal Change in Southeast Australia**” has not previously been submitted for a degree nor has it been submitted as part of requirements for a degree to any other university or institution other than Macquarie University.

I also certify that the thesis is an original piece of research and it has been written by me. Any help and assistance that I have received in my research work and the preparation of the thesis itself have been appropriately acknowledged.

In addition, I certify that all information sources and literature used are indicated in the thesis.

Thomas Mortlock (42733855)

20th November 2015

ACKNOWLEDGEMENTS

This research was funded by an International Macquarie University Research Excellence Scholarship (iMQRES) number 2011128, in association with an Australian Research Council Linkage Project (ARC LP) grant number 100200348 to Ian D Goodwin and Ian L Turner entitled "Australian coastal observation network: monitoring and forecasting coastal erosion in a changing climate". Acknowledgements specific to each study within this thesis are given at the end of each chapter.

I have been fortunate enough to spend time studying my passion; wind, waves and the coast. Growing up and windsurfing on the Thames Estuary was where it began for me. The ever-changing winds, tides and sand banks always fascinated me. I then managed (and was even paid) to spend many hours surveying beaches on the English south coast at first and last light, in rain and shine. The boundary been land and water at first light is an amazing experience and always different.

There is probably no better place to do a PhD in coastal science than on the Australian east coast. Aside from its stunning natural beauty, much of it is empty and the potential for frontier science is immense. The legacy of ocean-goers from Polynesians to Europeans is an inspiration when staring out to sea. 'Fieldwork' (official or otherwise) is a joy. No need for waders or woollies, bring on the jetski and pack the surfboard!

Both the beginning and end of this PhD were only possible thanks to a number of people. Firstly, many thanks goes to my supervisor Ian Goodwin for his critical guidance over the past 3 ½ years. In particular, his continued enthusiasm for coastal and climate science, and the autonomy he allowed me to explore my own research ideas made this PhD an exciting journey. I would also like to thank my adjunct supervisor, Ian Turner, for his guidance and support leading up to and during the PhD.

I of course thank my parents, Kathryn and Robert, for putting up with (whilst being responsible for) my wanderlust. Sending me to Central America at the age of 17 was pivotal for me, but also as it turns out for them! The move to Australia was difficult, and I thank them for understanding the importance of being able to pursue one's passions if given the chance to do so. Now a dad myself, I appreciate the selfless way you bought us up. Thank you to my brother James, my sister Hannah, aunty Marga and uncle John for your love and support.

También queiro mostrar mi gratitud para mi familia Mexicana/Alamana, sin su precencia aquí en Australia este tesis nunca hubiera sido terminado. A Mario, Elke, Karsten y Karina, les quiero mucho y aprecio de veras todo su apoyo. Siguiendo con el tema de las costas, espero con anticipación de explorar las de Baja California, Oaxaca y Chiapas con ustededs, Nadia and Jacob algún dia pronto.

Finally, and most importantly, to my wife Nadia and my son Jacob. This PhD has been a selfish exercise, competing for time and attention with both of you. Jacob, I managed to finish both despite your intermissions and because of them. If nothing else, this PhD has allowed me to spend precious time with you and watch you growing up. Each time you gave me a beaming smile or looked in wonder at something ordinary, you reminded me the simplest things in life are the best.

Nadia, you have encouraged and supported me every step of the way and even before this PhD began. You gave up your job in Southampton to be with me in Sydney. You've put up with my single-mindedness and stress. Physically, mentally and financially it just would not have been possible without you. This thesis is as much yours as it is mine, thank you.

Perfecting the survey technique at Palm Beach

CHAPTER 1

The Nambucca River

INTRODUCTION

1 INTRODUCTION

1.1 RELEVANCE OF THE THESIS

Wave climate change is a major driver of coastline stability in south east Australia from event- to centennial timescales. In the short-to-medium-term, changes to the storm wave climate can affect coastal inundation, beach erosion, damage to property and marine structures, and risk to public safety. In the medium-to-long-term, changes to the modal wave climate can enhance or dampen the effects of a rising tidal plane on coastal systems by modulating the delivery of sediment to the coast. An understanding of the variability and trends in both storm and modal wave conditions, and their relationship to atmospheric climate, is thus imperative for projecting and managing coastal change in the coming century.

There is an ever-increasing societal and economic risk associated with climate change in the coastal zone in south east Australia. The collective value of properties in the state of New South Wales (NSW) threatened by coastal processes within planning timeframes has been estimated at over $1 billion, partly a result of 85% of the population living on the coastal fringe (Department of Climate Change, 2009; Department of the Environment, 2015). The Sydney metropolitan area alone is projected to increase its population by 37% between 2011 - 2031 (Department of Planning and Environment, 2014). Other major conurbations such as Wollongong, Newcastle, Coffs Harbour and Brisbane, with their associated ports and maritime commerce, are also located along the eastern seaboard and thus vulnerable to changes in wave climate.

Despite the obvious need to understand climate-change related coastal impacts, the deterministic wave climate forecasting approach to coastal hazard assessment is associated with significant uncertainties. While uncertainty originates from a number of sources (discussed in Chapter 2), the main problems exist with imperfect climate and wave model physics, and the stochastic to semi-chaotic nature of the climate system. As an alternative, this thesis advocates a surrogate-observational approach to investigating wave climate and coastal change along the south east Australian shelf.

1.2 GENERAL BACKGROUND AND THEORY

While a background specific to each chapter is provided throughout the thesis, this section gives an overview of the description and modelling of surface ocean wind-waves, their transformation in coastal waters and the maturation of the science of wind-wave modelling. In addition, two of the most important signatures of anthropogenic climate change for the Pacific subtropics are introduced; an expansion of the tropical belt and the changing behaviour of El Niño Southern Oscillation. Finally, the concept of wave climate change modulating the coastal response to sea level rise is introduced.

1.2.1 Description of Surface Ocean Wind-Waves

This thesis is concerned with wind-generated surface gravity waves, which are defined as those ocean surface waves which propagate at frequencies of between ~ 0.03 and 1 Hz, or ~ 30 to 1 s (Munk, 1950). They are generated by winds acting on the surface of the ocean and move according to gravitational acceleration (*g*, 9.81 m/s). Gravity waves exist in a continuum of ocean waves according to propagation frequency (Figure 1.1), and can be decomposed into two types; 1) longer-period and far-generated, 'mature' swell, and 2) shorter-period, locally-generated 'young' wind-sea. The Tasman Sea (within which this thesis operates) represents a mixed wind-sea and swell environment.

Wind-waves can be described at several spatial scales, from one wave length (hundreds of metres), to ocean basins (thousands of kilometres), and at several spatial scales, from one wave period (seconds) to a wave climate (seasons to years or more) (Holthuijsen, 2007). An appropriate assessment of scale is the first step in the description and modelling of wind-waves.

1.2.1.1 Small Scales and the Full Sea Surface Variance

For studies of surf-zone dynamics or breakwater design, the full sea-surface variance is best described at the scale of a single wave length in a phase-resolving approach. Localised and non-linear wave processes such as diffraction, reflection or wave-wave interactions can only then be fully resolved. While fully deterministic, this approach is computationally intensive and thus only suitable for a limited number of cases and over small spatial domains. At these scales (and often shallow water depths), models based on linear wave theory often break down. Instead, models based on non-linear Boussinesq equations need to be used.

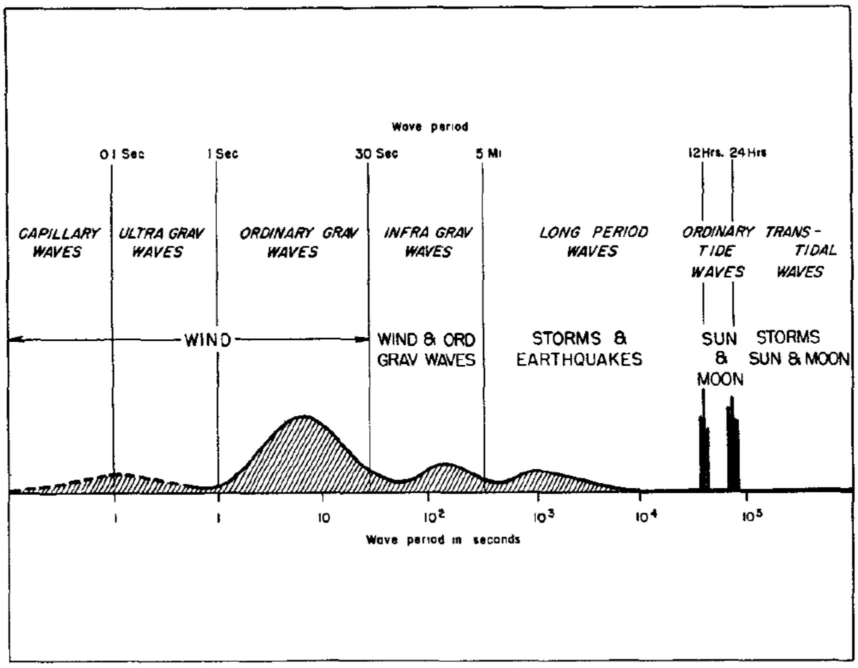

Figure 1.1 "Tentative classification of ocean waves according to wave period" proposed by Walter Munk in 1950, and still used today. Figure taken from Munk (1950).

1.2.1.2 Intermediate Scales and the Wave Spectrum

For event-to-seasonal scale studies (i.e. individual storms to seasonal wave climates) over regional spatial scales (i.e. shelf seas), describing the full sea-surface motion is impractical. Instead, the statistical properties of the sea surface are more efficiently described by the wave spectrum. The concept of the one-dimensional variance density spectrum is based on the notion that the variance of the sea-surface elevation over a certain length of time (usually one hour) can be described by the amount of energy density that exists in a prescribed number of frequency bins; $E(f)$, measured in $m^{2/}$Hz. A time series of the measured sea surface elevation can be readily transformed to an $E(f)$ spectrum using a Fourier transform. If directional measurements are available, the wave spectrum can be extended to two dimensions to describe how wave energy is distributed across both frequencies and directions; $E(f, \theta)$, in $m^{2/}$Hz/Degrees, or $m^{2/}$Hz/Radians (Figure 1.2).

Often, the spectral shape is repeatable and therefore predictable for certain sea-states that are produced by the same synoptic climate patterns. This means a probabilistic description of the sea surface elevation for certain sea states can be used, which is far more efficient that explicitly modelling the full sea-surface variance.

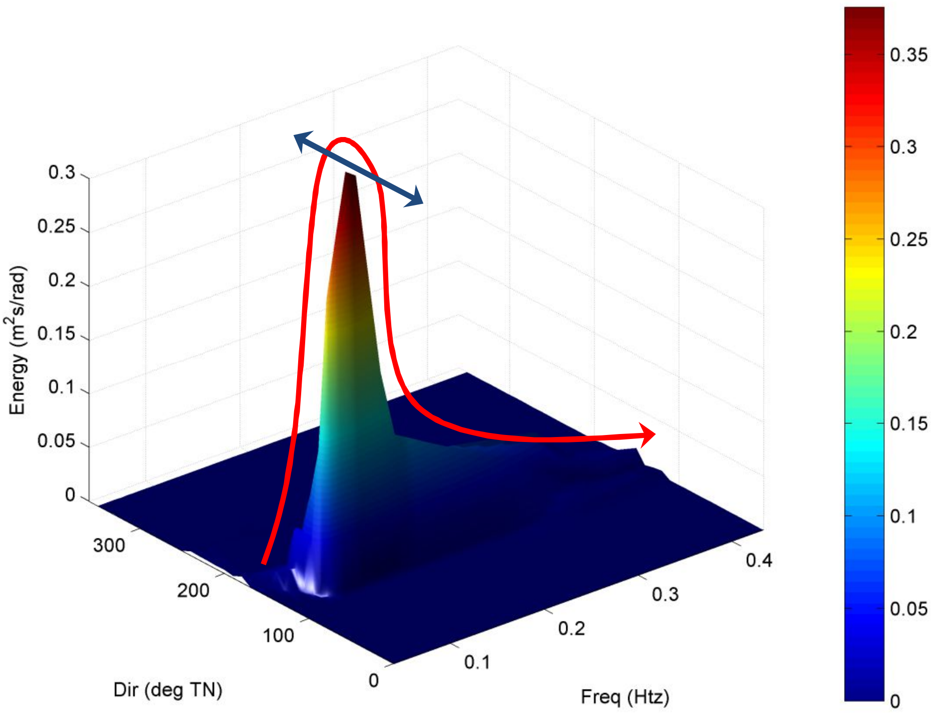

Figure 1.2 A two-dimensional wave energy spectrum generated from data captured at the Wamberal Directional WaveRider buoy. The energy peak is around 140 ° True North (TN), and 0.1 Hz (10 s). The spectrum is single peaked and follows a JONSWAP shape with high frequency tail (red line). Blue line shows directional spread.

Spectral wave models can use either parametric wave information or near-surface marine winds as boundary input to build and propagate a wave spectrum through different wave depths. Alternatively, a full spectrum can be used to start the model, derived from either another model run, or from observations. While this is a very efficient way of obtaining wave information over a large spatial area, it requires the assumption that wave conditions conform to a prescribed spectral shape, with a single and uni-directional spectral peak, and constant directional spreading across frequencies. The JONSWAP spectrum is often used for young sea states, whereas the Pierson-Moskowitz (PM) spectral shape is applied for fully developed seas.

The JONSWAP spectrum was derived from the Joint North Sea Wave Project (Hasselmann *et al.*, 1973). Observations during this study showed that as fetch (distance from wave generation) increases, the peak of the wave spectrum evolves from high to low frequencies (short to long wave periods; sea to swell) (Figure 1.3).

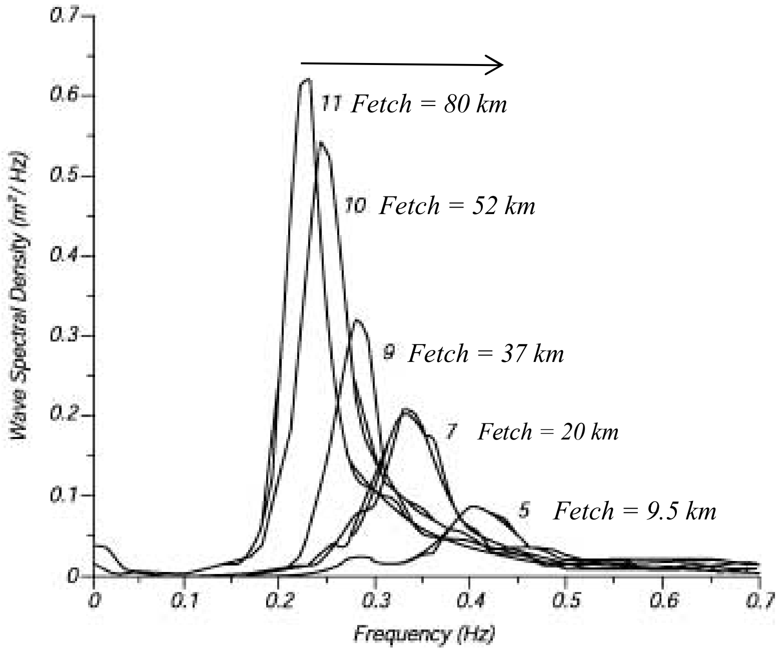

Figure 1.3 Spectra observed during the JONSWAP project. Original numbering refers to observation station in the North Sea; the equivalent fetch for each is added. As fetch is reduced, the wave spectrum evolves from low to high frequencies. Figure from Hasselmann *et al*. (1973).

A key finding was that as the one-dimensional spectrum evolves with fetch, the broad shape remains constant. Although this does not at first appear to be the case from Figure 1.3, once normalised, the shape is conserved for each fetch length. Even so, most spectral wave models allow the modification of the JONSWAP spectrum with shape and peakiness parameters, if observed spectra are shown to deviate from the default shape. The JONSWAP spectrum is valid for fetch-limited (i.e. mixed sea-swell conditions) in deep water. It also been shown to apply to storm conditions in deep water. This is because, for sufficiently steep waves, the quadruplet wave-wave interactions (see Chapter 2) tend to stabilise the shape of the spectrum into a JONSWAP shape (Holthuijsen, 2007). The use of a JONSWAP spectrum, and phase-averaged spectral wave models in general, are not appropriate for shallow water where the non-linear energy transfer among spectral components due to triad interactions occurs

(Eldeberky and Battjes, 1996). The JONSWAP spectrum also does not apply to pure-swell conditions with negligible fetch-limitations across ocean basins.

For ocean basin applications, the PM spectral shape (Pierson and Moskowitz, 1964) is more appropriate (as verified later by Alves and Banner, 2003). It assumes that if the wind blows steadily enough for a long period of time over a large area, then the waves will eventually reach a point of equilibrium with the wind. The peak frequency only depends on the wind speed, and not the fetch (Figure 1.4).

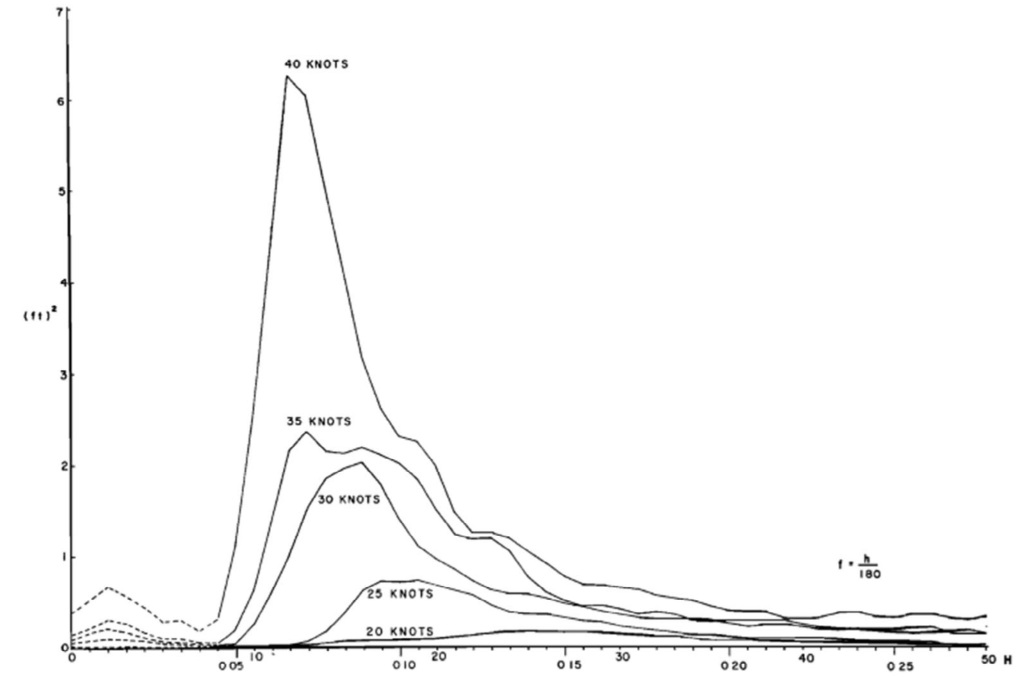

Figure 1.4 Wave spectra for a fully-developed sea for different wind speeds. X-axis scale is frequency (Hz), y-axis is wave spectral density (m^2/Hz). While there is no migration of the spectral peak as with JONSWAP, the peakiness of the spectrum increases with increasing wind speed. Figure from Moskowitz (1964).

The shape of the PM high frequency tail is similar to that of the JONSWAP spectrum, although the exact shape (whether it is a f^{-5} or f^{-4}) is still a point of contention, as some believe it scales with wind speed (e.g. Toba, 1973). However, the effect on energy distribution is barely noticeable (Holthuijsen, 2007) so for most applications the original f^{-5} tail is used.

The Tasman Sea is similar in part to the North Sea in that it is a partially open marginal sea with most wave generation fetch-limited by New Zealand or south west Pacific islands. Therefore, the JONSWAP formulation is the most appropriate spectral case. However, in instances where bi--modal sea states exist (i.e. a local and short-period wind sea superimposed on a far-field and long-period swell), the use of the single-peaked JONSWAP spectrum does not account for any wave energy associated with secondary peaks. In addition, bi-modal conditions are often also bi-directional, with the sea and swell components propagating from different directions. A classic example of this along the south east Australian shelf (SEAS) is when an anti-cyclonic high pressure system creates a short-period, locally generated wind-sea from the north-east, while at the same time a longer-period southerly swell generated from extra-tropical lows (whose equatorward track is blocked by the adjacent anti-cyclone) propagates from south (Figure 1.5).

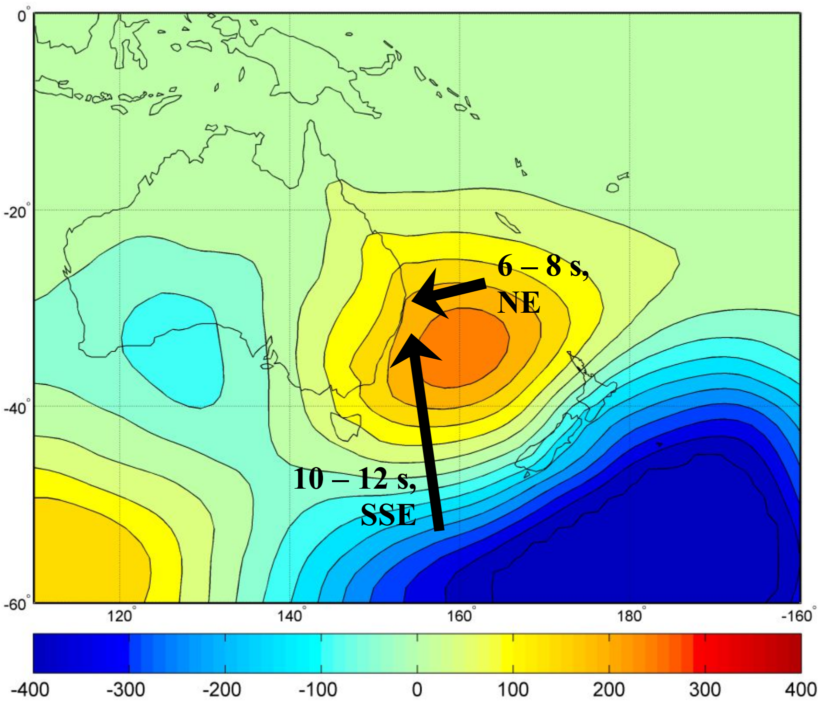

Figure 1.5 The synoptic arrangement for classic bi-modal wave conditions along the south east Australian shelf. Warm (cool) colours show anomalous high (low) sea surface pressure (hPa). This plot is explained in detail in Chapters 4 and 5.

In such instances, the use of a JONSWAP spectrum can lead to an under-representation of directional wave energy for coastal hazard definition and engineering design because only the primary spectral peak is accounted for.

1.2.1.3 Large Scales and Wave Parametric Data

On longer timescales (years or more), energy associated with sub-dominant spectral peaks is smoothed over time and the wave climate is most efficiently described by the time-averaged (usually hours or days) trivariate parameters of height, period and direction. The wave height distribution is Rayleigh-distributed (Figure 1.6).

While there are a number of parameters used to describe the wave height distribution (mean height, H_{mean}, root mean squared height, H_{rms}, significant height, H_s, average of top 10% of heights, H_{10}, and maximum height, H_{max}) H_s is widely used (and used in this thesis) and represents the mean of the highest one-third of waves in the wave record. H_s (also denoted $H_{1/3}$) is well correlated with the wave height that is visually estimated by experienced observers (Holthuijsen, 2007). Under a Rayleigh distribution, H_s is only exceeded 1 % of the time (Figure 1.6). While H_{max} cannot be derived from a Rayleigh distribution (as it goes to infinity), it is empirically related to H_s, in $H_{max} \approx 2.H_s$.

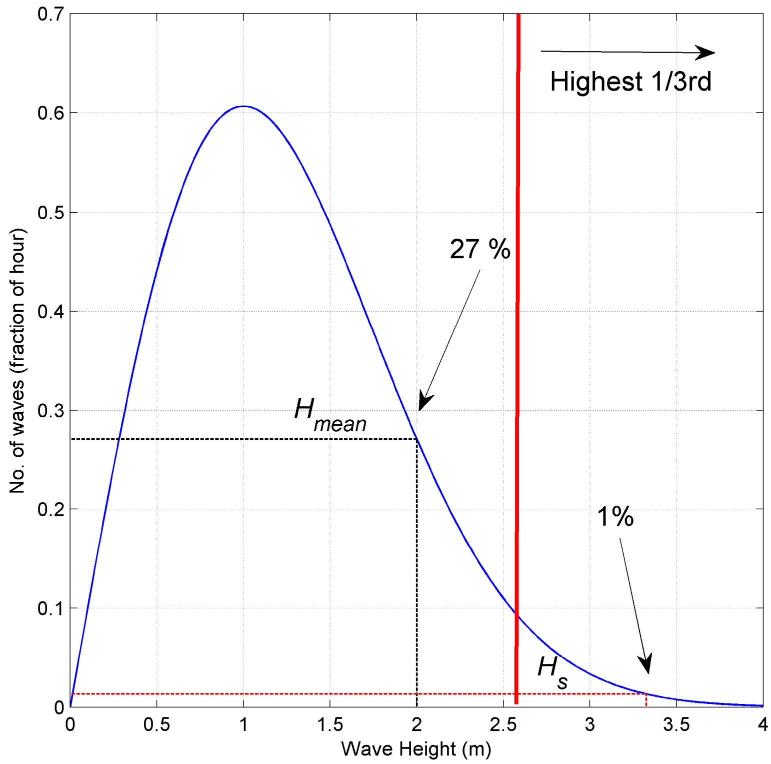

Figure 1.6 A Rayleigh distribution of wave heights observed in one hour, showing the probability of exceedance of H_{mean} (27% of the time), and H_s (1% of the time).

H_s can be calculated using the zero up-crossing method, whereby wave heights are first calculated from a measured time series of the sea surface elevation, then ranked by height, and the average height of the waves that comprise the top 33% is taken as H_s (Figure 1.7). This is how H_s is derived from all wave buoy observations used in this thesis.

The significant wave height can also be estimated from the wave spectrum:

$$H_{m0} \approx 4\sqrt{m_0} \tag{1.1}$$

Where m_0 is the zeroth-order moment of the variance density spectrum, $E(f)$. This method of estimating the significant wave height is used by spectral wave models, and is the parameter compared to buoy-observed H_s during model validation in this thesis. However, the two values are not exactly the same. Observations have shown that H_{m0} is typically 5 – 10% larger than the value of H_s estimated from measured time series (Holthuijsen, 2007).

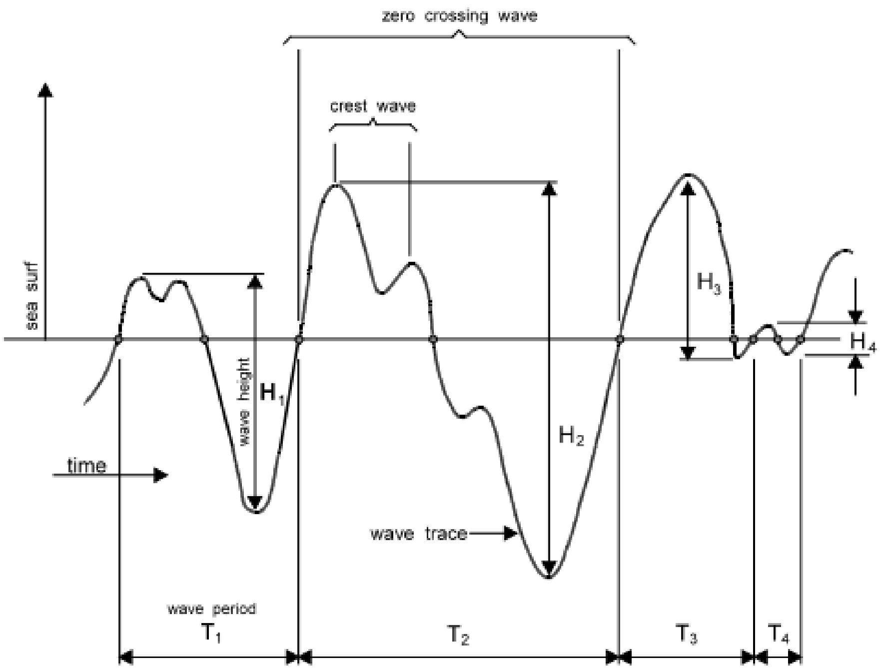

Figure 1.7 Zero up-crossing method of obtaining wave height and period statistics from a trace of the observed sea surface elevation (SSE). The wave height is defined as the crest to subsequent trough; the wave period is defined as the time taken for the SSE to down-cross and then up-cross the zero elevation line (mean sea level). Image from Kulmar (2013).

As with wave height, the wave period distribution (the distribution of the time intervals between the start and end of each wave in a time series) can be described by a number of parameters, and can be derived from both measured time series (Figure 1.7) and the wave spectrum. Two of the most important wave period parameters are the mean period (the zero-crossing period, T_z, from measured time series, and T_{m02} or T_{m01} from the wave spectrum), and the peak spectral wave period, T_p. When validating wave model output, the mean period, rather than the peak period, is the most robust comparison to make (see Chapter 2). T_z is the mean wave period parameter used throughout this thesis from buoy observations. T_{m02} and T_{m01} are the two comparable spectrally-derived mean wave periods that are given from wave model results. T_{m02} is defined as:

$$T_{m02} = \sqrt{\frac{m_0}{m_2}} \tag{1.2}$$

where m_2 is the second moment of the wave energy spectrum. However, the value of m_2 (and therefore estimates of T_{m02}) are sensitive to small errors in the analysis technique, because higher-order moments are more sensitive to noise in the high-frequency range of the spectrum (Holthuijsen, 2007). Therefore, T_{m01} may be considered a more reliable model output value to use, as it uses a lower-order moment which is less dependent on high-frequency noise:

$$T_{m01} = \left(\frac{m_1}{m_0}\right)^{-1} \tag{1.3}$$

Except for wave model validation, the T_p parameter is always used in this thesis for statistical analyses of wave buoy observations. This is because, for uni-modal conditions, T_p describes the frequency at which the bulk wave energy propagates at. This is the most suitable parameter for calculating wave power (Chapter 4), wave orbital velocities and wave-induced sediment transport (Chapter 6) for seasonal to multi-decadal wave climates. Likewise, the wave direction that corresponds to the primary spectral peak is used (MWD_{tp1}, abbreviated to MWD throughout). T_z is likely to under-estimate all frequency-dependent parameters since $T_p \approx 1.2\ T_z$ for a JONSWAP spectrum. T_z is also sensitive to bi-modal energy peaks; when there is near-equal energy in the swell and sea component of the spectrum, T_z is an average of the two and almost meaningless.

1.2.2 The Maturation of Wind-Wave Modelling

While the study of ocean wave dynamics is truly ancient (Aristotle and Leonardo de Vinci both made significant early contributions), interest in wave prediction grew during the first half of the 20th Century arising from the practical need for knowledge of the sea state during landing operations in the two World Wars (Komen *et al.*, 1994). The subject of wind-wave generation began in the modern era when Jeffrey (1924, 1925) assumed that air flowing over the ocean surface was sheltered by waves on their lee side. Sverdrup and Munk (1947) first introduced a parametrical description of the sea state to “forecast sea and swell from weather data” for US Navy operations. The concept of the wave spectrum was later introduced by Pierson *et al.* (1955), but took seven years before the application for modelling was achieved (Hasselmann, 1962). Prior to this, only ‘first-generation’ wave models existed, in which nonlinear wave interactions (the re-distribution of energy in the wave spectrum with wind and fetch due to quadruplets) was ignored (SWAMP Group, 1985). Second generation models included them, but only in parameterized form and not in two-dimensions (frequency-direction). Third-generation models were then developed, which model the full two-dimensional wave spectrum, explicitly representing all physical processes for wave evolution (SWAMP Group, 1985). The application of third-generation models requires considerable computational power, which has also recently become available. In addition, the development of altimeter and scatterometer techniques for global-scale measurements of the sea surface has allowed for real-time and hindcast assimilation and calibration of these models.

Despite much progress having been made in modelling the wave spectrum, the underlying concept is flawed. All present spectral models rely on one basic idea; the sea surface is the sum of many sinusoidal waves, each one characterized by its own height (i.e. energy), period (hence length and frequency), and direction (Cavaleri, 2006). Except for the case of pure swell conditions, this is obviously not true. According to Cavaleri (2006) and the WISE Group (2007), there is a growing feeling in the wave modelling community that spectral-based wave models cannot be much further improved in their representation of the actual sea surface than at present. Instead, a more deterministic approach, or the use of hybrid spectral-deterministic modelling, is the thought to be the direction of future advances in the field (Cavaleri, 2006).

Notwithstanding this obvious deficiency, the parametric information derived from modern spectral wave models is often very good. This is in part because the default physics in these models have undergone almost half a century of empirical-based calibration. It is also because spectral wave models only describe the statistical properties of the sea surface, rather than the sea surface form itself, and for this reason are computationally efficient (and widely-used) over a large spatial area. Thus, while the conceptual basis of spectral wave models is imperfect, the results for most engineering and coastal process applications are acceptable.

1.2.3 The Physical Basis of Spectral Wave Models

Most spectral wave transformation models can be classified into three categories depending on the governing equations that are used; the mild slope equation (Kirby, 1986), Boussinesq equations (Madsen *et al.*, 1991; Madsen and Sorensen, 1992), and the wave action balance (WAB) equation. Most oceanic and coastal-zone wave models are based on the WAB equation, such as WAM (WAMDI Group, 1988), MIKE 21 SW (Warren and Bach, 1992), TOMAWAC (Benoit *et al.*, 1996), SWAN (Booij *et al.*, 1999), and WAVEWATCH III (Tolman, 2009). This is largely because of their computational efficiency over large areas because they are phase-averaged (i.e. they have a spatial resolution that is much greater than one wave length). In contrast, the REF/DIF model (Kirby and Dalrymple, 1983) is an example of the use of the mild slope equation, while MIKE 21 BW (DHI, 2014) and FUNWAVE (Shi *et al.*, 2012) are two widely used examples of Boussinesq models. Both mild-slope and Boussinesq models are phase-resolved.

Phase-averaged WAB models assume all relevant information about the sea surface is contained in the two-dimensional energy density spectrum $E\ (f,\ \theta)$. They therefore determine the probabilistic evolution of wave energy in space and time. Specifically, it is the evolution of the action density that is calculated, rather than the energy density, because these models also account for wave-current interactions. Action density is conserved during wave propagation in the presence of ambient currents, whereas energy density is not (Whitham, 1974; SWAN, 2011a). The change in action density is computed in five dimensions in a model run; in time, x-space, y-space, wave direction-space and frequency-space. In order to solve the action balance equation, various sources and sinks are used to account for three principle processes; 1) the effects of wave energy generation (by wind), 2) energy transfer across frequencies, and 3) energy dissipation. Wave diffraction, which is not explained by the WAB equation, can be still be modelled using a phase-decoupled refraction-diffraction approximation (Holthuijsen *et al.*, 2003) (as in MIKE 21 SW and SWAN). In this approach, the wave amplitude is replaced by the square root of the spectral energy density. However, it is important to note that this is only a coarse approximation of diffraction, and in areas where diffraction dominates (i.e. in the vicinity of a breakwater), alternative modelling techniques need to be used (Section 1.2.2.3).

In contrast, models which solve the parabolic form of the mild slope equation (e.g. REF/DIF) can simulate the effects of shoaling, refraction and diffraction explicitly because the solution technique is phase-resolving. However, accurate results are restricted to waves propagating on a mild bottom slope within 45 º of the mean wave direction (Kirby and Dalrymple, 1983). Models based on Boussinesq equations (e.g. MIKE 21 BW, FUNWAVE) are also phase-resolving, and can simulate almost all linear and non-linear nearshore processes including reflection and transmission, which mild-slope models cannot. However, they are often limited to a water depth, d, to deep water wave length, L_0, ratio of $d/L_0 \leq 0.5$, meaning they are only practically applicable on small scales (e.g. harbours or surf zone).

For oceanic (deep water) applications, only WAB models are currently practical for modern computing. Modelling waves in oceanic waters is much simpler than in the coastal environment. Ocean wave models do not need to account for any bottom energy dissipation and the principle physical parameter is wave energy generation by wind. White-capping is the only energy dissipation source term needed, although it remains the least understood part of wave evolution and often becomes the tuning parameter of ocean wave models (WISE Group, 2007). Wave energy transfer between frequencies due to quadruplet wave-wave interactions is the third important process in deep water (Table 1.1).

Table 1.1 The relative importance of various processes affecting wave evolution in oceanic and coastal waters (after Battjes, 1994).

Process	Oceanic waters	Coastal waters	
		Shelf seas	Nearshore
Wind generation	✓✓✓	✓✓✓	✓
Quadruplet wave-wave interactions	✓✓✓	✓✓✓	✓
White-capping	✓✓✓	✓✓✓	✓
Bottom friction	×	✓✓	✓✓
Current refraction / energy bunching	×	✓	✓✓
Bottom refraction / shoaling	×	✓✓	✓✓✓
Breaking (depth-induced)	×	✓	✓✓✓
Triad wave-wave interactions	×	×	✓✓
Reflection	×	×	✓✓
Diffraction	×	×	✓✓

✓✓✓ = dominant, ✓✓ = significant but not dominant, ✓ = of minor importance, × = negligible

In coastal waters, many more processes need to be considered (Table 1.1). ‘Coastal waters’ specifically refers to the shoaling zone which extends from wave base to the seaward edge of the surf zone. Wave base depth is when the surface wave form begins to be affected by the seabed topography, and is defined as when $d \leq 0.5\ L_0$, where L_0 can be approximated as $gT^2\ /\ (2\pi)$. Therefore, wave base depends on wave period, T (and wave celerity). The mean annual wave period along the SEAS is ~ 10 s, so wave base is ~ 80 m. This is approximate to the mooring depth of the mid-shelf wave buoy network along the shelf (Figure 1.8).

The shoaling zone extends shoreward from wave base to the seaward edge of the surf zone (defined by Ruessink *et al.* (2011) as where H_s/d = 0.33). In this zone, wave energy dissipation also occurs due to bottom friction and depth-induced breaking as well as white-capping. By accurately representing bottom friction, the effect of shoaling and refraction on wave amplitude and direction can be derived. Shoaling and refraction are the two principle wave transformation processes in shelf seas. In the lee of headlands, islands or breakwaters, diffraction also becomes important.

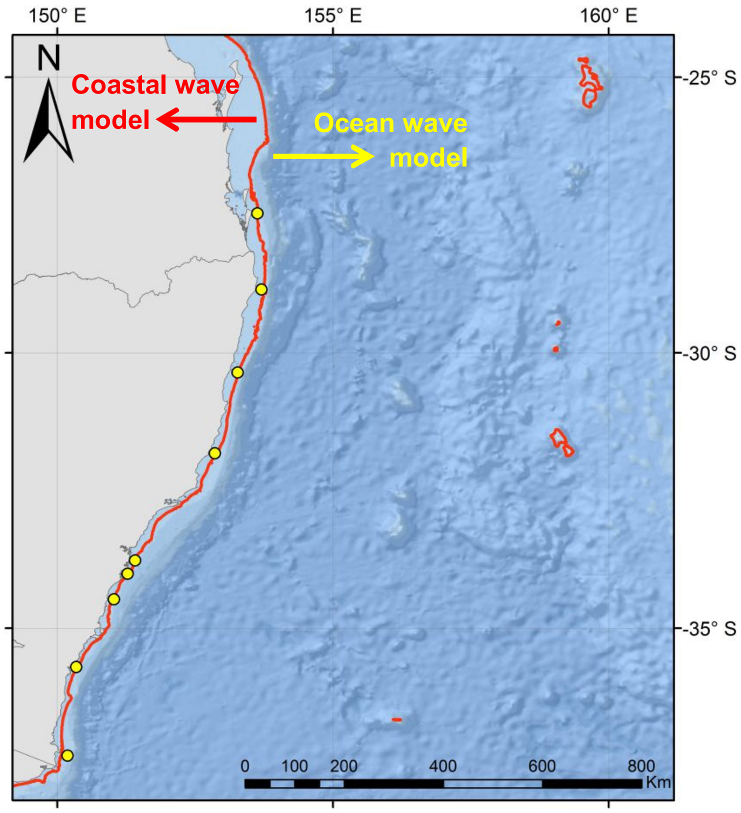

Figure 1.8 Tasman Sea and south east Australian shelf with 80 m depth contour (mean annual wave base) shown in red, delineating the boundary between coastal and ocean wave modelling. Positions of mid-shelf wave buoy moorings from Port Kembla in the south to North Stradbroke Island (Brisbane) in the north are shown in yellow.

1.2.2.1 Shoaling

Shoaling is the variation of waves in their direction of propagation due to depth-induced changes of the *group* velocity *in that direction* (Holthuijsen, 2007). Generally, the decrease in the wave group velocity in shallow water increases the wave amplitude (and height), leading to 'energy bunching' where wave energy is compacted into higher frequencies as the wave train slows down. The description of shoaling by linear wave theory breaks down, however, on approaching the shoreline, as the phase-averaged wave amplitude goes to infinity. WAB models use a high-frequency cut-off to prevent this from happening, but for proper representation of the shoaled wave in the surf zone, a phase-resolved approach is required.

1.2.2.2 Refraction

In order to calculate the effect of shoaling on wave energy, the direction of wave propagation must be known. Refraction describes the change in wave direction due to depth-induced changes in the *phase* velocity *along the wave crest* (Holthuijsen, 2007). The wave crest always turns towards shallower water (i.e. the coast) because the crest moves faster in deeper water than it does in shallower water. For harmonic, long-crested waves propagating over shore-parallel depth contours, the wave direction can be computed simply using Snel's law. However, if the depth contours are not shore-parallel (as is often the case), the wave direction needs to be computed using wave rays. This is done by computing the change in wave amplitude along the wave crest with depth, to find the rate of change in wave direction, and thus the curvature along the wave ray.

Munk and Traylor (1947) were one of the first to realise the dominant role refraction has on alongshore gradients in breaker wave height, longshore and rip currents, over a submarine canyon (Figure 1.9 a) and ridge (Figure 1.9 b) in La Jolla, southern California.

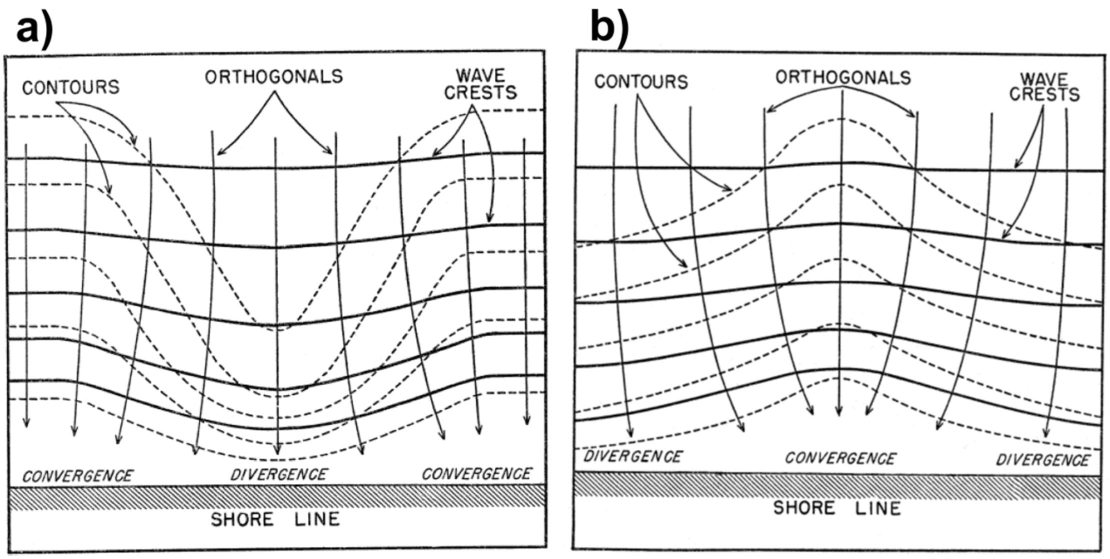

Figure 1.9 Refraction of waves by a submarine ridge (a) and submarine canyon (b), after Munk and Traylor (1947).

They showed that waves move faster over deep water (a canyon) than shallow water (a ridge) causing divergence (low waves) over the mouth of the canyon and convergence (high waves) on either side. They proceeded to show that refraction diagrams for the coastal zone can be drawn from deriving offshore wave periods and directions from meteorological maps. Sixty years on, this is essentially the same theory used by modern spectral wave models when using near-surface marine winds as input boundary conditions to refract waves to the nearshore.

1.2.2.3 Diffraction

The depth-induced changes in wave amplitude and direction that occur with shoaling and refraction are usually sufficiently slow (small over the distance of one wave length) that linear wave theory can be used. However, when waves propagate around surface-piercing obstacles the wave amplitude varies considerably and on scales close to or smaller than one wave length. Diffraction describes the sharp turning of waves into areas with lower amplitude because of rapid variation in wave amplitude along the crest line.

Such horizontal variations of the wave amplitude can also generate currents and thus affect sediment transport, especially in shallow water depths. It is therefore especially important to account for diffraction where shoaling and refraction is minimal (i.e. in a harbour setting where water depth is constant). Because this process occurs on sub-wave length scales, it can only be fully accounted for in phase-resolved models. This thesis uses a phase-averaged modelling approach, even in the lee of headlands. This is because Daly *et al* (2013) showed that diffraction is a secondary driver of shoreline change in the lee of headlands, to refraction and shoaling. In addition, the phase-decoupled diffraction approximation used in both SWAN and MIKE 21 SW is deemed sufficient to model the weakly diffractive processes around headlands (Holthuijsen, 2013).

While the change in wave energy in the coastal zone has been discussed with regard to variations in bathymetry, tides and currents can also influence the wave amplitude, frequency and direction. Time-varying water depths and ambient currents can thus contribute to the processes of shoaling, refraction, diffraction and ultimately sediment transport on continental shelves. However, their effect is often secondary and this thesis considers wave-only forcing because of the relatively large time (seasons to decades) and spatial scales (shelf seas) on which the investigations take place.

1.2.4 A Poleward Expansion of the Tropics

Changes to large-scale atmospheric circulation and wind patterns ultimately determine changes to the nearshore wind-wave climate, wave-induced sediment transport and coastal behaviour. This relationship is particularly strong on open-ocean and wave-dominated coastlines. In order to model future coastal change, projections of changes to atmospheric climate is thus of paramount importance. While there is high uncertainty related to climate modelling in general (Cai *et al.*, 2015b), one of the most robust signatures of recent and near-future climate change is an expansion of the tropical belt (Seidel *et al.*, 2008, England *et al.*, 2014).

The width of the tropics is measured by the meridional extent of the tropical Hadley circulation. The Hadley cell migrates between the northern and southern hemispheres on a seasonal basis, according to the position of the inter-tropical convergence zone (ITCZ). During the Austral summer (winter), the ITCZ is in the southern (northern) hemisphere, and the Austral tropics migrate poleward (equatorward). There is also a latitudinal displacement of the sub-tropics, in particular the position of the sub-tropical ridge (STR), defined as the latitude of highest pressure in the East Australian region (Timbal and Drosdowsky, 2013). Figure 1.10 shows how the STR in the Southern Hemisphere shifts south during the Austral summer, displacing high pressure anti-cyclones into the central Tasman Sea, and tropical low pressure systems into the Coral Sea. Likewise, the mid-latitude westerlies and extra-tropical cyclones in the Southern Ocean are displaced further poleward as the ITCZ moves into the Southern Hemisphere.

1.2.4.1 Magnitude and Causes of Expansion

There has been an observed expansion of the global tropics since 1979 by 2 to 5 degrees latitude in each hemisphere (Seidel *et al.* 2008; Allen *et al.*, 2014), with an average trend of approximately 0.5 to 1 degree per decade (Lucas *et al.*, 2014). While most Global Climate Models (GCM) agree that tropical expansion will continue with greenhouse warming, the magnitude of this expansion is largely under-estimated (Allen *et al.*, 2014). GCM rates of expansion remain significantly less than observed due to short observational record, large natural variability and/or model deficiencies (Johanson and Fu, 2009; Allen *et al.*, 2012). Even the most recent GCM model ensemble, CMIP5, continues to under-estimate observed tropical expansion, probably because of an under-estimation of the climate effect of anthropogenic aerosols (Bond *et al.*, 2013). In particular, systematic model biases in CMIP5 (and previous CMIP3) relate to Indo-Pacific and western tropical Pacific variability (Grose *et al.*, 2014), leading to low confidence in regional projections for south east Australia.

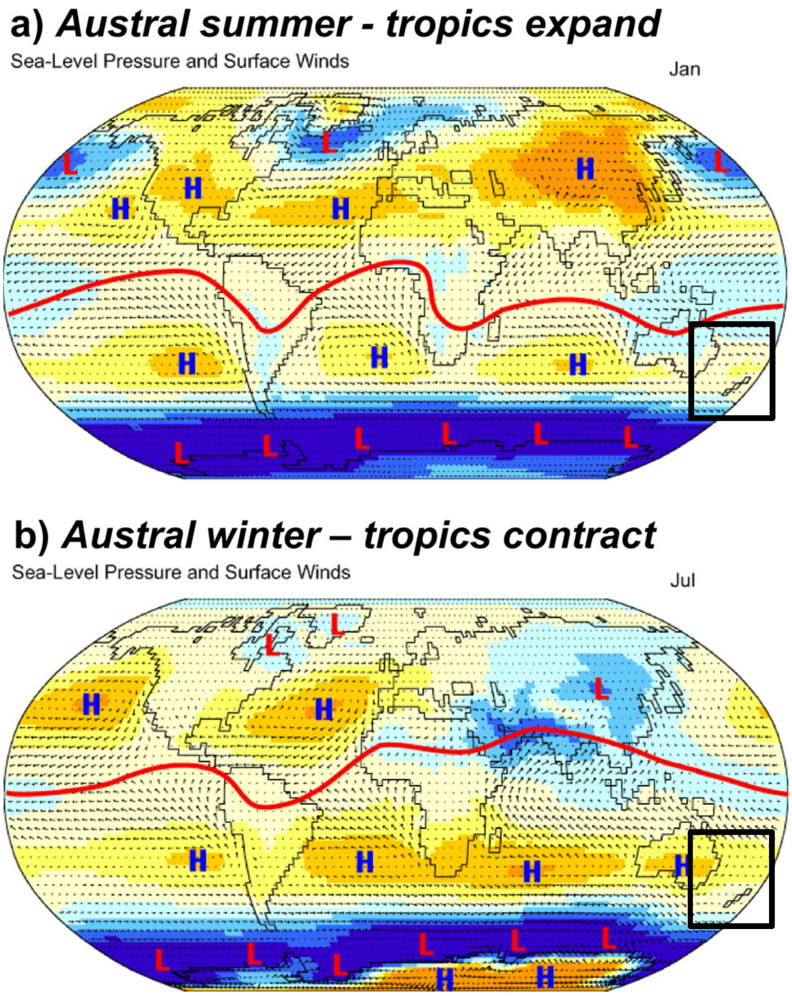

Figure 1.10 Mean sea level pressure and surface wind vectors during Austral summer (a) and winter (b). Warm (cool) colours represent areas of high (low) surface pressure. Red line denotes approximate position of sub-tropical ridge in Southern Hemisphere as tropics expand/contract. Black box shows area of Tasman and Coral Seas. Image from Laughlin (1997).

Multiple factors have been identified as potential drivers of tropical expansion, including increasing greenhouse gases, stratospheric ozone depletion and anthropogenic aerosols. In the past decade, the shift towards the La Nina-like state of the Pacific Decadal Oscillation has enhanced the expansion effect, and is likely to modulate the Pacific tropical belt width in the future (Allen *et al.*, 2014).

In the Southern Hemisphere in particular, ozone depletion in the high latitudes has played an important role in the meridional expansion of the tropics and associated poleward contraction of the extra-tropics over the last few decades (Polvani *et al*., 2011). Thus far, ozone depletion and greenhouse forcing have combined to produce strong positive trend in the Southern Annular Mode (SAM) in summer (Marshall *et al*, 2003). A positive (negative) SAM represents a poleward (equatorward) shift in the mid-latitude westerlies and contraction (expansion) of the extra-tropics towards (away from) Antarctica. The trend towards positive SAM is currently in-phase with an expanding tropics, leading to a poleward shift in the large-scale meridional circulation of the Southern Hemisphere. However, with the ozone hole projected to recover over this century, ozone and greenhouse gas forcing will oppose each other with ozone recovery leading to negative SAM trends and greenhouse gases continuing to shift the SAM towards positive values (Arblaster *et al*., 2011). Therefore, ozone healing may lead to weaker coupling between tropical and extra-tropical meridional change in the future.

1.2.4.2 Implications for Wave Climate in the Subtropics

The position of the STR, and associated STAC, significantly modulate the directional wave climate along the SEAS (Chapter 4). A sustained expansion of the tropics represents a move towards a more summer-like atmospheric circulation and wave climate (Figure 1.10). A first-pass conceptual analysis suggests this should lead to an anti-clockwise rotation of the mean wave direction. The displacement of the STAC into the central Tasman Sea produces more easterly winds and waves generated in the sub-tropics. At the same time, the poleward migration of mid-latitude extra-tropical cyclones means southerly wave generation is more distal for south east Australia, and southerly wave events are less frequent. Studies using GCM ensemble and wave modelling come to similar conclusions (Mori *et al*., 2010; Hemer *et al*. 2013a; Hemer *et al*., 2013b), although the 'spin-up' in the mid-latitude westerlies and thus Southern Ocean wave generation is another consideration for future wave climate along the SEAS. While an increase in Southern Ocean wave heights have been observed (Young *et al*., 1999) and modelled (Mori *et al*., 2010) with greenhouse forcing, the location of wave generation will be more poleward (distal) potentially leading to a less-frequent but longer-period southerly swell wave climate. The impacts of tropical expansion on the modal and storm wave climate, and implications for sediment transport, are discussed in more detail in Chapters 4 and 6.

1.2.5 Changing Behaviour of El Niño Southern Oscillation

While tropical expansion is a robust observed and modelled signal of anthropogenic climate change, another significant trend for Pacific coasts is the change in behaviour of El Niño Southern Oscillation (ENSO). Tropical expansion represents a change in the meridional atmospheric circulation (Hadley Cell), while ENSO modulates the zonal circulation (Walker Cell) in the Pacific. The impact of shifts in ENSO asymmetry and amplitude on wave climate and coasts is the focus of Chapter 5. Here, a brief background to ENSO dynamics and future changes is given.

ENSO is a highly complex, coupled atmospheric-oceanic phenomenon. El Niño or La Niña events are characterised by a positive feedback that occurs between trade wind intensity and zonal gradients in sea surface temperatures (SST), known as Bjerknes feedbacks (after Bjerknes, 1966). During ENSO neutral and La Niña phases (Figure 1.11 a and c), the trade winds pile up warm surface water in the western Pacific and upwell colder sub-surface water in the eastern Pacific along the equator and off the west coast of South America. This causes an east-west gradient in the ocean thermocline, and is responsible for bringing nutrients to the ocean surface and sustaining fisheries in the eastern Pacific. The atmospheric circulation associated with this pattern describes the zonal Walker Cell over the Pacific. The resultant east-west surface temperature gradient reinforces an east-west air pressure difference across the Pacific basin that in turn drives the easterly trade winds (Cai *et al.*, 2015b).

During La Niña events, the Walker circulation strengthens (Figure 1.11 c) and north and east Australia experiences increased rainfall, warmer SSTs and more tropical cyclone storm events. Very broadly, the coastal zone is impacted by increased fluvial discharge and ebb tidal delta growth, and increased storminess.

During El Niño events, the trade winds weaken, and the Walker circulation breaks down as atmospheric pressure rises in the western Pacific and falls in the eastern Pacific (Figure 1.11 b). During El Niño, the Bjerknes feedback operates in reverse, with weakened trade winds and SST warming east to west along the Equator reinforcing one another (Cai *et al,* 2015b). Under these conditions, upwelling and the thermocline is supressed in the eastern Pacific. El Niño is associated with drier than normal conditions in north and east Australia and cooler than normal SSTs in the Coral Sea and equatorial Pacific. As a result, there is reduced tropical and sub-tropical origin storminess and generally calmer wave conditions.

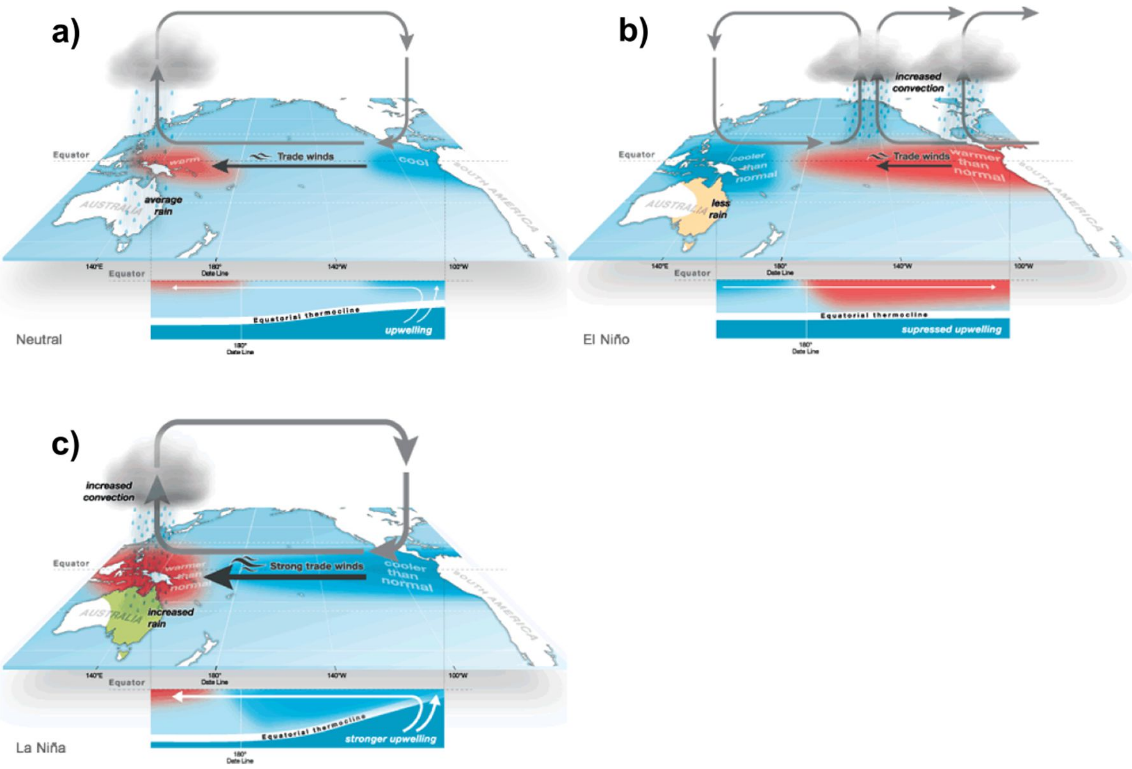

Figure 1.11 Coupled atmosphere-ocean response during ENSO neutral phase (a), El Niño event (b) and La Niña event (c). Dark blue in (a) and (c) represents the 'eastern Pacific cold tongue' and red denotes the 'western Pacific warm pool'. Images from Bureau of Meteorology (2015, http://www.bom.gov.au/climate/enso/history/ln-2010-12/three-phases-of-ENSO.shtml).

La Niña events tend to follow El Niños, but not the other way around. A La Niña can last for more than a year thus affecting the year-round wave climate, but an El Niño tends to end abruptly in late Austral summer or autumn (Takashimi *et al.*, 2011). It remains unclear what causes this quasi-oscillatory behaviour and breaks the positive feedback cycle of each ENSO phase; whether it is self-sustaining or triggered by stochastic forcing (Neelin *et al.*, 1998). One theory that has persisted is the "delayed oscillator theory" (Schopf and Suarez, 1988; Battisti and Hirst, 1989). This suggests that a growing warm event in the central and eastern tropical Pacific (El Niño) generates slow-moving, westward-propagating surface ocean Rossby waves. These are then downwelled and reflected off the Indonesian landmass on the western Pacific boundary, and return to the eastern Pacific as subsurface water Kelvin waves. The Kelvin waves are upwelled against South America, shallowing the thermocline. It takes Rossby waves ~ 200 days to cross the Pacific basin (phase speed ~ 0.9 m/s, distance ~ 18,000 km), and Kelvin waves ~ 70 days to return eastward (phase speed ~ 2.9 m/s). The peak amplitude of the cold event (La Niña) is about 6 months after the peak of the warm event (El Niño), or about 18 months after the onset of El Niño (Mantua and Battisti, 1994). While this theory explains the evolution and shutdown of a warm event (El Niño) and the subsequent onset of a cold event (La Niña), it does not indicate what causes the initial onset of the warm event. The cause of El Niño events remains a fundamental uncertainty in the prediction and modelling of ENSO behaviour.

ENSO amplitude is modulated by the background climate state in the Pacific (McPhaden *et al*., 2006; Collins *et al*., 2010). The Pacific Decadal Oscillation (PDO) measures the background oceanic state of the (specifically, east) Pacific; whether it is in a warm "El Niño-like" state (PDO positive) or a cool "La Niña-like state" (PDO negative). The mid-1970s phase shift of the PDO from a colder to warmer tropical eastern Pacific saw stronger ENSO amplitude (Federov and Philander, 2000), marked by the 1982/1983 and 1997/1998 extreme El Niño events, and the 1988/1989 and 1998/1999 extreme La Niña events. The PDO shifted back to a cool phase in the mid-2000, and has been associated with a period of subdued ENSO activity. Very recently (2015), it seems the PDO has swung back to its positive phase, with a contemporaneous large El Niño event building in Austral autumn 2015.

Since the 1970s there has been a trend towards ENSO anomalies developing in the central rather than eastern Pacific (Figure 1.12), which some believe to be a separate mode to the classic Canonical ENSO pattern (e.g. Ashok *et al*., 2007). Others consider it to be part of ENSO asymmetry (Takahashi *et al*., 2011, Takahashi and Dewitte, 2015), perhaps representing a stalling of the ENSO cycle. Both central Pacific-type ENSO (Yeh *et al*., 2009) and extreme ENSO events (Cai *et al*., 2014; 2015a) are projected to increase in the future with greenhouse warming, associated with a weakening of the Walker circulation (Vecchi *et al*., 2006; Xie *et al*., 2010). The impact of a shift from eastern to central Pacific ENSO on wave climate and coastal stability in Australia is the focus of Chapter 5.

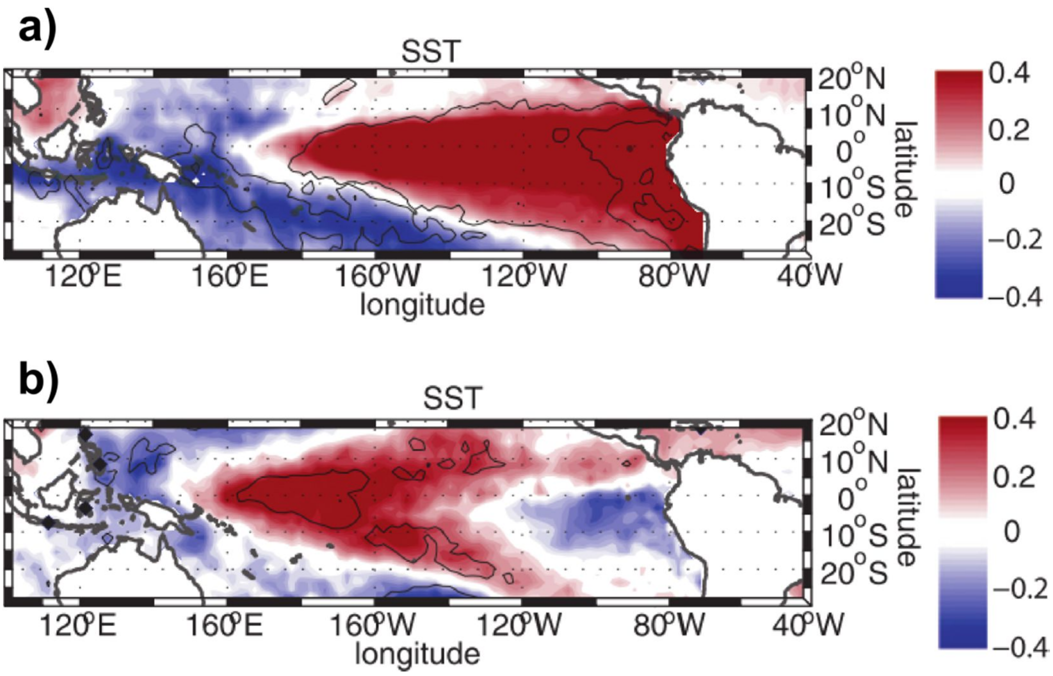

Figure 1.12 Sea Surface Temperature (SST) composite anomalies during an eastern Pacific ENSO pattern (a) and a central Pacific pattern (b), from Taschetto and England (2009).

1.2.6 Coastal Response to Sea Level Rise with Wave Climate Change

Wave climate change with greenhouse warming is considered the dominant process impacting shoreline change on high-energy sandy coastlines from interannual to multidecadal timescales (Slott *et al.*, 2006, Coelho *et al.*, 2009), while sea level rise (SLR) becomes the dominant process from centuries to millennia.

Global (eustatic) SLR is the sum of thermal expansion of the oceans and the loss of land-based ice (glaciers, ice caps and ice sheets in Greenland and Antarctica) due to increased melting. Global average sea level could rise by between 0.28 and 0.98 m by 2100 (compared to a 1986 – 2005 baseline), depending on which emissions scenario is followed (IPCC, 2014). Local rates of SLR may differ from global rates, because of isostatic adjustments to land, climate variability and oceanographic processes, all of which can affect the relative rate of rise. SLR poses a substantial threat to coastal communities in Australia (Department of Climate Change, 2009), and SLR research has largely eclipsed that of wave climate change over the past decade (Nicholls, 2007).

In south east Australia, coastal sea levels are influenced by variability in ENSO, the PDO and the strength of the easterly trade winds, both directly, and through their effect on the East Australian Current (EAC). The EAC is a poleward-flowing western boundary current, running down the length of the SEAS from north to south. The flow speed and position of the EAC is dependent on the westward-flowing South Equatorial Current, which in turn depends on the strength of the easterly trade winds (and thus sensitivity to ENSO variability). Holbrook *et al* (2011) showed that variability in ENSO, EAC transport and coastal sea level at Fort Denison, Sydney, are all significantly correlated and the linking mechanism is westward-propagating oceanic Rossby waves. The long-term coastal sea level rise (~ 1 cm/decade) observed at Fort Dension is coupled to the strengthening and poleward extension observed in the EAC. The poleward extension of the EAC (350 km in 60 years, Ridgway, 2007) is driven by a southward shift of the Southern Hemisphere subtropical ocean gyre (Gillet and Thompson, 2003), associated with the trend towards positive SAM (i.e. a poleward contraction of the mid-latitude westerly winds) (Marshall *et al*., 2003).

The coastal response to SLR is traditionally assessed using the Bruun Rule (Bruun, 1954; 1962), largely due to its simplicity and lack of easy-to-use alternatives (Ranasinghe *et al*., 2007). Dean and Maurmeyer (1983) extended the Bruun Rule to obtain a Standard Bruun Rule that applies to mainland beach systems with no backbarrier. The Standard Bruun Rule relates shoreline retreat, R, to SLR, S, by the dimensions of the active cross-sectional beach profile, which can be approximated by the distance offshore from the high tide shoreline, L, to the depth of closure, h_c:

$$R = \frac{L.S}{h_c} \tag{1.4}$$

The annual depth of closure (DOC) is usually taken to be ~ 12 m along most of the south east Australian coast (Short, 1999). As discussed in Chapter 6, a representative active profile slope is ~ 0.02, therefore L in this case is 600 m. For a 1 m SLR, plausible along the SEAS by 2100 (IPCC, 2015), the Standard Bruun Rule predicts a recession of the high tide shoreline of ~ 50 m. Because a beach slope of 0.01 to 0.02 is common for many of the world's coastlines (Ranasinghe *et al*., 2007), 50 x S or 100 x S is commonly applied as a rule of thumb in engineering practice (SCOR, 1991).

However, there are significant uncertainties as to whether this provides a realistic assessment of long-term coastal response along high-energy, wave-dominated coastlines. This is because the Bruun Rule make two major assumptions; 1) that the profile shape is conserved (i.e. in equilibrium) as sea level rises, and 2) that all sediment eroded is transported seaward of the active profile and does not form part of the profile response. It does not consider any alongshore exchange of sediment (Ranasinghe *et al*., 2012), storm-induced overwash (Rosati *et al*., 2013) or wave-induced onshore sediment transport during storm events.

The Bruun Rule also does not account for the influence of lower shoreface disequilibrium stress on the active profile over the longer term (Wright, 1995). The extent to which the lower shoreface is in equilibrium with the long-term wave climate and sea level can be conceptualised in the context of the shelf regime. The shelf can be classified into three different modes (underfit, overfit or graded) by comparing the measured cross-sectional profile of the lower shoreface against a theoretical equilibrium profile. In cases where the shelf profile is underfit, it is deeper or steeper than the equilibrium profile for the prevailing sea-level, wave climate and sediment characteristics. This indicates the lower shoreface is under-filled with sediment and there is positive accommodation space for deposition (Daley and Cowell, 2012). In this instance, cross-shelf transport away from the lower shoreface to the upper shoreface is unlikely. On overfit shelves, the opposite applies, where the lower shoreface is shallower or flatter than the equilibrium profile. Under these conditions, the lower shoreface is overfilled with sediment, there is negative accommodation space, and conditions for a cross-shelf transfer of sediment from the lower to upper shoreface exist. A graded profile exists when the measured shelf profile approximates to the equilibrium profile.

Disequilibrium stress comes about because of geomorphic relaxation – the time required for the shoreline to attain equilibrium with a new set of forcing conditions (Cowell *et al*., 1999). The effect of disequilibrium stress is relevant to chronic problems in coastal management such as systematic shoreline erosion, but often overlooked in coastal process studies (Daley and Cowell, 2012). If the shelf state is overfit (underfit), then an accretionary (erosional) regime for the upper shoreface exists. Results from Chapters 4 and 6 suggest that both modal and storm wave climate change associated with greenhouse forcing will increase the potential for onshore sediment transport from the lower shoreface along the SEAS, potentially lowering overfit shelves towards equilibrium. These findings and their implications for the long-term coastal response to SLR are explored in Chapter 7.

While the simplicity of the Bruun Rule is a major part of the attraction, a relaxation of the assumptions can make these type of models more generally applicable (Cowell *et al.*, 2006). Direct modifications to the Bruun Rule have been proposed to accommodate alongshore sediment exchange between the beach profile and tidal inlets along inlet-interrupted coastlines (Ranasinghe *et al.*, 2012), and barrier overwash and Aeolian transport (Rosati *et al.*, 2013). More complex geometric mass-balance models such as the Shoreface Translation Model (Cowell *et al.*, 1992; 1995) have also been developed to simulate the translation of a coastal sand body over a variable substrate with SLR, taking into account shoreface geometry and accommodation potential.

1.3 AIMS AND OBJECTIVES

The overall aim of this thesis is to improve the understanding of how variability and shifts in atmospheric climate impact directional wave conditions and coastal behaviour along the south east Australian shelf (SEAS). Wave-driven currents are the principle mechanism for sand transport on the SEAS (Goodwin, 2005). Therefore, there should be a robust causative relationship between atmospheric climate, wind-waves and coastal stability. Specifically, three research hypotheses were considered:

Hypothesis 1:

> The current state-of-the-art of regional downscaling of Global Climate Model (GCM) output is the best approach to forecasting nearshore wave climate and coastal change along the SEAS.

Hypothesis 2:

An expansion of the tropical belt projected with anthropogenic climate change will cause a shift in the directional wave climate and impact coastal behaviour along the SEAS.

Hypothesis 3:

A change in El Niño Southern Oscillation (ENSO) behaviour projected with anthropogenic climate change will cause a shift in the directional wave climate and impact coastal behaviour along the SEAS.

Responses to these three hypotheses and the extent to which they have been answered in the thesis are considered in Chapter 7 (Conclusions).

1.4 STRUCTURE AND APPROACH

1.4.1 Thesis Structure

This thesis contains five separate scientific studies as chapters. The findings of each study inform the relevance and direction of the next, thus forming one coherent thesis. While each chapter includes an independent introduction and conclusion, an overall introduction and background is given in this (the first) chapter, and key findings of the thesis as a whole are discussed in the final chapter.

Each chapter begins with an overview of the study, key findings, and statement of publication and author contribution in cases where collaborative material is presented. Published papers and manuscripts submitted for publication are provided as Appendices. A scientific format (Introduction – Methods – Results – Discussion – Conclusions) is followed in each chapter.

- **Chapter 1** states the relevance of the thesis, provides a general background to the work, and sets out the aims, objectives, structure and approach taken;
- **Chapter 2** explores the uncertainties and limitations related to numerical wave models within a regional downscaling framework, and examines what this means for the projection of nearshore wave climate and coastal change;

- **Chapter 3** evaluates the feasibility of obtaining nearshore wave information from shore-based video imagery as an alternative to the downscaling approach in Chapter 2;
- **Chapter 4** develops a wave climate typology that relates modal wave conditions to synoptic climate, which is then used to investigate mid-shelf wave climate change with tropical expansion;
- **Chapter 5** uses the typology developed in Chapter 4 to investigate wave climate and coastal change associated with shifts in El Niño Southern Oscillation;
- **Chapter 6** investigates potential changes to the storm wave climate and storm-driven cross-shelf transport with an expansion of the tropical belt;
- **Chapter 7** discusses the key findings of the thesis as a whole

1.4.2 Approach Taken

In light of significant uncertainties in regionally-downscaled and video-derived nearshore wave climates highlighted in Chapters 2 and 3, a combined observational-modelling approach is taken from Chapter 4 onwards. This approach uses deepwater wave observations as boundary forcing for numerical wave and morphodynamic modelling across the SEAS, in order to investigate wave climate impacts on the coast. A surrogate-observational approach is advocated whereby observed wave conditions and modelled coastal impacts are used as proxies for future climate change states. This method provides a range of scenarios for an uncertain future, and moves away from the deterministic model that is reliant on downscaled GCM output for projections of coastal impacts.

1.4.3 Numerical Modelling

The approach taken in this thesis is made possible by the availability of a latitudinal array of wave buoys along the SEAS that have been collecting spectral wave information since the mid-1970s. Long-term, continuous and directional wave data are available for mid-shelf locations from 27.5 to 37.3 ° S. Statistical analyses of this dataset, combined with numerical modelling, form the underlying methodology of this thesis.

Throughout the thesis, wave and sediment transport modelling is used to project wave climate impacts on the coast. In Chapter 2, the SWAN and WaveWatch III models are used; in Chapter 3, a MIKE 21 Boussinesq Wave model; in Chapter 5, a MIKE 21 Spectral Wave and MIKE 21/3 Coupled Flow model; and in Chapter 6, a MIKE 21 Spectral Wave model. All these models used the same (or sub-sets of) bathymetric information, and were validated against the same nearshore wave observations. Here, a summary of the bathymetries used and nearshore validation is given to support modelling in each chapter.

1.4.3.1 Bathymetries

Two independent model domains were created for wave and sediment transport modelling; one covering the Sydney region (extending from Bate Bay to the south, to Foresters Beach to the north) and a second covering the Coffs Harbour region (extending from Hat Head to the south to Coffs Harbour breakwater to the north) (Figure 1.13). These model domains are separated by ~ 2.5 º of latitude, which is the magnitude of tropical expansion predicted by some GCMs for the coming century.

Both domains extend from the shoreline to the depth contour on which the mid-shelf wave buoys at Sydney and Coffs Harbour are moored (~ 90 m). During most applications, the models were forced with boundary wave conditions from these buoys; therefore, an inherent assumption of this modelling approach is that wave conditions are identical along the same shore-parallel isobaths at this depth. This assumption is valid for most modal wave conditions, for which 90 m depth is beyond wave base (Section 1.2.3).

All available bathymetries were sourced, quality-controlled and mosaicked into one dataset for each model domain. The mosaics comprised four bathymetry types from 19 separate surveys; shore-normal single-beam echosounder (SBES) survey lines, multi-beam echosounder (MBES) soundings, airborne LIDAR bathymetry and seabed contours digitized from navigational charts. This included one survey that was conducted by me at Scotts Head, on the mid-north coast of NSW, in 2014. Metadata and extents of bathymetries used for both regions are given in Table 1.2 and Figure 1.14.

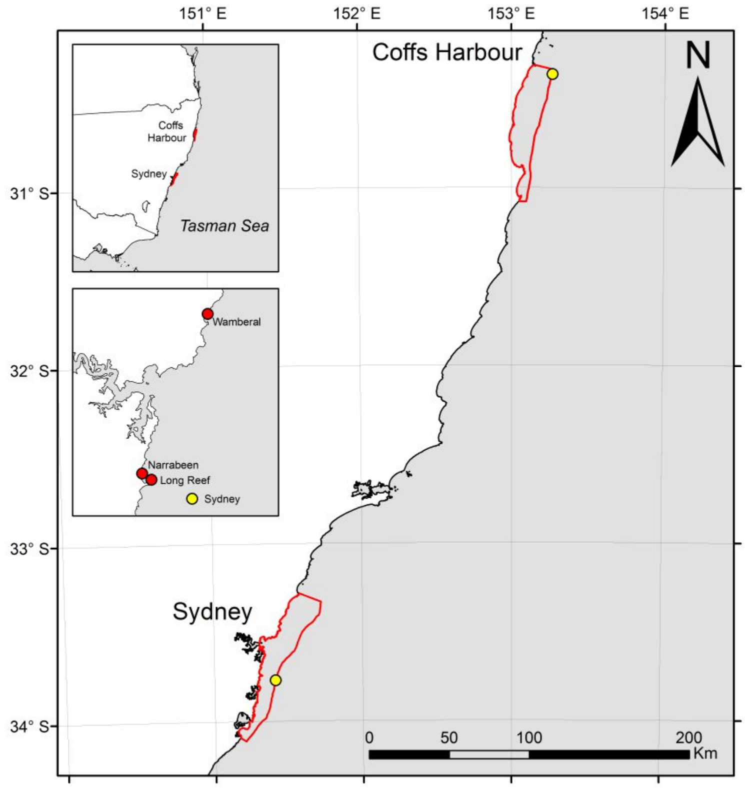

Figure 1.13 Locations of Sydney and Coffs Harbour model domains (red) with position of mid-shelf wave buoys also shown (yellow). Domains are separated by ~ 2.5 º latitude. Top inset shows domain locations in relation to south east Australia. Bottom inset shows location of Sydney and nearshore wave buoys used for model validation.

Table 1.2 Bathymetries used *, in year order for shoreface and inner shelf.

Year	Type (ownership)	Coverage	Resolution (m)	Depth (m AHD)
Shoreface				
1988	SBES (OEH)	Trial Bay (bay)	50 m lines	0 - 30
2008/11	LADS (OEH)	Wamberal (bay)	5 m point cloud	0 – 40
2008	LADS (OEH)	South West Rocks	5 m point cloud	0 - 40
2011	SBES (OEH)	Narrabeen (bay)	50/100 m lines	0 – 40
2011	SBES (OEH)	Bate Bay (bay)	250 m lines	0 – 45
2012	SBES (OEH)	Manly (bay)	50/100 m lines	0 – 45
2012	SBES (OEH)	Wanda (surfzone)	50 m lines	0 – 15
2013	MBES (OEH)	Sawtell (Deep Reef)	5 m point cloud	0 – 40
2011/14	SBES (OEH)	Sawtell (surfzone)	50 m lines	0 – 15
2014	SBES (OEH)	Narrabeen (surfzone)	50 m lines	0 - 15

2014	MBES (OEH)	Syd. Northern Beaches	5 m point cloud	5 – 50
2014	SBES (OEH)	Dee Why (surfzone)	50 m lines	0 – 15
2014	SBES (OEH)	Bongin (surfzone)	50 m lines	0 – 15
2014	SBES (OEH)	Bilgola (surfzone)	50 m lines	0 – 15
2014	MBES (OEH)	Nambucca Heads	5 m point cloud	0 – 40
2014	SBES (MQU)	Scotts Head	25/50 m lines	0 – 15
Inner shelf				
Multiple	AusBathy (GSA)	Australian shelf	250 m gridded	0 – 140
1972	SBES (RAN)	NSW inner shelf	3000 m lines	0 – 95
1984	Fairsheets (OEH)	Sydney region	2 m contours	0 – 85

* AHD – Australian OEH – Office of Environment and Heritage (NSW), MQU – Macquarie University, LADS – Laser Airborne Depth Sounder, SBES – Single Beam Echo Sounder, MBES – Multi Beam Echo Sounder, GSA – GeoScience Australia, RAN – Royal Australian Navy, AHO – Australian Hydrographic Office, Fairsheets – Navigational Charts.

In areas where no sounding information was available in depths greater than ~50 m, gaps were filled using the GeoScience Australia Bathymetric and Topographic (AusBathy) grid (Whiteway, 2009) after it was found in Chapter 2 that depth differences of up to 10 m existed when AusBathy was compared with other bathymetries in depths shoreward of ~50 m in both the Sydney and Coffs Harbour regions. AusBathy is a 9 arc-second bathymetric grid for the entire Australian shelf (Whiteway, 2009), and is not intended for use in the nearshore where bathymetric observations are sparse. All data gaps shoreward of ~50 m depth were instead filled by digitizing contour extensions between adjacent soundings. A buffer-overlap method was used when mosaicking to ensure no elevation stepping occurred between adjacent bathymetries.

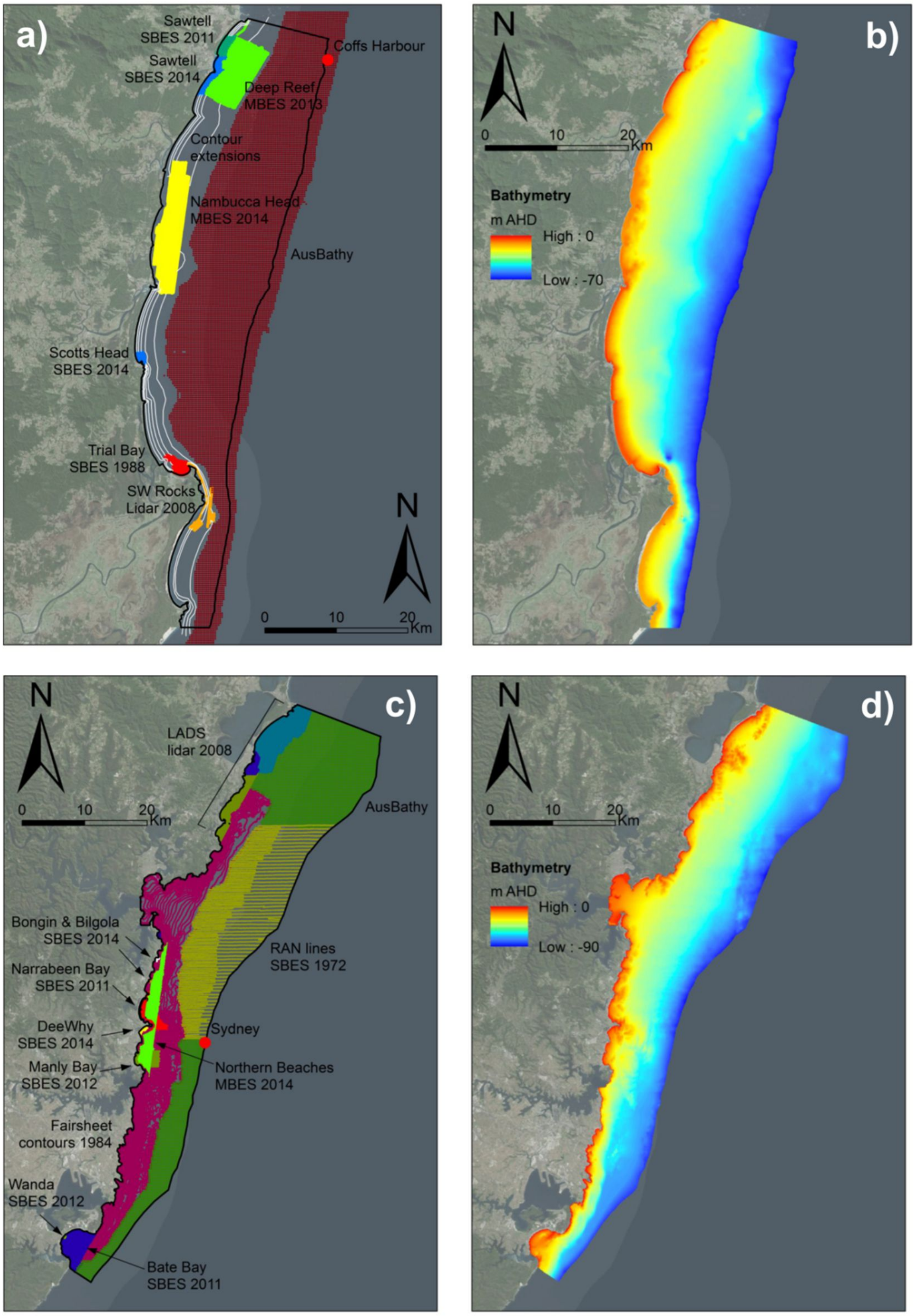

Figure 1.14 Extent of bathymetries used (a, c) and gridded product (b, d) for Coffs Harbour region (a,b) and Sydney region (c,d). Locations of Coffs Harbour and Sydney mid-shelf wave buoys are shown in (a) and (c).

As can be seen in Figure 1.14, some datasets are of higher spatial resolution than others. The Sydney region has a greater amount of good quality bathymetries available than

Coffs Harbour. In particular, airborne LIDAR and vessel-based MBES surveys provide a very high quality representation of the seabed. While all information was down-sampled for modelling, a flexible Delaunay mesh in the MIKE by DHI modelling suite allowed the high resolution of some bathymetries to be retained where needed (e.g. in areas of complex seabed topography and/or shallow water) with coarser resolution elsewhere.

Areas where high-resolution information was available include; Sydney Northern Beaches, Avoca and Terrigal-Wamberal compartments, Nambucca Heads and Deep Reef, off Sawtell. The most continuous of these is Sydney Northern Beaches (Figure 1.15).

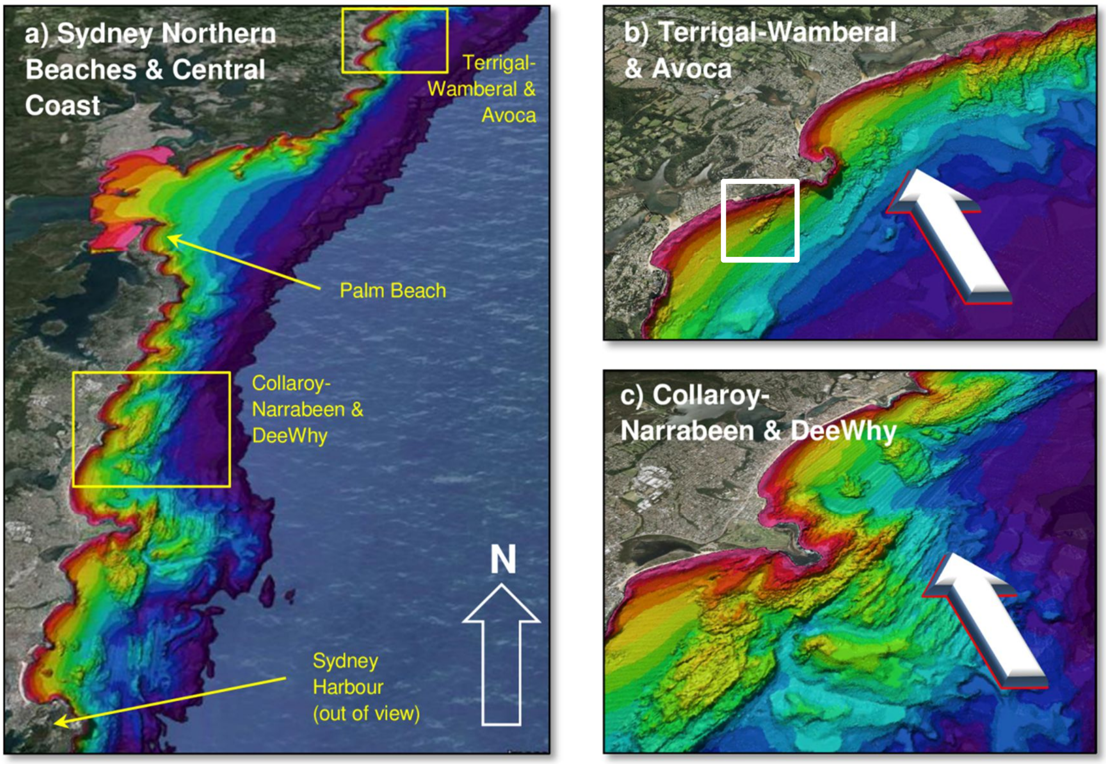

Figure 1.15 Exert of the Sydney regional model bathymetry for a) Sydney Northern Beaches and part of Central Coast NSW. Locations of study sites at Collaroy-Narrabeen (b) and Terrigal-Wamberal (c) are shown. Arrows show direction of mean wave propagation (south-east). Locations of other sites referred to in this thesis are shown in (a). Data was gridded at 10 m^2, interpolated in Fledermaus software and projected in GoogleEarth.

While beyond the scope of this thesis, it is interesting to note the highly complex rock reef, palaeo river valleys and sea cliffs that exist below the water line along the

Northern Beaches. It demonstrates why Collaroy-Narrabeen is so sheltered from southerly wave events, with Long Reef extending far beyond the headland. It also shows that only small pockets of sand exist within each embayment and that each must have a closed sediment budget, with subaqueous reef and a steep slope preventing a regular sediment exchange between compartments. The feature that can be seen in the Avoca compartment (white box) is the sunken HMAS Adelaide, now a dive site. While the features themselves are peripheral to the thesis, it demonstrates the high quality datasets on which wave and sediment transport modelling is based.

1.4.3.2 Validation

All models used in this thesis were validated in the nearshore by observations from three Datawell WaveRider buoys deployed in the Sydney region (locations Figure 1.14). The Narrabeen and Wamberal buoys were moored in ~ 12 m water depth, and the Long Reef buoy was moored in ~ 20 m depth. The Narrabeen and Wamberal buoys measured hourly directional wave spectra, while the Long Reef buoy was non-directional. The Narrabeen and Long Reef buoys recorded from July to November 2011, while the Wamberal buoy recorded from August 2011 to March 2012. I carried out two other buoy deployments at Sawtell and Scotts Head, on the mid-north coast of NSW. However, deployment lengths were short (1 – 2 days) and not suitable for model validation.

With the exception of Chapter 2, the MIKE by DHI model suite was used. In each case, wave refraction across the shelf was provided by a MIKE 21 Spectral Wave model, thus nearshore validation of this model is given here. Nearshore validation for SWAN is given separately in Chapter 2. Model outputs of significant wave height, H_{m01}, mean wave period, T_{m01}, and mean wave direction, θ, were compared against the equivalent parameters available for the nearshore buoys (significant wave height, H_s, mean wave period, T_z, and mean wave direction, *MWD*). Comparative wave statistics are discussed in Section 1.2.1.3 (this chapter) and Section 2.7.3 (Chapter 2).

To obtain an understanding of spatial model bias, validation was performed over the period when all buoys were recording simultaneously (i.e. August to November 2011). Validation therefore takes place during an Austral winter-spring wave climate that is typically dominated by extra-tropical and oblique wave energy. Figure 1.16 shows the wave height and direction recorded at the mid-shelf Sydney wave buoy over this period.

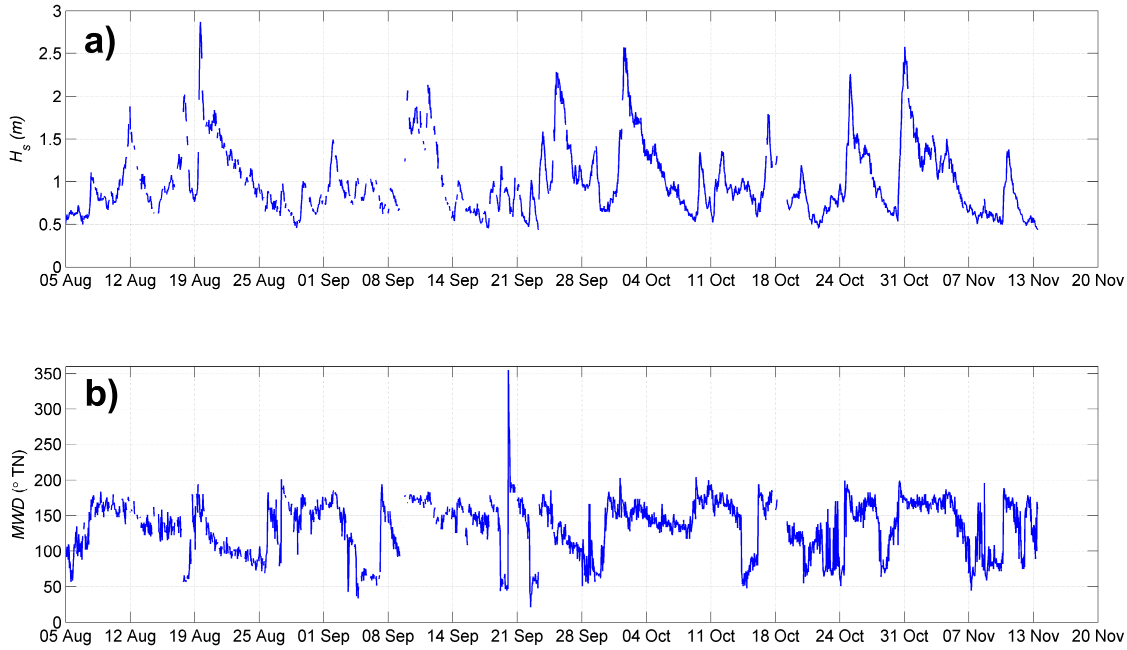

Figure 1.16 Wave height (a) and direction (b) recorded at the mid-shelf Sydney wave buoy during the modal validation period.

The validation period contains five events where the hourly H_s exceeded 2 m, and these are all associated with south-south-east (~ 160 °) wave conditions, typical of this time of year. Outside these events, the modal wave direction is south-east (~ 135 °), with some easterly (shore-normal) events occurring. This gives a good directional and energy range with which to validate the model.

The model was run with hourly parametric deepwater wave data from the Sydney Waverider buoy during the validation period. A JONSWAP spectrum with a directional spreading function equivalent to approximately 20 ° of spreading was used to replicate a mixed sea-swell environment. All model settings were largely left as default. Chapter 2 shows that calibrating the internal physics of third-generation wind-wave models against observations is largely inconsequential in open coastal locations. This is because the physical parameters that make up the models have been well calibrated and tuned over approximately 50 years of wind-wave model development (see Section 1.2.2). Instead, effort is better directed towards maximising the quality of input boundary conditions (waves, bathymetry), and bias-adjusting output against observations.

Model skill was assessed using five validation metrics; Pearson's squared correlation, R^2, Root mean squared error, *RMSE*, Bias (mean error), Scatter Index, *SI*, and Symmetric slope, *m*. An explanation of the significance of these metrics is given in Section 2.7.4 in Chapter 2. Figure 1.17 compares the quantiles between modelled and measured results and Table 1.3 details the verification metrics.

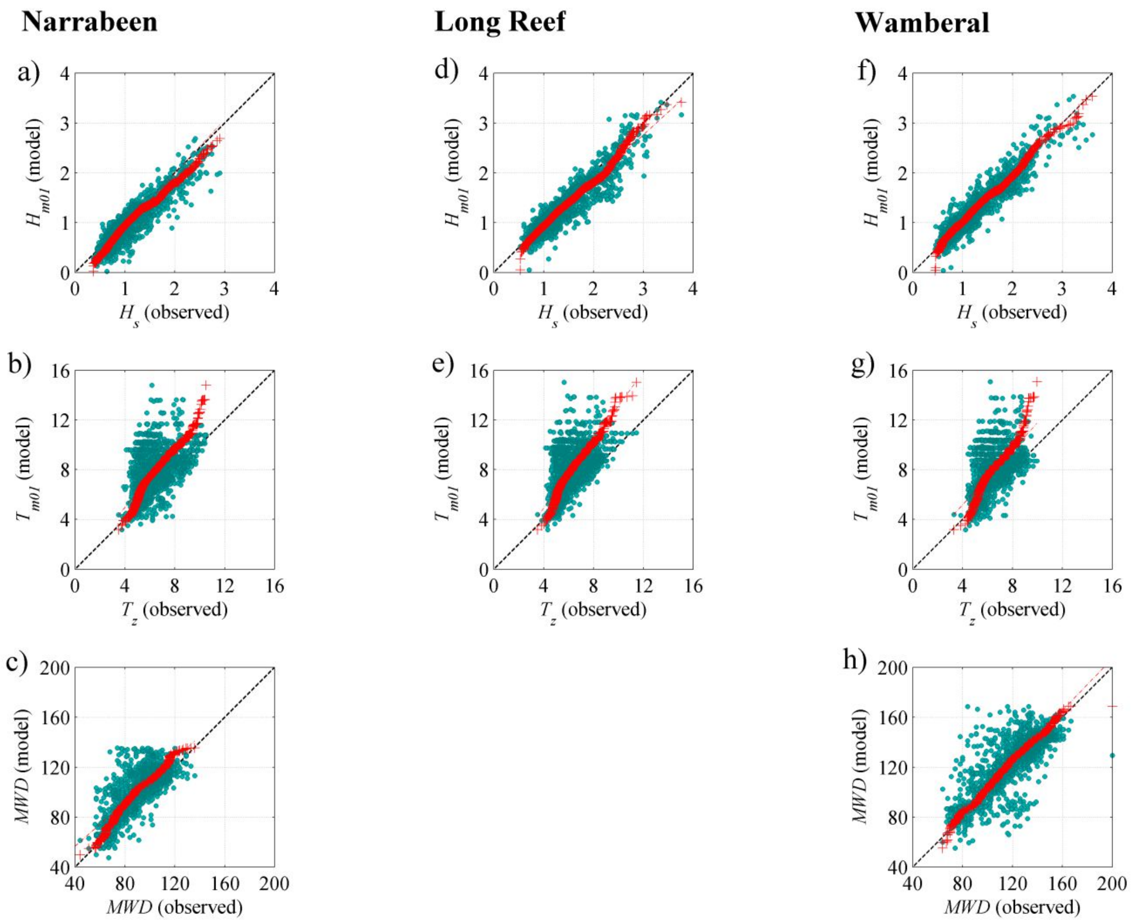

Figure 1.17 Validation of MIKE 21 Spectral Wave model at Narrabeen (a – c), Long Reef (d – e) and Wamberal (f – h) for modelled wave height (a, d, f), period (b, e, g), and direction (c, h) against hourly buoy measurements over the overlapping deployment period. Quantiles are shown in red, data points in green.

The model performs well in the prediction of nearshore wave heights at all buoy locations (R^2 0.91 to 0.93, $p < 0.05$). *RMSE* is consistently low ($\leq$ 0.07 m) at all three sites, and prediction is good for all range of wave heights measured (low bias, high slope and consistent quantile comparison). However, at the most exposed locations (Long Reef and Wamberal), Figure 1.17 indicates a trend towards slight under-estimation of $H_s > 3$ m.

Table 1.3 Model validation metrics.

	Narrabeen (n = 2010)			Long Reef (n = 2093)			Wamberal (n = 1842)		
	H_{m01}	T_{m01}	MWD	H_{m01}	T_{m01}	MWD^{**}	H_{m01}	T_{m01}	MWD
$R^{2\,*}$	0.91	0.44	0.76	0.93	0.50		0.94	0.48	0.81
$RMSE$	0.07	0.65	4.46	0.07	0.69		0.06	0.65	4.38
Bias	-0.01	0.13	0.88	-0.01	0.16		0.00	0.14	0.39
SI	0.06	0.10	0.05	0.05	0.11		0.05	0.10	0.04
m	0.88	0.59	0.79	0.88	0.75		0.90	0.72	0.82

* All R^2 values are to $p < 0.05$.
** Long Reef buoy is non-directional.

Comparisons of wave period show similar biases between sites, suggesting a systematic error. The over-prediction of wave period by the model is probably due to the absence of a local wind field being applied with waves at the model boundary. Another contributing factor could be that the JONSWAP spectrum assumed in the model contains more energy in the low frequency tail than may actually occur. This low frequency would propagate into the nearshore more efficiently exaggerating an initially small difference. Quantile plots indicate the over-prediction is most non-linear for short-period seas (T_{m01} < 7 s) and long-period swells (T_{m01} > 11 s), and best (i.e. linear with a constant offset ~ 1s) for intermediate conditions.

Since this error is systematic, it can be corrected for using a cumulative distribution function (CDF) matching approach (after Brocca *et al.*, 2011), with a 4th order polynomial of coefficients as shown in Figure 1.18. A 4th-order polynomial describes the mean offset between measured and modelled quartiles of the mean wave period at all three sites:

$$T_{m01} = aT_z^4 + bT_z^3 - cT_z^2 + dT_z - f \tag{1.5}$$

where a = -0.00082, b = 0.087, c = 1.7, d = 13 and f = 27. The quartic equation can be solved for T_z so that an adjustment to the modelled wave period can be made to agree with observations;

$$T_z\left(T_{m01}\right) = 26.524 + \frac{1}{2}\sqrt{1432.06 + \frac{\beta}{\alpha^{\frac{1}{3}}} + 1.103\,\alpha^{\frac{1}{3}}} - \frac{1}{2}\sqrt{2864.119 - \frac{\beta}{\alpha^{\frac{1}{3}}} - 1.103\,\alpha^{\frac{1}{3}} + \frac{110325.862}{\sqrt{1432.06 + \frac{\beta}{\alpha^{\frac{1}{3}}} + 1.103\,\alpha^{\frac{1}{3}}}}} \quad (1.6)$$

$$\alpha = -2.322\times10^{7} + 2.60\times10^{6}\,\mathrm{T}_{m01} + 11.619\sqrt{4.241\times10^{12} + \mathrm{T}_{m01}\left(-9.251\times10^{11} + \left(5.135\times10^{10} - 1.764\times10^{7}\,\mathrm{T}_{m01}\right)\mathrm{T}_{m01}\right)}$$

$$\beta = -35540.421 + 1473.613\,\mathrm{T}_{m01}$$

Equation 1.6 has been written as a Matlab function and is provided in Appendix 8 so that the wave period output by MIKE 21 SW can be corrected in the nearshore. It is only valid for Tm_{01} between 4 and 15 s, for exposed nearshore locations in the Sydney region (that are outside zones of dominant diffraction), and for MIKE 21 SW results when the model is run with boundary waves only (no wind field).

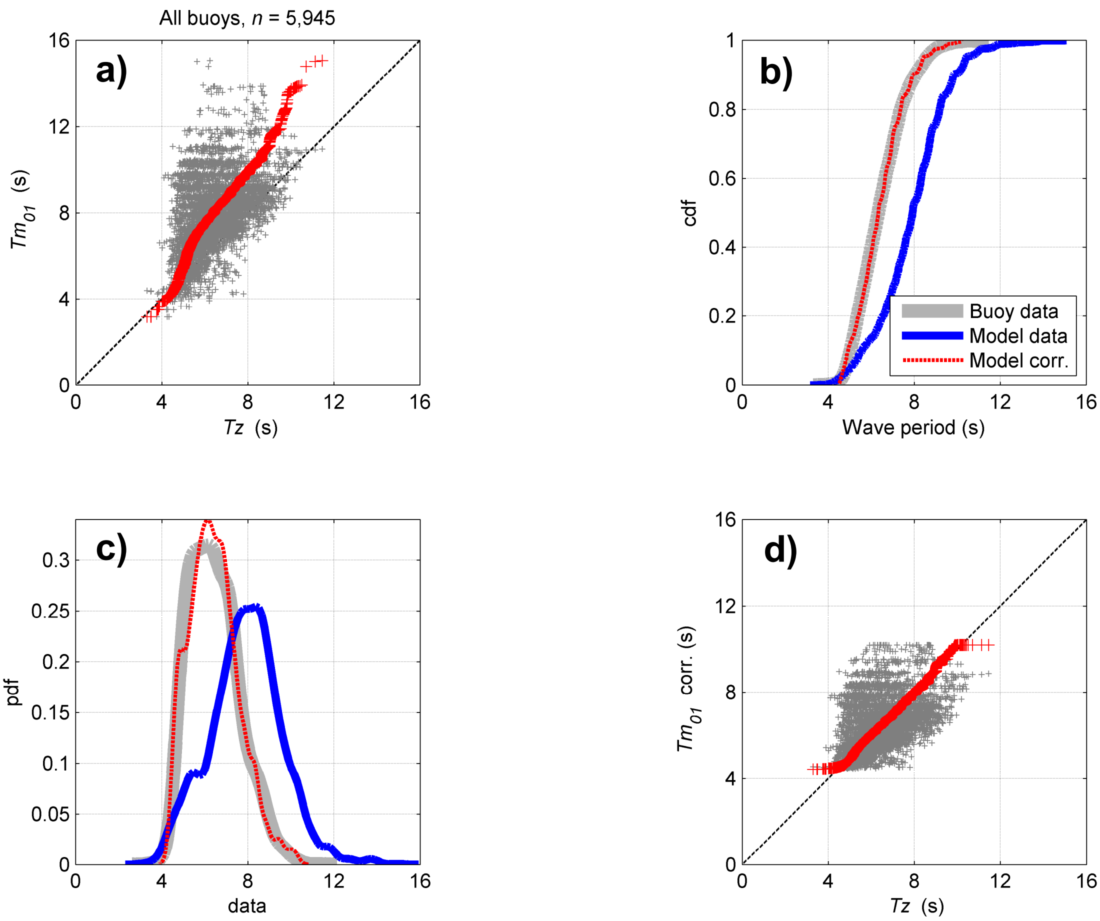

Figure 1.18 Modelled wave period correction by CDF matching using observed wave period at all nearshore buoys; a) comparison of observed and modelled wave period (grey) and quantiles (red) at all buoy locations, b) cumulative distribution and c) probability density of wave period

observed at the buoys (grey), modelled (blue) and model-corrected (red), and d) resultant comparison of model-corrected wave period against buoy-observed wave period.

Mean wave direction is well represented by the model (*RMSE* < 5 °) at the locations of the two directional buoys, Narrabeen and Wamberal. A very good directional distribution (R^2 0.81, $p < 0.05$) is modelled at the Wamberal buoy, which is moored at the northern end of the embayment, directly exposed to the modal south-easterly wave climate. There is therefore high confidence in the prediction of directional power at exposed nearshore sites. At Narrabeen, a central embayed location, waves south of ~130 ° are not recorded due to the shadowing of Long Reef headland. Onshore wave directions (~80 ° and 120 °), however, require 5 ° to 10 ° further anti-clockwise refraction to agree with buoy measurements.

There is no nearshore validation available for the southern end of embayments that are in headland diffraction zones with the south-easterly modal wave climate. A phase-averaged model such as MIKE 21 SW cannot fully resolve diffraction (Section 1.2.2.3), and is therefore a source of unquantified uncertainty. However, a phase-decoupled refraction-diffraction formulation is included, appropriate for approximating diffractive processes around headlands (Holthuijsen *et al.*, 2003).

CHAPTER 2

Little Bay, Smokey Cape

LIMITATIONS AND UNCERTAINTIES OF REGIONAL WAVE CLIMATE DOWNSCALING

2 LIMITATIONS AND UNCERTAINTIES OF REGIONAL WAVE CLIMATE DOWNSCALING

2.1 CHAPTER OVERVIEW

Spectral wave modelling is a common dynamical approach to transform offshore wave climates to the nearshore zone for coastal process studies and hazard definition. Common practice is to adopt a nesting approach, whereby a nearshore wave model sits within a regional and then global wave model domain. For future projections of wave climate change, the global wave model is usually coupled to surface marine wind output from ensembles of Ocean-Atmosphere Global Climate Models (GCMs). For wave climate hindcasts, a similar configuration is required.

The downscaling method of obtaining nearshore wave climates, while conceptually sound, is reliant on a wide range of input parameters and is sensitive to the biases and errors of each. It is also sensitive to the internal numerics and physics of the wave models themselves. Knowledge of the limitations and uncertainties related to regional downscaling is thus of paramount importance to projecting future nearshore wave climate and coastal change.

This chapter explores the uncertainties related to numerical wave models within a regional downscaling framework. The validation and nearshore sensitivities of a SWAN model at Terrigal-Wamberal, a classic parabolic shaped headland-bay beach in south east Australia, are investigated when the model is nested within a regional and global WaveWatch III (WW-III) model, compared to model forcing from simultaneous offshore buoy observations. While a validation of GCM marine surface winds is beyond the scope of this chapter, an overview of the key limitations for projecting wave climate and coastal change is discussed. An alternative surrogate-observational approach for projecting wave climate and coastal change is advocated.

2.2 KEY FINDINGS

The nearshore SWAN model achieved good results for nearshore wave heights (R^2 0.86, RMSE 0.2 m), but under-estimated mean wave period by approximately 1 s. Default SWAN physics were found to be largely appropriate. The inclusion of hindcast winds introduced a systematic over-estimation of high frequency (low period) wind-sea but improved the shape of the wave period distribution. Transformations of WW-III spectra through SWAN suggests that oblique swell is under-represented by WW-III at this location, with only wave directions between 80 and 150° accounted for.

For morphodynamic modelling, the longshore transport component which is driven by oblique long-period wave energy, would be under-estimated while shorter-period wind-waves that favour cross-shore sediment transport is preferenced. The mis-representation of the cross/along-shore wave energy balance is likely a result of imperfect model physics, near-coast bathymetries, and boundary winds/waves. The opportunity for error propagation becomes greater when wave climate downscaling is driven by GCM-based winds for forecasting.

2.3 PUBLICATION AND AUTHOR CONTRIBUTION

This chapter was published, in modified form in: **Mortlock, T.R.**, Goodwin, I.D. and Turner, I.L. (2014). Nearshore SWAN model sensitivities to measured and modelled offshore wave scenarios at an embayed beach compartment, NSW, Australia. *Australian Journal of Civil Engineering,* 12(1), 67-82. DOI: 10.7158/C14-016.2014.21.1. This publication is provided in Appendix 1.

This work was also presented at Coast and Ports conference 2013: **Mortlock, T.R.**, Goodwin, I.D and Turner, I.L. (2013). Calibration and sensitivities of a nearshore SWAN model to measured and modelled wave forcing at Wamberal, New South Wales, Australia. *Coast and Ports Conference*, *Engineers Australia, Manly, Sydney, September, 2013*. This publication is provided in Appendix 2.

This study began as a consulting report in 2012 for Office of Environment and Heritage (OEH) NSW, in collaboration with consultants Cardno. The project report was published as: **Mortlock, T.R.** and Goodwin, I.D. (2013). *Calibration and sensitivities of nearshore SWAN model performance for measured and modelled wave forcing scenarios, Wamberal, Australia.* Climate Futures at Macquarie. A report prepared for the Office of Environment and Heritage NSW.

As lead author, I carried out all analysis and wrote the chapter/publications. The original concept for this study was developed jointly between me, IDG and OEH NSW. IDG contributed to the interpretation of results and edits to the chapter/publications. ILT contributed to edits to the chapter/publications. Cardno provided data and technical support.

2.4 INTRODUCTION

Knowledge and prediction of nearshore wave climates is vital for sustainable shoreline management and structural design in the coastal zone. This is especially so for high-energy sandy coastlines, like the coast of south east Australia, where shoreline change on event timescales is predominantly driven by the passage of synoptic weather patterns and their storm-wave climates. Extreme wave events, such as the 1974 ‘Sygna Storm’, 1997 ‘Mother’s Day Storm’ and 2007 ‘Pasha Bulker Storm’ have caused coastal inundation, beach erosion, damage to property and marine structures, and risk to public safety (Shand *et al*, 2011). The ‘ambient’ wave climate that persists between storm events is predominantly responsible for post-storm beach recovery, long-term delivery of sediment and shoreline orientation. Although some authors predict a decrease in storm event frequency along the south east Australian coast (Dowdy *et al*, 2014), future wave climate change in the region remains uncertain (Hemer *et al*, 2013).

In 2009, the collective value of NSW properties threatened by coastal processes within planning timeframes was estimated at over $1 billion, partly a result of 80% of the NSW population living on the coastal fringe (Department of Climate Change, 2009). The Sydney region alone is projected to increase its population by 40% in the next 30 years (Department of Planning, 2008), only serving to increase coastal vulnerability to extreme wave events along the central NSW coastline. The accurate description of nearshore wave patterns, both storm and ambient, is therefore crucial to coastal hazard definition and prediction in NSW. In acknowledgement of this, the Office of Environment and Heritage (OEH) NSW in 2011 tendered for the development of a cross-shelf wave model system to cover the length of the NSW coast. This model aims to provide a wave hindcast baseline for local coastal process studies across NSW.

A coupled WW-III/SWAN model system for the NSW continental shelf was delivered to OEH by Cardno in 2013 (Cardno, 2012, 2013). This consisted of a nested global-to-regional WW-III model, with a nested SWAN grid to refract deep-water waves across the shelf. Although Cardno carried out wave calibration against a set of seven deep-water Directional WaveRider (DWR) buoys, limited nearshore calibration was undertaken due to lack of suitable shallow-water buoy data. The only nearshore calibration performed was against two DWR buoys operated by Newcastle Port Corporation, moored in 10 to 15m water depths outside the entrance to the Hunter River, Newcastle. Although peak storm wave height agreement was good (Cardno, 2012), the buoy locations for the purposes of model calibration were not ideal as they were moored on the edge of a dredged channel and adjacent to a training wall. These structures likely increase shoaling, reflection and non-linear interactions recorded at the buoy, which are not representative beyond that locality.

In light of this, OEH contracted the Marine Climate Risks Group at Macquarie University to provide a nearshore validation of the coupled WW-III/SWAN model system, using a Datawell DWR buoy deployed inside the Terrigal-Wamberal embayment, a headland-bay beach 60 km north of Sydney (Figure 2.1) as part of this PhD research. The focus of the report provided to OEH (Mortlock and Goodwin, 2013) was to validate the nearshore performance of the Cardno/OEH model system. However, the availability of simultaneous nearshore and offshore buoy observations, and a global-to-local wave downscaling framework, also afforded the rare opportunity to investigate the limitations and uncertainties related to numerical wave models within a regional downscaling framework.

This chapter describes the nearshore validation and sensitivities of a standalone SWAN model when forced with offshore buoy-measured wave information, and modelled WW-III waves. An evaluation of the sensitivities of WW-III/SWAN coupling is widely relevant to both hindcast and forecast coastal process and wave climate studies in a cross-shelf environment.

This chapter is presented in six sections. The introduction is followed by a description of the study site, the regional wave climate and wave model dynamics. The next section describes the boundary data applied to the SWAN model, after which the methodology of model validation is outlined. The results of the validation and sensitivity analyses are then presented. Lastly, the implications of using regionally downscaled wave climates for coastal process studies are discussed, as are the key limitations related to GCM marine winds for projecting wave climate change with scenarios of greenhouse warming.

2.5 BACKGROUND

2.5.1 Location

The Terrigal-Wamberal compartment (hereafter referred to as 'Wamberal') is located on the central NSW coast, approximately 60 km north-east of Sydney, on the south east coast of Australia (Figure 2.1). The compartment comprises a 2.8 km stretch of barrier sands that block the entrance of two adjacent drowned river valleys, now occupied by Wamberal and Terrigal lagoons (Short, 2006). The planform forms a classic parabolic beach shape, with curvature increasing with proximity to Terrigal Headland at the southern end of the embayment.

The repetition of embayed geomorphology along large parts of the NSW coast (e.g. Short, 1999) means the results of this study can be assumed broadly representative for these areas. Moreover, a collaborative project with this PhD research has demonstrated that shoreline behaviour at Terrigal-Wamberal is synonymous with other compartments in south east Australia (Bracs *et al*., in review).

The Wamberal DWR buoy (inset Figure 2.1) was deployed in August 2011 for eight months as part of an Australian Research Council (ARC) linkage project in association with this PhD research. The buoy recorded hourly directional wave spectra with a 93%

recovery rate. Full spectral data were transmitted to a land receiving station, post-processed by Manly Hydraulics Lab (MHL) and provided as hourly wave parameters for this study.

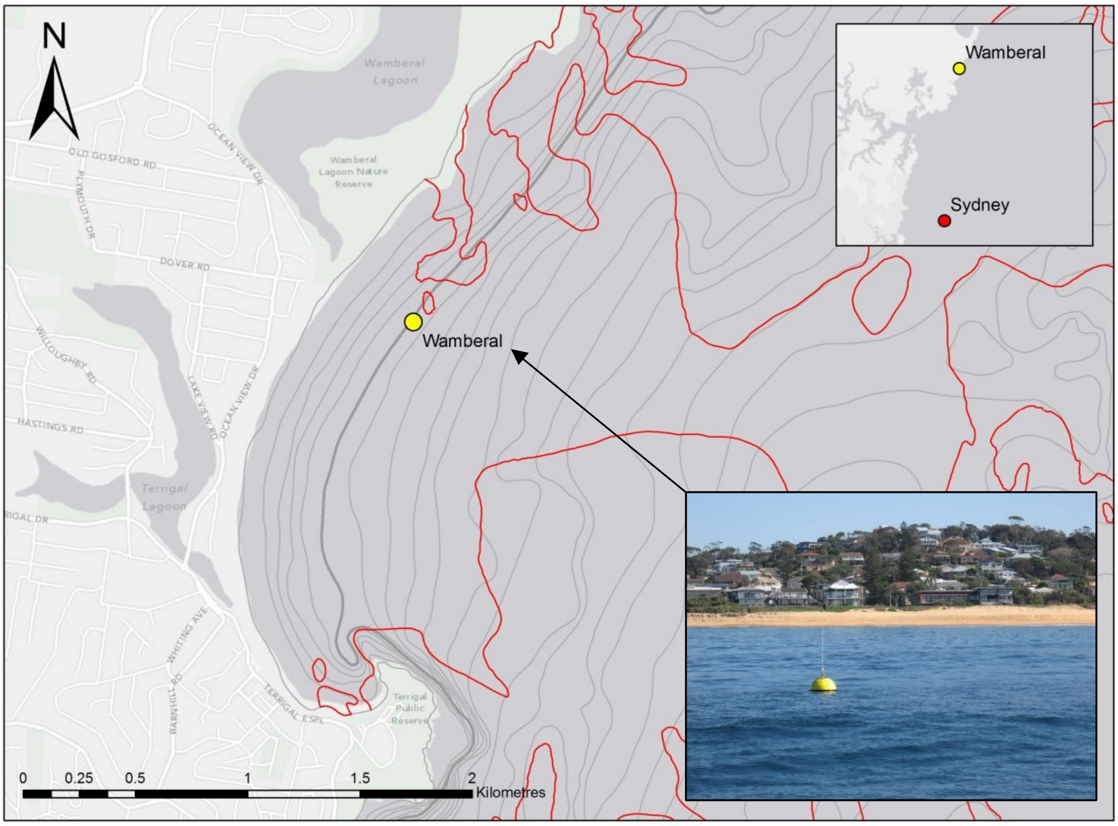

Figure 2.1 Terrigal-Wamberal compartment with buoy location (circled), depth contours (light grey) and exposed rock reef outline (dark grey). The 12 m depth contour is highlighted. Depth contours and rock reef location are from digitised bathymetric and seabed charts (see Jordan *et al*., 2010). Top inset shows locations of Wamberal compartment in relation to Sydney deep-water DWR buoy location. Bottom inset shows buoy as deployed at Wamberal (image courtesy of MHL).

The Wamberal wave buoy record represents largely shoaled but pre-broken shallow-water (~12 m depth) waves. The buoy location is exposed to the modal south-easterly wave climate, outside the influence of major headland diffraction, and is moored adjacent to a non-engineered shoreline. The embayment is characterised by mixed sand and exposed rock reef substrates, the outline of which is denoted in Figure 2.1. The rocky outcrops complicate wave refraction patterns towards the buoy especially under north-east seas and swells.

2.5.2 Inshore Wave Climate

The south east coast of Australia receives a near-field wave climate from the marginal Tasman Sea with far-field wave energy originating from mid-latitude cyclones in the Southern Ocean and tropical low pressure systems in the Coral Sea/Equatorial Pacific (Chapter 4). In addition, a further eight major storm types have been identified by Shand *et al* (2011) which can be broadly grouped into those of extra-tropical and tropical origin (Chapter 6).

The inshore wave climate at Wamberal is further complicated by localised refraction, shoaling and headland shadowing (Chapter 5). To illustrate this, Figure 2.2 shows the refraction patterns of waves entering the Wamberal compartment under typical storm conditions from the east (90 °), south-east (135 °) and south (180 °).

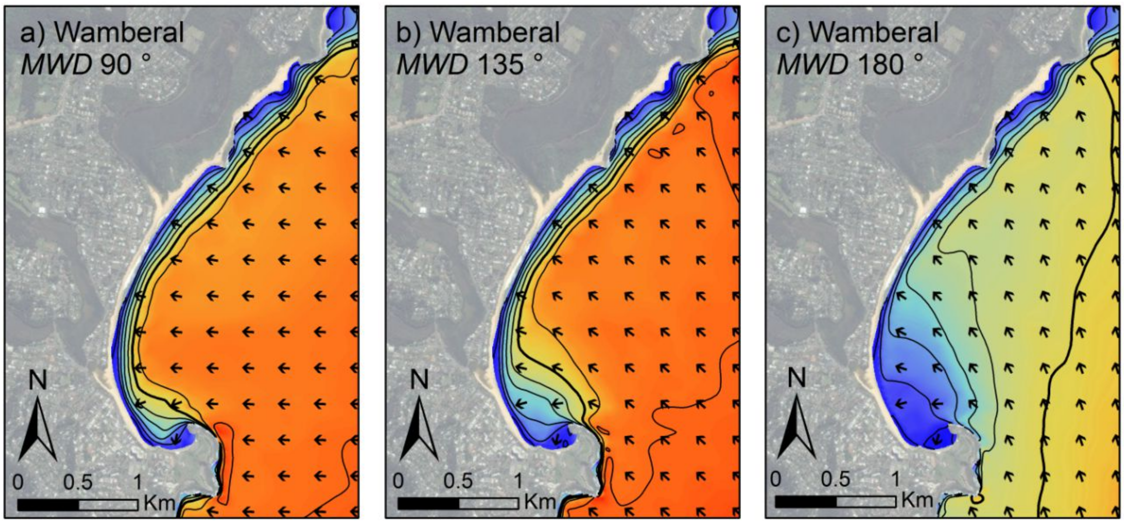

Figure 2.2 Nearshore wave refraction patterns from SWAN at Wamberal for a storm event with H_s 4.5 m, T_p 11 s, and *MWD* of 90, 135 and 180 °. Contours show 0.5 m intervals of H_s with the 3.0 m contour highlighted in each case for reference.

As shown, oblique offshore wave conditions produces a steep alongshore wave height gradient in the embayment, which is less pronounced during east and south-east wave directions. Southerly storm events also lead to reduced nearshore wave energy in the embayment, not only due to headland shadowing, but also because of high cross-shelf refraction. Therefore, the accurate modelling of wave direction is paramount in obtaining a nearshore wave energy field that is representative of the true conditions.

The Wamberal buoy is located at the northern (most exposed) end of the embayment where refraction is low. This means results from this study are not necessarily applicable to the headland shadow zones of such parabolic bay beaches, where high refraction and diffraction contribute to the nearshore wave climate (Daly *et al.*, 2014).

The Wamberal buoy record shows that, over the study period, waves were refracted into a predominantly uni-directional, low-energy and south-easterly nearshore wave climate (Figure 2.3). This is typical of the NSW coast during the Austral spring/summer. As winter ends, the sub-tropical ridge migrates poleward and anti-cyclonic blocking over the Tasman Sea produce a lower energy, south-easterly wind-sea (Chapter 4). A local sea breeze may be responsible for the residual north-easterly component shown in Figure 2.3 b. Over the study period, average significant wave height, H_s, was 1.2 m, average peak spectral wave period, T_{p1}, was 9.8 s and mean wave direction at the spectral peak, MWD_{tp1}, was 118 ° at the Wamberal buoy.

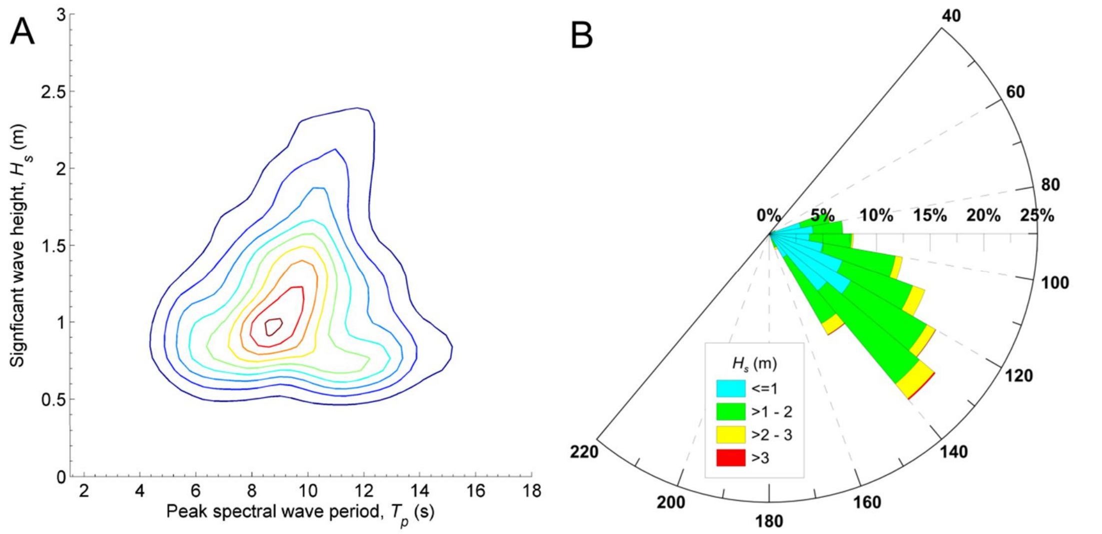

Figure 2.3 Joint Probability Density Function (JPDF) of wave height (H_s) and wave period (T_p) with linear regression of scatter data (a), and directional distribution of hourly wave heights, at the Wamberal DWR buoy from August 2011 to March 2012 (b).

2.5.3 SWAN Model

SWAN (Simulating WAves Nearshore) is a third generation fully-spectral wind-wave model developed at the Delft University of Technology (Booij *et al.*, 1999) that computes random, short-crested wind-generated waves in coastal regions and inland waters based on linear wave theory. SWAN solves the spectral balance equation of wave energy in terms of the wave action density spectrum. The implicit assumption of this equation means variability in bathymetry and currents should be orders of magnitude higher than a single wavelength. SWAN is one of the most widely used and interrogative wave refraction models, with the ability to be nested within global-scale wave models or driven by offshore wave observations. SWAN version 40.85 (June 2011) was used to be comparable with the deep-water calibration methodology of the WW-III/SWAN grid carried out by Cardno (2012).

In SWAN, bottom and current-induced shoaling and refraction are properly accounted for. Since SWAN is a phase-averaged spectral wave model and not a phase-resolved Boussinesq-type model, diffraction can only be approximated and is not fully resolved. Therefore results within diffraction zones should be treated with precaution. SWAN models wind generation, quadruplet wave-wave interactions, white-capping and bottom friction identically to the open-ocean WAM model (see WAMDI, 1988) with the addition of depth-induced breaking and triad wave-wave interactions for nearshore applications (Holthuijsen, 2007).

2.5.4 WaveWatch III Model

WaveWatch III (WW-III) is a WAM-type third generation fully-spectral wind-wave model developed by NCEP (Tolman 1997; 1999; 2009). Like SWAN, WW-III uses the wave action density spectrum to solve the wave energy balance equation. While the physics of WW-III are similar to SWAN, WW-III is primarily designed for oceanic large-scale applications and is optimised for efficient computing, rather than high-resolution coastal applications (Tolman, 2009).

The biggest difference between SWAN and WW-III used to be the modelling of shallow water physics, but now with version 3.14 WW-III can resolve all shallow water (including surf zone) processes in a similar fashion to SWAN. This means that it is now possible to use WW-III in both oceanic and coastal environments, although surf zone capabilities are still fairly rudimentary. Likewise, the capability of using spherical coordinates in SWAN (since version 40.11) means this model can also be practicably used for oceanic applications as well.

While both models have a similar physics base, the most important practical differences relate to the numerical scheme and grids used (Montoya *et al.*, 2013). SWAN uses an implicit numerical solution which behaves better for shallow water applications than explicit schemes, but is less efficient for deep water. Conversely, WW-III employs a largely explicit numerical scheme. Within SWAN, unstructured grids can be used which is very useful for resolving complex coastline orientation or nearshore bathymetries. WW-III however uses an unstructured grid scheme. Because of these design differences, the current state-of-the-art is to couple WW-III to a nearshore wave model (such as SWAN) to refract waves into shallow water.

2.6 DATASETS

2.6.1 Offshore Waves - Measured

A network of seven offshore DWR buoys records the mid-shelf, deep-water wave climate along the NSW continental shelf (Kulmar *et al*, 2013). The Sydney DWR is the nearest deep-water buoy to the Wamberal compartment, moored approximately 45 km south-east in ~90 m water depth (Figure 2.1). Hourly wave parametric data of H_s, T_{p1} and MWD_{tp1} from the Sydney buoy were used to force the ocean boundary of the SWAN model over the validation period.

2.6.2 Offshore Waves - Modelled

Modelled wave spectra were provided by Cardno from the output of a nested WW-III model system (version 3.14). A Tasman Sea WW-III model was run on a 0.05 ° x 0.05 ° grid (~ 5 km) covering the whole NSW coast (blue rectangle, Figure 2.4). This regional model was coupled to an Australian national model (0.25 ° x 0.25 ° grid, red rectangle Figure 2.4) which was likewise nested within a global scale (1.0 ° x 1.0 ° grid) WW-III model.

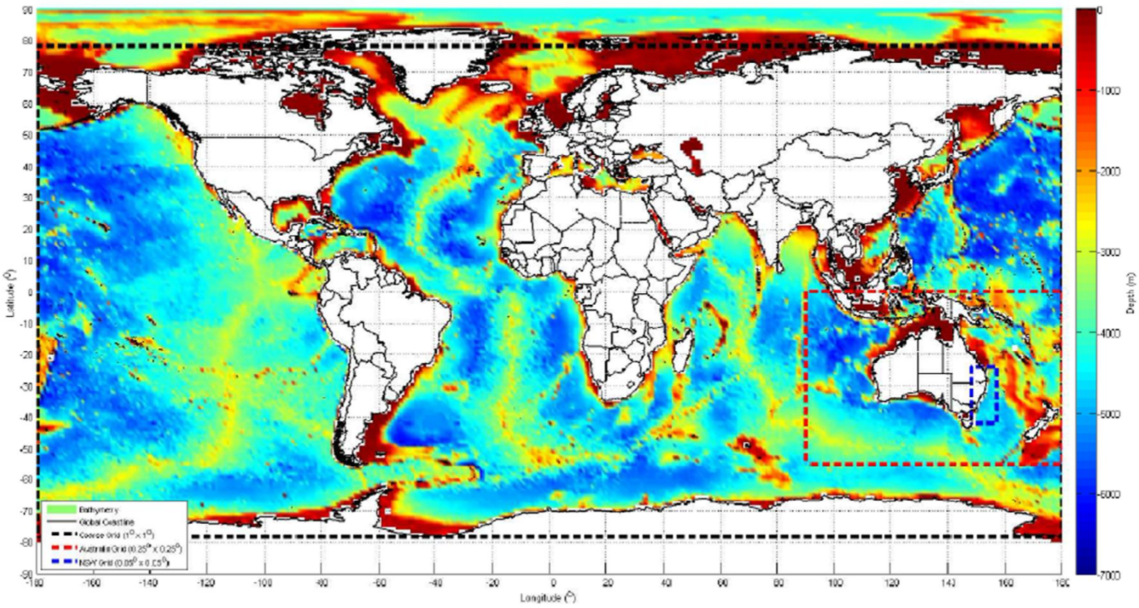

Figure 2.4 Global-to-regional WaveWatch III model framework configured by Cardno. The Tasman Sea nested WW-III model was coupled to a standalone SWAN model at Wamberal for this study. Image courtesy of Cardno (2012).

Since the regional WW-III grid points did not intersect exactly with the SWAN seaward boundary, spectra were interpolated to seven equidistant locations along the boundary (Figure 2.5). In order to evaluate SWAN/WW-III coupling depths, WW-III spectra were supplied at locations representative of the 90, 75 and 60 m depth contours. The SWAN grid was aligned to depth contours offshore of Wamberal accordingly.

The nesting of SWAN into WW-III requires the WW-III spectra to fall within a limited distance either side of the SWAN seaward boundary. However, the SWAN source code reduces the spectral location values to two decimal places, forcing a migration of the locations outside of tolerance. The SWAN source code was thus modified to retain accuracy. Line number 5919 in the source code of *swanmain.ftn* was modified from *"901 FORMAT (A12,2F7.2,F10.1,2(F7.2,F6.1))"* to *"901 FORMAT (A12,2F15.10,F10.1,2(F7.2,F6.1))"*.

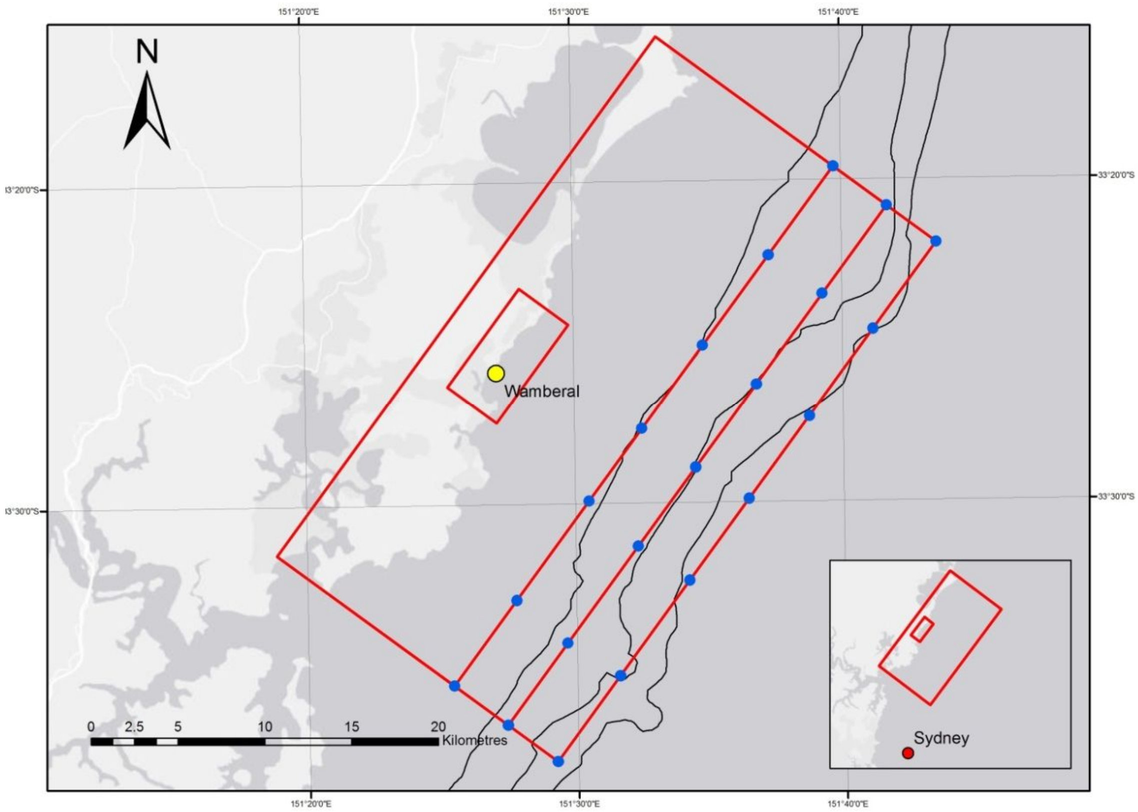

Figure 2.5 WW-III interpolated output locations (blue points) on SWAN computational grid (red). SWAN model boundaries intersect the 90, 75 and 60 m isobars (shown in black).

2.6.3 Bathymetry

Five bathymetric datasets were used in this study to interpolate to a computational grid in SWAN (Table 1). Figure 2.6 a illustrates the extents of available bathymetries. Soundings were edited in ArcGIS, and interpolated in the Delft3D RGFGRID module. Sensitivity testing suggested interpolation errors between methods (TIN to Grid, Natural Neighbour and Kriging) were negligible for the extents of the model domain, each having a mean absolute error of +/- 0.08m when compared to original soundings. The TIN to Grid method was chosen to align with the methodology used by Cardno (2012).

Table 2.1 Bathymetries used to interpolate to a SWAN grid.

Bathymetry	Data Type	Year
Australian Hydrographic Office (AHO) single-beam echosounder (SBES)	Shore-normal survey lines (3km spaced)	1972
AHO digitised fairsheets	Digitised contours	1984

	(2m contour spacing)	
Laser Airborne Depth Sounder (LADS) lidar soundings	Point cloud (5m spacing)	2008
GeoScience Australia (GA) AusBathy	Pre-gridded (250m)	2009
LADS lidar soundings	Point cloud (50m spacing)	2011

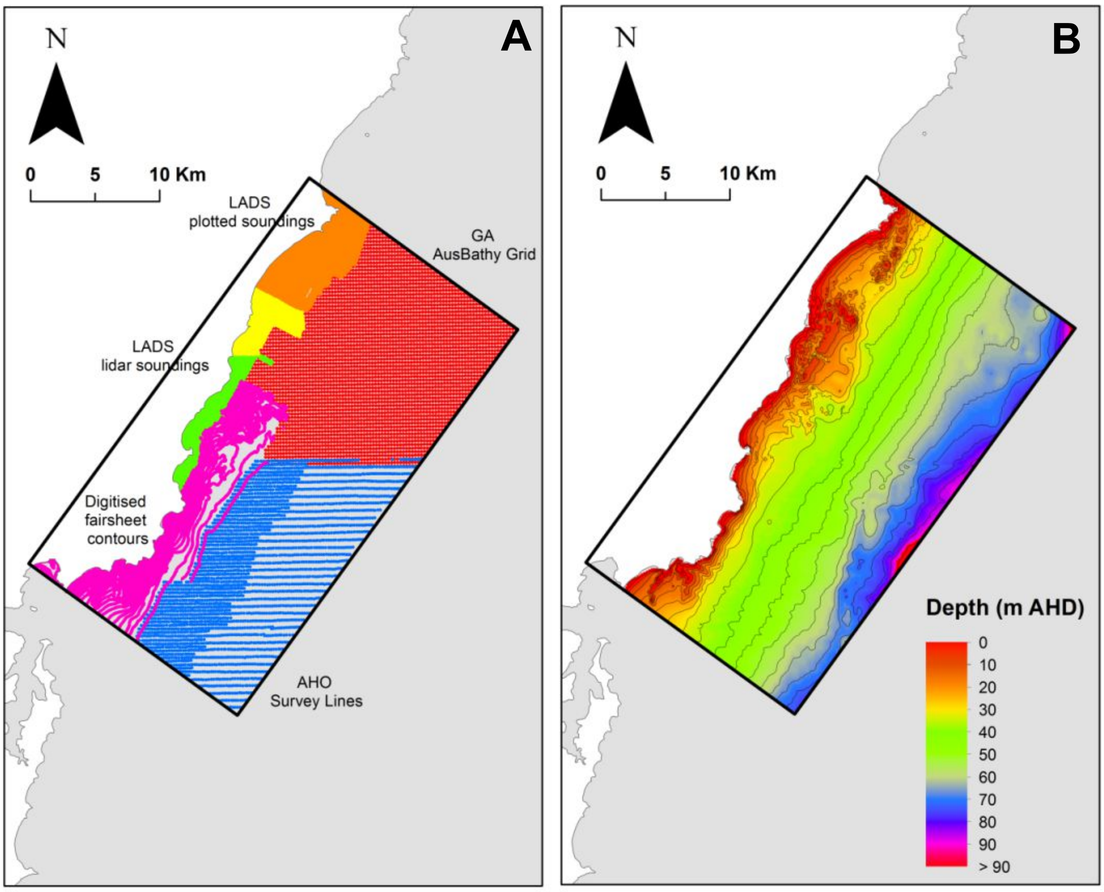

Figure 2.6 Extents (a) and interpolation (b) of available bathymetries.

A buffer-overlap technique was used to minimise stepping effects between bathymetries during merging. However, stepping was particularly apparent between the GA AusBathy grid and adjacent bathymetries. The 250 m pre-gridded AusBathy data covers all Australian marine territories and is composed of multiple datasets (Whiteway, 2009). Analysis here suggests that the AusBathy depths in the nearshore are too shallow by approximately 10 m (when compared with LADS lidar) and that this depth difference is maintained in some areas of the computational domain out to the (true) 50 m depth contour. Despite being interpolated to the shoreline, the AusBathy grid is not designed for nearshore use and has thus been limited, where possible, to depths beyond the mean wave base in this study.

2.6.4 Hindcast Winds

Cardno (2012) evaluated the nearshore performance of multiple sources of hindcast winds along the central NSW coast. Results suggested the Climate Forecast System Reanalysis (CFSR) dataset best represented measured conditions, although showed a positive bias at higher wind speeds and some directional discrepancies. Between 1979 and 2010, CFSR hindcast winds were generated on a global 0.3 ° x 0.3 ° grid at hourly intervals (Suranjana *et al,* 2010). From 2010 onwards, a second version (CFSv2) is available, generated on higher spatial and temporal resolutions. A scaling procedure of nearshore wind velocities was applied to the CFSv2 winds by Cardno (2012) to conform better to observed winds. Within 30 km of the NSW coast, wind speeds were scaled up by 20% of the original CFSv2 winds. This hourly up-scaled CFSv2 wind data was extracted by Cardno at the closest grid point to the Wamberal SWAN seaward boundary to provide a continuous time-series for wind forcing over the SWAN model domain.

2.6.5 Tides

Hourly tidal data from Middle Head (HMAS Penguin) tidal gauge (Sydney Harbour) was provided by Manly Hydraulics Lab (MHL) for the study period. Since tides reach NSW almost incident to the coast, time lags in tide are negligible.

2.7 METHODS

2.7.1 Model Configuration

SWAN was run in non-stationary mode with a domain centred on the Wamberal embayment. A nested rectilinear grid approach was used, allowing for higher computational resolution in the nearshore. The outer grid was 200 m^2 resolution, while the nested grid was 100 m^2. The grid resolutions were chosen to be comparable to the methodology of Cardno (2012, 2013).

In order that wave parameters from the Sydney buoy could be realistically applied to the seaward boundary of the model, the SWAN domain was extended to, and aligned with, the 90 m depth contour (20 km offshore). It is an inherent assumption of the model that wave conditions at the model boundary and the Sydney buoy are consistent. Linear wave theory suggests this to be the case (Mortlock and Goodwin, 2013). For sensitivity testing of WW-III spectra, the SWAN domain was incrementally narrowed from the 90 m to 60 m depth contour.

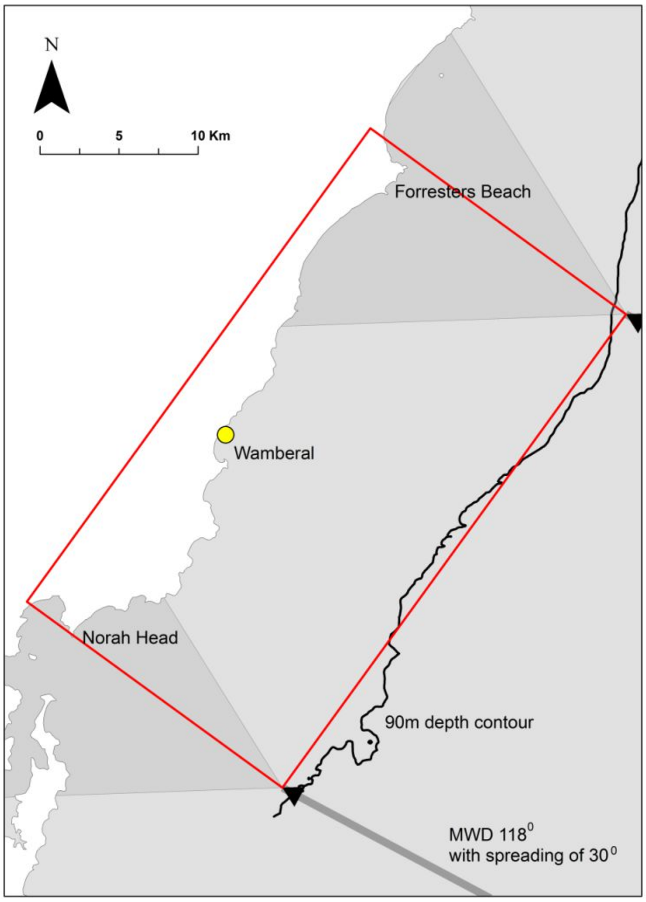

Figure 2.7 Nested model domain extents with 90 m seabed contour and shadow zones representative of the *MWD* shown. Contour extracted from AusBathy grid (Whiteway, 2009).

Both the measured (Sydney buoy) and modelled (WW-III spectra) boundary waves were applied to all three ocean boundaries. Since this is not necessarily a good approximation of the wave conditions along the lateral sides of the grid, especially in shallower waters, the domain was created with sufficient distance either side of the Wamberal-Terrigal embayment to minimise the propagation of lateral boundary errors into the area of interest (Figure 2.7). The lateral error shadow zones were calculated based on 30 ° of wind-sea spreading (SWAN, 2011a) around the offshore MWD_{tp1} (118 °) for the study period. Sustained periods of oblique waves may cast a wider nearshore shadow.

2.7.2 Model Calibration and Validation

A primary application of the Cardno/OEH wave model was extreme wave hindcasting. Nearshore model calibration and validation was therefore biased to storm conditions where possible. Storm events were detected in the Wamberal buoy record using the Peaks-Over-Threshold (POT) method. POT identifies storm events that exceed a significant wave height threshold; that are maintained for a minimum storm duration; and that are separated by a minimum storm recurrence interval. This approach was preferred over the Annual Maximum (AM) method due to the deficiencies of the latter in returning a low storm count for relatively short timeseries (Goda, 2010).

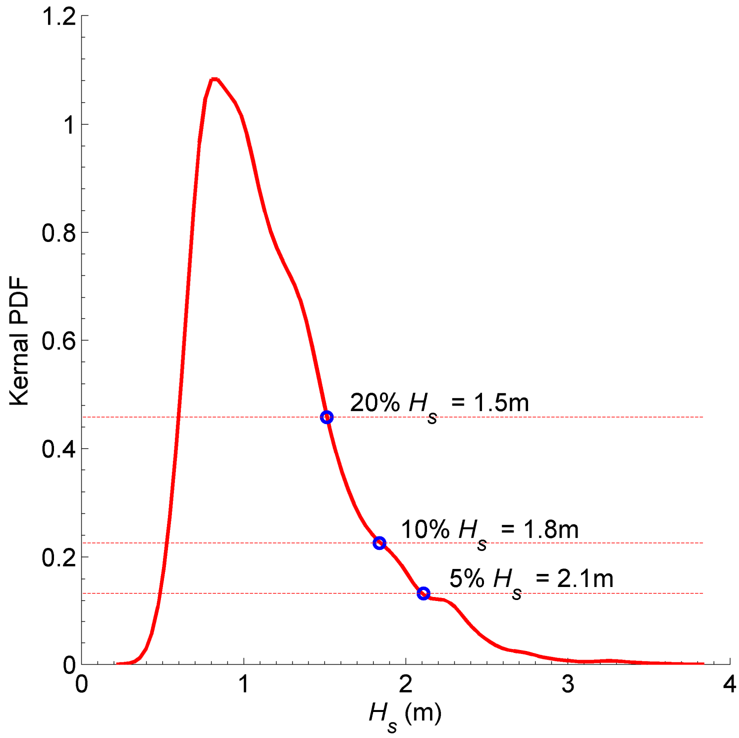

Figure 2.8 Wave height distribution at the Wamberal buoy (following a Rayleigh distribution, as discussed in Section 1.2.1.3).

A nearshore storm H_s threshold was set at 1.8m, equivalent to the hourly 10% exceedance H_s recorded at the Wamberal buoy (Figure 2.8). Previous regional studies (e.g. BBW, 1985, You and Lord, 2008, Rollason and Goodwin, 2009, Shand *et al*, 2011, Dowdy *et al*, 2014) have all used thresholds between 2 and 3 m, approximate to respective 10% exceedance values. Here, the absolute threshold is lower due to the nearshore position of the wave buoy. The use of the 10 % exceedance wave height is also validated in Chapter 4.

Despite the aforementioned studies adopting a 72 hour minimum storm duration, there were no periods in the Wamberal buoy record in which the storm threshold was exceeded for this length of time. The minimum duration was therefore reduced to 36 hours to enable storm detection. In line with previous studies (above), the minimum storm reoccurrence interval was set to 24 hours. Figure 2.9 shows the Wamberal buoy record with storm events detected using these POT conditions.

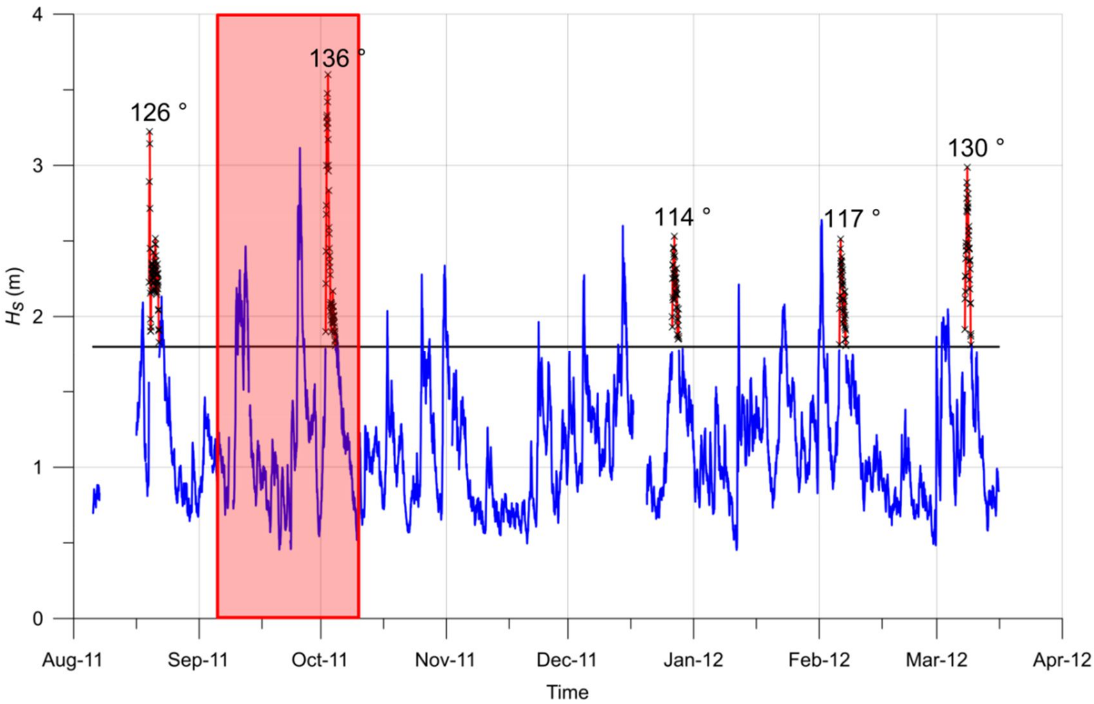

Figure 2.9 Wave height time series at the Wamberal buoy with storm events and storm threshold highlighted. The *MWD* of the storm event is annotated. Calibration sub-set is also highlighted (box).

As shown in Figure 2.9, there are five storm events detected in the buoy record, with hourly peak H_s values between 2.5 to 3.6m. Storm duration ranged between 37 and 60 hours. The largest storm events had a *MWD* of around 130 ° (SE), whereas the smaller storms were more ESE in origin (~ 115 °). Since the Wamberal buoy is exposed to both these storm wave directions, the variation in storm magnitude is more likely due to synoptic origin than localised shoaling and refraction. Thus, SWAN calibration can be assumed regionally representative for those storm types detected in the buoy record.

A continuous one month sub-set of the buoy record was used to calibrate the SWAN model (red box, Figure 2.9). This period was chosen to cover both modal and storm conditions, including the largest storm event detected in the record. The data capture rate during the calibration sub-set was also very good (99%). The remaining 'unseen' portion of the buoy record was used to validate the calibrated SWAN model.

2.7.3 Comparative Wave Statistics

SWAN modelled H_s, mean wave period (Tm_{02}) and MWD were compared to measured H_s, mean wave period (T_z) and MWD_{tp1} from the Wamberal buoy. Mean, rather than peak spectral statistics were used because the SWAN peak statistics are unstable parameters with a tendency of switching rapidly between high and low frequencies, especially in bi-modal seas. The mean statistics provides a better indication of how the bulk of the wave energy is being described in the model. Mean wave direction was not a statistic provided by MHL in the buoy wave data, so MWD_{tp1} was used instead. The SWAN T_{m02} parameter is the mean wave period as calculated from the second and zeroth spectral moments of the wave energy spectrum and is generally comparable to T_z. The T_z statistic is the average zero-crossing period based on upward zero crossing of the still water line. One of the limitations of using the T_z statistic, however, is the poor definition of wave period during bi- or multi-modal seas.

2.7.4 Validation Metrics

Five statistical metrics were used to assess nearshore SWAN model performance against the buoy observations. These included Pearson's squared correlation (R^2), root mean squared error ($RMSE$), bias, scatter index (SI) and symmetric slope (m), and are described below. These metrics are used throughout the thesis when validating model performance against observations.

2.7.4.1 Pearson's Squared Correlation

Pearson's squared correlation (R^2) is a measure of the statistical relation between two sets of independent variables. An R^2 value of 1 indicates a perfect correlation between the two datasets, whereas a value of 0 suggests no correlation at all. This metric however should be treated as a first-pass validation method only, as the significance level of the correlation is not implicit. It is given as:

$$R^2 = \frac{\sum_{i=1}^{n}\left([m_i - \bar{m}_i][o_i - \bar{o}_i]\right)}{\sum_{i=1}^{n}\left([m_i - \bar{m}_i]\right)} \tag{2.1}$$

Where m_i is the modelled wave parameter and o_i is the observation.

2.7.4.2 Root Mean Squared Error

The root mean squared error (*RMSE*) is a measure of the difference between the expected value and the true value of a parameter. It provides a measure of the magnitude of the difference between the modelled and the measured values. It is squared and root-squared so the sign of the residual error does not affect the error value. It is given as:

$$RMSE = \sqrt{\frac{1}{n}\sum_{i=1}^{n}\left([m_i - o_i]\right)^2} \tag{2.2}$$

2.7.4.3 Bias

The Bias, or Mean Error (ME), is the mean of the residual errors between modelled and measured data. Unlike RMSE, ME retains the sign of the mean residual error. Bias is a measure of the difference between the expected value and the true value of a parameter. An unbiased model has a zero bias, otherwise the model is said to be positively or negatively biased, an indication as to whether the model is persistently over or under-predicting the physical conditions. It is given as:

$$Bias = \frac{1}{n}\sum_{i=1}^{n}\left([m_i - o_i]\right) \tag{2.3}$$

2.7.4.4 Scatter Index

The scatter index (SI) is the RMSE normalised by the mean of the observations. It provides an indication of the scatter of the modelled data around the mean. It is given as:

$$SI = \frac{\sqrt{\frac{1}{n}\sum_{i=1}^{n}\left(\left[m_i - o_i\right]\right)^2}}{\overline{o}} \tag{2.4}$$

2.7.4.5 Symmetric Slope

The symmetric slope gives an indication of the symmetry between two compared variables and is denoted by *m* in the linear model equation $x=mx+c$. A slope value of 1 indicates perfect symmetry between modelled and measured data at all values (magnitudes) of the wave parameters whereas values close to zero indicate poor symmetry between datasets. The symmetry slope is calculated from the general linear regression model between two datasets.

2.8 RESULTS

2.8.1 Calibration of SWAN Numerics

Calibration was undertaken to assess the numerical scheme and numerical accuracy of the SWAN model developed for the study. SWAN was initially run using the default high-order Stelling and Leendertse (S&L) scheme but it became apparent that it was leading to poor wet grid point accuracy and long iteration intervals. Instead therefore, the lower-order more diffusive Backward-Space Backward-Time (BSBT) scheme was used. This scheme is computationally more efficient over smaller domains (< 100 km) and promotes better wet grid point accuracy (SWAN, 2011b).

Improved numerical accuracy was achieved by lowering the computation interval and increasing the iteration maxima. Grid cell computations were first run at hourly intervals, equal to the timestep of model output. However, the required wet grid point accuracy (98%) was not being met. At 15 minute computations, the required accuracy was met after, on average, five iterations. This meant that model runs were not only computationally more accurate, but also more efficient; computations at 15 minute intervals were in fact 25% faster than computations at hourly intervals due to the lower average number of iterations.

The iteration maxima were also increased from the SWAN default. It was found that the default of one-iteration-per-timestep rarely gave the required accuracy for all wet grid points, but when the computational process was extended to 15 iterations per timestep, the required numerical accuracy was achieved.

2.8.2 Calibration of SWAN Physics

Frequency and direction discretization, wind growth, and non-linear interactions (quadruplets and triads) were calibrated for. Frequency and direction discretization determines the resolution with which the model calculations are made. It was found that a doubling of the default discretization gave only a negligible improvement in modelled results, while model runs took almost twice as long to compute. Therefore the default discretization was taken as optimal.

Energy transfer to higher frequencies during wave propagation within SWAN is described (as default) by the wind growth model of Komen *et al*. (1994). A widely-used alternative is the Janssen model (1989; 1991). When the Janssen model was used, 55% of model runs did not converge above the required 95% threshold before 15 iterations. There was also an increase in the higher frequency energy. This not only led to dis-equilibrium with nearshore measurements, but also meant that model runs took on average 80% longer than when the Komen model was used. The Komen model was therefore taken as optimal.

Nonlinear wave interactions describe the redistribution of energy over the spectrum by resonant sets of waves. In deep and intermediate waters, four-wave interactions (quadruplets) are important, whereas three-wave interactions (triads) become more important in in shallow water (SWAN, 2011b). SWAN computes quadruplets using the Discrete Interaction Approximation (DIA) after Hasselmann *et al*. (1985). The lambda (λ) coefficient (default 0.2) in the quadruplet approximation can be modified to control the resonant frequencies at which quadruplets interact. It was found that increasing λ to 0.45 considerably improved model performance.

In shallow waters, triad wave interactions become more important by transferring energy to higher frequencies, resulting in wave breaking (Holthuijsen, 2007). SWAN computes triads using the Lumped Triad Approximation (LTA) derived by Eldeberky (1996), although triads are not accounted for in SWAN as default. The inclusion of triads in computations had very little effect on model performance, probably because the water depth at the Wamberal buoy is still too deep for the breaking of almost all waves.

2.8.3 Sensitivity to Hindcast Winds

The application of a wind field in SWAN accounts for wind-wave growth over the model domain. Table 2.2 shows the change in model performance when SWAN is run with and without the up-scaled CFSv2 hindcast winds over the eight-month buoy recording period, when compared with the Wamberal buoy data. Figure 2.10 shows the modelled distribution of mean wave periods with and without winds applied, and the measured distribution at the Wamberal buoy.

Table 2.2 Model sensitivity to hindcast winds where *W* = wind and *NW* = no wind scenario.

	Up-scaled CFSv2 hindcast winds					
n = 5015	H_s		Tm_{02}		MWD	
	W	NW	W	NW	W	NW
R^2	0.86	0.84	0.53	0.33	0.68	0.68
RMSE	0.23	0.21	1.26	1.88	13.50	14.67
Bias	0.22	0.14	-0.45	1.81	14.43	15.02
SI %	19.4	17.4	20.4	30.4	11.4	12.4
m	0.99	0.97	0.82	0.85	0.77	0.90

Results indicate that while the addition of a boundary wind field has only a minimal impact on modelled wave heights, the prediction of wave periods is generally improved. Hindcast winds reduce the modelled scatter (30% to 20%) and improve the shape of the frequency distribution (Figure 2.10). However, winds introduce too much higher frequency wave energy to the spectrum. Results also suggest that the addition of a wind field degrades the consistency of modelled wave directions (reduced slope, m 0.90 to 0.77), although the bias and scatter show negligible change.

2.8.4 Sensitivity to Bottom Friction

Bottom friction determines the amount of drag and energy dissipation a wave experiences when in contact with the seabed (i.e. where depth ≥ ½ deep-water wavelength, L_0). The default JONSWAP friction can be calculated using a coefficient for wind-sea (0.067 m^2s^{-3}) or swell-wave conditions (0.038 m^2s^{-3}). When the JONSWAP coefficient was set to the swell-wave value in SWAN, minor improvements to the modelled wave heights were seen but with equally minor detrimental effects for modelled wave directions and periods. Therefore, the default sea value was used in the optimised configuration.

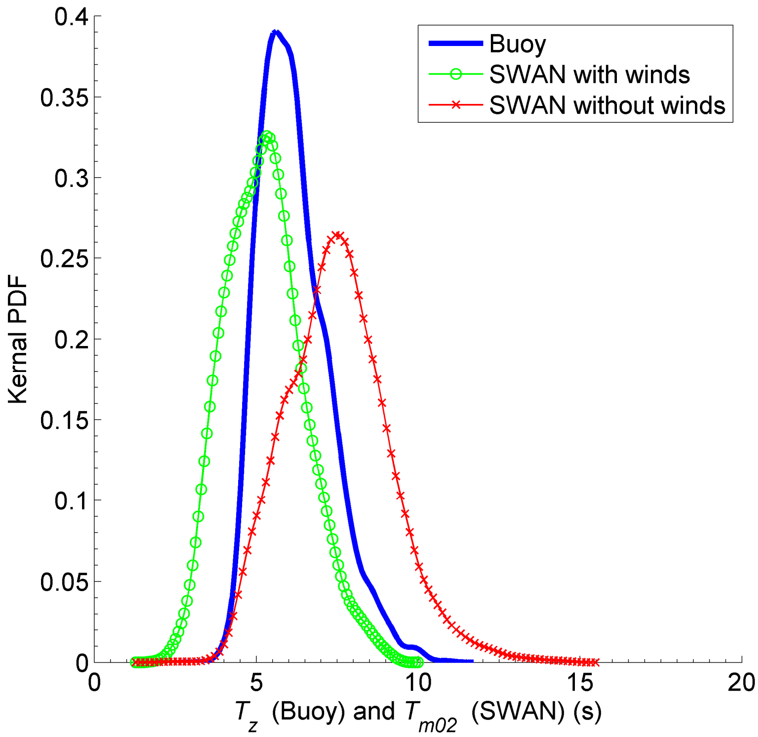

Figure 2.10 Distribution of mean wave period as measured at the Wamberal buoy (T_z) and modelled by SWAN (Tm_{02}) with and without hindcast winds.

2.8.5 Sensitivity to Grid Resolution

A more highly-resolved nested grid was used inside the model domain to investigate the effect of grid resolution on modelling. A higher resolved grid should not only better describe the seabed topography, but will better spatially resolve the surface waves.

SWAN was run with a non-nested rectilinear grid configuration of 200 m^2 to the shoreline, and a nested configuration in which spectra from a 200 m^2 outer grid were interpolated to the boundary of a 100 m^2 and 50 m^2 nested grid, and refracted to the shoreline. Figure 2.11 shows the difference in inshore bathymetric resolution when gridded at 100 and 200 m^2. Despite a substantial increase in computational demand and an obvious improvement in the representation of the seabed topography (Figure 2.11), only minimal improvements in modelled results were seen using the 100 m^2 and 50 m^2 nested approach. Indeed, improvements were so small as to be considered partly a result of the stochastic wind growth in the model.

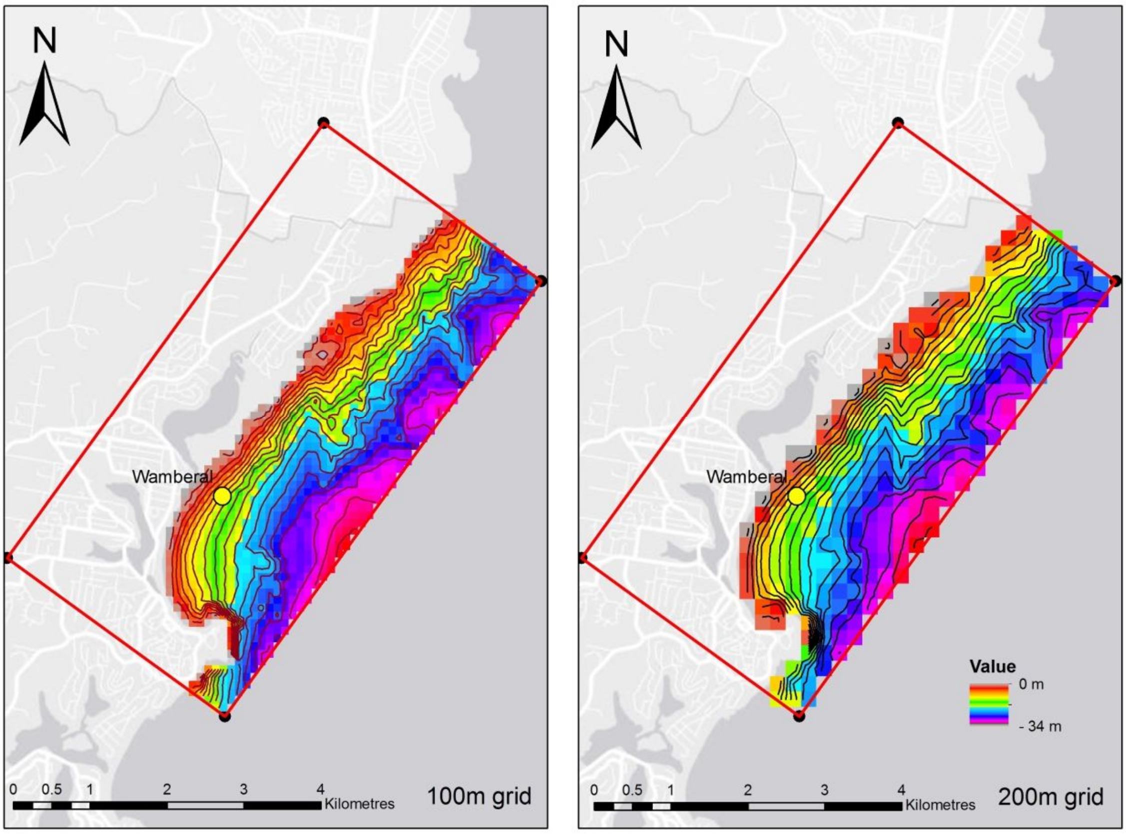

Figure 2.11 Difference in representation of the inshore seabed topography when gridded at 100 and 200 m resolution in the Wamberal embayment.

2.8.6 Sensitivity to Tides

Since measured and modelled wave data was input at hourly intervals, the influence of tide at the nearshore site was considered. However, the application of a measured hourly tide curve to SWAN made only negligible differences to modelled wave parameters.

2.8.7 Validation of WaveWatch III Spectra

Hourly wave spectra from the Tasman Sea WW-III wave model were refracted to the shoreline using the optimised standalone SWAN model to investigate nearshore performance and bias. Table 2.3 shows the change in SWAN performance when WW-III wave spectra are applied in place of offshore buoy boundary forcing. Figure 2.12

shows the modelled distribution of *MWD* when SWAN is forced with measured and modelled boundary waves, compared with the measured distribution at the Wamberal buoy.

Table 2.3 Performance of WW-III spectra when transformed through SWAN, where *A* = results from SWAN run forced with Sydney buoy (measured) and *B* = SWAN forced with WW-III (modelled) boundary waves.

	WW-III spectra (applied at the 90 m contour)					
n = 5015	H_s		T_{m02}		*MWD*	
	A	B	A	B	A	B
R^2	0.86	0.75	0.53	0.42	0.68	0.45
RMS	0.23	0.25	1.26	2.18	13.50	15.58
Bias	0.22	0.01	-0.45	-1.52	14.43	9.40
SI %	19.4	21.1	20.4	35.4	11.4	13.2
m	0.99	0.91	0.82	0.59	0.77	0.39

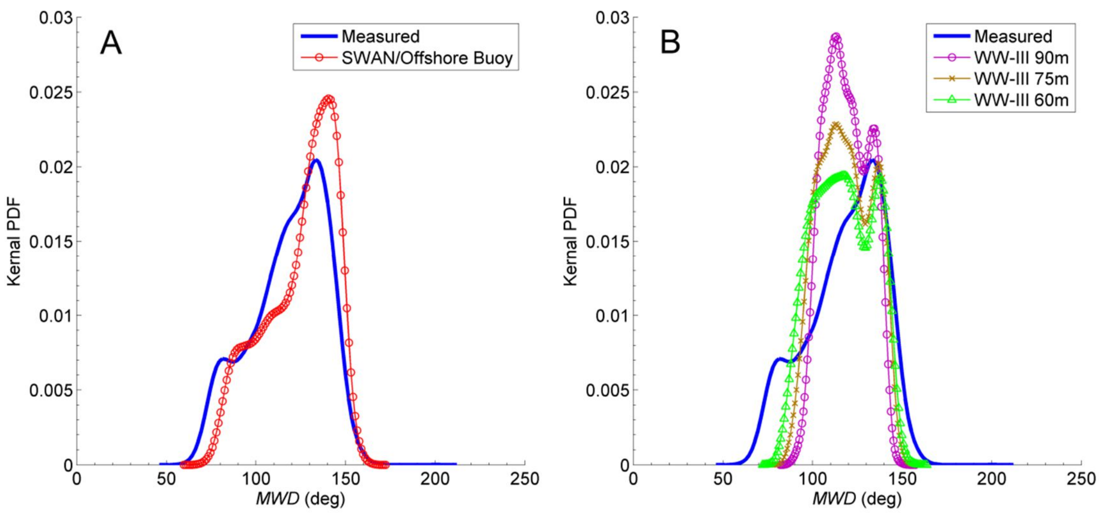

Figure 2.12 Distribution of *MWD*, as measured by the Wamberal buoy, compared against (A) SWAN-modelled *MWD* distribution when forced with buoy-measured offshore waves, and (B) SWAN-modelled *MWD* distribution when forced with modelled WW-III spectra along the 90 m, 75 m and 60 m depth contours.

Results indicate significantly better nearshore performance is achieved with offshore buoy parametric input, rather than WW-III spectral input, at the SWAN offshore boundary. Most noticeable is the poor estimation of nearshore wave direction with WW-III forcing. Despite a slight incremental improvement when applied at shallower depths, Figure 2.12 suggests the WW-III spectra under-estimates the directional spread and only account for wave directions between 80 and 150 °. The buoy-forced SWAN model better represents the measured directional spread, albeit for a consistent but small (10 °) southerly bias and an over-estimation at the modal peak.

2.9 DISCUSSION

2.9.1 Nearshore SWAN Model Performance

The optimised SWAN model achieved good nearshore correlation with measured wave heights (R^2 0.86, *m* 0.99) but a slight negative bias (1 s) in mean wave period and a 10 ° southerly directional bias (Figure 2.13). Other studies (e.g. Ris *et al*, 1999, Bottema and Bayer, 2001, Caires *et al.*, 2006) have also reported a habitual tendency for SWAN to under-estimate the mean wave period. This is because the decay of the primary spectral peak and regeneration of high-frequency energy are both over-predicted. While the errors at the high and low frequencies cancel each other out to return a good estimate of wave height, this is the main cause of the under-estimation of wave period (Ris *et al.*, 1999). This is an important consideration in the calculation of modelled nearshore wave power for morphodynamic modelling of costal impacts, which would be under-estimated even if all boundary forcing within the downscaling framework were perfect.

The default SWAN physics were largely found to be appropriate for exposed, nearshore sites in embayed compartments that are outside the influence of diffraction or shadowing. The applicability for sites along the NSW coast is therefore large. Whilst the default numerics can be improved by adopting a more diffusive scheme, increasing the iteration maxima (to 15) and lowering the computational interval (to 15 minutes), optimal physics were mostly found to be as default. The exception of this is the lambda coefficient for quadruplet calculations, which vastly improved modelled results when increased to 0.45 from the default value of 0.2.

SWAN was found to be largely insensitive to variations in JONSWAP bottom friction coefficients. This concurs with findings by Cardno (2012) when configuring a SWAN model at Newcastle, 70 km north-east of the Wamberal compartment. However, the

JONSWAP model does not explicitly account for bottom substrate type. Rather, it describes bottom dissipation based on the wave orbital motion instead of the substrate roughness length. Given the complex extents of exposed rock reef around the approaches to and inside the Wamberal embayment, bottom friction would be assumed variable. Two other models, the drag model of Collins (1972) and the eddy viscosity model of Madsen *et al*. (1988) might thus be more appropriate in these nearshore circumstances. These two latter models are allowed to vary spatially with bottom type and can therefore be input as a grid over the computational domain in SWAN. Expressing bottom dissipation in terms of a spatially variable roughness length, rather than a spatially-static orbital velocity term, may improve model performance and is currently being investigated.

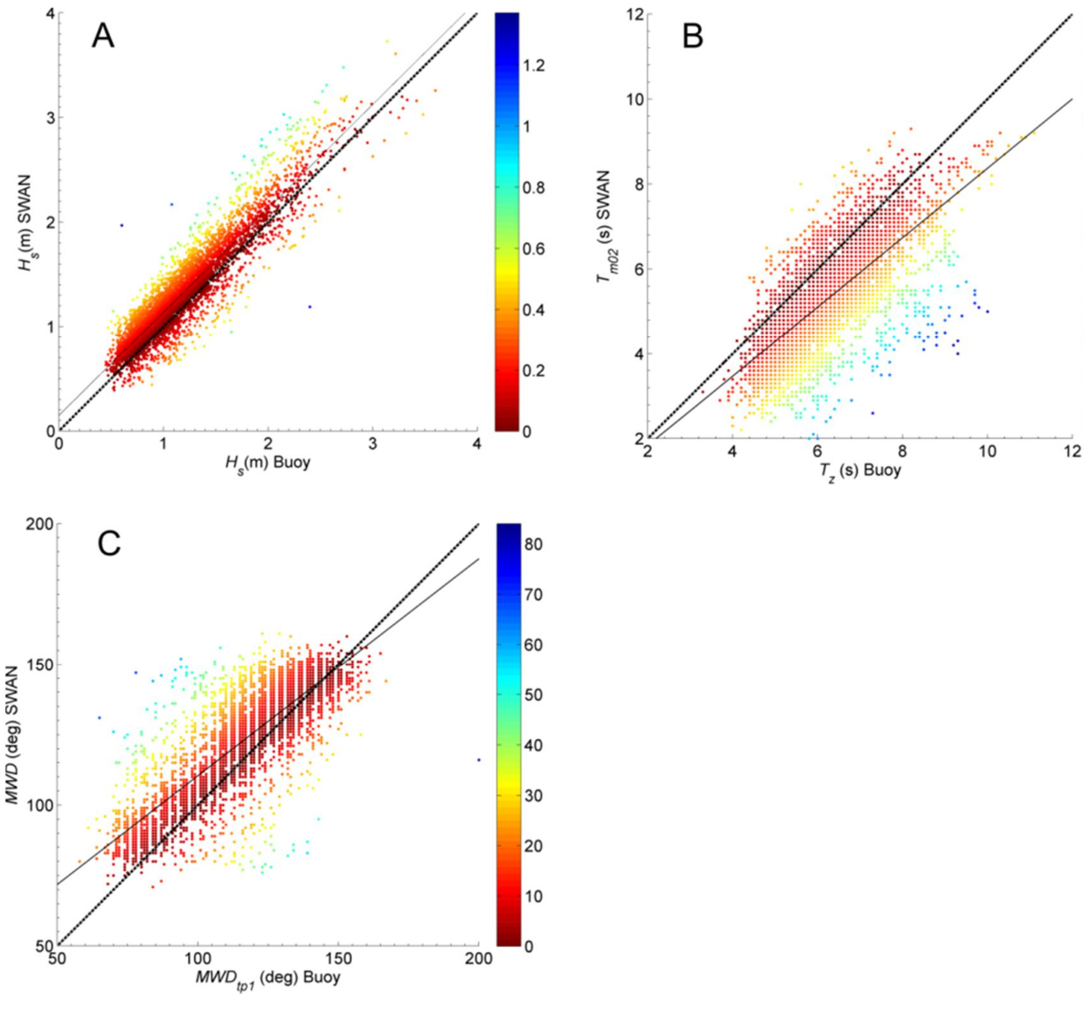

Figure 2.13 Scatter plots showing comparisons between SWAN modelled and buoy measured waves for (a) significant wave height, (b) mean wave period and (c) mean wave direction.

Colour bars indicate the residual error of modelled data. The linear regression (solid black) and best correlation lines (dotted) are also shown.

The inclusion of hindcast winds generally improved the modelled wave period distribution although a systematic over-estimation of high-frequency wind-sea was seen at all measured wave periods. A similar finding was reported by Cardno (2012) for deep-water locations along the NSW coast. This suggests the up-scaled CSFRv2 hindcast winds slightly over-estimated nearshore wind speeds during the eight-month study period. The addition of hindcast winds also slightly reduced the model's (already underlying) southerly directional wave bias of 10 ° by approximately 1 °. This indicates that only a small part of the directional disparity is due to surface wind-driven refraction.

The remainder of the directional bias could be due to inaccurate representation of seabed bathymetry. If this were the case, it is unlikely a result of improper bathymetric resolution. Results indicate that SWAN is largely insensitive to an improved grid resolution from 200 to 50 m^2 at the buoy location. This suggests that all necessary information on the variability of seabed topography is captured in a 200 m^2 grid. Although there is much more detail to be described beyond 200 m^2, bed features with length-scales much smaller than the mean wave length (around 140 m for the average T_z of 9.5 s) are unlikely to affect refraction, and therefore their resolution in a bathymetric grid is redundant.

If the directional bias is bathymetric-driven, then the source of error may be the intrusion of the AusBathy grid into intermediate waters north-east of the Wamberal-Terrigal compartment. Although this was unavoidable due to lack of overlapping soundings, there is a known depth error in this dataset for depths shoreward of approximately 50m. Indeed, the directional discrepancy is most noticeable for waves in the NE to E quadrants. A southerly bias suggests under-refraction due to artificial deepening caused by the inclusion of this dataset. In order to correct for this, offshore wave cases from this quadrant could be bias-adjusted using linear regression, or by modifying the cumulative distribution of modelled waves to the observed distribution (e.g. Piani *et al*, 2010). OEH are also currently undertaking swath bathymetry to fill in and update this area.

The transformation of WW-III spectra through SWAN suggested an under-representation of longer-period oblique waves and a preference for shore-normal (80 to 150 °) shorter-period wind-sea. This was the case at all WW-III/SWAN coupling depths. This suggests that, at least over the study period, the typically longer-period oblique swell waves generated by Southern Tasman Lows were under-represented in the WW-III model. Instead, preference was given to more locally-generated, shorter period wave climates with higher-frequency wave energy from the central Tasman Sea region. This is also manifest in the persistent bias towards shorter period sea seen in both this study and in Cardno (2012).

The apparent preference of WW-III spectra for high-frequency uni-directional wave energy can have consequences for shoreline modelling applications when waves are transformed to nearshore locations. The longshore transport component, typically driven by oblique long-period (constructive) wave energy, is likely to be under-estimated when preference is given to shorter-period, steeper incident (destructive) waves that promote cross-shore transport.

Frequency/directional discrepancies in WW-III are a result of composite errors in model source terms and imperfect wind forcing. A 10% error in the estimation of surface winds can lead to 10-50% errors in wave energy (Cavaleri, 1994). Whereas Cardno (2012) used WW-III v. 3 physics and CFSR winds, other regional WW-III based products such as the Bureau of Meteorology's AUSWAVE model (Durrant and Greenslade, 2011), and CSIRO's CAWCR Wave Hindcast (Hemer *et al*, 2013), have used v.3 (v. 4) physics and CFSR (ACCESS) synthetic winds. Thus, the same directional bias may not be apparent in all regional WW-III products. While it is beyond the scope of this study to locate the source of the directional error in WW-III, this work has provided a rare opportunity to evaluate the propagation of global-to-regional WW-III spectra into the nearshore zone.

2.9.2 Implications for Projections of Wave Climate and Coastal Change

As shown, the ability of global-to-local wave downscaling to accurately reproduce nearshore wave climates is largely a function of the accuracy of model physics, bathymetry, boundary winds and waves. In order to project future wave climate change, the state-of-the-art is to drive global-to-local wave downscaling with marine surface winds from GCMs (e.g. Erikson *et al*., in press). The nearshore information can then be passed from wave to shoreline modelling for the projection of coastal impacts.

However, large uncertainties in this process are inherited from climate modelling. Ocean-atmosphere coupled GCMs attempt to replicate highly complex, non-linear and stochastic processes on a global scale, which inevitably leads to model-, and regional-specific bias and error. In order to minimise the impact of bias, the ensemble mean is the safest metric for climate projections. Each ensemble comprises ~ 40 GCMs (e.g. CMIP5) and uses radiative forcing from one Representative Concentration Pathway (RCP) to describe how future greenhouse warming will change boundary climate conditions. There are currently four RCP scenarios (mitigation, low stabilisation, high stabilisation and high emission) that attempt to encapsulate a range of very different global futures. Each RCP is based on a best-guess estimate of six 'driving forces' of global change; population, economy, technology, energy, land use and agriculture.

Therefore even before GCM winds are downscaled to forecast regional wave climates, uncertainty exists in multiple forms; inter-ensemble model spread, inter-RCP spread and internal climate variability. In the near-future, internal climate variability (particularly in the equatorial Pacific) is the primary source of uncertainty in climate modelling as highlighted by the recent 'global warming hiatus' missed by most GCMs (Kosaka and Xie, 2013). For the mid-future (2020 – 2050) inter-model spread becomes more important. For projections beyond 2050, spread between RCP scenarios is the greatest source of uncertainty (Hawkins, 2013).

Because uncertainty originates from a large number of sources and is exchanged between research communities (economic, climate, wave and shoreline modelling), compound error in nearshore wave climates used to model coastal evolution is at best under-estimated. While conceptually sound, an alternative to the regional downscaling approach to coastal change forecasting is needed in light of significant uncertainties. Even with perfect model physics, the semi-chaotic nature of climate warrants a less deterministic approach.

2.10 CONCLUSIONS

A SWAN model was set up and calibrated for an exposed nearshore location in a headland-bay beach configuration on the south east coast of Australia. Model sensitivities to measured and modelled offshore wave scenarios within a regional wave downscaling framework were evaluated. Key findings include;

- Default SWAN physics are largely appropriate for modelling at exposed nearshore locations in embayed compartments, beyond the influence of diffraction and shadowing. The exception to this is the lambda (λ) coefficient for quadruplet nonlinearities. Default SWAN numerics, however, were found to be sub-optimal for computational efficiency.

- SWAN provided a good representation of nearshore wave heights, but under-estimated wave period by approximately 1 s. Other studies have also reported similar nearshore results. Ris *et al*. (1999) suggests the main cause is the over-prediction of both the decay in the primary spectral peak decay and regeneration of high-frequency energy by SWAN.

- A southerly directional bias in NE-E waves is a result of depth errors incurred in the inclusion of the AusBathy grid to the NE of the Wamberal compartment. It is suggested that if this bathymetry is used in subsequent regional wave modelling, a linear or distribution-based bias adjustment is applied to waves from the NE/E quadrant.

- Bathymetric resolutions of 200 m^2 sufficiently captured all necessary information on seabed variability for SWAN. Although higher-resolved grids better described seabed topography, this was redundant information with regards to improved model performance at the nearshore buoy location.

- Up-scaled CFSRv2 hindcast winds improved the modelled frequency distribution but introduced a systematic under-prediction of wave period (1 s) suggesting wind velocities in this dataset are over-estimated for this locality.

- The transformation of WW-III spectra to the nearshore suggested an under-representation of longer-period oblique waves and a preference for shore-normal shorter-period wind-sea.

The apparent preference of WW-III spectra for high-frequency shore-normal wave energy may lead to an under-estimation of alongshore transport if used for morphodynamic modelling. Likewise, the cross-shore transport component driven by shore-normal wave energy may be over-represented. The mis-representation of the cross/along-shore wave energy balance is a function of imperfect model physics, near-coast bathymetries, and boundary winds/waves. The opportunity for error propagation becomes greater when wave climate downscaling is driven by GCM-based winds for forecasting.

2.11 ACKNOWLEDGEMENTS

All tidal and wave data were supplied and quality-controlled by Manly Hydraulics Laboratory. The Wamberal nearshore buoy deployment was funded by ARC Linkage project LP100200348 granted to IDG and ILT. All bathymetric data was supplied and quality-controlled by Office of Environment and Heritage (OEH) NSW. WW-III wave spectra and upscaled CFSv2 hindcast winds were provided by Cardno. SWAN v.40.85 with modified source code, and technical support, was provided by Baird Australia. Special thanks to Michael Kinsela at OEH for technical feedback.

CHAPTER 3

Long Reef

INSHORE WAVE CLIMATES FROM ARCHIVE VIDEO IMAGERY

3 INSHORE WAVE CLIMATES FROM ARCHIVE VIDEO IMAGERY

3.1 CHAPTER OVERVIEW

The quality of inshore wave climates obtained by dynamical downscaling is primarily a function of wave model physics, near-coast bathymetries and boundary conditions (Chapter 2). The alternative of wave buoy deployments in the nearshore only provides *in situ* observations, is costly, and often suffers from data gaps during extreme wave events. Coastal imaging technology, however, provides a practical means for sustained, autonomous inshore wave monitoring without the need for dynamical modelling or expensive buoy deployments. However, existing, scientifically-proven systems are limited in their application due to cost and required infrastructure. A potential alternative was identified in the existing surfcam networks operating at over 100 sites around Australia and many sites around the world. This chapter reports a critical evaluation of this new, low-cost monitoring method which has the potential to capture both real-time and hindcast (archive) inshore wave information.

In this study, surfcam-derived inshore wave heights and periods are compared to three months of concurrent hourly nearshore (depth ~12 m) wave buoy measurements at two camera sites; Collaroy-Narrabeen and Terrigal-Wamberal on the south east coast of Australia. The feasibility of this method as an alternative to regional downscaling and nearshore wave buoy deployments is assessed.

3.2 KEY FINDINGS

Initial evaluation of the wave measurement capability of single and low-angle surfcams suggests a consistent over-estimation of smaller waves and under-estimation of larger waves. Wave period (and thus wave length and speed) is poorly represented, and in all cases scatter (precision) is low. In addition, only non-directional inshore wave information is currently available.

It is suggested that the “bottom-heavy” measurements of breaker wave heights are due to pixel rectification error associated with obliquity from a single low-angle camera; and the high variability in measurements due to beach and wave type. Measurement accuracy may be improved by using a dual-camera system, with the second camera mounted considerably higher above the water line. While the adoption of coastal camera infrastructure to provide two-dimensional inshore wave climates remains an attractive end-goal, it is currently not a viable observational source for this thesis.

3.3 PUBLICATION AND AUTHOR CONTRIBUTION

This chapter was published, in modified form in: Mole, M., **Mortlock, T.R.**, Turner, I.L., Goodwin, I.D., Splinter, K.D., Short, A.D. (2013). Capitalizing on the surfcam phenomenon: a pilot study in regional-scale shoreline and inshore monitoring utilizing existing camera infrastructure, *Journal of Coastal Research,* SI65 (ICS2013), 1433-1438. doi: 10.2112/SI65-242. This publication is provided in Appendix 3.

This study formed part of a government-industry-university ARC Linkage Project grant number 100200348 to IDG and ILT, “Australian coastal observation network: monitoring and forecasting coastal erosion in a changing climate”. Some project partners are listed in the above publication. This publication assessed the capability of coastal imaging technology to capture both shoreline and inshore wave climate information. MM carried out all analysis, presentation and interpretation of shoreline monitoring results, and I carried out all analysis, presentation and interpretation of inshore wave monitoring results. Therefore, only the assessment of inshore wave monitoring is included in this chapter. Other listed authors contributed to the original concept for this study, and edits to the final publication.

3.4 INTRODUCTION

Knowledge of inshore wave climates is crucial for coastal management, process studies and engineering design. Buoy deployments for nearshore wave monitoring can be time-consuming and expensive, and as a result sustained deployment campaigns are sparse. In addition, buoys only record *in situ* wave information. For a typical coastal compartment, alongshore gradients in wave power and direction mean *in situ* measurements do not capture embayment-wide variability and are only valid for the deployment locality. In addition, instrumentation error and thus data gaps often occur during extreme wave events, for which data is most sought for beach management. Notwithstanding, buoy-derived wave measurements are considered the most reliable source of surface spectral wave information (Holthuijsen, 2007). Shore-based remote sensing methods, however, offer a practical and relatively inexpensive option for sustained monitoring of inshore and embayment-wide wave conditions. Because of their installation above the water line, they also do not suffer from data loss during storm conditions. However, data quality and reliability are not standardised and vary between location and system used.

The present ‘state of the art’ in coastal imaging is the Argus video system that includes one or more fixed cameras per site, on-site data acquisition and control systems and a comprehensive data analysis suite (Holman and Stanley, 2007). For two decades, Argus systems have been applied to meet a range of monitoring and research needs around the world and inspired the development of similar systems (see Nieto *et al.*, 2010).

Optical techniques to estimate surf zone wave parameters are not new. Manual analyses of video imagery (photogrammetry) for coastal applications began in the 1950s with Cox and Munk (1954), but it is only over the past decade that this process has become automated and digital. Recent efforts to advance shore-based remote measurement of breaking waves have typically utilised a dual-camera (or ‘stereo-pair’) system (e.g. de Vries *et al.*, 2011; Shand *et al.*, 2012), where the overlapping field of view allows the simultaneous solution of position and water surface elevation by stereometric intersection (Holland *et al.*, 1997). Time-stacked analysis of stereo-pair imagery has been used to measure wave celerity and amplitude (e.g. Piepmeier and Waters, 2004) and, via linear dispersion theory, inverted to estimate local bathymetry (e.g. Bell, 1999, Stockdon and Holman, 2000, Catalan and Haller, 2008).

More recently, some studies (Browne *et al.*, 2005, de Vries *et al.*, 2011, Shand *et al.*, 2012) have proposed a two-camera photogrammetric approach to estimate breaker position and breaker height (and a simple inference of wave period). Of these studies, Browne *et al.* (2005) gives a purely conceptual overview of the technique, de Vries *et al.* (2011) is a lab-based approach with no field verification of wave height estimates, and Shand *et al.* (2012) describe a field-developed and verified approach.

Single-camera systems for breaking wave height measurement, rather than stereo-pairs, have also been developed to estimate surf zone wave parameters. Single-camera systems have been proposed by Hilmer (2005), Lane *et al.* (2010) and Almar *et al.* (2012). The main source of uncertainty with a single camera set-up is the accuracy with which a conversion from oblique-view pixels to real-world coordinates (rectification) can be made, and hence the accuracy of locating the rectified breaker position. The more low-set the camera is above the water line, the higher the obliquity error and distortion with distance from the camera. Errors in estimation of breaker position (defined as the position at which white water first appears) leads to errors in the calculation of breaker height.

Hilmer (2005) overcame this problem by assuming a fixed breaker position in order to estimate breaker height. This assumption is applicable to the reef environment in which the study took place, but is limited in a barred beach setting. Conversely, the method proposed by Almar *et al.* (2012) explicitly locates the breaker position by using a pixel intensity–threshold algorithm applied to timestack imagery. However, significant assumptions about the wave shape are made in order to estimate breaker height. In addition, the lab-based single camera system had no field verification and so its applicability to real-world wave conditions is unknown.

Coastal imaging systems have proved a useful tool for the integration of research and coastal zone management practice (e.g. Davidson *et al.*, 2007; Kroon *et al.*, 2007; Turner and Anderson, 2007). These systems are presently restricted in their usage due to installation and ongoing running expenses, and the requirement for a high beach-front platform at the site of interest. In recent years, there has been a move toward lower cost, more customisable systems, which are accessible to a wider user group in more locations (e.g. Nieto *et al.*, 2010).

The development of a low-cost, multi-purpose, easily accessible monitoring system, deployed at many sites simultaneously, could address the scarcity of high temporal resolution inshore wave data along the south east Australian coast. If wave information derived from such a network could be proved reliable, it would provide an invaluable archive for nearshore wave model validation, shoreline model boundary forcing and understanding of surf zone dynamics.

In this chapter, the opportunistic use of pre-existing ‘surfcams’ for inshore wave monitoring is explored. The aim is to report the first rigorous and independent assessment of a new wave monitoring capability based on an existing, low elevation, surfcam network. After introducing the study area, this chapter goes on to address the ability of the surfcams to provide information on inshore wave conditions.

3.5 BACKGROUND AND METHODS

3.5.1 Surfcam Network

The surfcam network utilized in this study is operated by Coastal Conditions Observation and Monitoring Solutions (CoastalCOMS) and includes 80 cameras around Australia. The cameras are SonyRZ50 pan-tilt-zoom internet protocol cameras, mounted inside small unobtrusive housings, usually located on 1-2 storey surfclub buildings. Surfcams are the only on-site equipment deployed, with all data acquisition, storage and analysis carried out on the Amazon cloud. Each site has a single camera, which is mechanically rotated between preset aim points for wave measurements. The surfcam sites used in this study are both “low-angle” with a lower limit of 7 m above mean sea level (0 m Australian Height Datum, AHD), presently specified by CoastalCOMS as suitable for wave monitoring.

3.5.2 Wave Detection Method

Lane *et al.* (2010) described a low-angle single camera wave height processing system "Wave Pack", which employs surfcam video from the CoastalCOMS network to derive the wave parameters assessed in this study. In order to extract wave measurements, each CoastalCOMS camera must be geo-referenced to a suitable datum and grid. Through the Wave Pack system, timeseries of video images are collected and a timestack image (e.g. Shand *et al.*, 2012) is created from the central pixel column. Breaking waves are detected by pixel intensity threshold algorithms and combined with known camera elevation and tilt angle to calculate distance to break position and wave height in metres. Waves are also counted to allow measurement of local wave periods.

Lane *et al.* (2010) presented a preliminary verification of the Wave Pack system at Narrowneck Beach, Gold Coast, Australia. The authors claim proven applicability in a barred beach environment, having verified their results with (i) nearshore wave buoy data (at 16 m water depth), (ii) nearshore SWAN model results, (iii) (manual) linear wave transformations and (iv) recorded observations by experienced practitioners. They reported an R^2 value of 0.82 between Wave Pack breaking wave height (H_b) and wave buoy significant wave height (H_{sig}) and R^2 of 0.53 between the Wave Pack maximum period (T_{max}) and wave buoy peak period (T_p).

3.5.3 Study Sites

For this study, inshore wave information was derived from CoastalCOMS surfcams installed at the Collaroy-Narrabeen (hereafter referred to as Narrabeen) and Terrigal-Wamberal (referred to as Wamberal) embayments (Figure 3.1) in south east Australia.

The Narrabeen embayment is a 3.6 km long, east-facing embayed beach compartment, located 17 km north of Sydney. The bathymetry is predominantly sand to 20 m water depth, interrupted by distinct rock reef outcrops. Long Reef is a large rock headland to the south with extensive sub-aqueous reef extending to the north. This feature is responsible for wave shadowing of the southern half of the embayment under oblique wave conditions (see Figure 2.2 in Chapter 2).

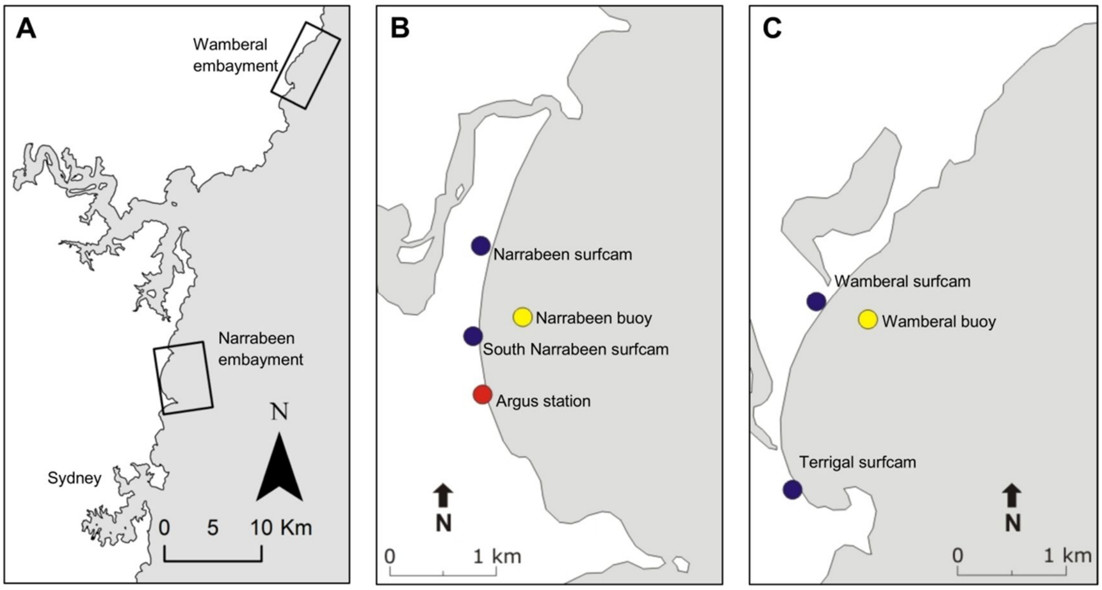

Figure 3.1 Location of study sites in relation to Sydney (a), Narrabeen embayment (b), and Wamberal embayment (c). Locations of wave buoys and surfcams are shown in (a) and (b). The South Narrabeen surfcam was used for this study at Narrabeen.

Boussinesq wave modelling of the embayment under the mean annual offshore wave conditions (Figure 3.2) shows wave focussing also occurs at North Narrabeen (north of wave buoy location) as wave energy is funnelled between two rock reefs. This is probably a contributing factor to the high surf amenity of this beach section. Therefore, the *in situ* buoy measurements cannot capture the embayment-wide spectrum of wave conditions important for beach management.

The Wamberal embayment is a 2.7 km long, south-east facing parabolic headland-bay beach located a further 35 km north of Narrabeen (Figure 3.1). The bathymetry is predominantly sand out to 20 m water depth. While exposed, subaqueous rock reef extends from Terrigal headland in the south of the embayment, the headland and associated reefs are smaller than Long Reef at Narrabeen and therefore the headland shadowing effect is reduced. The absence of significant reefs in the centre of the embayment means alongshore differences in the inshore wave climate are more uniform than at Narrabeen. For this reason, this site is the focus location for studies also in Chapters 2, 5 and 6. A more detailed description of the Wamberal embayment can be found in these chapters. A recent study has shown that shoreline response to wave forcing is comparable between these two sites (Braccs *et al*., in review).

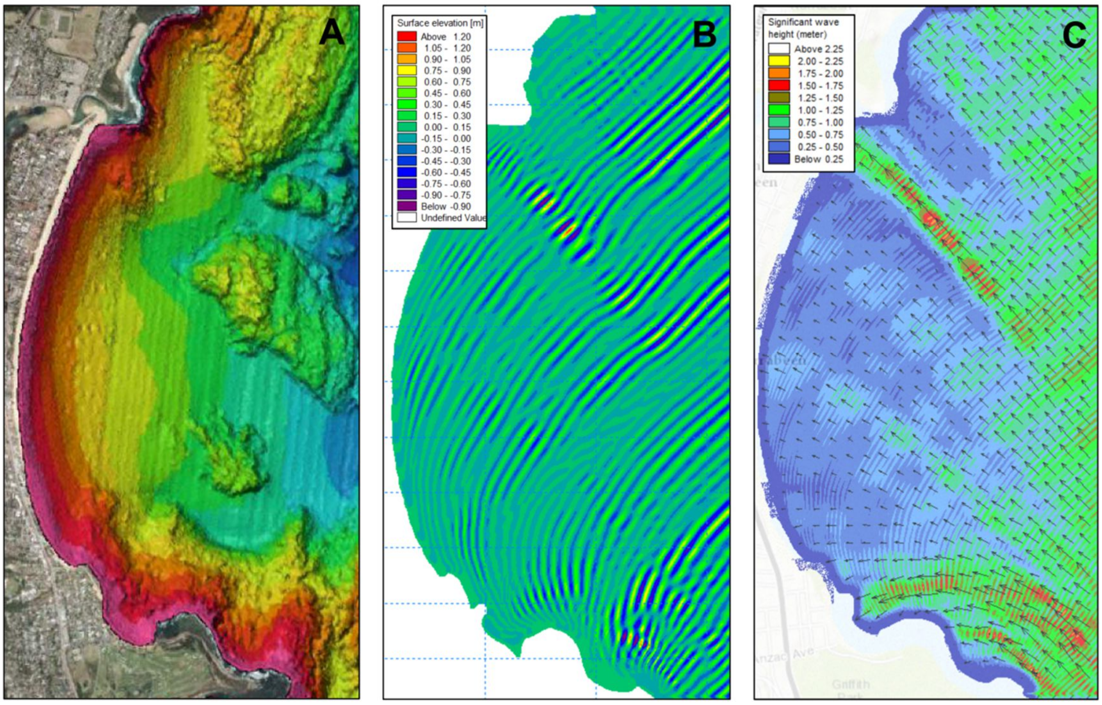

Figure 3.2 Narrabeen embayment bathymetry (a) from multiple sources (see Section 1.4.3.1, Chapter 1) surface water elevation (b) and wave parametric data (c) from Boussinesq wave modelling of the embayment under mean annual wave conditions.

3.5.4 Video-Derived Inshore Waves

Non-directional inshore wave statistics were produced through the Wave Pack system from 18-minute video recordings for 11 daylight hours per day over an 88 day period (Aug – Oct 2011) at the South Narrabeen and Wamberal surfcams. Data return at both sites was ~65%, resulting in 661 (639) hourly records for comparison at Narrabeen (Wamberal). Image quality control and data processing were undertaken by CoastalCOMS and the wave statistics provided to this study included wave height (mean, significant, 75th percentile, 90th percentile, maximum) and wave period (minimum, 5th percentile, mid, 95th percentile, maximum). Other available parameters include number of break zones, wave count, distance to breaker zone from camera, shoaling distance and tidal elevation.

3.5.5 Buoy-Derived Nearshore Waves

Wave Pack data was compared with hourly wave data simultaneously recorded at two nearshore Datawell directional WaveRider buoys (Figure 3.3, locations Figure 3.1).

Figure 3.3 Datawell directional WaveRider buoys deployed at Narrabeen (a) and Wamberal (b). Images courtesy of Manly Hydraulics Laboratory (MHL).

The wave buoys recorded sea surface elevation change for 34 minutes every hour, from which directional wave statistics were calculated. Data return rates for both buoys exceeded 90%. The Narrabeen buoy was 500 m east-northeast, and the Wamberal buoy 500 m east-southeast, of the corresponding surfcam (Figure 3.1), in water depths of 10-12 m. During data capture, mean (max) significant wave heights were 1.1 m (2.9 m) at Narrabeen and 1.2 m (3.6 m) at Wamberal. Mean nearshore wave direction was east-southeast at Narrabeen and southeast at Wamberal, resulting in predominantly shore-normal waves.

Due to the impracticalities of buoy deployment in the surf zone, wave buoy data represents shoaled but unbroken nearshore, shallow water waves whereas video-derived inshore wave data represents waves at the break point and within the surf zone. A linear relationship with a y-intercept offset would be expected for positive validation of the surfcam-derived wave data, as negligible wave generation occurs landwards of the buoy locations. The time lag between waves passing the buoys and entering the camera field of view should also be negligible. Therefore, the wave buoy statistics represent waves seen by the surfcam during the same timestack image.

3.5.6 Validation Method

Hourly mean wave height, H_{mean}, significant wave height, H_s, 10% exceedance wave height, H_{10}, and maximum wave height, H_{max}, observed at the buoys were regressed against all combinations of the same parameters derived from Wave Pack. The mean (zero-crossing) wave period, T_z, and the peak spectral wave period, T_p, were regressed against all combinations of the Wave Pack-derived minimum wave period, T_{min}, the average wave period, T_{mid}, and the maximum wave period, T_{max}. See Section 1.2.1.3 (Chapter 1) for significance of wave parameters.

In addition, the residuals from the above regressions were themselves regressed against (i) tidal stage, (ii) shoaling distance from the surf cam, (iii) wave count (number of waves identified per recording) as recorded by Wave Pack, and (iv) wave direction recorded at the buoy. This was in order to investigate whether any of these factors has a significant impact on the Wave Pack validation.

3.6 RESULTS

Figure 3.4 shows the comparison of hourly wave statistics between Wave Pack and the wave buoys at Narrabeen and Wamberal. At both sites Wave Pack over-estimated wave height and period for smaller waves (H_{sig} < 2 m, T_z < 7 s) and under-estimated for larger waves (up to H_{sig} = 3.6 m in this study). Some wave height over-estimations were more than four times the wave buoy value and in all cases scatter was high (i.e. low precision).

The metrics of R^2 and m (slope) were used to determine statistical relationships, with m used in addition to R^2 to investigate whether there was a systematic trend between wave data from the two methods (see Section 2.7.4 in Chapter 2 for a definition of R^2 and m). Tables 3.1 (3.2) show compared parameters and corresponding R^2 and m values at Narrabeen (Wamberal).

Results show all weak (R^2 < 0.6) but most significant (to 95% level) statistical relationships. However, the Durbin-Watson test shows positive autocorrelation of residuals (d = ~1.2, 95% confidence), indicating that the hourly wave statistics are not entirely independent, leading to under-estimation of the statistical significance level.

In all cases, residual errors of wave height and period showed no linear correlation with wave count, tidal stage, breaker distance from surfcam, or wave direction, indicating that wave measurement accuracy was independent of these physical conditions.

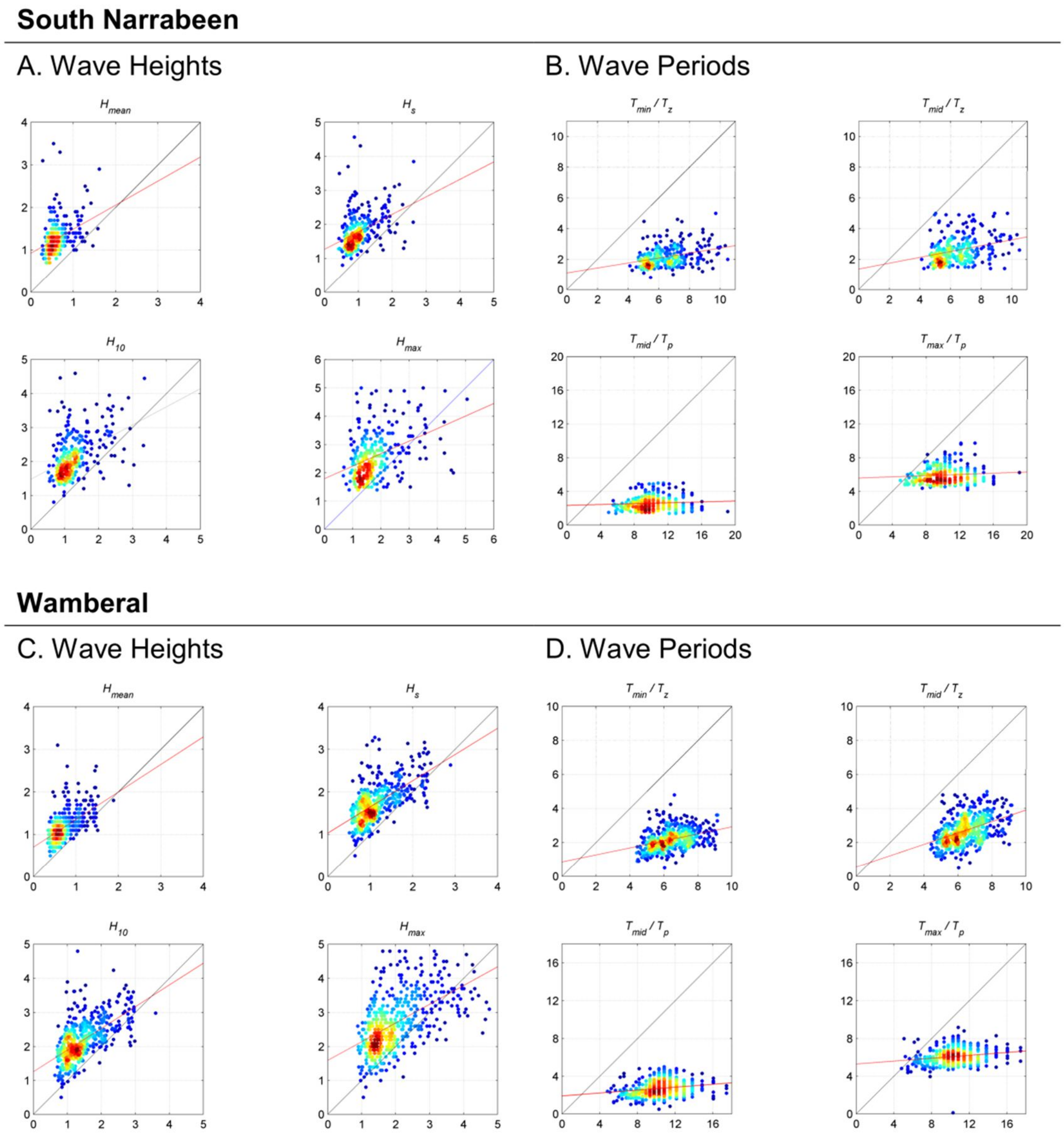

Figure 3.4 Comparison of Wave Pack wave parameters with buoy-measured parameters. Scatter plot colours show data point density. Wave height comparisons are (clockwise) H_{mean}, H_s, H_{10}, and H_{max} for South Narrabeen (a) and Wamberal (c). Wave period comparisons are (clockwise) T_{min}/T_z, T_{mid}/T_z, T_{mid}/T_p and T_{max}/T_p for South Narrabeen (b) and Wamberal (d). Buoy (Wave Pack) measurements are on x (y) axis.

Table 3.1 Comparison between Wave Pack and wave buoy output at Narrabeen (bold - $\boldsymbol{R^2}$ and italic - *slope*). For n = 500, using Student t-test, critical R^2 at 95% level = ~ 0.07.

		Wave Buoy						
		H_{mean}	H_s	H_{10}	H_{max}		T_z	T_p
Wave Pack	H_{mean}	**0.16**	**0.16**	**0.16**	**0.15**	T_{min}	**0.17**	**0.01**
		0.61	*0.37*	*0.29*	*0.19*		*0.30*	*0.05*
	H_s	**0.16**	**0.16**	**0.16**	**0.15**	T_{mid}	**0.33**	**0.04**
		0.86	*0.53*	*0.42*	*0.27*		*0.48*	*0.09*
	H_{10}	**0.17**	**0.18**	**0.18**	**0.16**	T_{max}	**0.54**	**0.14**
		1.10	*0.69*	*0.54*	*0.35*		*0.75*	*0.20*
	H_{max}	**0.17**	**0.18**	**0.17**	**0.16**			
		1.40	*0.89*	*0.70*	*0.45*			

Table 3.2 Comparison between Wave Pack and wave buoy output at Wamberal (bold - $\boldsymbol{R^2}$ and italic - *slope*).

		Wave Buoy						
		H_{mean}	H_s	H_{10}	H_{max}		T_z	T_p
Wave Pack	H_{mean}	**0.36**	**0.35**	**0.35**	**0.33**	T_{min}	**0.16**	**0.07**
		0.66	*0.41*	*0.33*	*0.22*		*0.35*	*0.11*
	H_s	**0.37**	**0.37**	**0.37**	**0.34**	T_{mid}	**0.36**	**0.11**
		0.95	*0.60*	*0.48*	*0.32*		*0.58*	*0.15*
	H_{10}	**0.34**	**0.34**	**0.34**	**0.31**	T_{max}	**0.35**	**0.19**
		1.20	*0.77*	*0.61*	*0.41*		*0.66*	*0.24*
	H_{max}	**0.30**	**0.31**	**0.31**	**0.28**			
		1.50	*0.98*	*0.79*	*0.53*			

3.7 DISCUSSION

There was a weak but significant statistical relationship between the hourly Wave Pack parameters and those simultaneously recorded by the nearshore buoys with high scatter evident. While buoy measurements represent nearshore, unbroken waves and Wave Pack measures waves at the break point and in the surf zone, if Wave Pack measurements were robust, a systematic offset would be expected against buoy data. In all cases, there was an over-estimation of smaller waves and an under-estimation of larger waves. Reasons for this skewed distribution were investigated by comparing the number of waves per recording, tidal stage and breaker distance from the surfcam with the residual errors of Wave Pack outputs. Weak correlations suggested that these factors did not significantly influence the inshore wave measurements.

Without a fixed reference in any dimension, rectification from pixels to real-world coordinates is difficult from a single camera, rather than a stereo-pair. The obliquity of low-angle cameras increases the margin for error in the cross-shore location of breakpoint and subsequently in the calculation of breaking wave height (e.g. Shand *et al.*, 2012). Results suggest the rectification process applied real-world lengths that were too small for distant pixels and too large for foreground pixels, so larger waves breaking further out were under-estimated and smaller waves breaking closer to shore were over-estimated. A second overlapping camera field of view may resolve this distortion.

Between the two locations, Wave Pack measurements are marginally improved at Wamberal. This may be because this site is located at the northern (most exposed) end of the embayment, receiving waves with less refraction and thus reduced obliquity on entering the surf zone. While there was no significant correlation between Wave Pack accuracy and wave direction measured at the buoy, there was a non-significant trend of greater error with north-easterly (oblique) waves. This trend was not significant because of high scatter in the residuals, but may indicate that wave obliquity on entering the surf zone is a contributing, but not over-riding, factor in the inaccuracies of wave height measurements from Wave Pack.

Observed scatter in all comparisons may be partly due to beach or wave type. Plunging waves are most easily detected, changing rapidly from a dark green (breaker face) to white at the break point. On reef systems plunging waves follow a more repeatable breaker line (Hilmer, 2005), but on multi-barred sandy beaches, both breaker type and position are more dynamic. Spilling or surging breakers leave large areas of white water, have no steep measurable face and break and re-form multiple times. Narrabeen and Wamberal are intermediate beaches (after Wright and Short, 1984), the former exhibiting a rhythmic bar and trough morphology and the latter a welded bar and rip system. Multiple break zones, spilling wave type and large areas of white water may all impede accurate measurement of breaking waves.

3.8 CONCLUSIONS

Wave measurements derived from low-angle surfcams have been validated against concurrent nearshore wave buoy observations at two embayments in south east Australia. Results indicate that the wave monitoring capabilities currently do not provide an adequate representation of inshore wave conditions. Comparisons indicate the surfcam method tends to over-estimate smaller waves and under-estimate larger waves, possibly due to rectification error and beach/wave type, and there is potential to improve Wave Pack algorithms by accommodating these factors.

While the adoption of this existing and extensive coastal camera infrastructure to provide real-time and hindcast inshore wave climates remains an attractive end-goal, it is currently not an option to pursue for this thesis. In addition to the current poor accuracy of wave heights and periods, this method does not provide any information of wave direction which is vital for the modelling of alongshore sediment transport.

After an assessment of uncertainties related to regional wave climate downscaling in Chapter 2, a surrogate-observational approach to investigating wave climate change and coastal impacts was advocated. This present chapter has shown that observations of inshore wave climates cannot reliably be obtained from surfcam observations currently available at beaches in south east Australia. Therefore, the rest of this thesis uses observational analyses of both mid-shelf and nearshore wave buoy data, with two-dimensional wave and morphodynamic modelling, to build scenarios of wave climate and coastal change for future climate states.

3.9 ACKNOWLEDGEMENTS

This research was funded by the Australian Research Council (LP100200348 to IDG and ILT), with additional support from partners the University of Plymouth (UK), NSW Office of Environment and Heritage, CoastalCOMS (particularly C. Lane for establishment and ongoing development of the surfcam network), Warringah Council, Gosford City Council. All Wave Pack data was processed and quality-controlled by C. Lane at CoastalCOMS. The Matlab freeware function *dscatter* (Eilers and Goeman, 2004) was used in the creation of Figure 3.4.

CHAPTER 4

Grassy Head Beach

MODAL WAVE CLIMATE VARIABILITY ALONG THE SOUTHEAST AUSTRALIAN SHELF

4 MODAL WAVE CLIMATE VARIABILITY ALONG THE SOUTHEAST AUSTRALIAN SHELF

4.1 CHAPTER OVERVIEW

Variability in the modal (non-storm) wave climate is a key process driving large-scale coastal behaviour on moderate- to high-energy sandy coastlines, and is strongly related to variability in synoptic climate drivers. However, in a semi-enclosed sea environment such as along the Southeast Australian Shelf (SEAS), isolating directional wave climates is hindered by a complex mixed sea-swell environment. Until now, only qualitative assessments of the SEAS wave climate have been made, with no explicit link to synoptic climate drivers.

This chapter presents a directional wave climate typology for the Tasman Sea using mid-shelf wave buoy observations along the SEAS to link wave observations to synoptic climate and wave generation. In addition, projections of regional wave climate change for the Sydney region with tropical expansion (as observed and modelled with greenhouse forcing) are made, based on a surrogate-buoy approach. This approach represents an alternative to the dynamical downscaling method explored in Chapter 3 for investigating future shifts in wave climate.

4.2 KEY FINDINGS

A statistical-synoptic analysis of wave buoy observations indicates that five synoptic-scale wave climates exist during winter, and six during summer. These can be clustered into easterly (Tradewind), south-easterly (Tasman Sea) and southerly (Southern Ocean) wave types, each with distinct wave power signatures.

Results show that a southerly shift in the sub-tropical ridge (STR) and trade-wind zone, consistent with an observed poleward expansion of the tropics, forces an increase in the total wave energy flux in winter for the central New South Wales shelf of 1.9 GJ m^{-1}

wave-crest-length for one degree southerly shift in the STR, and a reduction of similar magnitude (approximately 1.8 GJ m^{-1}) during summer. In both seasons there is an anti-clockwise rotation of wave power towards the east and south-east at the expense of southerly waves.

Reduced obliquity of constructive wave power would promote a general disruption to northward alongshore sediment transport, with the cross-shore component becoming increasingly prevalent. Results are of global relevance to sub-tropical east coasts where the modal wave climate is influenced by the position of the zonal STR.

4.3 PUBLICATION AND AUTHOR CONTRIBUTION

This chapter was published, in modified form, in: **Mortlock, T.R.** and Goodwin, I.D. (2015). Directional wave climate and power variability along the Southeast Australian shelf. *Continental Shelf Research*, 98, 36-53. doi: 10.1016/j.csr.2015.02.007. This publication is provided in Appendix 4.

This work was first presented at AGU Ocean Sciences Meeting 2014: **Mortlock, T.R.** and Goodwin, I.D. (2014). Marginal sea wave climate variability at Sydney, Australia. *Ocean Sciences Meeting, American Geophysical Union, Honolulu, Hawaii, February 2013*.

As lead author, I carried out all analysis and wrote the chapter/paper. The original concept for this study was developed jointly between me and IDG. IDG contributed to the interpretation of results and edits to the chapter/paper.

4.4 INTRODUCTION

Wave climate change, rather than sea-level rise, is presently expected to be the dominant process impacting shoreline change on moderate- to high-energy sandy coastlines in the coming decades (Slott *et al.*, 2006, Coelho *et al.*, 2009; Hemer *et al.*, 2012). It has long been realised that variations in the deep-water ocean wave field directly modulate the power that forces the evolution of coastal morphology (e.g. Johnson, 1919). However, there remains a stronger research focus on sea-level rise (Nicholls *et al.*, 2007) than studies on wave climate change globally, leading to only low confidence in projected changes (Hemer *et al*., 2013, Church *et al*., 2014).

Definition of wave climate and directional wave power is a key component in the fields of marine renewables (Hughes and Heap, 2010), shipping (Semedo *et al.*, 2011), coastal and ocean engineering (Callaghan *et al.*, 2008), marine ecology (Storlazzi *et al.*, 2005) and coastal management (Nicholls *et al.*, 2013). A wave climate can be defined simply as the long-term (a decade or more) statistical characteristics of the waves at any one location (Holthuijsen, 2007). Often, the bulk wave climate (seasonal to centennial) is composed of a number of wave types, originating from a range of synoptic weather systems that produce distinct surface wind-wave signatures.

The bulk wave climate will therefore comprise a mixture of wave types and distributions. Often it is desirable to decompose the wave climate into component groups - a process known as wave climate typing. For example, statistical or dynamical downscaling of long-term offshore wave information is frequently required for coastal process or maritime engineering studies. The computational inefficiency of down-scaling all available data requires that a small number of representative sea states are determined, which are later propagated to shallow water (Camus *et al.*, 2011a).

Wave climate typing can be approached either synoptically or statistically. Basic synoptic typing of wave climates was first proposed by Munk and Traylor (1947). This has since evolved towards the identification of dominant patterns of synoptic-scale weather systems based on large-scale synoptic evolution and atmospheric pressure gradients (Browning and Goodwin, 2013, Goodwin *et al*., in prep), or using Empirical Orthogonal Functions (EOF) of mean sea level pressure (MSLP) fields (Speer *et al*., 2009, Hemer *et al*., 2008).

A limitation of EOF analysis applied to climate data, is that it is often difficult to attribute specific synoptic conditions or mechanisms to the orthogonal datasets. Even in cases where EOFs adequately explain weather pattern variance, multiple synoptic types will not necessarily produce statistically dissimilar wave climates, but rather characterise the different synoptic evolution of wave generation. Moreover, EOF analyses will typically discard a large portion of the original dataset not described by the primary EOFs.

An alternative approach is statistical typing of parametric wave data. This involves the decomposition of a continuous wave timeseries without explicitly linking the wave types to their synoptic generation source. A major advantage of statistical typing is that 100% of the variance in the geophysical dataset is used. The most common approach is to define the empirical joint probability density function (PDF) of wave height and period for a given directional bin, and to visualise the results using two-dimensional histograms (Holthuijsen, 2007). The draw-back to this method is the subjectivity with which the position and width of directional bins are chosen. Unsuitable directional bins may split a wave climate in two, or merge adjacent wave climates. In addition, transient wave generation often results in the tails of the distribution being mixed with those of their neighbours.

An alternative statistical approach is to use clustering algorithms to obtain a wave typology. Clustering aims to group multivariate wave data into *n* number of classes ('wave climates') in an optimised manner such that dissimilarity between cluster groups is maximised. Cluster models such as K-Means, Partitioning Around Medoids (PAM), Self-Organised Mapping (SOM) and Maximum Dissimilarity are currently the principle algorithms used to characterise wave climates for coastal engineering applications (Hamilton, 2010, Camus *et al*. 2011a, 2011b, Guanche *et al*., 2013). Alternatively, Camus *et al*. (2014) have shown that clustering of hindcast MSLP fields (rather than direct clustering of a wave timeseries) can yield accurate wave climate types, by relating the clusters to sea states based on linear regressions built between MSLP and dynamical ocean wave hindcasts.

The principle disadvantage of wave cluster analysis is that the optimal number of wave clusters, *k*, is unknown. For open coast examples, where there is a clear distinction between far-field swells and localised wind-sea, clustering is often visually discernible from plotting. In these cases *k* can be estimated and fitted to a cluster model of choice. Western Australia (Masselink and Pattiaratchi, 2001), Southern California (Storlazzi and Wingfield, 2005) and the Iberian Peninsula (Camus *et al*., 2011b, Gaunche *et al.*, 2013) are all global open coast examples where the number of wave climates have been visually determined for conceptual or statistical description.

In semi-enclosed sea environments the distinction between wave climates is not so clear. The complexity of discerning between fetch-limited sea and swell in these environments has been acknowledged by authors in the North Sea (Boukhanovsky *et al*., 2007), Gulf of Mexico (Wang and Hwang, 2001), and Mediterranean Sea (Alomar *et al*., 2014).

The Tasman Sea is open to the north and south, borders the east coast of Australia, and is partially blocked from the Southwest Pacific Ocean by the New Zealand landmass (Figure 4.1). It extends from the mid latitudes to where it meets the Coral Sea in the north, at approximately 30° S (IHO, 1953). Waves propagating in water depths exceeding 5,000 m in the Tasman Sea rapidly shoal to around 100m at the East Australian shelf, which at Sydney is only 35km wide. This rapid shoaling conserves much of the offshore wave energy upon transformation across the shelf, leading to a high-energy nearshore wave climate and wave-dominated sediment transport.

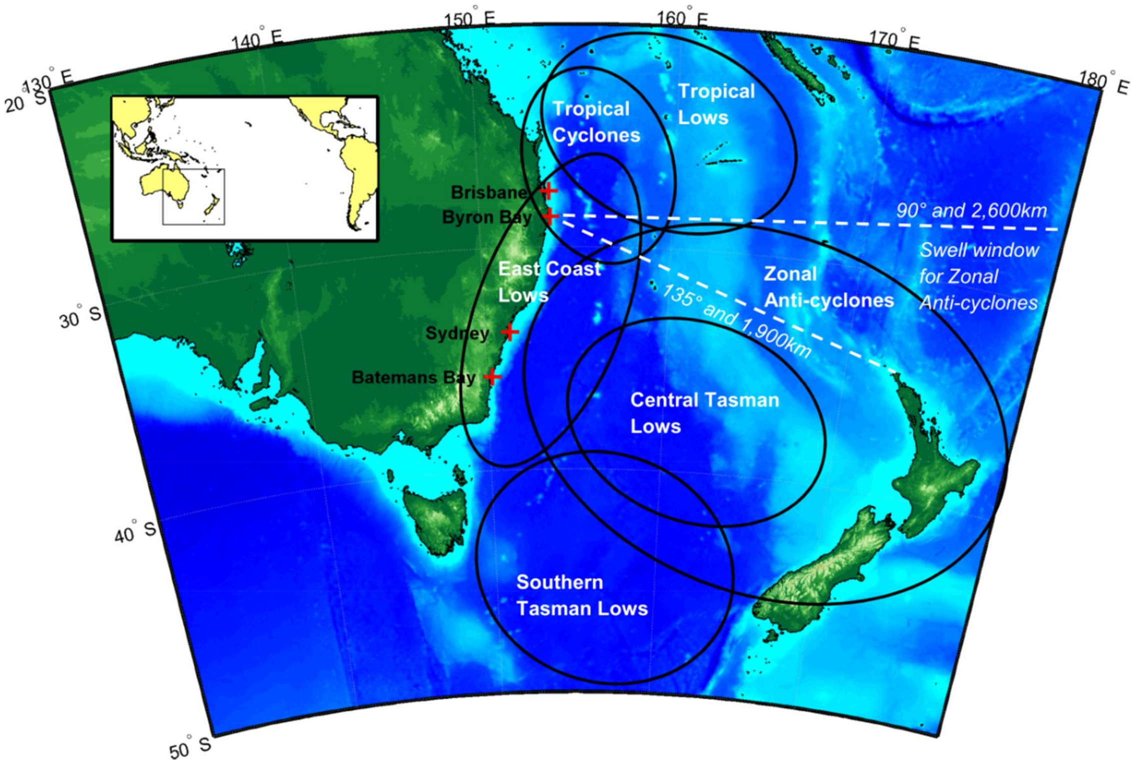

Figure 4.1 Approximate area of influence of wave-producing meteorological types in the Tasman and Coral Seas, based on work by Short and Treneman (1992) and Shand *et al* (2011a). Also shown is the potential swell window for zonal anti-cyclones outside the Tasman Sea. Inset shows position of study area in relation to Pacific Basin. ETOPO01 imagery courtesy of NOAA (Amante and Eakins, 2009).

The Southeast Australian Shelf (SEAS) experiences a mainly marginal sea wave climate produced by weather systems in, or peripheral to the Tasman Sea (Figure 4.1). Although it is possible for longer-period swells generated in the South Indian Ocean sector of the Southern Ocean to propagate through the Tasman Sea on a southwest – northeast trajectory on great circle paths (Munk *et al,* 1994), they cannot undergo sufficient refraction to be felt along the SEAS. Conversely, the west coast of New Zealand experiences a higher proportion of Southern Ocean swells than the SEAS due to the prevailing westerly movement of these systems. Likewise, there is no swell window for Northern Pacific waves generated during the boreal winter to propagate into the Tasman Sea due to the myriad of island chains and rises in the Equatorial Pacific.

Multiple studies (BBW, 1985, Short and Trenaman, 1992, Harley *et al*., 2010, Shand *et al*, 2011a) have led to a general acceptance of five to six synoptic wave-producing weather patterns that impact the SEAS. These include Tropical Cyclones, Tropical Lows, Anti-cyclonic Intensification, East Coast Lows, Southern Tasman Lows and Southern Secondary Lows (Figure 4.1). Since the majority of wave generation is within, or adjacent to, the Tasman Sea wave periods are fetch-limited and are rarely sustained above 12-13s over a 24-hour period. However, northern New South Wales and southeast Queensland receive a small percentage of swells between 12 – 16 seconds that are generated to the north east of New Zealand during anti-cyclonic intensification (Figure 4.1). A meso-scale sea-breeze is also recognisable during the summer months along the coastal fringe. Despite a wealth of observational buoy data, directional wave parameters and wave power signatures representing each type have never been isolated.

Previous studies have shown there to be considerable inter-annual modulation of the regional wave climate by El Niño Southern Oscillation (ENSO) and the Southern Annular Mode (SAM) (Harley *et al*., 2010), and multi-decadal forcing by ENSO and the Interdecadal Pacific Oscillation (IPO) (Goodwin, 2005), and the Indian Ocean Dipole (IOD) (Goodwin *et al*, 2010). The sub-tropical ridge (STR), the location of highest pressure that varies seasonally between 29°S in winter to 40°S in summer over Eastern Australia (Timbal and Drosdowsky, 2013), also exerts a strong influence on seasonal to inter-annual wave generation in the Tasman Sea (Browning and Goodwin, 2013), effectively dividing the region into easterly vs westerly generated wind-waves (Goodwin *et al*., 2013b).

However, due to the fetch-limiting influence of regional geography and equidistance of wave generation sources, there is no clear distinction between many of these meteorological patterns in the wave record. When joint probabilities of wave height and period were compared across storm types, Goodwin *et al* (in prep) found that a variety of different meteorological forcings produced statistically similar wave patterns across the New South Wales coast. For example, all types of East Coast Lows identified (Easterly Trough Lows, Southern Secondary Lows, Continental Lows and Inland Trough Lows) were indistinguishable in their joint distribution of wave height and period. This highlights the problem of using synoptic evolution to identify unique wave climates in semi-enclosed seas, although the approach is useful for description of meteorological forcing of extreme wave events.

This study has taken an alternative approach. The primary focus is on modal wave climate and power as the main driver of large-scale coastal behaviour to support future studies on long-term beach recovery and on-shore sediment transport from the lower shoreface. While storm waves are responsible for instantaneous coastal inundation and beach erosion, the modal (or 'ambient') wave climate that persists between storms is predominantly responsible for post-storm beach recovery, long-term delivery of sediment across the shoreface, and shoreline planform orientation (Ranasinghe *et al*., 2004, Harley *et al*, 2011). Additionally, New South Wales and southeast Queensland have a relatively small number of extreme events relative to the modal climate, when compared to the more energetic southern margin of Australia (Hemer and Griffin, 2010, Hughes and Heap, 2010). Despite this, there has been a lack of focus on modal variations in the Tasman Sea in favour of extreme wave events (BBW, 1985, You and Lord, 2008, Shand *et al*., 2011a, b, Cardno, 2012).

Statistical clustering was first performed on wave buoy records along the East Australian shelf in order to identify the dominant modes of directional wave climate variability. A Gaussian Mixture Model (GMM) was then used to assess the resolution of the clustering technique and further isolate 'synoptic-scale' wave climates. MSLP composites were then used to investigate wave climate relationships with large-scale climate drivers. The seasonal variability in directional wave power, and future changes associated with shifts in the STR, were then described and related to coastal processes. Results are of global relevance to coastlines where the modal wave climate is influenced by the position of a zonal STR, especially other mid-latitude, Southern Hemisphere east coasts with comparable wave climate genesis and sediment transport.

4.5 DATASETS

4.5.1 Available Buoy Records

Directional wave information recorded at four Datawell Directional WaveRider (DWR) buoys in south (Batemans Bay), central (Sydney) and north (Byron Bay) New South Wales and Southeast Queensland (North Stradbroke Island) was used (Figure 4.1). The North Stradbroke Island buoy is moored 40 km west of Brisbane, and is hereafter referred to as 'Brisbane'. This dataset provided observational coverage of approximately 1,000 km of mid-shelf, deep-water waves (60 – 100 m depth), along the western boundary of the Tasman and Coral Seas between 27 and 37° S.

Although buoy records are considered one of the most reliable sources of wave observations, they can suffer from periods of data loss. All four buoys used in this study have 90 - 95% data recovery rates, with the majority of non-recovery occurring during extreme wave conditions. Since this study is focussed on the modal wave climate, this is unlikely to affect results.

4.5.2 Wave Data Preparation

Hourly wave parameters were provided by Manly Hydraulics Laboratory (MHL), and the Queensland Department of Science, Information Technology, Innovation and the Arts (DSITIA). All directional wave information was averaged to daily values.

Significant wave height, H_s, primary peak spectral wave period, T_p and mean wave direction at the primary spectral peak, MWD_{Tp}, were used to describe the daily peak wave energy conditions at each buoy location. These parameters were extracted using spectral analysis by both MHL and DSITIA (where $H_s \approx$ four times the square root of the zeroth moment). Distributions of these parameters usually exhibit some type of skew-normal distribution, with occasional secondary modal peaks. As such, reference to the median value and inter-quartile range (IQR) is used in their description.

The wave data was reduced to resolutions of 0.01m (Hs), 0.1s (Tp_1) and 1.0° (MWD_{Tp1}) in line with buoy heave/direction (Datawell, 2014) and MHL data sampling (Wyllie and Kulmar, 1995) resolutions. Since this study concerns wave climate impacts on coastal behaviour, all offshore-propagating wave energy was extracted before clustering.

Each buoy record was split into (Austral oceanic) summer (January, February, March) and winter (July, August, September) seasons. Autumn and spring data were not included as wave patterns during these months represent a mixture of both winter and summer climatologies.

4.6 METHODS – STORM EVENT SEPERATION

Any statistical analysis of wave climate requires a separate treatment of storm (extreme) and modal (ambient) conditions because often the two will exhibit distinctly different distributions, due to the different underlying physical drivers (Holthuijsen, 2007). Defining an optimal separation between these two regimes, however, is a non-trivial task.

The procedure used here is based on the Peaks-Over-Threshold (POT) method. POT aims to identify storm events in a continuous wave record that exceed a significant wave height threshold; that are maintained for a minimum storm duration; and that are separated by a minimum storm recurrence interval. This approach was preferred over the Annual Maximum (AM) method due to the deficiencies of the latter in returning a low storm count for relatively short inter-annual timeseries (Goda, 2010).

4.6.1 Minimum Storm Duration

A minimum storm duration of three days was chosen, after other Tasman Sea wave climate analyses (Hemer, 2010, Shand *et al.*, 2011a, Shand *et al.*, 2011b, Cardno, 2012). Apart from tropical cyclones which are highly transient systems, synoptic storm types have similar residence times in the Tasman Sea (Browning and Goodwin, 2013), thus a single storm duration for all buoy locations is sufficient.

4.6.2 Minimum Storm Recurrence Interval

An appropriate recurrence interval ensures that a single storm event is not split into shorter component events if the H_s value dips briefly below the storm threshold. In doing so, it maintains the statistical and synoptic integrity of the storm timeseries. A 24 hour recurrence interval was used, according to the regional progression of synoptic events (Speer *et al.*, 2009, Browning and Goodwin, 2013).

4.6.3 Wave Height Threshold

Separate summer and winter storm wave height thresholds were determined for each DWR buoy to accommodate seasonal variation and localised effects (i.e. shoaling or wave focussing) in the wave height distributions. One criticism of the POT method is the subjectivity with which the height of the threshold can be chosen. This is especially important in this study as a threshold set too high will dilute the clustering of modal conditions.

Several studies (Mathiesen *et al.* 1994, Mazas and Hamm, 2011, Bernadara *et al.*, 2014) have attempted to determine a standard method to verify the statistical robustness of the threshold level based on the goodness-of-fit of the peak storm values with various extreme distributions (Coles, 2001). The Generalised Pareto Distribution (GPD) is now recommended (Hawkes *et al.*, 2008) and widely used (Méndez *et al.*, 2006, Thompson *et al.*, 2009, Mazas and Hamm, 2011) as the most appropriate extreme distribution for threshold validation.

A GPD approach to storm threshold selection was applied, with a modified Mazas and Hamm (2011) method. First, a range of thresholds was explored to locate a statistically robust storm threshold (u_3), starting from an under-estimated value of u_3 (u_0) to an over-estimated value of u_3 (u_1). Here, u_0 = 1m, which roughly equates to the 95% exceedance 24-hourly H_s for all buoy records, and u_1 = 3m, approximate to the 5% exceedance 24-hourly H_s for all buoy records. This reduces the data set to only include storms of a reasonably wide range of intensities, and also reduces serial correlation to make the statistical assessment more robust.

Next, the set of exceedances of storm peak wave height above threshold is fitted to a GPD, for a range of thresholds between u_0 and u_1. A final storm threshold (u_3), above which storms exhibit statistically extreme behaviour (i.e. begin to deviate from a GPD), is located between $u_0 - u_1$ using the GPD shape, k, and modified scale, σ^*, parameters, and a guide value (u_2). u_2 is chosen to match the average annual storm frequency (λ) for each buoy record, as reported in a separate synoptic-typing analysis by Shand *et al.* (2011). This process is detailed below in Figure 4.2.

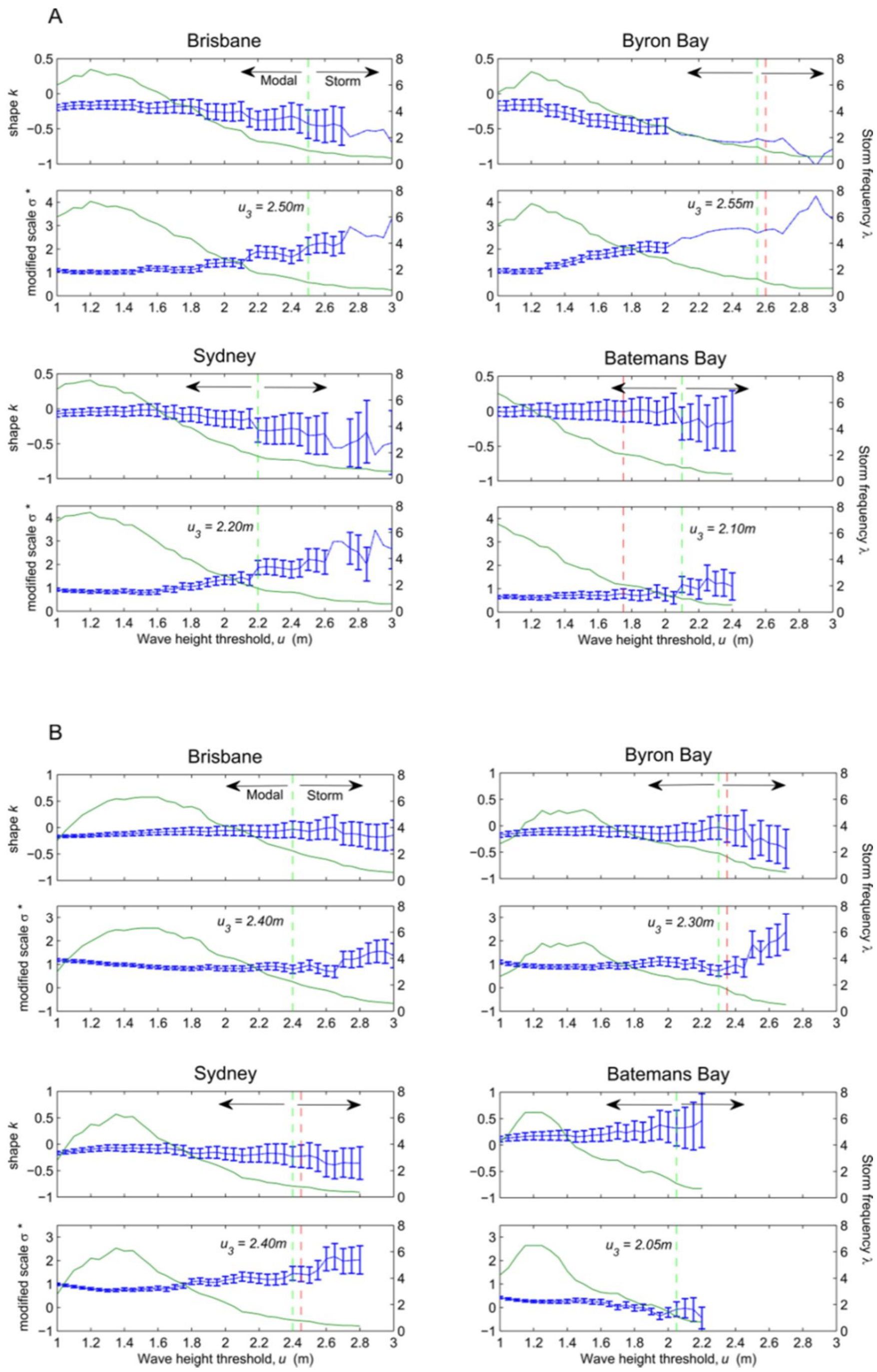

Figure 4.2 Storm threshold detection method used for (A) winter and (B) summer H_s distributions at the four buoy locations. The shape parameter, k, and the modified scale

parameter, σ^*, of the GPD were calculated at each 0.05m u interval (blue line with confidence intervals, CI, on top plot for k and bottom plot for σ^*) between u_0 (1m) and u_1 (3m). The mean annual storm frequency, λ, for each u interval between u_0 and u_1, is also shown (dark green solid line) and as expected, λ decreases with increasing u. The guide threshold, u_2, (green dotted line), and the final threshold, u_3, (red dotted line), are also given. If $u_2 = u_3$, only u_3 is shown. Note that for some higher u values, maximum likelihood used to estimate the GPD parameters cannot reliably compute CIs. Also, GPD statistics for u values towards 3m H_s in some instances are not shown (e.g. Batemans Bay winter/summer and Byron Bay/Sydney summer) because no storms were identified using these higher thresholds.

Figure 4.2 gives k and σ^* for 0.05m increments of H_s between $u_0 - u_1$, u_2 (red dotted line) and u_3 (green dotted line), for each buoy location for (A) winter and (B) summer. u_3 is determined using the guide value (u_2), and by identifying "domains of stability" in k and σ^* close to u_2. If the wave height distribution follows a GPD, both k and σ^* will remain relatively constant when u increases, and successive "domains of stability" can be seen (Mazas and Hamm, 2011). The point at which k and σ^* begin to deviate from GPD 'stability' is the idealised storm threshold value. Locating the final domain of stability before extreme behaviour is apparent, is subjective process (although automated methods have been proposed e.g. Thompson *et al*., 2009). Instead, u_2 is used as a guide. As it is desirable to minimise dilution of the modal wave climate with extreme events, the lowest u value of the domain of stability on which u_2 lies is selected as u_3.

Results indicate that the statistical storm thresholds (u_3) are very similar to those derived by Shand *et al* (2011) using a synoptic typing method. They are also approximate to the daily 10% exceedance wave heights at each buoy (H_{s10}), indicating that H_{s10} can be used as a general storm threshold guide for the Southeast Australian shelf. Other studies in New South Wales have used comparable values of H_s 2.0m (Shand *et al*, 2011a, 2011b), 2.5m (BBW, 1985, Rollason and Goodwin, 2009) and H_s 3.0m (You and Lord, 2008, Shand *et al*, 2011a, 2011b, Goodwin *et al*, in prep). All the aforementioned studies, however, included no statistical verification of the threshold value.

Storm thresholds vary between sites not only because of latitudinal differences in storm frequency, but also due to localised effects. Larger u_3 values (i.e. when a larger wave height threshold is required to meet the expected storm frequency, λ) indicate a more exposed buoy location, whereas smaller u_3 values suggest a more shoaled and/or sheltered climatology. This is particularly evident at Batemans Bay where significantly lower u_3 values are needed to match the required Λ than at other sites.

4.7 METHODS – CLUSTER ANALYSIS

4.7.1 Cluster Preparation

Once storm events were separated out, the trivariate modal wave timeseries (*Hs*, T_p, MWD_{Tp}) was normalised using the method proposed by Camus *et al.* (2011a). The first two parameters are scalar variables (*Hs* and T_p), while the third one (MWD_{Tp1}) is a circular variable. As noted by Camus *et al*. (2011a), the circular variable entails a problem for cluster application, since 1° True North (TN) and 359° TN are supposed to be completely different. While this is not always a problem for the analysis of New South Wales/Queensland buoy data, as they only receive a largely 180° directional spectrum because of coastal orientation, the Euclidean-Circular (EC) distance solution proposed by Camus *et al.* (2011a) was applied for clustering. Pre-cluster normalisation is necessary in order that Euclidean distances (or pairwise dissimilarities) used in the cluster model are not skewed by the difference in absolute variance between wave parameters. The wave data were subsequently de-normalised after clustering.

4.7.2 Cluster Model Selection

Cluster model selection depends on the quality of the clustering, and this can usually be assessed visually. Cluster models can be divided into those that use hierarchical and non-hierarchical schemes. Hierarchical clustering produces a tree of *k* first-order clusters which are divided into *n* number of sub-groups, and are commonly illustrated in the form of a dendrogram. Although visually useful, timeseries wave data cannot be indexed with a cluster number when using a dendrogram. The number of clusters shown is also heavily dependent on sensitivity settings such as the number of leaf nodes and the maximum linkage between levels. In contrast, non-hierarchical methods return a single set of cluster groups and each data point is assigned to a cluster. This indexing is needed when examining the variability of clusters over time.

K-means is one of the most widely used non-hierarchical cluster methods. The algorithm finds the optimal Voronoi cells in uni- or multi-dimensional datasets for *k* clusters, and returns a centroid for each cluster. Voronoi cells take the form of irregular polyhedra, and describe the multi-dimensional space occupied by each cluster. Voronoi cells are determined by minimising the sum of dissimilarities (squared errors) between each object and its corresponding centroid. The centroid is not an actual observation in the dataset; rather, it is an average value which acts as the central reference point for each cluster.

K-means, however, has certain sensitivities which can influence data partitioning. Firstly, the algorithm can be sensitive to outliers (Velmurugan and Santhanam, 2010) meaning the shape of Voronoi cells may be distorted in datasets with high scatter or noise. Secondly, the cluster search is prone to local minima (Pelleg and Moore, 2000). This means that, since the first iteration of centroids is chosen at random, cluster assignment is never exactly the same when the algorithm is repeated. This can affect re-clustering of small samples, although is barely noticeable for larger and Gaussian-distributed datasets.

An alternative to k-means, which aims to reduce sensitivity to outliers, is k-medoids. Instead of taking the mean value of the objects in a cluster as a central reference point, a medoid is used. A medoid is the most centrally located object in a cluster (and therefore is an observation that actually exists within the dataset, rather than a mean). The most common realisation of k-medoids is the Partitioning Around Medoids (PAM) algorithm. Unlike K-means, PAM is not sensitive to local minima – that is, re-clustering even small and scattered datasets with PAM will yield the same cluster assignment each time.

Here, both k-means and PAM were used to cluster daily wave parameters from the Sydney buoy in order to evaluate cluster quality between methods. In order to minimise the effect of local minima when using K-means, the algorithm was iterated 100 times and the iteration that returned the lowest mean squared error between cluster groups was chosen. Results indicated that k-means provides a clearer cluster separation across all wave directions than PAM. For this study, therefore, k-means clustering was used.

4.7.2 Determination of *k* Clusters

While the choice of a cluster model determines the cluster quality, it does not provide any indication of the optimal number of clusters in a dataset (*k*). The optimal cluster number should minimise the within-cluster variance, while also minimising the number of cluster groups. Since the within-cluster variance reduces as the number of clusters increases (to the point at which each data point is represented by its own cluster), this is a difficult computational task. *k* is thus often determined ad-hoc or based on practical experience (Hamerly and Elkan, 2003). There are, however, a number of statistical methods proposed in the literature to estimate *k*.

Here, a group of five cluster evaluation indices was used to make a first-pass estimation of the optimal number of wave climates that exist at each buoy location. In this way, cluster selection is not constrained by a single definition of optimality; rather, the choice is spread across indices. Indices included; Silhouette (Rousseeuw, 1987), Calinski-Harabasz (1974), Dunn (1974), Krzanowski-Lai (1985) and the C-Index (Hubert and Levin, 1976). The indices were chosen based on their ubiquity of use and performance; both as reported in the literature (Milligan and Cooper, 1985, Gordon, 1999) and after sensitivity testing as part of this study.

K-means clustering was repeated using a sensible range of possible numbers of wave climate clusters (here, between two to ten clusters). Each cluster index evaluates the strength of the clustering for every repetition of K-means. Visual inspection of a Dendrogram was then used to add to the index group. A range of optimal cluster numbers was thus obtained (denoted $\sim k_1$). The highest k value in the range of $\sim k_1$ was then chosen as a first-pass estimate of the optimal number of wave climates. This 'over-fitting' ensures no statistically similar wave climates are merged.

4.7.3 Cluster Evaluation

Once k_1 was determined, the wave buoy record was re-clustered with k_1 number of clusters. If both the T_p and MWD_{Tp} centroids of adjacent clusters were within one standard deviation (σ) of each other (+/- 0.1 s for T_p and +/- 1 ° for MWD_{Tp} for instrument accuracy), then they were assumed to represent the same wave field and merged.

In mixed sea-swell environments the tails of adjacent wave climates tend to overlap because transient, near-field meteorological types produce a wide spread of wave directions. In order to limit inter-cluster spreading, and aid conceptualisation, outliers below (above) the lower (upper) adjacents of the distribution were removed. The lower (upper) adjacent is defined as the first (third) quartile of the distribution minus (plus) 1.5 times the inter-quartile range (*IQR*). The tails represent the weakest members of the wave cluster, since they lie furthest away from the centroid.

4.8 RESULTS AND DISCUSSION (1) – WAVE FIELDS DETERMINED FROM CLUSTERING

Three directional wave fields of the modal wave climate were identified at all buoy locations from clustering. These include one from the east (Mode 1), a second spreading east-south-east through to south-south-east (Mode 2), and a third spreading south-east through to south-south-east (Mode 3). In addition, a second easterly wave field (Mode 1 *swell*) was superimposed on Mode 1 at Brisbane during summer.

Wave roses for each buoy location are given in Figure 4.3 a (winter) and b (summer). The non-directional wave fields are analysed in the form of joint probability density (JPD) functions in Figure 4.4 a (winter) and b (summer). Since the wave buoys are located mid-shelf, the directional distribution of each mode varies between sites due to cross-shelf refraction. However, each is distinguishable from another by the directional space it occupies, in combination with the shape of the non-directional PDF.

The storm wave climate represents the extreme tail of the modal distribution. The vastly smaller sample size for the storm tail means the directional wave fields returned by clustering are not reliable. Therefore, attention is directed here to the modal wave climate, which accounts for 91 – 95% of all wave days recorded.

4.8.1 Mode One (East)

Mode 1 is omnipresent throughout the year at all buoy locations. It constitutes the shortest-period wave climate of all the wave fields (Tp_1 8 – 9s), with the widest directional spread and *IQR*, suggesting a near-field origin. This wave field occupies a directional band between 85 and 105°, with minimal seasonal rotation.

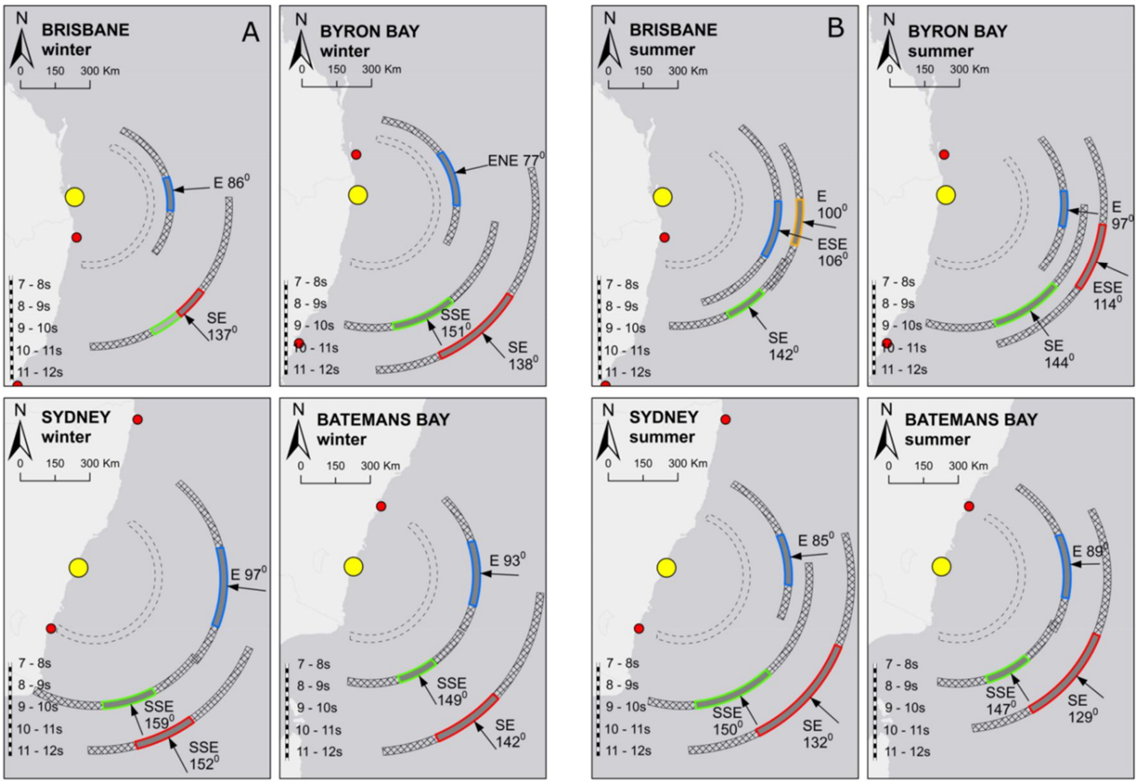

Figure 4.3 Primary wave modes at the four buoy locations for winter (A) and summer (B), as determined from clustering. Modes are plotted on a circular scale radiating out from each buoy location. The scale represents the mean T_p of the wave climate in 1s increments. Local wind-sea is shown as a dotted box covering the directional range observed at each buoy, and is indicative only. The principle buoy location for each sub-plot is shown as a yellow circle, while neighbouring buoys are red. The *IQR* of each wave field is shown in solid grey, while the tails of the distribution (excluding outliers) are hatched blocks. The *IQR* contains the central 50% of the cluster distribution. The position of the *IQR* indicates the directional skew, whereas the width indicates the directional spread. The approximate *MWD* for each mode is shown as a black arrow.

During summer, Brisbane is the only location that experiences a longer period (Tp_1 9 - 10s) wave field from the east (Mode 1 *swell*) that is superimposed on Mode 1. It is distinguishable as swell by its narrower *IQR*, lower directional spread, and skew towards longer wave periods (Figures 4.3 B and 4 B). Since Brisbane is beyond the fetch-limiting influence of New Zealand, it is open to the potential of longer-period wave propagation from the Equatorial Pacific and Coral Sea.

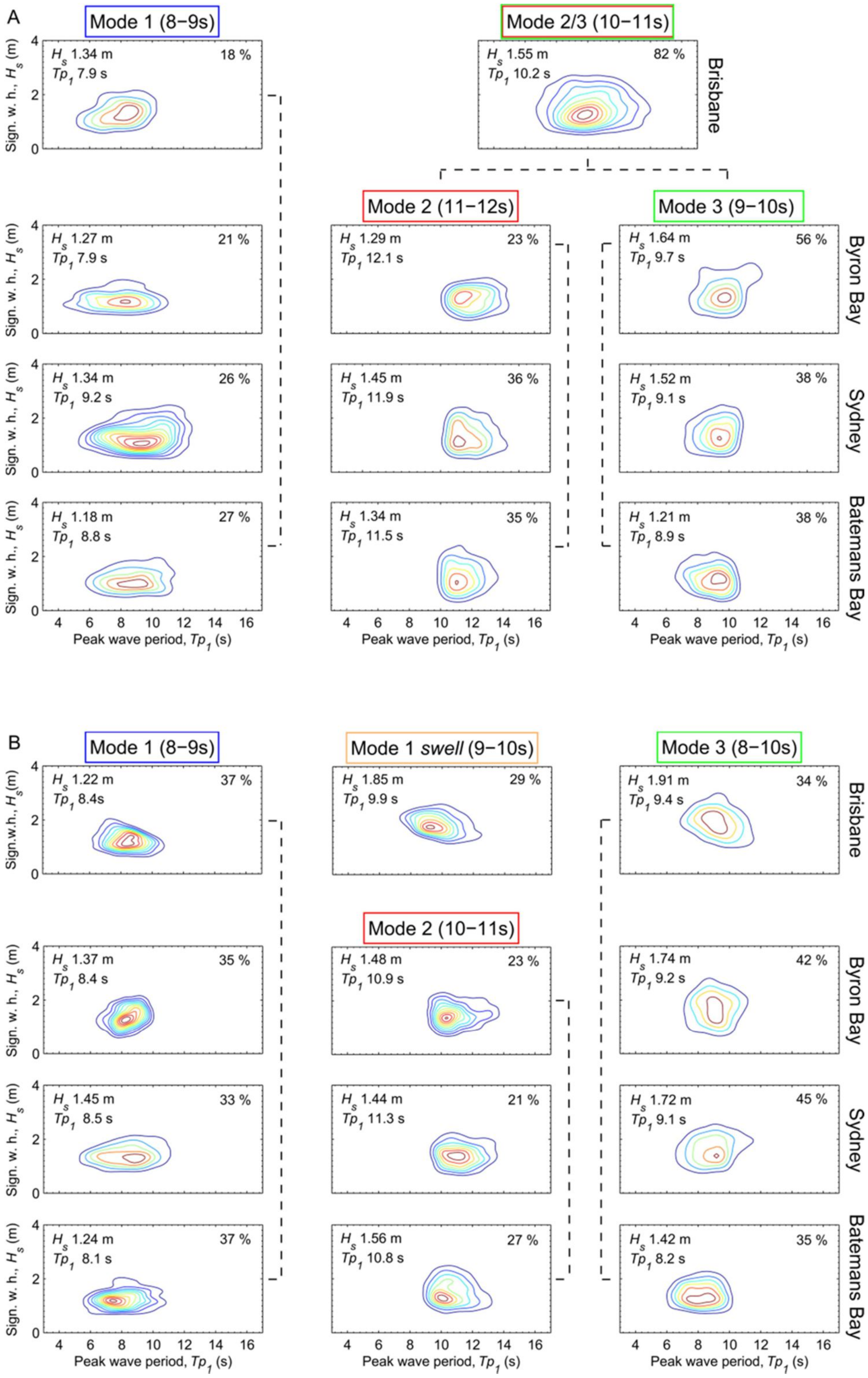

Figure 4.4 JPD functions of wave height, H_s (m), and period, T_p (s), for each wave field during (A) winter and (B) summer at the four buoy locations. Plots show the probabilities of joint occurrence for each wave field, as determined by clustering. Contours of joint occurrence are given for every 20% increment in probability density. The H_s and T_p centroid values for each

wave cluster are shown with the dominance (percentage occurrence, %) of each cluster during the respective buoy/season record.

4.8.2 Mode Two (South-East)

Mode 2 constitutes the longest period wave field identified by clustering. It contains a moderate amplitude (*Hs* 1.3–1.6m), long-period (Tp_1 11–12s) wave field that is incident onshore for much of the Southeast Australian coast throughout the year. Therefore, cross-shelf refraction is small. As a result, both directional and non-directional parameters are consistent between buoy locations. The narrow *IQR* and wave period skew towards higher values both suggest this is predominantly a far-field, but fetch-limited, wave field.

4.8.3 Mode Three (South)

Mode 3 is a moderate-period (Tp_1 9 - 10s), oblique (140 to 160°) wave field that operates adjacent to Mode 2. However, Mode 3 is distinguishable with shorter wave periods and higher amplitudes than Mode 2, suggesting a more proximal wave generation source.

The Batemans Bay and Brisbane buoys are partially shadowed from the most southerly portion of Mode 3 due to wave obliquity and shoreline geometry. A local northward indentation from Cape Green to the south, to Jervis Bay to the north, is probably responsible for wave shadowing at Batemans Bay. Storm separation in Section 4.6 also suggested the wave climate is more shoaled and/or sheltered at this location. As a result, the *MWD* of Mode 3 at Batemans Bay is 10° anti-clockwise of that recorded at Sydney, and the mean H_s is 0.3m lower.

From Cape Byron north, the coastline trends north-west, meaning the most southerly portion of Mode 3 is refracted across the shelf before it reaches Brisbane. As a result, Mode 3 is not separable by clustering from Mode 2 at Brisbane during winter. Instead, they are clustered as a single south-easterly wave field, accounting for over 80% of daily wave conditions.

4.8.4 Seasonal Variability in the Modal Wave Climate

During winter, 75% of the modal wave climate can be explained by variance in the south-east and south components (Modes 2 and 3), and 25% by the east component (Mode 1). In summer, Mode 1 increases in occurrence by approximately 10%, all modes rotate anti-clockwise, and the wave field grades towards a steeper sea.

Because of the semi-enclosed nature of the Tasman Sea, seasonality in the wave climate is subtle. Although the central *IQR* of each wave field exhibits seasonal rotation, wave clusters are spread over a similar directional space throughout the year. This is especially evident at the southern buoys, which are opposite to the fetch-limiting influence of New Zealand. The northern buoys, which are beyond the semi-enclosed sea setting, show stronger bi-modality in both direction and period between the south-east and south components (Modes 2 and 3) and the east component (Mode 1).

4.9 RESULTS AND DISCUSSION (2) – WAVE TYPE CLUSTERS AND SYNOPTIC WAVE GENERATION

4.9.1 Decomposition of Wave Clusters

Although k-means provides a useful metric for describing the primary modes of wave climate variability, the clustered wave fields do not necessarily represent individual 'synoptic-scale' wave climates. By definition, these wave climates have one generation source originating from a recurring anomalous synoptic pattern.

In order to identify synoptic-scale wave climates, the joint direction-frequency distribution of each cluster was examined. Wave height was not used, since it is invariant across all directional sectors. A single wave climate should exhibit a broadly uni-modal joint distribution in direction and frequency, as it originates from a single wave generation source (synoptic anomaly). If multiple peaks in the joint distribution are observed, the clustered wave field may be a composite of multiple wave geneses. Where this is the case, component wave climates can be separated out from the cluster using a bivariate Gaussian Mixture Model (GMM).

A GMM identifies individual Gaussian components in a mixed bivariate distribution, for which the number of components is known. The directional distribution of each cluster is first examined to determine the number of modal peaks (Figure 4.5 a), where each peak represents a component wave climate. A joint PDF of direction/frequency is then generated (Figure 4.5 b) and the cluster is separated into component parts using the GMM (Figure 4.5 c). Figure 4.5 d compares the single-peaked components (wave climates) separated using the GMM against the original twin-peaked directional distribution.

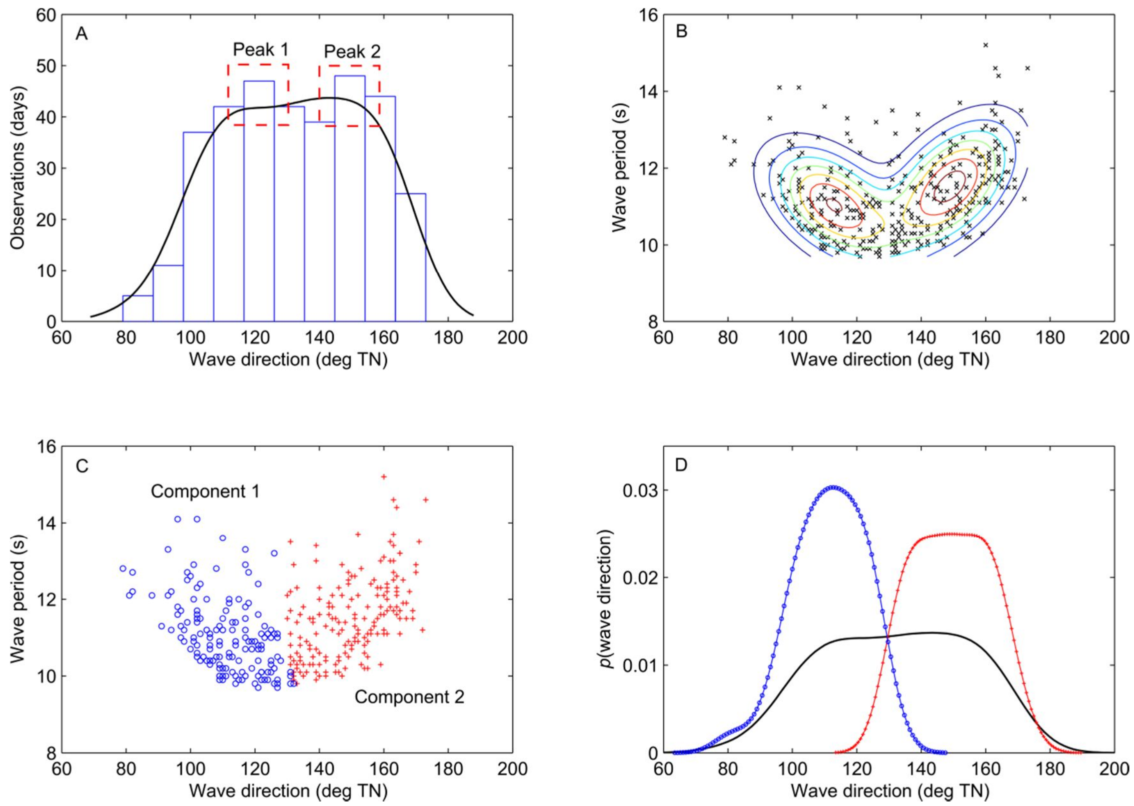

Figure 4.5 Application of a Gaussian Mixture Model (GMM) to a wave distribution originally clustered with k-means.

The ability of the components to represent individual synoptic-scale wave climates is then evaluated with composite anomalies of the Mean Sea Level Pressure (MSLP) field across the Tasman Sea, using the NCEP-NCAR Reanalysis (NNR) (Kalnay *et al*, 1996). Strong anomalous patterns for the composite days indicate coherent synoptic forcing and suggest the wave climate is produced by a single wave generation source. In order to avoid skewing the modal signal, storm conditions were again excluded from this process.

4.9.2 Synoptic Wave Climate Type Genesis

Results indicate that, of the three primary cluster modes described in Section 4.8, independently-generated wave climates can be further isolated at Sydney, Byron Bay and Brisbane during winter and summer. Sydney and Byron Bay best represent the latitudinal range of regional patterns as these buoys are the most exposed locations along the shelf, and are not affected by wave shadowing. Wave climate types were also isolated at the Brisbane buoy, although Mode 3 is not identifiable at this location due more to shoreline geometry than latitude (Section 4.8.3). This analysis was not undertaken at the Batemans Bay buoy because the regional representativeness of the wave climate is questionable (Section 4.8.3). The wave climate types identified at Sydney, Byron Bay and Brisbane, together with the associated synoptic anomalies across the South Pacific for each, are shown in Figures 4.6, 4.7 and 4.8 respectively.

Mode 1 was identified by clustering as a shorter-period easterly wave field, but GMM separation has identified two wave climates within this mode; North-Easterly Trade Winds (Mode 1a) and Zonal Easterly Trade Winds (Mode 1b). Both are formed with an anti-cyclonic anomaly in the Central Tasman that induces an easterly air flow. When the anomaly is more meridional, north-easterly waves from the Coral Sea are produced. A longer-period and more easterly wave climate prevails when the anomaly is more zonal. In both cases, the easterly wave climate is produced off the northern limb of the high pressure anomaly due to the anti-cyclonic air flow.

Mode 2 contains two wave climates, of which only one is identifiable in both winter and summer (Mode 2a). Mode 2a is a result of a surface pressure gradient between a Southern Tasman anticyclone to the south, and a Tropical Low adjacent to the north, producing a south-easterly wave climate. Mode 2b represents a summer Central Tasman Low, but is not identifiable as a separate wave type during winter. Although Central Tasman Lows are known to produce storm wave conditions throughout the year, results suggest they do not produce a dominant modal wave signal on a daily average scale during winter.

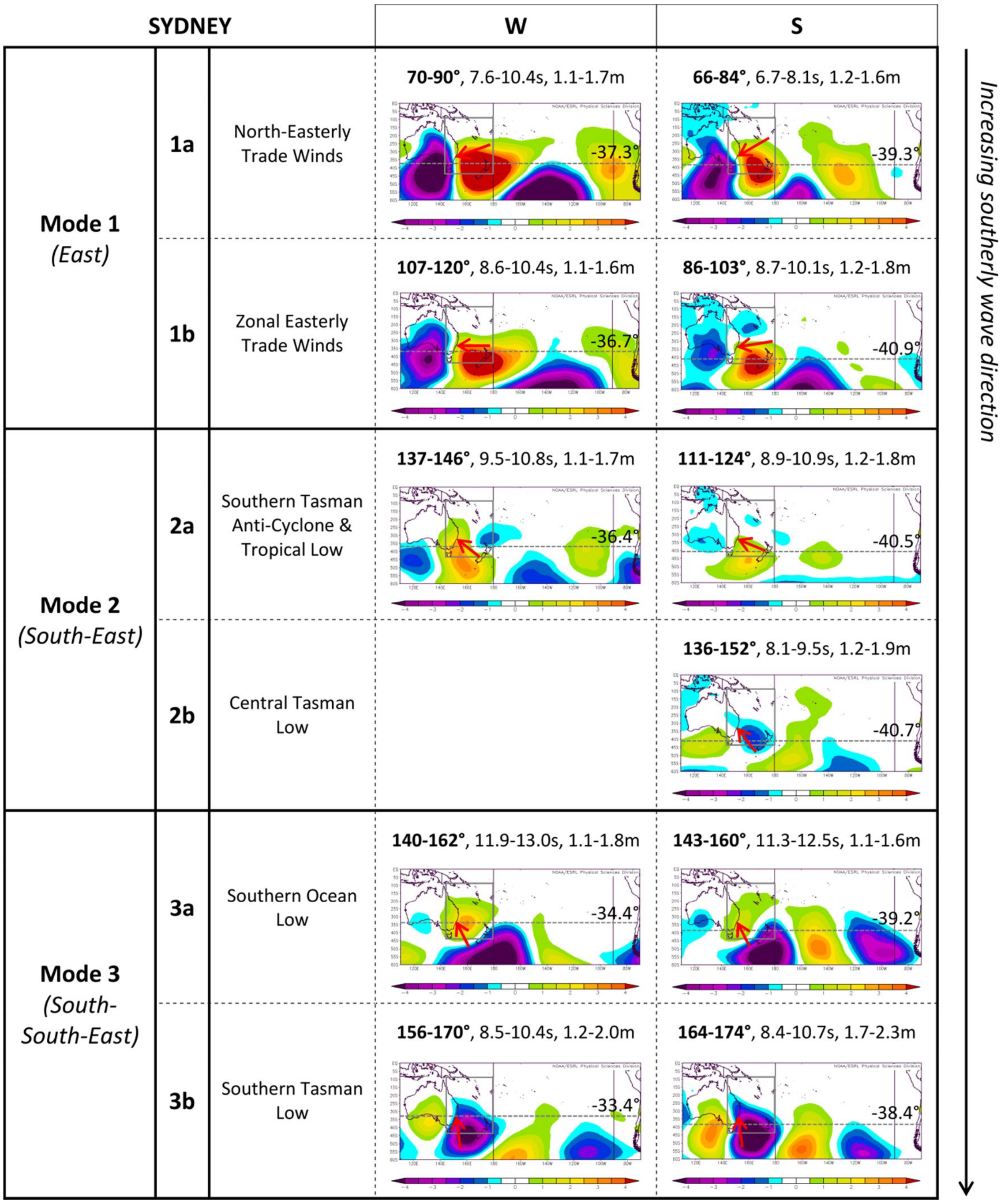

Figure 4.6 Wave climate types for winter (W) and summer (S) at Sydney. Cluster modes and wave climate sub-divisions are shown. MSLP anomalies from long-term climatology (1981 – 2010). A one-day lag has been applied to all composites to approximate wave travel time from source. Parametric data for each wave climate represents the *IQR* of the *MWD*, T_p and H_s distributions. The mean latitude of the STR (grey dashed line) and region of calculation (grey box) for each wave climate are denoted. STR was calculated as the latitude of highest pressure over the composite days over the Tasman and Coral Seas (150-180°E, 10-45°S), from the NNR reanalysis (Kalnay *et al*, 1996).

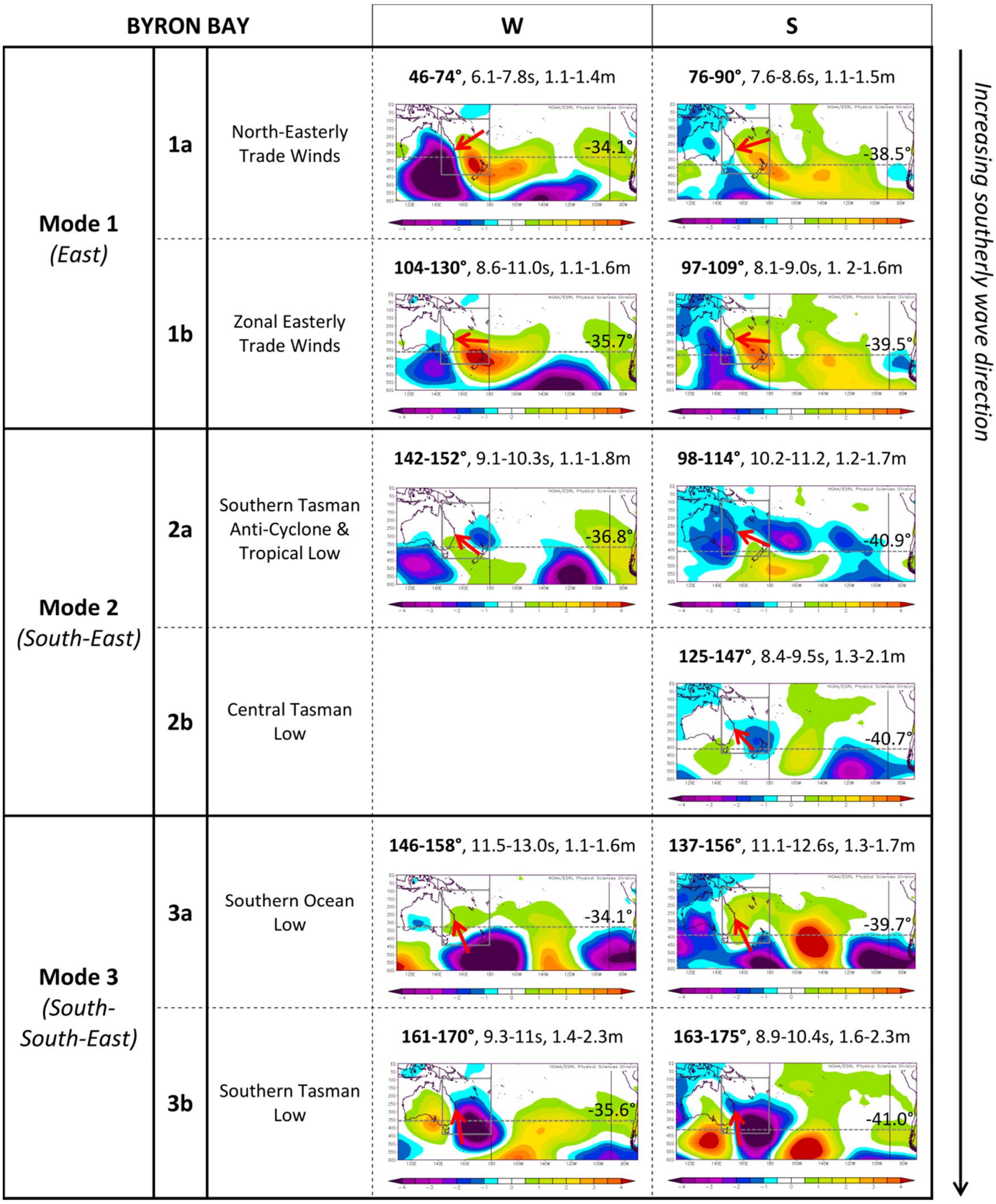

Figure 4.7 Wave climate types for winter (W) and summer (S) at Byron Bay.

Mode 3 represent the most oblique (southerly) wave field, and is composed of two wave climate types. Mode 3a is a long-period wave type produced from the south-west flow between a Tasman Sea anti-cyclone and a Southern Ocean Low. The synoptic arrangement for this wave type is most likely to produce bi-modal wave conditions, with a sub-dominant Mode 1 type wave field produced from the anticyclonic anomaly in the Central Tasman. Mode 3a does not exist at Brisbane because wave generation is too far field and wave propagation is blocked in the Central Tasman Sea. Mode 3b is an extreme southerly type, associated with Southern Tasman Low formation, and produces the largest wave heights of the modal wave climate at both Sydney and Byron Bay. Mode 3b is not seen at Brisbane because the oblique waves that run south to north up the SEAS cannot refract past the north-west trending shoreline north of Cape Byron.

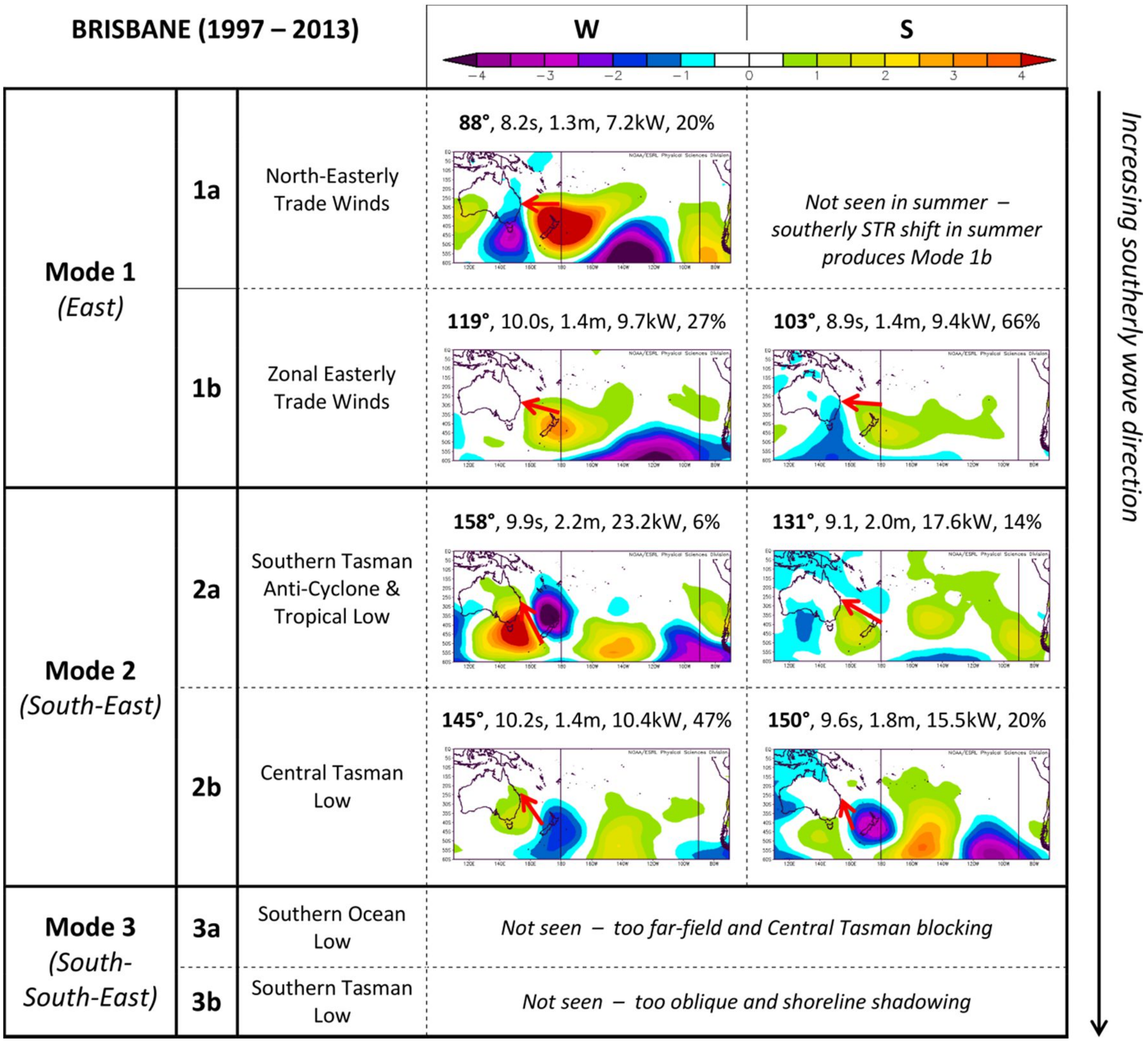

Figure 4.8 Wave climate types for winter (W) and summer (S) at Brisbane.

4.9.3 Transient Weather Pattern Wave Types

Further sub-divisions of Modes 1a and 1b were also identifiable (in a statistical sense, as per Section 4.9.1) at Byron Bay and Brisbane, but not at Sydney. These third-order wave climate types are shown in Figure 4.9 for Brisbane (valid also for Byron Bay) and represent transient weather pattern wave types rather than synoptically significant modes of variability.

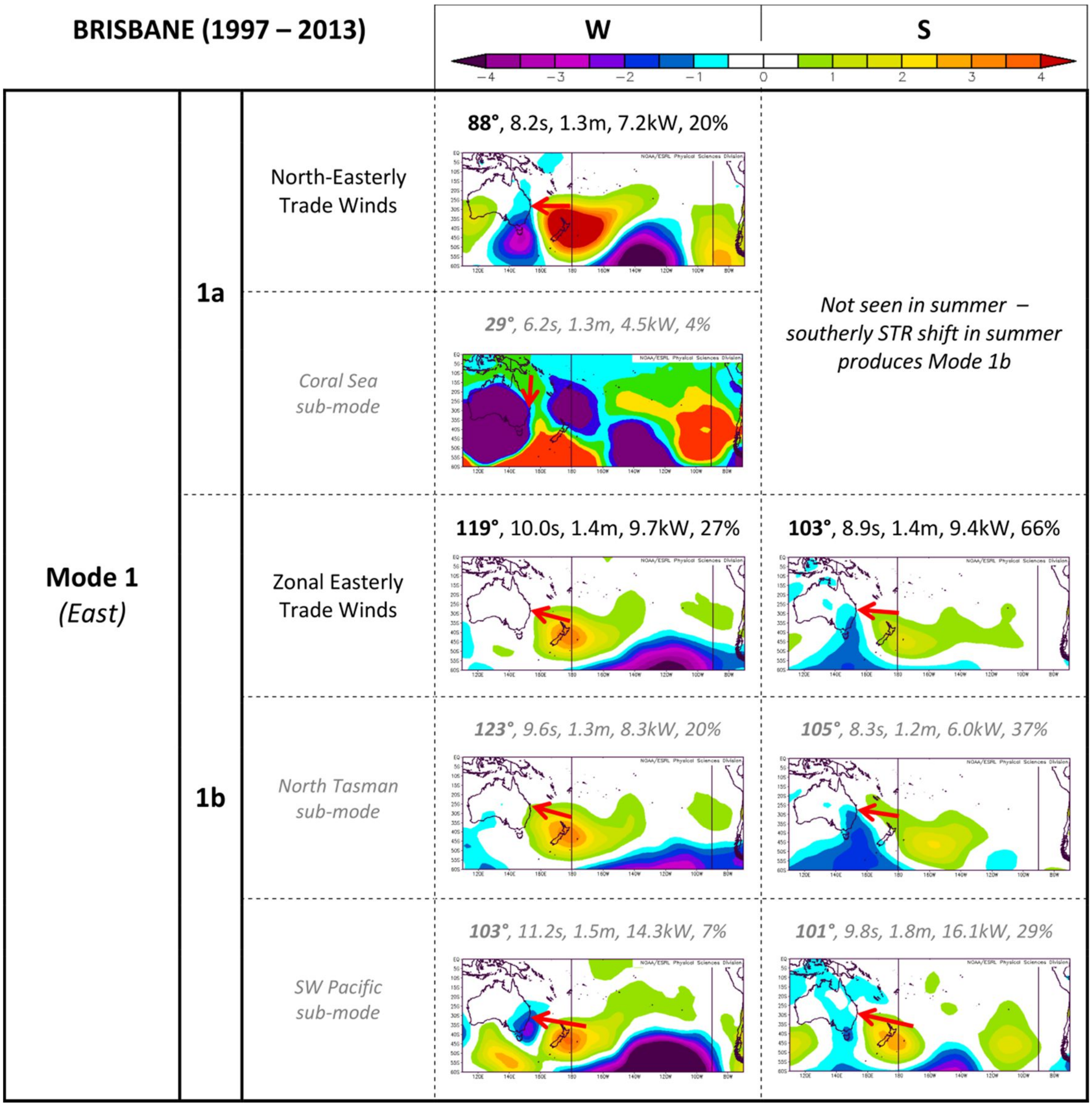

Figure 4.9 Sub-divisions of Mode 1a and 1b for winter (W) and summer (S) at Brisbane, representing transient weather pattern wave climates. Synoptic sub-divisions are also relevant for Byron Bay.

In winter, Mode 1a has a sub-dominant north-north-easterly (29 °), near-field (6.2 s) Coral Sea component at Brisbane and Byron Bay (Figure 4.9). This occurs when a low pressure front over the eastern seaboard strengthens and deflects the easterly trade winds to produce a north-north-easterly wind-wave climate. These are colloquially known as "September Northerlies" on the north coast of NSW and south east coast of Queensland. Because this is a very transient wave-generating synoptic arrangement, it is only visible when a three day lag is applied to the MSLP composites with respect to the time of wave observations. The synoptic arrangement produces a northerly airflow, but by the time the waves reach the Byron Bay and Brisbane buoys, they have refracted to a north-east direction. This sub-division does not exist during summer because as the STR shifts south, the more southerly position of the northern limb of the anti-cyclone produces easterly, rather than north-easterly wave conditions.

Mode 1b can be decomposed into two types of easterly waves in both winter and summer. The first is a fetch-limited North Tasman Sea generated easterly wave climate produced when the anti-cyclone is more south (Figure 4.9). The second is a south west Pacific longer-period swell wave climate produced by the northern limb of the anti-cyclone when in a more northerly position, with wave generation occurring to the north-east of the North Island of New Zealand.

While these weather-pattern wave types produce statistically distinct wave fields, their transient nature and low frequency of occurrence means they are superfluous to explain the relationship between wave generation and large-scale climate drivers. Therefore, the rest of this chapter includes no further consideration of these third-order wave types, and instead focusses on the synoptic-scale wave climate types (1a, 1b, 2a, 2b, 3a, 3b).

4.9.4 Relation to Large-Scale Climate Drivers

Synoptic patterns in Figures 4.6 to 4.8 suggest that Modes 1 and 3 are formed under Pacific-emanating atmospheric longwave patterns, while Mode 2 is a result of a longwave train emanating from the Indian Ocean sector. Specifically, Mode 1-type wave climates represent a spring-summer feature that is enhanced by La Niña-like climate. Mode 3 types represent a more autumn-winter-spring feature that is enhanced by El Niño-like climate. The wave climates of Modes 1 and 3 have a strong relationship with ENSO phases, as identified in Goodwin (2005). Accordingly, more southerly modal wave climates prevail under El Niño, while easterly conditions are more representative of La Niña phases. The Mode 2 wave types, with a strong central Tasman synoptic feature, represent either wave climates that occur during neutral ENSO conditions or where the Indian Ocean Dipole (IOD) or extension of the monsoon trough have a stronger influence on the Tasman Sea region. The coupling between ENSO and IOD has a significant effect on inter-annual wave climate variability at both sites (after Goodwin, 2005).

Figures 4.6 to 4.8 show no strong stratification of wave climate according to the latitude of the STR. However, the STR has a stronger influence on modulating the seasonal occurrence of, and latitudinal exposure to, different wave climate types. The latitudinal influence of the STR on wave climate along the SEAS can be demonstrated by comparing the wave climates between Sydney and Byron Bay. The differences between these two locations is largely a function of latitude, as the wave climates are not affected by localised wave shadowing (Batemans Bay) or changing shoreline aspect (Brisbane). Figure 4.10 shows the probability of occurrence of each wave mode for Sydney and Byron Bay in winter and summer.

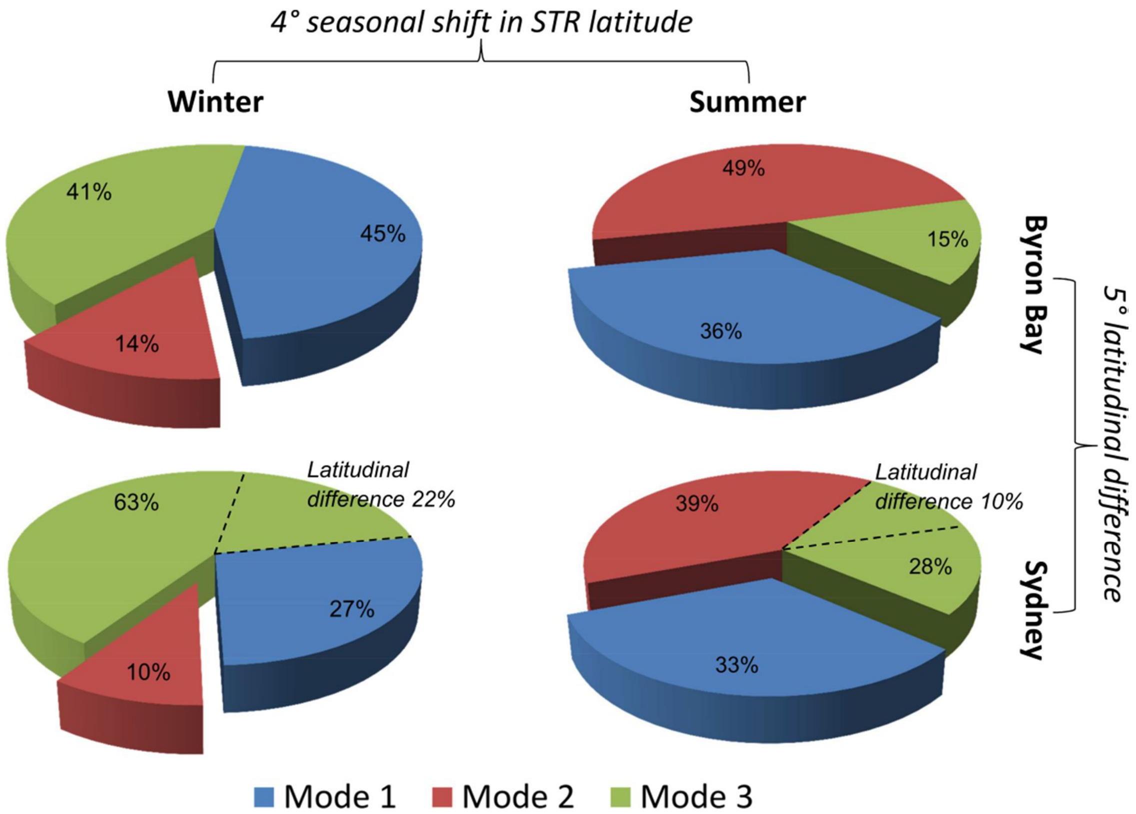

Figure 4.10 Probability of occurrence of seasonal wave climate modes at Sydney and Byron Bay. Those wave climates that co-vary between sites are adjoined, and their latitudinal difference shown (dotted line).

There is a 5° latitude separation between the Sydney (33.5°S) and Byron Bay (28.5°S) buoy locations. During winter, the mean latitude of the STR (over the period of analysis) is 35.4°S with a standard deviation of 6.6°, and 39.5°S with a standard deviation of 4.5° during summer. Hence, the seasonal shift in the STR latitude of 4° is comparable to the respective latitudinal difference between sites, and allowed us to examine the variance in modal wave climate clusters and synoptic types as a function of seasonal or latitudinal shifts.

During winter, Modes 1 and 3 co-vary between sites. At both Sydney and Byron Bay the sum total occurrence of these two modes is very similar and describes the bulk modal wave conditions (86-90%), with Mode 3 increasing with buoy location latitude south at the expense of Mode 1 (22% difference). Therefore, a poleward shift in the winter STR latitude decreases the occurrence of Mode 3-type wave climates in favour of Mode 1. The central wave field (Mode 2) is largely invariant between sites because the equatorward position of the STR means the wave generation region for this mode occupies the latitudes of both buoy locations. Latitudinal variability of the winter wave climate along the SEAS can therefore be described primarily by the STR control on the co-variance between the easterly (Mode 1) and southerly (Mode 3) wave types. Wave climate variability during winter therefore looks to be associated with the oscillation of coupled SAM and ENSO states.

During summer, Modes 2 and 3 co-vary between sites. The sum total occurrence of these two modes between Sydney and Byron Bay is the same (non-significant difference, $p < 0.05$), meaning a poleward shift in the summer STR latitude decreases the occurrence of Mode 3-type wave climates in favour of Mode 2. The easterly component (Mode 1) is invariant between sites (non-significant difference, $p < 0.05$) because the wave generation region occupies the latitudes of both buoy locations, due to the more poleward STR latitude. Latitudinal variability of the summer wave climate for the SEAS can therefore be described primarily by the STR control on the co-variance between the central (Mode 2) and southerly (Mode 3) wave types. Wave climate variability during summer may therefore be associated with coupling between the IOD and ENSO.

4.10 RESULTS AND DISCUSSION (3) – LATITUDINAL AND SEASONAL WAVE POWER VARIABILITY

The impact of wave climate variability on coastal processes can be assessed using the deep-water wave power, or the wave energy flux, P_0. P_0 was calculated for each daily wave event using the formula for irregular waves (from Holthuijsen, 2007):

$$P_0 = \frac{1}{16}\rho g H_s^{\,2} C_g \tag{4.1}$$

where ρ (kg m^{-3}) is the average density of seawater, g (m s^{-2}) is the acceleration due to gravity, H_s is the daily average significant wave height, and C_g (m s^{-1}) is the wave group velocity.

As the wave buoys are located in 60 – 100m water depth (mid-shelf), the deep-water wave assumption is not always valid for longer period swell where the wave base may be at times seaward of the buoy location. Therefore, C_g is determined using the equation:

$$C_g = \frac{n\lambda}{T_e} \tag{4.2}$$

where λ is the wavelength determined using the Newton-Raphson iterative solution, and T_e is the wave energy period. Here it is assumed $T_e = T_p$ (e.g. Hemer and Griffin, 2010), which is a good approximation for a standard JONSWAP spectrum (Cornett, 2008). Following Holthuijsen (2007), n varies from ½ in deep water to 1 in very shallow water and is defined as:

$$n = \frac{1}{2}\left(1 + \frac{4\pi d/\lambda}{\sinh\left(4\pi d/\lambda\right)}\right) \tag{4.3}$$

P_0 describes the power density expected from a single wave event that represents a certain wave climate or sea state and is expressed in kilowatts per metre wave-crest-length (kW m^{-1}). Here, wave climate wave power is expressed using the mean power of the respective wave climate distribution, P_W.

However, in order to assess wave power impacts on coastal processes, the probability of occurrence of each wave climate type (Figure 4.10) needs to be integrated. As such, the total, rather than mean, wave power (or energy flux) delivered by each wave climate in an average season (winter/summer) is a more useful metric. The total seasonal wave energy flux per wave climate type, E_W, is obtained by multiplying P_W (kW m^{-1}) by the time-integrated probability of occurrence (in seconds), dt, of each wave climate type, w, for each season, s:

$$E_W(w,s) = \int_0^t P_W(w,s)dt \tag{4.4}$$

Since power is integrated over time, E_W is expressed in gigajoules per metre (GJ m^{-1}) along a tangent to the mean wave climate crest. E_W is commonly used in renewable energy assessments to measure the total time-averaged wave energy resource. In modelling studies, E_W is calculated by integrating P_0 over all observations at a grid point and then dividing by the number of seasons or years in the record (Hughes and Heaps, 2010). However, since buoy records inevitably have data gaps, P_W needs to be integrated over the time equivalent of the mean percentage occurrence of each wave climate type instead, to obtain a representative total energy flux per season.

4.10.1 Inter-Site and Inter-Seasonal Wave Power Variability

Here the total seasonal wave energy flux delivered by each modal wave climate type, E_W, is compared between Sydney and Byron Bay. For a fair comparison, only wave observations for days when both buoys were recording simultaneously were used in the assessment. Both P_W and E_W are therefore mean values between 2000 and 2013 (Table 4.1).

Previous modelling studies have quantified P_W and E_W for New South Wales shelf waters. Cornett (2008), Hughes and Heap (2010) and Gunn *et al.* (2012) all report mean annual P_W values between 10 – 20 kW m^{-1}, and Hughes and Heap (2010) suggest mean annual E_W is around 510 GJ m^{-1}. P_W values are equivalent to those calculated by us in Table 4.1, and when approximated annually, the estimation of E_W is equivalent to that of Hughes and Heaps (2010) (when storm wave energy is included).

Table 4.1 Mean seasonal wave power, P_W (kW m^{-1}) and total seasonal wave energy flux, E_W (GJ m^{-1}) per wave climate type, for Sydney and Byron Bay buoys**.**

	Sydney			Byron Bay		
	P_W	n [1]	E_W	P_W	n [2]	E_W
Austral winter (JAS = 92 days)						
Mode 1	9.4	23	**18.3** [2]	9.9	39	**33.1** [3]
Mode 2	10.0	8	**7.2**	13.2	12	**13.7**
Mode 3	14.0	52	**63.3**	19.6	35	**59.0**
All Storms	58.9	9	44.0	64.8	6	34.7
TOTAL MODAL ENERGY			**88.8**			**105.8**
Austral summer (JFM = 90 days)						
Mode 1	9.2	28	**22.7**	8.4	29	**20.6**
Mode 2	12.4	34	**36.1**	13.9	39	**46.7**
Mode 3	18.6	24	**38.1**	19.7	12	**20.7**
All Storms	50.2	4	16.5	48.6	10	43.7
TOTAL MODAL ENERGY			**101.2**			**88.0**

[1] n is given here in average number of days per season but is converted to equivalent seconds to calculate E_W in GJ m^{-1} since one joule of energy = one watt of power exerted for n time in seconds.

[2] Only 13.2 GJ m^{-1} of this is comparable to Byron Bay for a wave climate change scenario.

[3] Only 20.2 GJ m^{-1} of this would be seen at Sydney under a wave climate change scenario.

During winter, the directionality of wave power delivery at both Sydney and Byron Bay is broadly the same (Figure 4.11 a). However, there is a greater total flux of wave energy (E_W difference of 18 GJ m^{-1}) at Byron Bay than at Sydney (Figure 4.11 a, using bracketed winter values). This is manifest in a greater easterly (Mode 1) and south-easterly (Mode 2) component, with a non-significant difference ($p < 0.05$) in southerly waves (Mode 3) between sites. This is explained by the mean winter position of the STR which is 7° south of Byron Bay, and 2° south of Sydney, meaning wave generation for Modes 1 and 2 is more proximal at Byron Bay than Sydney (see Figures 4.6 and

4.7). Mode 3 wave generation is still sufficiently northward in winter to remain the dominant winter wave climate type at Byron Bay as at Sydney. The dominance of the oblique southerly modal power component, and the north-south coastal alignment, enable potential northward longshore sediment transport.

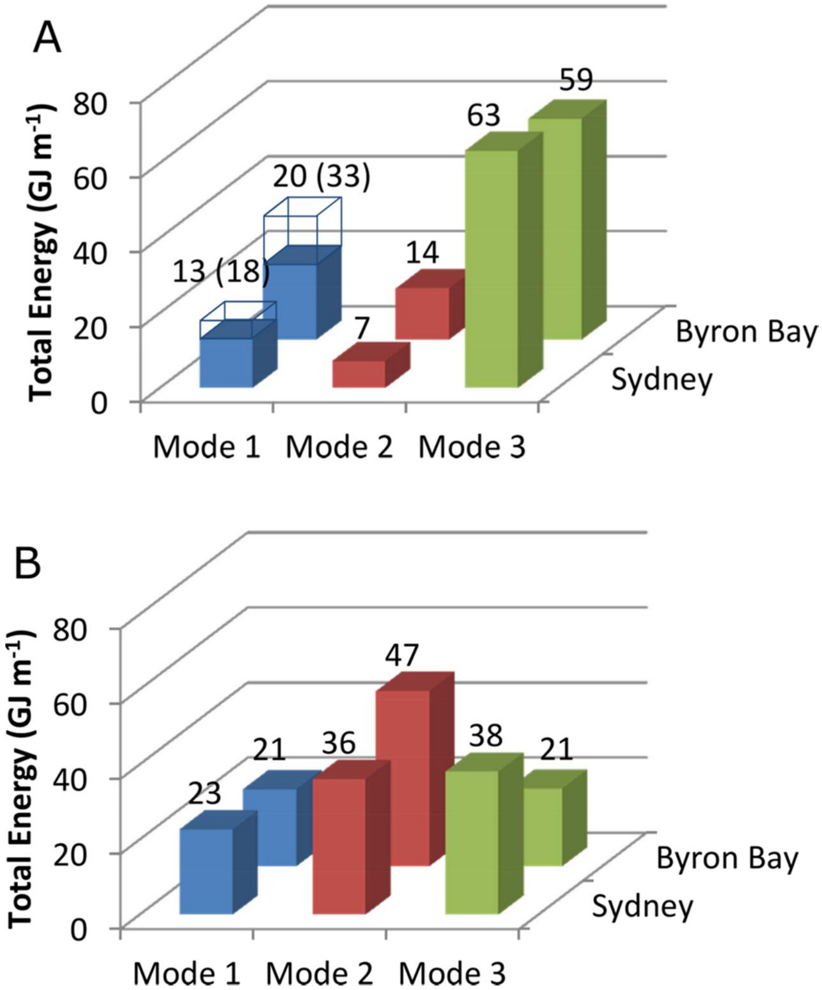

Figure 4.11 Mean winter (a) and summer (b) wave energy flux contribution from modal wave climates at Sydney and Byron Bay (shown to nearest GJ). The contribution of extra-Tasman swell propagation identified at Byron Bay for Mode 1 in winter is shown. Bracketed values are with extra-Tasman component (and corresponding days at Sydney) included.

The occurrence co-variance seen in Modes 1 and 3 between sites in winter (Section 4.9.4) does not translate to co-variance in a wave energy flux between these modes (Figure 4.11 a), since a reduction in occurrence of Mode 3-type waves at Byron Bay is compensated for by an increase in the mean wave height of Mode 3b waves. Analysis suggests that the highest wave heights are associated with the most southerly directions in the Mode 3b wave climate. Due to the alignment of the SEAS, high wave energy associated with these oblique directions propagates past Sydney but is received at Byron Bay.

In summer, there is less total flux of wave energy (E_W difference of 9 GJ m^{-1}) at Byron Bay than at Sydney. The directionality of energy delivery is also different. At Byron Bay, there is a greater occurrence of less-powerful south-easterly (Mode 2) waves and a lower occurrence of more powerful southerly (Mode 3) waves, with no significant difference in easterly (Mode 1) energy flux between sites.

There is also a covariance in total wave energy delivered by Mode 2 and Mode 3-types at Byron Bay between winter and summer (~70 GJ m^{-1}). This is a function of the seasonal proximity of Mode 2 and 3 wave generation to Byron Bay, which in turn is a function of the location of the STR (see Figure 4.7). The southerly STR shift in summer therefore drives a reduction in more powerful Mode 3-type wave events, in favour of, and broadly equivalent in energy to, the increase in Mode 2-type waves.

4.10.2 Inter-Annual Wave Power Variability

Indexing daily wave observations by wave climate type provides a means to investigate variability in synoptic wave generation over time. Figures 4.12 and 4.13 show the percentage contribution of each wave climate type to the total wave power of each winter (a) and summer (b) season over consecutive years, at Sydney and Byron Bay.

Analysis of the summer record at Sydney is hindered by insufficient data from 1997 to 1999. Despite this, Figure 4.12 indicates high variability in the directionality of wave power prior to 2002, as seen in the winter record over this period. From 2005 to 2009, there are successive summers with increasing Mode 1 and 2 wave power contributions, at the expense of Mode 3-types. This five-year period is similar to, but two years after, the five-year cycle of increasing Modes 1 and 2 wave power seen in the winter record. From 2010 (2008) onwards in summer (winter), results suggest this five year cycle is repeated.

A.

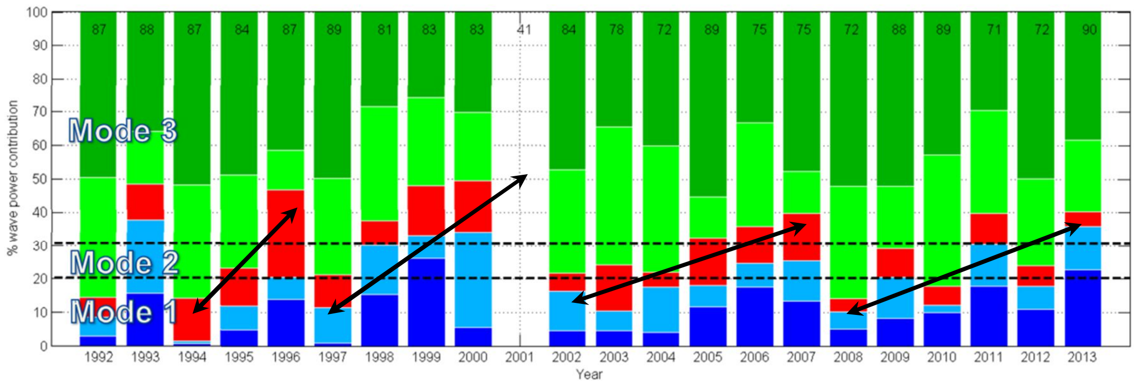

B.

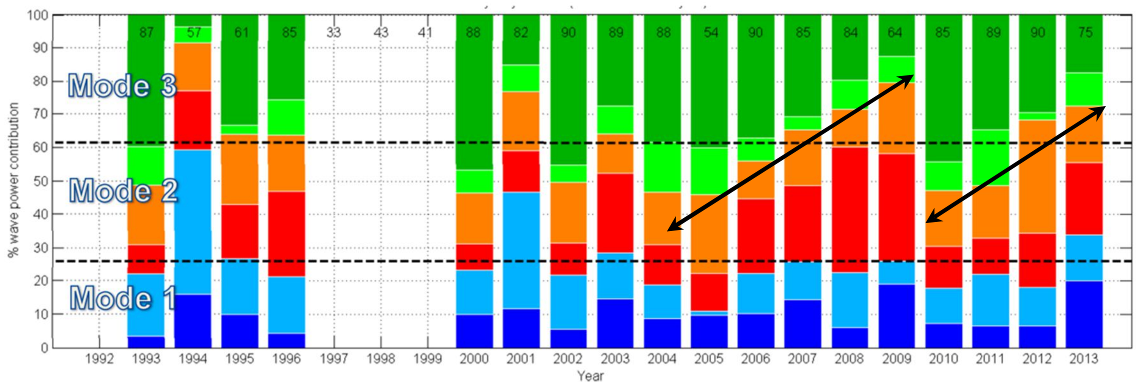

Figure 4.12 Inter-annual wave power variability at Sydney in winter (a) and summer (b), measured by the percentage contribution to the total wave energy flux, E_W, of each wave climate type for each year. Black dotted lines indicate mean percentage contribution for Modes 1, 2 and 3 between 1992 and 2013. Day count for each year is also shown. When the day count is lower than half the maximum for the season (winter 46, summer 45 days) results are considered not representative and are not plotted. Arrows indicate consecutive years with potential trend. Legend is provided in Figure 4.13.

The record at Byron Bay only begins at 2000. The summer record at Byron Bay is hindered by insufficient observations in 2003, 2004 and 2010. However, a period of increasing Modes 1 and 2 wave power at the expense of Mode 3-types is visible in successive years between 2005 and 2009. This five-year trend is the same as that seen in the Sydney summer record over the same time period. Although the Byron Bay record is cut at 2010, the re-initiation of this trend is seen between 2011 and 2013 –the same as the trend seen in the Sydney summer record successively from 2010 through to 2013. The trends seen in the Sydney winter wave climate between 2002 and 2013 are also visible in the Byron Bay winter wave climate.

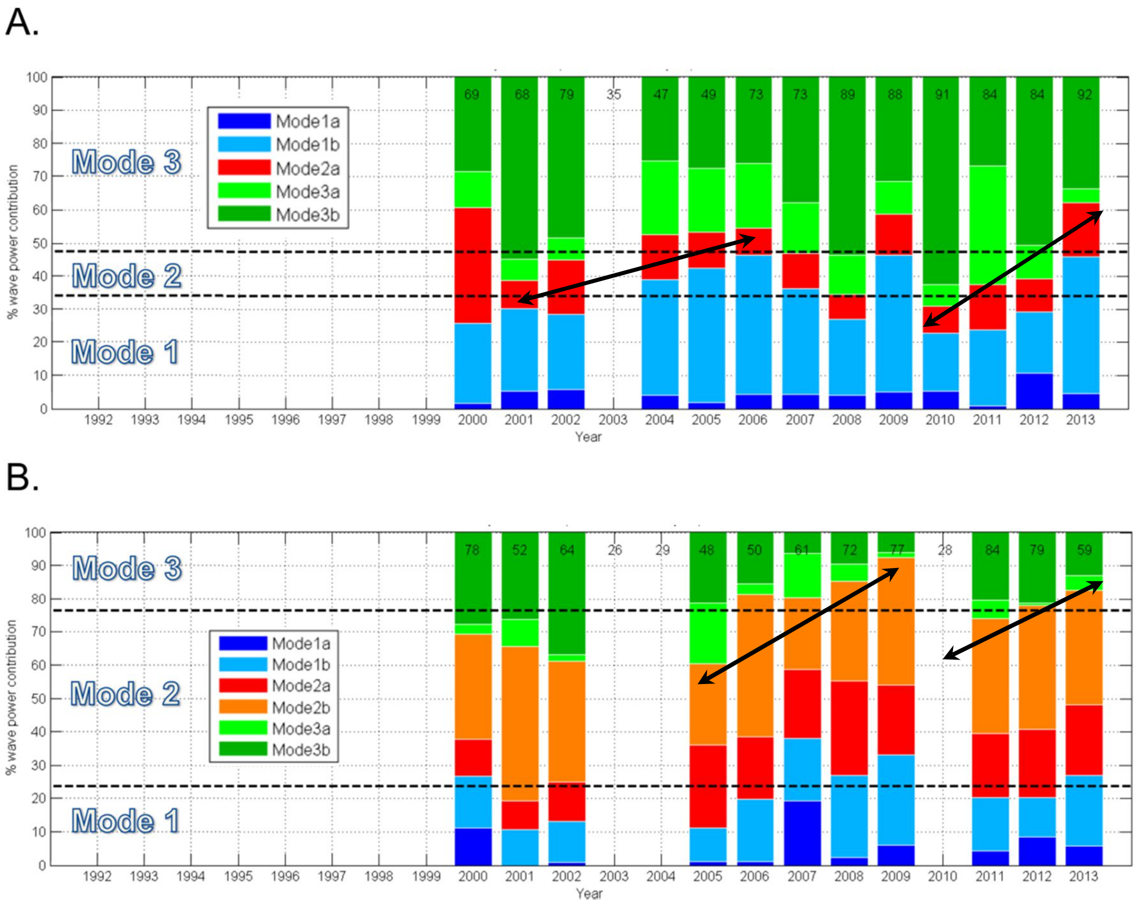

Figure 4.13 Inter-annual wave power variability at Byron Bay in winter (a) and summer (b), between 2000 and 2013. X axis runs from 1992 to facilitate comparison with Sydney.

Further analysis of the significance of these inter-annual trends, and climate attribution, is required but is beyond the scope of this chapter. Initial investigation suggests that although some trends are significant ($p < 0.1$), there is low confidence they are not just due to random variability, in most part due to the relatively short directional buoy record available. However, the fact that a quasi five-year cycle from Mode 3 (southerly) to Mode 1 (easterly) wave power is seen at both Sydney and Bryon Bay, suggests a regional and cyclical climate forcer. The potential link to ENSO and SAM forcing is a direction for further research. The method described in this section is used in Chapter 5 to define the directional wave power patterns during specific (central and eastern Pacific) ENSO climate.

4.10.3 Projecting Future Directional Wave Power Change for Central NSW

There is evidence to suggest that the atmospheric Hadley cell is expanding poleward, consistent with an enhanced greenhouse effect, ozone depletion (Seidel *et al*., 2008) due to anthropogenic aerosols, and the shift towards the La Nina-like state of the Pacific Decadal Oscillation (Allen *et al*., 2014). Coupled to this, the STR in the East Australian region is intensifying, although a coherent southerly shift is as yet unclear (Timbal and Drosdowsky, 2013). If a poleward shift in the Hadley cell and trade-wind zone continues, the present day wave climate at Byron Bay, 600 km equatorward of Sydney, may be used as a surrogate for future wave climate changes along the central NSW coast.

In using the Byron Bay wave climate as a surrogate for wave climate change at Sydney, the assumption is that all observed wave climate types at Byron Bay would be observed at Sydney. Although this is true for Modes 2 and 3 and the majority of Mode 1, there is a narrow swell window within Mode 1b where waves can be generated north-east of the north island of New Zealand and propagate towards Byron Bay (Figure 4.1). This was identified as a sub-division of Mode 1b in Section 4.8.3. Waves generated in this swell window would not be seen at Sydney under a southerly STR scenario because of the blocking effect of the New Zealand land mass. Mode 1a (in winter and summer) and Mode 1b (in summer) all are generated within the Tasman Sea.

Fetch-limited waves, such as those described by Mode 1, generated within the Tasman Sea cannot exceed T_p of 12-13 s due to a limiting maximum fetch of approximately 1,800 km between Byron Bay and New Zealand (assuming a 10 m/s wind, typical of trade wind-wave generation) (after Shore Protection Manual, 2002). Using this fetch threshold, only 11% of Mode 1b waves in winter (12.9 GJ m^{-1} of total winter wave energy, 8 days on average per winter) were found to propagate through a swell window above New Zealand between 90 and 135°. Therefore the majority of Mode 1b waves at Byron Bay in winter (89%) can be used as a surrogate for Sydney. Those wave evens in winter Mode 1b identified at Byron Bay as being generated outside the Tasman Sea are not included in the future scenario for Sydney. In order to maintain a linear comparison, the corresponding days on which these waves were observed at Byron Bay have been omitted from the totals at Sydney as well (Figure 4.11 a and Table 4.1).

The vast majority of wave events at Byron Bay (96% in winter, 100% in summer) are also seen at Sydney. However, there is a distinct change in wave climate north of Byron Bay as shown by the Brisbane buoy observations (Section 4.8). These show a relative increase in the percentage of the overall wave climate that is produced by 12-13s period swells generated in the southwest Pacific and Coral Sea (Mode 1 *swell*). Accordingly, a poleward expansion of the tropics would result in a progressive increase in percentage occurrence of Mode 1 waves at Byron Bay at the expense of a reduction in Mode 3 waves. This is consistent with GCM-based wave climate projections by Hemer *et al.* (2013), which indicates an anti-clockwise shift in annual *MWD* of up to 10°. The implications of a poleward shift in the STR on wave climate for the Sydney region is explored in the following section.

4.10.4 Implications for Directional Wave Power on the Central NSW Shelf

Results suggest that a poleward shift in the mean latitude of the STR would force an increase in total (modal) wave energy flux for the Sydney region of approximately 1.9 GJ m^{-1} wave-crest-length for a one degree latitude shift south during winter (Figure 4.14 a), and a reduction of similar magnitude (approximately 1.8 GJ m^{-1} for one degree latitude shift south) during summer (Figure 4.14 b).

The increase in total winter wave energy would be produced by heightened Mode 1 and Mode 2 wave fields, while the reduction in summer is manifest in a reduction of more-powerful Mode 3 in favour of less-powerful Mode 2. There is no change inferred in summer Mode 1 and winter Mode 3 wave energy.

A weaker Mode 2 (cross-shore) component in place of Mode 3 (along-shore) wave energy in summer will act to reduce the longshore transport component. In winter, although a total increase in modal (constructive) wave energy is inferred, this is also from the east and south-east, enhancing the cross-shore transport component at the expense of alongshore movement. Results from Chapter 6 on storm wave climate change with a southerly shift in the STR also indicate a similar preference for cross-shelf, rather than alongshore transport with a change in synoptic storm type frequency.

Reduced obliquity of constructive wave power throughout the year may promote a general disruption to the northward alongshore sediment transport along the central NSW coast. For those sections of coast sensitive to alongshore gradients in wave power, greater easterly wave power during winter favours shoreline planform embaymentisation, whereas an increase in south-easterly wave power during summer promotes planform flattening. There is evidence to suggest historical directional wave power change has forced considerable shoreline response along the Central to Northern

New South Wales coast. Studies of shoreface bathymetric change by Goodwin *et al* (2013a) in the Byron Bay area suggest that a trend towards a more south-easterly modal and storm wave climate during the late 1800s was responsible for planform flattening, nearshore bar welding and large sand supply rates to the shoreline during that period.

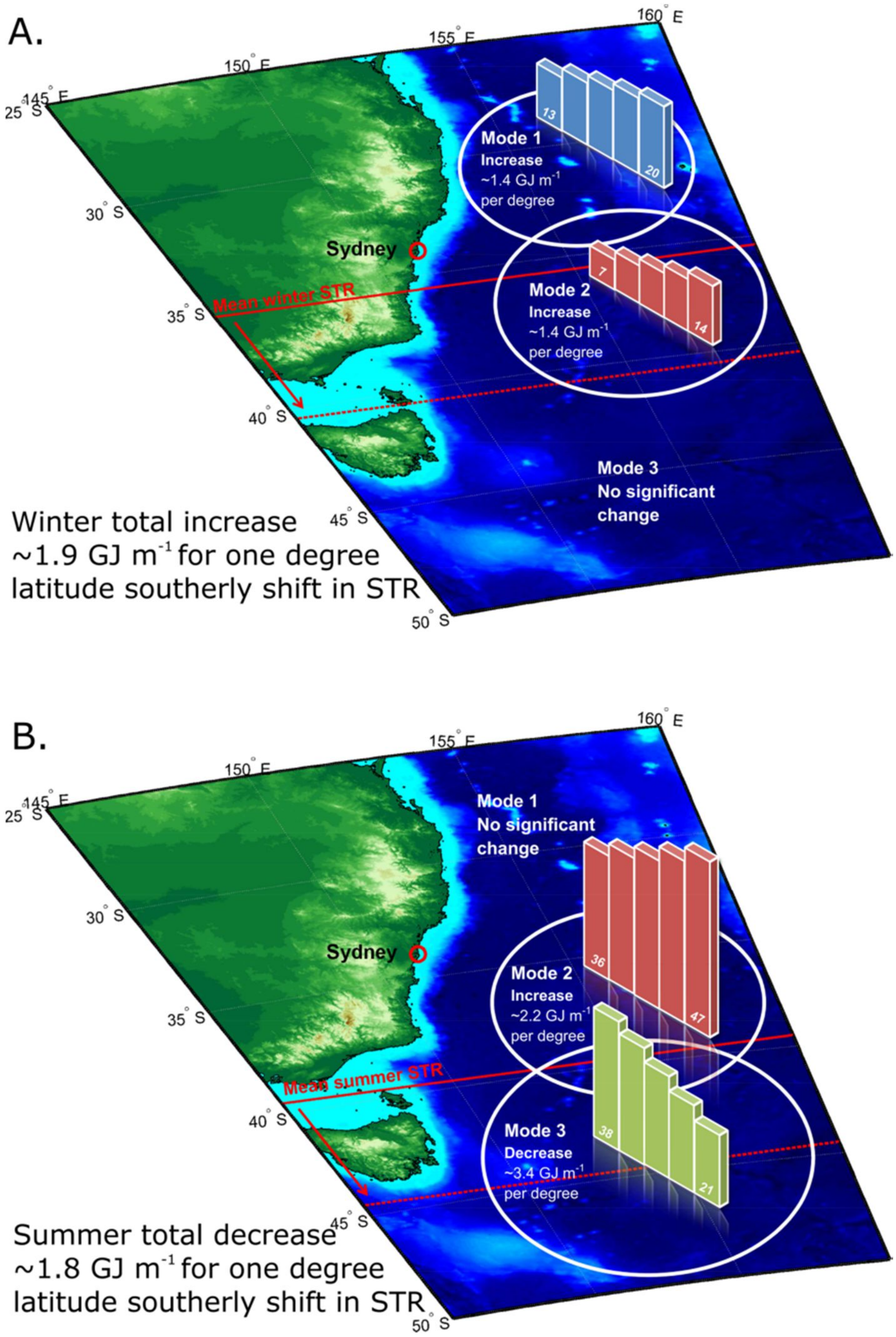

Figure 4.14 Future directional wave power change for the Sydney region with a southerly shift in the STR during (a) winter and (b) summer.

4.11 CONCLUSIONS

A combined statistical-synoptic typing approach of directional wave buoy records along the Southeast Australian shelf has isolated six modal wave climates and their respective generation sources. These include waves produced by North-Easterly Trade Winds, Zonal Easterly Trade Winds, a combination of Southern Tasman Anti-Cyclones and Tropical Lows, Central Tasman Lows, Southern Ocean Lows and Southern Tasman Lows. It is showed that these wave climates can be grouped into three distinct wave type clusters; Mode 1 (easterly), Mode 2 (south-easterly) and Mode 3 (southerly). K-means clustering with a best-guess estimate of the optimal wave climate number, *k*, was only able to identify the broad directional wave modes, rather than individual wave genesis. This is because multiple synoptic drivers produce statistically indifferent directional wave fields in a semi-enclosed sea environment. In order to isolate wave generation and ‘synoptic-scale’ wave climates, subsequent decomposition of the clusters using a Gaussian Mixture Model and analysis of the Mean Sea Level Pressure field was required.

Synoptic patterns suggest that Mode 1-type wave climates (easterly) and Mode 3-types (southerly) are formed under Pacific-dominant atmospheric longwave patterns and are related to ENSO phases. Mode 2-types (south-easterly) are a result of a longwave train originating from the Indian Ocean, and occur either during ENSO neutral conditions or when the IOD has a stronger influence on the Tasman Sea region. Occurrence co-variance between Modes 1 and 3 during winter suggests that a SAM/ENSO coupling is the dominant signal during winter, while co-variance between Modes 2 and 3 in summer indicate the IOD is more influential during summer.

The position of the STR modulates the seasonal occurrence of, and latitudinal exposure to, different wave climate types. A southerly migration of the STR is a plausible future scenario in line with an observed poleward expansion of the tropics cell due to anthropogenic forcing and natural variability. Results indicate that, under such a scenario, there would be an increase in the modal wave energy flux for the central NSW shelf of 1.9 GJ m^{-1} wave-crest-length for a one degree southerly shift in the STR during winter, and a reduction of similar magnitude (approximately 1.8 GJ m^{-1} for one degree latitude shift south) during summer.

In both seasons, a southerly shift in the STR forces a re-arrangement of the modal wave energy flux towards the east and south-east. This anti-clockwise rotation of the wave field is consistent with GCM-based wave climate projections (Hemer *et al*., 2013). Reduced obliquity of constructive wave power throughout the year would promote a general disruption to northward alongshore sediment transport for the central NSW coast. Under a southerly STR scenario, cross-shore sediment transport will become increasingly prevalent, with local-scale effects dependant on shoreface sediment availability. Results from this chapter are of primary application to investigating available wave energy for beach recovery after storm events, and mean shoreline configuration (as is done in Chapter 5).

This study is based on observational records on the East Australian shelf, but the understanding of the latitudinal gradient in modal wave climate may be applicable to other coastlines where the wave climate is influenced by the position of the zonal STR. In the northern hemisphere, Atlantic wave climates of the Iberian peninsula and Bay of Biscay are strongly influenced by the position and strength of the sub-tropical Azores high. Other Southern Hemisphere, continental east coasts along the mid-latitudes such South Africa/Mozambique and Uruguay/Brazil also have comparable wave genesis and sediment transport patterns.

4.12 ACKNOWLEDGEMENTS

All parametric wave data for NSW DWR buoys was provided by Manly Hydraulics Laboratory (MHL), and is funded by NSW Office of Environment and Heritage. Data for the Brisbane DWR buoy was provided by Queensland Department of Science, Information Technology, Innovation and the Arts (DSITIA). Stuart Browning at Macquarie University provided the Tasman Sea STR time series. During cluster evaluation, the freeware CVAP platform for Matlab (Wang *et al.*, 2009) was used. Comments from the anonymous reviewers of the paper on which this chapter is based significantly improved this study.

CHAPTER 5

Fisherman's Beach

ENSO WAVE CLIMATES AND COASTAL CHANGE IN SOUTHEAST AUSTRALIA

5 ENSO WAVE CLIMATES AND COASTAL RESPONSE IN SOUTHEAST AUSTRALIA

5.1 CHAPTER OVERVIEW

El Niño Southern Oscillation (ENSO) is a key driver of interannual wave climate variability and coastal behavior along the south east Australian shelf. This chapter investigates the impact of changing ENSO behavior on wave climate and coastal impacts, complementing findings in Chapter 4 of wave climate changes with tropical expansion. In particular, differences between central Pacific (CP) and eastern Pacific (EP) flavours of ENSO are explored. A background to ENSO dynamics and future projections is given in Section 1.2.5 in Chapter 1. This study uses the wave climate typology detailed in Chapter 4 to link observed patterns of ENSO directional wave power to synoptic climate and wave generation. A surrogate-observational and modelling approach, as advocated throughout this thesis, is used to assess the impacts of future shifts in ENSO behaviour as Global Climate Model-based projections of ENSO improve.

5.2 KEY FINDINGS

Wave climate and Pacific basin coastal behavior associated with ENSO is understood at a reconnaissance level, but the coastal response to different CP versus EP flavours of ENSO is unknown. Results from this study show that CP ENSO events produce significantly different patterns of directional wave power to EP ENSO along the southeast Australian shelf and southwest Pacific region, because of variability in trade-wind wave generation. The modulation of the trade wind wave climate during CP ENSO has thus far been neglected in existing coastal process studies.

Results also show that coastal change between CP and EP ENSO cannot be inferred from shifts in the deepwater wave climate, as previously assumed. This is because variability in trade-wind wave generation is masked in deepwater by the persistence of high power extra-tropical waves that have reduced impact on nearshore processes due to high wave refraction.

Morphodynamic modelling in a headland-bay beach indicates that CP ENSO leads to higher coastal erosion potential and slower post-storm recovery than EP ENSO during an El Niño/La Niña cycle. It is shown that the alongshore variability in beach morphological type can be used to model the static equilibrium planform response for each ENSO phase. Results indicate that shoreline response to ENSO in most headland-bay beach coasts is not as simple as the existing paradigm that (anti-) clockwise rotation occurs during El Niño (La Niña). This method provides a second-order approach to project coastal response to ENSO flavours.

5.3 PUBLICATION AND AUTHOR CONTRIBUTION

This chapter has been submitted for publication, in modified form in: **Mortlock, T.R.** and Goodwin, I.D. (in review). Impacts of Enhanced Central Pacific ENSO on Wave Climate and Headland-Bay Beach Morphology. *Continental Shelf Research*.

This work was first presented at Coastal Sediments 2015 conference: **Mortlock, T.R.** and Goodwin, I.D. (2015). Wave Climate Change Associated with ENSO Modoki and Tropical Expansion in Southeast Australia and Implications for Coastal Stability. *Coastal Sediments Conference, 11 - 15 May 2015, San Diego, USA.* doi: 10.1142/9789814689977_0198. The conference paper is provided in Appendix 5.

As lead author, I carried out all analysis and wrote the chapter/paper. The original concept for this study was developed jointly between me and IDG. IDG contributed to the interpretation of results and edits to the chapter/paper.

5.4 INTRODUCTION

There remains considerable uncertainty in the prediction of future shifts in ENSO behaviour from Global Climate Modelling (GCM) because of the non-linearity of ENSO and complex coupled feedbacks (Watanabe *et al*., 2012). Downscaled projections of regional wave climate inherit this uncertainty and are highly variable, especially for Pacific regions directly impacted by ENSO and on sub-annual timescales (Mori *et al*., 2013; Hemer *et al*., 2013). There remains, therefore, a significant knowledge gap in how Pacific coasts will respond to future changes in ENSO.

Multi-decadal wave buoy observations along the south east Australian shelf (SEAS), in the south west Pacific, have shown that ENSO significantly modulates wave climate directionality and intensity (Goodwin, 2005; Harley *et al*, 2010). In broad terms, El Niño promotes bi-directional south easterly and easterly wave conditions, while La Niña and ENSO-neutral phases are correlated with a more uni-directional south easterly wave climate. A greater number of storms occur during La Niña (Browning and Goodwin, 2013), in contrast to the eastern Pacific where El Niño is most damaging (Storlazzi and Griggs, 2000).

The poleward (equatorward) displacement of the Subtropical Ridge (STR), the latitude of highest pressure over East Australia, also exerts a strong influence on the seasonal wave climate (Mortlock and Goodwin, 2015) and impact of ENSO. ENSO wave climates are also coupled to the Southern Annular Mode (SAM) (Hemer *et al*., 2009), particularly during Austral winter. The SAM describes the see-saw of atmospheric mass between the mid-latitude westerlies and Antarctica (Marshall, 2003). Positive (negative) SAM represents a poleward (equatorward) displacement of the westerlies, and reinforces a La Niña (El Niño) wave climate through the modulation of Southern Ocean and Southern Tasman Sea wave generation.

Mortlock and Goodwin (2015) have showed that the directional wave climate along the SEAS can be encapsulated in three primary modes of variability (Figure 5.1 a). A sub-tropical easterly mode is modulated by south Pacific trade winds (Mode 1); a south-easterly mode is generated locally in the Tasman Sea (Mode 2) and an extra-tropical southerly mode is related to the strength of the mid-latitude westerlies (Mode 3).

Similar to other Southern Hemisphere coastlines, the south east Australian coast is meridionally oriented with a predominant south to north longshore sediment transport regime (Figure 5.1 a). Sediment transport cells are divided by prominent headlands, leading to the repetition of headland-bay beach morphology along much of the 1,200 km of coastline length. Under this configuration, the headland is located to the south, with the parabolic beach adjacent to the north. A Mode 1 wave climate produces cross-onshore wave conditions, Mode 2 onshore, and Mode 3 oblique (Figure 5.1 b). The planform geometry of these coastal sections is well described by the Parabolic Bay Shape Equation (PBSE) developed by Hsu and Evans (1989). Downdrift (north) of the parabola, the planform is oriented normal to the modal wave direction.

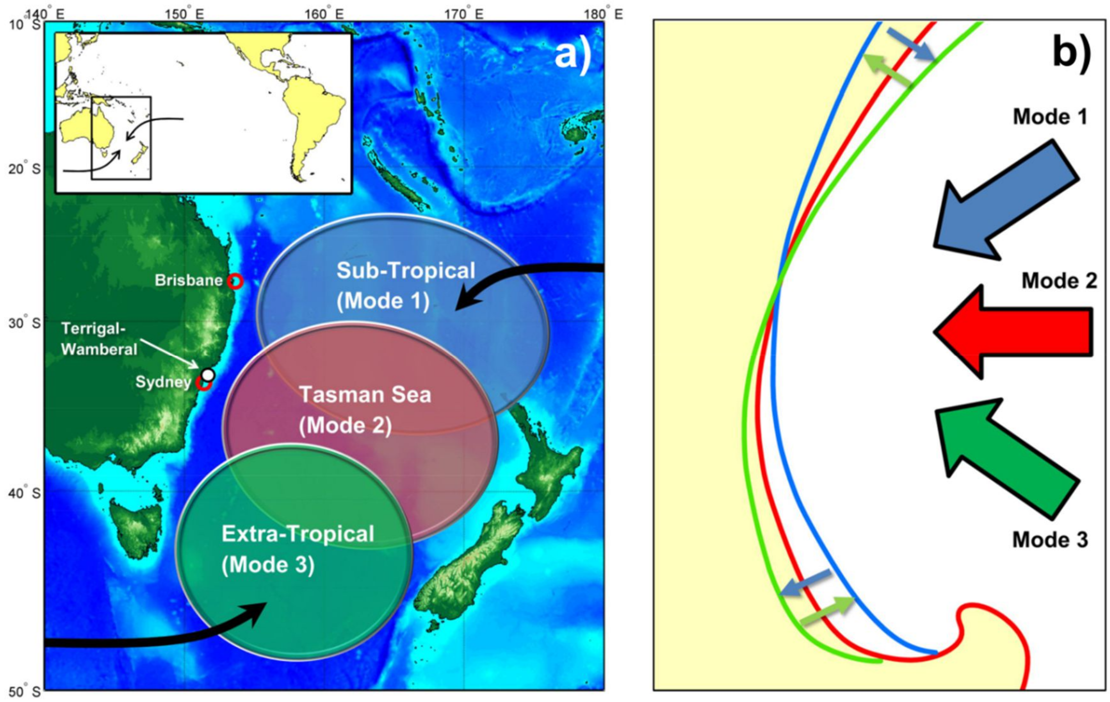

Figure 5.1 a) Three primary modes of wave climate variability in the Tasman Sea with locations of Sydney, Brisbane and Terrigal-Wamberal wave buoys. Inset shows relation to south Pacific and Southern Ocean; b) conceptualisation of planform rotation in a headland-bay beach in south east Australia.

Shifts in the orientation of headland-bay beach compartments are linked to directional variability in the SEAS wave climate with ENSO (Goodwin *et al.*, 2006; 2013). Collaroy-Narrabeen Beach and Palm Beach, two embayed compartments in Sydney, rotate clockwise (anti-clockwise) during biennial El Niño (La Niña) events (Short *et al.*, 2000; Ranasinghe *et al*., 2004), because of shifts in wave directionality (Ranasinghe *et al*., 2004; Harley *et al*., 2015). Recent research suggests that coastline fluctuations observed along this section of coast are part of a synchronous Pacific basin-wide response to ENSO forcing (Barnard *et al*., 2015).

While a connection between El Niño/La Niña wave climate and coastal response is established, the current understanding of coastal impacts on Pacific coastlines has not yet accounted for different flavours of ENSO. Most observational studies relate to an eastern Pacific (EP) El Niño (La Niña) climate that is characterised by a canonical pattern of surface warming (cooling) in the eastern Pacific. However, ENSO anomalies also develop in the central Pacific (CP). CP ENSO events (also known as ENSO Modoki) have become more frequent in recent decades (Lee and McPhaden, 2010) and some GCMs indicate this will continue with greenhouse warming (Yeh *et al*., 2009). It is therefore important to understand whether the wave climate and coastal response to CP ENSO is significantly different to EP ENSO.

Over 20 years of mid-shelf and directional buoy observations are used to examine shifts in wave power and wave generation with EP and CP ENSO along the south east Australian shelf. A morphodynamic model is used to investigate coastal response at Terrigal-Wamberal (33.4° S, 151.4° E), a classic parabolic shaped headland-bay beach 60 km north of Sydney. The extent to which the deepwater wave climate is a valid indicator of nearshore change is also investigated. The alongshore variability in surf-zone morphology is used as an indicator of coastal vulnerability and also as a measure of geometric planform change. This study focusses on the modal (non-storm) wave climate as a predictand of the ENSO Pacific climate state and as the principle driver of large-scale coastal behaviour. An ensemble of coupled ENSO wave climates and beach states are presented for an idealised headland-bay beach configuration, which can be used to model scenarios of coastal impacts as GCM projections of ENSO improve.

5.5 METHODS

5.5.1 Identification of ENSO Events

Austral oceanic summers (January to March, JFM) and winters (July to September, JAS) during either EP or CP El Niño/La Niña events were identified over the period of directional buoy observations, from the monthly Niño 3.4 index (NINO3.4) and El Niño Modoki Index (EMI) (Figure 5.2). The definition of CP ENSO in this study is therefore synonymous with ENSO Modoki after Ashok *et al.* (2007).

Where possible, a suitable coupling with the SAM and allowance for time lags between indices and wave climate response were considered. Selected EP ENSO periods were based on those identified by the Oceanic Niño Index (ONI). Selected CP ENSO events were cross-checked with those identified in the literature (e.g. Shinoda *et al.*, 2011). The wave climates of the selected ENSO periods are given in Table 5.1.

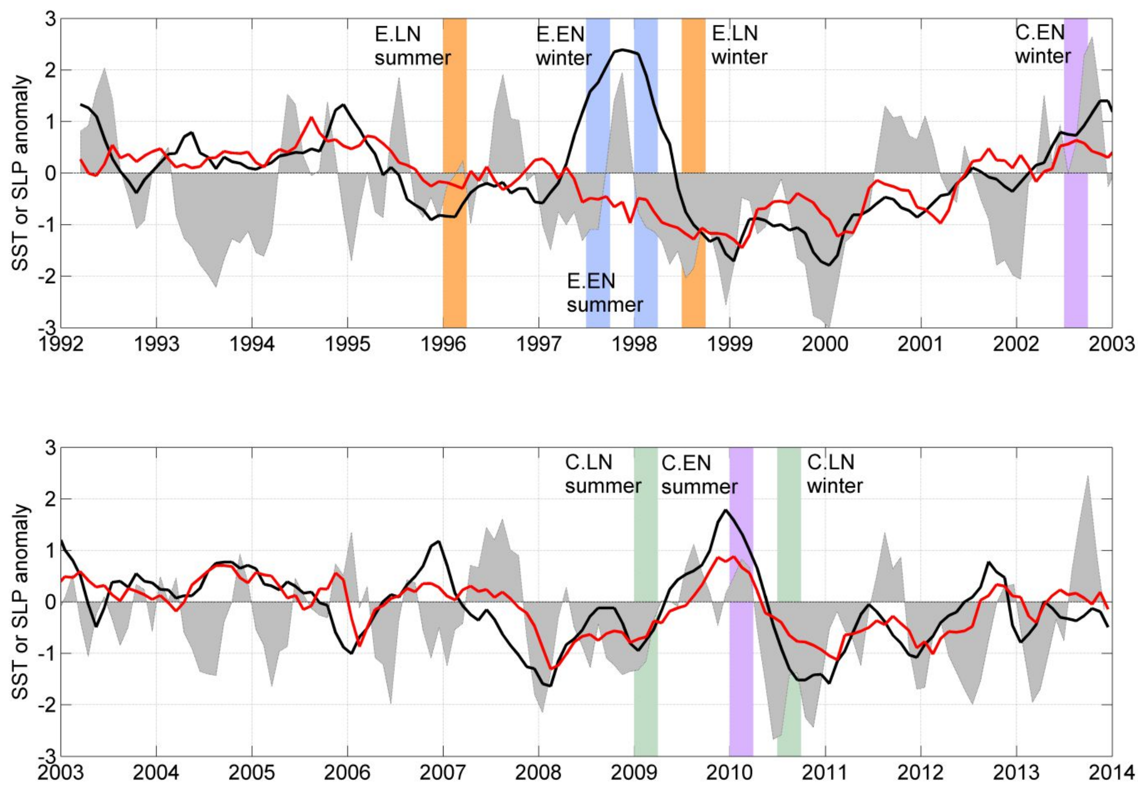

Figure 5.2 Monthly values of the EMI (red line), NINO3.4 (black line) and three-month running mean of the monthly SAM index (grey shade) over the period of directional buoy

operation. The sign of the SAM has been inverted for visualization of coupling with NINO3.4. Y-axis shows Sea Surface Temperature (SST) anomaly (in the case of the EMI and NINO3.4) and zonal mean SLP difference between 40° and 60° S (in the case of the SAM). Selected Austral oceanic summer (JFM) and winter (JAS) periods for EP El Niño (E.EN, blue), EP La Niña (E.LN, orange), CP El Niño (C.EN, purple) and CP La Niña (C.LN, green) are shown

Table 5.1 Three month periods used to represent ENSO wave climates from the available buoy record.

	Austral Summer	Austral Winter
EP El Niño	JFM 1998	JAS 1997
CP El Niño	JFM 2010	JAS 2002
EP La Niña	JFM 1996	JAS 1998
CP La Niña	JFM 2009	JAS 2010

.

5.5.2 Parametric Wave Data

Directional wave observations from buoys at Sydney (1992 – 2013) and North Stradbroke Island (40 km west of Brisbane, hereafter referred to as 'Brisbane') (1997 – 2013) were used to represent the mid-shelf (60 – 80m water depth) wave climates of ENSO periods along the SEAS (Figure 5.1 a). Daily-averaged significant wave height, H_s, peak spectral wave period, T_p, and mean wave direction, *MWD*, were used.

Since our focus is on the modal (non-storm) wave climate, all storm events were omitted from the buoy records using a Peaks-over-Threshold (PoT) method. The 10% daily exceedance H_s was used with a three-day minimum storm duration at Sydney, after Mortlock and Goodwin (2015) found this to return the best split between ambient and extreme wave distributions. At Brisbane, a second threshold using the 5% daily exceedance H_s with a 1-day minimum duration was also applied in order to filter high energy and transient tropical cyclone storm events from the record.

5.5.3 Directional Wave Hindcast

MWD at Brisbane was hindcast for summer 1996 using cumulative distribution function (CDF) matching (Brocca *et al.,* 2011) of summer wave directions at the Sydney buoy to capture the summer EP La Niña wave climate (Figure 5.3). Figure 5.3 d shows an improved correlation exists between CDF-matched Sydney wave directions and those observed at Brisbane, than between uncorrected Sydney wave directions and observations at Brisbane, over a blind test period (Figure 5.3 a).

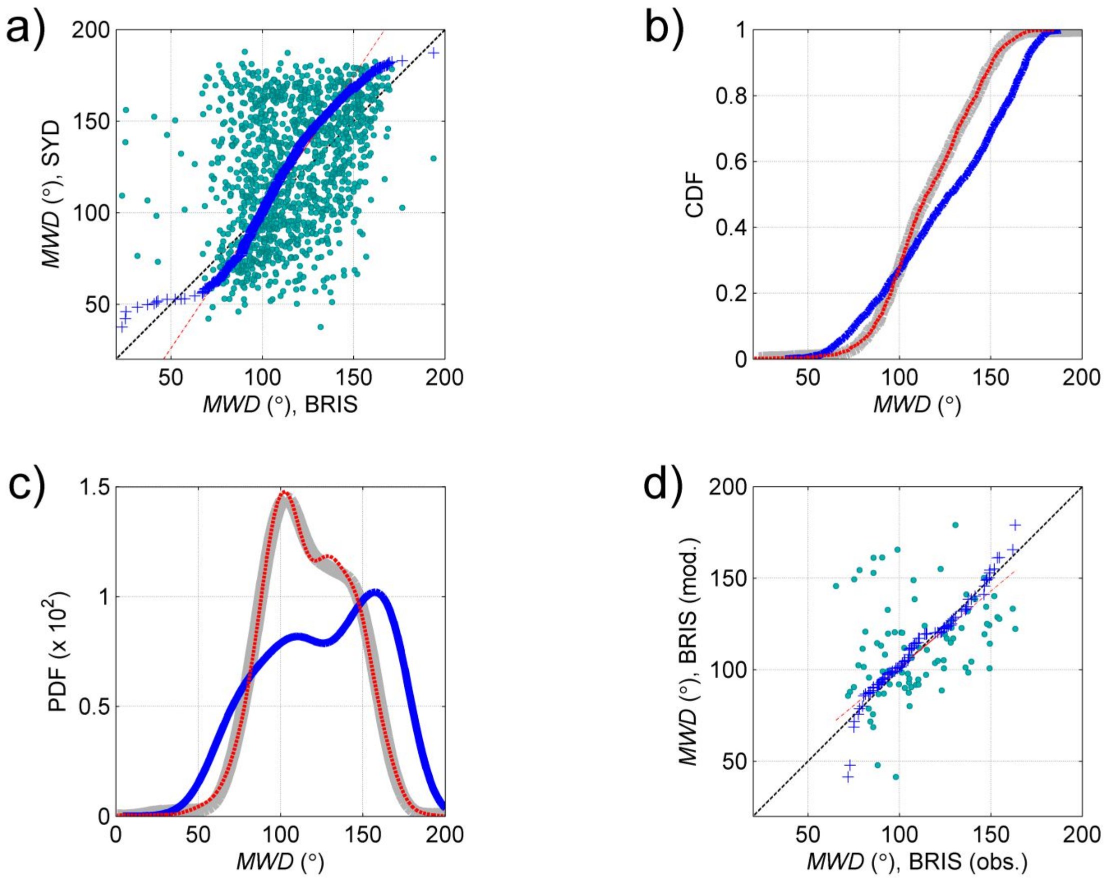

Figure 5.3 Cumulative Distribution Function (CDF) matching of Sydney summer *MWD* with Brisbane showing (a) scatter plot of Brisbane and Sydney daily summer *MWD* (1997 – 2012) used as model training dataset, with quantiles (blue) and linear regression (red line), (b) CDF of *MWD* observed at Brisbane (grey), observed at Sydney (blue), and CDF-matched for Brisbane (red), (c) the same for PDF of *MWD*, and (d) scatter plot with quantiles of Brisbane *MWD* observed (obs.) and modelled (mod.) for a blind test (using JFM 2013).

5.5.4 Wave Climate Typology

The three primary modes of wave climate variability presented in Figure 5.1 a were further decomposed into six synoptic-scale modal 'wave climate types' (WCT) using a combined statistical-synoptic typing method as presented in Chapter 4. Figure 5.4 shows the mean sea level pressure (MSLP) anomaly patterns for each of these WCTs over the Tasman Sea. All WCTs are identifiable in both Austral summer and winter, apart from Mode 2b which at Sydney only exists as a summer pattern. Modes 3a and 3b are not seen at the Brisbane buoy due to a north-west trending shoreline north of Cape Byron. A detailed discussion of each WCT is provided in Chapter 4. Here we use the WCT discretization to relate directional wave power to zonal Pacific circulation.

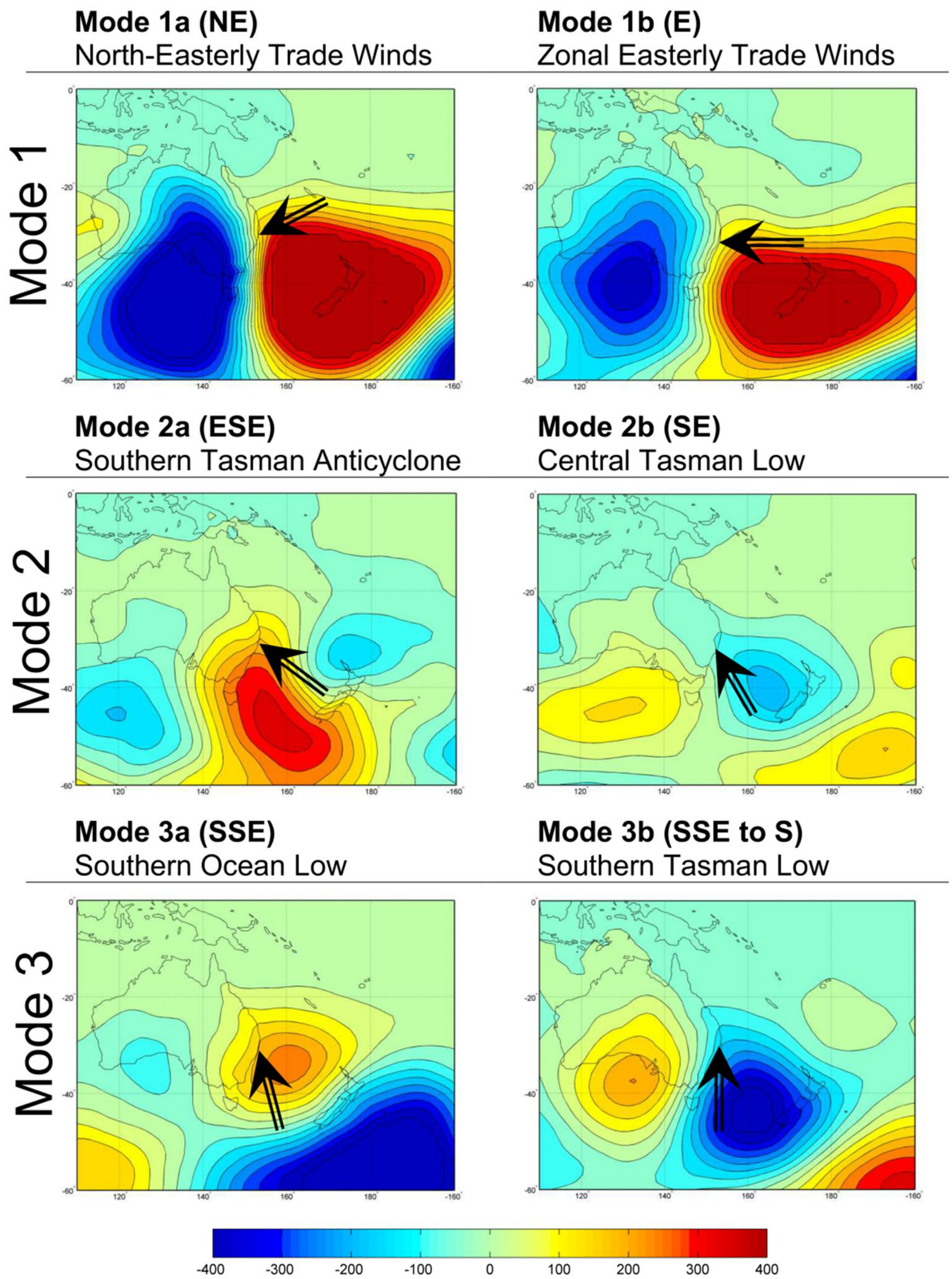

Figure 5.4 Composite anomalies (hPa) of mean sea level pressure using ERA-Interim Reanalysis 1979-2013 (Dee *et al.*, 2011) for synoptic-scale wave climate types in the Tasman Sea. Arrows are indicative of mean wave direction at the Sydney buoy.

A sub-tropical easterly mode is modulated by south Pacific trade winds (Mode 1); a south-easterly mode is generated locally in the Tasman Sea (Mode 2) and an extra-tropical southerly mode is related to the strength of the mid-latitude westerlies (Mode 3). Mode 1 produces east to north east wave conditions along the SEAS, Mode 2 south east, and Mode 3 south south east to south. In Chapter 4 these three modes were further decomposed into six synoptic-scale modal 'wave climate types' (WCT).

Figure 5.4 shows the mean sea level pressure (MSLP) anomaly patterns for each of these WCTs over the Tasman Sea. All WCTs are identifiable in both Austral summer and winter, apart from Mode 2b which at Sydney only exists as a summer pattern. Modes 3a and 3b are not seen at the Brisbane buoy due to a north-west trending shoreline north of Cape Byron. Chapter 4 provides a detailed discussion of each wave climate type. In the present study, storm events were omitted from the buoy records and modal wave data were decomposed into these six synoptic WCTs to relate directional wave power to zonal Pacific circulation.

5.5.5 Patterns of ENSO Directional Wave Power

The total wave power, P_W, delivered by each wave climate type was used to describe the pattern of directional wave power for each ENSO period. P_W is the integral of the wave power density of each daily wave event, P_0, over the duration of each WCT, t, given in megawatt-hours per metre wave-crest-length (MWh m^{-1}):

$$P_W = \int_0^t P_0 dt \qquad (5.1)$$

To ensure no bias of P_W away from periods with data gaps due to instrumental error, the frequency of occurrence of each WCT was up-scaled from the observed record to simulate 100% data recovery at the buoys. The frequency of occurrence of each WCT was then de-trended before calculating P_W.

A two-tailed student t-test was used to determine whether the difference between patterns of ENSO directional wave power was significant (to 90% confidence). This was based on the frequency of occurrence of each WCT during each ENSO period (Table 5.2). Significant differences between wave power generated by individual WCTs, rather than the wave climate as a whole, were also determined between EP and

CP ENSO climates. If differences exceeded one standard deviation of the interannual wave power variability for the respective WCT, it was considered significant to the 90% CI.

Table 5.2 Dissimilarity matrix of Austral summer (winter) ENSO wave climates using a two-tailed student t-test. 0 (1) = distributions are (not) dissimilar between ENSO types (to 90% CI).

	EP El Niño	CP El Niño	EP La Niña	CP La Niña
a) Sydney				
EP El Niño	n/a	0 (1)	0 (1)	0 (1)
CP El Niño	0 (1)	n/a	0 (1)	0 (1)
EP La Niña	0 (1)	0 (1)	n/a	1 (1)
CP La Niña	0 (1)	0 (1)	1 (1)	n/a
b) Brisbane				
EP El Niño	n/a	1 (0)	1 (0)	1 (0)
CP El Niño	1 (0)	n/a	1 (1)	1 (0)
EP La Niña	1 (0)	1 (1)	n/a	1 (0)
CP La Niña	1 (0)	1 (0)	1 (0)	n/a

5.5.6 Morphodynamic Modelling of a Headland-Bay Beach

ENSO wave climates at Sydney were transformed to Terrigal-Wamberal, 60 km north (Figure 5.5), to investigate shoreface response to ENSO in an idealised headland-bay beach. A coupled MIKE21/3 model of the embayment was nested within a regional MIKE21 Spectral Wave (SW) model. MIKE21/3 dynamically couples a spectral wave, hydrodynamic and sand transport module to simulate bathymetric evolution by wave-driven currents based on Reynolds-averaged Navier-Stokes theory (DHI, 2014).

5.5.6.1 Model Configuration

The model was configured to isolate wave forcing, so no terrestrial sediment inputs, tides, local winds or ambient currents were included. Headland sand bypassing is essentially switched off for this experiment, since the embayed geometry of the regional coast and the incised nature of the Wamberal embayment prevent bypassing during modal wave conditions. High spatial resolution (5 m^2) LIDAR bathymetry (March 2008) was used to represent the shoreface to 30 m depth. All subaqueous reef around

Terrigal Headland was omitted, and only areas of the embayment with a sand bottom were modelled (Figure 5.5).

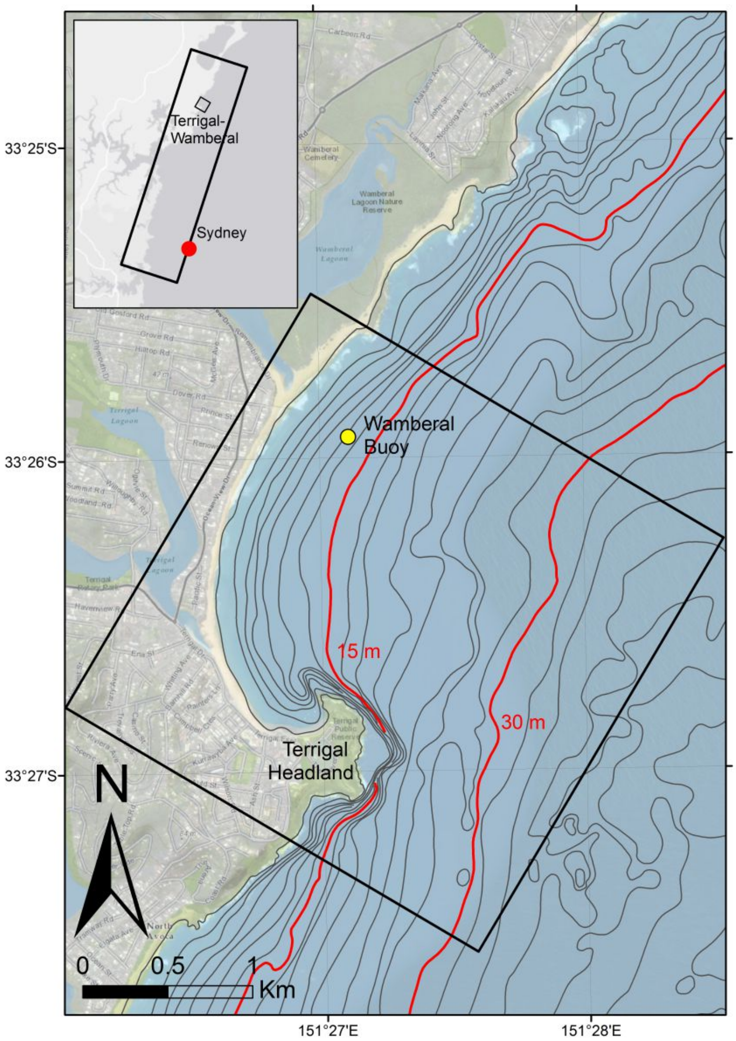

Figure 5.5 Location of Terrigal-Wamberal with upper and lower shoreface (15m isobar) and lower shoreface and inner shelf breaks (30m isobar). Extent of morphodynamic model (black rectangle) and nearshore buoy are shown. Inset shows extent of regional wave model and Sydney buoy.

5.5.6.2 Model Validation

Nearshore model performance was verified against eight months of hourly buoy observations (August 2011 to March 2012) at 12 m depth inside the Wamberal embayment (location Figure 5.5). For results of model validation and discussion of significance, see Section 1.4.3.2 in Chapter 1.

5.5.6.3 Boundary Wave Forcing

A three-month time series of daily offshore modal wave conditions for each ENSO wave climate was generated for model boundary forcing (Figure 5.6). The observed time series at the Sydney buoy was first indexed by WCT for each ENSO season. This was done so that each wave day could be represented by the centroid parameters H_s, T_p and *MWD* of the WCT to which the observation belonged, rather than the actual observation. This method obtained a clearer signal of morphological response between ENSO types in what is a complex mixed sea-swell environment (Chapter 4). Centroid parameters were calculated separately for each ENSO period.

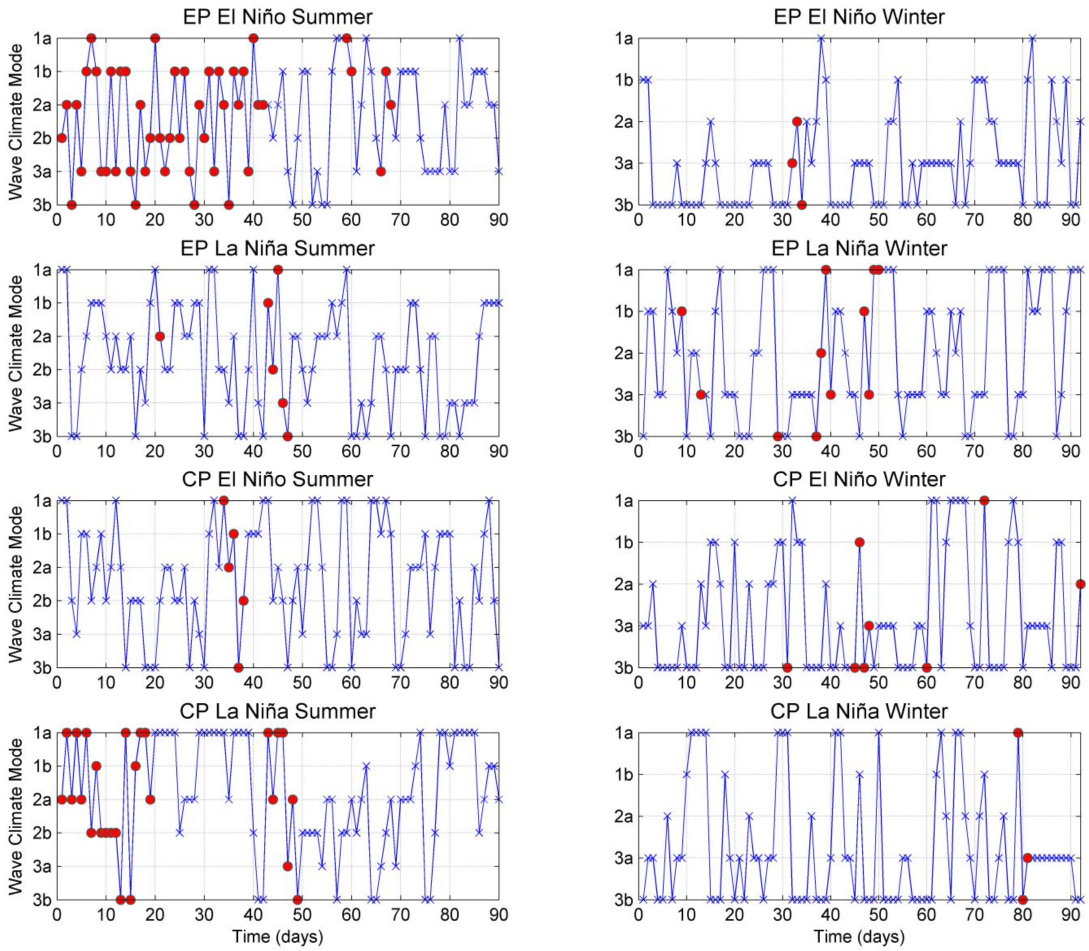

Figure 5.6 Time series of daily modal waves for each ENSO wave climate at the Sydney buoy. X-axis shows number of days (summers = 90 days, winters = 92 days), y-axis shows wave climate type (WCT). Red dots indicate location of missing wave days.

A continuous (gap-free) time series was required for modelling. However, missing wave days existed in the observed (buoy) record due to either instrument error at the buoy or omitted storm events. Missing days were filled by first calculating the number of extra days needed per WCT to maintain the frequency of occurrence of each WCT from the portion of the time series observed at the buoy. Each required wave day was then represented by the respective centroid parameters of the corresponding WCT. A random permutation of the required wave days was performed and then inserted into the locations of data gaps in the time series. This provides a 'nudged random' order of WCTs for data gap periods, as the randomness of the sequencing is already weighted by the number of wave days needed. The sequencing of the wave time series is as important as the wave climate itself (e.g. Southgate, 1995), as the morphological model dynamically couples waves, flow and bed elevation change at each time step. A six-month wave climate consisting of two cycles of the respective three-month time series was then used to force the model to allow sufficient time for an equilibrium beach state to develop.

5.5.6.4 Bed Elevation Change

Cumulative bed elevation change was normally-distributed for each ENSO case with a mean approximate to zero after outliers were removed. All values within one standard deviation of the mean were removed, with the remaining vertical difference considered to be significant to the 90% CI.

5.6 RESULTS AND DISCUSSION

5.6.1 Impact of ENSO on Seasonal Wave Climate

At locations where the winter wave climate is strongly influenced by the SAM (south of Cape Byron), patterns of ENSO wave power are most dissimilar during Austral summer when the STR migrates ~ 4° poleward, displacing the SAM (and southerly Mode 3 wave power) influence on the sub-tropics. During winter, the wave climate is dominated by Mode 3 power, masking the influence of ENSO.

This is evident at Sydney, where all ENSO wave climates are dissimilar from each other during summer, but not during winter (Table 5.2). The exception is between summer EP La Niña and CP La Niña, which are not dissimilar (at the 90% CI) although there is a significant increase in Mode 1a wave power during La Niña Modoki (Figure 5.7).

While the SAM does not influence the winter wave climate at Brisbane, an open fetch for Coral Sea and Southwest Pacific tradewind wave generation means easterly Mode 1 power dominates in all ENSO phases during summer (Figure 5.8). As a result, no ENSO wave climates are dissimilar during summer, whereas almost all types are discrete in winter (Table 5.2). The exception is between winter EP La Niña and CP El Niño, which are not dissimilar.

5.6.2 Impact of Central Pacific ENSO on Directional Wave Power

CP ENSO produces significantly different patterns of directional wave power from EP ENSO at Sydney and Brisbane (Table 5.2) primarily because of the modulation of Mode 1 wave power between the different flavours of ENSO. At both locations, east to north east wave power is greater during EP El Niño than CP El Niño, and CP La Niña than EP La Niña in Austral summer, while the opposite is true in winter (Figure 5.7 for Sydney, Figure 5.8 for Brisbane).

The modulation of Mode 1 wave power represents variability in longer-period south west Pacific trade-wind wave generation and is associated with the position and strength of the sub-tropical Anticyclone (STAC). East to north east wave power is maximised when the STAC is located to the north east of the North Island of New Zealand (summer EP El Niño/CP La Niña, or winter EP La Niña/CP El Niño), and weakest when in the central Tasman Sea (summer EP La Niña/CP El Niño) or over south east Australia (winter EP El Niño/CP La Niña).

As a result, prolonged periods of CP La Niña enhance wave climate seasonality over successive summer/winters at Sydney and Brisbane, in comparison with EP La Niña. This is manifest in an anti-clockwise (clockwise) rotation of modal wave power during summer (winter). At Sydney, persistent CP La Niña results in lower total modal wave power for consecutive summer/winters (Figure 5.7), while at Brisbane there is an increase in total wave power in summer but a decrease the following winter (Figure 5.8).

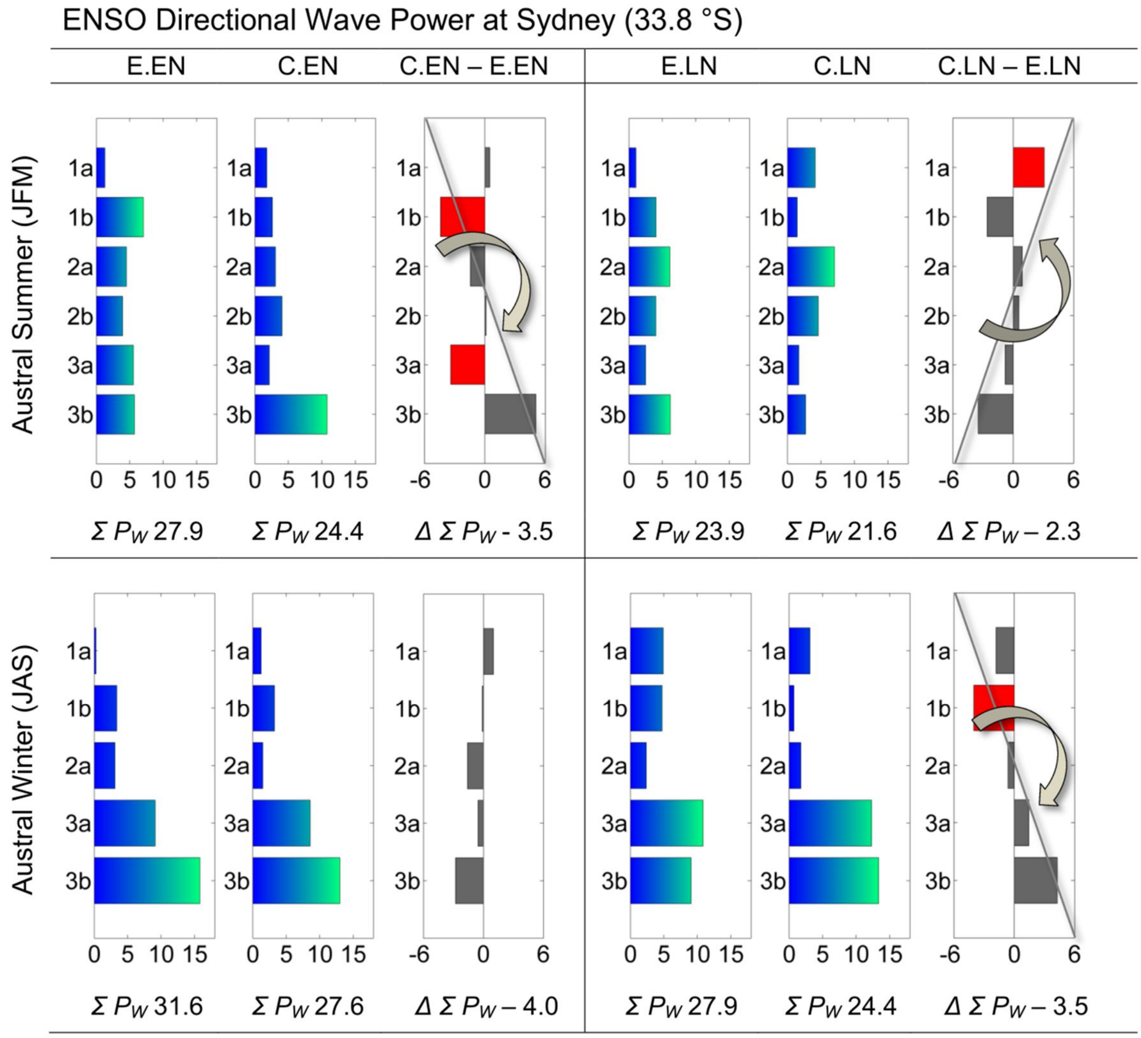

Figure 5.7 Directional (mid-shelf) wave power, P_W (MWh m^{-1}), discretised by wave climate type during summer and winter EP El Niño (E.EN), EP La Niña (E.LN), CP El Niño (C.EN) and CP La Niña (C. LN) events at Sydney. Anomalous P_W between EP and CP ENSO is shown with significant anomalies in red. Total P_W for each ENSO period (ΣP_W) and the difference between EP and CP ENSO ($\Delta\Sigma P_W$) is also shown.

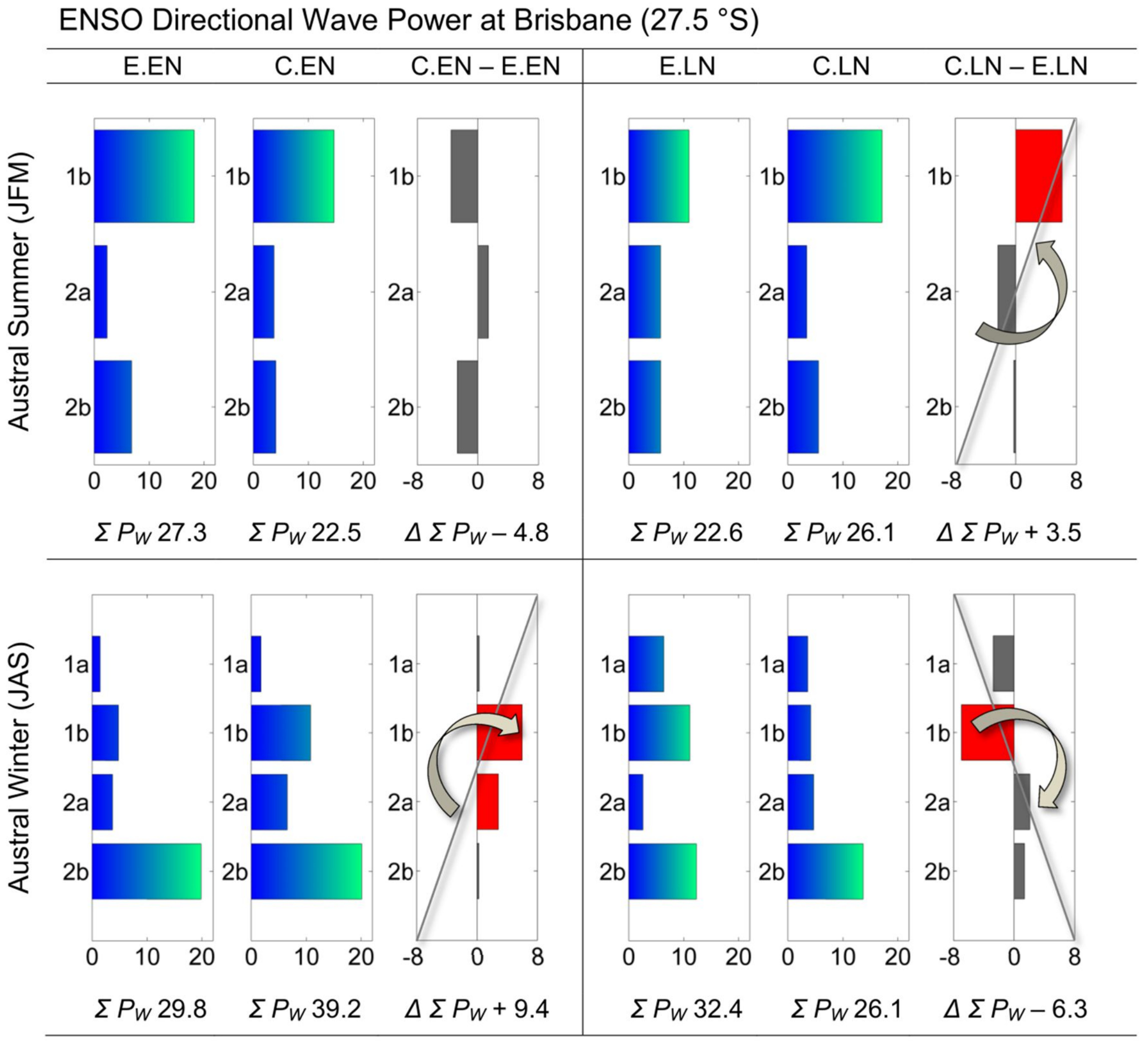

Figure 5.8 Directional (mid-shelf) wave power, P_W (MWh m^{-1}), at Brisbane discretised by wave climate type.

5.6.3 Nearshore Sensitivity to Shifts in the Deepwater Wave Climate

While discrete patterns of wave power exist in deep water, changes to the nearshore wave climate are more subtle. The nearshore wave climate was output along the seaward edge of the surf zone (5m contour) in the south, centre and north of the embayment. Figure 5.9 (5.10) shows nearshore results for summer (winter) ENSO model runs with corresponding deepwater boundary wave climate. Results show the nearshore zone is relatively insensitive to shifts in offshore wave direction due to shoaling processes. On average, a one degree shift in the direction of waves entering the surf zone requires a ~35 ° shift offshore. At the northern (most exposed) end of the embayment, only 50 % of total offshore wave power reaches the surf zone, while in the headland shadow zone this is reduced to 11 % after refraction.

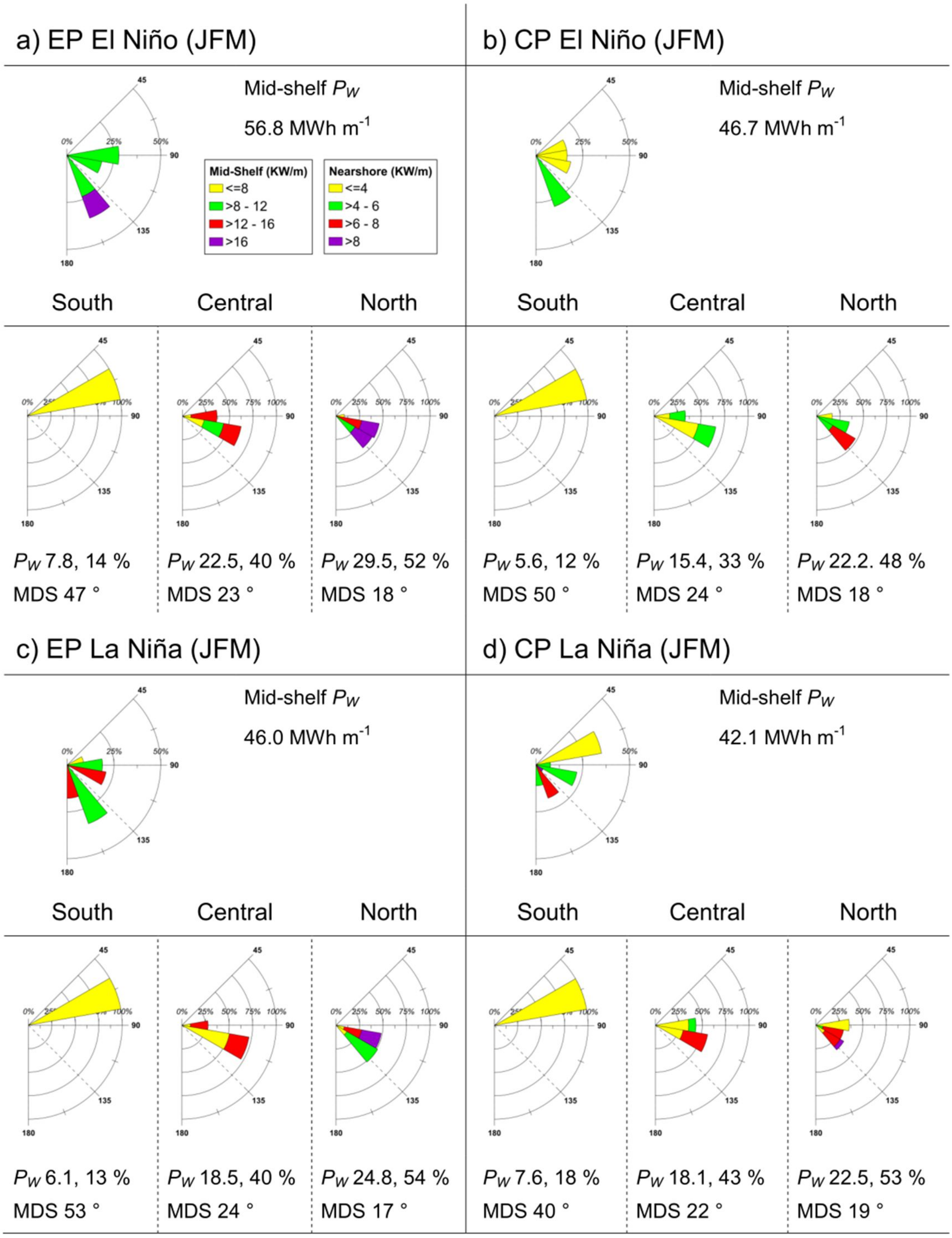

Figure 5.9 Directional wave power at Terrigal-Wamberal during Austral summer (JFM). Wave roses show wave power density (kW m^{-1}) for 20° directional bins. The cumulative wave power of the six-month boundary wave time series is shown for each ENSO case (mid-shelf P_W, MWh

m^{-1}). Percentage values below wave roses represent the proportion of offshore power retained at the nearshore point over the six-month period. The Mean Directional Sensitivity (MDS) value refers to the shift in the offshore wave direction needed to force a 1° directional change in the nearshore, and is calculated as the root mean squared difference between the offshore and nearshore mean wave direction.

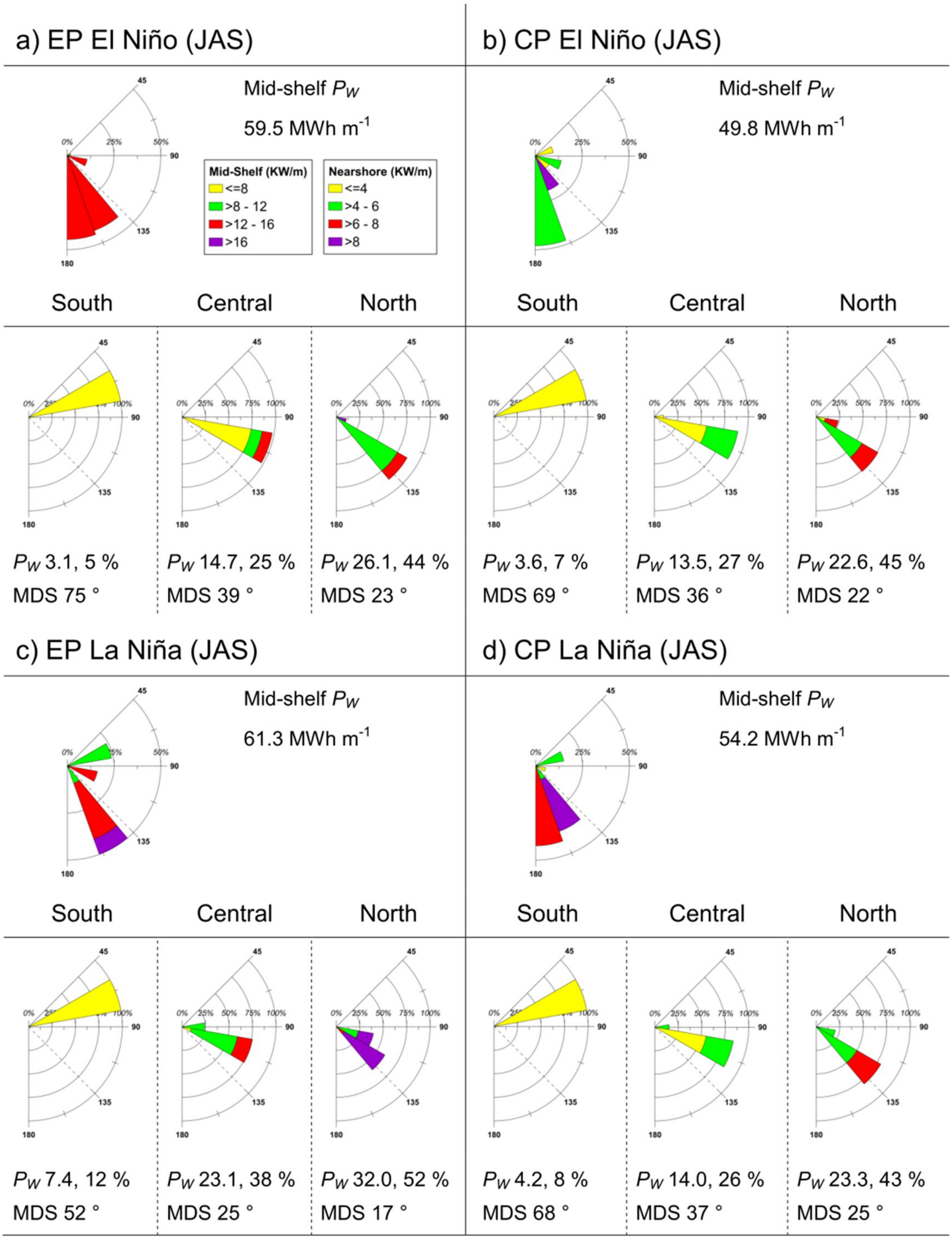

Figure 5.10 Mid-shelf and nearshore directional wave power at Wamberal during Austral winter.

Both wave power and directional sensitivity vary considerably in the south and centre of the embayment with wave obliquity. When the deepwater mean wave direction is (anti-) clockwise of shore-normal south-east, a ~55 ° (30 °) degree shift is required for a one degree change in the centre/south of the embayment, and ~15 % (30 %) of total deepwater wave power reaches the surf zone in this area. The nearshore is therefore more sensitive to variability in east and north east trade-wind waves than southerly extra-tropical waves, despite the latter having much greater total power in deepwater. This indicates that ENSO-related coastal impacts cannot be directly inferred from the deepwater wave climate because the importance of trade-wind waves is masked in deepwater by the persistence of extra-tropical and oblique wave conditions.

5.6.4 Beach Morphological Response to ENSO

Figure 5.11 shows how the surf zone morphology in a headland-bay beach may equilibrate according to the persistence of different ENSO climate states. Morphologies can be divided into two mean states; those produced under north east to south east ENSO wave climates (typical of summer), and those with a significant southerly wave component (typical of winter). The differences between morphologies can be viewed in terms of the alongshore variation in the Wright and Short (1984) beach state classification.

North east to south east ENSO wave climates (summer EP El Niño, EP La Niña and CP La Niña and winter EP La Niña) produce a shore-normal, more energetic nearshore wave climate and rhythmic bar and beach (RBB) morphology along the majority of the planform. In the headland shadow zone sand is transferred from the beach toe to a low tide terrace (LTT) with a rip channel separating adjacent morphology to the north. To the east, negligible wave energy produces a reflective beach state with deeper water directly off the toe. The transfer of sand to the LTT is greatest during east to north east wave conditions and may contribute to an apparent anti-clockwise rotation of the shoreline, as proposed by Ranasinghe *et al.* (2004) at Collaroy-Narrabeen, 30 km south of Terrigal-Wamberal. If this is the mechanism for rotation at the southern end of the embayment, the sand is only moved a few metres below the water line.

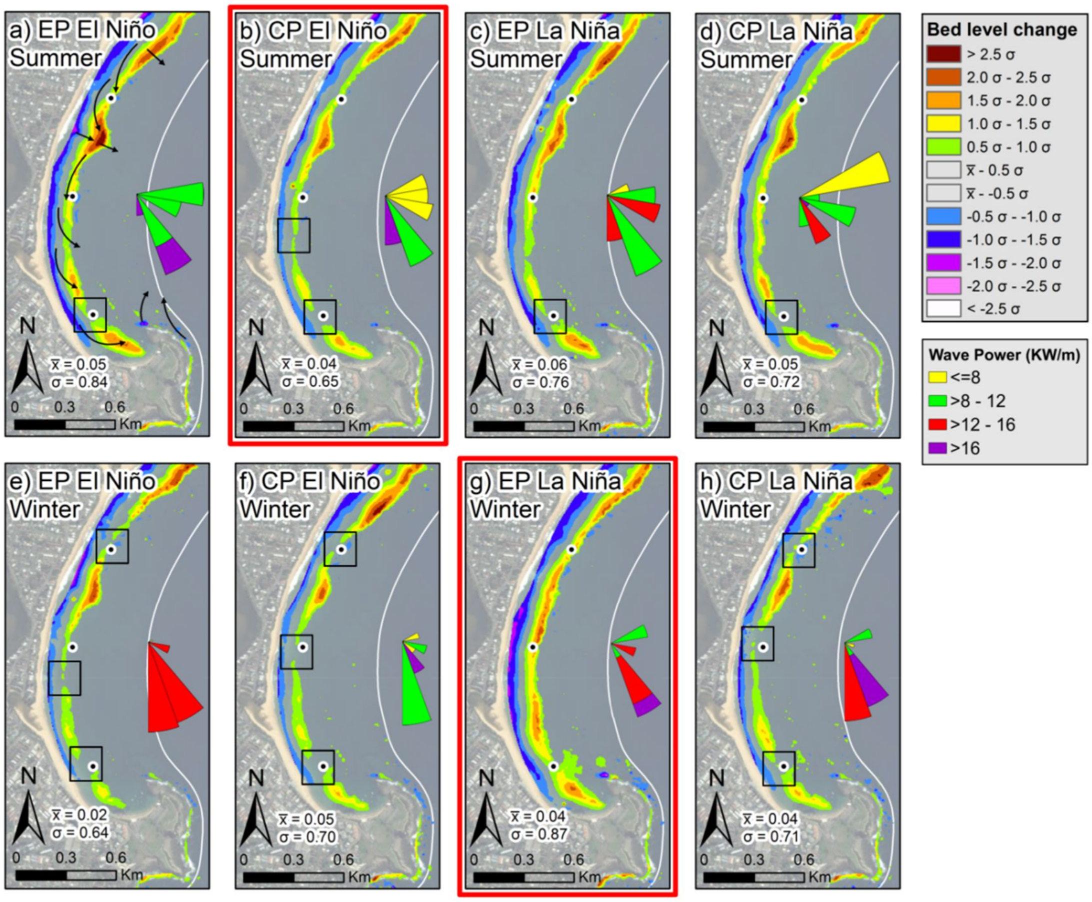

Figure 5.11 ENSO surf zone morphology at Terrigal-Wamberal. Cumulative bed level change > one standard deviation, σ, around the mean, $\bar{x}$, is shown in 0.5σ increments, where σ and $\bar{x}$ are given for each case. Wave roses show offshore directional wave power density. White line shows seaward limit of upper shoreface (15 m isobar), black circles show nearshore wave output points (Figures S6 – S7), and boxes show locations of erosion hotspots. Vectors in a) indicate time-averaged sand transport direction over the simulation period for all cases. Red boxes show greatest seasonal difference.

In contrast, southerly ENSO wave climates (winter EP El Niño, CP El Niño and CP La Niña and summer CP El Niño) produce a steep alongshore gradient in nearshore wave power and a reduced-energy wave environment in the south and centre of the embayment, despite having the highest cumulative power offshore. This leads to a transverse bar and rip (TBR) morphology for most of the planform, grading to RBB at the (most exposed) northern end. Less sand is transferred to a LTT in the headland shadow zone during oblique wave conditions.

Only CP El Niño summer and EP La Niña winter lead to seasonal changes in the beach state, despite all summer wave climates being discrete in deep water. CP El Niño summer contains a reduced easterly component producing a more winter-like beach state than other ENSO summers. EP La Niña winter is a bi-directional north east and south east wave climate (Figure 5.7) producing a more summer-like beach state than other ENSO winters.

The starting bathymetry was captured two weeks after a cluster of small (one year return period) southerly storms. In all cases, an initial period of rapid (± 0.4 m/day) shoreface recovery lasted eight to ten weeks (from end of storm) before the rate of change significantly slowed and the morphology attained an equilibrium with ambient wave conditions. Recovery was most rapid when the modal wave direction was close to the antecedent storm direction.

5.6.5 Coastal Vulnerability with Future ENSO Behaviour

Results represent inter-annual ENSO wave climates coupled to variability in the SAM in the extra-tropics. A view of ENSO impact is also presented under a specific large-scale regime in terms of the STR, which is poleward of its mean position for the last 1,000 years (Goodwin *et al.*, 2014). While both these scenarios are anomalous in the long-term, they are relevant for projections for the coming century as greenhouse warming is likely to force a continued expansion of the tropics (Seidel, 2008; Allen *et al.*, 2014) and maintain a strong coupling between SAM and ENSO (Thompson and Wallace, 2000; Wang and Cai, 2013), enhanced by a continued trend towards positive SAM with ozone healing (Mayewski *et al.*, 2015).

Despite recent improvements in GCM modelling, there is still no consensus on how ENSO will change with greenhouse warming (Cai *et al.*, 2015b), and regionally downscaled projections inherit this uncertainty. This affords little confidence in assessing future ENSO-related impacts. Therefore, a scenarios-based approach is required to account for this uncertainty. Results can be used with GCM-based projections of ENSO to model coastal impacts.

One scenario is an increase in ENSO amplitude, with more frequent extreme El Niño events (that influence the Austral summer wave climate) followed by extreme La Niña events (impacting the following winter and summer wave climates) (Cai *et al.*, 2015a).

There is no robust projection of whether an EP or CP pattern is more likely, although extreme La Niña tends to be a central Pacific phenomenon and CP ENSO events have become more frequent in recent decades (Lee and McPhaden, 2010). The coastal impact of both EP and CP ENSO sequences can be idealised based on the coupled wave climate and beach states presented in this chapter (Figure 5.12). The alongshore variability in surf-zone morphology can be used as a measure of coastal vulnerability.

For an EP pattern, a longshore bar forms along most of the planform during the first El Niño summer, with greater bar building at the northern end because of an east and south easterly wave climate (Figure 5.12 a). During the subsequent La Niña winter, a rhythmic bar also forms with greater bar-building in the south/centre of the embayment than during the preceding El Niño phase because of a north easterly wave component (Figure 5.12 b). The second (La Niña) summer wave climate is more uni-directional south easterly, leading to a longshore bar in the centre/north of the embayment, and a transverse bar and rip cell pattern in the southerly third (Figure 5.12 c).

For a CP pattern, the first El Niño summer is characterised by the persistence of transverse bar and rip in the south/centre of the embayment due to (unseasonal) south south easterly wave power with a sub-dominant easterly component (Figure 5.12 d). The following La Niña winter is also south south easterly, but the absence of an easterly component extends the bar-and-rip morphology of the preceding summer across the whole planform (Figure 5.12 e). A longshore bar eventually forms during the second (La Niña) summer under a north-easterly wave climate (Figure 5.12 f).

The absence of a continuous bar during the first summer to winter affords less storm wave dissipation during CP ENSO. Moreover, the rip cells focus wave energy and correspond to erosion hotspots. South-easterly storms occur more often during winter and La Niña phases in south east Australia (Browning and Goodwin, 2013). Therefore, the embayment is most vulnerable to storm damage during CP La Niña winter, especially if the preceding summer is a CP El Niño pattern. By comparison, the EP ENSO wave climates provide better storm protection for the sub-aerial beach.

Shoreface recovery from storm cut is most rapid when subsequent modal wave direction is similar to the antecedent storm direction. Therefore, the CP ENSO sequence may lead to slower rates of recovery after La Niña winter storms, because the modal wave climate of the following summer is low power and from the north east while storms are south easterly. In contrast, EP La Niña summer is higher power south easterly and better placed to return sand to the surf zone.

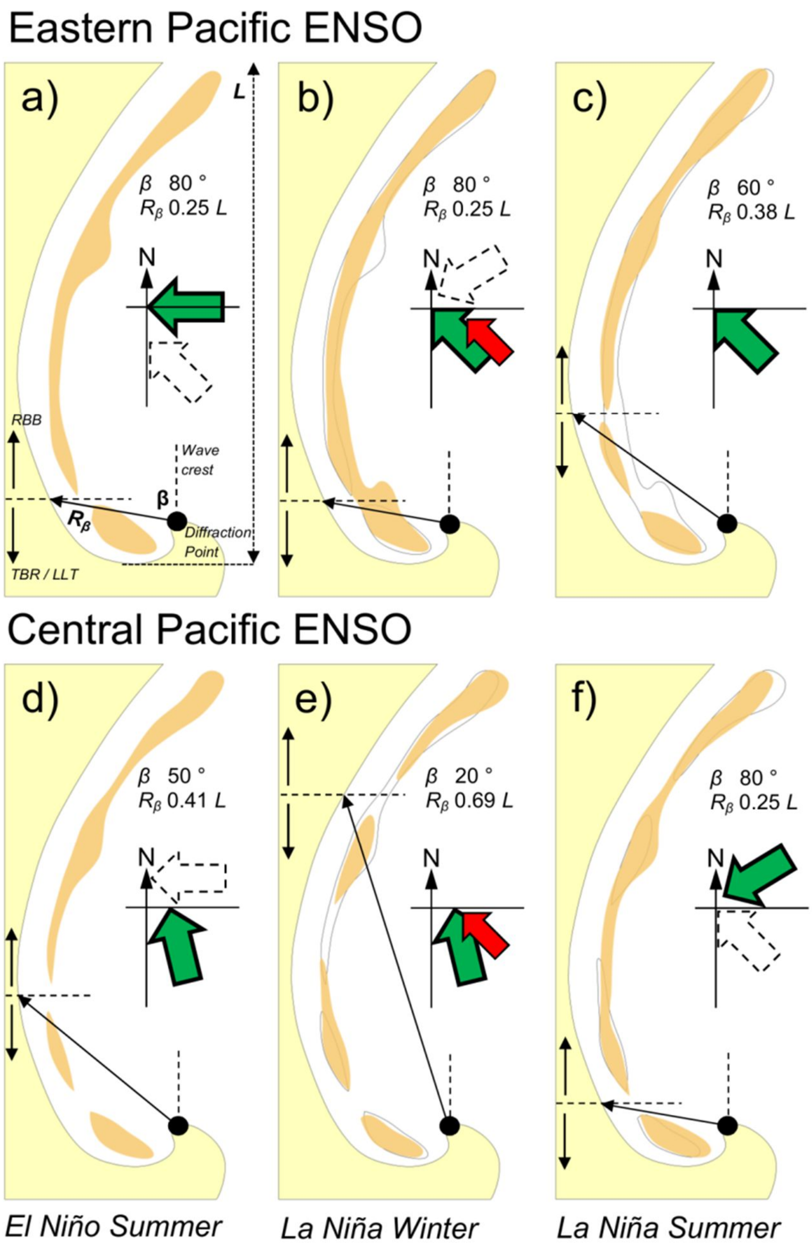

Figure 5.12 Idealised model of surf zone change during a summer-to-summer El Niño/La Niña cycle for EP and CP ENSO climate. Arrows represent wave direction; green (white) arrows indicate direction of (sub) dominant modal wave power (cumulative for season); red arrows indicate mean storm wave direction during La Niña winter. Areas of accretion are shown in orange with the outline of the preceding season's pattern below. Plots also show location of

diffraction point, wave obliquity, β, and control line length, R_β according to change in surf zone morphology from TBR / LLT to RBB. R_β is given relative to compartment length, L.

5.6.6 Modelling Planform Geometry with Long-Term Shifts in ENSO

We suggest that the alongshore variability in surf zone morphology can be used to locate the downcoast control point needed to model a Static Equilibrium Planform. Locating the downcoast control point has always been a major source of uncertainty in applying the Parabolic Bay Shape Equation (PBSE) to determine the SEP (Lausman *et al.*, 2010). We propose that the change from either Low Tide Terrace (LTT) or Transverse Bar and Rip (TBR) to Rhythmic Bar and Beach (RBB) morphology represents the point at which the planform ceases to follows a parabola to where it aligns normal to the wave orthogonal as an equilibrium shoreline response to the persistence of each ENSO wave climate (Figure 5.12). By locating this point the angle of wave obliquity, β, and the control line length, R_β can be found, from which the Parabolic Bay Shape Equation (PBSE) can be solved. Here R_β is expressed in terms of the compartment length, L for the method to be expanded to other compartments in south east Australia.

The change in surf zone morphology represents the point at which nearshore wave power grades from highly diffracted and subsequently refracted (moving away from the headland) to shore normal. The gradation in nearshore wave power in the lee of the headland is essentially the process that governs the development of a parabolic beach shape. Thus, the use of surf zone morphology to define the geometric alignment of the shoreline is appropriate.

This method reduces computationally intense, two-dimensional morphodynamic modelling of the embayment to a one-line expression of the shoreline for each ENSO climate. It also allows the complexity of bi-modal wave conditions (and thus more than one diffraction point) to be incorporated into the equilibrium planform for each ENSO type, which has also been a difficulty when applying the PBSE to real-world wave conditions.

While headland sand bypassing is essentially switched off in this experiment (Section 5.5.6.1), the control line and downdrift control point also represents the bypass strand and re-attachment point, respectively, for the cross-embayment transport of sand where it occurs. This pathway forms the connector between sand transported in the outer surf zone and the down-coast, littoral transport when sand bypasses the headland from an updrift compartment (Goodwin *et al*., 2013).

Results can be scaled up to conceptualise Static Equilibrium Planforms that are representative of the long-term persistence of each ENSO wave climate. An EP El Niño summer wave climate confines the parabolic shoreline to the first quarter of the planform (Figure 5.12 a). This leads to an anti-clockwise rotation of the shoreline in the lee of the headland, while the rest of the planform is flattened under predominantly shore-normal wave conditions. EP La Niña winter-type conditions lead to a similar pattern (Figure 5.12 b), while the persistence of an EP La Niña summer-type wave climate produces a clockwise rotation at both ends of the embayment (Figure 5.12 c).

In comparison, CP El Niño summer and in particular La Niña winter wave conditions lead to a substantial clockwise rotation in the planform (Figure 5.12 d and e). In CP La Niña winter, the parabolic shoreline describes almost 70 % of the embayment length. The CP El Niño summer response is geometrically similar to EP La Niña winter. Conversely, CP La Niña summer wave climate produces an anti-clockwise rotation of the planform (Figure 5.12 f) that is geometrically similar to EP El Niño summer. Therefore, the shoreline response to ENSO wave forcing in an embayed beach is more complex than the simple paradigm that (anti-) clockwise rotation occurs during El Niño (La Niña) for an idealised bathymetry. The complex geometric response is due to real-world shoaling processes, bi-modal wave conditions and the emergence of different flavours of ENSO climate variability.

5.7 CONCLUSIONS

While a link between ENSO, wave climate and coastal behaviour is understood at a reconnaissance level, uncertainties remain as to the coastal responses of CP versus EP ENSO. Using over 20 years of directional and mid-shelf buoy observations, we show that CP ENSO produces significantly different patterns of directional wave power to EP ENSO along the south east Australian shelf, in the south west Pacific, and differences are primarily due to the modulation of easterly, trade-wind generated wave power. The strength of trade-wind wave power is related to the position of the sub-tropical anticyclone which varies between CP and EP ENSO events.

Changes to the nearshore wave climate and coastal morphology are more subtle. Using a wave and morphodynamic model, we show that only CP El Niño summers and EP La Niña winters lead to seasonal changes in the surf zone morphology of a headland-bay beach. The nearshore is more sensitive to changes in east and north-east trade-wind waves than oblique extra-tropical wave conditions. In deep water, the importance of the trade wind wave climate is masked by the persistence of high power extra-tropical wave conditions that have a reduced impact on nearshore processes due to high refraction. As a result, ENSO-related coastal impacts cannot be directly inferred from shifts in offshore wave direction as previously assumed.

The alongshore variability in surf-zone morphology produced by each ENSO climate state can be used as a measure of coastal vulnerability. During an Austral summer-to-summer El Niño/La Niña cycle, a CP ENSO pattern leads to potentially higher storm erosion and slower post-storm recovery than EP ENSO. This is because CP ENSO wave climate is unseasonably oblique before and during the shore-normal La Niña winter storm season. This leads to a bar and rip cell morphology that affords less wave energy dissipation and more energy focussing than during EP ENSO. The following La Niña summer wave climate is significantly more north easterly and low power during CP ENSO than EP ENSO, and slower to return sand to the surf zone.

In addition, it is proposed in this chapter that the alongshore variability in beach morphological type can be used to locate the cross-embayment bypass strand and thus construct static equilibrium planforms for each ENSO phase. This method can be used to resolve two major uncertainties related to the application of the Parabolic Bay Shape Equation; (i) the location of the downcoast control point and; (ii) the incorporation of real-world wave conditions. Results indicate that the shoreline response to ENSO wave forcing in an embayed beach is not as simple as (anti-) clockwise rotation during El Niño (La Niña) as previously suggested, because of shoaling processes, bi-modal wave conditions and the emergence of different flavours of ENSO. On open ocean coastlines in the north and south east Pacific exposed to long-fetch wave climates, the response of coastal geometry to ENSO wave climate flavours may be amplified when compared to our findings for the fetch limited Tasman Sea.

5.8 ACKNOWLEDGEMENTS

The Sydney buoy is funded by Office of Environment and Heritage (OEH) NSW and operated by Manly Hydraulics Laboratory. Data is available from https://www.mhl.nsw.gov.au/DataRequest. The Brisbane buoy is funded by State of Queensland, Department of Science, Information Technology, Innovation and the Arts. Data is available at https://data.qld.gov.au/dataset/coastal-data-system-waves-brisbane. The Wamberal buoy was funded by Australian Research Council (ARC) Linkage Project (grant number LP100200348 to Ian D Goodwin and Ian L Turner), and data is available from the authors. Bathymetries were supplied by OEH NSW and are available on request. The NINO3.4 index was sourced from NOAA Climate Prediction Center; the EMI from the Japan Agency for Marine-Earth Science and Technology; the SAM index from National Environment Research Council, UK. An Educational MIKE by DHI Software License was used. Thanks to Will Hibberd at DHI Gold Coast for technical support.

CHAPTER 6

Curl Curl Beach

STORM WAVES AND CROSS-SHELF TRANSPORT WITH TROPICAL EXPANSION IN SOUTHEAST AUSTRALIA

6 STORM WAVES AND CROSS-SHELF TRANSPORT WITH TROPICAL EXPANSION IN SOUTHEAST AUSTRALIA

6.1 CHAPTER OVERVIEW

Tropical expansion is a potential amplifier of coastal change in the subtropics because of associated changes to storm type frequency. Storm wave climate change has important consequences for nearshore wave power, cross-shelf sediment supply and coastal stability. Most Global Climate Models (GCM) agree that an expansion of the tropics will continue with greenhouse warming, although the magnitude of this expansion is largely under-estimated. This chapter extends the surrogate-observational approach advocated throughout this thesis to the storm wave climate along the south east Australian shelf (SEAS), and investigates scenarios of storm wave climate change with an expanding tropical belt. A discussion of the observed and modelled trends of tropical expansion is given in Section 1.2.4 in Chapter 1.

First, the latitudinal distribution of storm wave types along the SEAS and their refraction patterns across the shoreface are investigated using a hybrid approach of meteorological typing and statistical clustering. The statistical robustness of synoptic storm wave climate typing is assessed. This is followed by a first-pass assessment of potential changes to storm-induced cross-shelf sediment transport with tropical expansion and implications for coastal stability along the SEAS.

6.2 KEY FINDINGS

A continued expansion of the tropics in the south-west Pacific region will lead to a latitudinal shift in storm wave generation and propagation patterns. A 2.5° poleward migration of the sub-tropical ridge (STR) (as projected in some GCMs) may result in the SEAS experiencing more frequent north-easterly generated and shore-normal storm waves, and less frequent southerly generated and shore-oblique storm waves. This study finds that a poleward migration in the STR may cause: an increase in average storm wave power associated with Easterly Trough Lows (ETL) becoming the most frequent storm type; an anticlockwise shift of the coastal planform, together with a reduction in headland bypassing; and a greater cross-shelf sand transport component. Shorelines in the lee of southern headlands will be most vulnerable to changes in the storm wave climate with tropical expansion, especially those located on the Mid-North and North Coasts of New South Wales (NSW). This is because of increased exposure and storm cut during ETL events, and reduced headland bypassing required for shoreline stability as oblique, extra-tropical storm events become less frequent.

6.3 PUBLICATION AND AUTHOR CONTRIBUTION

Some of this chapter has been submitted for publication in: Goodwin, I.D., **Mortlock, T.R.**, Browning, S., Shand, T. (in review). Contrasting Tropical and Extratropical-Origin Storm Wave Types, Their Propagation on the Inner Shelf and Influence on the East Australian Longshore Sand Transport System. *Journal of Geophysical Research: Oceans*.

As second author, I carried out the majority of data analysis and made a significant contribution to writing the paper and interpretation of results. Only sections of the paper for which I was the lead contributor are included in this chapter, plus additional material which is my sole work that was not part of the paper. The only elements of this chapter which were not produced by me are some sections of the introduction, which were written by IDG, and Figure 6.10 a, which was generated by SB. The synoptic typing of storm events was undertaken by IDG and SB as part of Shand *et al*. (2011).

6.4 INTRODUCTION

Extreme storm waves are an important driver of coastal stability, and can be hazardous to offshore and coastal infrastructure. Studies have shown that storm wave heights have been increasing in the North Pacific (Komar and Allan, 2008; Ruggiero *et* *al*., 2010; Bromirski *et al*., 2013), North Atlantic (Wang *et al*., 2012; Bertin *et al*., 2013, Bromirski and Cayan, 2015), and the Southern Ocean (Young, 1999; Hemer, 2010) in association with a shift towards strengthening extratropical wind fields (Cai *et al*., 2005; Thompson and Solomon, 2002).

Whilst there is increasing attention towards the projection of future storm wave climates and extreme values globally under a changing climate (Ruggiero *et al*., 2010; Hemer *et al*., 2013; Dowdy *et al*., 2014), a major unknown is whether the poleward expanding tropics (Seidel *et al*., 2008) will be associated with a shift in the relative frequency and magnitude of tropical or extratropical storm waves. Most Global Climate Models (GCM) agree that an expansion of the tropics will continue with greenhouse warming, although the magnitude of this expansion is largely under-estimated (Lucas *et al*., 2014). A first-order impact is wave climate and coastal response in the sub-tropics.

Changes to storm type frequency with tropical expansion have important consequences for the nearshore propagation of wave power and cross-shelf sediment transport. While storm events usually have a net-destructive effect on the sub-aerial beach and lead to shoreline recession at the event-scale, they also move sediment to the upper shoreface from deeper water that is otherwise out of reach during less energetic, modal wave conditions. The cross-shelf delivery of sediment during extreme wave events ultimately facilitates the process of beach recovery from previous storm events, and acts to balance the seasonal sediment budget. Because onshore sediment transport on continental shelves is highly episodic (Harris and Wilberg, 2002), changes to the storm wave climate with climate change are thus critical to determining long-term shoreline stability with sea-level rise (assuming an adequate shelf sediment supply).

Recent studies projecting storm wave climate change for the coming century have grouped all storm wave events into either Tropical Cyclones or East Coast Cyclones (Hemer *et al*., 2013; Dowdy *et al*., 2014). Since these storms evolve from a complex interaction of tropical and extratropical drivers, it is important to differentiate between storm types based either on their synoptic genesis, or by a statistical evaluation of observed storm wave parameters. This way, scenarios of future storm wave climate dominated by either tropical or extratropical origin storm types can be investigated.

In the south-west Pacific region, extreme waves are generated from either: (i) poleward-moving tropical cyclones in the Coral Sea; (ii) in the Tasman Sea from East Coast Cyclones (ECC) of both subtropical and extratropical origin; or, (iii) in the Southern Tasman Sea by extratropical lows cut-off from the circumpolar trough (Browning and Goodwin, 2013). Shand *et al*. (2011) further identified eight different storm types along the Southeast Australian Shelf (SEAS) based on the synoptic genesis of the storm, storm track and the synoptic pattern at the time of the observed peak storm wave conditions (Table 6.1). The approximate location of wave genesis in the Tasman Sea for these storm types is illustrated in Figure 4.1 (Chapter 4).

Table 6.1 Storm type definitions along the SEAS (from Shand *et al*., 2011). Abbreviations of storm types are used throughout this chapter.

Abbreviation	Full Name	Storm Description
TC	Tropical Cyclone	Swell related to named Tropical Cyclones forming in the Coral Sea between 5-10° latitude.
TL	Tropical Low	Low pressure systems forming in the Coral Sea but not reaching the low pressure intensity of a named tropical cyclone
ACI	Anti-Cyclone Intensification	Form when a high across the Tasman Sea directs onshore E to SE winds to the coast
ETL	Easterly Trough Low	Cyclonic depressions generated primarily along the central NSW coast between 25° and 40° latitude
ITL	Inland Trough Low	Originate in the quasi-permanent low pressure trough over inland Qld, their movement to the east coast is often associated with STL
CL	Continental Low	Storms originating in Western Australia of the Great Australian Bight and moving overland, often re-intensify upon crossing the east coast
SSL	Southern Secondary Low	Form as a secondary cut off extratropical low in the Southern Tasman sea
STL	Southern Tasman Low	Major lows in the Southern Ocean south of 38°S

In this study, the extreme wave event database compiled by Shand *et al*. (2011) is used to investigate the distribution of storm types along the SEAS, and their refraction patterns across the shoreface. In addition, the meteorological-based storm type groupings are re-classified based on a statistical assessment of the wave parametric data rather than their synoptic genesis. The implications of a changing storm wave climate with tropical expansion are then assessed in terms of nearshore wave power, cross-shelf sediment supply and coastal stability.

Results from this study can be applied to either reanalyzed climate data, or synoptically downscaled GCM output, to improve the understanding of probable future trends in the storm wave types and coastal impacts. Findings are relevant for other Southern Hemisphere east coasts in South America and Africa, and Northern Hemisphere west coasts in North America and Europe with similar mid-shelf wave climate and sediment transport regimes in the sub-tropics.

6.5 METHODS

6.5.1 Instrumental Wave Data

Along the SEAS, instrumental wave data have been collected since the mid-1970s when the New South Wales (NSW) and Queensland (QLD) Governments commenced wave monitoring. Long-term, continuous and directional wave data are available for mid-shelf locations at (north to south) Byron Bay, Coffs Harbour, Crowdy Head, Sydney, Port Kembla, Batemans Bay and Eden (Figure 6.1).

In addition, Sydney Ports Corporation has maintained a wave buoy offshore of Botany Bay since 1971. Further north, the Queensland Department of Science, Information Technology, Innovation and the Arts (DSITIA) maintains a network of 12 wave buoys along the QLD coastline. A wave buoy located offshore of Brisbane (Point Lookout on North Stradbroke Island) since 1976 improves the evaluation of subtropical wave climate in far north NSW, and is used in this study. Table 6.2 shows the length of directional and non-directional wave observations for each buoy used in this study (after Kulmar *et al*., 2013).

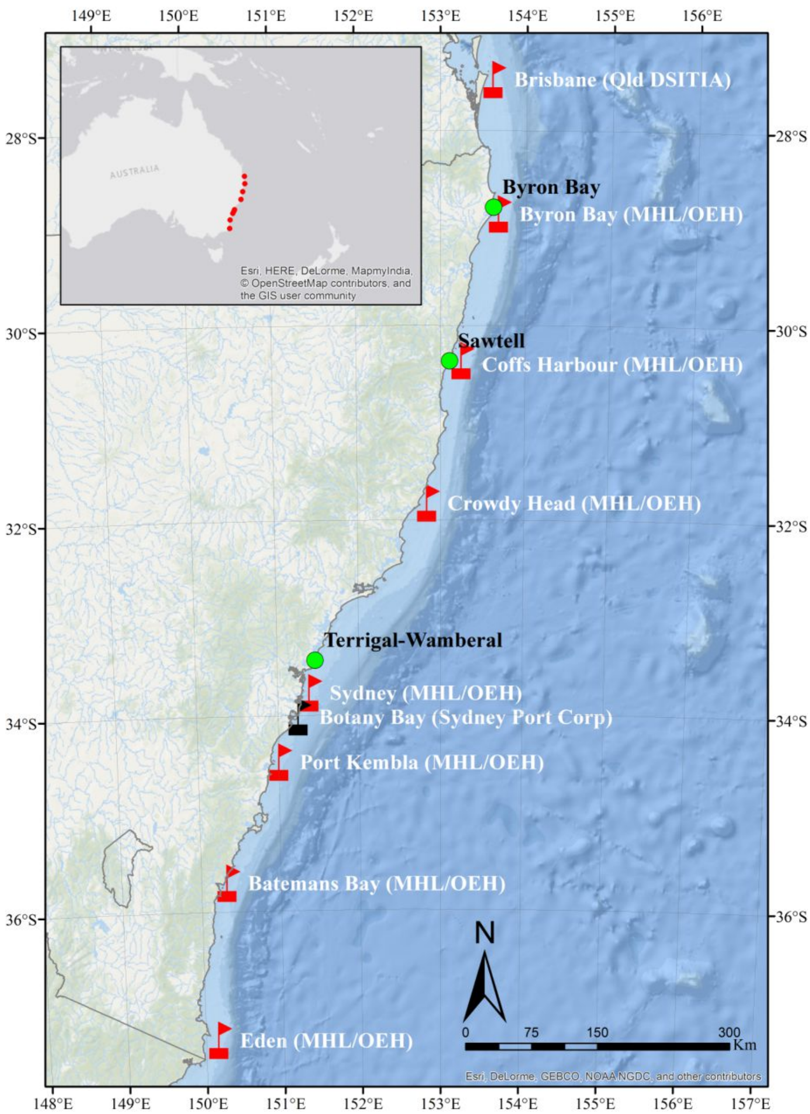

Figure 6.1 Location of mid-shelf wave buoys and study sites. Red symbols indicate a part-directional wave buoy record that was used in this study, black symbols indicate a non-directional record. Study site locations are denoted by green circles.

Table 6.2 Directional and non-directional buoy record used in this study. Water depths reflect current moored position.

Wave Station (N to S)	Latitude (dec. dgs)	Water Depth (m)	Date Site Commissioned	Directional Buoy Deployed
Brisbane	- 27.48	70	31-Oct-1976	20-Jan-1997
Byron Bay	- 28.85	62	14-Oct-1976	26-Oct-1999
Coffs Harbour	- 30.35	72	26-May-1976	14-Feb-2012
Crowdy Head	- 31.81	79	10-Oct-1985	19-Aug-2011

Sydney	- 33.77	92	17-Jul-1987	03-Mar-1992
Botany Bay	- 34.04	75	08-Apr-1971	14-Jan-2015
Port Kembla	- 34.47	80	07-Feb-1974	20-Jun-2012
Batemans Bay	- 35.70	73	27-May-1986	23-Feb-2001
Eden	- 37.30	100	08-Feb-1978	16-Dec-2011

This dataset provides observational coverage of approximately 1,000 km of mid-shelf waves (60 – 100 m depth), along the western boundary of the Tasman and Coral Seas from 27 to 37° S. All buoys measure hourly wave spectra, from which timeseries parametric data is derived. In this study, the 1-hourly significant wave height, H_s (m), wave period at the primary spectral peak, T_p (s), and mean wave direction, *MWD* (degrees True North, ° TN) are used to describe storm wave characteristics. Although most modal wave conditions are likely to be deep-water waves at the buoy locations (where water depth is greater than half the wavelength, $d > L/2$), this condition is not always satisfied for storm waves travelling at periods of 10 s or more. This study therefore deals with a mid-shelf, intermediate-to-deepwater storm wave climatology.

6.5.2 Extreme Value Analysis

An extreme value analysis of this instrumental wave data archive (start of record to December, 2009) was reported in Shand *et al.* (2011) and the database was made available for this study. A Peak over Threshold (PoT) analysis was undertaken to define storm events for 1-hourly significant wave height, H_s, of greater than 2.0 m (approximate to the 10% exceedance wave height along the NSW/QLD coast) with a minimum exceedance duration of three days. A second higher threshold of 3.0 m (5% exceedance threshold) with no minimum duration was also used to capture intense but transient storms (e.g. tropical cyclones). A minimum interval between storms was set at one day to prevent single storms being split into two or more events if wave height temporarily drops below the threshold. The storm event frequency returned using these values was tested in Chapter 5 and found to give a statistically robust split between storm and modal wave conditions.

The length of this wave data spanning ~40 years is considered appropriate for the study of extreme waves, as it is sampled from both phases of the IPO that has been previously shown to influence the SEAS wave climate (Goodwin, 2005).

6.5.3 Synthesis of Storm Wave Parameters

Average storm-peak parameters H_s, T_p and *MWD* for each storm type were determined using the database of Shand *et al*. (2011) (Table 6.3).

Table 6.3 Average offshore storm-peak parameters, wave base and mean frequency of occurrence for the four most frequent storm types in central, mid-north and north coast NSW.

Storm Type	Average Storm Peak H_s (m)	Average Storm Peak T_p (s)	Average Storm Peak *Dir* (°)	Wave Base for Storm Peak H_s (m)
Sydney / Port Kembla				
STL (36 %)	3.8	11.1	172	96
SSL (28 %)	4.3	11.0	170	95
ITL (18 %)	4.2	10.4	157	85
ETL (7 %)	5.3	11.8	153	109
Coffs Harbour				
ITL (25 %)	4.1	10.5	142	86
ETL (23 %)	4.6	11.5	116	103
SSL (21 %)	3.9	11.1	149	96
STL (14%)	3.6	11.3	161	100
Byron Bay				
SSL (26 %)	3.8	11.1	167	96
AI (23 %)	3.4	9.5	139	71
ITL (15 %)	3.9	10.4	156	85
ETL (12 %)	4.3	10.6	115	88

For the Central Coast NSW, average storm peak H_s and T_p parameters were derived from storm events identified from the Sydney and Port Kembla buoy records (1974 – 2009), and *MWD* from the available (1992 - 2009) directional Sydney record. For the Mid North Coast NSW, average storm peak H_s and T_p were derived from storm events identified from the Coffs Harbour buoy record (non-directional 1976 - 2009), and *MWD* was hindcast from the directional portion of the Byron Bay record (2000 - 2009) (method Section 6.5.4). For the North Coast NSW, average storm peak parameters were derived from the Byron Bay buoy (non-directional from 1977, directional from 2000), except for ETLs where the peak storm wave direction was determined from the

Brisbane buoy record. This was because observed ETLs are understood to be under-sampled at Byron Bay due to issues of buoy submergence during early deployments (Shand *et al.,* 2011). The number of ETLs recorded at Brisbane and Byron Bay is comparable between sites.

6.5.4 Storm Wave Direction Hindcast

Since the Coffs Harbour buoy only became directional in 2012, no directional information for storm types was available in the original Shand *et al.* (2011) report, which was concluded in 2009. Instead the directional portion of the Byron Bay buoy record, 190 km north of Coffs Harbour, was used to hindcast *MWD* for storms back to 2000 at Coffs Harbour. The Byron Bay buoy is the nearest mid-shelf buoy with an interannual directional record.

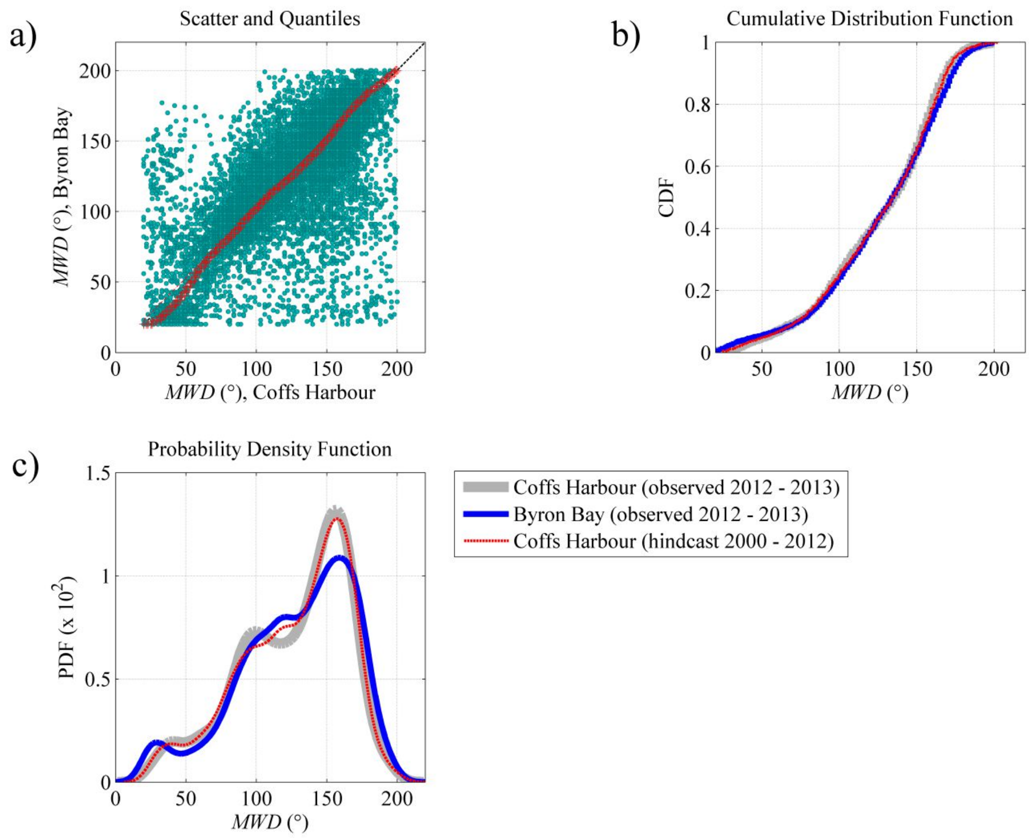

Figure 6.2 *MWD* hindcast at Coffs Harbour by CDF matching using *MWD* at Byron Bay; a) hourly observations of *MWD* (green) and quantiles (red) at Coffs Harbour and Byron Bay (Feb 2012 – Dec 2013), b) cumulative distribution and c) probability density of *MWD* observed at Coffs Harbour and Byron Bay, and resultant hindcast at Coffs Harbour for 2000 – 2012.

A cumulative distribution function (CDF) matching approach (Brocca *et al.*, 2011) was used (as in Chapter 5) between the overlapping directional records at Byron Bay and Coffs Harbour (February 2012 – December 2013), giving a training dataset of over 12,000 hourly observations (Figure 6.2). Only wave directions between 20 and 200 ° (i.e. onshore-propagating energy) were used to train the model. Although *MWD* is broadly comparable between the two sites (Figure 6.2 a), bias-adjustment using a 5th-order polynomial function was found to better describe the *MWD* distribution, especially the peaks around 40 and 150° characteristic of the Coffs Harbour record (Figure 6.2 c). Once *MWD* was hindcast for the non-directional portion of the Coffs Harbour record (back to 2000), average peak-storm *MWD* for each storm type could be determined (Table 6.3).

6.5.5 Modelling Storm Wave Shoreface Refraction Patterns

A MIKE21 Spectral Wave (SW) model was used to transform offshore peak storm wave parameters of the four most frequent storm types (Table 6.3) to three characteristic coastal compartments: (i) Central Coast NSW (Terrigal-Wamberal Beach); Mid North Coast NSW (Sawtell Beach); and, (iii) North Coast NSW (Byron Bay) (locations Figures 6.1 and 6.3).

MIKE21 SW is a third-generation, phase-averaged spectral wind-wave model that computes random, short-crested wind-waves in coastal and inland regions (DHI, 2014). In this instance, the model solves the wave action conservation equation using a directional decoupled parametric formulation. A JONSWAP spectrum was used to propagate spectral information through the model domain based on boundary parameters of peak storm H_s, T_p and *MWD* for each storm type. A directional spreading function equivalent to approximately 20 ° of spreading was used to replicate a mixed sea-swell environment characteristic of storm wave conditions. The seabed topography was described using a mosaic of best-available bathymetries from the depth of offshore buoys (~ 90 m) to the shoreline. Where no localised bathymetries were available, gaps were filled using the GeoScience Australia AusBathy grid (Whiteway, 2009). Information on model configuration, bathymetries used and nearshore validation is provided in Section 1.4.3 in Chapter 1.

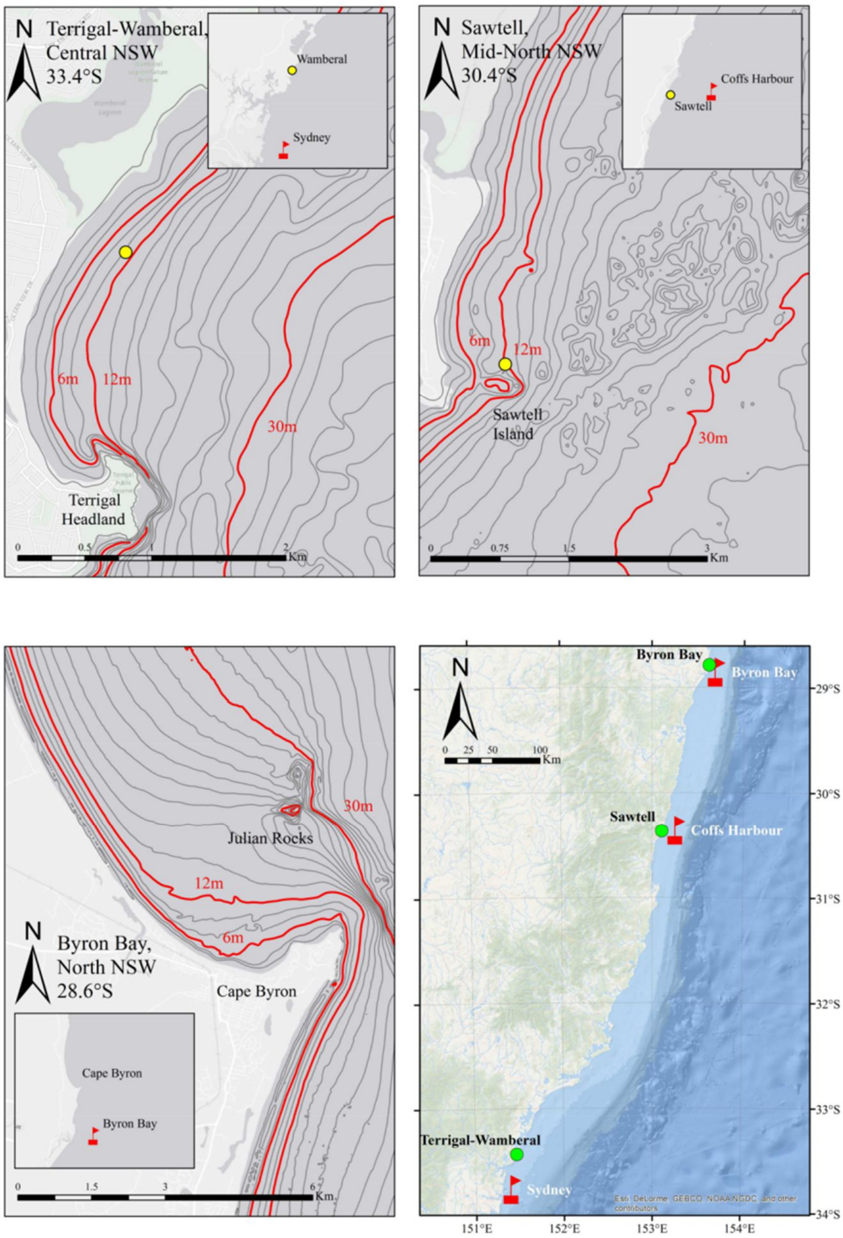

Figure 6.3 Sites for refraction modelling of storm types and regional map. 2 m spaced bathymetry from 0 m contour shown. Yellow circles (red flags) indicate nearshore (offshore) buoy locations. A variable scale is used between sites due to differences in alongshore compartment length. The 6, 12 and 30 m contours are highlighted at each site to denote the approximate seaward extent of the surf zone, upper/lower shoreface and lower shoreface/inner shelf boundary. Study sites are denoted as green circles in regional map.

6.5.6 Modelling Storm-Induced Sediment Transport on the Shoreface

Patterns of sediment mobilisation on the shoreface during SSL and ETL storm types were calculated at Terrigal-Wamberal and Byron Bay to demonstrate potential impacts of changes to the storm wave climate with tropical expansion. A first pass approach was used, based on the modelled wave refraction patterns of peak storm wave conditions for each storm type (Section 6.5.5). Airy wave theory was used to calculate wavelength (λ) and bottom wave orbital velocity (U_b) from the surface wave parameters H_s and T_p retrieved from MIKE 21 SW at each grid point in the model domain:

$$\lambda = \left(gT_p^{\,2}/2\pi\right)\tanh\left(2\pi d/\lambda\right) \tag{6.1}$$

$$U_b = \pi H_s \Big/ \left[T_p \sinh\left(2\pi d/\lambda\right)\right] \tag{6.2}$$

where g is the acceleration due to gravity and d is water depth. Wavelength was calculated iteratively using the Newson-Raphson routine. While the choice of wave height parameter makes a substantial difference to the overall pattern of sediment mobilization (Griffin *et al.*, 2008), H_s is used here because under a Rayleigh distribution it is only exceeded 1% of the time (see Section 1.2.1.3, Chapter 1) and therefore a robust indicator of storm conditions.

The initiation of sediment motion can be calculated (as a short-cut to calculating skin-friction shear stress) by the exceedance of a critical bottom velocity (U_{cr}). This method has been used by other authors (Porter-Smith *et al.*, 2004; Griffin *et al.*, 2008) as a first pass to investigate patterns of sediment entrainment (sediment is entrained when $U_b > U_{cr}$). Griffin *et al.* (2008) shows this rapid approach compares well (within 10%) with the more complex skin-friction shear stress method on the SEAS. For spherical, cohesionless quartz grains U_{cr} is given after Clifton and Dingler (1984):

$$U_{cr} = 0.337\left(g^2 T_p D_s\right)^{0.33} \tag{6.3}$$

for grain sizes, D_s, < 0.5 mm. In this study, a single D_s value (0.19 mm) is used after Stephens and Roy (unpublished Geological Survey of NSW report, 1980), who show outer nearshore deposits are composed of quartz sands of this grain size across the central to north NSW shelf (Stephens and Roy, unpublished Geological Survey of NSW report, 1980). As such, cross-shore changes in sediment characteristics are not considered here.

6.6 RESULTS AND DISCUSSION (1) – STORM TYPE DISTRIBUTION AND SHOREFACE REFRACTION PATTERNS

6.6.1 Latitudinal Gradients in Storm Types

Figure 6.4 a shows the latitudinal distribution of storm type occurrence across all buoy records. North of 31.5° S latitude (Crowdy Head, Coffs Harbour, Byron Bay and Brisbane buoys) over 50% of storm variance is described by AIs (23%), SSLs (19%) and ITs (16%). Storms observed at the northern buoys tend to exhibit longer durations, with mean storm duration at Brisbane of 90 hours and mean durations of over 70 hours for Byron Bay, Coffs Harbour and Crowdy Head.

On the central coast NSW from 32° S to 34° S (Sydney/Botany Bay and Port Kembla buoys) the most frequent storm types are STLs (33%) and SSLs (28%). The central coast is subject to the highest number (~24) of storm events per year as well as the largest mean and maximum storm peak height, both of which were associated with ETLs.

South of 34° S (Batemans Bay and Eden buoys) the most frequent storm waves are generated by STLs (39%) and ITs (25%). Storm wave events at these latitudes exhibit mean durations under 70 hours, with Batemans Bay having a mean storm duration of 57 hours. The STLs produce mid-shelf waves in excess of 5 m but not reaching 6 m, and longer period oblique swell along the central and northern NSW coasts. The Batemans Bay buoy record is sheltered from the most southerly storm directions due to a local indentation of the coastline and consequent wave shadowing (Coughlan *et al.*, 2011). The occurrence of each storm type was regressed against buoy latitude to examine statistical significance of latitudinal gradients in storm type occurrence. Those storm types that had a significant ($p \leq 0.02$) latitudinal (north to south) gradient in occurrence include AI (decrease), ETL (decrease), TC (decrease) and STL (increase).

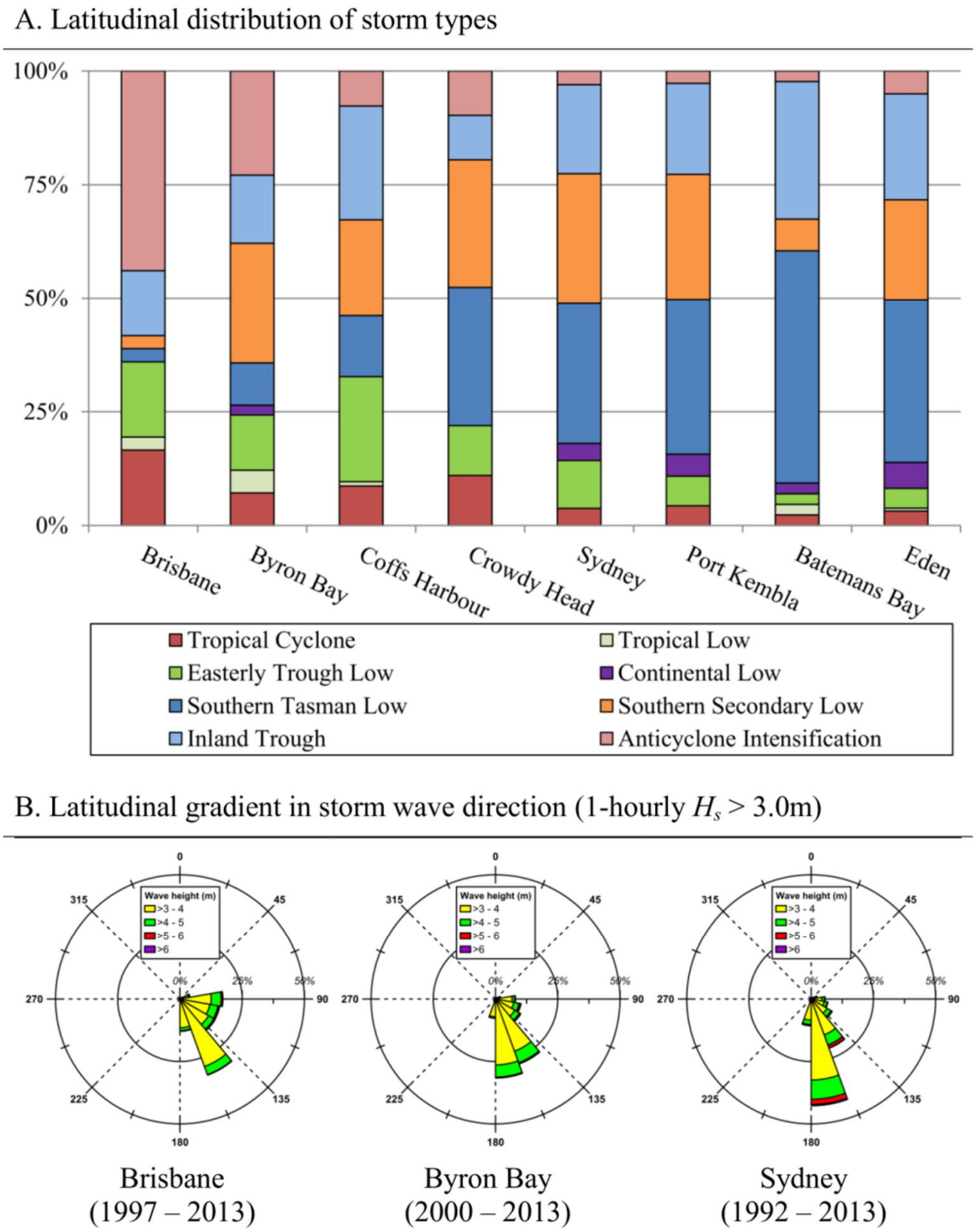

Figure 6.4 Latitudinal (a) distribution of storm types and (b) gradient in storm wave direction (for (a), Sydney includes Botany Bay buoy record).

Figure 6.4 b illustrates the latitudinal gradient in storm wave direction for those buoys with a suitable directional record (Brisbane, Byron Bay and Sydney buoys). The Batemans Bay buoy has also been directional since 2001, but is not comparable to the exposed locations of the other directional records, as previously discussed. Mean storm wave direction is 129 ° at Brisbane 147 ° at Byron Bay and 153 ° at Sydney, thus rotating clockwise with latitude south. While a significant south-east component is visible at all three buoys, Sydney receives the largest storm waves from the south-south-east and Brisbane from the east-north-east, reflecting the proximity to different storm wave genesis (i.e. from Figure 6.4 a, storm wave genesis of AIs, TCs and ETLs is most proximal at Brisbane, and STLs and SSLs are most proximal at Sydney).

6.6.2 Statistical Evaluation of Synoptic Storm Type Classification

The storm wave classification of Shand *et al* (2011) discretised East Coast Low storms into eight different types based on the analysis of the meteorological evolution of each storm event in the buoy record (Table 6.1). While this approach is useful for a climatological analysis of extreme wave events, it does not provide a range of statistically discrete surface wave parameters which is necessary for modelling storm-induced cross-shelf transport.

To address this, the joint probability density functions (JPDF) of peak storm H_s and T_p (Figure 6.5) and peak storm H_s and storm duration (Figure 6.6) were estimated for each storm type. The probability density of joint occurrence is illustrated in the form of contours produced from binning observations into bivariate histograms. Probability densities were estimated using bivariate Gaussian kernel densities implemented in Matlab by Cao (2008). Bins sizes are based on the optimization method of Bowman and Azzalini (1997), approximate to $\Delta H_s \approx 0.01$ m and $\Delta T_p \approx 0.10$ s. Contours represent every 20% increment in probability density.

The latitudinal gradient in bivariate distributions for each storm type were examined by splitting the analysis first using data from all NSW buoys (Figures 6.5 a and 6.6 a), then north NSW (Byron Bay, Coffs Harbour, Crowdy Head) (Figures 6.5 b and 6.6 b), central NSW (Sydney, Botany Bay, Port Kembla) (Figures 6.5 c and 6.6 c) and south NSW (Batemans Bay, Eden) buoy groupings (Figures 6.5 d and 6.6 d). The Brisbane buoy record was not used because it is open to a distinctly different wave climate from the Coral Sea and Equatorial Pacific, after the coastline trends NW north of Cape Byron (Chapter 4). The analysis was not extended to include *MWD* for each storm type because there was insufficient directional data from enough buoys to enable a statistically robust analysis.

Figures 6.5 and 6.6 show that when the meteorological discrimination of storm events is removed (i.e. storm type distributions are amalgamated from all buoy records), the storm types identified by Shand *et al*. (2011) can be combined to form five discrete groups based on joint distributions of peak storm H_s, peak storm T_p, and storm duration. These groups are (i) STL/SSL/CL, (ii) ITL, (iii) ETL, (iv) AI, and (v) TC and TL. STL/SSL/CLs can all be described with centroid values of 3-4 m peak storm H_s, 8-11 s T_p, and 20-60 hour duration; ITLs, 3-4.5 m, 9-10.5 s, and 20-60 hours; ETLs, 4-6.5 m, 10-12 s, and 20-120 hours;. AIs, 3-3.5 m, 8.5-9.5 s, and 20-60 hours; and TC and TLs, 3.5-4 m, 9-11 s, and 30-90 hours.

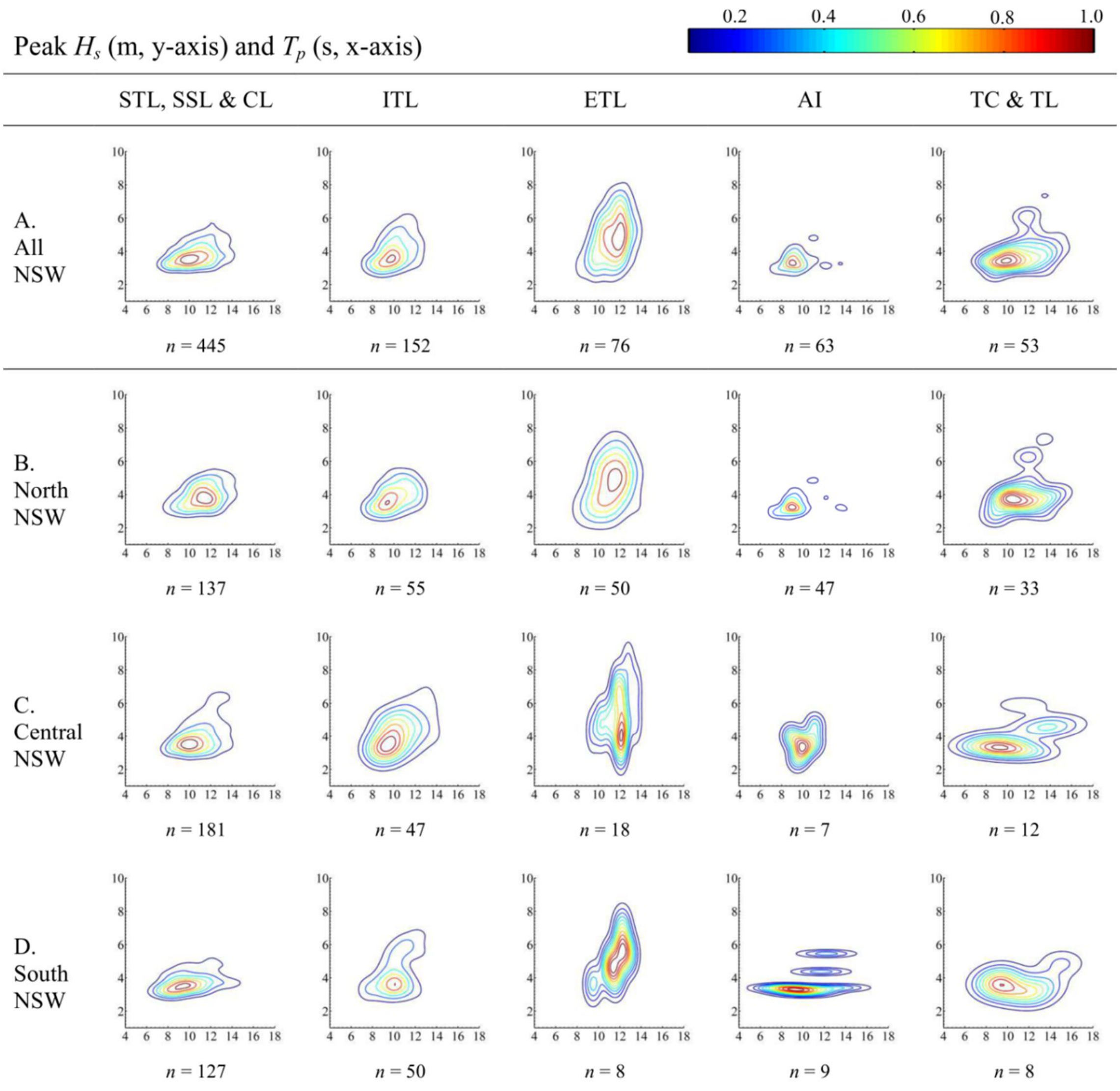

Figure 6.5 Bivariate distributions of peak storm H_s and peak storm T_p for five discrete storm groups. Probability density is represented by contour colours. The number of observations for

each synoptic group, *n*, is given. There were no TLs recorded for Central NSW, therefore 'TL & TC' group in this case only represents the distribution of TCs.

The highest peak wave heights of 7-8 m and periods of 11-13 s are produced by the ETL type. ETL storms also produce up to twice the storm duration at significantly higher peak storm wave heights, than all other storm types. The longer duration of ETL storm waves is associated with a slow-moving long-wave atmospheric circulation during the storm's transition from the tropics to extra-tropics.

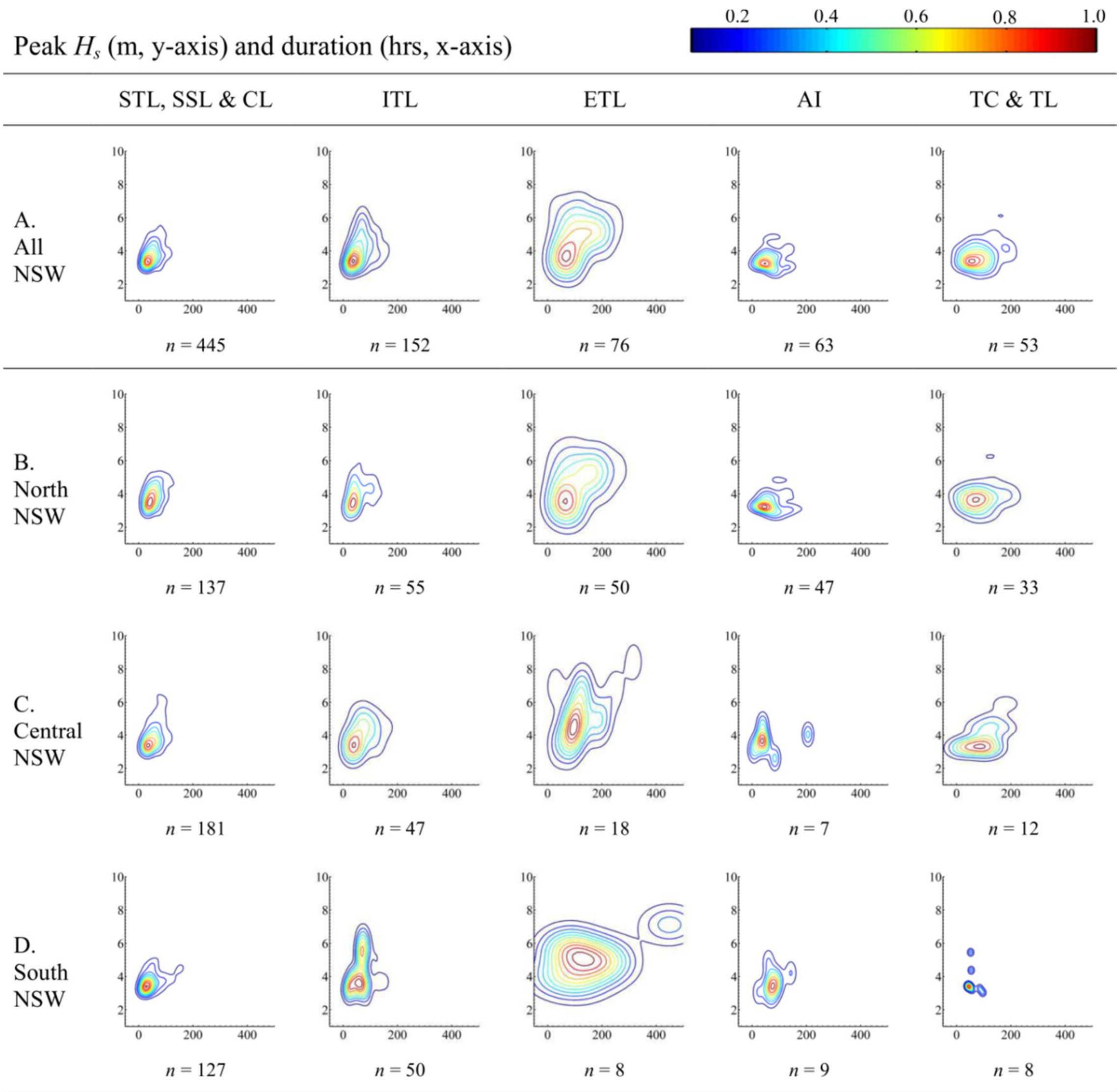

Figure 6.6 Bivariate distributions of peak storm H_s and storm duration.

6.6.3 Patterns of Storm Wave Power on the Shoreface

Numerical wave transformation modelling of the four most commonly-occurring storm types was conducted on the central, mid-north and north coast of NSW (where the greatest range of storm wave directional variability occurs). Figures 6.7 to 6.9 show the pattern of directional wave power for each storm type at Terrigal-Wamberal (Central Coast NSW), Sawtell (Mid North Coast NSW) and Byron Bay (North Coast NSW) when offshore peak-storm wave parameters for the four most frequent storm types at each location (Table 6.3) were refracted across the shelf.

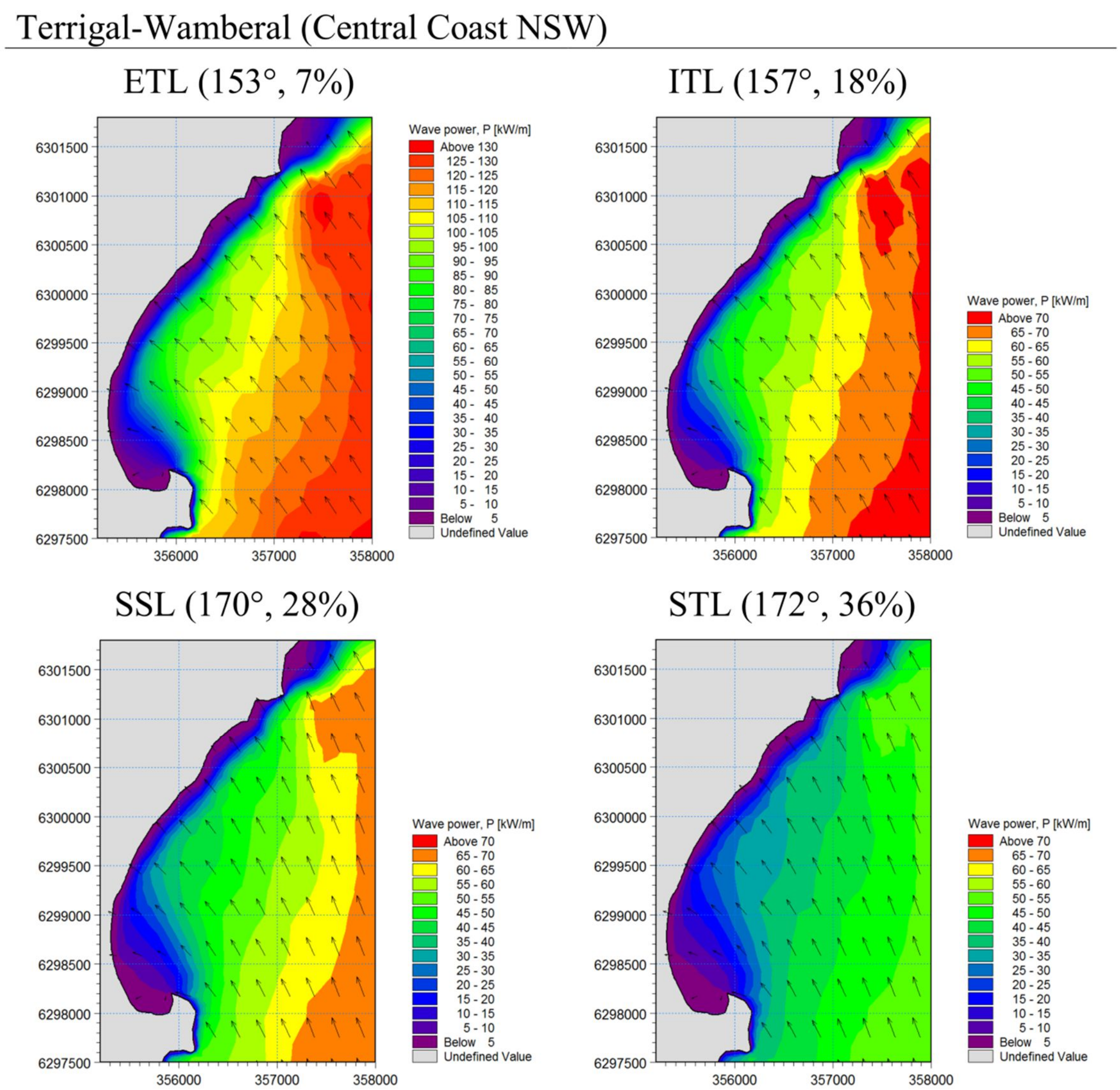

Figure 6.7 Refraction patterns for the four most commonly-occurring storm types at Terrigal-Wamberal, showing gradients in P_0 and vectors of *MWD*. The average peak-storm *MWD*

(offshore) and mean percentage occurrence of each storm type is shown. Storm types are ordered following a clockwise rotation of *MWD* (top left to bottom right).

At each location, the four most frequent storm types describe over 75% of the variability in the storm wave climate, after which the storm type sample size drops considerably. ETLs, ITLs, SSLs and STLs are the most common storm types along the SEAS, apart from on the North Coast NSW (Byron Bay) where AIs replace STLs. The replacement of STLs for AIs at Byron Bay reflects the closer proximity to AI storm wave generation on the north coast.

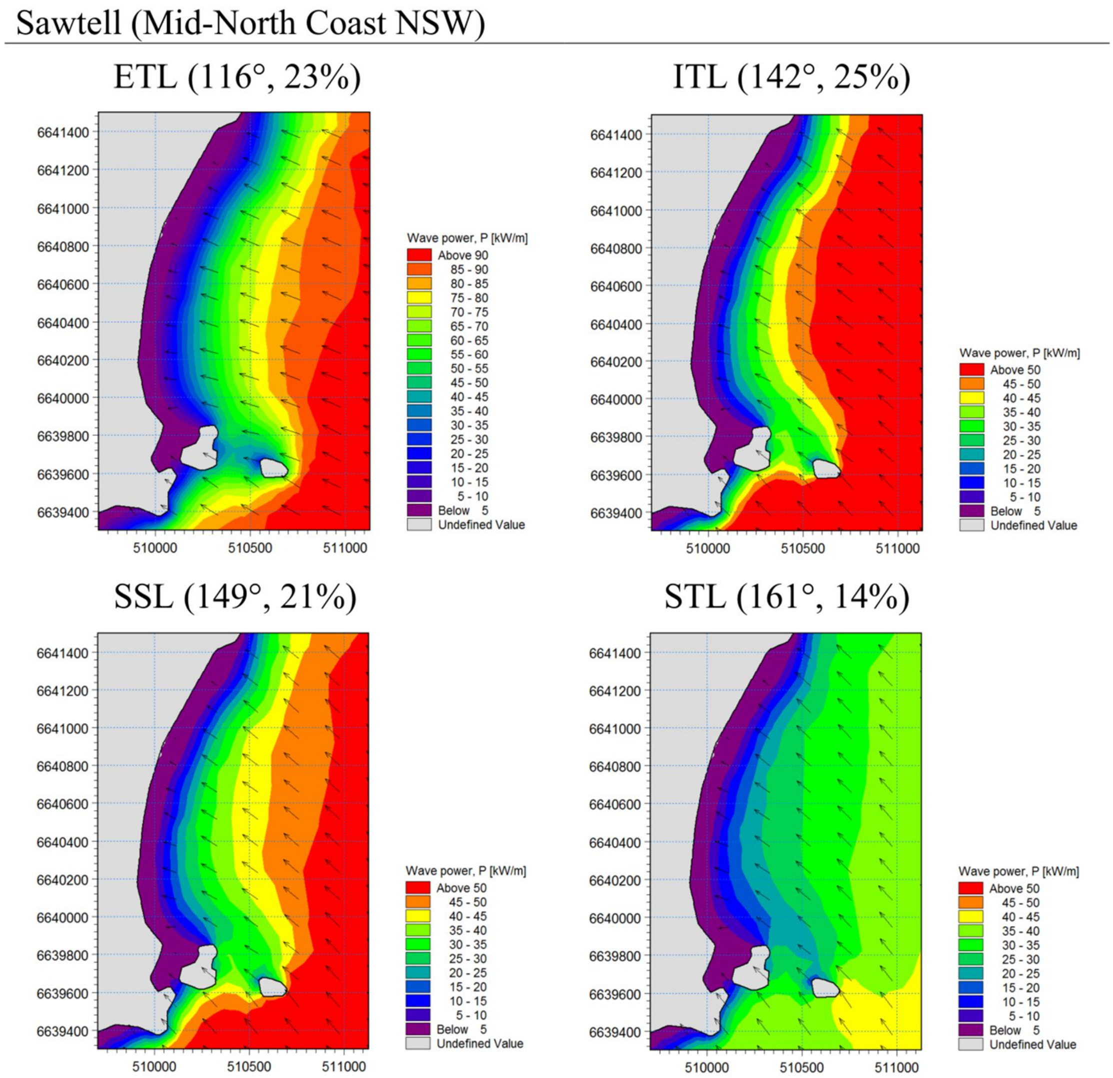

Figure 6.8 Refraction patterns for the four most commonly-occurring storm types at Sawtell.

Average peak-storm wave parameters in Table 6.3 show that for each storm type, offshore H_s decreases with a clockwise rotation in the *MWD*. Since the buoys are mid-shelf, high energy storm waves are already partially refracted before reaching the buoy locations; therefore, most wave energy dissipation occurs during oblique storm wave conditions. ETLs are the most powerful storm type across the shoreface at all sites, due to the highest offshore wave height and most shore-normal wave direction.

Because of the southerly wave generation of the most common storm types along the SEAS, there is a south-to-north latitudinal wave power gradient on the shoreface (Figures 6.7 to 6.9). The Central Coast NSW receives more shoreface wave power from all storm types than on the Mid North and North Coast.

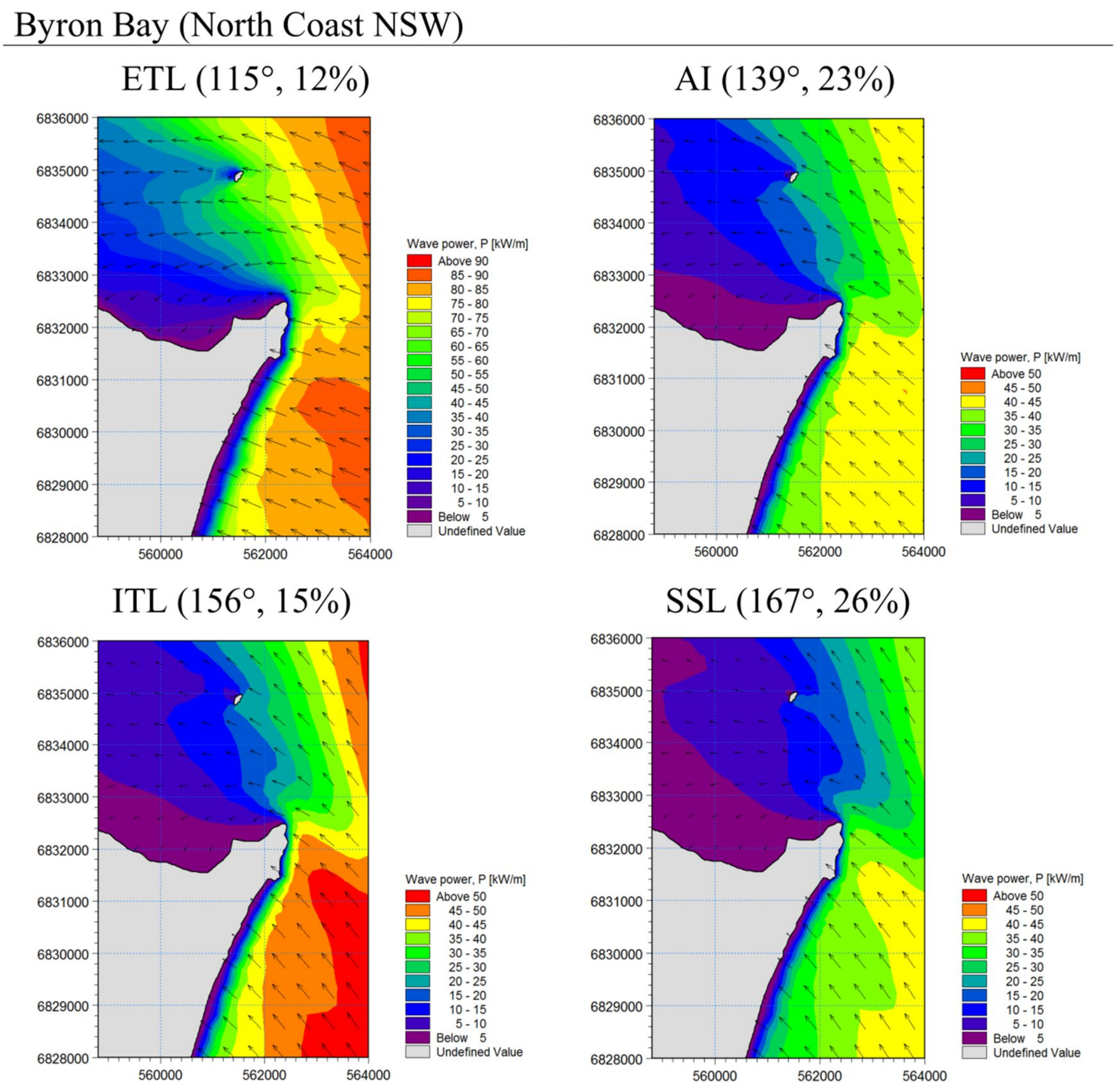

Figure 6.9 Refraction patterns for the four most commonly-occurring storm types at Byron Bay.

The difference in refraction patterns between sites is also a function of shoreface slope and aspect at each location (as can be seen in Figure 6.3). The mean upper (lower) shoreface slope and aspect at Wamberal is approximately 2.2% (1.4%) and SE, at Sawtell and Byron Bay is 1.9% (0.6%) and ESE and NE, respectively. A steeper, narrower shoreface, and planform orientation towards the mean storm wave direction at Wamberal, combined with the proximity to southerly storm wave generation, increases the exposure to high nearshore storm wave power especially at the northern end of the embayment. A shadowing effect from Terrigal Headland is evident under all storm types (Figure 6.7) which extends north with increasing wave obliquity (greatest during STLs).

Despite having a wider and shallower shoreface, high (> 90 kW/m for ETLs) storm wave power still propagates to the upper shoreface at Sawtell. This is because the embayment is oriented towards the mean storm wave direction which is more easterly in the Coffs Harbour region than at Sydney. Lower wave obliquity and less energy dissipation leads to a high power nearshore environment especially during ETLs. A localised shadowing effect by Sawtell Island can be seen under all storm types (Figure 6.8), most pronounced during STLs, but not as prominent as at Wamberal, due to reduced wave obliquity.

The pattern of nearshore wave power at Byron Bay is influenced by refraction around Cape Byron, Julian Rocks and a prominent shoal east of Cape Byron, identified as an offshore sand lobe on the lower shoreface/inner shelf break by Goodwin *et al* (2013). These three features dissipate wave energy producing much lower wave power to propagate onto the upper shoreface than at Wamberal and Sawtell. Lower offshore wave heights for each storm type at Byron Bay, due to the increased distance from southerly storm wave generation (for SSL, ITL and STLs) or less intense storm type (for AIs), also contribute to a lower energy nearshore environment during storm events.

6.7 RESULTS AND DISCUSSION (2) – IMPLICATIONS OF TROPICAL EXPANSION FOR STORM WAVE CLIMATE AND SEDIMENT TRANSPORT

6.7.1 Changes to Storm Type Frequency with Tropical Expansion

Observations and GCMs indicate that a poleward expansion of the tropics and an intensification of the tradewinds are signatures of recent and near-future climate change (Seidel *et al*., 2008, England *et al*., 2014). In the past decade, the shift towards the La Nina-like state of the Pacific Decadal Oscillation and Interdecadal Pacific Oscillation (Allen *et al*., 2014) has enhanced the tradewind intensification. These changes are associated with the poleward shift of the sub-tropical ridge (STR) or intensification of the sub-tropical anticyclone (STAC) in the East Australian region (Timbal and Drosdowsky, 2013) and a poleward contraction of the mid-latitude westerlies (Marshall *et al*, 2003; Arblaster *et al*., 2011).

Future poleward shifts in the STR latitude and the modal wave climate are characterized by an increased frequency of easterly and north-easterly trade-wind generated waves replacing Southern Tasman and Southern Ocean wave climates (Hemer *et al*., 2013, Chapter 4 this thesis). Likewise, a continued expansion of the tropics may lead to ex-TC and warm season ETLs forming at more southerly latitudes, in place of extra-tropical STL and SSL storm types as the wave generation source migrates poleward and away from the SEAS. Whilst previous studies using GCM projections such as Dowdy *et al* (2014) and Abbs and McInnes (2004) indicate an overall decline of East Coast Low storm events later this century, changes in the occurrence of different storm types will impact the directionality and magnitude of storm waves, and thus coastal stability.

This section investigates the impacts of a reduction in SSL storms and increase in ETL storms with a poleward expansion of the tropics. The impacts on nearshore wave power and shoreface sediment transport at the two most latitudinally separate sites, Wamberal and Byron Bay, are explored.

6.7.2 Implications for Nearshore Wave Power and Shoreline Rotation

Figure 6.10 shows the difference in storm wave propagation along the SEAS (a), and the gradients in nearshore wave power (b) in the headland shadow zones of Wamberal and Byron Bay. SSL events are more common at both Wamberal (28% frequency of occurrence) and Byron Bay (26%) than ETL events (7 and 12%, respectively), and produce larger wave heights in the central Tasman Sea (Figure 6.10 a). Despite less energetic oceanic conditions, ETL events are associated with higher wave power in both the mid-shelf environment (Figures 6.5 and 6.6) and in the nearshore (Figures 6.7 to 6.9), when compared with SSLs. This is because the direction of wave propagation is significantly more shore-normal, thus less wave energy dissipation due to shoaling/refraction takes place across the shelf.

For east-facing headland-bay beach compartments such as at Wamberal and Byron Bay, an anti-clockwise rotation of the mean storm wave direction associated with a shift from SSL to ETL storm type leads to greater wave power propagation into the southern hook environment (Figure 6.10 b). The southern hook refers to the parabolic bay beach shape in the lee (to the north) of a southern headland, and is often the most sensitive section of the shoreline to shifts in wave directionality (Chapter 5).

In Chapter 5, it was shown that shoreline rotation in a headland bay beach configuration can be elucidated from the alongshore change in surf zone morphology. The change in morphological type is in turn a function of the alongshore gradient in nearshore wave power. Other observational studies (e.g. Quartel, 2009; Price and Ruessink, 2013; Lageweg *et al.,* 2013) have also shown that surf zone morphology is coupled to shoreline patterns. Therefore as a first pass, changes to the position of nearshore wave power contours should be indicative of the alongshore extent of shoreline rotation in a headland-bay beach that results from a shift in wave direction. In Figure 6.10 b, the 5 kW/m wave power contour during peak storm wave conditions of SSL and ETL storm types is shown, starting from the approximate diffraction point at the headland. The 5kW/m contour was chosen after the wave power refraction pattern showed this contour to be most representative of the upper shoreface isobaths, and thus most indicative of the long-term shoreline response.

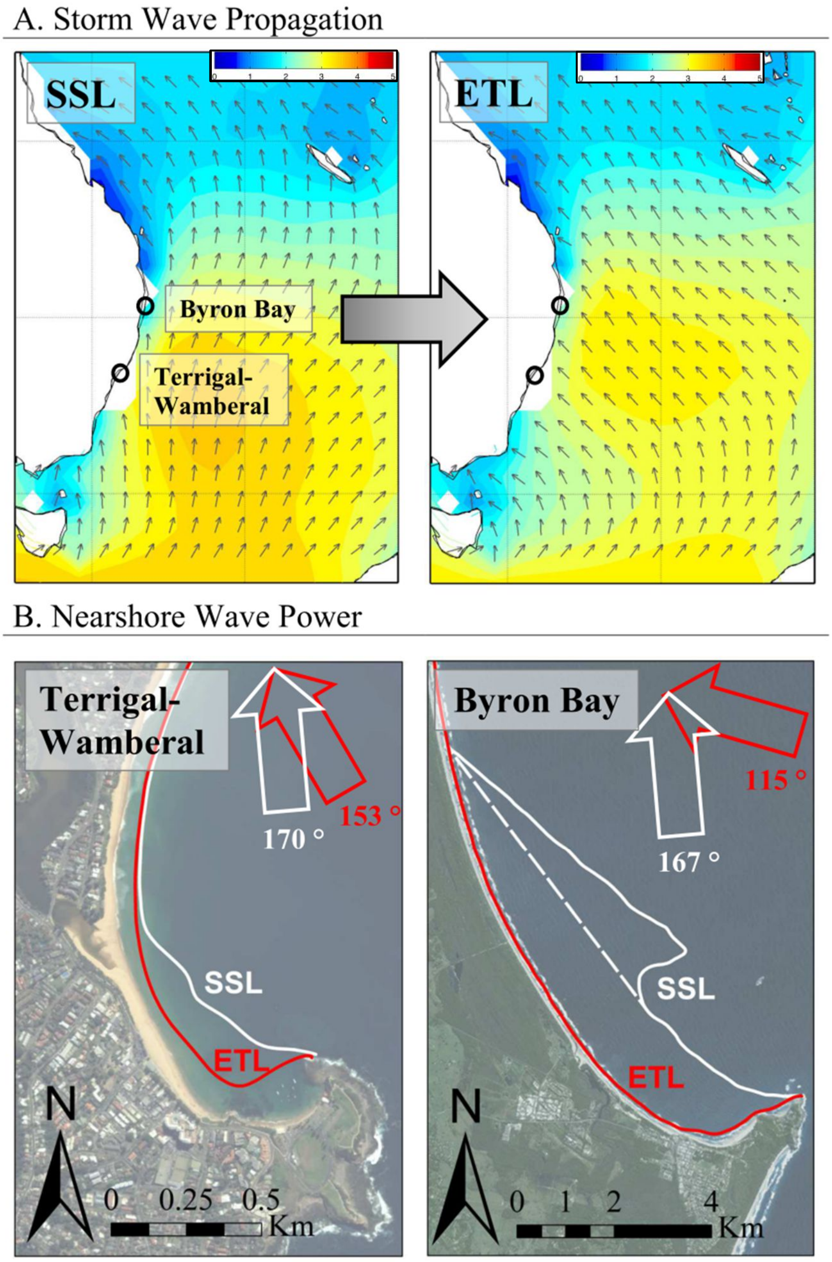

Figure 6.10 Difference between Southern Secondary Low (SSL) and Easterly Trough Low (ETL) storm wave propagation patterns on the SEAS (a), and 5 kW/m nearshore wave power gradients (b) in headland shadow zones at Terrigal-Wamberal and Byron Bay. Propagation plots in (a) represent composite H_s (contour plot) and *MWD* (wave vectors) for all recorded storm wave events for each storm type, using the ERA-Interim gridded wave data (1980 - 2011). Arrows in (b) represent the average peak storm mid-shelf wave direction for SSL (white) and ETL (red) at Sydney (for Terrigal-Wamberal) and Byron Bay buoys. The dotted white line at Byron Bay illustrates the 5 kW/m power gradient for SSL without the shadowing effect of Julian Rocks.

At both sites, greater propagation of wave power into the southern hook with ETL storm events leads to an anti-clockwise rotation of the planform. The alongshore extent of this rotation can be approximated to where the wave power contours of SSL and ETL storms converge. At Byron Bay, the alongshore extent of planform rotation is greater than at Wamberal. This is because the difference in mid-shelf wave direction between these two storm types is considerably greater at the Byron Bay buoy (52 º) than at the Sydney buoy (17 º), due to the more northerly locus of wave generation for ETL storms in the Tasman Sea (Figure 6.10 a).

Therefore, a shift in storm type with tropical expansion from SSL to ETL storms would lead to greater mid-shelf and nearshore wave power along the SEAS and thus an overall increase in magnitude of the storm wave climate. Because of the more northerly location of wave generation of ETL storms, the mid-north and north coasts of NSW would experience a greater anti-clockwise rotation in the storm wave direction, and thus a more extensive anti-clockwise rotation of the shoreline planform, than on central coast NSW sections.

6.7.3 Implications for Cross-Shelf Sediment Supply

Figure 6.11 (6.12) shows the patterns of sediment mobilisation during peak storm wave conditions of ETL and SSL storm types at Byron Bay (Wamberal). The rate of sediment mobilisation will scale according to the exceedance of the wave-induced bottom orbital velocity (U_b) over a critical threshold for entrainment (U_{crit}) as described in Section 6.5.6. Only patterns of $U_b > U_{crit}$ exceedance greater than one standard deviation above U_{crit} (~ 0.4 m/s) are shown, to illustrate significant differences in entrainment patterns between storm types.

Results represent a cross-shore and wave-only case where surf zone circulation, ambient shelf currents, surface winds, grain size gradation, bed forms or alongshore transport is not accounted for. While wave energy is the dominant mechanism for sediment transport on most shelf environments (Butman *et al.*, 1979; Drake and Cachione, 1985), Griffin *et al* (2008) have shown that extreme wind events on the SEAS (often associated with storm wave events) extend the seaward limit of sediment entrainment from mid- to outer-shelf depths. While patterns of sediment entrainment are shown, zones of net accretion/erosion and thus the transport volume rate cannot be calculated without using a fully deterministic morphodynamic model.

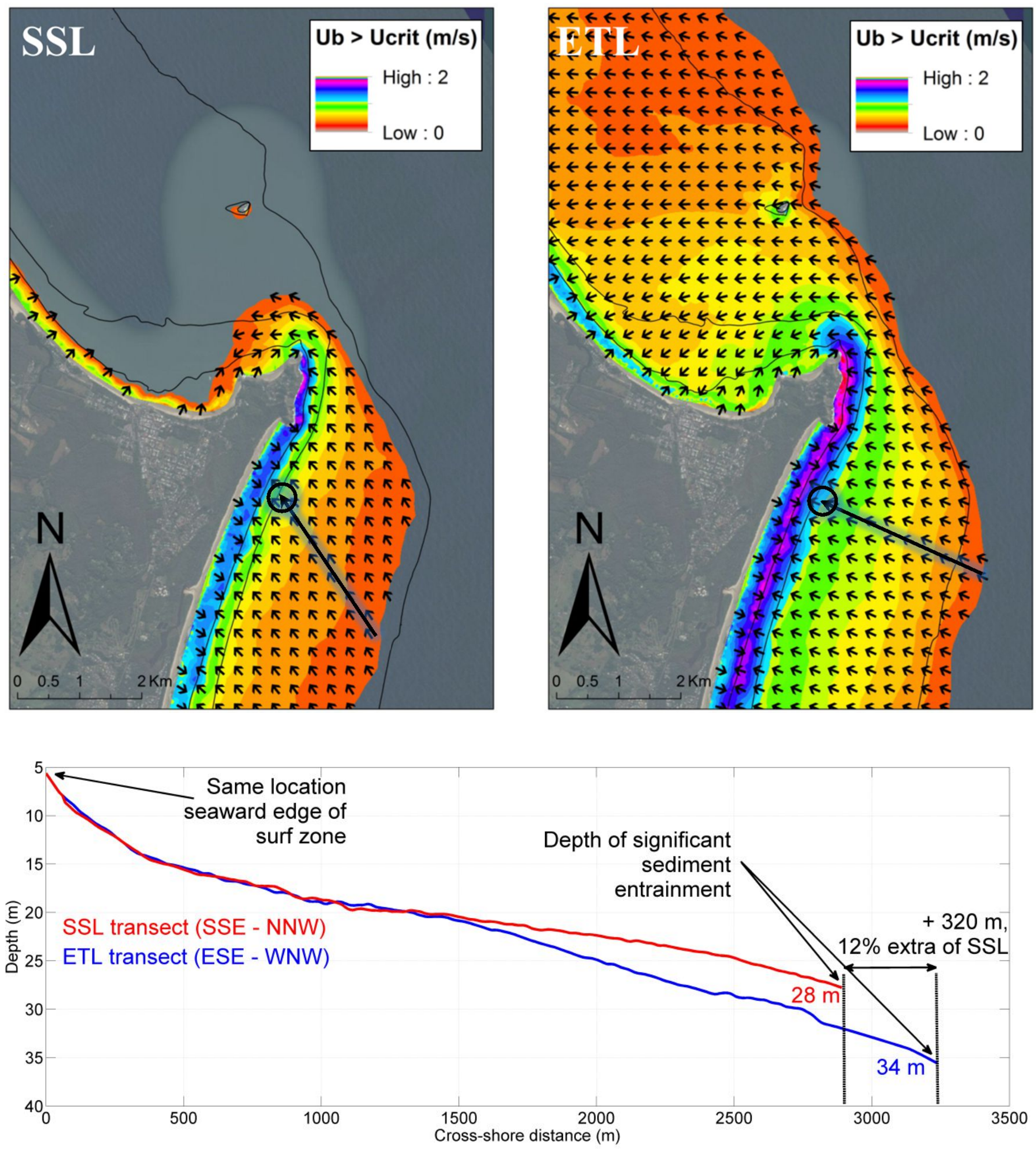

Figure 6.11 Patterns of sediment mobilisation during peak storm wave conditions for SSL and ETL storm types at Byron Bay. Exceedance velocity of $U_b > U_{crit}$ is shown. Vectors represent approximate direction of cross-shore transport (onshore in shoaling zone, offshore in surf zone). 5, 12 and 30 m contours are shown to represent seaward limit of surf zone, upper shoreface and lower shoreface. Black lines show location of transects taken through the bathymetric surface, representing idealised cross-shore transport routes for SSL and ETL storm events from the

depth of significant sediment entrainment to the same location on the seaward edge of the surf zone. The cross-section profiles are shown in the bottom panel.

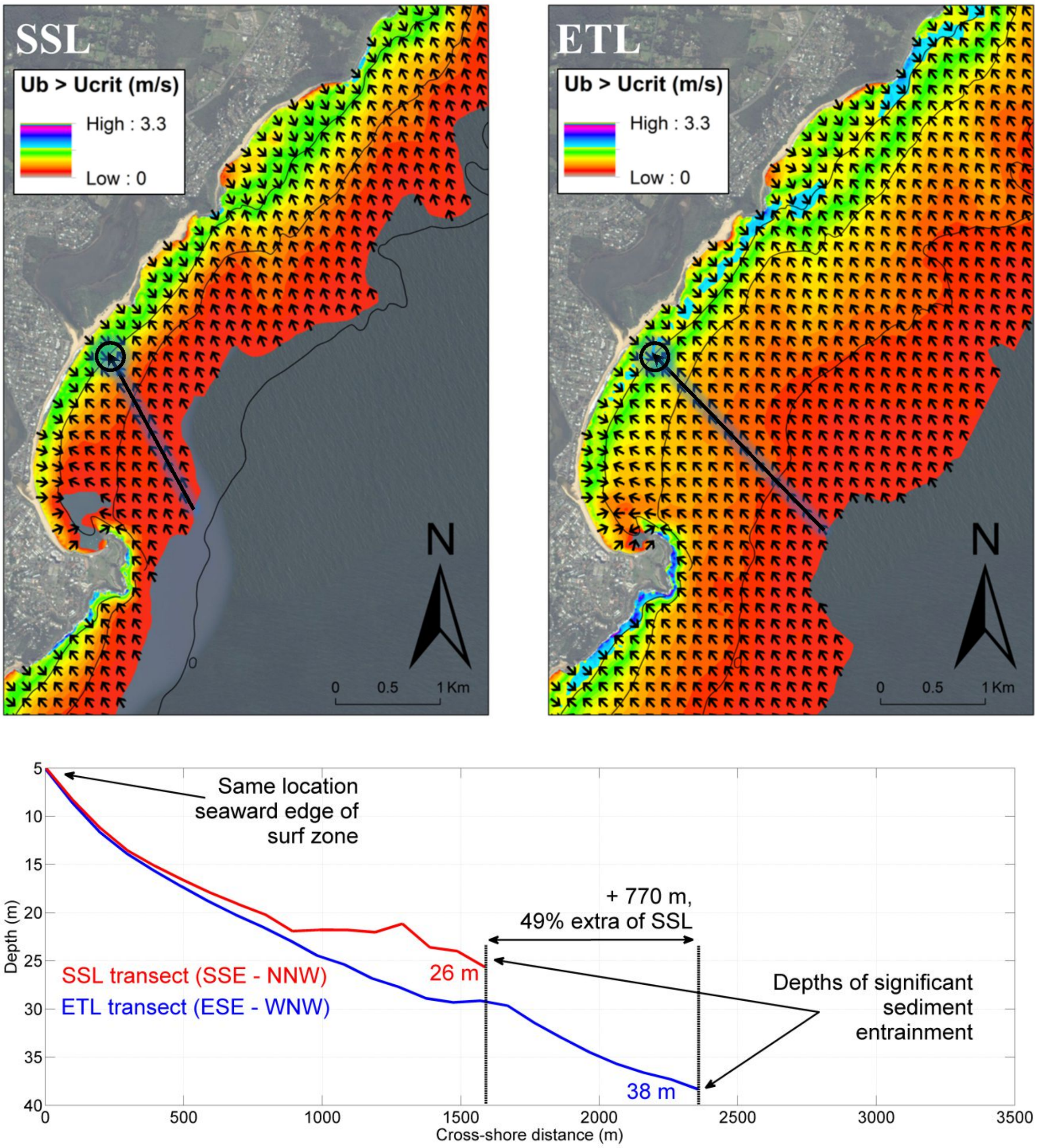

Figure 6.12 Patterns of sediment mobilisation during peak storm wave conditions for SSL and ETL storm types at Wamberal (as Figure 6.11). 5, 15 and 30 m contours are shown.

In the shoaling zone (from the seaward edge of the surf zone to wave base), the direction of near-bed wave orbital motion is determined by the velocity skewness of the wave profile (Ruessink *et al.*, 2012). Waves with shorter, higher crests and longer, shallower troughs have higher velocities in the crest, promoting onshore-directed orbital motion. As the wave shoals further, velocity skewness is replaced by velocity asymmetry as the wave pitches forward with a steep front face and gentle rear face, until it breaks. Both velocity skewness and asymmetry (almost always) lead to onshore sand transport (Ribberink and Al-Salam, 1994; O'Donoghue and Wright, 2004; Ruessink *et al.*, 2011). Therefore, the direction of wave-induced cross-shore sediment transport in the shoaling zone, once entrained, is approximate to the direction of wave propagation (Figures 6.11 and 6.12).

In the surf zone (defined as landward of the 5 m isobath), it is assumed that net transport under storm conditions is offshore and thus opposite to the wave direction (Figures 6.11 and 6.12). While not modelled explicitly in this study, energetic wave conditions in the surf zone commonly lead to offshore bar formation because of strong undertow and rip circulation that occurs in depths where critical shear stress and entrainment is achieved by every wave.

In all cases, Figures 6.11 and 6.12 show a cross-shore gradient in wave-generated sediment mobilisation where bed exceedance velocities (and thus inferred sediment mobilisation rate) increase with proximity to the coast. This is because wave orbital motion at the seafloor, and thus bed shear stress required for entrainment, increases with decreasing water depth. Such cross-shore transport gradients are characteristic of most wave-dominated sloping shelf environments (Harris and Wilberg, 2002). Because ETL events are more energetic, significant sediment mobilisation begins in deeper water (and further offshore) than during SSL events. The pattern of sediment mobilisation, however, is also a function of the cross-shelf bathymetric profile and the direction of storm wave propagation.

At Byron Bay, the obliquity of wave power during SSL storms leads to a large north-south divide in the cross-shore extent of mobilised sediment. South of Cape Byron, sediment is entrained shoreward from ~ 28 m depth, compared to ~ 34 m during ETL events. This equates to an extra ~ 12 % of shelf area over which ETL storms cause significant sediment mobilisation where SSL events do not (Figure 6.11). North of Cape Byron, onshore-directed sediment mobilised during SSL events only occurs in the immediate lee of the headland. North of this, results suggest that highly refracted, lower storm wave power means only offshore-directed transport in the surf zone occurs during SSL events, with no significant onshore movement of sand in adjacent deeper water. During ETL storm events, higher and more shore-normal wave power means sediment continues to be entrained from ~ 34 m depth both south and north of Cape Byron. This large difference in onshore-directed transport capacity between storm types north of Cape Byron equates to ~ 5 km in cross-shore distance.

At Wamberal, there is much less alongshore variability in sediment entrainment than at Byron Bay because the regional shoreline is oriented normal to the wave direction of both storm types. Also, the cross-shelf bathymetric profile is steeper at Wamberal (Figure 6.12, bottom panel) than at Byron Bay (Figure 6.11) meaning the offshore wave power signatures of both storm types are retained further inshore because less energy is dissipated across the shelf. Because ETL events are significantly more powerful than SSL events (Table 6.3), there is a large depth difference at which sediment is mobilised (~ 38 m depth during ETL events, ~ 26 m during SSL events). This equates to an extra ~ 49 % of shelf area over which ETL storms cause significant sediment mobilisation where SSL events do not.

These preliminary results indicate that, if the effects of tropical expansion on the storm wave climate were sustained in the long-term, a move towards ETL events becoming the most frequent storm type along the SEAS could help the coastline keep pace with sea-level rise by being a more effective agent of cross-shelf transport. East to north-easterly storm waves with large wave heights (ETLs), in place of south south east storm waves with lower wave heights (SSLs) are better placed to deepen the lower shoreface, transferring sediment to the upper shoreface and active profile, bringing an overfit shelf regime towards equilibrium.

6.8 CONCLUSIONS

This study has investigated the distribution of storm wave types along the south east Australian shelf (SEAS), and their refraction patterns across the shoreface, using a hybrid approach of meteorological typing and statistical clustering. The statistical assessment of wave parametric data showed that the eight synoptic storm types developed by Shand *et al* (2011) can be reduced to five groups along the SEAS with joint distributions of peak storm H_s, peak storm T_p, and storm duration. These groups in respective order from extratropical to tropical origin are (i) Southern Tasman

Lows/Southern Secondary Lows/Continental Lows, (ii) Inland Trough Lows, (iii) Easterly Trough Lows, (iv) Anticyclonic Intensifications, and (v) Tropical Cyclones and Tropical Lows.

Refraction modelling of storm types across the shoreface highlights the importance of wave direction for storm magnitude in both the mid-shelf and nearshore environments. For each storm type along the SEAS, the mid-shelf H_s decreases with a clockwise rotation in the *MWD*. Because of shore-normal wave propagation, Easterly Trough Lows are the most powerful storm type for the central to north coast NSW. Extra-tropical origin storms such as Southern Tasman Lows and Southern Secondary Lows produce shore-oblique (southerly) wave conditions and thus lower mid-shelf and nearshore power, despite producing some of the highest wave heights in the Tasman Sea. Because of the southerly wave generation of the most common storm types along the SEAS, there is a south-to-north latitudinal wave power gradient on the shelf and shoreface.

A continued expansion of the tropics in the south-west Pacific region will lead to a latitudinal shift in the synoptic type of storm wave generation and propagation. A 2.5° poleward migration of the STR (as projected in some GCMs) would result in the SEAS experiencing more frequent north-easterly generated and shore-normal storm waves (AI, ETL and TC/TL), and less frequent southerly generated and shore-oblique storm waves (STL, SSL and CL).

Results indicate that a sustained trend towards more ETL and less frequent SSL/STL storm waves will have a significant impact on nearshore wave power, cross-shelf sediment supply and coastal stability. On the event-scale, higher wave power propagation into protected southern sections of coastal compartments during ETL storm events leads to storm cut and an anti-clockwise rotation in the southern planform. The Mid-North and North Coasts of NSW would experience more extensive anti-clockwise rotation of the shoreline planform than on the Central Coast because of the more northerly location of wave generation of ETL storms.

Modelling suggests that ETL storms have the capacity to entrain and transport sediment over a significantly wider area of the shelf than SSL storms. This suggests that in the long-term, an increase in the occurrence of ETL storm events along the SEAS would be beneficial for those shorelines that require a cross-shore sediment supply for stability, to keep pace with sea-level rise. An ETL-dominant storm wave climate, with more shore-normal and higher wave energy, is certainly a more effective agent of lower to upper shoreface sediment transfer. While not modelled explicitly, a reduction in oblique SSL storms also reduces the number of episodic, high-energy wave events required for headland bypassing between compartments and alongshore transport.

Shorelines in the lee of southern headlands will be most vulnerable to changes in the storm wave climate with tropical expansion, especially those located on the mid-north and north coasts. This is because of increased exposure and storm cut during ETL events, and reduced headland bypassing required for shoreline stability as oblique, extra-tropical storm events become less frequent. Results can be applied to other Southern Hemisphere east coasts in South America and Africa, and Northern Hemisphere west coasts in North America and Europe impacted by tropical expansion in the sub-tropics.

6.9 ACKNOWLEDGEMENTS

Wave data from all NSW buoys is funded by NSW Office of Environment and Heritage (OEH) and is operated by Manly Hydraulics Laboratory (MHL). Wave data from the Brisbane buoy is funded by State of Queensland, Department of Science, Information Technology, Innovation and the Arts (DSITIA) and distributed by Coastal Impacts Unit - Science Delivery Division, DSITIA. Nearshore buoy deployments in the Sydney region and at Sawtell Beach were funded by Australian Research Council (ARC) Linkage Project (grant number LP100200348 to IDG and Ian L Turner). Thanks to Sonny Tisdell and Sawtell SLS Club for help with buoy deployments at Sawtell Beach. All bathymetry used for refraction modelling was supplied by NSW OEH. A Macquarie University (MQU) academic license for MIKE by DHI software was used. The paper on which this chapter is based is a contribution to the Eastern Seaboard Climate Change Initiative – East Coast Lows (ESCCI-ECL) Project 4, and an NSW OEH and NSW Environmental Trust Grant to IDG.

CHAPTER 7

Hat Head National Park

OVERALL CONCLUSIONS

7 OVERALL CONCLUSIONS

7.1 KEY THESIS FINDINGS

This thesis has made a distinct contribution to the field of coastal science, particularly in advancing the understanding of how wave climates and coasts in south east Australia will respond to a changing climate. It has assessed the accuracy of nearshore wave information derived from both archive video imagery and spectral wave models, and the implications of using these data sources for modelling coastal processes (Chapter 2 and 3). It has also developed a new wave climate typology for the Tasman Sea region based on a novel statistical-synoptic typing method that is readily transferable to other marginal sea settings (Chapter 4). Importantly, this typology has allowed the relationship between synoptic climate forcing, observed wave parametric data and coastal response to be investigated.

The wave climate and coastal impacts of two key regional climate signals have been investigated; an expansion of the tropical belt (Chapters 4 and 6), and the changing behaviour of El Niño Southern Oscillation (Chapter 5). Results have informed a preliminary assessment of the role of a changing storm wave climate in modulating coastal evolution with sea level rise (Chapter 6). A new link between surf zone morphology and the shoreline equilibrium profile of headland-bay beaches has also been made, which allows the Parabolic Bay Shape Equation (PBSE) to be applied to real-world wave conditions with a greater level of objectivity (Chapter 5).

Responses to the three research hypotheses posed in Section 1.3 are implicit in the sections below, which summarise the key findings of this thesis. Overall, Hypothesis 1, *"The current state-of-the-art of regional downscaling of Global Climate Model (GCM) output is the best approach to forecasting nearshore wave climate and coastal change along the SEAS"*, was concluded not to be true because of significant uncertainties in the regional wave downscaling approach. Instead, a surrogate-observational method was adopted throughout the thesis which facilitated a scenarios-based approach to forecasting wave climate and coastal change.

Hypothesis 2, *"An expansion of the tropical belt projected with anthropogenic climate change will cause a shift in the directional wave climate and impact coastal behaviour along the SEAS"*, was concluded to be true in that tropical expansion was found to force an overall anti-clockwise rotation of the wave field, and impact the cross/alongshore sediment transport balance along the SEAS.

Hypothesis 3, *"A change in El Niño Southern Oscillation (ENSO) behaviour projected with anthropogenic climate change will cause a shift in the directional wave climate and impact coastal behaviour along the SEAS"*, was concluded to be true in that different 'flavours' of ENSO were found to produce statistically different wave climates along the SEAS and coastal responses in a headland-bay beach setting.

7.1.1 Accuracy of Nearshore Wave Information

Nearshore wave information was evaluated from two standalone coastal wave models (SWAN and MIKE 21 SW), a global-to-coastal wave downscaling framework (using WaveWatch III and SWAN) and a pre-existing network of shore-based camera stations. In all cases, wave data was validated against an array of nearshore, directional WaveRider buoy observations.

The spectral wave models provided a far superior representation of the nearshore wave field than archive 'surfcam' video imagery. This was because only low-angled, single camera installations were available which impeded pixel rectification and the correct measurement of waves. Single-camera systems have been successfully used in the past, but only in either wave flume (Almar *et al.*, 2012) or reef (Hilmer, 2004) environments where the breaker type and position is well defined. The current best-practice for remote measurement of breaking waves in a beach environment is to use a dual-camera (high- and low-mount) system where the dynamic breaker position can be properly located by triangulation (e.g. Piepmeier and Waters, 2004; de Vries *et al.*, 2011; Shand *et al.*, 2012). Results suggest that at present, the network of oblique and single-camera surfcams installed at Australian beaches cannot be used to derive wave parametric data for coastal process studies.

In contrast, both SWAN and MIKE 21 SW (with sufficiently high quality bathymetric and boundary wave information) can replicate nearshore wave height distributions very well using default configurations (SWAN R^2 0.86 m 0.99, MIKE 21 SW R^2 0.94 m 0.90

at Terrigal-Wamberal, on the central NSW coast). The mean wave direction is also reasonably well modelled (SWAN R^2 0.68 m 0.90, MIKE 21 SW R^2 0.81 m 0.82).

The correct estimation of wave heights and directions indicate that energy dissipation due to bottom effects, and thus shoaling and refraction, is well represented in the models. There are deficiencies however in the prediction of wave period, indicating that the energy distribution across wave frequencies is not correct. The mis-representation of the mean wave period in spectral wave models is well reported (e.g. Ris *et al*., 1999; Strauss *et al*., 2007; Moeini and Etemad-Shahidi, 2007), and is a function of; a) the quality of boundary wind and wave forcing, b) the representation of energy bunching with shoaling, and c) the validity of the starting spectral shape used in the model.

Validation results for SWAN and MIKE 21 SW in the Sydney region show that; wave height is the most accurate output parameter; wave period is the least accurate; and an indicative level of directional accuracy (independent of error propagating from boundary wind/waves) is ± 5 º (RMSE, averaged across buoys and models; when using high-quality nearshore bathymetries; for exposed nearshore locations outside zones of diffraction).

7.1.2 Implications for Coastal Process Modelling

While residual errors are unavoidable when modelling the wave spectrum (Section 1.2.2), numerical wind-wave models still provide the most practical and accurate method for obtaining nearshore wave information in two-dimensional space. Spectral models have undergone almost half a century of empirical improvement, and the default configurations of both SWAN and MIKE 21 SW were found to be largely appropriate where validated.

Nevertheless, the spectral approach to wind-wave modelling may have reached its limit (Liu *et al*., 2002; Cavaleri, 2006; WISE Group, 2007) and incremental improvements to model physics are slowing. While models can be further calibrated to agree with observations (often by modifying the level of energy dissipation in the model), the 'improvements' are only relevant for the vicinity and period of *in situ* observations. Instead, an appreciation of residual errors in nearshore wave data and implications for modelling coastal processes is required.

Two parameters that have been used throughout this thesis to relate wave climate change to coastal evolution are wave power, P_0 (Equations 4.1 to 4.3), and wave-induced bottom orbital velocity, U_b (Equations 6.1 to 6.2). P_0 scales with the square of the wave height, and is therefore more sensitive to uncertainties in the modelled significant wave height, H_{m01}, while U_b (and thus calculations of sediment transport) is considerably more sensitive to errors in the modelled mean wave period, T_{m01}. Since wave height is a more robust modelled parameter than wave period (Section 7.1.1), it follows that there is more confidence in the prediction of P_0 than U_b. In this respect, the method of relating nearshore wave power contours to shoreline rotation proposed in Chapter 6 is vindicated because it is less sensitive to errors in wave period.

Errors in the nearshore wave period can propagate from boundary wind and wave forcing as well as due to internal physics. This can occur when a coastal wave model is coupled to output from a global ocean model (Chapter 2). Errors in the modelled wave direction may also be related to the inability of the global wave model to replicate both far- and near-field synoptic wave generation simultaneously. However, small directional errors in deepwater may have no significant impact on the modelling of coastal processes because of the insensitivity of the nearshore to shifts in offshore wave direction (Snel's law). Results from Chapter 5 indicate that, for the more exposed sections of a typical embayed beach, shifts in the deepwater (mid-shelf) wave direction need to be greater than 35 º to change the nearshore wave direction by more than 1 º (although this varies alongshore and with wave obliquity).

Coastal process modelling is least sensitive to errors by global wave models in representing extra-tropical, southerly (oblique) wave generation because these wave conditions are highly refracted across the shelf, and are therefore more likely to reach the surf zone in the same or adjacent directional bins, with or without errors. Conversely, the coastal zone is most sensitive to errors in locally-generated easterly and south-easterly (shore-normal) wave generation because these wave conditions experience less directional change from shelf to shore. This highlights an important drawback of using regionally downscaled modelled waves for coastal process modelling in southeast Australia; the representation of local wave growth is most important to get right, but often localised weather (and thus wave) patterns are the least well resolved in regional climate models for the Australian region (Grose *et al*., 2012).

7.1.3 A Wave Climate Typology for the Tasman Sea

A major contribution to this thesis has been the development of a combined statistical-synoptic typing approach of directional wave buoy records along the southeast Australian shelf (SEAS). Prior to this, only meteorological-based descriptions of the regional wave climate were available (BBW, 1985, Short and Trenaman, 1992, Shand *et al*, 2011a). The problem with meteorological typing in the Tasman Sea is that multiple synoptic drivers can produce statistically indifferent directional wave fields because of the predominance of localised wave generation and fetch-limitations. Therefore, an alternative approach was required to identify unique wave patterns along the SEAS.

It was found that the directional wave climate could be encapsulated by three primary modes of variability. A sub-tropical easterly mode is modulated by south Pacific trade winds (Mode 1); a south-easterly mode is generated locally in the Tasman Sea (Mode 2) and an extra-tropical southerly mode is related to the strength of the mid-latitude westerlies (Mode 3). These three primary modes were further decomposed into six synoptic-scale 'wave climate types' that represented; North-Easterly Trade Winds, Zonal Easterly Trade Winds, a combination of Southern Tasman Anti-Cyclones and Tropical Lows, Central Tasman Lows, Southern Ocean Lows and Southern Tasman Lows.

While a statistical clustering approach may be adequate for defining sea states in an open-ocean setting (e.g. Camus *et al*., 2011; 2014), results from this thesis suggest that clustering alone cannot isolate synoptic-scale wave climates in a marginal sea environment. To overcome this problem, a novel combination of Gaussian Mixture Modelling and analysis of the Mean Sea Level Pressure fields was used to decompose the k-means clusters and identify unique patterns of wave generation.

The resultant typology facilitated the observational-based study of climate change impacts on wave climate and coastal behaviour for the rest of the thesis. Each daily wave observation in the buoy record was indexed by a wave climate type, so wave parametric data could be directly linked to wave generation and climate drivers.

7.1.4 Wave Climate Change Impacts for Coastal Stability in Southeast Australia

Two of the most important signatures of anthropogenic climate change for the Pacific subtropics include an expansion of the tropical belt (and associated southerly migration of the sub-tropical ridge, STR) and the changing behaviour of El Niño Southern Oscillation (ENSO). While both of these phenomena have been studied with respect to the hydrological cycle over east Australia (e.g. Taschetto and England, 2009; Timbal and Drosdowski, 2013), the impacts on wave climate and coastal stability have received little attention. Using the wave climate typology developed in Chapter 4, the impacts of tropical expansion and changing ENSO asymmetry on the modal wave climate, the storm wave climate, sediment transport patterns and coastline stability along the SEAS were explored.

7.1.4.1 Tropical Expansion

A surrogate-buoy approach was used to examine the poleward migration of wave climate with tropical expansion, whereby modern wave parameters from more equatorward buoys were taken as surrogate data to project future wave impacts at more poleward locations. This circumnavigates the need for regional wave climate downscaling and related uncertainties. Where a latitudinal array of buoys is available, this approach can be easily extended to a number of expansion scenarios.

The impacts on the modal (non-storm) wave climate were first investigated. Results indicate that for every one degree poleward shift in the STR there will be an increase in total modal wave energy for the central SEAS of 1.9 GJ m^{-1} wave-crest-length during the Austral winter, and a reduction of similar magnitude (~ 1.8 GJ m^{-1}) during summer. This is based on using a (modified) wave climate observed at the Byron Bay buoy as surrogate for the Sydney region, divided by number of degrees latitude of separation between the two sites. In both seasons, tropical expansion leads to an anti-clockwise rotation of the wave field which is consistent with GCM-based wave climate projections (Hemer *et al.*, 2013a; 2013b).

A continued expansion of the tropics in the south west Pacific region would lead to a poleward shift in storm wave generation and propagation patterns, as with the modal wave climate. If this were the case, the SEAS would experience more frequent north-easterly generated and shore-normal storm wave types such as Easterly Trough Lows

(ETL) and less frequent southerly-generated and shore-oblique storm wave types such as Southern Secondary Lows (SSL).

The overall impact of a poleward shift of the STR on the SEAS ultimately depends on the interaction between storm and non-storm conditions. Results suggest that both the modal and storm wave direction will rotate anti-clockwise, at the expense of extra-tropical, southerly wave generation. The magnitude and duration of individual storm events, and thus the cumulative power of each storm, will increase with ETLs becoming the most frequent storm type. However, previous studies using GCM projections such as Abbs and McInnes (2004) and Dowdy *et al.* (2014) indicate a reduction in storm frequency along the SEAS for the coming century. Therefore, a plausible future wave climate may consist of longer periods of ambient wave conditions from the east and south-east that are of shorter period and lower energy, punctuated by less frequent but higher magnitude storm events from the east to north-east. Hemer *et al*. (2013a; 2013b) show that greater Southern Ocean wave generation is another regional hallmark of climate-change, although the south-westerly wave direction, and the sheltering effect of Tasmania, means these wave events do not affect the wave climate along the SEAS.

Overall, these changes leads to a reduced along-shore transport component and greater cross-shore transport along the SEAS. Shoreline sections in the lee of southern headlands (headland-bay beaches) would be most vulnerable. These planforms are exposed to north-easterly ETL events but currently equilibrated with a much lower-energy (highly-refracted) south-easterly modal wave climate. Headland-bay beaches also require a combination of high energy oblique storm events for episodic headland sand bypassing, with subsequent shore-normal modal conditions to transport the bypassed sand shoreward (Goodwin *et al*., 2013). A reduction in oblique storms and bypassing events, and longer periods of shore-normal ambient conditions, would at first deflate bypass deposits on the shoreface to feed the beach face (Figure 7.1).

A remaining unknown is whether the sediment transported offshore during ETL storms would be then re-worked back on the beach during (more frequent) easterly modal conditions, or deposited at depths that are out of reach of less energetic non-storm waves (Figure 7.1). This is an interesting avenue for further research.

Headland-bay beach sections on the mid-north and north coasts of NSW would experience the greatest impacts of these changes because of the more northerly locus of ETL storm wave generation in the Tasman Sea, and thus higher wave power locally during these events. This poses a significant challenge for coastal management in north NSW since most townships and related infrastructure are located in the lee of southern headlands.

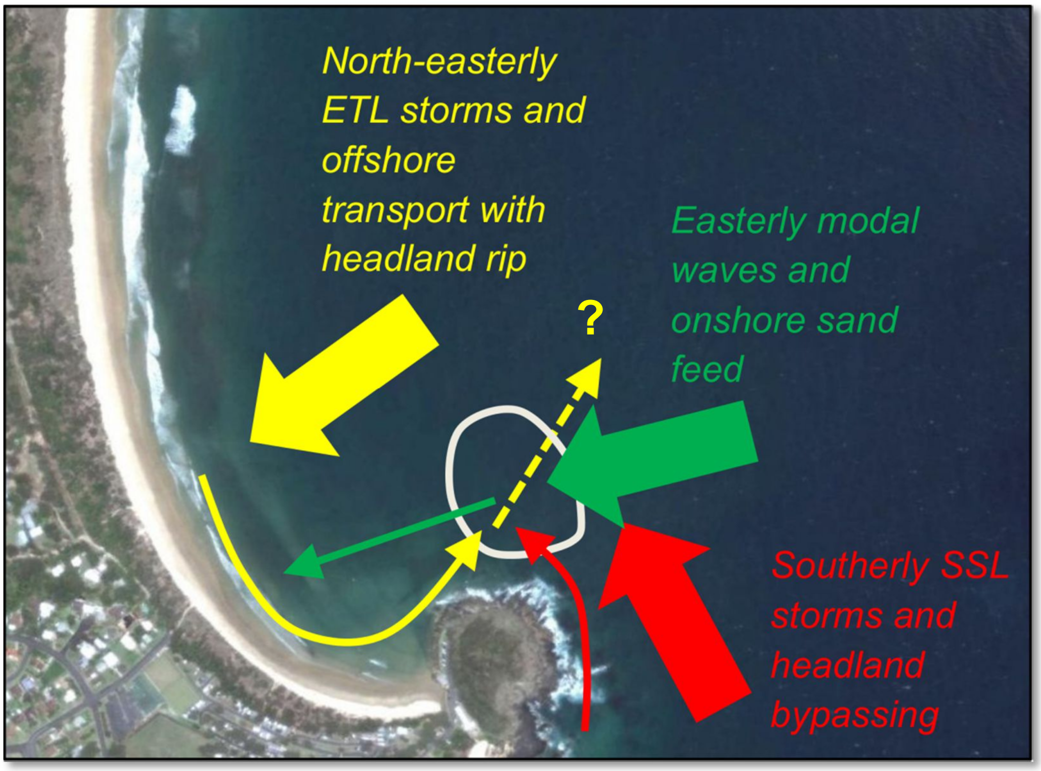

Figure 7.1 Schematic of wave climate change impacts for a headland-bay beach (Scotts Head, mid-north coast NSW). White polygon represents location of bypass lobe (not to scale). Background image from GoogleEarth (2015).

7.1.4.2 Changing Behaviour of ENSO

Superimposed on the long-term anti-clockwise rotation in the wave field with tropical expansion is the interannual modulation of wave climate by ENSO. There is evidence to suggest ENSO is changing, with central Pacific (CP) type ENSO and extreme ENSO events both becoming more frequent with greenhouse forcing (Yeh *et al*., 2009; Lee and McPhaden, 2010; Cai *et al*., 2014; 2015a). The impact of a shift from eastern to central Pacific ENSO on wave climate and coastal stability in southeast Australia has thus far been neglected in existing coastal process studies.

Using an array of directional buoy observations in combination with the wave typology developed in Chapter 4, it was showed that CP ENSO events produce significantly different patterns of directional wave power to eastern Pacific (EP) ENSO events along the SEAS, and this is because of the modulation of trade-wind wave generation. The strength of trade-wind wave power is related to the position of the sub-tropical anticyclone which varies between CP and EP ENSO events. Since the modulation of the easterly trade winds is an integral part of ENSO dynamics (Section 1.2.5), it is logical to suggest that it should also drive the wave climate response in the south west Pacific.

A coupled spectral wave–hydrodynamic–sediment transport model was used to project ENSO wave climates on coastal processes in a headland-bay beach setting (Terrigal-Wamberal on the central NSW coast). The alongshore variability in surf-zone morphology produced by each ENSO climate state was then used as a measure of coastal vulnerability.

This approach yielded three key findings. First, that CP ENSO leads to higher coastal erosion potential and slower post-storm recovery than EP ENSO during an El Niño/La Niña cycle. Second, that the shoreline response to ENSO in a headland-bay beach is not as simple as the existing paradigm that (anti-) clockwise rotation occurs during El Niño (La Niña) (e.g. Ranasinghe *et al.*, 2004; Harley *et al*, 2011; 2015), because of shoaling processes, bi-modal wave conditions and the emergence of different flavours of ENSO. Third, that coastal change between ENSO phases cannot be inferred from shifts in the deepwater wave climate, as previously assumed (e.g. Ranasinghe *et al.*, 2004). This is because variability in trade-wind wave generation is masked in deepwater by the persistence of high power extra-tropical waves that have reduced impact on nearshore processes due to high wave refraction.

As the tropics expand, the influence of the easterly trade winds and ENSO variability on wave climate will become more direct for the SEAS. As was found in Chapter 4, the fetch-limitations in the Tasman Sea complicate the investigation of wave genesis, synoptic climate forcing and coastal response. On open-ocean coastlines in the north and south east Pacific that are exposed to long-fetch wave climates, the response of coastal geometry to ENSO wave climate variability and tropical expansion may be amplified when compared to findings for the Tasman Sea.

7.1.5 Implications of Storm Wave Climate Change for Coastal Evolution with Sea Level Rise

Storm events usually have a net-destructive effect on the sub-aerial beach and lead to shoreline recession at the event-scale, but they also move sediment to the upper shoreface from deeper water that is otherwise out of reach during more frequent but less energetic ambient wave conditions. Over the same timescales on which sea-level rise affects coasts, cross-shelf storm wave transport provides an important mechanism that links shelf sand bodies to coastal evolution. Because onshore sediment transport on continental shelves is highly episodic (Harris and Wilberg, 2002), changes to the storm wave climate with climate change are critical to determining long-term shoreline stability with sea-level rise (assuming an adequate shelf sediment supply). The process of a long-term sediment feed onto the active profile from the lower shoreface is not currently considered in estimates of shoreline recession due to sea-level rise that use the Bruun Rule.

Modelling in Chapter 6 suggests that a move towards ETL events becoming the most frequent storm type along the SEAS would lead to greater quantities of cross-shelf sand movement as resuspension events, across a wider area, for longer durations. ETL storms can entrain sand between 34 to 38 m depth (at study sites Byron Bay and Wamberal, respectively), compared to 26 to 28 m depth during SSL events. This equates to ETL events having the capacity to mobilise sediment over an extra 12% (Byron Bay) to 49% (Wamberal) of the lower shoreface than SSL events (the large difference between sites is a function of bathymetry and storm wave energy dissipation). Therefore, while storm event frequency as a whole is projected to decrease, the capacity of each event to move sand shoreward may be greater with tropical expansion. The net effect of lower frequency but higher magnitude storm events on coastal evolution with sea level rise is unclear. What this thesis has shown, however, is that ETL storm events are a more effective agent of cross-shelf sand transport from the lower to upper shoreface, which has the potential to facilitate coastal evolution with sea level rise. Chapter 6 represents a first step towards quantifying this, but a more deterministic approach that involves two- or three-dimensional process modelling is required.

7.1.6 A Link between Beach Morphology and Equilibrium Shorelines for Headland-Bay Beaches

Results from Chapters 4 to 6 indicate that headland-bay beach sections, particularly those located on the mid-north to north coast of NSW, are most vulnerable to directional wave climate changes associated with both tropical expansion and changing ENSO behaviour. Modelling the headland-bay beach response to a variable wave climate can be approached in two ways; either by two-dimensional modelling of hydrodynamic processes in the surf-zone, or by using the Parabolic Bay Shape Equation (PBSE) developed by Hsu and Evans (1989) to describe the Static Equilibrium Planform (SEP). The one-line modelling approach (using models such as LITPACK by DHI, XBEACH by Deltares, or GENESIS by US Army Corp of Engineers) cannot be applied in areas with high planform curvature because the planform is described by an alongshore set of shore-normal profiles that begin to overlap when the coastline is not straight. In addition, the one-line approach only incorporates alongshore, and not cross-shore processes when modelling the shoreline position.

Instead, two-dimensional modelling accounts for all sediment transport in the surf zone. However, there is usually no representation of the sub-aerial portion of the beach and no sediment exchange across the water line. This means it is often difficult to extract a representative shoreline from this type of model because the zero metre contour is static. Instead, the equilibrium (long-term) shoreline shape of headland-bay beaches can be described using the PBSE. However, the PBSE is only valid for idealised wave climates (monochromatic, uni-directional swell), and there is no control on the downcoast limit of the parabolic shoreline (Lausman *et al*., 2010).

In Chapter 5, it was proposed that the downcoast control point needed for the PBSE could be located by using alongshore changes in surf zone morphology (either observed or modelled). Modelling suggested that the change from either Low Tide Terrace or Transverse Bar and Rip to Rhythmic Bar and Beach morphology (after Wright and Short, 1984) represents the point at which the planform ceases to follows a parabola to where it aligns normal to the wave orthogonal. By locating this point the angle of wave obliquity and the control line length can be found, from which the PBSE can be solved. The coupling between surf zone sandbars and shoreline position is readily observable in the field, and has been used in process studies to measure the long-term shoreline position on straight coastlines (Price and Ruessink, 2013; van der Lageweg *et al*., 2013). However, the link between surf zone morphology and shoreline shape on parabolic beaches has thus far been neglected.

To ascertain the equilibrium planforms for range of ‘real-world’ wave climates, a two-dimensional process model could first be run over the area of interest until the morphology attained a dynamic equilibrium with the wave conditions (as in Chapter 5). The alongshore delineation between surf zone morphological types could be then made to locate the downcoast control point and solve the PBSE. This method is described in Figure 5.12. This method does not require any directional wave information for the PBSE, as it is inferred from the control line angle drawn from the diffraction point to the downcoast control point. It also means that the complexity of a variable and bi-modal wave climate can be incorporated into the PBSE through the process model.

REFERENCES

Abbs, D.J., and K.L. McInnes (2004), The impact of climate change on extreme rainfall and coastal sea levels over south-east Queensland. Part 1, Analysis of extreme rainfall and wind events in a GCM. A project undertaken for the Gold Coast City Council, CSIRO Atmospheric Research. Aspendale, Victoria, 48 pp.

Allen, M. A. and J. Callaghan (2000), Extreme wave conditions for the South East Queensland coastal region. Technical Report 32. Queensland Environmental Protection Agency, Brisbane, Queensland.

Allen, R. J., S. C. Sherwood, J. R. Norris and C. S. Zender (2012), Recent Northern Hemisphere tropical expansion primarily driven by black carbon and tropospheric ozone. Nature 485(7398), 350-354.

Allen, R. J., J. R. Norris and M. Kovilakam (2014), Influence of anthropogenic aerosols and the Pacific Decadal Oscillation on tropical belt width. Nature Geoscience 7(4): 270-274.

Almar, R., Cienfuegos, R., Catalan, P.A., Michallet, H., Castelle, B., Bonneton, P. and Marieu, V., (2012), A new breaking wave height direct estimator from video imagery. Coastal Engineering, 61, 42-48.

Alomar, M., Sánchez-Arcilla, A., Bolaños, R, Sairouni, A. (2014), Wave growth and forecasting in variable, semi enclosed domains. Continental Shelf Research 87(15), 28-40.

Alves, J. H. G. M., M. L. Banner and I. R. Young (2003), Revisiting the Pierson–Moskowitz Asymptotic Limits for Fully Developed Wind Waves. Journal of Physical Oceanography 33(7): 1301-1323.

Amante, C. and B.W. Eakins, (2009), ETOPO1 1 Arc-Minute Global Relief Model: Procedures, Data Sources and Analysis. NOAA Technical Memorandum NESDIS NGDC-24. National Geophysical Data Center, NOAA. [access date 30/07/2014].

Arblaster, J. M., G. A. Meehl and D. J. Karoly (2011), Future climate change in the Southern Hemisphere: Competing effects of ozone and greenhouse gases. Geophysical Research Letters 38(2).

Ashok, K., S. K. Behera, S. A. Rao, H. Y. Weng and T. Yamagata (2007), El Nino Modoki and its possible teleconnection. Journal of Geophysical Research-Oceans 112(C11).

Barnard, P. L., A. D. Short, M. D. Harley, K. D. Splinter, S. Vitousek, I. L. Turner, J. Allan, M. Banno, K. R. Bryan, A. Doria, J. E. Hansen, S. Kato, Y. Kuriyama, E. Randall-Goodwin, P. Ruggiero, I. J. Walker and D. K. Heathfield (2015), Coastal vulnerability across the Pacific dominated by El Niño/Southern Oscillation. Nature Geoscience, 8, 801-807.

Battisti, D.S. and A.C. Hirst (1989), Interannual variability in a tropical atmosphere-ocean model: Influence of the basic state, ocean geometry and nonlinearity, Journal of Atmospheric Science, 46, 1687-1712.

BBW [Blain, Bremner and Williams] (1985). Elevated ocean levels, storms affecting the NSW coast 1880-1980. A report prepared for the NSW Public Works Department Coastal Branch in conjunction with Weatherex Meteorological Services, PWD Report No. 85041.

Bell, P.S. (1999), Shallow water bathymetry derived from an analysis of X-band marine radar images of waves. Coastal Engineering, 37(3-4), 513-527.

Benoit, M., F. Marcos, and F. Becq (1996), Development of a third generation shallow-water wave model with unstructured spatial meshing, Proceedings of the 25th International Conference on Coastal Engineering, Orlando, 465–478, ASCE.

Bernadara, P., F. Mazas, X. Kergadallan, and L.Hamm (2014), A two-step framework for over-threshold modelling of environmental extremes. Natural Hazards and Earth System Sciences, 14, 635-647.

Bertin, X., E. Prouteau and C. Letetrel (2013). A significant increase in wave height in the North Atlantic Ocean over the 20th century. Global and Planetary Change 106: 77-83.

Bjerknes, J. (1966), A possible response of the atmospheric Hadley circulation to equatorial anomalies of ocean temperature. Tellus, 18(4), 820-829.

Bond, T. C., S. J. Doherty, D. W. Fahey, P. M. Forster, T. Berntsen, B. J. DeAngelo, M. G. Flanner, S. Ghan, B. Kärcher, D. Koch, S. Kinne, Y. Kondo, P. K. Quinn, M. C. Sarofim, M. G. Schultz, M. Schulz, C. Venkataraman, H. Zhang, S. Zhang, N. Bellouin, S. K. Guttikunda, P. K. Hopke, M. Z. Jacobson, J. W. Kaiser, Z. Klimont, U. Lohmann, J. P. Schwarz, D. Shindell, T. Storelvmo, S. G. Warren and C. S. Zender (2013), Bounding the role of black carbon in the climate system: A scientific assessment. Journal of Geophysical Research: Atmospheres 118(11): 5380-5552.

Booij, N., R.C. Ris and L.H. Holthuijsen (1999), A third-generation wave model for coastal regions 1. Model description and validation. Journal of Geophysical Research, 104, 7649 - 7666.

Bottema, M. and D. Bayer (2001), Evaluation of the Swan Wave Model for the Dutch Ijsselmeer Area. Proceedings of the Fourth International Symposium on Ocean Wave Measurement and Analysis, Waves 2001, San Francisco, California, September 2-6, 2001.

Boukhanovsky, A.V., L.J. Lopatoukhin, and C. Guedes Soares (2007), Spectral wave climates of the North Sea. Applied Ocean Research, 29(3), 146-154.

Bowman, A.W. & A. Azzalini (1997), Applied Smoothing Techniques for Data Analysis: The Kernel Approach with S-Plus Illustrations. Oxford University Press, Oxford, U.K, pp 204.

Boyd, R., K. Ruming, I.D. Goodwin, M. Sandstrom, and C. Schroeder-Adams (2008), Highstand Transport of Coastal Sand to the Deep Ocean: A Case Study from Fraser Island, southeast Australia. Geology, 36 (1): 15-18.

Brocca, L., S. Hasenauer, T. Lacava, F. Melone, T. Moramarco, W. Wagner, W. Dorigo, P. Matgen, J. Martínez-Fernández, P. Llorens, J. Latron, C. Martin and M. Bittelli (2011), Soil moisture estimation through ASCAT and AMSR-E sensors: An intercomparison and validation study across Europe. Remote Sensing of Environment 115(12), 3390-3408.

Bromirski, P. D., D. R. Cayan, J. Helly and P. Wittmann (2013), Wave power variability and trends across the North Pacific. Journal of Geophysical Research: Oceans 118(12), 6329-6348.

Bromirski, P. D., and D. R. Cayan (2015), Wave power variability and trends across the North Atlantic influenced by decadal climate patterns, Journal Geophysical Research: Oceans, 120.

Browne, M., M. Blumenstein, R. Tomlinson and D. Strauss (2005), An intelligent system for remote monitoring and prediction of beach safety. Proceedings of Artificial Intelligence and Applications. Feb 14 – 16 Innsbruck, Austria.

Browning, S. A. and I. D. Goodwin (2013), Large-Scale Influences on the Evolution of Winter Subtropical Maritime Cyclones Affecting Australia's East Coast. Monthly Weather Review 141(7), 2416-2431.

Bruun, P. (1954), Coast erosion and the development of beach profiles. Beach Erosion Board Technical Memorandum 44.US Army Corps of Engineers, Washington DC.

Bruun, P. (1962), Sea level rise as a cause of shore erosion. Journal of Waterways and Harbors Division, ASCE 88, 117–130.

Butman, B., M. A. Noble and D. W. Folger (1979), Long-term observations of bottom current and bottom sediment movement on the mid-Atlantic continental shelf. Journal of Geophysical Research: Oceans 84(C3), 1187-1205.

Cai, W., G. Shi, T. Cowan, D. Bi and J. Ribbe (2005), The response of the Southern Annular Mode, the East Australian Current, and the southern mid-latitude ocean circulation to global warming. Geophysical Research Letters 32, L23706.

Cai, W., S. Borlace, M. Lengaigne, P. van Rensch, M. Collins, G. Vecchi, A. Timmermann, A. Santoso, M. J. McPhaden, L. Wu, M. H. England, G. Wang, E. Guilyardi and F.-F. Jin (2014), Increasing frequency of extreme El Niño events due to greenhouse warming. Nature Climate Change 4(2), 111-116.

Cai, W., G. Wang, A. Santoso, M. J. McPhaden, L. Wu, F.-F. Jin, A. Timmermann, M. Collins, G. Vecchi, M. Lengaigne, M. H. England, D. Dommenget, K. Takahashi and E.

Guilyardi (2015a), Increased frequency of extreme La Niña events under greenhouse warming. Nature Climate Change 5(2), 132-137.

Cai, W., A. Santoso, G. Wang, S.-W. Yeh, S.-I. An, K. M. Cobb, M. Collins, E. Guilyardi, F.-F. Jin, J.-S. Kug, M. Lengaigne, M. J. McPhaden, K. Takahashi, A. Timmermann, G. Vecchi, M. Watanabe and L. Wu (2015b), ENSO and greenhouse warming. Nature Climate Change 5(9), 849-859.

Caires, S., J. Groeneweg, and A. Sterl (2006), Changes in the North Sea extreme waves. Proceedings of the Ninth International Workshop on Wave Hindcasting & & Forecasting, Victoria, B.C. Canada, September 24-29, 2006.

Calinski, T. & J. Harabaz (1974), A dendrite method for cluster analysis. Communications in Statistics, 3, 1-27.

Callaghan, D. P., P. Nielsen, A. Short, and R. Ranasinghe (2008), Statistical simulation of wave climate and extreme beach erosion. Coastal Engineering, 55, 375-390.

Callaghan, J. and P. Helman (2008), Severe storms on the east coast of Australia 1770-2008. Griffith Centre for Coastal Management, Griffith University, Gold Coast, Queensland, p240.

Camus, P., F. J. Mendez, R. Medina and A.S. Cofiño (2011a), Analysis of clustering and selection algorithms for the study of multivariate wave climate. Coastal Engineering, 58, 453-462.

Camus, P., A. Cofiño, F.J. Mendez and R. Medina (2011b), Multivariate wave climate using self-organizing maps. Journal of Atmospheric and Oceanic Technology, 28, 1554-1658.

Camus, P., M. Menéndez, F. J. Méndez, C. Izaguirre, A. Espejo, V. Cánovas, J. Pérez, A. Rueda, I. J. Losada and R. Medina (2014), A weather-type statistical downscaling framework for ocean wave climate. Journal of Geophysical Research: Oceans 119(11), 7389-7405.

Cao, Y. (unpublished, 2008), Bivariate Kernel Density Estimation (V2.1) - a tool for bivariant pdf, cdf and icdf estimation using Gaussian kernel function (20 March 2008, updated 12 August 2013). Retrieved from MATLAB file exchange on 7th January 2014, http://www.mathworks.com/matlabcentral/fileexchange/19280-bivariant-kernel-density-estimation--v2-1-/content/gkde2.zip.

Cardno (2012), NSW coastal waves: numerical modelling final report. A report prepared for the Office of Environment and Heritage NSW. Report No. LJ2949/R2745.

Cardno (2013), NSW Coastal Wave Modelling - Phase II. Report prepared for Office of Environment and Heritage NSW.

Catálan, P. A. and M. C. Haller (2008), Remote sensing of breaking wave phase speeds with application to non-linear depth inversions. Coastal Engineering 55(1): 93-111.

Cavaleri, L. (2006), Wave Modeling: Where to Go in the Future. Bulletin of the American Meteorological Society 87(2): 207-214.

Church, J.A., P.U. Clark, A. Cazenave, J.M. Gregory, S. Jevrejeva, A. Levermann, M.A. Merrifield, G.A. Milne, R.S. Nerem, P.D. Nunn, A.J. Payne, W.T. Pfeffer, D. Stammer and A.S. Unnikrishnan, (2013), Sea Level Change. In: Climate Change 2013: The Physical Science Basis. Contribution of Working Group I to the Fifth Assessment Report of the Intergovernmental Panel on Climate Change [Stocker, T.F., D. Qin, G.-K. Plattner, M. Tignor, S.K. Allen, J. Boschung, A. Nauels, Y. Xia, V. Bex and P.M. Midgley (eds.)]. Cambridge University Press, Cambridge, United Kingdom and New York, NY, USA.

Coelho, C., R. Silva, F. Veloso-Gomes, and F. Taveira-Pinto (2009), Potential effects of climate change on northwest Portuguese coastal zones. ICES Journal of Marine Science, 66, 1497–1507.

Coghlan, I., M. A. Mole, T. D. Shand, J. T. Carley, W. L. Peirson, B. Miller, M. Kulmar, E. Couriel, B. Modra and B. You (2011), High Resolution Wave Modelling (HI-WAM) for Batemans Bay Detailed Wave Study. Proceedings of the 20th Australasian Coastal and Ocean Engineering Conference, Institution of Engineers Australia, Perth, Australia, 215 – 221.

Coles, S. (2001), An introduction to statistical modelling of extreme values. Springer, London, pp 209.

Collins, J.I. (1972), Prediction of shallow water spectra. Journal of Geophysical

Research, 77, 2693-2707.

Collins, M., S.-I. An, W. Cai, A. Ganachaud, E. Guilyardi, F.-F. Jin, M. Jochum, M. Lengaigne, S. Power, A. Timmermann, G. Vecchi and A. Wittenberg (2010), The impact of global warming on the tropical Pacific Ocean and El Nino. Nature Geoscience 3(6), 391-397.

Cornett A.M. (2008). A global wave energy resource assessment. 18th International Society of Offshore and Polar Engineers (ISOPE) Conference, Vancouver, Canada, ISOPE-2008-TPC-579.

Cowell, P. J., P.S. Roy and R.A. Jones (1992), Shoreface Translation Model: Computer Simulation of Coastal Sand-Body Response to Sea Level Rise. Mathematics and Computers in Simulation, 33, 603-608.

Cowell, P. J., P.S. Roy and R.A. Jones (1995), Simulation of Large Scale Coastal Change Using a Morphological Behaviour Model. Marine Geology, 126, 45-61.

Cowell, P. J., D.J. Hanslow and J.F. Meleo (1999), The Shoreface. In: Short, A. D. (ed.) Handbook of Beach and Shoreface Morphodynamics. New York: John Wiley.

Cowell, P. J., B. G. Thom, R. A. Jones, C. H. Everts and D. Simanovic (2006), Management of Uncertainty in Predicting Climate-Change Impacts on Beaches. Journal of Coastal Research, 221, 232-245.

Cox, C. and W. Munk (1954), Measurement of the Roughness of the Sea Surface from Photographs of the Sun's Glitter. Journal of the Optical Society of America, 44 (11), 835-850.

Daley, M. and P.J. Cowell (2012), Long-Term Shoreface Response to Disequilibrium-Stress: A Conundrum for Climate Change. Proceedings of the 21st NSW Coastal Conference, Kiama, NSW, Australia.

Datawell (2014). Directional Waverider MkIII Specifications. Datawell BV.

Davidson, M., M.V. Koningsveld, A. de Kruif, J. Rawson, R. Holman, A. Lamberti, R. Medina, A. Kroon and S. Aarninkhof (2007), The CoastView project: developing coastal video monitoring systems in support of coastal zone management. Coastal Engineering, 54, 463–475.

de Vries, S., D.F. Hill, M.A. Schipper and M.J.F. Stive (2011), Remote sensing of surf zone waves using stereo imaging. Coastal Engineering 58(3), 239-250.

Dean, R.G. (1991), Equilibrium Beach Profiles: Characteristics and Applications. Journal of Coastal Research, 7 (1), 53-84.

Dean, R.G. and E.M. Maurmeyer, (1983), Models of beach profile response. In: P. Komar and J. Moore (Editors), CRC Handbook of Coastal Processes and Erosion. CRC Press, Boca Raton, FL, 151-165.

Dean, R. G. and R.A. Dalrymple (2004), Coastal Processes with Engineering Applications. Cambridge University Press, Cambridge, U.K. pp 489.

Dee, D. P., S. M. Uppala, A. J. Simmons, P. Berrisford, P. Poli, S. Kobayashi, U. Andrae, M. A. Balmaseda, G. Balsamo, P. Bauer, P. Bechtold, A. C. M. Beljaars, L. van de Berg, J. Bidlot, N. Bormann, C. Delsol, R. Dragani, M. Fuentes, A. J. Geer, L. Haimberger, S. B. Healy, H. Hersbach, E. V. Hólm, L. Isaksen, P. Kållberg, M. Köhler, M. Matricardi, A. P. McNally, B. M. Monge-Sanz, J. J. Morcrette, B. K. Park, C. Peubey, P. de Rosnay, C. Tavolato, J. N. Thépaut and F. Vitart (2011), The ERA-Interim reanalysis: configuration and performance of the data assimilation system. Quarterly Journal of the Royal Meteorological Society 137(656): 553-597.

Department of Climate Change (2009), Climate Change Risks to Australia's Coasts - a First Pass National Assessment. Department of Climate Change (DECC), Australian Government.

Department of Planning (2008), New South Wales State and Regional Population Projections, 2006-2036: 2008 Release. Sydney: Department of Planning, Australian Government.

Department of Planning and Environment (2014), 2014 NSW Population Projections data. Department of Planning and Environment, Australian Government. Available http://www.planning.nsw.gov.au/projections. Accessed 07/11/2015.

Department of the Environment (2015), Climate Change in the Future: Sea Level.

Department of the Environment, Australian Government. Available at https://www.environment.gov.au/climate-change/climate-science/climate-change-future/sea-level. Accessed 07/11/2015.

DHI (2014), MIKE21 SW Spectral Wave Model FM User Guide, MIKE by DHI, Danish Hydraulics Institute, Denmark, 122 pp.

DHI (2014), MIKE21/3 Coupled Model FM User Guide, MIKE by DHI, Danish Hydraulics Institute, Denmark, 52 pp.

Dowdy, A. J., G. A. Mills, B. Timbal and Y. Wang (2014), Fewer large waves projected for eastern Australia due to decreasing storminess. Nature Climate Change 4(4): 283-286.

Drake, D. E. and D. A. Cacchione (1985), Seasonal variation in sediment transport on the Russian River shelf, California. Continental Shelf Research 4(5), 495-514.

Drosdowsky, W. (2005), The latitude of the subtropical ridge over Eastern Australia: The L index revisited. International Journal of Climatology 25(10), 1291-1299.

Dunn, J. C. (1974), Well separated clusters and optimal fuzzy partions. Journal Cybernetics, 4, 95-104.

Durrant, T. and D. Greenslade (2011), Evaluation and implementation of AUSWAVE. Centre for Australian Weather and Climate Research (CAWCR) Technical Report No041.

Eilers, P.H.C. and J.J. Goeman (2004), Enhancing scatterplots with smoothed densities Bioinformatics, 20, 623 - 628.

Eldeberky, Y. (1996), Nonlinear transformation of wave spectra in the nearshore zone, Ph.D. thesis, Delft University of Technology, Department of Civil Engineering, The Netherlands

Eldeberky, Y. and J. A. Battjes (1996), Spectral modelling of wave breaking: application to Boussinesq equations, Journal of Geophysical Research., 101, C1, 1253–1264.

England, M. H., S. McGregor, P. Spence, G. A. Meehl, A. Timmermann, W. Cai, A. S. Gupta, M. J. McPhaden, A. Purich and A. Santoso (2014), Recent intensification of wind-driven circulation in the Pacific and the ongoing warming hiatus. Nature Climate Change 4(3), 222-227.

Erikson, L. H., C. A. Hegermiller, P. L. Barnard, P. Ruggiero and M. van Ormondt (in press), Projected wave conditions in the Eastern North Pacific under the influence of two CMIP5 climate scenarios. Ocean Modelling.

Fedorov, A. and S.G. Philander (2000), Is El Niño changing? Science 288, 1997–2002.

Foster, D., A. D. Gordon and N. V. Lawson (1975), The Storms of May-June 1974, Sydney NSW. Proceedings of the 2nd Australian Conference on Coastal and Ocean Engineering, Institution of Engineers Australia, Publication 75/2, Gold Coast, Australia, 1-11.

Gagan, M.K., A.R. Chivas, A.L. Herczeg (1990), Shelf-wide erosion, deposition, and suspended sediment transport during Cyclone Winifred, Central Great Barrier Reef, Australia. Journal of Sedimentary Research 60(3), 456-470.

Geoscience Australia and ABARE (2010). Australian Energy Resource Assessment, Canberra. Department of Resources, Energy and Tourism, Australian Government.

Gillett, N. P., and D. W. J. Thompson (2003), Simulation of recent Southern Hemisphere climate change, Science, 302, 273 – 275.

Goda, Y. (2010), Random seas and design of maritime structures. World Scientific, Singapore, pp 464.

Goodwin, I. D. (2005), A mid-shelf, mean wave direction climatology for southeastern Australia, and its relationship to the El Niño—Southern Oscillation since 1878A.D., International Journal of Climatology, 25(13), 1715-1729.

Goodwin, I. D., M. A. Stables and J. M. Olley (2006), Wave climate, sand budget and shoreline alignment evolution of the Iluka–Woody Bay sand barrier, northern New South Wales, Australia, since 3000 yr BP, Marine Geology 226(1-2), 127-144.

Goodwin, I.D., R. Freeman, K. Blackmore (2010), Decadal wave climate variability and implications for interpreting New South Wales Coastal Behaviour. Proceedings of the Australian Wind Waves Research Science Symposium, 19-20 May 2010, Gold Coast, Queensland, Australia, pp 58-61.

Goodwin, I. D., R. Freeman and K. Blackmore (2013a), An insight into headland sand bypassing and wave climate variability from shoreface bathymetric change at Byron Bay, New South Wales, Australia. Marine Geology 341: 29-45.

Goodwin, I.D., T.R. Mortlock, and S. Browning (2013b), Tasman Sea Wave Climate Variability Associated with Shifts in the Subtropical Ridge. 2nd Australasian wind-wave symposium, Melbourne, June, 2013.

Goodwin, I., S. Browning, A. Lorrey, P. Mayewski, S. Phipps, N. N. Bertler, R. Edwards, T. Cohen, T. van Ommen, M. Curran, C. Barr and J. C. Stager (2014), A reconstruction of extratropical Indo-Pacific sea-level pressure patterns during the Medieval Climate Anomaly, Climate Dynamics 43(5-6), 1197-1219.

Goodwin, I.D., T.R. Mortlock, S. Browning and T. Shand (in review), Tropical and Extratropical-Origin Storm Wave Types and Their Contrasting Directional Power Distribution on the Inner Shelf. Continental Shelf Research.

Gordon, A. D. (1999), Classification: 2nd Edition. Chapman and Hall/CRC Press, New York, pp 272.

Griffin, J. D., M. A. Hemer and B. G. Jones (2008), Mobility of sediment grain size distributions on a wave dominated continental shelf, southeastern Australia. Marine Geology 252(1-2): 13-23.

Grose, M. R., M. J. Pook, P. C. McIntosh, J. S. Risbey and N. L. Bindoff (2012), The simulation of cutoff lows in a regional climate model: reliability and future trends. Climate Dynamics, 39(1-2), 445-459.

Grose, M. R., J. N. Brown, S. Narsey, J. R. Brown, B. F. Murphy, C. Langlais, A. S. Gupta, A. F. Moise and D. B. Irving (2014), Assessment of the CMIP5 global climate model simulations of the western tropical Pacific climate system and comparison to CMIP3. International Journal of Climatology 34(12), 3382-3399.

Guanche, Y., R. Mínguez and F.J. Méndez (2013), Climate-based Monte Carlo simulation of trivariate sea states. Coastal Engineering, 80, 107-121.

Gunn, K. and C. Stock-Williams (2012), Quantifying the global wave power resource. Renewable Energy, 44, 296-304.

Hamerly, G., and C. Elkan (2003), Learning the k in k-means. Advances in Neural Information Processing Systems, 16, 2526 – 2532.

Hamilton, L.J. (2010), Characterising spectral sea wave conditions with statistical clustering of actual spectra. Applied Ocean Research, 32, 332-342.

Harley, M. D., I. L. Turner, A. D. Short and R. Ranasinghe (2010), Interannual variability and controls of the Sydney wave climate. International Journal of Climatology, 30, 1332-1335.

Harley, M.D., I.L. Turner, A.D. Short and R. Ranasinghe (2011), A reevaluation of coastal embayment rotation: the dominance of cross-shore versus alongshore sediment transport processes, Collaroy-Narrabeen Beach, southeast Australia, Journal of Geophysical Research, 116, FO04033.

Harley, M. D., I. L. Turner, and A. D. Short (2015), New insights into embayed beach rotation: the importance of wave exposure and cross-shore processes. Journal of Geophysical Research: Earth Surface, 120(8), 1470-1484.

Harris, C. K. and P. Wiberg (2002), Across-shelf sediment transport: Interactions between suspended sediment and bed sediment. Journal of Geophysical Research: Oceans, 107(C1).

Hasselmann, K. (1962), On the nonlinear energy transfer in a gravity-wave spectrum. Part 1. General theory, Journal of Fluid Mechanics., 12, 481–500.

Hasselmann, K., T. P. Barnett, E. Bouws, H. Carlson, D. E. Catrtwright, K. Enke, J. A. Ewing, H. Gienapp, D. E. Hasselmann, P. Kruseman, A. Meerburg, P. Muller, D. J. Olbers, K. Richter, W. Sell and H. Walden (1973), Measurements of wind-wave growth and swell decay during the Joint North Sea Wave Project (JONSWAP). Deutches Hydrographisches Institut.

Hasselmann, S., K. Hasselmann, J.H. Allender, and T.P. Barnett (1985), Computations and parameterizations of the nonlinear energy transfer in a gravity wave spectrum. Part II: Parameterizations of the nonlinear transfer for application in wave models, Journal of Physical Oceanography, 15, 1378-1391.

Hawkes, P., D. Gonzalez-Marco, A.Sánchez-Arcilla and P. Prinos (2008), Best practice for the estimation of extremes: a review. Journal of Hydraulic Research, 46 (2), 324-332.

Hawkins, E. (2013), Sources of uncertainty in CMIP5 projections. Climate Lab Book, Open climate science blog. Available http://www.climate-lab-book.ac.uk/2013/sources-of-uncertainty/, Accessed 08/11/2015.

Helman, P. (2007), Two Hundred Years of Coastline Change and Future Change, Fraser Island to Coffs Harbour, East Coast Australia. Unpublished PhD Thesis, Southern Cross University, Australia.

Hemer, M. A. (2010), Historical trends in Southern Ocean storminess: Long-term variability of extreme wave heights at Cape Sorell, Tasmania. Geophysical Research Letters, 37(18), l18601.

Hemer, M. A., I. Simmonds and K. Keay (2008), A classification of wave generation characteristics during large wave events on the Southern Australian margin. Continental Shelf Research, 28, 634-652.

Hemer, M. A., J. A. Church and J. R. Hunter (2009), Variability and trends in the directional wave climate of the Southern Hemisphere. International Journal of Climatology, 30, 475-491.

Hemer, M. A. and D.A. Griffin (2010), The wave energy resource along Australia's Southern margin. Journal of Renewable and Sustainable Energy 2 (4) 043108.

Hemer, M. A., K. McInnes and R. Ranasinghe (2012), Climate and variability bias adjustment of climate model-derived winds for a southeast Australian dynamical wave model. Ocean Dynamics, 62, 87-104.

Hemer, M. A., J. Katzfey and C. E. Trenham (2013a), Global dynamical projections of surface ocean wave climate for a future high greenhouse gas emission scenario. Ocean Modelling, 70, 221-245.

Hemer, M. A., Y. Fan, N. Mori, A. Semedo and X. L. Wang (2013b), Projected changes in wave climate from a multi-model ensemble. Nature Climate Change 3(5), 471-476.

Hilmer, T. (2005), Measuring breaking wave heights using video, PhD Thesis, The University of Hawai'i at Manoa.

Holbrook, N. J., I. D. Goodwin, S. McGregor, E. Molina and S. B. Power (2011), ENSO to multi-decadal time scale changes in East Australian Current transports and Fort Denison sea level: Oceanic Rossby waves as the connecting mechanism. Deep Sea Research Part II: Topical Studies in Oceanography, 58(5), 547-558.

Holland, K.T, R.A. Holman, T.C. Lippman, J. Stanley, and N. Plant (1997), Practical use of video imagery in nearshore oceanographic field studies. IEEE Journal of Oceanic Engineering, 22(1), 81-92.

Holman, R.A. and J, Stanley (2007), The history and technical capabilities of Argus. Coastal Engineering, 54, 477-491.

Holthuijsen, L. H. (2007), Waves in oceanic and coastal waters. Cambridge University Press, Cambridge, U.K. pp 387.

Holthuijsen, L. H., A. Herman and N. Booij (2003), Phase-decoupled refraction–diffraction for spectral wave models. Coastal Engineering, 49(4), 291-305.

Hopkins, L. C. and G. J. Holland (1997), Australian heavy-rain days and associated east coast cyclones: 1958-92. Journal of Climate, 10(4), 621-635.

Hsu, J.R.C., and C. Evans (1989), Parabolic bay shapes and applications. Proceedings of the Institute of Civil Engineers, 87 (2). Thomas Telford, London, pp. 557-570.

Hu, Y. and Q. Fu (2007), Observed poleward expansion of the Hadley circulation since 1979, Atmospheric Chemistry and Physics, 7(19), 5229-5236.

Hubert, L. J., & Levin, J. R. (1976), A general statistical framework for assessing categorical clustering in free recall. Psychological Bulletin, 83, 1072-1080.

Hughes, M. G., and A.D. Heap (2010), National-scale wave energy resource assessment for Australia. Renewable Energy, 35, 1783-1791.

International Hydrographic Organization (IHO), (1953), Limits of Oceans and Seas, International Hydrographic Organization, Bremerhaven, PANGAEA, pp 44.

IPCC, 2014 Climate Change 2014: Synthesis Report. Contribution of Working Groups I, II and III to the Fifth Assessment Report of the Intergovernmental Panel on Climate Change [Core Writing Team, R.K. Pachauri and L.A. Meyer (eds.)]. IPCC, Geneva, Switzerland, 151 pp.

Janssen, P.A.E.M. (1991), Quasi-linear theory of wind-wave generation applied to wave forecasting, Journal of Physical Oceanography, 21, 1631-1642.

Jeffreys, H. (1924), On the formation of waves by wind. Proceedings of the Royal Society A 107, 189–206.

Jeffreys, H. (1925), On the formation of waves by wind. II. Proceedings of the Royal Society A 110, 341–347.

Johanson, C. M. and Q. Fu (2009), Hadley cell widening: Model simulations versus observations, Journal of Climate, 22, 2713–2725.

Johnson, D. (1919), Shore Processes and Shoreline Development. Wiley, New York, pp 617.

Jordan, A., P. Davies, T. Ingleton, E. Foulsham, J. Neilson, T. Pritchard (2010), Seabed Habitat Mapping of the Continental Shelf of NSW. Department of Environment, Climate Change and Water (DECCW). Australian Government.

Kalnay, E., M. Kanamitsu, R. Kistler, W. Collins, D. Deaven, L. Gandin, M. Iredell, S. Saha, G. White, J. Woollen, Y. Zhu, M. Chelliah, W. Ebisuzaki, W. Higgins, J. Janowiak, K. C. Mo, C. Ropelewski, J. Wang, A. Leetmaa, R. Reynolds, R. Jenne and D. Joseph (1996), The NCEP/NCAR 40-year reanalysis project. Bulletin of the American Meteorological Society, 77(3), 437-471.

Kirby, J.T. (1986), Higher-order approximations in the parabolic equation method for water waves, Journal of Geophysical Research, 91(C1), 933–952.

Kirby, J.T. and R.A. Dalrymple (1983), A parabolic equation for the combined refraction-diffraction of Stokes waves by mildly-varying topography, Journal of Fluid Mechanics, 136, 453-466.

Komar, P. D. and J. C. Allan (2008), Increasing hurricane-generated wave heights along the US East Coast and their climate controls. Journal of Coastal Research, 24(2), 479-488.

Komen, G. J., L. Cavaleri, M. Donelan, K. Hasselmann, S. Hasselmann and P. A. E. M. Janssen (1994), Dynamics and modelling of ocean waves. Cambridge University Press, pp 556.

Kosaka, Y. and S.-P. Xie (2013), Recent global-warming hiatus tied to equatorial Pacific surface cooling. Nature 501(7467), 403-407.

Kroon, A., M.A. Davidson, S.G.J. Aarninkhof, R. Archetti, C. Armaroli, M. Gonzalez, S. Medri, A. Osorio, T. Aagaard, R.A. Holman, and R. Spanhoff (2007), Application of remote sensing video systems to coastline management problems. Coastal Engineering, 54, 493-505.

Krzanowski, W.J. and Y.T. Lai (1985), A criterion for determining the number of groups in a data set using sum-of-squares clustering. Biometrics, 44, 23-34.

Kulmar, M. (2013), NSW Wave Climate and Coastal Air Pressure Annual Summary 2012 – 2013. Report MHL2221.Manly Hydraulics Lab Report.

Kulmar, M., B. Modra and M. Fitzhenry (2013), The New South Wales Wave Climate Improved Understanding through the Introduction of Directional Wave Monitoring Buoys. Proceedings of the Coasts and Ports Conference, 11-13 September, 2012.

Lane, C., Y. Gal, M. Browne, A.D. Short, D. Strauss, K. Jackson and C. Tan (2010), A new system for break zone location and the measurement of breaking wave heights and periods. Proceedings of IEEE International Geoscience and Remote Sensing Symposium (Honolulu, Hawaii, USA), pp. 2234-2236.

Laughlin, G.P. (1997), The user's guide to the Australian coast. Frenchs Forest, NSW, New Holland, pp 213.

Lausman, R., A. H. F. Klein and M. J. F. Stive (2010), Uncertainty in the application of the Parabolic Bay Shape Equation: Part 1. Coastal Engineering, 57(2), 132-141.

Lawson, N.V. and C.L. Abernethy (1975), Long Term Wave Statistics off Botany Bay. Second Australian Conference on Coastal and Ocean Engineering: The Engineer, the Coast and the Ocean, Institution of Engineers Australia, Sydney, 169-178.

Lee, T. and M. J. McPhaden (2010), Increasing intensity of El Niño in the central-equatorial Pacific. Geophysical Research Letters 37(14).

Liu, P. C., D. J. Schwab and R. E. Jensen (2002), Has wind-wave modeling reached its limit?, Ocean Engineering, 29(1), 81-98.

Lord D.B. and M. Kulmar (2000), The 1974 Storms Revisited: 25 Years' Experience in Ocean Wave Measurement Along the South-East Australian Coast, Proceedings International Conference of Coastal Engineering, pp 559-572, American Society of Civil Engineers, USA.

Lucas, C., B. Timbal and H. Nguyen (2014), The expanding tropics: a critical assessment of the observational and modeling studies. Wiley Interdisciplinary Reviews: Climate Change 5(1), 89-112.

Madsen, O.S., Y.K. Poon and H.C. Graber (1988), Spectral wave attenuation by bottom friction: Theory. Proceedings of the 2st International Conference on Coastal Engineering, ASCE, 492-504.

Madsen, P. A., R. Murray and O. R. Sørensen (1991), A new form of the Boussinesq equations with improved linear dispersion characteristics. Coastal Engineering, 15(4), 371-388.

Madsen, P. A. and O. R. Sørensen (1992), A new form of the Boussinesq equations with improved linear dispersion characteristics. Part 2: a slowly-varying bathymetry, Coastal Engineering, 18, 3–4, 183–205.

Mantua, N. J. and D. S. Battisti (1994), Evidence for the Delayed Oscillator Mechanism for ENSO: The "Observed" Oceanic Kelvin Mode in the Far Western Pacific. Journal of Physical Oceanography, 24(3), 691-699.

Marshall, G. J. (2003), Trends in the southern annular mode from observations and reanalyses. Journal of Climate, 16(24), 4134-4143.

Masselink, G. and C.B. Pattiaratchi (2001), Characteristics of the sea-breeze system in Perth, Western Australia, and its effect on the nearshore wave climate. Journal of Coastal Research, 17(1), 173-187.

Mathiesen, M., Y. Goda, P.J. Hawkes, E. Mansard, M.J. Martín, E. Peltier, E.F. Thompson, G. Van Vledder (1994), Recommended practice for extreme wave analysis. Journal of Hydraulic Research, 32 (6), 803–814.

Mayewski, P. A., T. Bracegirdle, I. Goodwin, D. Schneider, N. A. N. Bertler, S. Birkel, A. Carleton, M. H. England, J. H. Kang, A. Khan, J. Russell, J. Turner and I. Velicogna (2015), Potential for Southern Hemisphere climate surprises. Journal of Quaternary Science, 30(5), 391-395.

Mazas, F., and L. Hamm (2011), A multi-distribution approach to POT methods for determining extreme wave heights. Coastal Engineering, 58(5), 385-394.

McPhaden, M. J., S. E. Zebiak, and M.H. Glantz (2006), ENSO as an integrating concept in Earth science. Science, 314, 1740–1745.

Méndez, F.J., M. Menéndez, A. Luceño, I.J. Losada (2006), Estimation of long-term variability of extreme significant wave height using a time-dependent Peaks Over Threshold (POT) model. Journal of Geophysical Research, 111(C07), C07024.

Milligan, G., and M. Cooper (1985), An examination of procedures for determining the number of clusters in a data set. Psychometrika, 50(2), 159-179.

Moeini, M. H. and A. Etemad-Shahidi (2007), Application of two numerical models for wave hindcasting in Lake Erie. Applied Ocean Research, 29(3), 137-145.

Montoya, R.D., A. Osorio Arias, J.C. Ortiz Royero, F.J. Ocampo-Torres (2013), A wave parameters and directional spectrum analysis for extreme winds. Ocean Engineering, 67, 100-118.

Mori, N., T. Shimura, T. Yasuda and H. Mase (2013), Multi-model climate projections of ocean surface variables under different climate scenarios—Future change of waves, sea level and wind. Ocean Engineering, 71, 122-129.

Mortlock, T.R. and I.D. Goodwin (2013), Calibration and Sensitivity of Nearshore SWAN Model Performance for Measured and Modelled Wave Forcing Scenarios, Wamberal, Australia. Climate Futures at Macquarie. Report prepared for Office of Environment and Heritage NSW.

Mortlock, T.R. and I.D. Goodwin (2015), Directional Wave Climate and Power Variability along the Southeast Australian Shelf. Continental Shelf Research, 98, 36-53.

Moskowitz, L. (1964), Estimates of the power spectrums for fully developed seas for wind speeds of 20 to 40 knots. Journal of Geophysical Research, 69(24), 5161-5179.

Munk, W. H. (2010), Origin and Generation of Waves. Proceedings of First Conference on Coastal Engineering, Long Beach, California, October, 1950.

Munk, W. H., and M. Traylor (1947), Refraction of ocean waves: a process linking underwater topography to beach erosion. The Journal of Geology, 55(1), 1-14.

Munk, W. H., R.C. Spindel, A. Baggeroer, and T.G. Birdsall (1994), The Heard Island Feasibility Test. The Journal of the Acoustical Society of America, 96(4), 2330-2342.

Neelin, J. D., D. S. Battisti, A. C. Hirst, F.-F. Jin, Y. Wakata, T. Yamagata and S. E. Zebiak (1998), ENSO theory. Journal of Geophysical Research: Oceans, 103(C7), 14261-14290

Nicholls, R.J., P.P.Wong, V.R. Burkett, J.O. Codignotto, J.E. Hay, R.F. McLean, S. Ragoonaden and C.D.Woodroffe, 2007: Coastal systems and low-lying areas. Climate Change 2007: Impacts, Adaptation and Vulnerability. Contribution ofWorking Group II to the Fourth Assessment Report of the Intergovernmental Panel on Climate Change, M.L. Parry, O.F. Canziani, J.P. Palutikof, P.J. van der Linden and C.E. Hanson, Eds., Cambridge University Press, Cambridge, UK, 315-356.

Nicholls, R. J., I.H. Townend, A. Bradbury, D. Ramsbottom, and S.A. Day (2013), Planning for long-term coastal change: experiences from England and Wales. Ocean Engineering, 71, 3-16.

Nieto, M.A., B. Garau, S. Balle, G. Simarro, G.A. Zarruk, A. Ortiz, J. Tintore, A. Alvarez-Ellacuria, L. Gomez-Pujol, and A. Orfila (2010), An open-source, low cost video-based coastal monitoring system. Earth Surface Processes and Landforms, 35(14), 1712-1719.

O'Donoghue, T. and S. Wright (2004), Flow tunnel measurements of velocities and sand flux in oscillatory sheet flow for well-sorted and graded sands. Coastal Engineering, 51(11–12), 1163-1184.

Peixoto, J. and A. Oort (1992), Physics of Climate, American Institute of Physics, New York, USA, pp 520.

Pelleg, D., and A. Moore (2000), X-means: extending k-means with efficient estimation of the number of clusters. Proceedings of the Seventeenth International Conference on Machine Learning, San Francisco, USA, 727-734.

Piani, C., J.O. Haerter, and E. Coppola (2010), Statistical bias correction for daily precipitation in regional climate models over Europe. Theoretical and Applied Climatology, 99, 187 – 192.

Piepmeier, J. A. and J. Waters (2004), Analysis of Stereo Vision-Based Measurements of Laboratory Water Waves. Proceedings of the IGARSS Geoscience and Remote Sensing Symposium, 2004, IEEE International (Volume 5), 3588 – 3591.

Pierson, W. J., G. Neumann and R. W. James (1955), Practical Methods for Observing and Forecasting Ocean Waves by Means of Wave Spectra and Statistics, Washington, U.S.Navy Hydrographic Office, Publication No. 603 (reprinted 1960), 284 pp.

Pierson, W. J. and L. Moskowitz (1964), A proposed spectral form for fully developed wind seas based on the similarity theory of S. A. Kitaigorodskii, Journal of Geophysical Research, 69(24), 5181–5190.

Pittock, A.B. (1973), Global meridional interactions in stratosphere and troposphere. Quarterly Journal of the Royal Meteorological Society, 99(421), 424–437.

Polvani, L. M., D. W. Waugh, G. J. P. Correa and S.-W. Son (2011), Stratospheric Ozone Depletion: The Main Driver of Twentieth-Century Atmospheric Circulation Changes in the Southern Hemisphere. Journal of Climate, 24(3), 795-812.

Price, T.D. and B.G. Ruessink (2013), Observations and conceptual modelling of morphological coupling in a double sandbar system. Earth Surface Processes and Landforms, 38, 477-489.

PWD (1986), Elevated ocean levels – Storms affecting the NSW coast 1980-1985. Report prepared by Lawson and Treloar Pty. Ltd. for the NSW Public Works Department Coastal Branch, in conjunction with Weatherex Meteorological Services, PWD Report No. 86026.

Quartel, S. (2009), Temporal and spatial behaviour of rip channels in a multiple-barred coastal system. Earth Surface Processes and Landforms, 34, 163 – 176.

Ranasinghe, R., R. McLoughlin, A. Short and G. Symonds (2004), The Southern Oscillation Index, wave climate, and beach rotation. Marine Geology, 204(3-4), 273-287.

Ranasinghe, R., P. Watson, D. Lord, D. Hanslow, and P. Cowell (2007), Sea Level Rise, Coastal Recession and the Bruun Rule. Proceedings of Coast and Ports Conference, Melbourne, Australia, Engineers Australia.

Ranasinghe, R., T. M. Duong, S. Uhlenbrook, D. Roelvink and M. Stive (2012), Climate-change impact assessment for inlet-interrupted coastlines. Nature Climate Change, 3(1), 83-87.

Ribberink, J. S. and A. A. Al-Salem (1994), Sediment transport in oscillatory boundary layers in cases of rippled beds and sheet flow. Journal of Geophysical Research: Oceans, 99(C6), 12707-12727.

Ridgway, K. R. (2007), Long-term trend and decadal variability of the southward penetration of the East Australian Current. Geophysical Research Letters, 34(13).

Ris, R.C., L.H. Holthuijsen and N. Booij (1999), A third-generation wave model for coastal regions 2. Verification. Journal of Geophysical Research, 104, 7667 - 7681.

Rollason, V., and I.D. Goodwin (2009), Coffs Harbour Coastal Processes Progress Report. BMT WBM and Climate Futures at Macquarie, Macquarie University. Report prepared for Coffs Harbour City Council.

Rosati, J. D., R. G. Dean and T. L. Walton (2013), The modified Bruun Rule extended for landward transport. Marine Geology, 340, 71-81.

Rousseeuw, P. (1987), Silhouettes: a graphical aid to the interpretation and validation of cluster analysis. Journal of Computational and Applied Mathematics, 20(1), 53-65.

Roy, P.S. and A.W. Stephens (1980), Regional geological studies of the N.S.W. inner continental shelf: summary results. Geological Survey Report No GS 1980/028. Geological Survey of New South Wales, Department of Mines, Sydney Australia.

Ruessink, B. G., H. Michallet, T. Abreu, F. Sancho, D. A. Van der A, J. J. Van der Werf and P. A. Silva (2011), Observations of velocities, sand concentrations, and fluxes under velocity-asymmetric oscillatory flows. Journal of Geophysical Research: Oceans 116(C3).

Ruessink, B. G., G. Ramaekers and L. C. van Rijn (2012), On the parameterization of the free-stream non-linear wave orbital motion in nearshore morphodynamic models. Coastal Engineering, 65, 56-63.

Ruggiero, P., P. D. Komar and J. C. Allan (2010), Increasing wave heights and extreme value projections: The wave climate of the U.S. Pacific Northwest. Coastal Engineering 57(5), 539-552.

Saha, S., S. Moorthi, H.-L. Pan, X. Wu, J. Wang, S. Nadiga, P. Tripp, R. Kistler, J. Woollen, D. Behringer, H. Liu, D. Stokes, R. Grumbine, G. Gayno, J. Wang, Y.-T. Hou, H.-Y. Chuang, H.-M. H. Juang, J. Sela, M. Iredell, R. Treadon, D. Kleist, P. Van Delst, D. Keyser, J. Derber, M. Ek, J. Meng, H. Wei, R. Yang, S. Lord, H. Van Den Dool, A. Kumar, W. Wang, C. Long, M. Chelliah, Y. Xue, B. Huang, J.-K. Schemm, W. Ebisuzaki, R. Lin, P. Xie, M. Chen, S. Zhou, W. Higgins, C.-Z. Zou, Q. Liu, Y. Chen, Y. Han, L. Cucurull, R. W. Reynolds, G. Rutledge and M. Goldberg (2010), The NCEP Climate Forecast System Reanalysis. Bulletin of the American Meteorological Society, 91(8), 1015-1057.

SCOR (1991), The response of beaches to sea level changes: a review of predictive models. Journal of Coastal Research, 7, 895-921.

Schopf, P.S. and M.J. Suarez (1988), Vacillations in a coupled ocean-atmosphere model. Journal of Atmospheric Science, 45, 549-566.

Seidel, D. J., Q. Fu, W. J. Randel and T. J. Reichler (2008), Widening of the tropical belt in a changing climate. Nature Geoscience, 1(1), 21-24.

Semedo, A., K. Sušelj, A. Rutgersson and A. Sterl (2011), A global view on the wind-sea and swell climate and variability from ERA-40. Journal of Climate, 24(5), 1461-1479.

Shand, T. D., I. D. Goodwin, M. A. Mole, J. T. Carley, S. A. Browning, I. Coghlan, M. D. Harley and W. J. Pierson (2011a), NSW Coastal Inundation Hazards Study: Coastal Storms and Extreme Waves, Water Research Laboratory & Climate Futures at Macquarie University, WRL Technical Report 2010/16, University of New South Wales, pp 75.

Shand, T., M.A. Mole, J.T. Carley, W.L. Peirson, and R.J. Cox (2011b), Coastal storm data analysis: provision of extreme wave data for adaptation planning. Water Research Laboratory, University of New South Wales.

Shand, T.D., D.G. Bailey, and R.D. Shand (2012), Automated detection of breaking wave height using an optical technique. Journal of Coastal Research, 28(3), 671-682.

Shi, F., J. T. Kirby, J. C. Harris, J. D. Geiman and S. T. Grilli (2012), A high-order adaptive time-stepping TVD solver for Boussinesq modeling of breaking waves and coastal inundation. Ocean Modelling, 43-44, 36-51.

Shinoda, T., H. E. Hurlburt and E. J. Metzger (2011), Anomalous tropical ocean circulation associated with La Niña Modoki. Journal of Geophysical Research, 116(C12).

Short, A.D. (1999), Handbook of Beach and Shoreface Morphodynamics. John Wiley & Sons, California, pp 392.

Short, A.D. (2007), Beaches of the New South Wales coast: a guide to their nature, characteristics, surf and safety (2nd edition), Sydney University Press, Sydney, pp 398.

Short, A. D., and N.L. Trenaman (1992), Wave climate of the Sydney region, an energetic and highly variable ocean wave regime. Marine and Freshwater Research, 43, 765-791.

Short, A.D., A.C. Trembanis, I.L. Turner (2000), Beach oscillation, rotation and the Southern Oscillation, Narrabeen Beach, Australia. Proceedings 27th International Coastal Engineering Conference. ASCE, Sydney, pp. 2439-2452.

Slott, J. M., A.B. Murray, A.D. Ashton, and T.J. Crowley (2006), Coastline responses to changing storm patterns. Geophysical Research Letters, 33, L18404.

Southgate, H. N. (1995), The effects of wave chronology on medium and long term coastal morphology. Coastal Engineering, 26, 251-270.

Speer, M. S., P. Wiles and A. Pepler (2009), Low pressure systems off the New South Wales coast and associated hazardous weather: establishment of a database. Australian Meteorological and Oceanographic Journal, 58, 29-39.

Stockdon, H. F. and R. A. Holman (2000), Estimation of wave phase speed and nearshore bathymetry from video imagery. Journal of Geophysical Research-Oceans 105(C9), 22015-22033.

Storlazzi, C.D. and G.B. Griggs, (2000), Influence of El Niño-Southern Oscillation (ENSO) events on the evolution of central California’s shoreline. Geological Society of America Bulletin, 112 (2), 236-249.

Storlazzi, C.D. and D.K. Wingfield (2005), Spatial and temporal variations in oceanographic and meteorologic forcing along the central Californian coast, 1980 – 2002. USGS Scientific Investigations Report 2005-5085.

Storlazzi, C.D., E. Brown, M.E. Field, K. Rodgers and P.L. Jokiel (2005), A model for wave control on coral breakage and species distribution in the Hawaiian Islands. Coral Reefs, 24(1), 43-55.

Strauss, D., H. Mirferendesk and R. Tomlinson (2007), Comparison of two wave models for Gold Coast, Australia. Journal of Coastal Research, 312-316.

Sverdrup, H. U. and W. H. Munk (1947), Wind, sea and swell : theory of relations for forecasting. Scripps Institute of Oceanography. Hydrographic Office, Washington D.C.

SWAMP Group (1985), Ocean Wave Modeling. Plenum Press, New York, p. 266.

SWAN (2011a), User Manual SWAN Cycle III version 40.85. Delft University of Technology, Netherlands.

SWAN (2011b), Technical Manual SWAN Cycle III version 40.85. Delft University of Technology, Netherlands.

Takahashi, K. and B. Dewitte (2015), Strong and moderate nonlinear El Niño regimes. Climate Dynamics.

Takahashi, K., A. Montecinos, K. Goubanova and B. Dewitte (2011), ENSO regimes: Reinterpreting the canonical and Modoki El Niño. Geophysical Research Letters, 38, L10704.

Taschetto, A. S. and M. H. England (2009), El Niño Modoki Impacts on Australian Rainfall. Journal of Climate, 22(11), 3167-3174.

Thompson, D. W. J. and J.M. Wallace (2000), Annular Modes in the Extratropical Circulation. Part I: Month-to-Month Variability. Journal of Climate, 13, 1000-1016.

Thompson, D.W.J. and S. Solomon (2002), Interpretation of recent Southern Hemisphere climate change. Science, 296, 895–899.

Thompson, P., Y. Cai, D. Reeve, J. Stander (2009), Automated threshold selection methods for extreme wave analysis. Coastal Engineering, 56, 1013–1021.

Timbal, B. and W. Drosdowsky (2013), The relationship between the decline of Southeastern Australian rainfall and the strengthening of the subtropical ridge. International Journal of Climatology, 33(4), 1021-1034.

Tolman, H. L. (2009), User Manual and System Documentation of WAVEWATCH III version 3.14. NOAA, US Department of Commerce.

Turner, I.L. and D.J. Anderson (2007), Web-based and ‘real-time’ beach management system. Coastal Engineering, 54, 555-565.

US Army Corps of Engineers (2002), Shore Protection Manual Volume 1. Coastal Engineering Research Center, Department of the Army, Mississippi, USA.

van de Lageweg, W. I., K. R. Bryan, G. Coco and B. G. Ruessink (2013), Observations of shoreline–sandbar coupling on an embayed beach. Marine Geology, 344, 101-114.

Vecchi, G. A., B. J. Soden, A. T. Wittenberg, I. M. Held, A. Leetmaa and M. J. Harrison (2006), Weakening of tropical Pacific atmospheric circulation due to anthropogenic forcing. Nature, 441(7089), 73-76.

Velmurugan, T. and T. Santhanam (2010), Computational Complexity between K-Means and K-Medoids Clustering Algorithms for Normal and Uniform Distributions of Data Points. Journal of Computer Science, 6(3), 363-368.

von Storch, H., and F.W. Zwiers, (1999). Statistical Analysis in Climate Research. Cambridge University Press, Cambridge, pp 484.

WAMDI group (1988), The WAM model – a third generation ocean wave prediction model, Journal of Physical Oceanography, 18(12), 1775–1810.

Wang, D.W. and P.A. Hwang (2001), An operational method for separating wind sea and swell from ocean wave spectra. Journal of Atmospheric & Oceanic Technology, 18(12), 2052 – 2063.

Wang, K., B. Wang and L. Peng (2009), CVAP: Validation for Cluster Analyses. Data Science Journal, 8, 88-93.

Wang, X. L., Y. Feng and V. R. Swail (2012), North Atlantic wave height trends as reconstructed from the 20th century reanalysis. Geophysical Research Letters 39(18), L18705.

Warren, I. R. and H. K. Bach (1992), MIKE 21: a modelling system for estuaries, coastal waters and seas. Environmental Software, 7, 229-240.

Watanabe, M., J.-S. Kug, F.-F. Jin, M. Collins, M. Ohba and A. T. Wittenberg (2012), Uncertainty in the ENSO amplitude change from the past to the future. Geophysical Research Letters, 39(20).

Webb, A. T. and M. A. Kulmar (1989), Coastal Wave Climate of New South Wales – An Update. 9th Australasian Conference on Coastal and Ocean Engineering. Adelaide, Australia, Institution of Engineers, Australia: 374-379.

Whiteway, T.G. (2009), Australian Bathymetry and Topography Grid. Geoscience Australia Report 2009/21. Australian Government. June 2009.

Whitham, G.B. (1974), Linear and nonlinear waves, Wiley, New York, pp. 636.

WISE Group (2007), Wave modelling - the state of the art. Progress in Oceanography, 75, 603–674.

Wright, L.D. and A.D. Short (1984), Morphodynamic Variability of Surf Zones and Beaches: A Synthesis. Marine Geology, 56(1-4), 93-118.

Wright, L.D. (1995), Morphodynamics of Inner Continental Shelves. CRC Press, Boca Raton, pp 241.

Wyllie, S.J., and M. Kulmar (1995), Coastal Wave Monitoring. Australian Marine Data Collection and Management Guidelines Workshop, Environmental Resources Information Network, Hobart, December 1995.

Xie, S.-P., Y. Du, G. Huang, X.-T. Zheng, H. Tokinaga, K. Hu and Q. Liu (2010), Decadal Shift in El Niño Influences on Indo–Western Pacific and East Asian Climate in the 1970s*. Journal of Climate, 23(12), 3352-3368.

Yeh, S. W., J. S. Kug, B. Dewitte, M. H. Kwon, B. P. Kirtman and F. F. Jin (2009), El Nino in a changing climate. Nature 461(7263), 511-514.

You, Z. and D. Lord (2008), Influence of the El-Nino-Southern Oscillation on NSW Coastal Storm Severity, Journal of Coastal Research, 24, 203-207.

Young, I. R. (1999), Seasonal variability of the global ocean wind and wave climate. International Journal of Climatology, 19(9), 931-950.

APPENDIX 1

Published Journal Article.

Mortlock, T.R., Goodwin, I.D. and Turner, I.L. (2014). Nearshore SWAN model sensitivities to measured and modelled offshore wave scenarios at an embayed beach compartment, NSW, Australia. *Australian Journal of Civil Engineering,* 12(1), 67-82. doi: 10.7158/C14-016.2014.21.1

Nearshore SWAN model sensitivities to measured and modelled offshore wave scenarios at an embayed beach compartment, NSW, Australia*

TR Mortlock† and ID Goodwin
Marine Climate Risks Group, Department of Environment and Geography, Macquarie University, North Ryde, NSW

IL Turner
Water Research Laboratory, School of Civil and Environmental Engineering, University of New South Wales, Sydney, NSW

ABSTRACT: *Spectral wave modelling is a common dynamical approach to transform offshore wave climates to the nearshore zone for coastal hazard definition and engineering design. Knowledge of model limitations and sensitivities are thus of paramount importance to appropriate use for coastal engineering. This study reports the calibration and nearshore sensitivities of a SWAN model at Wamberal-Terrigal on the central New South Wales coast, when the model is forced with wave information from a regional WaveWatch III (WW-III) model, compared to model forcing from simultaneous offshore buoy observations. SWAN achieved good results for nearshore wave heights (R^2 = 0.86, RMSE = 0.2 m), but under-estimated mean wave period by approximately 1 s. Default SWAN physics were found to be largely appropriate. The inclusion of hindcast winds introduced a systematic over-estimation of high frequency (low period) wind-sea but improved the shape of the wave period distribution. Transformations of WW-III spectra through SWAN suggests that oblique swell is under-represented by WW-III at this location, with only wave directions between 80° and 150° accounted for. In modelling cases, the long shore transport component, typically driven by oblique long-period wave energy, would likely be under-estimated while shorter-period wind-waves that favour cross-shore sediment transport is preferenced.*

KEYWORDS: Nearshore wave climate; wave refraction modelling; SWAN; WaveWatch III.

REFERENCE: Mortlock, T. R., Goodwin, I. D. & Turner, I. L. 2014, "Nearshore SWAN model sensitivities to measured and modelled offshore wave scenarios at an embayed beach compartment, NSW, Australia", *Australian Journal of Civil Engineering*, Vol. 12, No. 1, pp. 67-82, http://dx.doi.org/10.7158/C14-016.2014.12.1.

1 INTRODUCTION

Knowledge and prediction of nearshore wave climates is vital for sustainable shoreline management and structural design in the coastal zone. This is especially so for high-energy sandy coastlines, like that of the NSW coast, where shoreline change on event timescales is predominantly driven by the passage of synoptic weather patterns and their storm-wave climates. Extreme wave events, such as the 1974 "Sygna Storm", 1997 "Mother's Day Storm" and 2007 "Pasha Bulker Storm" have caused coastal inundation, beach erosion, damage to property and marine structures, and risk to public safety (Shand et al, 2011). The "ambient" wave climate that persists between storm events is predominantly responsible for post-storm beach recovery, long-term delivery of sediment and shoreline orientation. Although some authors predict a decrease in storm event frequency

* Reviewed and revised version of paper first presented at Coast and Ports Conference 2013, 11-13 September 2013, Sydney.

† Corresponding author Thomas Mortlock can be contacted at thomas.mortlock@mq.edu.au.

(not magnitude) along the east Australian coast (Dowdy et al, 2014), future wave climate change in the region remains unclear (Hemer et al, 2013).

In 2009, the collective value of New South Wales (NSW) properties threatened by coastal processes within planning timeframes was estimated at over $1 billion, partly a result of 80% of the NSW population living on the coastal fringe (Department of Climate Change, 2009). The Sydney region alone is projected to increase its population by 40% in the next 30 years (Department of Planning, 2008), only serving to increase coastal vulnerability to extreme wave events along the central NSW coastline. The accurate description of nearshore wave patterns, both storm and ambient, is therefore crucial to coastal hazard definition and prediction in NSW. In acknowledgement of this, the NSW Office of Environment and Heritage (OEH) in 2011 tendered for the development of a cross-shelf wave model system to cover the length of the NSW coast. This model aims to provide a wave hindcast baseline for local coastal process studies across NSW.

A coupled WW-III/SWAN model system for the NSW continental shelf was delivered to OEH by Cardno in 2013 (Cardno, 2012; 2013). This consisted of a nested global-to-regional WW-III model, with a nested SWAN grid to refract deep-water waves across the shelf. Although Cardno carried out wave calibration against a set of seven deep-water Directional WaveRider (DWR) buoys, limited nearshore calibration was undertaken due to lack of suitable shallow-water buoy data. The only nearshore calibration performed was against two DWR buoys operated by Newcastle Port Corporation, moored in 10 to 15 m water depths outside the entrance to the Hunter River, Newcastle. Although peak storm wave height agreement was good (Cardno, 2012), the buoy locations for the purposes of model calibration were not ideal as they were moored on the edge of a dredged channel and adjacent to a training wall. These structures likely increase shoaling, reflection and non-linear interactions recorded at the buoy, which are not representative beyond that locality.

In light of this, OEH contracted the Marine Climate Risks Group at Macquarie University to provide a nearshore validation of the coupled WW-III/SWAN model system, using a Datawell DWR buoy deployed for research purposes on the central NSW coast. Although this paper does not comment on the nearshore performance of the Cardno/OEH model (see Mortlock & Goodwin, 2013), it describes the nearshore calibration and sensitivities of a standalone SWAN model when forced with offshore buoy-measured wave information, and modelled WW-III waves. The sensitivities of WW-III/SWAN coupling in a cross-shelf environment will be of interest to practitioners in the coastal, marine and renewables fields.

This paper is presented in six sections. The introduction is followed by a description of the study site, the regional wave climate and wave model dynamics. Section 3 describes the boundary data applied to the SWAN model, while section 4 outlines the methodology of model calibration. The results of the calibration and sensitivity analyses are presented in section 5 and discussed in section 6.

2 BACKGROUND

2.1 Location

The Wamberal-Terrigal compartment is located on the central NSW coast, approximately 60 km northeast of Sydney, on the southeast coast of Australia (figure 1). The compartment comprises a 2.8 km stretch of barrier sands that block the entrance of two adjacent drowned river valleys, now occupied by Wamberal and Terrigal lagoons (Short, 2006). The planform curvature increases with proximity to Terrigal Headland at the southern end of the embayment. The repetition of embayed geomorphology along large parts of the NSW coast (eg. Short, 1999) means the results of this study can be assumed broadly representative for these areas.

The Wamberal DWR buoy (figure 2) was deployed in August 2011 for eight months as part of an Australian Research Council (ARC) linkage project. The buoy recorded hourly directional wave spectra with a 93% recovery rate. Full spectral data were transmitted to a land receiving station, post-processed by Manly Hydraulics Lab (MHL) and provided as hourly wave parameters for this study.

The Wamberal wave buoy record represents largely shoaled but pre-broken shallow-water (~12 m depth) waves. The buoy location is exposed to the modal south-easterly wave climate, outside the influence of major headland diffraction, and is moored adjacent to a non-engineered shoreline. The embayment is characterised by mixed sand and exposed rock reef substrates, the outline of which is denoted in figure 1. The rocky outcrops complicate wave refraction patterns towards the buoy especially under north-east seas and swells.

2.2 Wave climate

The southeast coast of Australia receives a near-field wave climate from the marginal Tasman Sea with far-field wave energy originating from mid-latitude cyclones in the Southern Ocean and tropical low pressure systems in the Coral Sea/Equatorial Pacific (Short & Trenaman, 1992). In addition, a further eight major storm types have been identified by Shand et al (2011) which can be broadly grouped into extra-tropical lows, tropical lows/cyclones and anticylonic intensification (Goodwin et al, 2014).

Figure 1: Wamberal-Terrigal compartment with buoy location (circled), depth contours (light grey) and exposed rock reef outline (dark grey). The 12 m depth contour is highlighted. Depth contours and rock reef location are from digitised bathymetric and seabed charts (see Jordan et al, 2010). Insert shows Sydney region with Sydney deep-water DWR buoy location.

Figure 2: Datawell MkII DWR buoy at Wamberal-Terrigal. Image courtesy of MHL.

The nearshore wave climate is further complicated by localised refraction, shoaling and shadowing effects. Figure 3 illustrates the refraction pattern of waves entering the Wamberal-Terrigal compartment under a typical storm swell (H_s = 2.5 m, T_p = 10 s) from the south (170°) and southeast (120°).

As shown in figure 3, oblique offshore swell produces a steep alongshore wave height gradient in the embayment, which is less pronounced with south-east swells. Even though there is a distinct shoaling differential between offshore swell directions at the buoy location, the refraction coefficient (ratio between offshore/nearshore mean wave direction (MWD)) remains close to 1 (ie. little to no refraction) at the buoy location. This cannot be said for areas within southern hook "shadow" zones, as highlighted in figure 3. Therefore, model calibration and sensitivities reported here may not be valid for these southern hook locations.

The Wamberal buoy record shows that, over the study period, a predominantly unidirectional low-energy southeasterly wave climate prevailed (figure 4). This is typical of the central NSW coast during the Australian spring/summer period. As winter ends, the subtropical ridge progresses southward and anti-cyclonic blocking highs over the Tasman Sea produce a lower energy, southeasterly wind-sea. A local sea breeze may be responsible for the residual north-easterly component seen in figure 4(b). Over the study period, average significant wave height, H_s, was 1.2 m, average peak spectral wave period, T_{p1}, was 9.8 s and MWD at the spectral peak, MWD_{tp1}, was 118° at the Wamberal buoy.

2.3 SWAN

SWAN (Simulating WAves Nearshore) is a third generation fully-spectral wind-wave model developed at the Delft University of Technology (Booij et al, 1999) that computes random, short-crested wind-generated waves in coastal regions and inland waters. SWAN is one of the most widely used and flexible wave refraction models, with the ability to be nested within global-scale wave models or driven by offshore wave observations. SWAN version 40.85 (June 2011) was used to be comparable with the deep-water calibration methodology of the WW-III/SWAN grid carried out by Cardno (2012).

In SWAN, bottom and current-induced shoaling and refraction are properly accounted for but diffraction is only coarsely resolved. SWAN models wind generation, quadruplet wave-wave interactions, white-capping and bottom friction identically to the open-ocean WAM model (see WAMDI, 1988) with the addition of depth-induced breaking and triad wave-wave interactions for nearshore applications (Holthuijsen, 2007).

2.4 WaveWatch III

WaveWatch III (WW-III) is a third-generation fully-spectral wind-wave model developed by NCEP

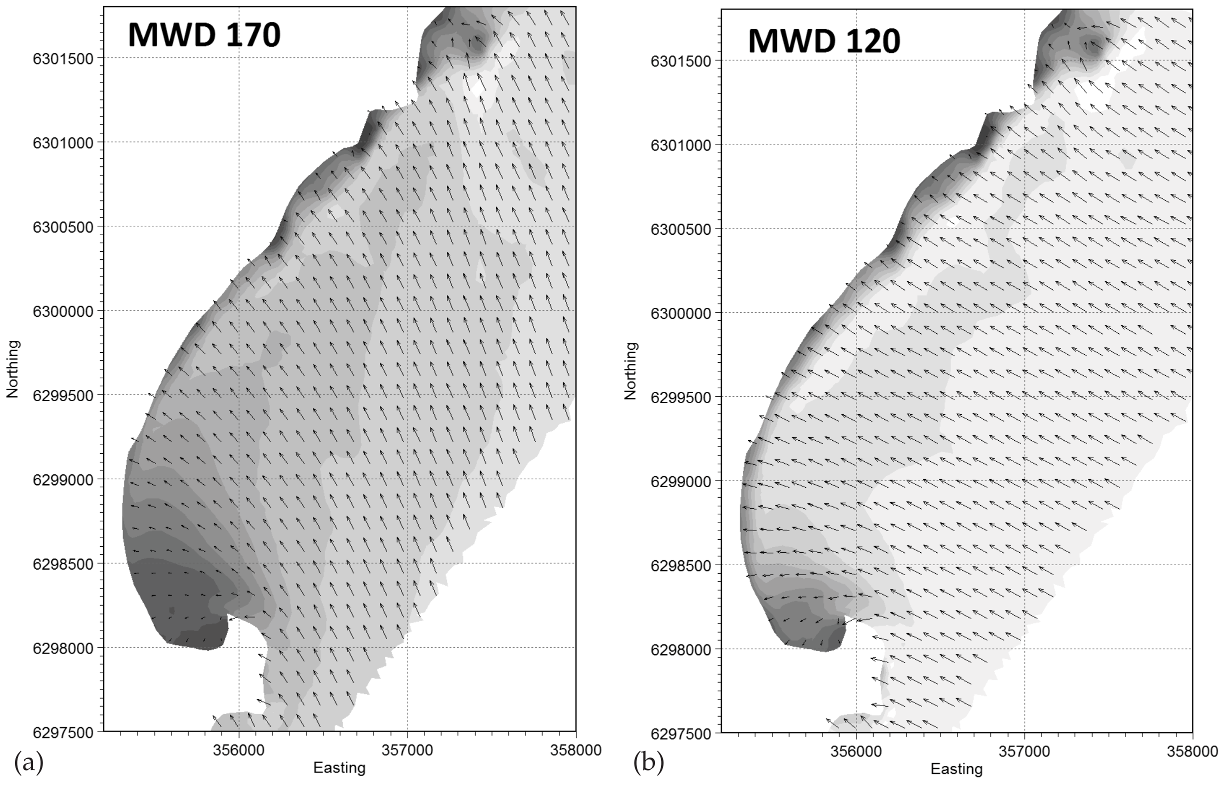

Figure 3: Refractograms of storm swells at Wamberal-Terrigal. Plots shows wave height distribution with mean wave direction (MWD) vectors superimposed. Darker shades of grey indicate progressively lower wave heights (at 0.2 m intervals, from 0 to 2.6 m).

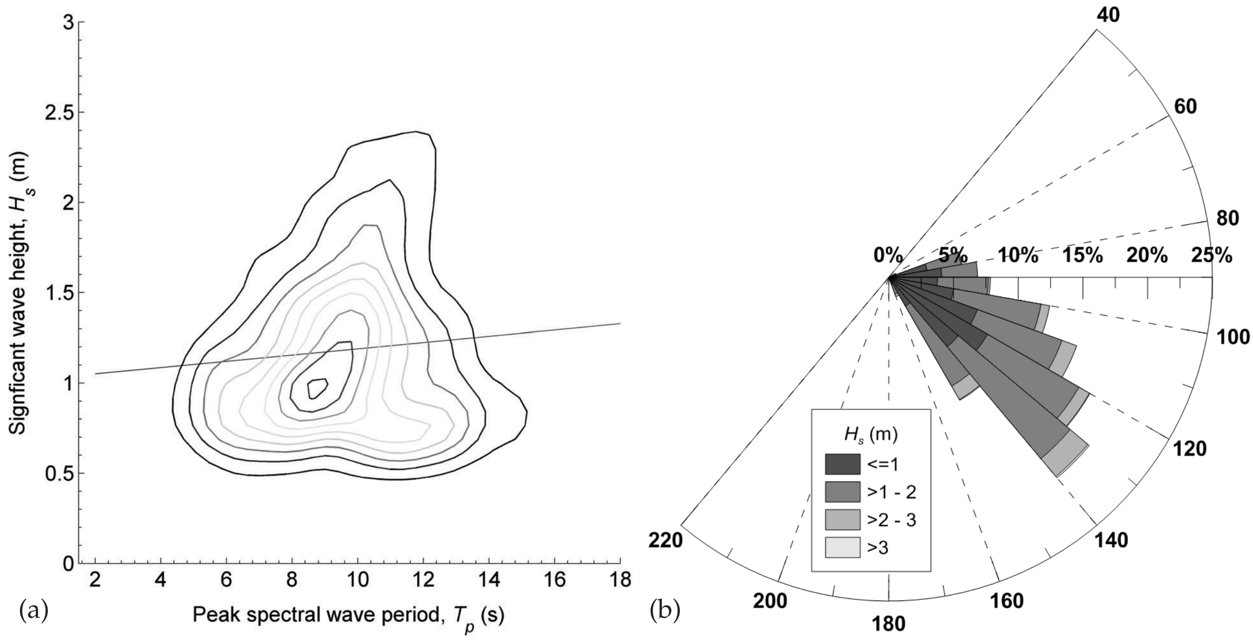

Figure 4: (a) Joint probability density function (JPDF) of wave height (H_s) and wave period (T_p) with linear regression of scatter data; and (b) directional distribution of 1-hour wave heights, at the Wamberal DWR buoy from August 2011 to March 2012.

(Tolman, 2009). WW-III is designed for oceanic large-scale applications and is optimised for efficient computing, rather than high-resolution coastal applications (Tolman, 2009). Therefore, it is common practice to couple a nearshore wave model (such as SWAN) to refract waves into shallow water.

3 DATASETS

3.1 Offshore waves: Measured

A network of seven offshore DWR buoys records the mid-shelf, deep-water wave climate along the NSW continental shelf (Kulmar et al, 2013). The Sydney DWR is the nearest deep-water buoy to the Wamberal-Terrigal compartment, moored approximately 45 km southeast in 90 m water depth. Hourly H_s, T_{p1} and MWD_{tp1} from the Sydney buoy were used to force the ocean boundary of the SWAN model.

3.2 Offshore waves: Modelled

Modelled wave spectra were provided by Cardno from the output of the nested WW-III model system. Since the regional WW-III grid points did not intersect exactly with the SWAN seaward boundary, spectra were interpolated to seven equidistant locations along the boundary. In order to evaluate SWAN/WW-III coupling depths, WW-III spectra were supplied at locations representative of the 90, 75 and 60 m depth contours. The SWAN grid was aligned to depth contours offshore of Wamberal accordingly.

The nesting of SWAN into WW-III requires the WW-III spectra to fall within a limited distance either side of the SWAN seaward boundary. However, the SWAN source code reduces the spectral location values to two decimal places, forcing a migration of the locations outside of tolerance. The SWAN source code was thus modified to retain accuracy. Line number 5919 in the source code of *swanmain.ftn* was modified from *"901 FORMAT (A12,2F7.2,F10.1,2(F7.2,F6.1))"* to *"901 FORMAT (A1 2,2F15.10,F10.1,2(F7.2,F6.1))"*.

3.3 Bathymetry

Five bathymetric datasets were used in this study to interpolate to a computational grid in SWAN (table 1). Figure 5 illustrates the extents of available bathymetries. Soundings were edited in ArcGIS, and interpolated in the Delft3D RGFGRID module. Sensitivity testing suggested interpolation errors between methods (TIN to Grid, Natural Neighbour and Kriging) were negligible for the extents of the model domain, each having a mean absolute error of ±0.08 m when compared to original soundings. The TIN to Grid method was chosen to align with the methodology used by Cardno (2012).

A buffer-overlap technique was used to minimise stepping effects between bathymetries during merging. However, stepping was particularly apparent between the GA AusBathy grid and adjacent bathymetries. The 250 m pre-gridded AusBathy data covers all Australian marine territories and is composed of multiple datasets (Whiteway, 2009). Analysis here suggests that the AusBathy depths in the nearshore are too shallow by approximately 10 m (when compared with LADS lidar) and that this depth difference is maintained in some areas of the computational domain out to the (true) 50 m depth contour. Despite being interpolated to the shoreline,

Table 1: Bathymetries used to interpolate to a SWAN grid.

Bathymetry	Data type	Year
Australian Hydrographic Office (AHO) single-beam echosounder (SBES)	Shore-normal survey lines (3 km spaced)	1972
AHO digitised fairsheets	Digitised contours (2 m contour spacing)	1984
Laser Airborne Depth Sounder (LADS) lidar soundings	Point cloud (5 m spacing)	2008
GeoScience Australia (GA) AusBathy	Pre-gridded (250 m)	2009
LADS lidar soundings	Point cloud (50 m spacing)	2011

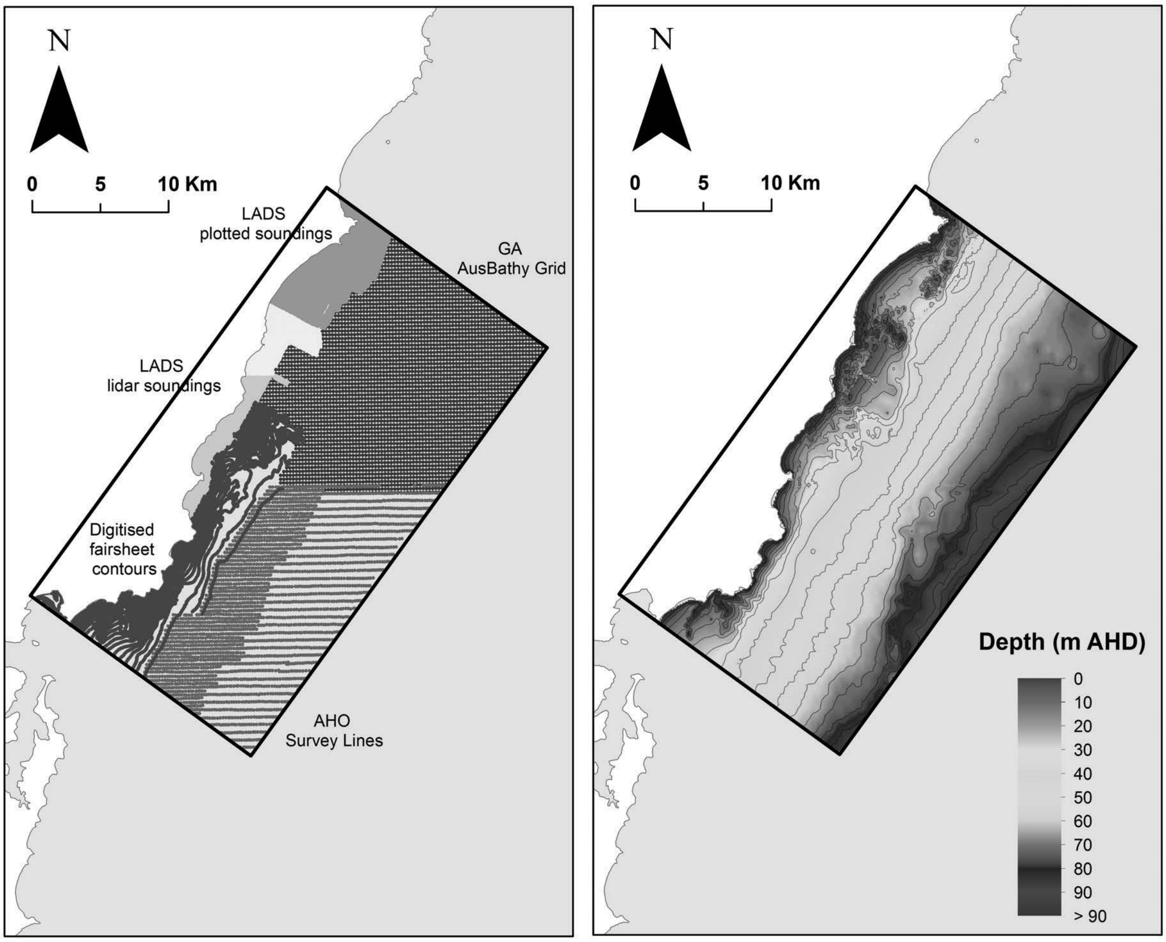

Figure 5: Extents (left) and interpolation (right) of available bathymetries.

the AusBathy grid is not designed for nearshore use and has thus been limited, where possible, to depths beyond the mean wave base.

3.4 Hindcast winds

Cardno (2012) evaluated the nearshore performance of multiple sources of hindcast winds along the central NSW coast. Results suggested the Climate Forecast System Reanalysis (CFSR) dataset best represented measured conditions, although showed a positive bias at higher wind speeds and some directional discrepancies. Between 1979 and 2010, CFSR hindcast winds were generated on a global 0.3125° × 0.3125° grid at hourly intervals (Saha et al, 2010). From 2010 onwards, a second version (CFSv2) is available, generated on higher spatial and temporal resolutions. A scaling procedure of nearshore wind velocities was applied to the CFSv2 winds by Cardno (2012) to conform better to observed winds. Within 30 km of the NSW coast, wind speeds were scaled up by 20% of the original CFSv2 winds. This hourly up-scaled CFSv2 wind data was extracted by Cardno at the closest grid point to the Wamberal SWAN seaward boundary to provide a continuous time-series for wind forcing in the SWAN model.

3.5 Tides

Hourly tidal data from Middle Head (HMAS Penguin) tidal gauge (Sydney Harbour) was provided by MHL for the study period. Since tides reach NSW almost incident to the coast, time lags in tide between Middle Head and Wamberal are negligible.

4 METHODS

4.1 Model setup

SWAN was run in non-stationary mode with a domain centred on the Wamberal embayment. A nested rectilinear grid approach was used (figure 6), allowing for higher computational resolution in the nearshore. The outer grid was 200 m^2 resolution, while the nested grid was 100 m^2. The grid resolutions were chosen to be comparable to the methodology of Cardno (2012; 2013).

In order that wave parameters from the Sydney buoy could be realistically applied to the seaward boundary of the model, the SWAN domain was extended to, and aligned with, the 90 m depth contour (20 km offshore). It is an inherent assumption of the model that wave conditions at the model boundary and the Sydney buoy are consistent. Linear wave theory suggests this to be the case (Mortlock & Goodwin, 2013). For sensitivity testing of WW-III spectra, the SWAN domain was incrementally narrowed from the 90 to 60 m depth contour.

Both the measured (Sydney buoy) and modelled (WW-III spectra) boundary waves were applied to all three ocean boundaries. Since this is not necessarily a good approximation of the wave conditions along the lateral sides of the grid, especially in shallower waters, the domain was created with sufficient distance either side of the Wamberal-Terrigal embayment to minimise the propagation of lateral boundary errors into the area of interest. The lateral error shadow zones shown in figure 6 were calculated based on 30° wind-sea spreading (SWAN, 2011a) around the offshore MWD_{tp1} (118°) for the study period. Sustained oblique waves may cast a wider nearshore shadow.

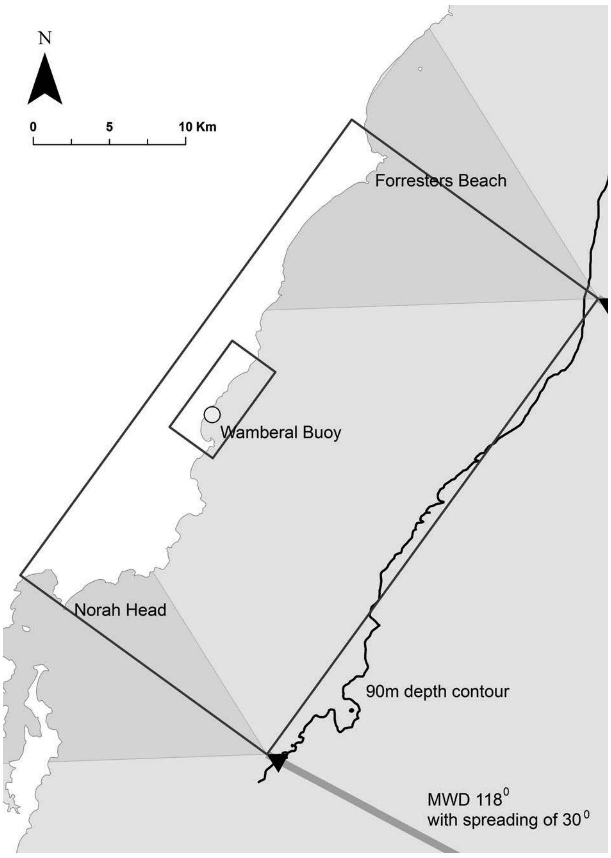

Figure 6: Nested model domain extents with 90 m seabed contour and shadow zones representative of the MWD shown. Contour extracted from AusBathy grid (Whiteway, 2009).

4.2 Model calibration

A primary application of the Cardno/OEH wave model is extreme wave hindcasting. This involves recreating the past 50 years of extreme wave events along the NSW coast using offshore metocean data, such as wind field reanalyses. Considering the application of the model, nearshore calibration was, where possible, biased to storm conditions. Storm events were detected in the Wamberal buoy record using the peaks-over-threshold (POT) method. POT identifies storm events that exceed a significant wave height threshold; that are maintained for a minimum storm duration; and that are separated by a minimum storm recurrence interval. This approach was preferred over the annual maximum method due to the deficiencies of the latter in returning a low storm count for relatively short time series (Goda, 2010).

A storm wave height threshold was set at 1.8 m, equivalent to the hourly 10% exceedance H_s recorded at the Wamberal buoy (figure 7). Previous regional studies (eg. BBW, 1985; You & Lord, 2008; Rollason & Goodwin, 2009; Shand et al, 2011; Dowdy et al, 2014) have all used thresholds between 2 and 3 m, roughly equivalent to respective 10% exceedance values. Here, the absolute threshold is lower due to the nearshore position of the wave buoy. Despite

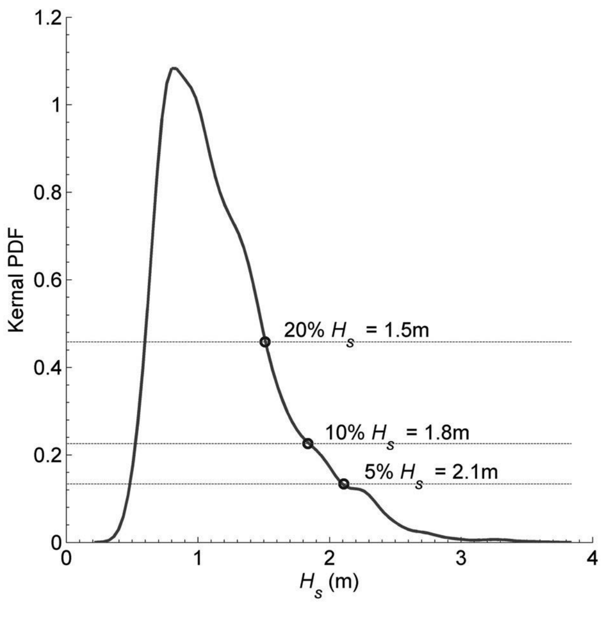

Figure 7: Wave height distribution at the Wamberal buoy.

the aforementioned studies adopting a 72 hour minimum storm duration, there were no periods in the Wamberal buoy record in which the storm threshold was exceeded for this length of time. The minimum duration was therefore reduced to 36 hours to enable storm detection. In line with previous studies (above), the minimum storm reoccurrence interval was set at 24 hours. Figure 8 shows the Wamberal buoy record with storm events detected using these POT conditions.

As shown in figure 8, there are five storm events detected in the buoy record, with hourly peak H_s values between 2.5 to 3.6 m. Storm duration ranged between 37 and 60 hours. The largest storm events had a MWD of around 130° (southeast), whereas the smaller storms were more east-southeast in origin (around 115°). Since the Wamberal buoy is exposed to both these storm wave directions, the variation in storm magnitude is more likely due to synoptic origin than localised shoaling and refraction. Thus, SWAN calibration can be assumed regionally representative for those storm types detected in the buoy record.

A continuous one month sub-set of the buoy record was used to calibrate the SWAN model (figure 8). This period was chosen to cover both modal and storm conditions, including the largest storm event detected in the record. The data capture rate during the calibration sub-set was also very good (99%). The remaining "unseen" portion of the buoy record was used to validate the calibrated SWAN model.

4.3 Comparative wave statistics

Modelled H_s, mean wave period (Tm_{02}) and MWD were compared to measured H_s, mean wave period (T_z) and MWD_{tp1} from the Wamberal buoy. Mean, rather than peak spectral statistics were used because the SWAN peak statistics are unstable parameters with a tendency of switching rapidly between high and low frequencies, especially in bi-modal seas. The mean statistics provides a better indication of how the bulk of the wave energy is being described in the model. MWD was not a statistic provided by MHL in the buoy wave data, so MWD_{tp1} was used instead. The SWAN T_{m02} statistic is the mean wave period as calculated from the second and zeroth spectral moments of the wave energy spectrum and is generally comparable to T_z (Cardno, 2012). The T_z statistic is the average zero-crossing period based on upward zero crossing of the still water line. One of the limitations of using the T_z statistic, however, is the poor definition of wave period during bi- or multi-modal seas.

5 RESULTS

5.1 Calibration of SWAN numerics

Calibration of the model was undertaken to assess the numerical scheme and numerical accuracy of the SWAN model developed for the study. SWAN was initially run using the default high-order Stelling

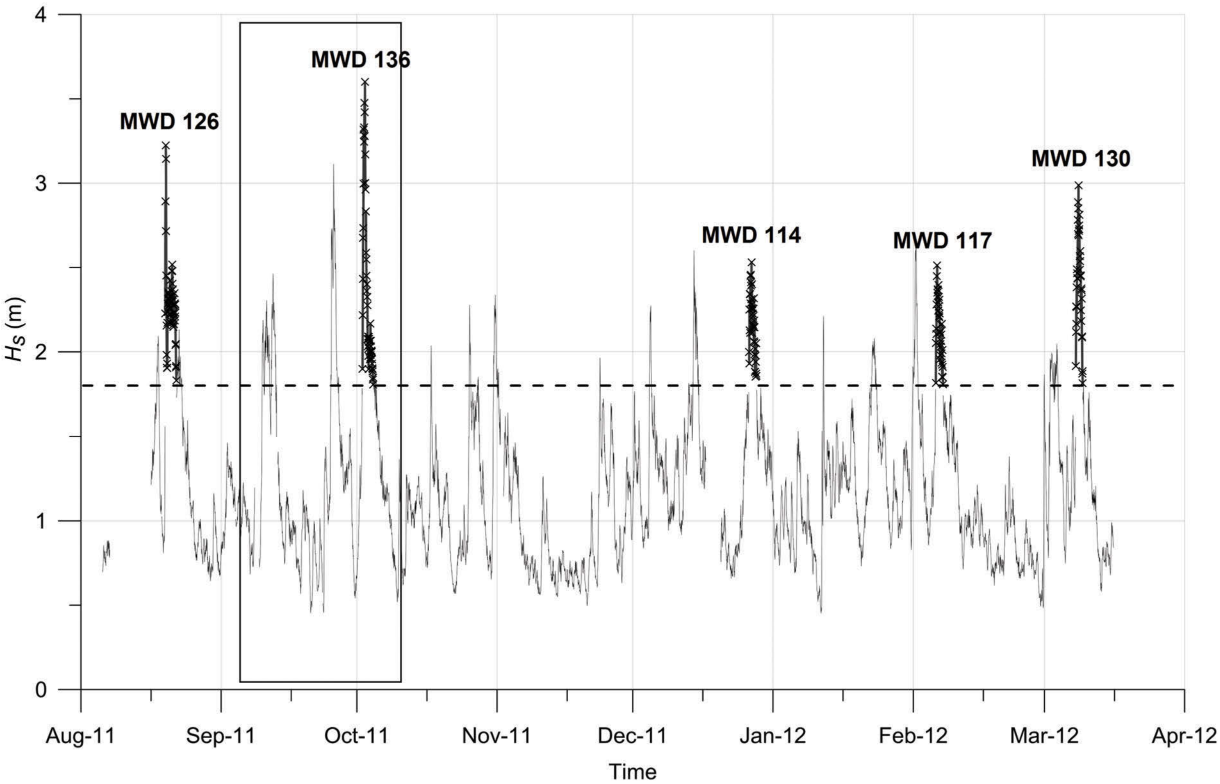

Figure 8: Wave height time series at the Wamberal buoy with storm events and storm threshold highlighted. The MWD of the storm event is annotated. Calibration sub-set is also highlighted (box).

and Leendertse scheme but it became apparent that it was leading to poor wet grid point accuracy and long iteration intervals. Instead therefore, the lower-order more diffusive backward-space backward-time scheme was used. This scheme is computationally more efficient over smaller domains (< 100 km) and promotes better wet grid point accuracy (SWAN, 2011b).

Improved numerical accuracy was achieved by lowering the computation interval and increasing the iteration maxima. Grid cell computations were first run at hourly intervals, equal to the time-step of model output. However, the required wet grid point accuracy (98%) was not being met. At 15 minute computations, the required accuracy was met after, on average, five iterations. This meant that model runs were not only computationally more accurate, but also more efficient; computations at 15 minute intervals were in fact 25% faster than computations at hourly intervals due to the lower average number of iterations.

The iteration maxima were also increased from the SWAN default. It was found that the default of one-iteration-per-time-step rarely gave the required accuracy for all wet grid points, but when the computational process was extended to 15 iterations per time-step, the required numerical accuracy was achieved.

5.2 Calibration of SWAN physics

Frequency and direction discretisation, wind growth, and non-linear interactions (quadruplets and triads) were calibrated for. Frequency and direction discretisation determines the resolution with which the model calculations are made. It was found that a doubling of the default discretisation gave only a negligible improvement in modelled results, while model runs took almost twice as long to compute. Therefore the default discretisation was taken as optimal.

Energy transfer to higher frequencies during wave propagation within SWAN is described (as default) by the wind growth model of Komen et al (1994). A widely-used alternative is the Janssen model (1989; 1991). When the Janssen model was used, 55% of model runs did not converge above the required 95% threshold before 15 iterations. There was also an increase in the higher frequency energy. This not only led to dis-equilibrium with nearshore measurements, but also meant that model runs took on average 80% longer than when the Komen model was used. The Komen model was therefore taken as optimal.

Non-linear wave interactions describe the redistribution of energy over the spectrum by resonant sets of waves. In deep and intermediate waters, four-wave interactions (quadruplets) are important, whereas three-wave interactions (triads) become more important in in shallow water (SWAN, 2011b). SWAN computes quadruplets using the discrete interaction approximation after Hasselmann et al (1985). The lambda (λ) coefficient (default 0.2) in the quadruplet approximation can be modified to control the resonant frequencies at which quadruplets interact. It was found that increasing λ to 0.45 considerably improved model performance.

In shallow waters, triad wave interactions become more important by transferring energy to higher frequencies, resulting in wave breaking (Holthuijsen, 2007). SWAN computes triads using the lumped triad approximation derived by Eldeberky (1996), although triads are not accounted for in SWAN as default. The inclusion of triads in computations had very little effect on model performance, probably because the water depth at the Wamberal buoy is still too deep for the breaking of the vast majority of waves.

5.3 Sensitivity to hindcast winds

The application of a wind field in SWAN accounts for wind-wave growth over the model domain. Table 2 shows the change in model performance when SWAN is run with and without the up-scaled CFSv2 hindcast winds over the eight-month buoy recording period, when compared with the Wamberal buoy data. Figure 9 shows the modelled distribution of mean wave periods with and without winds applied, and the measured distribution at the Wamberal buoy.

Results indicate that while the addition of a boundary wind field has only a minimal impact on modelled wave heights, the prediction of wave periods is generally improved. Hindcast winds reduce the modelled scatter (30% to 20%) and improve the shape of the frequency distribution (figure 9). However, winds introduce too much higher frequency wave energy to the spectrum. Results also suggest that the addition of a wind field degrades the consistency of modelled wave directions (reduced slope, m = 0.90 to 0.77), although the bias and scatter show negligible change.

Table 2: Model sensitivity to hindcast winds where W = wind and NW = no wind scenario.

n = 5015	Up-scaled CFSv2 hindcast winds					
	H_s		Tm_{02}		*MWD*	
	W	NW	W	NW	W	NW
R^2	0.86	0.84	0.53	0.33	0.68	0.68
RMSE	0.23	0.21	1.26	1.88	13.50	14.67
Bias	0.22	0.14	–0.45	1.81	14.43	15.02
SI %	19.40	17.40	20.40	30.40	11.40	12.40
m	0.99	0.97	0.82	0.85	0.77	0.90

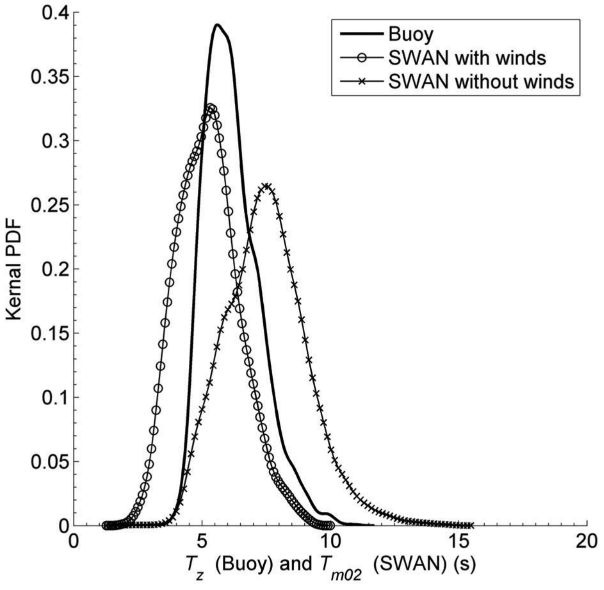

Figure 9: Distribution of mean wave period as measured at the Wamberal buoy (T_z) and modelled by SWAN (Tm_{02}) with and without hindcast winds.

5.4 Sensitivity to bottom friction

Bottom friction determines the amount of drag and energy dissipation a wave experiences when in contact with the seabed (ie. where depth ≥ half deep-water wavelength, L_0). The default JONSWAP friction can be calculated using a coefficient for wind-sea (0.067 m^2s^{-3}) or swell-wave conditions (0.038 m^2s^{-3}).

When the JONSWAP coefficient was set to the swell-wave value in SWAN, minor improvements to the modelled wave heights were seen but with equally minor detrimental effects for modelled wave directions and periods. Therefore, the default sea value was used in the optimised configuration.

5.5 Sensitivity to grid resolution

A more highly-resolved nested grid was used inside the model domain to investigate the effect of grid resolution on modelling. A higher resolved grid should not only better describe the seabed topography, but will better spatially resolve the surface waves.

SWAN was run with a non-nested rectilinear grid configuration of 200 m^2 to the shoreline, and a nested configuration in which spectra from a 200 m^2 outer grid were interpolated to the boundary of a 100 and 50 m^2 nested grid, and refracted to the shoreline.

Despite a substantial increase in computational demand, only minimal improvements in modelled results were seen using the 100 and 50 m^2 nested approach. Indeed, improvements were so small as to be considered partly a result of the stochastic wind growth in the model.

5.6 Sensitivity to tides

Since measured and modelled wave data was input at hourly intervals, the influence of tide at the nearshore site was considered. However, the application of a measured hourly tide curve to SWAN made only negligible differences to modelled wave parameters.

5.7 Validation of WW-III wave spectra

WW-III spectra from the Cardno/OEH wave model were refracted to the shoreline using the optimised SWAN model to investigate nearshore performance and bias. Table 3 shows the change in SWAN performance when WW-III wave spectra are applied in place of offshore buoy boundary forcing. Figure 10 shows the modelled distribution of MWD when SWAN is forced with measured and modelled boundary waves, compared with the measured distribution at the Wamberal buoy.

Results indicate significantly better nearshore performance is achieved with offshore buoy parametric input, rather than WW-III spectral input, at the SWAN offshore boundary. Most noticeable is the poor estimation of nearshore wave direction with WW-III forcing. Despite a slight incremental improvement when applied at shallower depths, figure 10 suggests the WW-III spectra under-estimates the directional spread and only account for wave directions between 80° and 150°. The buoy-forced SWAN model better represents the measured directional spread, albeit for a consistent but small (10°) southerly bias and an over-estimation at the modal peak.

6 DISCUSSION

The optimised SWAN model achieved good nearshore correlation with measured wave heights (R^2 = 0.86, m = 0.99) but a slight negative bias (1 s) in mean wave period and a 10° southerly directional bias (figure 11).

Table 3: Performance of WW-III spectra when transformed through SWAN, where A = results from SWAN run forced with Sydney buoy (measured) and B = SWAN forced with WW-III (modelled) boundary waves.

	WW-III spectra (applied at the 90 m contour)					
n = 5015	H_s		Tm_{02}		*MWD*	
	A	**B**	**A**	**B**	**A**	**B**
R^2	0.86	0.75	0.53	0.42	0.68	0.45
RMSE	0.23	0.25	1.26	2.18	13.50	15.58
Bias	0.22	0.01	–0.45	–1.52	14.43	9.40
SI %	19.40	21.10	20.40	35.40	11.40	13.20
m	0.99	0.91	0.82	0.59	0.77	0.39

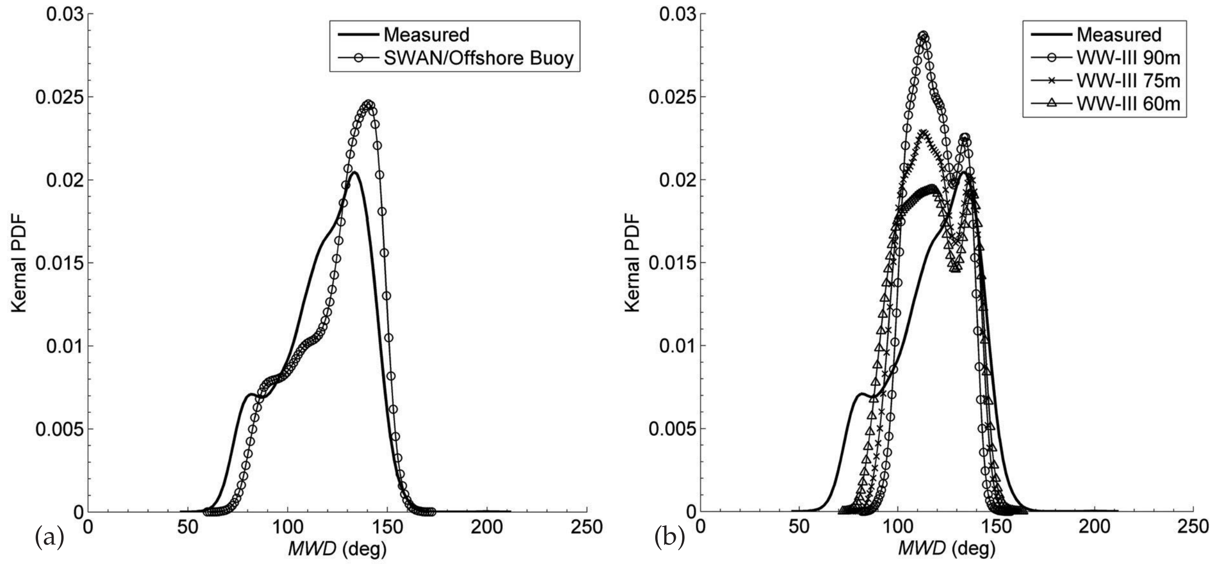

Figure 10: Distribution of MWD, as measured by the Wamberal buoy, compared against (a) SWAN-modelled MWD distribution when forced with buoy-measured offshore waves, and (b) SWAN-modelled MWD distribution when forced with modelled WW-III spectra along the 90, 75 and 60 m depth contours.

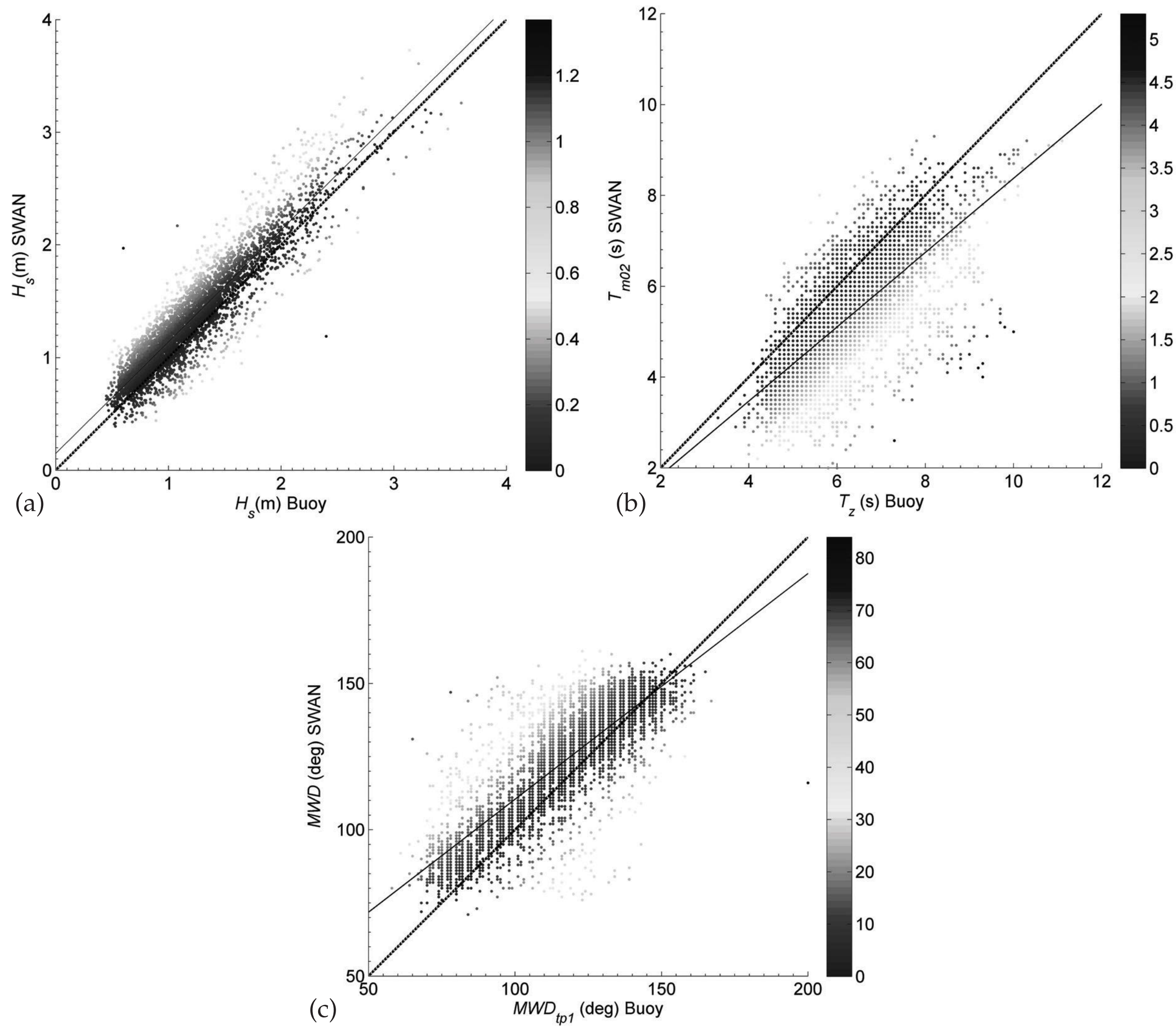

Figure 11: Scatter plots showing comparisons between SWAN and Wamberal buoy measured waves for (a) significant wave height, (b) mean wave period and (c) MWD. Colour bars indicate the residual error of modelled data. The least-squared line (solid black) and best correlation line (dotted) is also shown.

Residual errors seen in the model may be due to either deficiencies in (i) model physics and/or (ii) in boundary data. Other studies (eg. Ris et al, 1999; Bottema & Bayer, 2001; Caires et al, 2006) have also reported a habitual tendency for SWAN to under-estimate the mean wave period. This suggests the underestimation seen here is likely a product of deficiencies in model physics rather than boundary errors.

The default SWAN physics were largely found to be appropriate for exposed, nearshore sites in embayed compartments that are outside the influence of diffraction or shadowing. The applicability for sites along the NSW coast is therefore large. While the default numerics can be improved by adopting a more diffusive scheme, increasing the iteration maxima (to 15) and lowering the computational interval (to 15 minutes), optimal physics were mostly found to be as default. The exception of this is the lambda coefficient for quadruplet calculations, which vastly improved modelled results when increased to 0.45 from the default value of 0.2.

SWAN was found to be largely insensitive to variations in JONSWAP bottom friction coefficients. This concurs with findings by Cardno (2012) when configuring a SWAN model at Newcastle, 70 km north-east of the Wamberal-Terrigal compartment. However, the JONSWAP model does not explicitly account for bottom substrate type. Rather, it describes bottom dissipation based on the wave orbital motion instead of the substrate roughness length. Given the complex extents of exposed rock reef around the approaches to and inside the Wamberal-Terrigal embayment, bottom friction would be assumed variable. Two other models, the drag model of Collins (1972) and the eddy viscosity model of Madsen et al (1988) might thus be more appropriate in these nearshore circumstances. These two latter models are allowed to vary spatially with bottom type and can therefore be input as a grid over the computational domain in SWAN. Expressing bottom dissipation in terms of a spatially variable roughness length, rather than a spatially-static orbital velocity term, may improve model performance and is currently being investigated.

The inclusion of hindcast winds generally improved the modelled wave period distribution although a systematic over-estimation of high-frequency wind-sea was seen at all measured wave periods. A similar finding was reported by Cardno (2012) for deep-water locations along the NSW coast. This suggests the up-scaled CSFRv2 hindcast winds slightly over-estimated nearshore wind speeds during the eight-month study period. The addition of hindcast winds also slightly reduced the model's (already underlying) southerly directional wave bias of 10° by about 1°. This indicates that only a small part of the directional disparity is due to surface wind-driven refraction.

The remainder of the directional bias could be due to inaccurate representation of seabed bathymetry. If this were the case, it is unlikely a result of improper bathymetric resolution. Results indicate that SWAN is largely insensitive to an improved grid resolution from 200 to 50 m^2 at the buoy location. This suggests that all necessary information on the variability of seabed topography is captured in a 200 m^2 grid. Although there is much more detail to be described beyond 200 m^2, bed features with length-scales much smaller than the mean wave length (around 140 m for the mean T_z of 9.5 s) are unlikely to affect refraction, and therefore their resolution in a bathymetric grid is redundant.

If the directional bias is bathymetric-driven, then the source of error may be the intrusion of the AusBathy grid into intermediate waters northeast of the Wamberal-Terrigal compartment. Although this was unavoidable due to lack of overlapping soundings, there is a known depth error in this dataset for depths shoreward of approximately 50 m. Indeed, the directional discrepancy is most noticeable for waves in the northeast to east quadrants. A southerly bias suggests under-refraction due to artificial deepening caused by the inclusion of this dataset. In order to correct for this, offshore wave cases from this quadrant could be bias-adjusted using linear regression, or by modifying the cumulative distribution of modelled waves to the observed distribution (eg. Piani et al, 2010). OEH are also currently undertaking swath bathymetry to fill in and update this area.

The transformation of WW-III spectra through SWAN suggested an under-representation of longer-period oblique waves and a preference for shore-normal (80° to 150°) shorter-period wind-sea. This was the case at all WW-III/SWAN coupling depths. This suggests that, at least over the study period, the typically longer-period oblique swell waves generated by Southern Tasman Lows were under-represented in the WW-III model. Instead, preference was given to more locally-generated, shorter period wave climates with higher-frequency wave energy from the central Tasman Sea region. This is also manifest in the persistent bias towards shorter period sea seen in both this study and in Cardno (2012).

The apparent preference of WW-III spectra for high-frequency unidirectional wave energy can have consequences for shoreline modelling applications when waves are transformed to nearshore locations. The long-shore transport component, typically driven by oblique long-period (constructive) wave energy, is likely to be under-estimated when preference is given to shorter-period, steeper incident (destructive) waves that promote cross-shore transport.

Frequency/directional discrepancies in WW-III are a result of composite errors in model source terms and imperfect wind forcing. A 10% error in the estimation of surface winds can lead to 10-50% errors in wave energy (Cavaleri, 1994). Whereas Cardno (2012) used WW-IIIv3 physics and CFSR winds, other regional WW-III based products such as the Bureau of Meteorology's AUSWAVE model (Durrant & Greenslade, 2011), and CSIRO's CAWCR Wave Hindcast (Hemer et al, 2013), have used v3 (v4) physics and CFSR (ACCESS) synthetic winds. Thus, the same directional bias may not be apparent in all regional WW-III products. While it is beyond the scope of this study to locate the source of the directional error in WW-III, this work has provided a rare opportunity to evaluate the propagation of global-to-regional WW-III spectra into the nearshore zone.

7 CONCLUSIONS

A SWAN model was set up and calibrated for an exposed nearshore location in a typical embayed compartment on the central NSW coast. Model sensitivities to measured and modelled offshore wave scenarios were evaluated. Key findings include:

- Default SWAN physics are largely appropriate for modelling at exposed nearshore locations in embayed compartments, beyond the influence of diffraction and shadowing. The exception to this is the lambda (λ) coefficient for quadruplet non-linearities. Default SWAN numerics, however, were found to be sub-optimal for computational efficiency.
- Bathymetric resolutions of 200 m^2 sufficiently captured all necessary information on seabed variability for SWAN. Although higher-resolved grids better described seabed topography, this was redundant information with regards to improved model performance at the nearshore buoy location.
- A southerly directional bias in northeast to east waves is a result of depth errors incurred in the inclusion of the AusBathy grid to the northeast of the Wamberal compartment. It is suggested that if this bathymetry is used in subsequent regional wave modelling, a linear or distribution-based bias adjustment is applied to waves from the northeast/east quadrant.
- Up-scaled CFSRv2 hindcast winds improved the modelled frequency distribution but introduced a systematic under-prediction of wave period (1 s) suggesting wind velocities in this dataset are over-estimated for this locality.
- The transformation of WW-III spectra to the nearshore suggested an under-representation of longer-period oblique waves and a preference for shore-normal shorter-period wind-sea. If used for coastal process modelling, this bias could influence the cross/long-shore wave energy balance at the shoreline.

ACKNOWLEDGEMENTS

The Wamberal nearshore buoy deployment was funded by ARC linkage project LP100200348. All tidal and wave data were supplied and quality controlled by Mark Kulmar at MHL. All bathymetric data was supplied and quality-controlled by OEH. WW-III wave spectra and upscaled CFSv2 hindcast winds were provided by Cardno. SWAN v.40.85 with modified source code, and technical support, was provided by David Taylor and Sean Garber at Baird Australia. Financial assistance for Cardno and Baird Australia's participation in data provision was funded by OEH through a grant from the Natural Disaster Relief Program (NDRP). Special thanks to Michael Kinsela at OEH for technical feedback. Financial support provided by OEH contributed directly to this work. T Mortlock is funded by a Macquarie University International Research Excellence Scholarship.

REFERENCES

BBW, 1985, *Elevated Ocean Levels, Storms Affecting the NSW Coast 1880-1980*, Report prepared for the NSW Public Works Department Coastal Branch in conjunction with Weatherex Meteorological Services, PWD Report No. 85041.

Booij, N., Ris, R. C. & Holthuijsen, L. H. 1999, "A third-generation wave model for coastal regions 1. Model description and validation", *Journal of Geophysical Research*, Vol. 104, pp. 7649-7666.

Bottema, M. & Bayer, D. 2001, "Evaluation of the Swan Wave Model for the Dutch Ijsselmeer Area", *Proceedings of the Fourth International Symposium on Ocean Wave Measurement and Analysis (Waves 2001)*, San Francisco, California, 2-6 September .

Caires, S., Groeneweg, J. & Sterl, A. 2006, "Changes in the North Sea extreme waves", *Proceedings of the Ninth International Workshop on Wave Hindcasting & Forecasting*, Victoria, B.C. Canada, 24-29 September.

Cardno, 2012, *NSW Coastal Waves: Numerical Modelling Final Report*, report prepared for Office of Environment and Heritage NSW.

Cardno, 2013, *NSW Coastal Wave Modelling – Phase II*, report prepared for Office of Environment and Heritage NSW.

Cavaleri, L. 1994, "Wave models and input wind", *Wave Dynamics and Modelling of Ocean Waves*, Komen, G. J., Hasselmann, S., Donelan, M., Cavaleri, L. & Janssen, P. (editors), Cambridge University Press, pp. 283-284.

Collins, J. I. 1972, "Prediction of shallow water spectra", *Journal of Geophysical Research*, Vol. 77, pp. 2693-2707.

Department of Climate Change, 2009, *Climate Change Risks to Australia's Coasts – a First Pass National Assessment*, Australian Government.

Department of Planning, 2008, *New South Wales State and Regional Population Projections, 2006-2036: 2008 Release*, Australian Government, Sydney.

Dowdy, A. J., Mills, G. A., Timbal, B. & Wang, Y. 2014, "Fewer large waves projected for eastern Australia due to decreasing storminess", *Nature Climate Change*, Vol. 4, pp. 283-286.

Durrant, T. & Greenslade, D. 2011, *Evaluation and implementation of AUSWAVE,* Centre for Australian Weather and Climate Research Technical Report No. 041.

Eldeberky, Y. 1996, "Nonlinear transformation of wave spectra in the nearshore zone", PhD Thesis, Delft University of Technology, Department of Civil Engineering, The Netherlands.

Goda, Y. 2010, *Random Seas and Design of Maritime Structures*, World Scientific, Singapore.

Goodwin, I. D., Browning, S., Mortlock, T. R., Shand, T. & Braccs, M. 2014, "Synoptic drivers of extreme waves and their latitudinal propagation along the south-eastern Australian shelf", *Journal of Continental Research*, submitted for review, May.

Hasselmann, S., Hasselmann, K., Allender, J. H. & Barnett, T. P. 1985, "Computations and parameterizations of the nonlinear energy transfer in a gravity wave spectrum. Part II: Parameterizations of the nonlinear transfer for application in wave models", *Journal of Physical Oceanography*, Vol. 15, pp. 1378-1391.

Hemer, M. A., Fan, Y., Mori, N., Semedo, A. & Wang, X. L. 2013, "Projected changes in wave climate from a multi-model ensemble", *Nature Climate Change*, Vol. 3, pp. 471-476.

Holthuijsen, L. H. 2007, *Waves in Oceanic and Coastal Waters*, Cambridge University Press.

Janssen, P. A. E. M. 1989, "Wave-induced stress and the drag of air flow over sea waves", *Journal of Physical Oceanography*, Vol. 19, pp. 745-754.

Janssen, P. A. E. M. 1991, "Quasi-linear theory of wind-wave generation applied to wave forecasting" *Journal of Physical Oceanography*, Vol. 21, pp. 1631-1642.

Jordan, A., Davies, P., Ingleton, T., Foulsham, E., Neilson, J. & Pritchard, T. 2010, *Seabed Habitat Mapping of the Continental Shelf of NSW*, Department of Environment, Climate Change and Water, Australian Government.

Komen, G. J., Cavaleri, L., Donelan, M., Hasselmann, K., Hasselmann, S. & Janssen, P. A. E. M. 1994, *Dynamics and Modelling of Ocean Waves*, Cambridge University Press.

Kulmar, M., Modra, B. & Fitzhenry, M. 2013, "The New South Wales Wave Climate Improved Understanding through the Introduction of Directional Wave Monitoring Buoys", *Coasts & Ports*, Engineers Australia, Sydney, 11-13 September.

Madsen, O. S., Poon, Y.-K. & Graber, H. C. 1988, "Spectral wave attenuation by bottom friction: Theory", *Proceedings of the 2nd International Conference on Coastal Engineering*, ASCE, pp. 492-504.

Mortlock, T. R. & Goodwin, I. D. 2013, "Calibration and Sensitivity of Nearshore SWAN Model Performance for Measured and Modelled Wave Forcing Scenarios, Wamberal, Australia", Climate Futures at Macquarie, report prepared for Office of Environment and Heritage NSW.

Piani, C., Haerter, J. O. & Coppola, E. 2010, "Statistical bias correction for daily precipitation in regional climate models over Europe", *Theoretical and Applied Climatology,* Vol. 99, pp. 187-192.

Ris, R. C., Holthuijsen, L. H. & Booij, N. 1999, "A third-generation wave model for coastal regions 2. Verification", *Journal of Geophysical Research*, Vol. 104, pp. 7667-7681.

Rollason, V. & Goodwin, I. D. 2009, *Coffs Harbour Coastal Processes Progress Report*, BMT WBM and Climate Futures at Macquarie, Macquarie University, report prepared for Coffs Harbour City Council.

Saha, S., Moorthi, S., Pan, H.-L., Wu, A., Wang, J., Nadiga, S., Tripp, P., Kistler, R., Woollen, J., Behringer, D., Liu, H., Stokes, D., Grumbine, R., Gayno, G., Wang, J., Hou, Y.-T., Chuang, H.-Y., Juang, H.-M. H., Sela, J., Iredell, M., Treadon, R., Kleist, D., Van Delst, P., Keyser, D., Derber, J., Ek, M., Meng, J., Wei, H., Yang, R., Lord, S., Van Den Dool, H., Kumar, A., Wang, W., Long, C., Chelliah, M., Xue, Y., Huang, B., Schemm, J.-K., Ebisuzaki, W., Lin, R., Xie, P., Chen, M., Zhou, S., Higgins, W., Zou, C.-Z., Liu, Q., Chen, Y., Han, Y., Cucurull, L., Reynolds, R. W., Rutledge, G. & Goldberg, M. 2010, "The NCEP Climate Forecast System Reanalysis", *Bulletin of the American Meteorology Society*, Vol. 91, pp. 1015-1057.

Shand, T. D., Goodwin, I. D., Mole, M. A., Carley, J. T., Browning, S., Coghlan, I. R., Harley, M. D., Peirson, W. L., You, Z.-J. & Kulmar, M. A. 2011, *NSW Coastal Inundation Hazard Study: Coastal Storms and Extreme*

Waves, Water Research Laboratory, University of New South Wales & Climate Futures, Macquarie University.

Short, A. D. 1999, *Handbook of Beach and Shoreface Morphodynamics*, John Wiley & Sons.

Short, A. D. 2006, *Beaches of the New South Wales Coast*, Sydney University Press.

Short, A. D., & Trenaman, N. L. 1992, "Wave climate of the Sydney region, an energetic and highly variable ocean wave regime", *Marine and Freshwater Research*, Vol. 43, pp. 765-791.

SWAN, 2011a, *User Manual SWAN Cycle III version 40.85*, Delft University of Technology, Netherlands.

SWAN, 2011b, *Technical Manual SWAN Cycle III version 40.85*, Delft University of Technology, Netherlands.

Tolman, H. L. 2009, *User Manual and System Documentation of WAVEWATCH III version 3.14*, NOAA, US Department of Commerce.

WAMDI, 1988, "The WAM Model – a third generation ocean wave prediction model", *Journal of Physical Oceanography*, Vol. 18, pp. 1775-1809.

Whiteway, T. G. 2009, *Australian Bathymetry and Topography Grid*, Geoscience Australia Report 2009/21, Australian Government, June.

You, Z. & Lord, D. 2008, "Influence of the El-Nino-Southern Oscillation on NSW Coastal Storm Severity", *Journal of Coastal Research*, Vol. 24, pp. 203-207.

THOMAS MORTLOCK

Thomas Mortlock has six years' professional experience in the fields of coastal process science, metocean and oceanography. He is currently undertaking a PhD at the Marine Climate Risks Group, Macquarie University, Sydney. His research focuses on the modelling and description of wave climate change impacts for the east Australian coast, by applying regional-scale climatology with coastal engineering techniques. Thomas has experience in the collection and analysis of multiple metocean and coastal monitoring datasets, and using spectral and Boussinesq wave modelling for coastal hazard definition and management. He has published his research in international and national journals and conferences. Prior to his PhD, Thomas was employed as a Coastal Process Scientist in the UK. He has professional experience in using coastal process science and monitoring for engineering design, and is a Chartered (Marine) Engineer. He has also been involved in the delivery of shoreline management plans and environmental impact assessments for local and central government, and various small- to medium-scale coastal capital and maintenance works.

IAN GOODWIN

Ian Goodwin is Associate Professor in Climate and Coastal Risk and is a member of the Climate Futures Research Centre at Macquarie University, as well as a researcher at the Sydney Institute of Marine Science. Ian leads the Marine Climate Risk Group at Climate Futures. He has 30 years research experience in the fields of climatology, paleoclimatology and climate change science, coastal and marine geoscience, coastal oceanography, polar glaciology, environmental hazard definition and impact management throughout eastern Australia and the southwest Pacific. His papers have documented decadal climate variability, mechanisms for sea-level change, wave climate change, regional coastal evolution, coral reef evolution, extratropical storm climatology, reanalysis and reconstructions of Southern Hemisphere climate, Antarctic ice sheet dynamics. Ian is a foundation member of the scientific advisory committees for the Eastern Seaboard Climate Change Initiative and is researching coastal processes and climate change at numerous sites in northern NSW and southeast Queensland.

IAN TURNER

Ian Turner is the Deputy Director (Research) of the Water Research Laboratory (WRL), School of Civil and Environmental Engineering, University of New South Wales (UNSW), Sydney, and is responsible for the research direction and output. He is also a Senior Coastal Specialist in WRL's coast and estuary investigations group. Ian is trained in both the fields of coastal engineering and coastal geomorphology, with a PhD in Marine Science (Sydney University) and a Masters degree in Environmental Engineering Science (UNSW). Ian's current research interests include beach groundwater dynamics and sediment transport at the beach face, monitoring of coastal change and impacts of climate variability, coastal erosion control and coastal management, and coastal aquifer hydrogeology. In recognition of Ian's leadership in the field of coastal engineering, since 2005 he has been an active member of the Engineers Australia's National Committee on Coastal and Ocean Engineering.

APPENDIX 2

Published Conference Paper.

Mortlock, T.R., Goodwin, I.D and Turner, I.L. (2013). Calibration and sensitivities of a nearshore SWAN model to measured and modelled wave forcing at Wamberal, New South Wales, Australia. *Coast and Ports Conference*, *Engineers Australia, Manly, Sydney, September, 2013*.

Calibration and sensitivities of a nearshore SWAN model to measured and modelled wave forcing at Wamberal, New South Wales, Australia

Thomas R. Mortlock[1], Ian D. Goodwin[1], Ian L. Turner[2]
[1] Department of Environment and Geography, Macquarie University, North Ryde, Australia; thomas.mortlock@mq.edu.au
[2] Water Research Laboratory, School of Civil and Environmental Engineering, UNSW, Sydney, Australia

Abstract
A SWAN model was configured and calibrated at Wamberal on the central New South Wales (NSW) coast. The model was verified against a nearshore Datawell WaveRider buoy (WRB) located at an exposed shallow-water site at the northern end of an embayed compartment. Model sensitivities to bed roughness, tide and hindcast winds were investigated. The optimised SWAN model achieved good results for nearshore wave heights (R^2 0.86 m 0.99) with low RMS error (0.2m). Up-scaled CFSv2 hindcast winds introduced a systematic over-estimation of high frequency (low period) wind sea and contributed to a consistent negative bias in modelled mean wave periods of 0.5 to 1s. However, the inclusion of hindcast winds appeared to generally improve the shape of the wave period distribution. Spectral wave information from a regional WaveWatch III (WW-III) model was also transformed to the nearshore buoy location. Over the study period, the WW-III wave spectra under-estimated the directional spread of waves, only accounting for wave directions between 100 and 140˚, suggesting that longer-period swell waves are under-represented at this location. The longshore transport component, typically driven by oblique long-period (constructive) wave energy produced by far-field storms, would likely be under-estimated while preference is given to shorter-period, steeper (destructive) waves that favour cross-shore sediment transport. Results are of significance for coastal management on the Australian East Coast in cases where hindcast modelled deepwater wave spectra are used to calibrate and drive shoreline models.

Keywords: nearshore wave climate, wave refraction modelling, SWAN, WW-III

1. Introduction

Knowledge of nearshore wave climates is vital for sustainable shoreline management. In 2007, the collective value of NSW properties threatened by coastal processes within planning timeframes was estimated at over $1 billion [4]. The Sydney region alone is projected to increase its population by 40% in the next 30 years [4]. Rising population pressure will only serve to increase coastal vulnerability to wave climate change in NSW. In response to this, the NSW Office of Environment and Heritage (OEH) commissioned a coastal wave model system to provide a storm-wave hindcast for NSW [2, 3]. This paper describes the calibration and sensitivities of a nearshore SWAN model set up at Wamberal to provide nearshore validation and calibration of this wave model system.

2. Background

2.1 Wamberal buoy

The Wamberal-Terrigal compartment is located on the central NSW coast, approximately 60km north-east of Sydney (Figure 1). The northern section of the Wamberal compartment, where the WaveRider Buoy (WRB) used in this study was located, is exposed to the modal south-easterly wave climate. The buoy was positioned near the 12m depth contour (AHD) towards the northern end of the embayment approximately 400m offshore. The buoy recorded hourly directional wave spectra between 05/08/2011 12:00 and 16/03/2012 08:00 (EST) with a 93% recovery rate (5015 of 5373 records recovered).

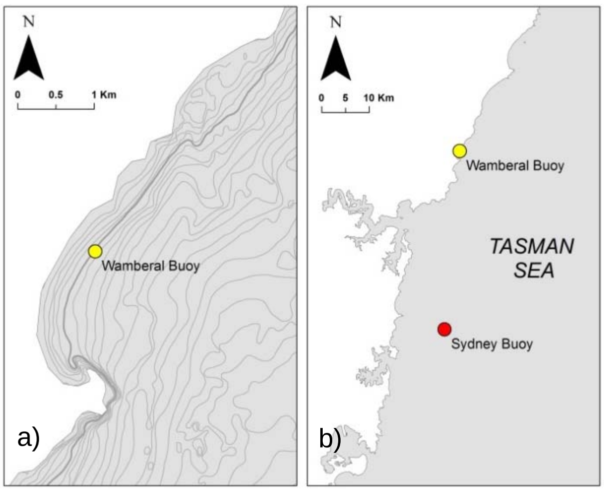

Figure 1 (a) WRB location at Wamberal-Terrigal with 2m depth contours and (b) in relation to Sydney region

2.2 Nearshore wave climate

The peaks over threshold (POT) method was employed to analyse the nearshore modal and storm wave climates from the Wamberal buoy, using the derived 5% exceedance wave height (~ 2m) with a minimum exceedance duration of six hours. A minimum interval between storm events was set at one half day (12 hours). Figure 2 shows the directional distribution of wave heights during the buoy deployment period for modal (≤2m H_s, 98% of record) and storm (≥2m H_s, 2% of record) waves in 10° directional bins. Both modal and storm wave climates have a strong south-east (130 to 140°) component. During storm waves, this band is even more concentrated within the south-east quadrant.

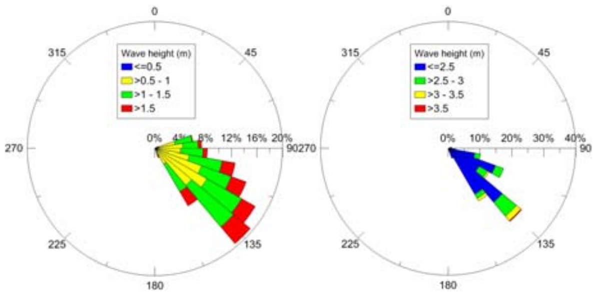

Figure 2 Wave directional distribution at Wamberal when $H_s < 2$m (left) and when $H_s \geq 2$m (right).

The predominantly uni-directional low-energy south-easterly wave climate seen at the buoy from August 2011 to March 2012 is typical of the central NSW coast during the austral spring/summer period. As winter ends, the subtropical ridge progresses southward and quasi-stable high pressure systems over the Tasman Sea block the northward progression of mid-latitude lows, reducing the longer period southerly wave component. Anticylonic intensification over the Tasman Sea produces a lower energy, more uni-modal south-easterly wave climate [5]. A local sea breeze may be responsible for the lower energy north-easterly component seen in the modal energy wave rose. During the measurement period, mean H_s was 1.2m, mean T_z was 6.2s and mean wave direction, *MWD*, was 118° (deg TN).

2.3 SWAN model

SWAN (Simulating WAves Nearshore) is a third generation fully-spectral wave model developed at the Delft University of Technology [1] that computes random, short-crested wind-generated waves in coastal regions and inland waters. Within the SWAN model, bottom and current-induced shoaling (energy bunching) and refraction are properly accounted for but diffraction is only approximated [7]. The dissipation of wave energy is accounted for in the formulations for whitecapping, bottom dissipation and surf breaking. SWAN version 40.85 was used in this study, which included a modified line in the source code (line 5919 in *swanmain.ftn*) to enable WW-III spectra to be accurately applied to the SWAN seaward boundary.

2.4 WW-III model

WW-III is a fully-spectral third generation wind-wave model developed by NCEP [9]. It is designed for oceanic large-scale applications and is optimised for efficient computing, rather than high-resolution coastal applications [9]. Cardno [2, 3] developed a global-to-regional WW-III model suite for OEH based on WW-III version 3.14 physics. This model suite consists of a series of nested grids from global, to national, to Tasman Sea and NSW-wide. The Tasman Sea model is run on a 0.05° x 0.05° grid (approximately 5km) covering the whole NSW coast. This regional model is coupled to a wider Australian national model (0.25° x 0.25° grid) which is likewise nested within a global scale (1.0° x 1.0° grid) WW-III model. Directional wave spectra, output from this wave model system, were applied to the standalone SWAN deep-water boundary and transformed to the Wamberal buoy location.

3. Data sources

3.1 Bathymetry

Five bathymetric datasets (Table 1) were used in this study in order to build a continuous bathymetric grid in SWAN. All bathymetric data was supplied by OEH, projected in WGS84 coordinates and referenced to Australian Height Datum (AHD).

Table 1 Bathymetric types

Bathymetry	Type	Year
Australian Hydrographic Office (AHO) survey lines	Survey lines (3km spaced)	1972
AHO digitised fairsheets	Digitised contours (2m contours)	1984
Laser Airborne Depth Sounder (LADS) soundings	Point cloud lidar (5m spacing)	2008
GeoScience Australia (GA) AusBathy	Pre-gridded (250m)	2009
LADS plotted soundings	Point cloud lidar (50m spacing)	2011

3.2 Offshore wave data - measured

Hourly spectral wave parameters from the Sydney WRB were provided by Manly Hydraulics Lab (MHL) over the period of the Wamberal buoy deployment. The peak spectral parameters of significant wave height, H_s, peak spectral wave period, Tp_1 and mean wave direction corresponding to the spectral peak, MWD_{tp1}, were input to the SWAN model at the deep-water boundary. The Sydney buoy is located at ~90m depth, approximately 45km south-east of the Wamberal buoy (Figure 1). Over this period, the Sydney record had a 93% data recovery rate.

3.3 Offshore wave data - modelled

Spectral wave information was provided by Cardno [2, 3] from the output of the OEH WW-III wave model system. Spectral data was provided in SWAN spectral format (.sp2) and applied along the deep-water SWAN boundary.

3.4 Hindcast winds

Cardno [2] evaluated the nearshore performance of multiple sources of hindcast winds along the central NSW coast. Results suggested the Climate

Forecast System Reanalysis (CFSR) dataset best represented measured conditions, although showed a positive bias at higher wind speeds and some directional discrepancies. Between 1979 and 2010, CFSR hindcast winds were generated on a global 0.3125° x 0.3125° grid at hourly intervals [7]. From 2010 onwards, a second (not full hindcast) version (CFSv2) is available, generated on higher spatial and temporal resolutions [7]. A scaling procedure of nearshore wind velocities was applied to the CFSv2 winds by Cardno [2] to conform better to observed winds. Within 30km of the NSW coast, wind speeds were scaled up by 20% of the original CFSv2 winds. This hourly up-scaled CFSv2 wind data was extracted by Cardno at the closest grid point to the Wamberal SWAN seaward boundary (151.600E, 33.425S) to provide a continuous time-series for wind forcing in the SWAN model.

3.5 Tides

Hourly tidal data from Middle Head (HMAS Penguin) tidal gauge (Sydney Harbour) was provided by MHL for the period of Wamberal wave buoy deployment. Since tides reach NSW almost incident to the coast, time lags in tide between Middle Head and Wamberal are negligible.

4. SWAN model domain

Figure 3 shows the extents of the computational grid used in the Wamberal SWAN model.

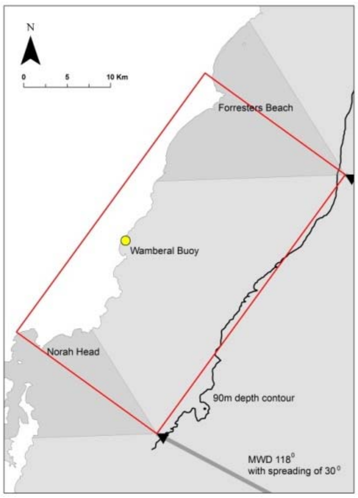

Figure 3 Wamberal SWAN model extent (red) with 90m depth contour and lateral error shadow zones estimated from the MWD (dark grey)

The SWAN model was centred around the Wamberal embayment and nearshore WRB. In order that wave parameters from the Sydney buoy could be realistically applied to the model, the SWAN domain extended to 90m depth (20km offshore) and was aligned to depth-contours offshore of Wamberal (54° rotation). It is therefore an inherent assumption of the model that wave conditions at 90m depth at the Sydney buoy and the model domain are consistent. The Sydney deep-water buoy wave parameters were applied to all three ocean boundaries. Since this is not necessarily a good approximation of the wave conditions along the lateral sides of the grid, especially in shallower waters, the domain was created with sufficient distance either side of the Wamberal embayment to minimise the propagation of lateral boundary errors into the area of interest.

5. Bathymetry preparation

Figure 4 illustrates the extents and gridded product of available bathymetries.

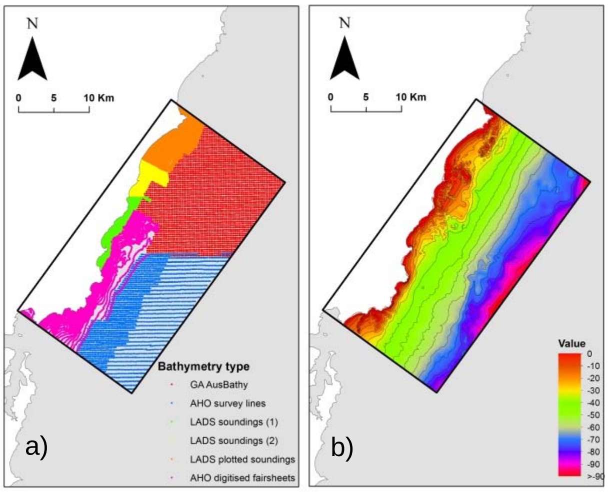

Figure 4 (a) Bathymetric types used for gridding in SWAN and (b) bathymetries gridded to an interpolated surface with 5m contours shown

Bathymetric soundings were edited in ArcGIS and exported in xyz format to Delft3D QUICKIN where they were interpolated to grids created in the Delft3D RGFGRID module. The gridded bathymetries were then converted to SWAN bot format. A number of bathymetry types were merged to provide sounding data for the entirety of the model domain. When merging bathymetries, care was taken that areas of data joins did not produce artificial steps in the seabed topography. Due to differences in sounding collection method, data point spacing and depth accuracy, sharp slopes can appear along join lines. This stepping effect was minimised by leaving a thin buffer of overlapping soundings at join lines so the interpolation process would smooth out any abrupt depth differences.

6. SWAN model calibration

6.1 Calibration period

The SWAN model was calibrated against a subset of the Wamberal nearshore WRB dataset. Since an underlying objective of the OEH NSW wave modelling project was to produce a storm-wave climatology for the NSW coast, the calibration sub-set was chosen with preference to storm-wave conditions. A continuous 27-day calibration sub-set (10/09/11 16:00 to 05/10/11 07:00) was chosen. This period included five of the 13 storm events (when H_s ≥ 2m, or the 5% exceedance wave height, for six hours or more) detected in the buoy record including the largest event (maximum hourly H_s = 3.60m) A 24-hour buffer period was provided for preceding the calibration period for model spin up and shock wave propagation. During the calibration period, the data capture rate at the Wamberal buoy was 99% with only eight dropouts in 625 hourly records.

6.2 Comparative wave statistics

Modelled significant wave height (H_s), mean wave period (Tm_{02}) and mean wave direction (*MWD*) were compared to significant wave height (H_s), mean wave period (T_z) and mean wave direction (MWD_{tp1}) from the Wamberal WRB. Mean, rather than peak spectral statistics were used because the SWAN peak statistics are unstable parameters with a tendency of switching rapidly between high and low frequencies, especially if the sea and swell portions of the sea state are near equal. The mean frequency-direction statistics provides a better indication of how the bulk of the wave energy is being described in the model. Mean wave direction was not a statistic provided by MHL in the Sydney or Wamberal wave data, so the mean wave direction at the spectral peak frequency was used (θ_{tp1}). The SWAN Tm_{02} statistic is the mean wave period as calculated from the second and zeroth spectral moments of the wave energy spectrum and is generally comparable to T_z [2]. The T_z statistic is the average zero-crossing period based on upward zero crossing of the still water line.

7. SWAN model sensitivities

Sensitivities of the SWAN model to bottom friction, tide, hindcast winds and WW-III spectra were investigated. Model sensitivities were quantified using a range of validation metrics. These metrics included Pearson's Squared Correlation (R^2), Root Mean Squared (RMS) error, Bias, Scatter Index (SI) and Slope (*m*). These metrics collectively provide a description of how the modelled nearshore wave parameters performed over the calibration period when compared with measured data at the Wamberal buoy location.

7.1 Bottom friction

SWAN can account for bottom friction by either using the JONSWAP dissipation approximation, the drag law formulae or the eddy viscosity model. The JONSWAP formulation is set as default and can be calculated using a coefficient for wind-sea (0.067 m^2s^{-3}) or swell-wave conditions (0.038 m^2s^{-3}). Table 2 gives the effect on nearshore modelled wave parameters of varying this coefficient. Only minor improvements to the RMS, Bias, SI and Slope of the modelled wave heights are seen when the swell coefficient is used, but there are equally small detrimental effects for modelled wave directions and periods. Correlation coefficients for all wave parameters were unaffected.

Table 2 Model sensitivity to JONSWAP bottom friction where *WS* = wind-sea and *S* = swell-wave coefficient

	JONSWAP bottom friction					
***n* = 586**	**H_s**		**Tm_{02}**		***MWD***	
	WS	***S***	***WS***	***S***	***WS***	***S***
R^2	0.90	0.90	0.38	0.38	0.74	0.74
RMS	0.22	0.21	1.97	2.01	11.98	11.99
Bias	0.09	0.08	-1.61	-1.66	4.62	4.60
SI %	16.2	15.8	28.7	29.2	9.7	9.7
m	0.93	0.94	0.61	0.62	0.78	0.77

7.2 Tide

Since measured and modelled wave data was available hourly, the influence of tide at the nearshore site was considered over the calibration period and results are detailed in Table 3.

Table 3 Model sensitivity to tide where *NT* = no tide and *T* = tide

	Tide					
***n* = 586**	**H_s**		**Tm_{02}**		***MWD***	
	NT	***T***	***NT***	***T***	***NT***	***T***
R^2	0.90	0.90	0.38	0.37	0.74	0.74
RMS	0.22	0.22	1.97	1.90	11.98	11.91
Bias	0.09	0.09	-1.61	-1.53	4.62	4.56
SI %	16.2	16.2	28.7	27.6	9.7	9.6
m	0.94	0.96	0.62	0.56	0.77	0.78

As seen in Table 3, the application of a measured hourly tide curve to SWAN made only negligible differences to modelled wave parameters. The majority of all calibration metrics remained the same, although there were minor improvements to the RMS error, bias and scatter of modelled wave periods and directions. Modelled wave heights remained unaffected.

7.3 Hindcast winds

The application of a wind field in SWAN accounts for wind-wave growth over the model domain and adds to higher-frequency spectral wave energy. Table 4 shows the change in model performance when SWAN is run with and without the coastal up-scaled CFSv2 hindcast winds over the full eight-month time-series, when compared with the Wamberal buoy data.

Table 4 Model sensitivity to hindcast winds where *W* = wind and *NW* = no wind

	Up-scaled CFSv2 hindcast winds					
***n* = 5015**	**H_s**		**Tm_{02}**		***MWD***	
	W	**NW**	**W**	**NW**	**W**	**NW**
R^2	0.86	0.84	0.53	0.33	0.68	0.68
RMS	0.23	0.21	1.26	1.88	13.50	14.67
Bias	0.22	0.14	-0.45	1.81	14.43	15.02
SI %	19.4	17.4	20.4	30.4	11.4	12.4
m	0.99	0.97	0.82	0.85	0.77	0.90

Figure 5 shows the modelled distribution of mean wave periods with and without winds applied, and the measured distribution at the Wamberal buoy. Results indicate that whilst the addition of a boundary wind field has only a minimal impact on modelled wave heights, the prediction of wave periods is generally improved.

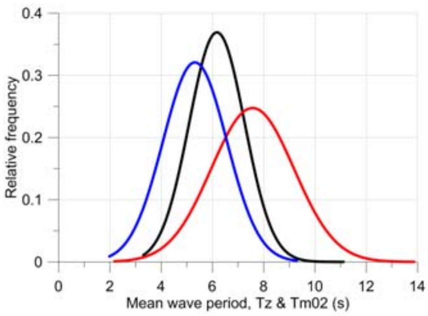

Figure 5 Distribution of mean wave period, T_z/Tm_{02}, as measured (black), and SWAN-modelled with hindcast winds (blue) and without hindcast winds (red)

Hindcast winds reduce the scatter seen in the model (from 30% to 20%) and improve the shape of the frequency distribution (blue curve, Figure 5). However, winds introduce too much higher frequency wave energy to the spectrum, causing a systematic under-prediction of wave periods (by around 0.5 to 1 second). Results also suggest that the addition of a wind field introduces a directional wave bias. Although the R^2, RMS error, bias and scatter remain relatively constant both with and without winds, the slope is much improved without winds (*m* 0.77 to 0.90) when compared to measured data. This suggests modelled waves of all directions best matched with observed values in the absence of the CFSv2 hindcast winds.

7.4 WW-III spectra

While all above sensitivities were investigated using measured parametric wave input from the Sydney deepwater buoy, WW-III spectral wave information from the Cardno/OEH wave model system was also transformed to the nearshore buoy location in SWAN over the full eight month timeseries to investigate nearshore performance and bias. Table 5 shows the change in SWAN performance when WW-III wave spectra are applied in place of buoy-measured parameters.

Table 5 Model sensitivity to WW-III spectra where *B* = buoy (measured) and *WW* = WW-III (modelled) input

	WW-III spectra					
***n* = 5015**	**H_s**		**Tm_{02}**		***MWD***	
	B	**WW**	**B**	**WW**	**B**	**WW**
R^2	0.86	0.75	0.53	0.42	0.68	0.45
RMS	0.23	0.25	1.26	2.18	13.50	15.58
Bias	0.22	0.01	-0.45	-1.52	14.43	9.40
SI %	19.4	21.1	20.4	35.4	11.4	13.2
m	0.99	0.91	0.82	0.59	0.77	0.39

Figure 6 shows the modelled distribution of mean wave directions when SWAN is forced with measured and modelled boundary waves, and the measured distribution at the Wamberal buoy. Results indicate better nearshore performance is achieved with Sydney WRB parametric input, rather than WW-III spectral wave input.

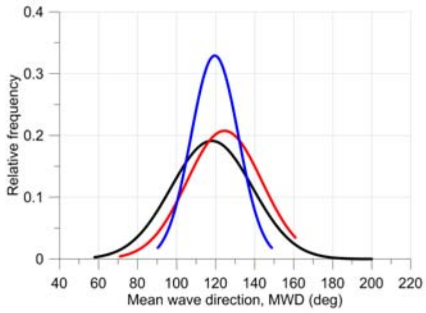

Figure 6 Distribution of mean wave direction *MWD*, as measured (black), and SWAN-modelled with WW-III spectra (blue) and buoy-measured parameters (red) as deepwater boundary input for SWAN

The R^2, RMS error, SI and slope of all three wave parameters in Table 5 worsen when the SWAN model is run with spectral WW-III input. Most noticeable, however, is the poor estimation of nearshore wave direction when the model is forced with WW-III spectra. Figure 6 suggests the WW-III spectra under-estimates the directional spread and only account for wave directions between 100 and 140° whereas the WRB-forced SWAN model better represents this directional spread.

8. Discussion

The calibrated SWAN model, when forced with deep-water buoy-measured wave statistics, achieved consistent nearshore correlation with measured wave heights (R^2 0.86, *m* 0.99) but a scattered (SI 20%) and slightly negatively biased (0.5s) estimate of wave period and a consistent 14° southerly directional bias. Residual biases may be due to either; a) biases in the buoy-measured waves and/or b) deficiencies in model physics. Because the Sydney buoy was located 45km outside the SWAN domain, the application of this dataset direct to the model may have introduced boundary errors. In addition, parametric, rather than full spectral wave input requires SWAN to assume a spectral shape which may not be accurate especially during multi-modal seas. Although the spectral shape was calibrated for (not reported here), a subsequent study will use full spectra to eliminate this error source.

SWAN was found to be largely insensitive to bottom friction at the Wamberal buoy location. This concurs with findings by Cardno [2] when configuring a SWAN model at Newcastle, 70km north-east of Wamberal. Considering the complex extents of exposed rock reef around the approaches to and inside the Wamberal embayment, bottom friction would be assumed to vary throughout the model domain. However, SWAN uses the empirical JONSWAP model of bottom energy dissipation as default, which does not explicitly account for bottom substrate type. Rather, it describes bottom dissipation based on the wave orbital motion instead of the substrate roughness length. Conversely, the drag model uses a bottom friction coefficient directly related to bottom substrate type. The eddy viscosity model similarly uses a friction factor estimated according to a variable bottom roughness length scale according to bottom substrate type. These two latter models in SWAN are allowed to vary spatially with bottom type and can therefore be input as a grid over the computational domain. Expressing bottom dissipation in terms of a spatially variable roughness length, rather than a spatially-static orbital velocity term, may improve model performance at Wamberal and is being investigated in a current study.

SWAN was equally insensitive to hourly tides; perhaps unsurprising considering the water depth at the buoy is around 12m and the mean spring tidal range at Sydney is only 1.3m. Energy dissipation due to earlier interaction with the seabed at lower tidal elevations may be plausible, but results suggest that any effect this has on wave celerity is averaged over the tidal cycle.

The inclusion of hindcast winds generally improved the modelled wave period distribution although a systematic over-estimation of high-frequency wind-sea was seen at all wave periods. A similar finding was reported by Cardno [2] for deep-water locations along the NSW coast. This suggests the hindcast winds slightly over-estimated nearshore wind speeds during the eight-month study period.

The application of WW-III spectra to SWAN suggested an under-representation of longer-period oblique waves and a preference for shore-normal (100 to 140°) shorter-period wind-sea. This suggests that, at least over the study period, the typically longer-period swell waves generated by Southern Tasman Lows and Tropical Lows were under-represented in the WW-III spectra as these wave generation systems produce wave climates with SSE and ENE waves along the central NSW coast, respectively. Instead, the WW-III spectra gave preference to more locally-generated, shorter period wave climates with higher-frequency wave energy from the central Tasman Sea region. This is also manifest in the persistent bias towards shorter period sea seen in both this study and in Cardno [2]. This apparent preference of WW-III spectra for high-frequency uni-directional wave energy can have consequences for shoreline modelling applications when waves are transformed to nearshore locations. The longshore transport component, typically driven by oblique long-period (constructive) wave energy, is likely to be under-estimated when preference is given to shorter-period, steeper incident (destructive) waves that promote cross-shore transport.

9. Summary

SWAN was largely insensitive to variations in bottom friction at the Wamberal buoy location despite a variable substrate over the model domain. This was concluded to be due to the JONSWAP dissipation term (default in SWAN) not directly accounting for bed roughness length. Further work is being undertaken to investigate the effect of applying a variable roughness grid in SWAN. The inclusion of up-scaled CFSv2 hindcast winds improved the modelled frequency distribution but introduced a systematic under-prediction of wave period (0.5s) suggesting wind velocities are over-estimated at this location. The forcing of the model with WW-III spectra suggested, for the duration of the study period, an under-representation of longer-period oblique waves and a preference for more locally-generated sea. If these deep-water spectra were used to feed shoreline modelling, the longshore component of sediment transport may be under-represented in favour of cross-shore movement.

10. Acknowledgements

All tidal and wave data were supplied and quality-controlled by Mark Kulmar at MHL. The Wamberal WRB deployment was funded by ARC linkage project LP100200348. All bathymetric data was supplied by OEH. Wave spectra and hindcast winds were provided by Cardno. SWAN v.40.85 with modified source code, and technical support, was provided by Mark Taylor and Sean Garber at SeaState Engineering. Special thanks go to Michael Kinsela at OEH for technical feedback.

11. References

[1] Booij, N., Ris, R. C., & Holthuijsen, L. H. (1999). A third-generation wave model for coastal regions 1. Model description and validation. *Journal of Geophysical Research, 104*(C4), 7649 - 7666.

[2] Cardno. (2012). NSW Coastal Waves: Numerical Modelling Final Report *Prepared for Office of Environment and Heritage (OEH)*. September 2012.

[3] Cardno. (2013). NSW Coastal Modelling – Phase II. *Prepared for Office of Environment and Heritage (OEH)*. April 2013.

[4] DECC. (2009). Climate Change Risks to Australia's Coasts. Department of Climate Change (DECC), Commonwealth of Australia.

[5] Goodwin, I. D. (2005). A mid-shelf wave direction climatology for south-eastern Australia, and its relationship to the El Nino – Southern Oscillation, since 1877 AD. *Int. J. Climatology. 25*, 1715-1729.

[6] Holthuijsen, L. H. (2007). Chapter 9. The SWAN Wave Model. In L.H. Holthuijsen (2007) *Waves in Oceanic and Coastal Waters*: Cambridge University Press. pp. 286 - 309

[7] Saha, S, Suranjana, M., & co-authors (2010). The NCEP Climate Forecast System Reanalysis. *Bull. Amer. Meteor. Soc.,* Vol 91, pp 1015.1057.

[8] The SWAN Team (2013). USER MANUAL SWAN Cycle III version 40.91: Delft University of Technology.

[9] Tolman, H. L. (2009). User manual and system documentation of WAVEWATCH III^{TM} version 3.14 *NOAA/NWS/NCEP/MMAB Technical Note 276*.

APPENDIX 3

Published Journal Article.

Mole, M., **Mortlock, T.R.**, Turner, I.L., Goodwin, I.D., Splinter, K.D., Short, A.D. (2013). Capitalizing on the surfcam phenomenon: a pilot study in regional-scale shoreline and inshore monitoring utilizing existing camera infrastructure, *Journal of Coastal Research,* SI65 (ICS2013), 1433-1438. doi: 10.2112/SI65-242

Capitalizing on the surfcam phenomenon: a pilot study in regional-scale shoreline and inshore wave monitoring utilizing existing camera infrastructure

Melissa A. Mole†, Thomas R.C. Mortlock‡, Ian L. Turner†, Ian D. Goodwin‡, Kristen D. Splinter† and Andrew D. Short∞

† School of Civil and Environmental Engineering, University of New South Wales, NSW 2052, Australia
m.mole@unsw.edu.au
ian.turner@unsw.edu.au
k.splinter@unsw.edu.au

‡ Marine Climate Risk Group, Department of Environment and Geography, Macquarie University, NSW 2109, Australia
thomas.mortlock@mq.edu.au
ian.goodwin@mq.edu.au

∞ CoastalCOMS,
Varsity Lakes, QLD 4227, Australia
andrew.short@coastalcoms.com

www.cerf-jcr.org

www.JCRonline.org

ABSTRACT

Mole, M.A., Mortlock, T.R.C., Turner, I.L., Goodwin, I.D., Splinter, K.S. and Short, A.D., 2013. Capitalizing on the surfcam phenomenon: a pilot study in regional-scale shoreline and inshore wave monitoring utilizing existing camera infrastructure. *In:* Conley, D.C., Masselink, G., Russell, P.E. and O'Hare, T.J. (eds.), *Proceedings 12th International Coastal Symposium* (Plymouth, England), *Journal of Coastal Research*, Special Issue No. 65, pp. xxx-xxx, ISSN 0749-0208.

Driven by dynamic inshore wave climates, sandy beaches oscillate around long term mean trends at daily (storm events) to inter-annual timescales (regional climate cycles). Coastal imaging technology provides a practical means for sustained, autonomous beach morphology and inshore wave monitoring at high temporal resolution. However, existing, scientifically-proven systems are limited in their application due to cost and required infrastructure. A potential alternative has been identified in the existing surfcam networks operating at 100+ sites around Australia and many sites around the world. This work reports a critical evaluation of this new, low-cost monitoring method which has the potential to significantly expand spatial coverage of coastal behavior; capturing both real-time forcing (waves) and effect (shoreline change). In this study, seven embayed beaches in New South Wales, Australia, are used to examine the potential for a sustainable regional monitoring network using existing surfcam infrastructure to provide daily measurements of shoreline position and inshore waves at the break point. Surfcam image-derived shorelines are compared at daily frequency over 10 months at one site to co-located Argus image-derived shorelines and at monthly frequency over 18 months at nine camera sites to concurrent on-ground RTK-GPS surveys. Preliminary comparisons to Argus image-derived and RTK-GPS surveyed shorelines indicated promising qualitative agreement. A simple geometric correction was shown to significantly improve the surfcam-derived shoreline measurements. Surfcam-derived inshore wave heights and periods are compared to three months of concurrent hourly nearshore (depth ~10m) wave buoy measurements at two camera sites. Initial evaluation of the wave measurement capability suggests a consistent over-estimation of smaller waves and under-estimation of larger waves. It is suggested that these "bottom-heavy" measurements are due to pixel rectification error associated with obliquity from a single low-angle camera; and the high variability in measurements due to beach and wave type.

ADDITIONAL INDEX WORDS: *coastal monitoring, daily beach variability, low mounted cameras, internet protocol cameras, coastal imaging, image processing, CoastalCOMS.*

BACKGROUND

Knowledge of shoreline location, history, and behaviour is crucial for the management of coastal settlements and a range of techniques have been applied to identify this dynamic land-sea boundary (Boak and Turner, 2005). While *in situ* beach surveying and nearshore wave monitoring can be time-consuming and expensive, shore-based remote sensing methods offer a practical and relatively inexpensive option for sustained coastal monitoring.

The present 'state of the art' in coastal imaging is the Argus video system that includes one or more fixed cameras per site, on-site data acquisition and control systems and a comprehensive data analysis suite (Holman and Stanley, 2007). For two decades, Argus systems have been applied to meet a range of monitoring and research needs around the world and inspired the development of similar systems (see Nieto *et al.*, 2010). The use of colour images has allowed the development of several shoreline detection techniques that have improved shoreline measurement in diverse environments (e.g. Plant *et al.*, 2007). Shoreline measurement is usually accomplished with a time-lapse image from a single camera, using established photogrammetric techniques to correct for lens distortion and incorporate camera position and rotation angles (azimuth, tilt, and roll) with recorded ground control points (GCPs) to transform two-dimensional image coordinates to corresponding three-dimensional geographic coordinates (e.g. Holland *et al.*, 1997). Shoreline elevation is often assumed equal to tidal elevation for convenience or more precisely determined from tide and wave-induced components (e.g. Aarninkhof *et al.*, 2003). A timeseries of hourly shorelines then forms an intertidal bathymetry and from this surface, a specific contour can be extracted for beach width monitoring, or the intertidal slope or sand volume may be calculated (e.g. Plant and Holman, 1997).

DOI: 10.2112/SI65-xxx.1 received 30 November 2012; accepted Day Month 2013.

Recent efforts to advance shore-based remote measurement of breaking waves have typically utilised a dual-camera system (e.g. de Vries *et al.*, 2011; Shand *et al.*, 2012), where the overlapping field of view allows the simultaneous solution of position and water surface elevation by stereometric intersection (Holland *et al.*, 1997). Single-camera systems for breaking wave height measurement have been validated under laboratory conditions (e.g. Almar *et al.*, 2012) and in the field on a fringing reef system where the horizontal position of breaking was reasonably constrained (Hilmer, 2005). A single, low-mounted camera system has also been tested in a multi-barred beach environment (Lane *et al.*, 2010), however uncertainty remains over the accuracy of geometric solution in this dynamic environment without a second camera or horizontally constrained breaking zone. The recent work by Shand *et al*. (2012) remains the only rigorously field-verified video system for breaker height measurements in a dynamic beach environment to date.

Coastal imaging systems have proved a useful tool for the integration of research and coastal zone management practice (e.g. Davidson *et al.*, 2007; Kroon *et al.*, 2007; Turner and Anderson, 2007). Through near continuous recording extending up to several kilometres along a coastline, high-end coastal imaging systems can provide image-derived data to investigate and quantify a diverse range of coastal processes. These systems are presently restricted in their usage due to installation and ongoing running expenses, and the requirement for a high beach-front platform at the site of interest; commonly a multi-storey building or purpose-built tower. In recent years, there has been a move toward lower cost, more customisable systems, which are accessible to a wider user group in more locations (e.g. Nieto *et al.*, 2010).

The development of a low-cost, multi-purpose, easily accessible monitoring system, deployed at many sites simultaneously, could address the scarcity of daily to multi-year coastal monitoring data currently available. In this present work, the opportunistic use of pre-existing ‘surfcams’ for inshore wave and shoreline monitoring is explored. In a previous study, the use of similar cameras specifically mounted at high locations for shoreline monitoring was reported (Splinter *et al.*, 2011). The aim of this study is to report the first rigorous and independent assessment of a new wave and shoreline monitoring capability based on an existing, low elevation, surfcam network. After introducing the study area, the paper is presented in two parts, addressing the surfcam ability to provide information on shorelines and nearshore waves.

STUDY AREA AND SURFCAM NETWORK

This present work is based in embayed beaches distributed along ~250 km of the New South Wales (NSW) coastline, Australia. Seven embayments (incorporating nine surfcam sites) were selected for this study with varying embayment length and orientation, which control the exposure of each site to the modal south-south-easterly wave climate. Study sites are indicated in Figure 1, with one surfcam per embayment, except at Narrabeen-Collaroy and Wamberal-Terrigal, where there are two cameras and inshore wave evaluations were also completed. The positions of the existing Argus station at Narrabeen-Collaroy and inshore wave-rider buoys at both sites are also shown.

The surfcam network utilized in this study is operated by Coastal Conditions Observation and Monitoring Solutions (CoastalCOMS) and includes 80 cameras around Australia. The cameras are SonyRZ50 pan-tilt-zoom internet protocol cameras, mounted inside small unobtrusive housings, usually located on 1-2 storey surfclub buildings. Surfcams are the only on-site equipment deployed, with all data acquisition, storage and analysis carried out on the Amazon cloud. Each site has a single camera, which is

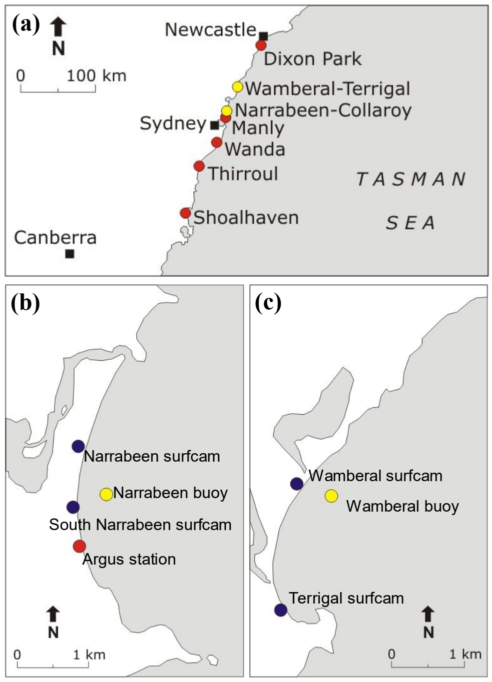

Figure 1. (a) Study sites (●) and major cities (■) along the NSW coastline; (b) Narrabeen-Collaroy embayment; (c) Wamberal-Terrigal embayment.

mechanically rotated between preset aim points (one for wave measurement and up to five for adjacent sections of the shoreline).

The nine surfcam sites are all “low-angle” with elevations ranging from 9 to 20 m above mean sea level (0 m Australian Height Datum, AHD), with a lower limit of 7 m presently specified by CoastalCOMS as suitable for wave monitoring. Surveyed beach widths at the nine sites over 18 months ranged from 40 to 118 m, resulting in angles between 6.3 and 14.6 degrees measured between the 0 m AHD contour and the camera, compared with measured intertidal zone slopes (between 0 and 2 m AHD) between 2.9 and 10.8 degrees. At times beach width and slope caused shorelines to be obscured, highlighting one of the inevitable limitations of low-angle cameras.

SHORELINE DATA COMPARISON

Shoreline Data Collection Program

This study builds on the existing coastal monitoring program at Narrabeen, including monthly RTK-GPS surveys of the sub-aerial beach and hourly Argus-derived shorelines (Harley *et al.*, 2011), which span across the surfcam site of South Narrabeen. The Argus system is used to map hourly (daylight) shorelines every day. These are interpolated to form a daily intertidal bathymetry, from which beach widths are calculated. At the six other embayments included here, RTK-GPS surveys of the sub-aerial beach spanning the cameras’ field of view have been carried out on a monthly basis since February 2011. Once per day at each surfcam site, a single mid-tide recording was made for each camera aim point and corresponding shoreline positions (at ~3 pre-defined cross-shore transects per image) reported by CoastalCOMS. Once per month, hourly recordings were made so that intertidal cross-shore profiles could be constructed, where each shoreline elevation was taken as the measured tidal elevation.

Shoreline Detection and Image Processing

The image analysis methods described here were developed in-house by CoastalCOMS, with the resulting beach width data supplied for independent evaluation. 640x480 pixel time-exposure images are produced by averaging 12 frames per second over five minutes of recorded video. The colour image is converted to an intensity image, based on the hue property, and a simple edge detection model is applied to locate the abrupt change in hue from sand to water. This technique often results in the detection of multiple edges in each image and manual review is required. If a dune or berm blocks the shoreline, the edge of this feature will be detected and result in an erroneous shoreline position.

Conventional image rectification (e.g. Holland *et al.*, 1997) is not used in this system and camera location and viewing angles are not calculated. The CoastalCOMS geometric solution for shoreline measurement requires GCPs to be recorded at a five metre interval along shore-normal transects that extend out to the shoreline at the time of the survey. Continuous shorelines are detected within each image and discrete shoreline positions are then calculated at points where these surveyed transects intersect the detected shoreline. Linear interpolation is carried out between the two closest GCPs on each transect to locate a detected shoreline position in real world coordinates. With typically three transects per image, 3 shoreline positions are measured (out of a total 640 pixels potentially available across each image).

The transect technique also restricts the image region for shoreline measurement, with short transects resulting in reduced data capture as the shoreline often falls beyond the narrow region where the transect was first surveyed. Daily data return across the individual transects at all nine surfcam sites varied from 1 to 97%, with site averages between 30 and 60% (Table 1). At longer, well positioned transects, data return exceeded 90%, reflecting the true potential of this system to capture shoreline variability.

Results of Daily Comparison at South Narrabeen

In this section, 10 months of surfcam-derived beach width data from South Narrabeen was assessed by comparison with Argus shorelines at the same location, where the accuracy and repeatability of this latter method is well established (Harley *et al.*, 2011). Dependant on wave conditions and detection technique, an image-derived shoreline will have a vertical offset from the tidal elevation (e.g. Plant *et al.*, 2007) and corresponding horizontal offset based on beach slope. Due to uncertainties in the surfcam geometric solution method, this offset cannot be established and it is assumed that surfcam mid-tide shorelines correspond to 0 m AHD. For the South Narrabeen Argus coastal imaging system, 0.7 m AHD is used for daily beach width monitoring as this elevation has been shown to correspond to the image-derived mid-tide shorelines routinely mapped at this site (Harley *et al.*, 2011) using the PIC detection technique (Aarninkhof *et al.*, 2003). Based on the average intertidal zone slope (6.8 degrees) and this 0.7 m vertical offset, a seaward horizontal offset of ~5.8 m of the surfcam shorelines from the Argus shorelines was expected.

In Figure 2, beach width is compared at a single "best case" alongshore position near the surfcam, as measured by both systems. In this comparison between daily surfcam- and Argus-derived shoreline data, a high correlation between the two timeseries was expected, as well as the offset described above. The general similarity in daily variability over this 10-month period is encouraging, although a time-varying landward bias in the reported surfcam beach widths is evident. This pattern was also observed at other points alongshore.

Based on the CoastalCOMS geometric solution technique, each selected pixel is assumed to represent a constant horizontal point in space (Easting, Northing of the corresponding GCP on the day it was measured). These points are fixed in pixel space but not in geographic space; as the elevation (vertical coordinate) of the beach changes over time, so too does the horizontal position represented by each pixel. Due to the obliquity of low-angle cameras to the beach surface, small errors in the vertical plane correspond to large horizontal errors. In this case, the omission of a vertical coordinate in the geometric solution results in reduced accuracy of the reported shorelines as the beach varies from the calibrated profile (Figure 3). A simple geometric correction was devised within this study to account for this induced horizontal error (Figure 3).

With this new cross-shore geometric correction applied to the surfcam data, Figures 2 and 3 show the substantial improvement that is achieved. This correction resulted in a halving of the root mean square error (RMSE) from 7.8 to 3.9 m at this location and an average improvement in RMSE of 2.6 m was achieved at 11 other transects near the surfcam. No improvement was achieved at six more distant (oblique) transects, where the alongshore (horizontal) errors induced by the same vertical errors, dominate and cannot simultaneously be corrected for.

Results of Monthly Comparison at Nine Sites

When combined with measured tidal elevation, hourly surfcam-derived beach widths form cross-shore profiles. In this study, cross-shore profiles were extracted from monthly RTK-GPS surveys at all nine camera sites for direct comparison with surfcam image-derived profiles. A point-by-point comparison was made to assess surfcam accuracy, quantified in terms of correlation-squared (R^2) and root mean square error (RMSE) (Table 1). The same cross-shore geometric correction was applied to account for

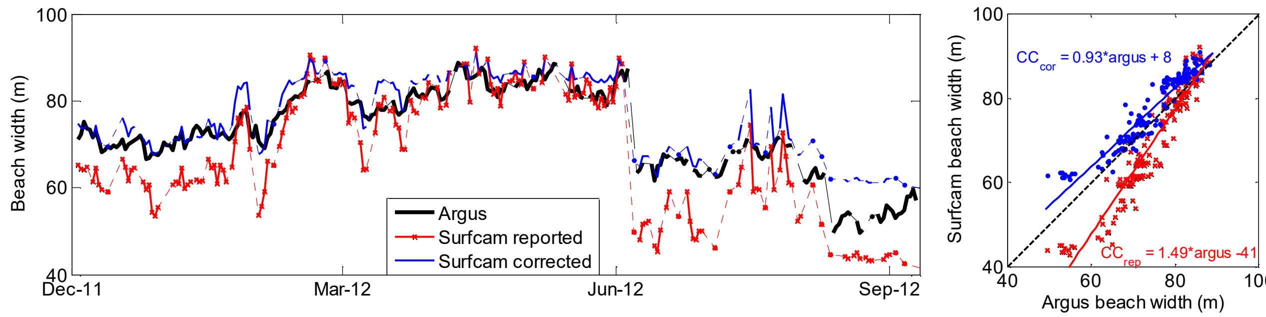

Figure 2. 10 months of daily image-derived beach widths from co-located surfcam (as reported and corrected) and Argus station for a single alongshore position at South Narrabeen (dashed lines indicate missing data). Results are typical for transects close to the camera.

Table 1. Summary of surfcam set up, reported and corrected shoreline data (shoreline elevation is assumed equal to measured tidal elevation). Z = elevation of camera (m AHD); D = average beach width (to 0 m AHD) seaward of camera; α = average intertidal slope (between 0 m and 2 m AHD); β = average angle from 0 m AHD to camera; BW = beach width (to 0 m AHD).

Surfcam site	Z (m)	D^* (m)	α^* (deg)	β^* (deg)	*Range in BW** *(m)*	*Mean R^2 reported BW*#	*RMSE reported BW*# *(m)*	*Mean {max} R^2 corrected BW*#	*RMSE corrected BW*# *(m)*	*Mean {max} data return*ˣ *(%)*
Dixon	20.6	106	5.7	11.0	24	0.46	10.5	0.65 {0.97}	7.6	30 {52}
Wamberal	15.2	108	6.3	8.0	29	0.38	10.6	0.63 {0.89}	5.9	43 {90}
Terrigal	9.1	70	4.6	7.4	19	0.39	15.5	0.72 {0.86}	8.8	61 {91}
Narrabeen	16.2	93	6.8	9.9	40	0.60	9.8	0.80 {0.90}	4.4	46 {72}
Sth Narrabeen	16.7	77	6.8	12.2	27	0.82	10.2	0.91 {0.96}	5.7	48 {83}
Manly	9.2	48	5.7	10.9	18	0.50	13.8	0.67 {0.97}	10.3	56 {86}
Wanda¤	14.5	65	5.1	12.6	21	-	-	-	-	38 {47}
Thirroul	9.7	69	4.0	8.0	21	0.41	15.7	0.58 {0.76}	7.2	61 {74}
Shoalhaven	15.6	102	4.0	8.7	22	0.49	24.8	0.72 {0.97}	16.4	38 {54}

* Calculated from monthly RTK survey data seaward of each surfcam between June 2011 and November 2012.
# Calculated from hourly recordings once per month compared to concurrent RTK survey data across all transects.
ˣ Number of daily surfcam shoreline measurements divided by number of days, excluding months when surfcam not operational.
¤ Due to an unresolved error at the Wanda site, shoreline accuracy cannot yet be determined.
Note: BW statistics may be biased by outliers due to small sample sizes (e.g. only 10 to 30 points for all Manly transects).

the landward/seaward bias in reported shoreline data caused by a more eroded/accreted beach profile (Figure 3). With this correction, R^2 values improved and RMSE were reduced at all sites. Max values are indicated as system performance varies greatly between transects and the best values represent the ideal (but achievable) application of this system in its present form.

The magnitude of remaining errors may be attributed to: unknown offset of the detected shoreline above the tidal elevation; alongshore errors which cannot be accounted for; berm obscuring the shoreline; poor pixel resolution near the shoreline when intertidal slope approaches angle to camera, or camera views are too zoomed out (this occurred at Shoalhaven and is presumed a

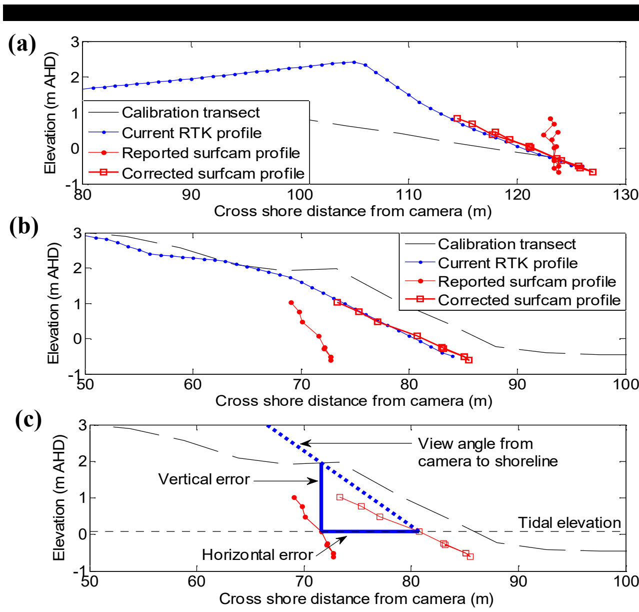

Figure 4. Example surveyed (RTK) profiles compared to calibration profiles, reported and corrected surfcam-derived profiles; (a) accretion causes seaward error; (b) erosion causes landward error; (c) example of geometric correction (for horizontal error) based on view angle from camera and elevation difference between calibration transect and tide (vertical error).

key factor in the large error). The observed cross-shore errors in beach width would collectively result in systematic under/over estimation of sand volume and any other derived parameters.

Discussion of Shoreline Monitoring Capability

The shoreline monitoring capability of the surfcam system investigated here is limited by CoastalCOMS adopted image processing techniques. The transect method under-utilizes the (potentially) available information determined from each image by dramatically restricting the image region where a detected shoreline position may be quantified. The assumption of static cross-shore profiles also results in larger cross-shore and alongshore errors the more the beach profile varies from the calibrated profile. Within the present study, a geometric correction was devised to resolve this cross-shore error, resulting in a significant improvement of the surfcam-derived beach widths for the more shore-normal view angles.

Data collection and image analysis were carried out by CoastalCOMS and, as with any new technology; extensive manual quality control is presently required. Significant development of the surfcam-based shoreline monitoring system has been achieved over the past two years and work is in progress to address the existing image processing shortcomings.

Camera sites must be selected with consideration of both height above mean sea level and the local beach width and slope. At present a minimum elevation of 7 m above mean sea level is adopted by CoastalCOMS, however there is no limit on minimum angle above the shoreline region of interest. For the further development and potentially wider adoption of the surfcam system to provide a practical and robust coastal monitoring capability, refinement of these criteria is required.

INSHORE WAVE DATA COMPARISON

Wave Detection Method

Lane *et al.* (2010) described a low-angle single camera wave height processing system "Wave Pack", which employs surfcam video to derive the wave parameters assessed in this study. In order to extract wave measurements, each camera must be geo-referenced to a suitable datum and grid. Through the Wave Pack system, timeseries of video images are collected and a timestack image (e.g. Shand *et al.*, 2012) is created from the central pixel column. Breaking waves are detected by pixel intensity threshold algorithms and combined with known camera elevation and tilt angle to calculate distance to break position and wave height in metres. Waves are also counted to allow measurement of local wave periods. Lane *et al.* (2010) presented a preliminary verification of the Wave Pack system at Narrowneck Beach, Gold Coast, Australia. They reported an R^2 value of 0.82 between Wave Pack breaking wave height (H_b) and wave buoy significant wave height (H_{sig}) and R^2 of 0.53 between the Wave Pack maximum period (T_{max}) and wave buoy peak period (T_p).

Wave Data Collection Program

In this study, non-directional inshore wave statistics were produced through the Wave Pack system from 18-minute video recordings for 11 daylight hours per day over an 88 day period (Aug – Oct 2011) at the Narrabeen-Collaroy and Wamberal-Terrigal sites (Figure 1). Data return at both sites was ~65%, resulting in 661 (639) hourly records for comparison at Narrabeen (Wamberal). Image quality control and data processing were undertaken by CoastalCOMS and the wave statistics provided to this study included wave height (mean, significant, 75th percentile, 90th percentile, maximum) and wave period (minimum, 5th percentile, mid, 95th percentile, maximum). Other available parameters include number of break zones, wave count, distance to breaker zone from camera, shoaling distance and tide.

Wave Pack data was compared with hourly and daily-averaged wave data simultaneously recorded at two nearshore Datawell directional waverider buoys (Figure 1). The wave buoys recorded sea surface elevation change for 34 minutes every hour, from which directional wave statistics were calculated. Data return rates for both buoys exceeded 90%. The Narrabeen buoy was 500 m east-northeast, and the Wamberal buoy 500 m east-southeast, of the corresponding surfcam, in water depths of 10-11 m. During data capture, mean (max) significant wave heights were 1.1 m (2.9 m) at Narrabeen and 1.2 m (3.6 m) at Wamberal. Mean nearshore wave direction was east-southeast at Narrabeen and southeast at Wamberal, resulting in predominantly shore-normal waves.

Due to the impracticalities of buoy deployment in the surf zone, wave buoy data represents unbroken nearshore, shallow water waves whereas video-derived inshore wave data represents waves at the break point and within the surf zone. A linear relationship with a y-intercept offset is expected as no significant sea or swell is generated landwards of the buoy locations. The time lag between waves passing the buoys and entering the camera field of view should be negligible, so the wave buoy statistics should represent waves seen by the surfcam during the same time.

Results of Hourly Wave Parameter Comparison

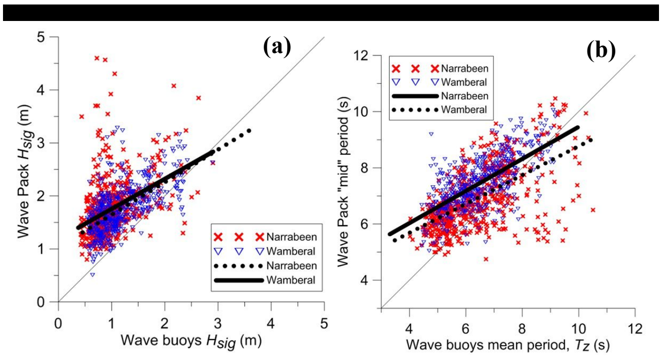

Figure 5. Wave Pack and wave buoy derived (a) significant wave height and (b) mean wave period at Narrabeen and Wamberal. Best fit lines for each dataset are indicated in black.

Table 2. Comparison between Wave Pack and wave buoy output at Narrabeen (bold - $\mathbf{R^2}$ and italic - *slope*). For n = 500, using Student t-test, critical R^2 at 95% level = ~ 0.07.

		Wave buoy parameters						
		H_{mean}	H_{sig}	H_{10}	H_{max}		T_z	T_{p1}
Wave Pack parameters	H_{mean}	**0.16**	**0.16**	**0.16**	**0.15**	T_{min}	**0.17**	**0.01**
		0.61	*0.37*	*0.29*	*0.19*		*0.30*	*0.05*
	H_{sig}	**0.16**	**0.16**	**0.16**	**0.15**	T_{mid}	**0.33**	**0.04**
		0.86	*0.53*	*0.42*	*0.27*		*0.48*	*0.09*
	H_{10}	**0.17**	**0.18**	**0.18**	**0.16**	T_{max}	**0.54**	**0.14**
		1.10	*0.69*	*0.54*	*0.35*		*0.75*	*0.20*
	H_{max}	**0.17**	**0.18**	**0.17**	**0.16**			
		1.40	*0.89*	*0.70*	*0.45*			

Table 3. Comparison between Wave Pack and wave buoy output at Wamberal ($\mathbf{R^2}$ and *slope*).

		Wave buoy parameters						
		H_{mean}	H_{sig}	H_{10}	H_{max}		T_z	T_{p1}
Wave Pack parameters	H_{mean}	**0.36**	**0.35**	**0.35**	**0.33**	T_{min}	**0.16**	**0.07**
		0.66	*0.41*	*0.33*	*0.22*		*0.35*	*0.11*
	H_{sig}	**0.37**	**0.37**	**0.37**	**0.34**	T_{mid}	**0.36**	**0.11**
		0.95	*0.60*	*0.48*	*0.32*		*0.58*	*0.15*
	H_{10}	**0.34**	**0.34**	**0.34**	**0.31**	T_{max}	**0.35**	**0.19**
		1.20	*0.77*	*0.61*	*0.41*		*0.66*	*0.24*
	H_{max}	**0.30**	**0.31**	**0.31**	**0.28**			
		1.50	*0.98*	*0.79*	*0.53*			

Figure 4 shows the comparison of hourly wave statistics between Wave Pack and the wave buoys at Narrabeen and Wamberal. At both sites Wave Pack over-estimated wave height and period for smaller waves (H_{sig} < 2 m, T_z < 7 s) and under-estimated for larger waves (up to H_{sig} = 3.6 m in this study). Some wave height over-estimations were more than four times the wave buoy value and in all cases scatter was high (i.e. low precision). The metrics of R^2 and m (slope) were used to determine statistical relationships, with m used in addition to R^2 to investigate whether there was a systematic trend between wave data from the two methods. Tables 2 and 3 show compared parameters and corresponding R^2 and m values, showing all weak (R^2 < 0.6) but most significant (to 95% level) statistical relationships. However, the Durbin-Watson test shows positive autocorrelation of residuals (d = ~1.2, 95% confidence), indicating that the hourly wave statistics are not entirely independent, leading to under-estimation of the statistical significance level.

The influence of wave count (number of waves identified per recording), tidal stage, and breaker distance from surfcam on residual error between Wave Pack and buoy measurements was investigated for all parameters. In all cases, residual errors of wave height and period show no linear correlation with these factors, indicating that wave measurement accuracy was independent of the number of waves counted, tidal stage and breaker distance from the surfcam. Daily-averaged wave statistics were also compared between the video and buoy data, however this made no significant difference to results.

Discussion of Wave Monitoring Capability

There was a weak but significant statistical relationship between the hourly Wave Pack parameters and those simultaneously recorded by the nearshore buoys with high scatter evident. If Wave Pack measurements were robust, a systematic offset would be expected against buoy data. In all cases, there was an over-estimation of smaller waves and an under-estimation of larger waves. Reasons for this skewed distribution were investigated by comparing the number of waves per recording, tidal stage and breaker distance from the surfcam with the residual errors of Wave Pack outputs. Weak correlations suggested that these factors did not significantly influence the inshore wave measurements.

Without a fixed reference in any dimension, rectification from pixels to real-world coordinates is difficult from a single camera, rather than a stereo-pair. The obliquity of low-angle cameras increases the margin for error in the cross-shore location of breakpoint and subsequently in the calculation of breaking wave height (e.g. Shand *et al.*, 2012). Results suggest the rectification process applied real-world lengths that were too small for distant pixels and too large for foreground pixels, so larger waves breaking further out were under-estimated and smaller waves breaking closer to shore were over-estimated. A second overlapping camera field of view may resolve this distortion.

Observed scatter may be partly due to beach or wave type. Plunging waves are most easily detected, changing rapidly from a dark green (breaker face) to white at the break point. On reef systems plunging waves follow a more repeatable breaker line (Hilmer, 2005), but on multi-barred sandy beaches, both breaker type and position are more dynamic. Spilling or surging breakers leave large areas of white water, have no steep measurable face and break and re-form multiple times. Narrabeen and Wamberal are intermediate beaches, the former exhibiting a rhythmic bar and trough morphology and the latter a welded bar and rip system. Multiple break zones, spilling wave type and large areas of white water may all impede accurate measurement of breaking waves. Statistics are a function of the number of waves per sample and the average 18 minute wave count was 50 (167 per hour) at Narrabeen and 62 (207 per hour) at Wamberal, with 8% of wave counts $\leq$ 10 ($\leq$ 33 per hour). As the mean wave period (T_z) measured by both buoys was ~6.5 s, a likely true wave count would be around 550 per hour. The lower the wave count, the lower the statistical significance of distribution-dependant wave parameters (H_{mean}, H_{sig}, H_{10}, H_{max}).

CONCLUDING REMARKS

Low-angle surfcams have been applied to routine shoreline and inshore wave monitoring at a selection of sites on the NSW coastline. The wave monitoring capabilities presently do not provide an adequate representation of wave conditions when compared with concurrent nearshore wave buoy measurements. Comparisons indicate the surfcam method tends to over-estimate smaller waves and under-estimate larger waves, possibly due to rectification error and beach/wave type, and there is potential to improve Wave Pack algorithms by accommodating these factors.

Application to shoreline monitoring was more successful, following the implementation of a new geometric correction that significantly improved accuracy. The transect method used for geometric transformation is the most significant limitation of the present operational system, reducing data return and accuracy, and utilizing only a small proportion of the shoreline information contained within raw images. The adoption of this existing and extensive coastal camera infrastructure in support of broad-scale coastal change monitoring remains an attractive end-goal. Further work is underway to explore the systematic improvement that can be achieved by combining images from the surfcam network with established image processing techniques.

ACKNOWLEDGEMENTS

This research is funded by the Australian Research Council (LP100200348), with additional support from partners the University of Plymouth (UK), NSW Office of Environment and Heritage, CoastalCOMS (particularly C. Lane for establishment and ongoing development of the surfcam network), Warringah Council, Gosford City Council. M. Mole is funded by a UNSW Faculty of Engineering, Women in Engineering Research Scholarship. T. Mortlock is funded by a Macquarie University International Research Excellence Scholarship.

LITERATURE CITED

Aarninkhof, S.G.J., Turner, I.L., Dronkers, T.D.T., Caljouw, M. and Nipius, L., 2003. A video-based technique for mapping intertidal beach bathymetry. *Coastal Engineering*, 49, 275-289.

Almar, R., Cienfuegos, R., Catalan, P.A., Michallet, H., Castelle, B., Bonneton, P. and Marieu, V., 2012. A new breaking wave height direct estimator from video imagery. *Coastal Engineering*, 61, 42-48.

Boak, E.H. and Turner, I.L., 2005. Shoreline definition and detection: a review. *Journal of Coastal Research*, 21(4), 688–703.

Davidson, M., Koningsveld, M.V., de Kruif, A., Rawson, J., Holman, R., Lamberti, A., Medina, R., Kroon, A. and Aarninkhof S., 2007. The CoastView project: developing coastal video monitoring systems in support of coastal zone management. *Coastal Eng.*, 54, 463–475.

de Vries, S., Hill, D.F., Schipper, M.A. and Stive, M.J.F., 2011. Remote sensing of surf zone waves using stereo imaging. *Coastal Engineering* 58(3), 239-250.

Harley, M.D., Turner, I.L, Short, A.D. and Ranasinghe, R., 2011. Assessment and integration of conventional, RTK-GPS and image-derived beach survey methods for daily to decadal coastal monitoring, *Coastal Engineering*, 58, 194-205.

Hilmer, T., 2005. "Measuring breaking wave heights using video", PhD Thesis, The University of Hawai'i at Manoa.

Holland, K.T, Holman, R.A., Lippman, T.C., Stanley, J. and Plant, N., 1997. Practical use of video imagery in nearshore oceanographic field studies. *IEEE Journal of Oceanic Engineering*, 22(1), 81-92.

Holman, R.A. and Stanley, J., 2007. The history and technical capabilities of Argus. *Coastal Engineering*, 54, 477-491.

Kroon, A., Davidson, M.A., Aarninkhof, S.G.J., Archetti, R., Armaroli, C., Gonzalez, M., Medri, S., Osorio, A., Aagaard, T., Holman, R.A. and Spanhoff, R., 2007. Application of remote sensing video systems to coastline management problems. *Coastal Engineering*, 54, 493-505.

Lane, C., Gal, Y., Browne, M., Short, A.D., Strauss, D., Jackson, K. and Tan, C., 2010. A new system for break zone location and the measurement of breaking wave heights and periods. *In*: *Proceedings of IEEE International Geoscience and Remote Sensing Symposium* (Honolulu, Hawaii, USA), pp. 2234-2236.

Nieto, M.A., Garau, B., Balle, S., Simarro, G., Zarruk, G.A., Ortiz, A., Tintore, J., Alvarez-Ellacuria, A., Gomez-Pujol, L. and Orfila, A., 2010. An open-source, low cost video-based coastal monitoring system, *Earth Surface Processes and Landforms*, 35(14), 1712-1719.

Plant, N.G., Aarninkhof, S.G.J., Turner, I.L. and Kingston, K.S., 2007. The performance of shoreline detection models applied to video imagery. *Journal of Coastal Research*, 23 (3), 658-670.

Plant, N.G. and Holman, R.A., 1997. Intertidal beach profile estimation using video images. *Marine Geology*, 140, 1-24.

Shand, T.D., Bailey, D.G. and Shand, R.D., 2012. Automated detection of breaking wave height using an optical technique. *Journal of Coastal Research*, 28(3), 671-682.

Splinter, K. D., Strauss, D. and Tomlinson, R., 2011. Assessment of post-storm recovery of beaches using video imaging techniques: A case study at Gold Coast, Australia. *IEEE Transactions on Geoscience and Remote Sensing,* 49, 4704-4716.

Turner, I.L. and Anderson, D.J., 2007. Web-based and 'real-time' beach management system. *Coastal Engineering*, 54, 555-565.

APPENDIX 4

Published Journal Article.

Mortlock, T.R. and Goodwin, I.D. (2015). Directional wave climate and power variability along the Southeast Australian shelf. *Continental Shelf Research*, 98, 36-53. doi: 10.1016/j.csr.2015.02.007

Continental Shelf Research 98 (2015) 36–53

Contents lists available at ScienceDirect

Continental Shelf Research

journal homepage: www.elsevier.com/locate/csr

Research papers

Directional wave climate and power variability along the Southeast Australian shelf

Thomas R. Mortlock*, Ian D. Goodwin

Marine Climate Risk Group, Department of Environmental Sciences, Macquarie University, North Ryde, NSW 2109, Australia

ARTICLE INFO

Article history:
Received 20 September 2014
Received in revised form
24 February 2015
Accepted 24 February 2015
Available online 5 March 2015

Keywords:
Wave climate
Wave power
Cluster analysis
Sub-tropical ridge
Southeast Australia
Tasman Sea

ABSTRACT

Variability in the modal wave climate is a key process driving large-scale coastal behaviour on moderate- to high-energy sandy coastlines, and is strongly related to variability in synoptic climate drivers. On sub-tropical coasts, shifts in the sub-tropical ridge (STR) modulate the seasonal occurrence of different wave types. However, in semi-enclosed seas, isolating directional wave climates and synoptic drivers is hindered by a complex mixed sea-swell environment. Here we present a directional wave climate typology for the Tasman Sea based on a combined statistical-synoptic approach using mid-shelf wave buoy observations along the Southeast Australian Shelf (SEAS). Five synoptic-scale wave climates exist during winter, and six during summer. These can be clustered into easterly (Tradewind), south-easterly (Tasman Sea) and southerly (Southern Ocean) wave types, each with distinct wave power signatures. We show that a southerly shift in the STR and trade-wind zone, consistent with an observed poleward expansion of the tropics, forces an increase in the total wave energy flux in winter for the central New South Wales shelf of 1.9 GJ m^{-1} wave-crest-length for 1° southerly shift in the STR, and a reduction of similar magnitude (approximately 1.8 GJ m^{-1}) during summer. In both seasons there is an anti-clockwise rotation of wave power towards the east and south-east at the expense of southerly waves. Reduced obliquity of constructive wave power would promote a general disruption to northward alongshore sediment transport, with the cross-shore component becoming increasingly prevalent. Results are of global relevance to sub-tropical east coasts where the modal wave climate is influenced by the position of the zonal STR.

1. Introduction

Wave climate change, rather than sea-level rise, is presently expected to be the dominant process impacting shoreline change on moderate- to high-energy sandy coastlines in the coming decades (Slott et al., 2006; Coelho et al., 2009; Hemer et al., 2012). It has long been realised that variations in the deep-water ocean wave field directly modulate the power that forces the evolution of coastal morphology (e.g. Johnson, 1919). However, there remains a stronger research focus on sea-level rise (Nicholls et al., 2007) than studies on wave climate change globally, leading to only low confidence in projected changes (Hemer et al., 2013; Church et al., 2013).

Definition of wave climate and directional wave power is a key component in the fields of marine renewables (Hughes and Heap, 2010), shipping (Semedo et al., 2011), coastal and ocean engineering (Callaghan et al., 2008), marine ecology (Storlazzi et al., 2005) and coastal management (Nicholls et al., 2013). A wave climate can be defined simply as the long-term (a decade or more) statistical characteristics of the waves at any one location (Holthuijsen, 2007). Often, the bulk wave climate (seasonal to centennial) is composed of a number of wave types, originating from a range of synoptic weather systems that produce distinct surface wind-wave signatures.

The bulk wave climate will therefore comprise a mixture of wave types and distributions. Often it is desirable to decompose the wave climate into component groups – a process known as wave climate typing. For example, statistical or dynamical down-scaling of long-term offshore wave information is frequently required for coastal process or maritime engineering studies. The computational inefficiency of down-scaling all available data requires that a small number of representative sea states are determined, which are later propagated to shallow water (Camus et al., 2011a).

Wave climate typing can be approached either synoptically or statistically. Basic synoptic typing of wave climates was first proposed by Munk and Traylor (1947). This has since evolved towards

* Correspondence to: Room 825, Building E7A, Macquarie University, North Ryde, NSW 2109, Australia.
E-mail address: thomas.mortlock@mq.edu.au (T.R. Mortlock).

http://dx.doi.org/10.1016/j.csr.2015.02.007
0278-4343/

the identification of dominant patterns of synoptic-scale weather systems based on large-scale synoptic evolution and atmospheric pressure gradients (Browning and Goodwin, 2013; Goodwin et al., submitted), or using Empirical Orthogonal Functions (EOF) of mean sea level pressure (MSLP) fields (Speer et al., 2009; Hemer et al., 2008).

A limitation of EOF analysis applied to climate data, is that it is often difficult to attribute specific synoptic conditions or mechanisms to the orthogonal datasets. Even in cases where EOFs adequately explain weather pattern variance, multiple synoptic types will not necessarily produce statistically dissimilar wave climates, but rather characterise the different synoptic evolution of wave generation. Moreover, EOF analyses will typically discard a large portion of the original dataset not described by the primary EOFs.

An alternative approach is statistical typing of parametric wave data. This involves the decomposition of a continuous wave timeseries without explicitly linking the wave types to their synoptic generation source. A major advantage of statistical typing is that 100% of the variance in the geophysical dataset is used. The most common approach is to define the empirical joint probability density function (PDF) of wave height and period for a given directional bin, and to visualise the results using two-dimensional histograms (Holthuijsen, 2007). The draw-back to this method is the subjectivity with which the position and width of directional bins are chosen. Unsuitable directional bins may split a wave climate in two, or merge adjacent wave climates. In addition, transient wave generation often results in the tails of the distribution being mixed with those of their neighbours.

An alternative statistical approach is to use clustering algorithms to obtain a wave typology. Clustering aims to group multivariate wave data into n number of classes ('wave climates') in an optimised manner such that dissimilarity between cluster groups is maximised. Cluster models such as K-means, Partitioning Around Medoids (PAM), Self-Organised Mapping (SOM) and Maximum Dissimilarity are currently the principle algorithms used to characterise wave climates for coastal engineering applications (Hamilton, 2010; Camus et al., 2011a, 2011b; Guanche et al., 2013). Alternatively, Camus et al. (2014) have shown that clustering of hindcast MSLP fields (rather than direct clustering of a wave timeseries) can yield accurate wave climate types, by relating the clusters to sea states based on linear regressions built between MSLP and dynamical ocean wave hindcasts.

The principle disadvantage of wave cluster analysis is that the optimal number of wave clusters, k, is unknown. For open coast examples, where there is a clear distinction between far-field swells and localised wind-sea, clustering is often visually discernible from plotting. In these cases k can be estimated and fitted to a cluster model of choice. Western Australia (Masselink and Pattiaratchi, 2001), Southern California (Storlazzi and Wingfield, 2005) and the Iberian Peninsula (Camus et al., 2011b; Guanche et al., 2013) are all global open coast examples where the number of wave climates have been visually determined for conceptual or statistical description.

In semi-enclosed sea environments the distinction between wave climates is not so clear. The complexity of discerning between fetch-limited sea and swell in these environments has been acknowledged by authors in the North Sea (Boukhanovsky et al., 2007), Gulf of Mexico (Wang and Hwang, 2001), and Mediterranean Sea (Alomar et al., 2014).

The Tasman Sea is open to the north and south, borders the east coast of Australia, and is partially blocked from the Southwest Pacific Ocean by the New Zealand landmass (Fig. 1). It extends from the mid latitudes to where it meets the Coral Sea in the north, at approximately 30°S (IHO, 1953). Waves propagating in water depths exceeding 5000 m in the Tasman Sea rapidly shoal to

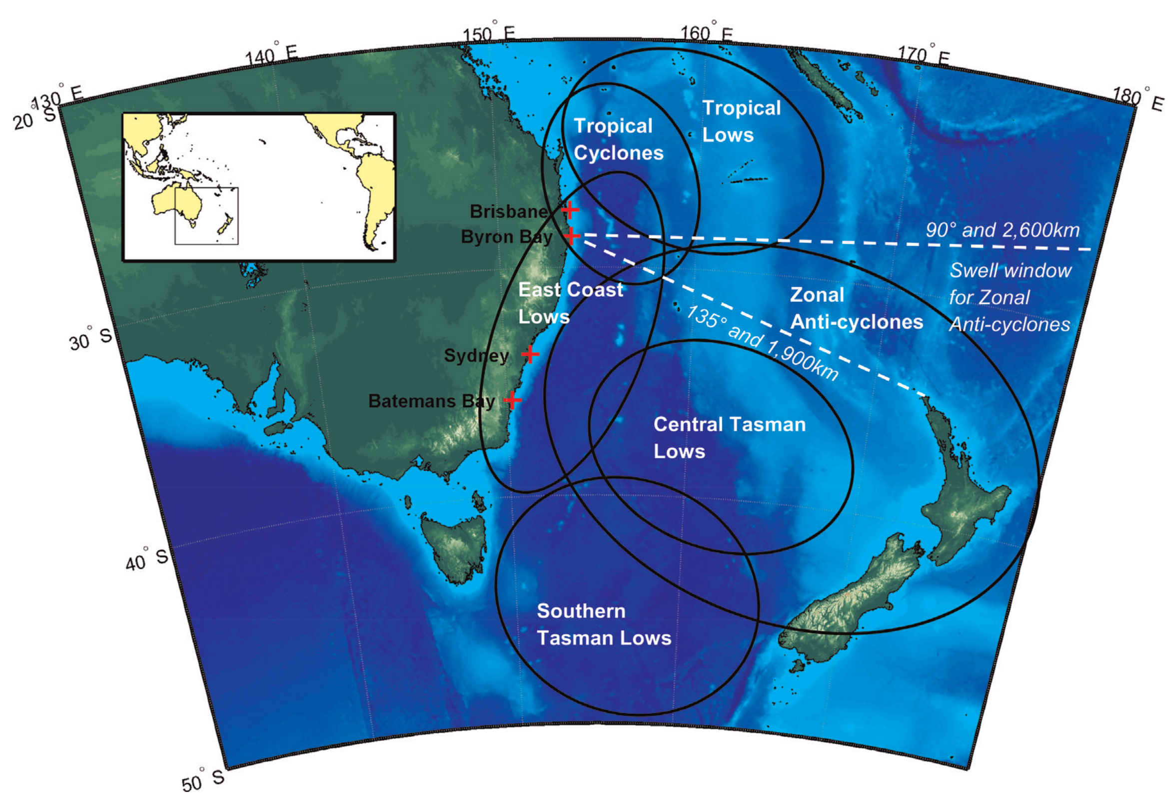

Fig. 1. Approximate area of influence of wave-producing meteorological types in the Tasman and Coral Seas, based on work by Short and Trenaman (1992) and Shand et al. (2011a). Also shown is the potential swell window for zonal anti-cyclones outside the Tasman Sea. Inset shows position of study area in relation to Pacific Basin. ETOPO01 imagery courtesy of NOAA (Amante and Eakins, 2009).

around 100 m at the East Australian shelf, which at Sydney is only 35 km wide. This rapid shoaling conserves much of the offshore wave energy upon transformation across the shelf, leading to a high-energy nearshore wave climate and wave-dominated sediment transport.

The Southeast Australian Shelf (SEAS) experiences a mainly marginal sea wave climate produced by weather systems in, or peripheral to the Tasman Sea (Fig. 1). Although it is possible for longer-period swells generated in the South Indian Ocean sector of the Southern Ocean to propagate through the Tasman Sea on a southwest – northeast trajectory on great circle paths (Munk et al., 1994), they cannot undergo sufficient refraction to be felt along the SEAS. Conversely, the west coast of New Zealand experiences a higher proportion of Southern Ocean swells than the SEAS due to the prevailing westerly movement of these systems. Likewise, there is no swell window for Northern Pacific waves generated during the boreal winter to propagate into the Tasman Sea due to the myriad of island chains and rises in the Equatorial Pacific.

Multiple studies (BBW, 1985; Short and Trenaman, 1992; Harley et al., 2010; Shand et al., 2011a) have led to a general acceptance of five to six synoptic wave-producing weather patterns that impact the SEAS. These include Tropical Cyclones, Tropical Lows, Anticyclonic Intensification, East Coast Lows, Southern Tasman Lows and Southern Secondary Lows (Fig. 1). Since the majority of wave generation is within, or adjacent to, the Tasman Sea wave periods are fetch-limited and are rarely sustained above 12–13 s over a 24- h period. However, northern New South Wales and southeast Queensland receive a small percentage of swells between 12 and 16 s that are generated to the northeast of New Zealand during anti-cyclonic intensification (Fig. 1). A meso-scale sea-breeze is also recognisable during the summer months along the coastal fringe. Despite a wealth of observational buoy data, directional wave parameters and wave power signatures representing each type have never been isolated.

Previous studies have shown there to be considerable inter-annual modulation of the regional wave climate by El Niño Southern Oscillation (ENSO) and the Southern Annular Mode (SAM) (Harley et al., 2010), and multi-decadal forcing by ENSO and the Interdecadal Pacific Oscillation (IPO) (Goodwin, 2005), and the Indian Ocean Dipole (IOD) (Goodwin et al., 2010). The sub-tropical ridge (STR), the location of highest pressure that varies seasonally between 29°S in winter and 40°S in summer over Eastern Australia (Timbal and Drosdowsky, 2013), also exerts a strong influence on seasonal to inter-annual wave generation in the Tasman Sea (Browning and Goodwin, 2013), effectively dividing the region into easterly vs westerly generated wind-waves (Goodwin et al., 2013b).

However, due to the fetch-limiting influence of regional geography and equidistance of wave generation sources, there is no clear distinction between many of these meteorological patterns in the wave record. When joint probabilities of wave height and period were compared across storm types, Goodwin et al. (submitted) found that a variety of different meteorological forcings produced statistically similar wave patterns across the New South Wales coast. For example, all types of East Coast Lows identified (Easterly Trough Lows, Southern Secondary Lows, Continental Lows and Inland Trough Lows) were indistinguishable in their joint distribution of wave height and period. This highlights the problem of using synoptic evolution to identify unique wave climates in semi-enclosed seas, although the approach is useful for description of meteorological forcing of extreme wave events.

This study has taken an alternative approach. We have focussed on the modal wave climate and power as the primary driver of large-scale coastal behaviour to support future studies on long-term beach recovery and on-shore sediment transport from the lower shoreface. While storm waves are responsible for instantaneous coastal inundation and beach erosion, the modal (or 'ambient') wave climate that persists between storms is predominantly responsible for post-storm beach recovery, long-term delivery of sediment across the shoreface, and shoreline planform orientation (Ranasinghe et al., 2004; Harley et al., 2011). Additionally, New South Wales and southeast Queensland have a relatively small number of extreme events relative to the modal climate, when compared to the more energetic southern margin of Australia (Hemer and Griffin, 2010; Hughes and Heap, 2010). Despite this, there has been a lack of focus on modal variations in the Tasman Sea in favour of extreme wave events (BBW, 1985; You and Lord, 2008; Shand et al., 2011a, 2011b; Dent et al., 2012).

Statistical clustering was first performed on wave buoy records along the East Australian shelf in order to identify the dominant modes of directional wave climate variability. A Gaussian Mixture Model (GMM) was then used to assess the resolution of the clustering technique and further isolate 'synoptic-scale' wave climates. MSLP composites were then used to investigate wave climate relationships with large-scale climate drivers. The seasonal variability in directional wave power, and future changes associated with shifts in the STR, were then described and related to coastal processes. Results are of global relevance to coastlines where the modal wave climate is influenced by the position of a zonal STR, especially other mid-latitude, Southern Hemisphere east coasts with comparable wave climate genesis and sediment transport.

2. Observational wave data

2.1. Available buoy records

Directional wave information recorded at four Datawell Directional WaveRider (DWR) buoys in south (Batemans Bay), central (Sydney) and north (Byron Bay) New South Wales and Southeast Queensland (Brisbane) was used (Fig. 1). This dataset provided observational coverage of approximately 1000 km of mid-shelf, deep-water waves (60–100 m depth), along the western boundary of the Tasman and Coral Seas between 27 and 37°S.

Although buoy records are considered one of the most reliable sources of wave observations, they can suffer from periods of data loss. All four buoys used in this study have 90–95% data recovery rates, with the majority of non-recovery occurring during extreme wave conditions. Since this study is focussed on the modal wave climate, this is unlikely to affect results.

2.2. Wave data preparation

Hourly wave parameters were provided by Manly Hydraulics Laboratory (MHL), and the Queensland Department of Science, Information Technology, Innovation and the Arts (DSITIA). All directional wave information was averaged to daily values.

Significant wave height, H_s, primary peak spectral wave period, T_p and mean wave direction at the primary spectral peak, MWD_{Tp}, were used to describe the daily peak wave energy conditions at each buoy location. These parameters were extracted using spectral analysis by both MHL and DSITIA (where $H_s \approx$ four times the square root of the zeroth moment). Distributions of these parameters usually exhibit some type of skew-normal distribution, with occasional secondary modal peaks. As such, reference to the median value and inter-quartile range (IQR) is used in their description.

The wave data was reduced to resolutions of 0.01 m (H_s), 0.1 s (T_{p1}) and 1.0° (MWD_{Tp1}) in line with buoy heave/direction (Datawell, 2014) and MHL data sampling (Wyllie and Kulmar, 1995) resolutions. Since our interest concerns wave climate impacts on coastal behaviour, all offshore-propagating wave energy was extracted before clustering.

Each buoy record was split into (austral oceanic) summer (January–March) and winter (July–September) seasons. Autumn and spring data were not included as wave patterns during these months represent a mixture of both winter and summer climatologies.

3. Storm event separation

Any statistical analysis of wave climate requires a separate treatment of storm (extreme) and modal (ambient) conditions because often the two will exhibit distinctly different distributions, due to the different underlying physical drivers (Holthuijsen, 2007). Defining an optimal separation between these two regimes, however, is a non-trivial task.

The procedure used here is based on the Peaks-Over-Threshold (POT) method. POT aims to identify storm events in a continuous wave record that exceed a significant wave height threshold; that are maintained for a minimum storm duration; and that are separated by a minimum storm recurrence interval. This approach was preferred over the Annual Maximum (AM) method due to the deficiencies of the latter in returning a low storm count for relatively short inter-annual timeseries (Goda, 2010).

3.1. Minimum storm duration

A minimum storm duration of three days was chosen, after other Tasman Sea wave climate analyses (Hemer, 2010; Shand et al., 2011a, 2011b; Dent et al., 2012). Apart from tropical cyclones which are highly transient systems, synoptic storm types have similar residence times in the Tasman Sea (Browning and Goodwin, 2013), thus a single storm duration for all buoy locations is sufficient.

3.2. Minimums storm recurrence interval

An appropriate recurrence interval ensures that a single storm event is not split into shorter component events if the H_s value dips briefly below the storm threshold. In doing so, it maintains the statistical and synoptic integrity of the storm timeseries. A 24 h recurrence interval was used, according to the regional progression of synoptic events (Speer et al., 2009; Browning and Goodwin, 2013).

3.3. Wave height threshold

Separate summer and winter storm wave height thresholds were determined for each DWR buoy to accommodate seasonal variation and localised effects (i.e. shoaling or wave focussing) in the wave height distributions.

One criticism of the POT method is the subjectivity with which the height of the threshold can be chosen. This is especially important in this study as a threshold set too high will dilute the clustering of modal conditions.

Several studies (Mathiesen et al., 1994; Mazas and Hamm, 2011; Bernadara et al., 2014) have attempted to determine a standard method to verify the statistical robustness of the threshold level based on the goodness-of-fit of the peak storm values with various extreme distributions (Coles, 2001). The Generalised Pareto Distribution (GPD) is now recommended (Hawkes et al., 2008) and widely used (Méndez et al., 2006; Thompson et al., 2009; Mazas and Hamm, 2011) as the most appropriate extreme distribution for threshold validation.

A GPD approach to storm threshold selection was applied, with a modified Mazas and Hamm (2011) method. First, a range of thresholds was explored to locate a statistically robust storm threshold (u_3), starting from an under-estimated value of u_3 (u_0) to an over-estimated value of u_3 (u_1). Here, $u_0=1$ m, which roughly equates to the 95% exceedance 24-hourly H_s for all buoy records, and $u_1=3$ m, approximate to the 5% exceedance 24-hourly H_s for all buoy records. This reduces the data set to only include storms of a reasonably wide range of intensities, and also reduces serial correlation to make the statistical assessment more robust.

Next, the set of exceedances of storm peak wave height above threshold is fitted to a GPD, for a range of thresholds between u_0 and u_1. A final storm threshold (u_3) above which storms exhibit statistically extreme behaviour (i.e. begin to deviate from a GPD) is located between u_0 and u_1 using the GPD shape, k, and modified scale, $\sigma*$, parameters, and a guide value (u_2). u_2 is chosen to match the average annual storm frequency (λ) for each buoy record, as reported in a separate synoptic-typing analysis by Shand et al. (2011a, 2011b). This process is detailed in Fig. 2.

Fig. 2 gives k and $\sigma*$ for 0.05 m increments of H_s between u_0 – u_1, u_2 (red dotted line) and u_3 (green dotted line), for each buoy location for (A) winter and (B) summer. u_3 is determined using the guide value (u_2), and by identifying 'domains of stability' in k and $\sigma*$ close to u_2. If the wave height distribution follows a GPD, both k and $\sigma*$ will remain relatively constant when u increases, and successive 'domains of stability' can be seen (Mazas and Hamm, 2011). The point at which k and $\sigma*$ begin to deviate from GPD 'stability' is the idealised storm threshold value. Locating the final domain of stability before extreme behaviour is apparent, is subjective process (although automated methods have been proposed e.g. Thompson et al. (2009)). Instead, we use u_2 as a guide. As it is desirable to minimise dilution of the modal wave climate with extreme events, the lowest u value of the domain of stability on which u_2 lies is selected as u_3.

Results indicate that the statistical storm thresholds (u_3) are very similar to those derived by Shand et al. (2011a, 2011b) using a synoptic typing method. They are also approximate to the daily 10% exceedance wave heights at each buoy (H_{s10}), indicating that H_{s10} can be used as a general storm threshold guide for the Southeast Australian shelf. Other studies in New South Wales have used comparable values of H_s 2.0 m (Shand et al., 2011a, 2011b), 2.5 m (BBW, 1985; Rollason and Goodwin, 2009) and H_s 3.0 m (You and Lord, 2008; Shand et al., 2011a, 2011b; Goodwin et al., submitted). All the aforementioned studies, however, included no statistical verification of the threshold value.

Storm thresholds vary between sites not only because of latitudinal differences in storm frequency, but also due to localised effects. Larger u_3 values (i.e. when a larger wave height threshold is required to meet the expected storm frequency, λ) indicate a more exposed buoy location, whereas smaller u_3 values suggest a more shoaled and/or sheltered climatology. This is particularly evident at Batemans Bay where significantly lower u_3 values are needed to match the required λ than at other sites.

4. Cluster analysis

4.1. Cluster preparation

Once storm events were separated out, the trivariate modal wave timeseries (H_s, T_p, MWD$_{Tp}$) was normalised using the method proposed by Camus et al. (2011a). The first two parameters are scalar variables (H_s and T_p), while the third one (MWD$_{Tp1}$) is a circular variable. As noted by Camus et al. (2011a), the circular variable entails a problem for cluster application, since 1° True North (TN) and 359° TN are supposed to be completely different. While this is not always a problem for the analysis of New South

Wales/Queensland buoy data, as they only receive a largely 180° directional spectrum because of coastal orientation, the Euclidean-Circular (EC) distance solution proposed by Camus et al. (2011a) was applied for clustering. Pre-cluster normalisation is necessary in order that Euclidean distances (or pairwise dissimilarities) used in the cluster model are not skewed by the difference in absolute variance between wave parameters. The wave data were subsequently de-normalised after clustering.

4.2. Cluster model selection

Cluster model selection depends on the quality of the clustering, and this can usually be assessed visually. Cluster models can be divided into those that use hierarchical and non-hierarchical schemes. Hierarchical clustering produces a tree of k first-order clusters which are divided into n number of sub-groups, and are commonly illustrated in the form of a dendrogram. Although visually useful, timeseries wave data cannot be indexed with a cluster number when using a dendrogram. The number of clusters shown is also heavily dependent on sensitivity settings such as the number of leaf nodes and the maximum linkage between levels. In contrast, non-hierarchical methods return a single set of cluster groups and each data point is assigned to a cluster. This indexing is needed when examining the variability of clusters over time.

K-means is one of the most widely used non-hierarchical cluster methods. The algorithm finds the optimal Voronoi cells in uni- or multi-dimensional datasets for k clusters, and returns a centroid for each cluster. Voronoi cells take the form of irregular polyhedra, and describe the multi-dimensional space occupied by each cluster. Voronoi cells are determined by minimising the sum of dissimilarities (squared errors) between each object and its corresponding centroid. The centroid is not an actual observation in the dataset; rather, it is an average value which acts as the central reference point for each cluster.

K-means, however, has certain sensitivities which can influence data partitioning. Firstly, the algorithm can be sensitive to outliers (Velmurugan and Santhanam, 2010) meaning the shape of Voronoi cells may be distorted in datasets with high scatter or noise. Secondly, the cluster search is prone to local minima (Pelleg and Moore, 2000). This means that, since the first iteration of centroids is chosen at random, cluster assignment is never exactly the same when the algorithm is repeated. This can affect re-clustering of small samples, although is barely noticeable for larger and Gaussian-distributed datasets.

An alternative to K-means, which aims to reduce sensitivity to outliers, is k-medoids. Instead of taking the mean value of the objects in a cluster as a central reference point, a medoid is used. A medoid is the most centrally located object in a cluster (and

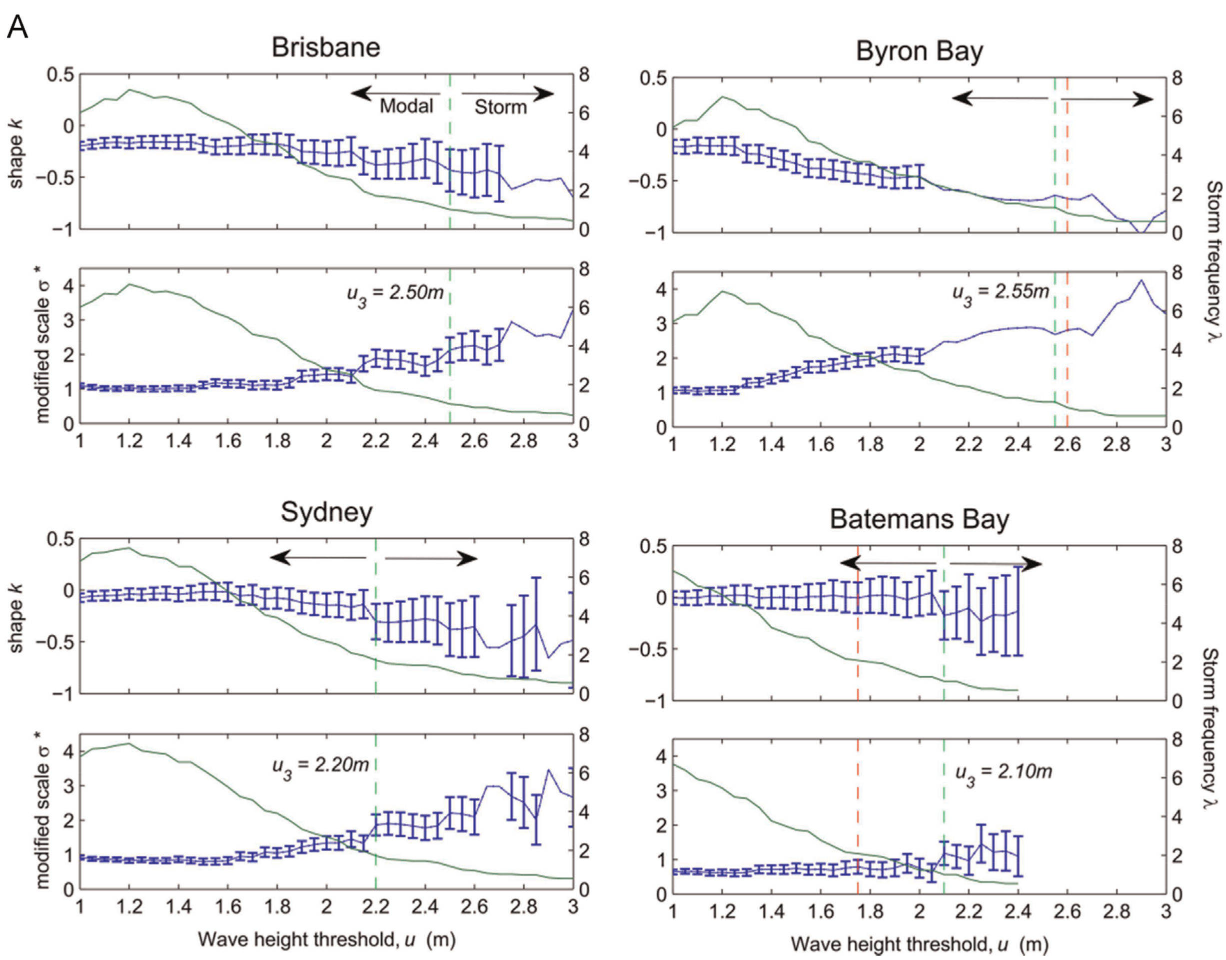

Fig. 2. Storm threshold detection method used for (A) winter and (B) summer H_s distributions at the four buoy locations. The shape parameter, k, and the modified scale parameter, σ^*, of the GPD were calculated at each 0.05 m u interval (blue line with confidence intervals, CI, on top plot for k and bottom plot for σ^*) between u_0 (1 m) and u_1 (3 m). The mean annual storm frequency, λ, for each u interval between u_0 and u_1, is also shown (dark green solid line) and as expected, λ decreases with increasing u. The guide threshold, u_2, (green dotted line), and the final threshold, u_3, (red dotted line), are also given. If $u_2=u_3$, only u_3 is shown. Note that for some higher u values, maximum likelihood used to estimate the GPD parameters cannot reliably compute CIs. Also, GPD statistics for u values towards 3 m H_s in some instances are not shown (e.g. Batemans Bay winter/summer and Byron Bay/Sydney summer) because no storms were identified using these higher thresholds. (For interpretation of the references to colour in this figure legend, the reader is referred to the web version of this article.)

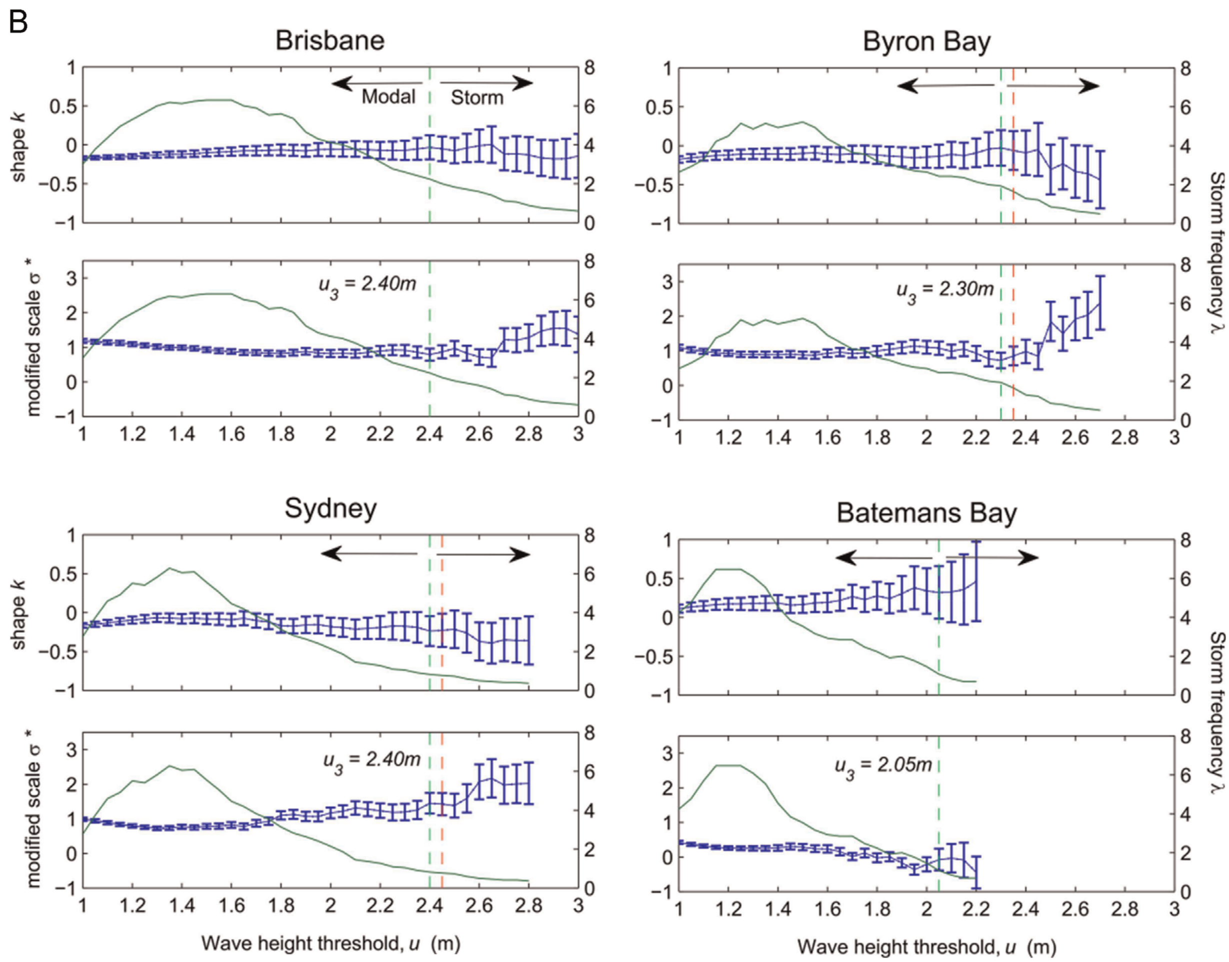

Fig. 2. (*continued*)

therefore is an observation that actually exists within the dataset, rather than a mean). The most common realisation of k-medoids is the Partitioning Around Medoids (PAM) algorithm. Unlike K-means, PAM is not sensitive to local minima – that is, re-clustering even small and scattered datasets with PAM will yield the same cluster assignment each time.

Here, both K-means and PAM were used to cluster daily wave parameters from the Sydney buoy in order to evaluate cluster quality between methods. In order to minimise the effect of local minima when using K-means, the algorithm was iterated 100 times and the iteration that returned the lowest mean squared error between cluster groups was chosen. Results indicated that K-means provides a clearer cluster separation across all wave directions than PAM. For this study, therefore, K-means clustering was used.

4.3. Determination of k clusters

While the choice of a cluster model determines the cluster quality, it does not provide any indication of the optimal number of clusters in a dataset (k). The optimal cluster number should minimise the within-cluster variance, while also minimising the number of cluster groups. Since the within-cluster variance reduces as the number of clusters increases (to the point at which each data point is represented by its own cluster), this is a difficult computational task. k is thus often determined ad-hoc or based on practical experience (Hamerly and Elkan, 2003). There are, however, a number of statistical methods proposed in the literature to estimate k.

Here, a group of five cluster evaluation indices was used to make a first-pass estimation of the optimal number of wave climates that exist at each buoy location. In this way, cluster selection is not constrained by a single definition of optimality; rather, the choice is spread across indices. Indices included; Silhouette (Rousseeuw, 1987), Calinski and Harabaz (1974), Dunn (1974), Krzanowski-Lai (1985) and the *C*-Index (Hubert and Levin, 1976). The indices were chosen based on their ubiquity of use and performance; both as reported in the literature (Milligan and Cooper, 1985; Gordon, 1999) and after sensitivity testing as part of this study.

K-means clustering was repeated using a sensible range of possible numbers of wave climate clusters (here, between two to ten clusters). Each cluster index evaluates the strength of the clustering for every repetition of K-means. Visual inspection of a Dendrogram was then used to add to the index group. A range of optimal cluster numbers was thus obtained (denoted $\sim k_1$). The highest k value in the range of $\sim k_1$ was then chosen as a first-pass estimate of the optimal number of wave climates. This 'over-fitting' ensures no statistically similar wave climates are merged.

4.4. Cluster evaluation

Once k_1 was determined, the wave buoy record was re-clustered with k_1 number of clusters. If both the T_p and MWD_{Tp} centroids of adjacent clusters were within one standard deviation (σ) of each other (± 0.1 s for T_p and $\pm 1°$ for MWD_{Tp} for instrument accuracy), then they were assumed to represent the same wave field and merged.

In mixed sea-swell environments the tails of adjacent wave climates tend to overlap because transient, near-field meteorological types produce a wide spread of wave directions. In order to limit inter-cluster spreading, and aid conceptualisation, outliers below (above) the lower (upper) adjacents of the distribution were removed. The lower (upper) adjacent is defined as the first (third) quartile of the distribution minus (plus) 1.5 times the inter-quartile range (IQR). The tails represent the weakest members of the wave cluster, since they lie furthest away from the centroid.

5. Wave fields determined from clustering

Three directional wave fields of the modal wave climate were identified at all buoy locations from clustering. These include one from the east (Mode 1), a second spreading east-south-east through to south-south-east (Mode 2), and a third spreading south-east through to south-south-east (Mode 3). In addition, a second easterly wave field (Mode 1 *swell*) was superimposed on Mode 1 at Brisbane during summer.

Wave roses for each buoy location are given in Fig. 3A (winter) and B (summer). The non-directional wave fields are analysed in the form of joint probability density (JPD) functions in Fig. 4A (winter) and B (summer). Since the wave buoys are located mid-shelf, the directional distribution of each mode varies between sites due to cross-shelf refraction. However, each is distinguishable from another by the directional space it occupies, in combination with the shape of the non-directional PDF.

The storm wave climate represents the extreme tail of the modal distribution. The vastly smaller sample size for the storm tail means the directional wave fields returned by clustering are not reliable. Therefore, attention is directed here to the modal wave climate, which accounts for 91–95% of all wave days recorded.

5.1. Mode one (east)

Mode 1 is omnipresent throughout the year at all buoy locations. It constitutes the shortest-period wave climate of all the wave fields (T_{p1} 8–9 s), with the widest directional spread and IQR, suggesting a near-field origin. This wave field occupies a directional band between 85° and 105°, with minimal seasonal rotation.

During summer, Brisbane is the only location that experiences a longer period (T_{p1} 9–10 s) wave field from the east (Mode 1 *swell*) that is superimposed on Mode 1. It is distinguishable as swell by its narrower IQR, lower directional spread, and skew towards longer wave periods (Figs. 3B and 4B). Since Brisbane is beyond the fetch-limiting influence of New Zealand, it is open to the potential

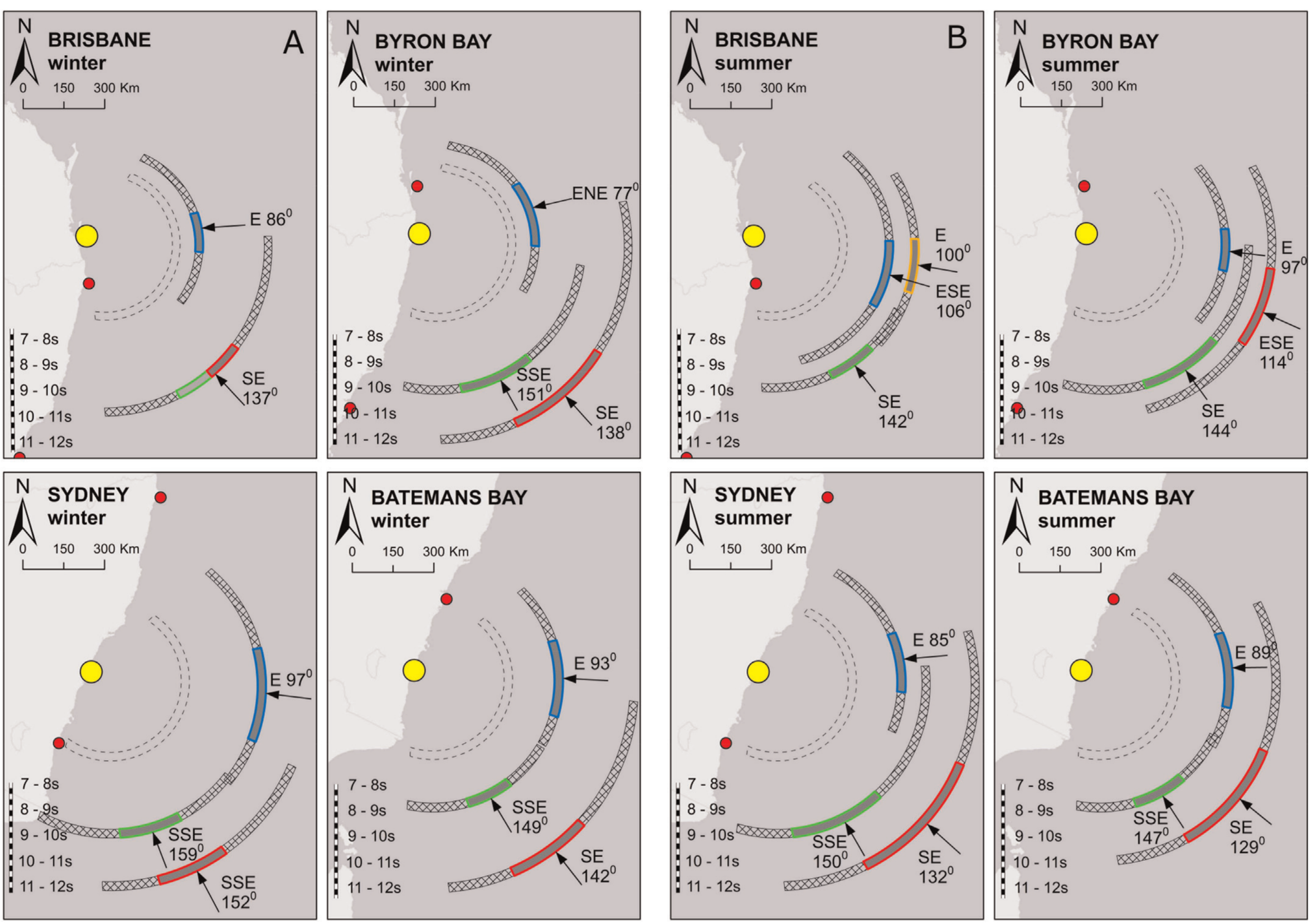

Fig. 3. Primary wave modes at the four buoy locations for winter (A) and summer (B), as determined from clustering. Modes are plotted on a circular scale radiating out from each buoy location. The scale represents the mean T_p of the wave climate in 1 s increments. Local wind-sea is shown as a dotted box covering the directional range observed at each buoy, and is indicative only. The principle buoy location for each sub-plot is shown as an yellow circle, while neighbouring buoys are red. The IQR of each wave field is shown in solid grey, while the tails of the distribution (excluding outliers) are hatched blocks. The IQR contains the central 50% of the cluster distribution. The position of the IQR indicates the directional skew, whereas the width indicates the directional spread. The approximate MWD for each mode is shown as a black arrow. (For interpretation of the references to colour in this figure legend, the reader is referred to the web version of this article.)

of longer-period wave propagation from the Equatorial Pacific and Coral Sea.

5.2. Mode two (south-east)

Mode 2 constitutes the longest period wave field identified by clustering. It contains a moderate amplitude (H_s 1.3–1.6 m), long-period (T_{p1} 11–12 s) wave field that is incident onshore for much of the Southeast Australian coast throughout the year. Therefore, cross-shelf refraction is small. As a result, both directional and non-directional parameters are consistent between buoy locations. The narrow IQR and wave period skew towards higher values both suggest this is predominantly a far-field, but fetch-limited, wave field.

5.3. Mode three (southerly)

Mode 3 is a moderate-period (T_{p1} 9–10 s), oblique (140–160°) wave field that operates adjacent to Mode 2. However, Mode 3 is distinguishable with shorter wave periods and higher amplitudes than Mode 2, suggesting a more proximal wave generation source.

The Batemans Bay and Brisbane buoys are partially shadowed from the most southerly portion of Mode 3 due to wave obliquity and shoreline geometry. A local northward indentation from Cape Green to the south, to Jervis Bay to the north, is probably responsible for wave shadowing at Batemans Bay, as suggested by Coghlan et al. (2011). Storm separation in Section 3 also suggested the wave climate is more shoaled and/or sheltered at this location. As a result, the MWD of Mode 3 at Batemans Bay is 10° anti-clockwise of that recorded at Sydney, and the mean H_s is 0.3 m lower.

From Cape Byron north, the coastline trends north-west, meaning the most southerly portion of Mode 3 is refracted across the shelf before it reaches Brisbane. As a result, Mode 3 is not separable by clustering from Mode 2 at Brisbane during winter. Instead, they are clustered as a single south-easterly wave field, accounting for over 80% of daily wave conditions.

5.4. Seasonal variability in the modal wave climate

During winter, 75% of the modal wave climate can be explained by variance in the south-east and south components (Modes 2 and 3), and 25% by the east component (Mode 1). In summer, Mode 1 increases in occurrence by approximately 10%, all modes rotate anti-clockwise, and the wave field grades towards a steeper sea.

Because of the semi-enclosed nature of the Tasman Sea, seasonality in the wave climate is subtle. Although the central IQR of each wave field exhibits seasonal rotation, wave clusters are spread over a similar directional space throughout the year. This is especially evident at the southern buoys, which are opposite to the fetch-limiting influence of New Zealand. The northern buoys, which are beyond the semi-enclosed sea setting, show stronger bi-modality in both direction and period between the south-east and south components (Modes 2 and 3) and the east component (Mode 1).

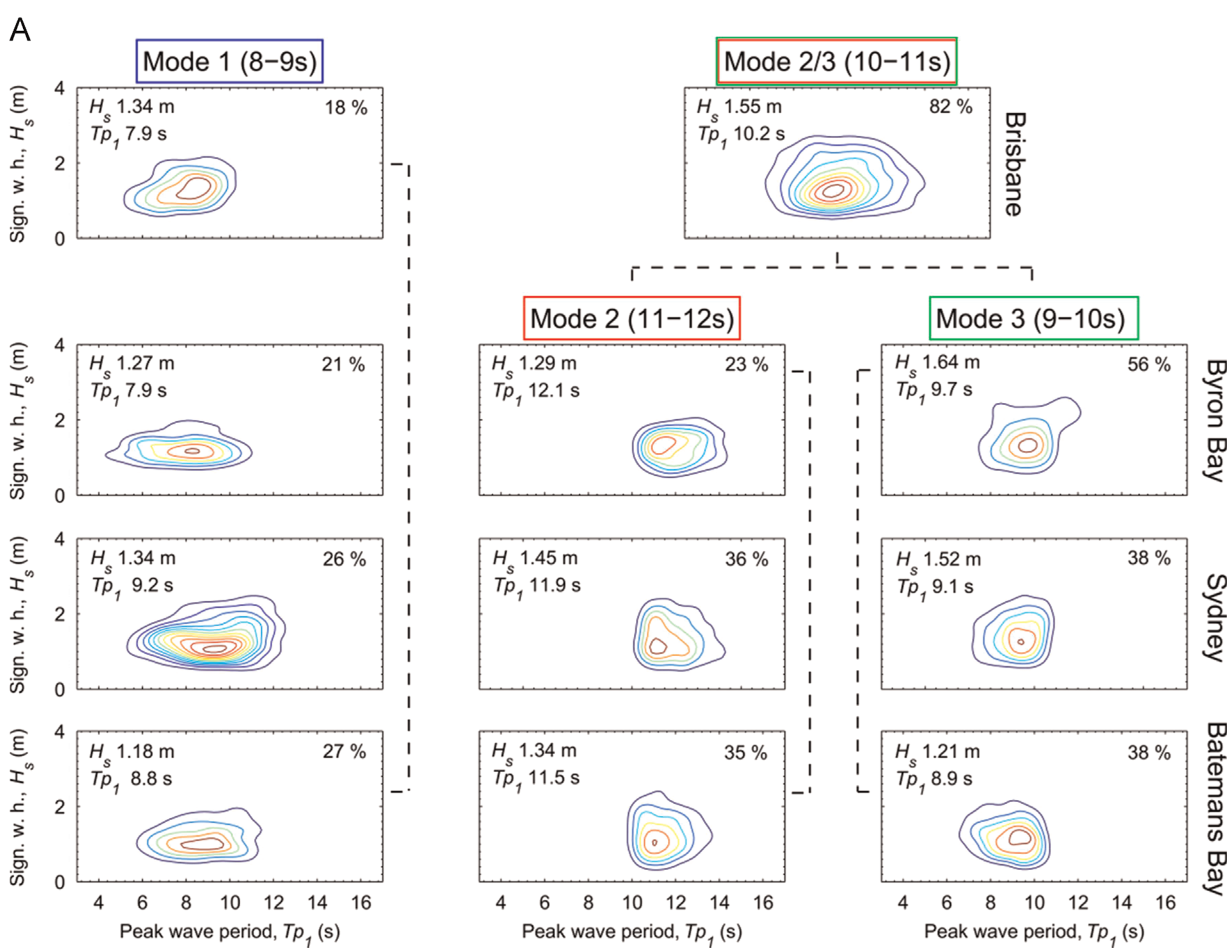

Fig. 4. JPD functions of wave height, H_s (m), and period, T_p (s), for each wave field during (A) winter and (B) summer at the four buoy locations. Plots show the probabilities of joint occurrence for each wave field, as determined by clustering. Contours of joint occurrence are given for every 20% increment in probability density. The H_s and T_p centroid values for each wave cluster are shown with the dominance (percentage occurrence, %) of each cluster during the respective buoy/season record.

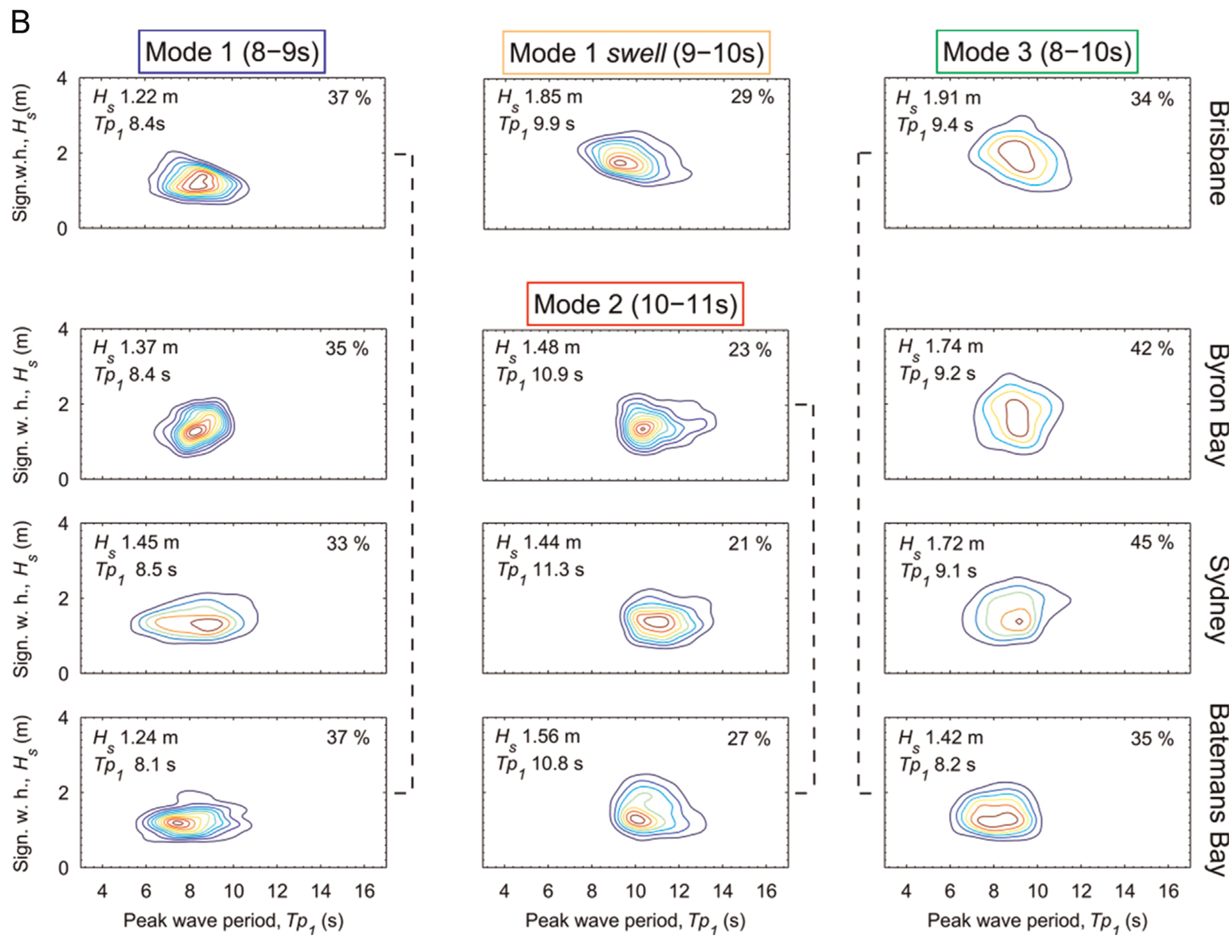

Fig. 4. (*continued*)

6. Wave type clusters and synoptic wave generation

6.1. Decomposition of wave clusters

Although K-means provides a useful metric for describing the primary modes of wave climate variability, the clustered wave fields do not necessarily represent individual 'synoptic-scale' wave climates. By definition, these wave climates have one generation source originating from a recurring anomalous synoptic pattern.

In order to identify synoptic-scale wave climates, the joint direction-frequency distribution of each cluster was examined. Wave height was not used, since it is invariant across all directional sectors. A single wave climate should exhibit a broadly unimodal joint distribution in direction and frequency, as it originates from a single wave generation source (synoptic anomaly). If multiple peaks in the joint distribution are observed, the clustered wave field may be a composite of multiple wave geneses. Where this is the case, component wave climates can be separated out from the cluster using a bivariate Gaussian Mixture Model (GMM).

A GMM identifies individual Gaussian components in a mixed bivariate distribution, for which the number of components is known. The directional distribution of each cluster is first examined to determine the number of modal peaks (Fig. 5A), where each peak represents a component wave climate. A joint PDF of direction/frequency is then generated (Fig. 5B) and the cluster is separated into component parts using the GMM (Fig. 5C). Fig. 5D compares the single-peaked components (wave climates) separated using the GMM against the original twin-peaked directional distribution.

The ability of the components to represent individual synoptic-scale wave climates is then evaluated with composite anomalies of the mean sea level pressure field across the Tasman Sea, using the NCEP-NCAR Reanalysis (NNR) (Kalnay et al., 1996). Strong anomalous patterns for the composite days indicate coherent synoptic forcing and suggest the wave climate is produced by a single wave generation source. In order to avoid skewing the modal signal, storm conditions were again excluded from this process.

6.2. Wave climate type genesis

Results indicate that, of the three primary cluster modes described in Section 5, independently-generated wave climates can be further isolated at Sydney and Byron Bay during winter ($n=5$) and summer ($n=6$). Sydney and Byron Bay best represent the latitudinal range of regional patterns as these buoys are the most exposed locations along the shelf, and are not affected by wave shadowing. The wave climate types identified at Sydney and Byron Bay, together with the associated synoptic anomalies across the South Pacific for each, are shown in Figs. 6 and 7 respectively.

Mode 1 was identified by clustering as a shorter-period easterly wave field, but GMM separation has identified two wave climates within this mode; North-Easterly Trade Winds (Mode 1a) and Zonal Easterly Trade Winds (Mode 1b). Both are formed with an anti-cyclonic anomaly in the Central Tasman that induces an easterly air flow. When the anomaly is more meridional, north-easterly waves from the Coral Sea are produced. A longer-period and more easterly wave climate prevails when the anomaly is more zonal. In both cases, the easterly wave climate is produced off the northern limb of the high pressure anomaly due to the anti-cyclonic air flow.

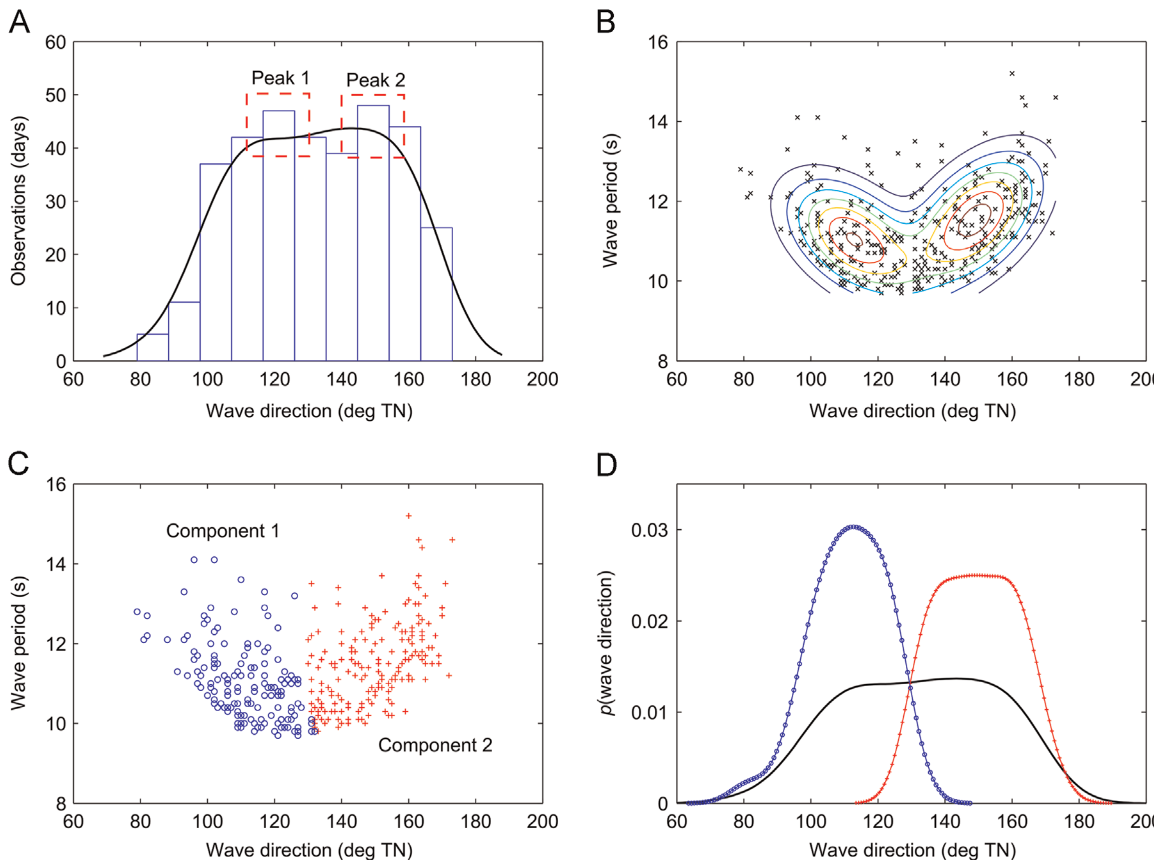

Fig. 5. Application of a Gaussian Mixture Model (GMM) to a wave distribution originally clustered with K-means.

Mode 2 contains two wave climates, of which only one is identifiable in both winter and summer (Mode 2a). Mode 2a is a result of a surface pressure gradient between a Southern Tasman anticyclone to the south, and a Tropical Low adjacent to the north, producing a south-easterly wave climate. Mode 2b represents a summer Central Tasman Low, but is not identifiable as a separate wave type during winter. Although Central Tasman Lows are known to produce storm wave conditions throughout the year, results suggest they do not produce a dominant modal wave signal on a daily average scale during winter.

Mode 3 represent the most oblique (southerly) wave field, and is composed of two wave climate types. Mode 3a is a long-period wave type produced from the south-west flow between a Tasman Sea anti-cyclone and a Southern Ocean Low. The synoptic arrangement for this wave type is most likely to produce bi-modal wave conditions, with a sub-dominant Mode 1 type wave field produced from the anticyclonic anomaly in the Central Tasman. Mode 3b is an extreme southerly type, associated with Southern Tasman Low formation, and produces the largest wave heights of the modal wave climate at both Sydney and Byron Bay.

6.3. Relation to large-scale climate drivers

Synoptic patterns shown in Figs. 6 and 7 suggest that Modes 1 and 3 are formed under Pacific-emanating atmospheric longwave patterns, while Mode 2 is a result of a longwave train emanating from the Indian Ocean sector. Specifically, Mode 1-type wave climates represent a spring–summer feature that is enhanced by La Niña-like climate. Mode 3 types represent a more autumn-winter-spring feature that is enhanced by El Niño-like climate. The wave climates of Modes 1 and 3 have a strong relationship with ENSO phases, as identified in Goodwin (2005). Accordingly, more southerly modal wave climates prevail under El Niño, while easterly conditions are more representative of La Niña phases. The Mode 2 wave types, with a strong central Tasman synoptic feature, represent either wave climates that occur during neutral ENSO conditions or where the Indian Ocean Dipole (IOD) or extension of the monsoon trough have a stronger influence on the Tasman Sea region. The coupling between ENSO and IOD has a significant effect on inter-annual wave climate variability at both sites (after Goodwin, 2005).

Figs. 6 and 7 show no strong stratification of wave climate according to the latitude of the STR. However, the STR has a stronger influence on modulating the seasonal occurrence of, and latitudinal exposure to, different wave climate types. Fig. 8 shows the probability of occurrence of each wave mode for Sydney and Byron Bay in winter and summer.

There is a 5° latitude separation between the Sydney (33.5°S) and Byron Bay (28.5°S) buoy locations. During winter, the mean latitude of the STR (over the period of analysis) is 35.4°S with a standard deviation of 6.6°, and 39.5°S with a standard deviation of 4.5° during summer. Hence, the seasonal shift in the STR latitude of 4° is comparable to the respective latitudinal difference between sites, and allowed us to examine the variance in modal wave climate clusters and synoptic types as a function of seasonal or latitudinal shifts.

During winter, Modes 1 and 3 co-vary between sites. At both Sydney and Byron Bay the sum total occurrence of these two modes is very similar and describes the bulk modal wave conditions (86–90%), with Mode 3 increasing with buoy location latitude south at the expense of Mode 1 (22% difference). Therefore, a poleward shift in the winter STR latitude decreases the occurrence of Mode 3-type wave climates in favour of Mode 1. The central wave field (Mode 2) is largely invariant between sites

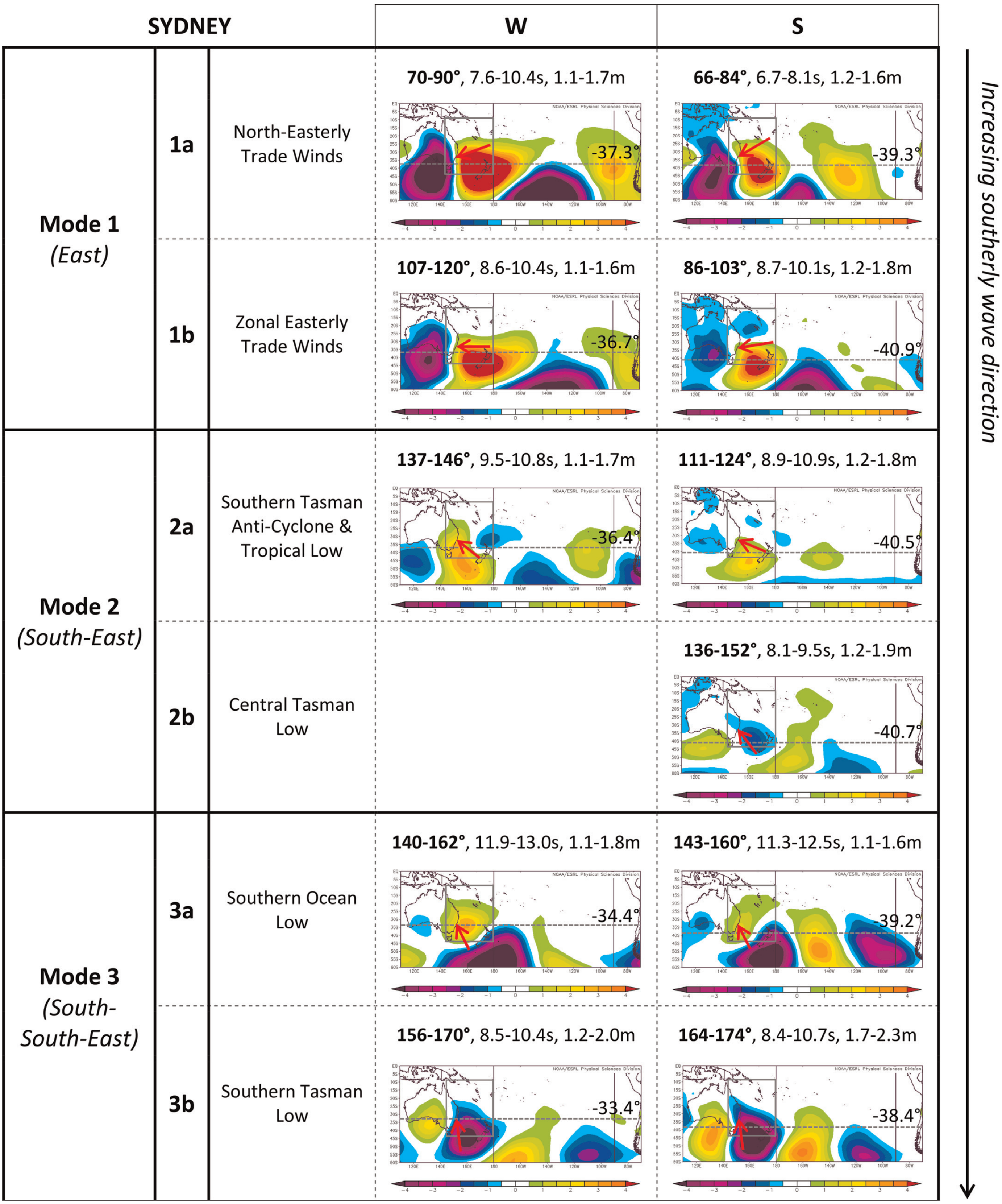

Fig. 6. Wave climate types for winter (W) and summer (S) at Sydney. The original cluster modes and respective wave climate sub-divisions are shown. MSLP anomalies represent the deviation of the synoptic pattern from the long-term climatology (1981–2010). Considering mid-Tasman wave generation, a one-day lag has been applied to all composites to approximate wave travel time from source. Parametric data for each wave climate represents the IQR of the MWD, T_p and H_s distributions. The mean latitude of the STR (grey dashed line) and region of calculation (grey box) for each wave climate are denoted. STR was calculated as the latitude of highest pressure over the composite days for a region covering the Tasman and Coral Seas (150–180°E, 10–45°S), from the NNR reanalysis (Kalnay et al., 1996).

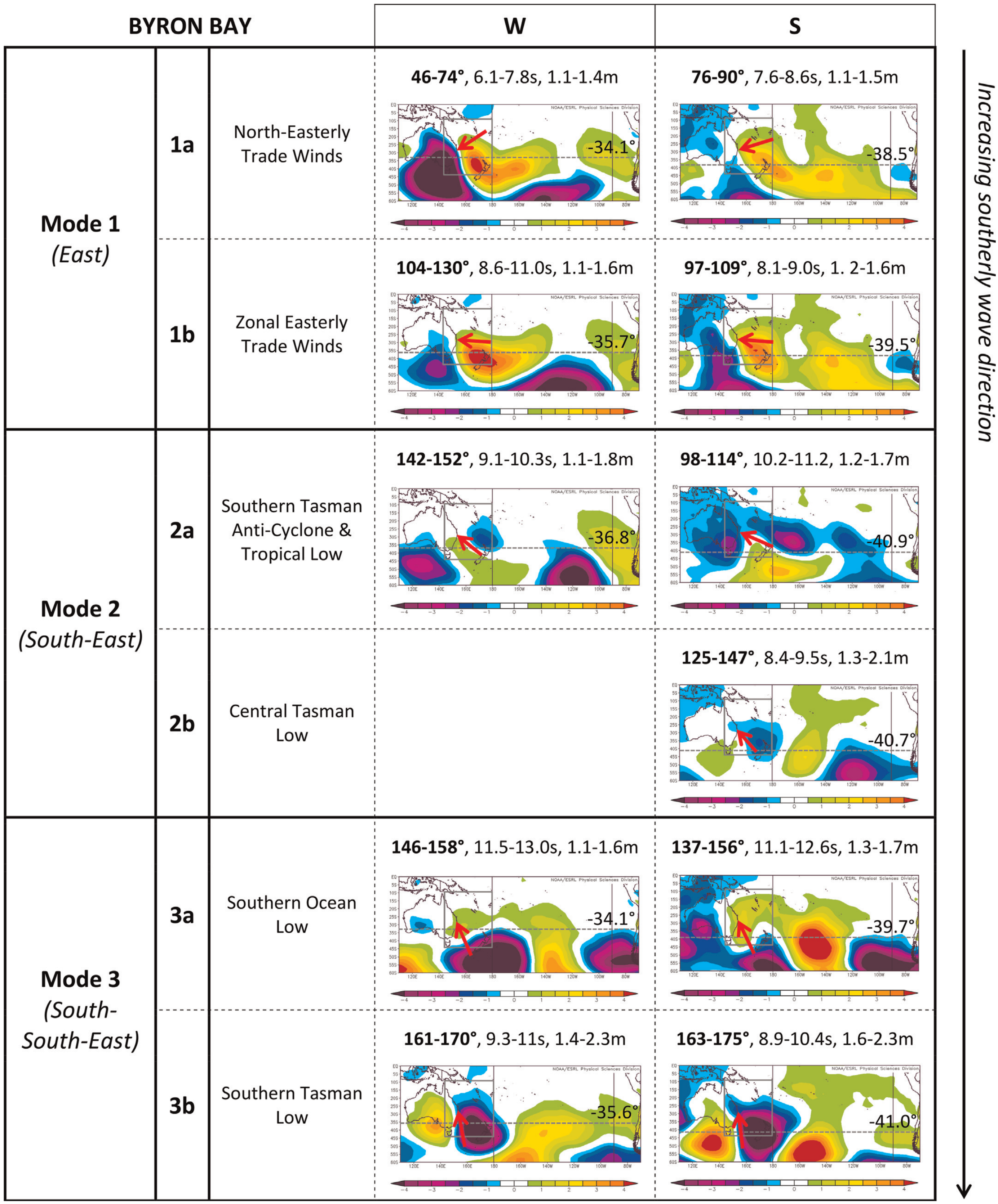

Fig. 7. Wave climate types for winter (W) and summer (S) at Byron Bay.

because the equatorward position of the STR means the wave generation region for this mode occupies the latitudes of both buoy locations. Latitudinal variability of the winter wave climate for Southeast Australia can therefore be described primarily by the STR control on the co-variance between the easterly (Mode 1) and southerly (Mode 3) wave types. Wave climate

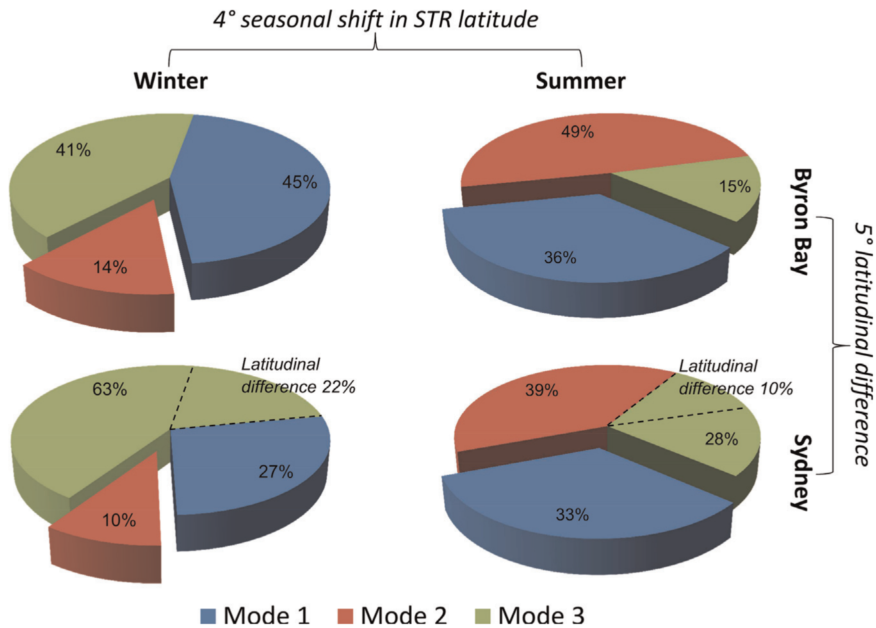

Fig. 8. Probability of occurrence of seasonal wave climate modes at Sydney and Byron Bay. Those wave climates that co-vary between sites are adjoined, and their latitudinal difference shown (dotted line).

variability during winter is therefore associated with the oscillation of ENSO states.

During summer, Modes 2 and 3 co-vary between sites. The sum total occurrence of these two modes between Sydney and Byron Bay is the same (non-significant difference, $p < 0.05$), meaning a poleward shift in the summer STR latitude decreases the occurrence of Mode 3-type wave climates in favour of Mode 2. The easterly component (Mode 1) is invariant between sites (non-significant difference, $p < 0.05$) because the wave generation region occupies the latitudes of both buoy locations, due to the more poleward STR latitude. Latitudinal variability of the summer wave climate for the SEAS can therefore be described primarily by the STR control on the co-variance between the central (Mode 2) and southerly (Mode 3) wave types. Wave climate variability during summer may therefore be associated with coupling between the IOD and ENSO.

7. Latitudinal and seasonal wave power variability

The impact of wave climate variability on coastal processes can be assessed using the deep-water wave power, or the wave energy flux, P_0. P_0 was calculated for each daily wave event using the formula for irregular waves (from Holthuijsen, 2007):

$$P_0 = \frac{1}{16}\rho g\, Hs^2 C_g \tag{1}$$

where ρ (kg m^{-3}) is the average density of seawater, g (m s^{-2}) is the acceleration due to gravity, H_s is the daily average significant wave height, and C_g (m s^{-1}) is the wave group velocity.

As the wave buoys are located in 60–100 m water depth (mid-shelf), the deep-water wave assumption is not always valid for longer period swell where the wave base may be at times seaward of the buoy location. Therefore, C_g is determined using the following equation:

$$C_g = \frac{n\lambda}{T_e} \tag{2}$$

where λ is the wavelength determined using the Newton–Raphson iterative solution, and T_e is the wave energy period. Here we assume $T_e = T_p$ (e.g. Hemer and Griffin, 2010), which is a good approximation for a standard JONSWAP spectrum (Cornett, 2008). Following Holthuijsen (2007), n varies from 1/2 in deep water to 1 in very shallow water and is defined as

$$n = \frac{1}{2}\left(1 + \frac{4\pi d/\lambda}{\sinh(4\pi d/\lambda)}\right) \tag{3}$$

P_0 describes the power density expected from a single wave event that represents a certain wave climate or sea state and is expressed in kilowatts per metre wave-crest-length (kW m^{-1}). Here, wave climate wave power is expressed using the mean power of the respective wave climate distribution, P_W.

However, in order to assess wave power impacts on coastal processes, the probability of occurrence of each wave climate type (Fig. 8) needs to be integrated. As such, the total, rather than mean, wave power (or energy flux) delivered by each wave climate in an average season (winter/summer) is a more useful metric. The total seasonal wave energy flux per wave climate type, E_W, is obtained by multiplying P_W (kW m^{-1}) by the time-integrated probability of occurrence (in seconds), n, of each wave climate type, w, for each season, s:

$$E_W(w, s) = P_W(w, s) \times n(w, s) \tag{4}$$

Since power is integrated over time, E_W is expressed in gigajoules per metre (GJ m^{-1}) along a tangent to the mean wave climate crest. E_W is commonly used in renewable energy assessments to measure the total time-averaged wave energy resource. In modelling studies, E_W is calculated by integrating P_0 overall observations at a grid point and then dividing by the number of seasons or years in the record (Hughes and Heaps, 2010). However, since buoy records inevitably have data gaps, P_W needs to be integrated over the time equivalent of the mean percentage occurrence of each wave climate type instead, to obtain a representative total energy flux per season.

7.1. Inter-site and inter-seasonal wave power variability

Here we compare the total seasonal wave energy flux delivered by each modal wave climate type, E_W, between Sydney and Byron Bay. For a fair comparison, only wave observations for days when

Table 1
Mean seasonal wave power, P_W (kW m^{-1}) and total seasonal wave energy flux, E_W (GJ m^{-1}) per wave climate type, for Sydney and Byron Bay buoys.

	Sydney	Byron Bay				
	P_W	n[a]	E_W	P_W	n	E_W
Austral winter (JAS=92 days)						
Mode 1	9.4	23	18.3[b]	9.9	39	33.1[c]
Mode 2	10.0	8	7.2	13.2	12	13.7
Mode 3	14.0	52	63.3	19.6	35	59.0
All storms	58.9	9	44.0	64.8	6	34.7
Total modal energy			88.8			105.8
Austral summer (JFM=90 days)						
Mode 1	9.2	28	22.7	8.4	29	20.6
Mode 2	12.4	34	36.1	13.9	39	46.7
Mode 3	18.6	24	38.1	19.7	12	20.7
All storms	50.2	4	16.5	48.6	10	43.7
Total modal energy			101.2			88.0

[a] n is given here in average number of days per season but is converted to equivalent seconds to calculate E_W in GJ m^{-1} since 1 J of energy=1 W of power exerted for n time in seconds.
[b] Only 13.2 GJ m^{-1} of this is comparable to Byron Bay for a wave climate change scenario.
[c] Only 20.2 GJ m^{-1} of this would be seen at Sydney under a wave climate change scenario.

both buoys were recording simultaneously were used in the assessment. Both P_W and E_W are therefore mean values between 2000 and 2013 (Table 1).

Previous modelling studies have quantified P_W and E_W for New South Wales shelf waters. Cornett (2008), Hughes and Heap (2010) and Gunn et al. (2012) all report mean annual P_W values between 10 and 20 kW m^{-1}, and Hughes and Heap (2010) suggest mean annual E_W is around 510 GJ m^{-1}. P_W values are equivalent to those calculated by us in Table 1, and when approximated annually, our estimation of E_W is equivalent to that of Hughes and Heaps (2010) (when we include storm wave energy).

During winter, the directionality of wave power delivery at both Sydney and Byron Bay is broadly the same (Fig. 9A). However, there is a greater total flux of wave energy (E_W difference of 18 GJ m^{-1}) at Byron Bay than at Sydney (Fig. 9A, using bracketed winter values). This is manifest in a greater easterly (Mode 1) and south-easterly (Mode 2) component, with a non-significant difference ($p<0.05$) in southerly waves (Mode 3) between sites. This is explained by the mean winter position of the STR which is 7° south of Byron Bay, and 2° south of Sydney, meaning wave generation for Modes 1 and 2 is more proximal at Byron Bay than Sydney (see Figs. 6 and 7). Mode 3 wave generation is still sufficiently northward in winter to remain the dominant winter wave climate type at Byron Bay as at Sydney. The dominance of the oblique southerly modal power component, and the north–south coastal alignment, enable potential northward longshore sediment transport.

The occurrence co-variance seen in Modes 1 and 3 between sites in winter (Section 6.3) does not translate to co-variance in a wave energy flux between these modes (Fig. 9A), since a reduction in occurrence of Mode 3-type waves at Byron Bay is compensated for by an increase in the mean wave height of Mode 3b waves. Analysis suggests that the highest wave heights are associated with the most southerly directions in the Mode 3b wave climate. Due to the alignment of the SEAS, high wave energy associated with these oblique directions propagates past Sydney but is received at Byron Bay.

In summer, there is less total flux of wave energy (E_W difference of 9 GJ m^{-1}) at Byron Bay than at Sydney. The directionality of energy delivery is also different. At Byron Bay, there is a greater occurrence of less-powerful south-easterly (Mode 2) waves and a

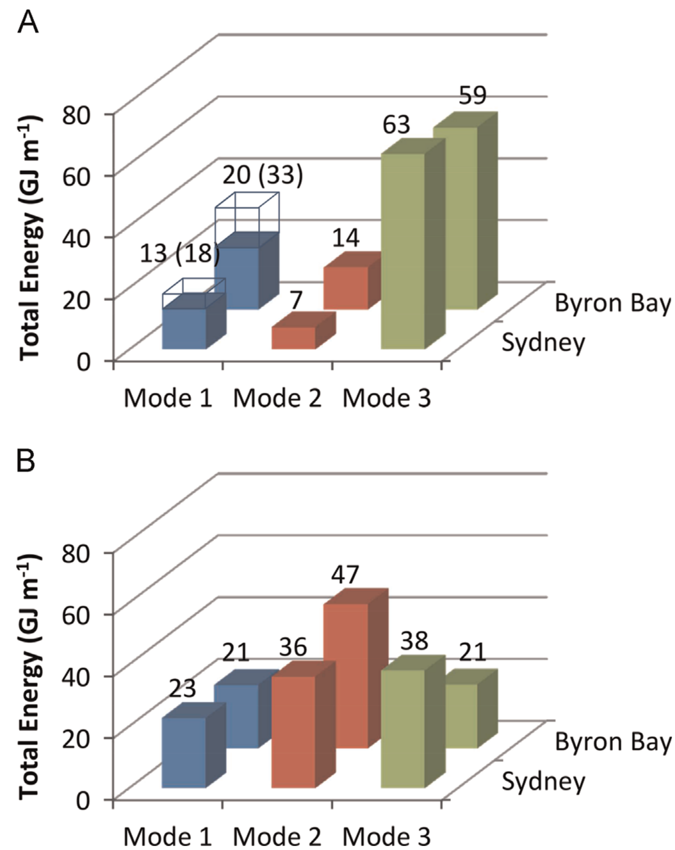

Fig. 9. Mean winter (A) and summer (B) wave energy flux contribution from modal wave climates at Sydney and Byron Bay (shown to nearest GJ). The contribution of extra-Tasman swell propagation identified at Byron Bay for Mode 1 in winter is shown. Bracketed values are with extra-Tasman component (and corresponding days at Sydney) included.

lower occurrence of more powerful southerly (Mode 3) waves, with no significant difference in easterly (Mode 1) energy flux between sites.

There is also a covariance in total wave energy delivered by Mode 2 and Mode 3-types at Byron Bay between winter and summer (~70 GJ m^{-1}). This is a function of the seasonal proximity of Mode 2 and 3 wave generation to Byron Bay, which in turn is a function of the location of the STR (see Fig. 7). The southerly STR shift in summer therefore drives a reduction in more powerful Mode 3-type wave events, in favour of, and broadly equivalent in energy to, the increase in Mode 2-type waves.

7.2. Projecting future directional wave power change for central NSW

There is evidence to suggest that the atmospheric Hadley cell is expanding poleward, consistent with an enhanced greenhouse effect, ozone depletion (Seidel et al., 2008) due to anthropogenic aerosols, and the shift towards the La Nina-like state of the Pacific Decadal Oscillation (Allen et al., 2014). Coupled to this, the STR in the East Australian region is intensifying, although a coherent southerly shift is as yet unclear (Timbal and Drosdowsky, 2013). If a poleward shift in the Hadley cell and trade-wind zone continues, the present day wave climate at Byron Bay, 600 km equatorward of Sydney, may be used as a surrogate for future wave climate changes along the central NSW coast.

In using the Byron Bay wave climate as a surrogate for wave climate change at Sydney, we are assuming that all observed wave climate types at Byron Bay would be observed at Sydney. Although this is true for Modes 2 and 3 and the majority of Mode 1, there is a

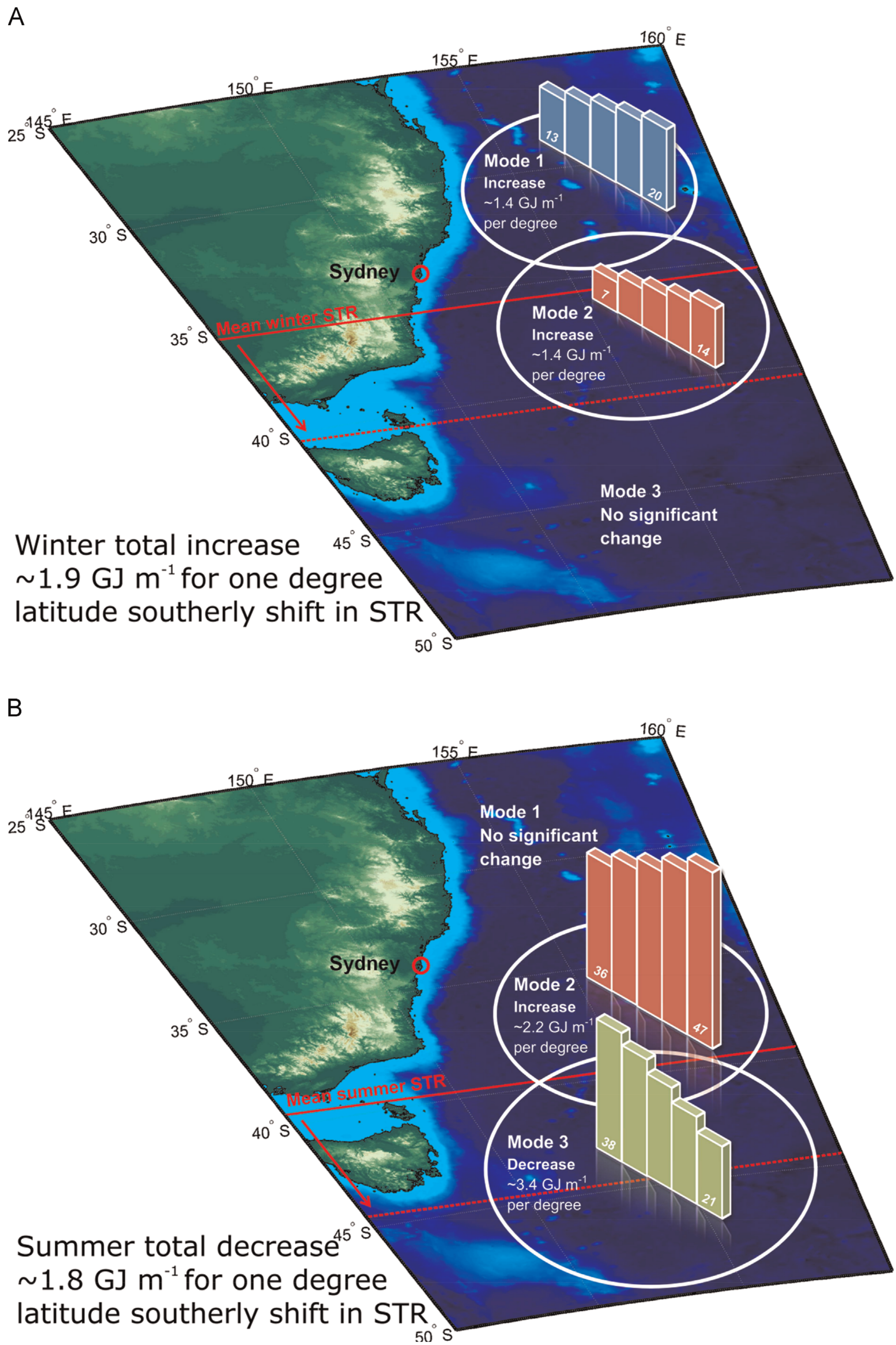

Fig. 10. Future directional wave power change for the Sydney region with a southerly shift in the STR during (A) winter and (B) summer. Bars represent projected change in modal wave climate type for the Sydney region per degree southerly shift in the STR, for up to 5 degrees southerly shift scenario.

narrow swell window within Mode 1b where waves can be generated north-east of the north island of New Zealand and propagate towards Byron Bay (Fig. 1). Waves generated in this swell window would not be seen at Sydney under a southerly STR scenario because of the blocking effect of the New Zealand landmass. Mode 1a (in winter and summer) and Mode 1b (in summer) all are generated within the Tasman Sea.

Fetch-limited waves, such as those described by Mode 1, generated within the Tasman Sea cannot exceed T_p of 12–13 s due to a limiting maximum fetch of approximately 1800 km between Byron Bay and New Zealand (assuming a 10 m s^{-1} wind, typical of trade wind-wave generation) (after US Army Corp of Engineers, 2002). Using this fetch threshold, only 11% of Mode 1b waves in winter (12.9 GJ m^{-1} of total winter wave energy, 8 days on average per winter) were found to propagate through a swell window above New Zealand between 90° and 135°. Therefore the majority of Mode 1b waves at Byron Bay in winter (89%) can be used as a surrogate for Sydney. Those wave evens in winter Mode 1b identified at Byron Bay as being generated outside the Tasman Sea are not included in the future scenario for Sydney. In order to maintain a linear comparison, the corresponding days on which these waves were observed at Byron Bay have been omitted from the totals at Sydney as well (Fig. 9A and Table 1).

The vast majority of wave events at Byron Bay (96% in winter, 100% in summer) are also seen at Sydney. However, there is a distinct change in wave climate north of Byron Bay as shown by the Brisbane buoy observations (Section 5). These show a relative increase in the percentage of the overall wave climate that is produced by 12–13 s period swells generated in the southwest Pacific and Coral Sea (Mode 1 *swell*). Accordingly, a poleward expansion of the tropics would result in a progressive increase in percentage occurrence of Mode 1 waves at Byron Bay at the expense of a reduction in Mode 3 waves. This is consistent with GCM-based wave climate projections by Hemer et al. (2013), which indicates an anti-clockwise shift in annual MWD of up to 10°. We explore the implications of a poleward shift in the STR on wave climate for the Sydney region in the following section.

7.3. *Implications for directional modal wave power for the central NSW shelf*

We estimate that a poleward shift in the mean latitude of the STR would force an increase in total (modal) wave energy flux for the Sydney region of approximately 1.9 GJ m^{-1} wave-crest-length for a 1° latitude shift south during winter (Fig. 10A), and a reduction of similar magnitude (approximately 1.8 GJ m^{-1} for 1° latitude shift south) during summer (Fig. 10B).

The increase in total winter wave energy would be produced by heightened Mode 1 and Mode 2 wave fields, while the reduction in summer is manifest in a reduction of more-powerful Mode 3 in favour of less-powerful Mode 2. There is no change inferred in summer Mode 1 and winter Mode 3 wave energy.

Assuming no change in storm synoptic type distribution (Goodwin et al., submitted), magnitude or clustering, a weaker Mode 2 (cross-shore) component in place of Mode 3 (along-shore) wave energy in summer will act to reduce the longshore transport component. In winter, although a total increase in modal (constructive) wave energy is inferred, this is also from the east and south-east, enhancing the cross-shore transport component at the expense of alongshore movement.

Reduced obliquity of constructive wave power throughout the year may promote a general disruption to the northward alongshore sediment transport along the central NSW coast. For those sections of coast sensitive to alongshore gradients in wave power, greater easterly wave power during winter favours shoreline planform embaymentisation, whereas an increase in south-easterly wave power during summer promotes planform flattening. There is evidence to suggest historical directional wave power change has forced considerable shoreline response along the Central to Northern New South Wales coast. Studies of shoreface bathymetric change by Goodwin et al. (2013a) in the Byron Bay area suggest that a trend towards a more south-easterly modal and storm wave climate during the late 1800 s was responsible for planform flattening, nearshore bar welding and large sand supply rates to the shoreline during that period.

8. Conclusions

A combined statistical-synoptic typing approach of directional wave buoy records along the Southeast Australian shelf has isolated six modal wave climates and their respective generation sources. These include waves produced by North-Easterly Trade Winds, Zonal Easterly Trade Winds, a combination of Southern Tasman Anti-Cyclones and Tropical Lows, Central Tasman Lows, Southern Ocean Lows and Southern Tasman Lows. We show these wave climates can be grouped into three distinct wave type clusters; Mode 1 (easterly), Mode 2 (south-easterly) and Mode 3 (southerly). K-means clustering with a best-guess estimate of the optimal wave climate number, *k*, was only able to identify the broad directional wave modes, rather than individual wave genesis. This is because multiple synoptic drivers produce statistically indifferent directional wave fields in a semi-enclosed sea environment. In order to isolate wave generation and 'synoptic-scale' wave climates, subsequent decomposition of the clusters using a Gaussian Mixture Model and analysis of the mean sea level pressure field was required.

Synoptic patterns suggest that Mode 1-type wave climates (easterly) and Mode 3-types (southerly) are formed under Pacific-dominant atmospheric longwave patterns and are related to ENSO phases. Mode 2-types (south-easterly) are a result of a longwave train originating from the Indian Ocean, and occur either during ENSO neutral conditions or when the IOD has a stronger influence on the Tasman Sea region. Occurrence co-variance between Modes 1 and 3 during winter suggests ENSO is the dominant signal during winter, while co-variance between Modes 2 and 3 in summer indicate the IOD is more influential during summer.

The position of the STR modulates the seasonal occurrence of, and latitudinal exposure to, different wave climate types. A southerly migration of the STR is a plausible future scenario in line with an observed poleward expansion of the tropics cell due to anthropogenic forcing and natural variability. Our results indicate that, under such a scenario, there would be an increase in the modal wave energy flux for the central NSW shelf of 1.9 GJ m^{-1} wave-crest-length for a 1° southerly shift in the STR during winter, and a reduction of similar magnitude (approximately 1.8 GJ m^{-1} for 1° latitude shift south) during summer.

In both seasons, a southerly shift in the STR forces a re-arrangement of the modal wave energy flux towards the east and south-east. This anti-clockwise rotation of the wave field is consistent with GCM-based wave climate projections (Hemer et al., 2013). Reduced obliquity of constructive wave power throughout the year would promote a general disruption to northward alongshore sediment transport for the central NSW coast. Under a southerly STR scenario, cross-shore sediment transport will become increasingly prevalent, with local-scale effects dependant on shoreface sediment availability. Our results are of primary application to investigating available wave energy for beach recovery after storm events, and mean shoreline configuration.

This study is based on observational records on the East Australian shelf, but our understanding of the latitudinal gradient in modal wave climate may be applicable to other coastlines where the wave climate is influenced by the position of the zonal STR. In the northern hemisphere, Atlantic wave climates of the Iberian peninsula and Bay of Biscay are strongly influenced by the position and strength of the sub-tropical Azores high. Other Southern Hemisphere, continental east coasts along the mid-latitudes such South Africa/Mozambique and Uruguay/Brazil also have comparable wave genesis and sediment transport patterns.

Acknowledgements

Parametric wave data from all NSW buoys is owned by NSW Office of Environment and Heritage (OEH) and is managed and collected by Manly Hydraulics Laboratory (MHL). Wave data from the Brisbane buoy is owned by State of Queensland, Department of Science, Information Technology, Innovation and the Arts (DSITIA) and distributed by Coastal Impacts Unit - Science Delivery Division, DSITIA. Thanks also to Stuart Browning at Macquarie University for provision of the Tasman Sea STR timeseries. During cluster evaluation, the freeware CVAP platform for Matlab (Wang et al., 2009) was used. We also thank the anonymous reviewers of this paper whose comments significantly improved the work. T. Mortlock is funded by a Macquarie University International Research Excellent Scholarship (MQiRES) in association with Australian Research Council (ARC) Linkage Project (LP100200348).

References

Allen, R.J., Kovilakam, M., 2014. Influence of anthropogenic aerosols and the Pacific Decadal Oscillation on tropical belt width. Nat. Geosci. 7 (4), 270–274.

Alomar, M., Sánchez-Arcilla, A., Bolaños, R., Sairouni, A., 2014. Wave growth and forecasting in variable, semi enclosed domains. Cont. Shelf Res. 87 (15), 28–40.

Amante, C., Eakins, B.W., 2009. ETOPO1 1 Arc-Minute Global Relief Model: procedures, data sources and analysis. NOAA Technical Memorandum NESDIS NGDC-24. National Geophysical Data Center, NOAA (accessed 30.07.14).

BBW (Blain, Bremner and Williams), 1985. Elevated ocean levels, storms affecting the NSW coast 1880-1980. A Report Prepared For The NSW Public Works Department Coastal Branch in Conjunction with Weatherex Meteorological Services. PWD Report No., 85041.

Bernadara, P., Mazas, F., Kergadallan, X., Hamm, L., 2014. A two-step framework for over-threshold modelling of environmental extremes. Nat. Hazards Earth Syst. Sci. 14, 635–647.

Boukhanovsky, A.V., Lopatoukhin, L.J., Guedes Soares, C., 2007. Spectral wave climates of the North Sea. Appl. Ocean Res. 29 (3), 146–154.

Browning, S.A., Goodwin, I.D., 2013. Large-scale influences on the evolution of winter subtropical maritime cyclones affecting Australia's east coast. Mon. Weather Rev. 141 (7), 2416–2431.

Calinski, T., Harabaz, J., 1974. A dendrite method for cluster analysis. Commun. Stat. 3, 1–27.

Callaghan, D.P., Nielsen, P., Short, A., Ranasinghe, R., 2008. Statistical simulation of wave climate and extreme beach erosion. Coast. Eng. 55, 375–390.

Camus, P., Mendez, F.J., Medina, R., Cofiño, A.S., 2011a. Analysis of clustering and selection algorithms for the study of multivariate wave climate. Coast. Eng. 58, 453–462.

Camus, P., Cofiño, A., Mendez, F.J., Medina, R., 2011b. Multivariate wave climate using self-organizing maps. J. Atmos. Oceanic Technol. 28, 1554–1658.

Camus, P., Menéndez, M., Méndez, F.J., Izaguirre, C., Espejo, A., Cánovas, V., Pérez, J., Rueda, A., Losada, I.J., Medina, R., 2014. A weather-type statistical downscaling framework for ocean wave climate. J. Geophys. Res.: Oceans 119 (11), 7389–7405.

Church, J.A., Clark, P.U., Cazenave, A., Gregory, J.M., Jevrejeva, S., Levermann, A., Merrifield, M.A., Milne, G.A., Nerem, R.S., Nunn, P.D., Payne, A.J., Pfeffer, W.T., Stammer, D., Unnikrishnan, A.S., 2013. Sea level change In: Stocker, T.F., Qin, D., Plattner, G.-K., Tignor, M., Allen, S.K., Boschung, J., Nauels, A., Xia, Y., Bex, V., Midgley, P.M. (Eds.), Climate Change 2013: The Physical Science Basis. Contribution of Working Group I to the Fifth Assessment Report of the Intergovernmental Panel on Climate Change. Cambridge University Press, Cambridge, United Kingdom, New York, NY, USA.

Coelho, C., Silva, R., Veloso-Gomes, F., Taveira-Pinto, F., 2009. Potential effects of climate change on northwest Portuguese coastal zones. ICES J. Marine Sci. 66, 1497–1507.

Coles, S., 2001. An Introduction to Statistical Modelling of Extreme Values. Springer, London, p. 209.

Coghlan, I., Mole, M., Shand, T., Carley, J., Pierson, W., Miller, B., et al., 2011. High resolution wave modelling (HI-WAM) for Batemans Bay detailed wave study: A Report Prepared for Manly Hydraulics Lab/Office of Environment and Heritage NSW.. Water Research Laboratory, University of Water Research Laboratory, University of New South Wales

Cornett, A.M., 2008. A global wave energy resource assessment. In: Proceedings of the 18th International Society of Offshore and Polar Engineers (ISOPE) Conference. Vancouver, Canada, ISOPE-2008-TPC-579.

Datawell, 2014. Directional Waverider MkIII Specifications. Datawell BV.

Dent, J., Taylor, D., Treloar, (on behalf of Cardno consultancy), 2001. NSW Coastal Waves: Numerical Modelling Final Report A Report Prepared for the Office of Environment and Heritage NSW. Report No. LJ2949/R2745.

Dunn, J.C., 1974. Well separated clusters and optimal fuzzy partions. J. Cybern. 4, 95–104.

Goda, Y., 2010. Random Seas and Design of Maritime Structures. World Scientific, Singapore, p. 464.

Goodwin, I.D., 2005. A mid-shelf, mean wave direction climatology for southeastern Australia, and its relationship to the El Niño Southern Oscillation since 1878 AD. Int. J. Climatol. 25, 1715–1729.

Goodwin, I.D., Freeman, R., Blackmore, K., 2010. Decadal wave climate variability and implications for interpreting New South Wales Coastal Behaviour. In: Proceedings of the Australian Wind Waves Research Science Symposium. Gold Coast, Queensland, Australia, 19–20 May 2010, pp. 58–61.

Goodwin, I.D., Freeman, R., Blackmore, K., 2013a. An insight into headland sand bypassing and wave climate variability from shoreface bathymetric change at Byron Bay. 341. Marine Geology, New South Wales, Australia, pp. 29–45.

Goodwin, I.D., Mortlock, T.R., Browning, S., 2013b. Tasman Sea wave climate variability associated with shifts in the subtropical ridge. In: Proceedings of the 2nd Australasian Wind-Wave Symposium. Melbourne, June 2013.

Goodwin, I.D., Mortlock, T.R., Browning, S., Shand, T., 2015. Extreme east coast waves, their propagation and refraction patterns on the Southeast Australian shelf. J. Geophys. Res.: Oceans (submitted).

Gordon, A.D., 1999. Classification, 2nd edition. Chapman and Hall/CRC Press, New York, p. 272.

Guanche, Y., Mínguez, R., Méndez, F.J., 2013. Climate-based Monte Carlo simulation of trivariate sea states. Coast. Eng. 80, 107–121.

Gunn, K., Stock-Williams, C., 2012. Quantifying the global wave power resource. Renew. Energy 44, 296–304.

Hamerly, G., Elkan, C., 2003. Learning the k in k-means. Adv. Neural Inform. Process. Syst. 16, 2526–2532.

Hamilton, L.J., 2010. Characterising spectral sea wave conditions with statistical clustering of actual spectra. Appl. Ocean Res. 32, 332–342.

Harley, M.D., Turner, I.L., Short, A.D., Ranasinghe, R., 2010. Interannual variability and controls of the Sydney wave climate. Int. J. Climatol. 30, 1322–1335.

Harley, M.D., Turner, I.L., Short, A.D., Ranasinghe, R., 2011. A reevaluation of coastal embayment rotation: the dominance of cross-shore versus alongshore sediment transport processes, Collaroy-Narrabeen Beach, southeast Australia. J. Geophys. Res. 116, FO04033.

Hawkes, P., Gonzalez-Marco, D., Sánchez-Arcilla, A., Prinos, P., 2008. Best practice for the estimation of extremes: a review. J. Hydraul. Res. 46 (2), 324–332.

Hemer, M.A., 2010. Historical trends in Southern Ocean storminess: long-term variability of extreme wave heights at Cape Sorell, Tasmania. Geophys. Res. Lett. 37 (18), L18601.

Hemer, M.A., Fan, Y., Mori, N., Semedo, A., Wang, X.L., 2013. Projected changes in wave climate from a multi-model ensemble. Nature Climate Change 3 (5), 471–476.

Hemer, M.A., Griffin, D.A., 2010. The wave energy resource along Australia's Southern margin. J. Renew. Sustain. Energy 2 (4), 043108.

Hemer, M.A., Simmonds, I., Keay, K., 2008. A classification of wave generation characteristics during large wave events on the Southern Australian margin. Cont. Shelf Res. 28, 634–652.

Hemer, M.A., McInnes, K., Ranasinghe, R., 2012. Climate and variability bias adjustment of climate model-derived winds for a southeast Australian dynamical wave model. Ocean Dyn. 62, 87–104.

Holthuijsen, L.H., 2007. Waves in Oceanic and Coastal Waters. Cambridge University Press, Cambridge, p. 387.

Hubert, L.J., Levin, J.R., 1976. A general statistical framework for assessing categorical clustering in free recall. Psychol. Bull. 83, 1072–1080.

Hughes, M.G., Heap, A.D., 2010. National-scale wave energy resource assessment for Australia. Renew. Energy 35, 1783–1791.

International Hydrographic Organization (IHO), 1953. Limits of Oceans and Seas. International Hydrographic Organization, Bremerhaven, Pangaea, p. 44.

Johnson, D., 1919. Shore Processes and Shoreline Development. Wiley, New York.

Kalnay, E., Kanamitsu, M., Kistler, R., Collins, W., Deaven, D., et al., 1996. The NCEP/NCAR 40-year reanalysis project. Bull. Am. Meteorol. Soc. 77, 437–470.

Krzanowski, W.J., Lai, Y.T., 1985. A criterion for determining the number of groups in a data set using sum-of-squares clustering. Biometrics 44, 23–34.

Masselink, G., Pattiaratchi, C.B., 2001. Characteristics of the sea-breeze system in Perth, Western Australia, and its effect on the nearshore wave climate. J. Coast. Res. 17 (1), 173–187.

Mathiesen, M., Goda, Y., Hawkes, P.J., Mansard, E., Martín, M.J., Peltier, E., Thompson, E.F., Van Vledder, G., 1994. Recommended practice for extreme wave analysis. J. Hydraul. Res., 32; , pp. 803–814.

Mazas, F., Hamm, L., 2011. A multi-distribution approach to POT methods for determining extreme wave heights. Coast. Eng. 58 (5), 385–394.

Méndez, F.J., Menéndez, M., Luceño, A., Losada, I.J., 2006. Estimation of long-term variability of extreme significant wave height using a time-dependent peaks over threshold (POT) model. J. Geophys. Res. 111 (C07), C07024.

Milligan, G., Cooper, M., 1985. An examination of procedures for determining the number of clusters in a data set. Psychometrika 50 (2), 159–179.

Munk, W.H., Traylor, M., 1947. Refraction of ocean waves: a process linking underwater topography to beach erosion. J. Geol. 55 (1), 1–14.
Munk, W.H., Spindel, R.C., Baggeroer, A., Birdsall, T.G., 1994. J. Acoust. Soc. Am. 96 (4), 2330–2342.
Nicholls, R.J., Wong, P.P., Burkett, R.V., Codignotto, J.O., Hay, J.E., McLean, R.F., et al., 2007. Coastal Systems and Low-lying Areas. IPCC Forth Assessment Report (AR4), Working Group II: Impacts. Adaptation and Vulnerability. Cambridge University Press (Chapter 6).
Nicholls, R.J., Townend, I.H., Bradbury, A., Ramsbottom, D., Day, S.A., 2013. Planning for long-term coastal change: experiences from England and Wales. Ocean Eng. 71, 3–16.
Pelleg, D., Moore, A., 2000. X-means: extending k-means with efficient estimation of the number of clusters. In: Proceedings of the Seventeenth International Conference on Machine Learning. San Francisco, USA, pp. 727–734.
Ranasinghe, R., McLoughlin, R., Short, A., Symonds, G., 2004. The Southern Oscillation Index, wave climate, and beach rotation. Mar. Geol. 204 (3-4), 273–287.
Rollason, V., Goodwin, I.D., 2009. Coffs Harbour Coastal Processes Progress Report. A Report Prepared for Coffs Harbour Council, BMT WBM.
Rousseeuw, P., 1987. Silhouettes: a graphical aid to the interpretation and validation of cluster analysis. J. Comput. Appl. Math. 20 (1), 53–65.
Seidel, D.J., Fu, Q., Randel, W.J., Reichler, T.J., 2008. Widening of the tropical belt in a changing climate. Nat. Geosci. 1 (1), 21–24.
Semedo, A., Sušelj, K., Rutgersson, A., Sterl, A., 2011. A global view on the wind-sea and swell climate and variability from ERA-40. J. Clim. 24 (5), 1461–1479.
Shand, T., Goodwin, I.D., Mole, M.A., Carley, J.T., Browning, S., Coghlan, I.R., et al., 2011a. NSW Coastal Inundation Hazard Study: Coastal Storms and Extreme Waves. Water Research Laboratory, University of New South Wales & Climate Futures, Macquarie University.
Shand, T., Mole, M.A., Carley, J.T., Peirson, W.L., Cox, R.J., 2011b. Coastal Storm Data Analysis: Provision of Extreme Wave Data for Adaptation Planning. Water Research Laboratory, University of New South Wales.
Short, A.D., Trenaman, N.L., 1992. Wave climate of the Sydney region, an energetic and highly variable ocean wave regime. Mar. Freshw. Res. 43, 765–791.
Slott, J.M., Murray, A.B., Ashton, A.D., Crowley, T.J., 2006. Coastline responses to changing storm patterns. Geophys. Res. Lett. 33, L18404.
Speer, M., Wiles, P., Pepler, A., 2009. Low pressure systems off the New South Wales coast and associated hazardous weather: establishment of a database. Aust. Meteorol. Oceanogr. J. 58, 29–39.
Storlazzi, C.D., Brown, E., Field, M.E., Rodgers, K., Jokiel, P.L., 2005. A model for wave control on coral breakage and species distribution in the Hawaiian Islands. Coral Reefs 24 (1), 43–55.
Storlazzi, C.D., Wingfield, D.K., 2005. Spatial and temporal variations in oceanographic and meteorologic forcing along the central Californian coast, 1980–2002. Scientific Investigation Report by the U.S. Geological Survey (USGS), 2005–5085.
Thompson, P., Cai, Y., Reeve, D., Stander, J., 2009. Automated threshold selection methods for extreme wave analysis. Coast. Eng. 56, 1013–1021.
Timbal, B., Drosdowsky, W., 2013. The relationship between the decline of Southeastern Australian rainfall and the strengthening of the subtropical ridge. Int. J. Climatol. 33 (4), 1021–1034.
US Army Corps of Engineers, 2002. Shore Protection Manual. vol. 1. Coastal Engineering Research Center, Department of the Army, Mississippi, USA.
Velmurugan, T., Santhanam, T., 2010. Computational complexity between K-means and K-medoids clustering algorithms for normal and uniform distributions of data points. J. Comput. Sci. 6 (3), 363–368.
Wang, D.W., Hwang, P.A., 2001. An operational method for separating wind sea and swell from ocean wave spectra. J. Atmos. Oceanic Technol. 18 (12), 2052–2063.
Wang, K., Wang, B., Peng, L., 2009. CVAP: validation for cluster analyses. Data Sci. J. 8, 88–93.
Wyllie, S.J., Kulmar, M., 1995. Coastal Wave Monitoring. Australian Marine Data Collection and Management Guidelines Workshop, Environmental Resources Information Network. Hobart, December 1995.
You, Z., Lord, D., 2008. Influence of the El-Nino-Southern oscillation on NSW coastal storm severity. J. Coast. Res. 24 (2B), 203–207.

APPENDIX 5

Published Conference Paper.

Mortlock, T.R. and Goodwin, I.D. (2015). Wave Climate Change Associated with ENSO Modoki and Tropical Expansion in Southeast Australia and Implications for Coastal Stability. *Proceeding of the Coastal Sediments Conference*, *11 - 15 May 2015*, *San Diego, USA*. doi: 10.1142/9789814689977_0198.

WAVE CLIMATE CHANGE ASSOCIATED WITH ENSO MODOKI AND TROPICAL EXPANSION IN SOUTHEAST AUSTRALIA AND IMPLICATIONS FOR COASTAL STABILITY

THOMAS R. MORTLOCK[1], IAN D. GOODWIN[1]

1. *Marine Climate Risk Group, Climate Futures and Department of Environmental Sciences, Macquarie University, North Ryde, NSW 2109, Australia.* thomas.mortlock@mq.edu.au.

Abstract: Large-scale shifts in Pacific Basin climate such as the expansion of the tropics and an increase in ENSO Modoki events have occurred in recent decades. We investigate associated wave climate changes in Southeast Australia using a multidecadal directional buoy record at Sydney. We find significant interannual trends in austral summer and winter modal wave climate type occurrence and power, consistent with a poleward expansion of the subtropics and associated changes in extra-tropical wave generation. We also find an increase in winter storm frequency and intensity, consistent with increasing Southern Ocean wave heights. Summer El Niño and La Niña Modoki and winter La Niña and El Niño Modoki conditions produce significantly different wave climates in the Tasman Sea region. All other combinations do not. Summer La Niña Modoki favours north-easterly modal waves, but a reduction in total energy. Winter El Niño Modoki favours southerly modal energy in place of southerly storm energy.

Introduction

Wave-driven currents are the principle mechanism for sand transport on the Southeast Australian Shelf (SEAS) and surf zone (Goodwin, 2005). Therefore, coastal stability is intrinsically linked to variability in sand transport pathways and the directionality of modal and storm wave conditions.

The directional wave climate of the Tasman Sea and western Pacific region, which borders the east coast of Australia (Figure 1), undergoes considerable inter-annual (Harley *et al.*, 2010) and multi-decadal (Goodwin, 2005) modulation with El Niño Southern Oscillation (ENSO). The annual mean wave direction at Sydney is significantly correlated to ENSO (Goodwin, 2005). El Niño phases promote a bi-directional southerly and easterly wave climate, while La Niña and ENSO-neutral phases are correlated with a more uni-directional south-easterly wave climate. La Niña is also associated with greater storm frequency and intensity (You and Lord, 2008).

Research by Short *et al*. (1995; 2000), Ranasinghe *et al*. (2004) and Harley *et al*. (2011) has shown embayed beach rotation on Sydney's northern beaches is related to wave climate modulation by ENSO. Only subtle changes in the modal wave direction between El Niño and La Niña (no more than 25%) are needed to cause a reversal in alongshore transport in such swash-aligned embayments (Harley *et al.*, 2011). In drift-aligned compartments in north New South Wales (NSW), larger rotations in wave direction are responsible for planform reorientation on multi-decadal to centennial timescales (Goodwin *et al*, 2013).

However, some studies (Ashok *et al.,* 2007; Yeh *et al.*, 2009) suggest the flavour of ENSO is changing. Classic ENSO refers to a canonical pattern of Sea Surface Temperature (SST) anomalies extending from the eastern Pacific, and is the first EOF of Pacific SST variance (50%) (Wang and Hendon, 2007). However, a second mode (12%) is represented by a tripolar SST pattern of warm anomalies in the central Pacific, flanked by cool anomalies either side. Ashok *et al.* (2007) refer to this as ENSO Modoki, and suggest a climate state now exists that favours more frequent Modoki events due to changes in the zonal slope of the equatorial thermocline caused by global warming since the late 1970s.

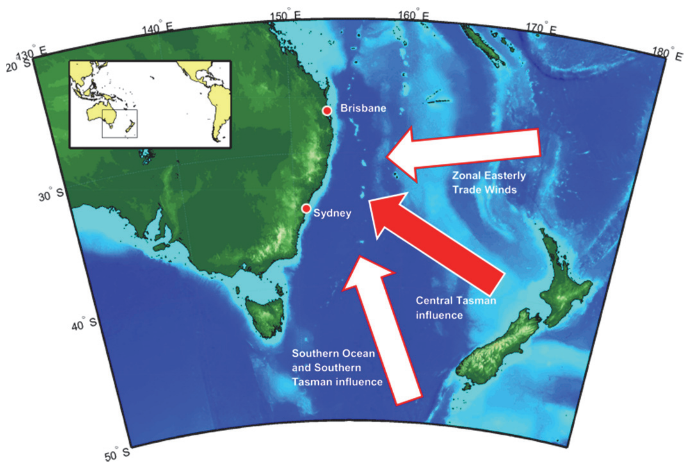

Fig. 1. Wave directions associated with ENSO phases in the Tasman Sea.

In addition, there is evidence to suggest the Hadley cell and trade wind zone is expanding poleward, consistent with an enhanced greenhouse effect, ozone depletion (Seidel *et al.*, 2008), and the shift towards the La Nina-like state of the Pacific Decadal Oscillation (Allen *et al.*, 2014). Coupled to this, the STR in the East Australian region is intensifying (Timbal and Drosdowsky, 2013). Mortlock and Goodwin (submitted) suggest this would lead to an increase in tropical wave generation (easterly wave direction) at the expense of extra-tropical (southerly) sources along the SEAS, although evidence for such changes already occurring has not yet been investigated.

The aims of this paper are to examine a) whether wave climates associated with Modoki-like ENSO are significantly different from classic ENSO, b) whether a tropical expansion scenario is visible in the observational record, and c) what the coupled impact may be for coastal stability in Southeast Australia.

Data and Methods

Observational Wave Climate

The directional wave climate was clustered from daily-averaged wave parametric data (1992 – 2013) from the Sydney Directional WaveRider (DWR) buoy by Mortlock and Goodwin (submitted). Sydney is the focus for coastal management in NSW, and the buoy record provides the longest directional wave observations along the SEAS.

The modal wave climate was clustered into three primary types for austral oceanic winter (JAS) and summer (JFM) seasons. These include an easterly Trade-Wind (Mode 1), a south-easterly Central Tasman Sea (Mode 2), and a south-south-easterly Southern Ocean (Mode 3) wave clusters. These were further decomposed into five (six) synoptic-scale modal wave climate types for the austral winter (summer) (Table 1).

Table 1. Wave climate types for the central NSW shelf, their power and direction.

Mode		**Generation**	P_W (kW m^{-1}) *	**Directional quadrant**
Mode 1	1a	North-Easterly Trade Winds	9.5 (7.5)	NE
	1b	Zonal Easterly Trade Winds	9.4 (11.7)	E
Mode 2	2a	Southern Tasman Anti-Cyclone	11.0 (12.2)	ESE
	2b	Central Tasman Low	(11.7)	SE
Mode 3	3a	Southern Ocean Low	16.3 (12.3)	SE/SSE
	3b	Southern Tasman Low	13.3 (20.7)	SSE
Storms events		Not classified **	57.6 (54.0)	SE/SSE

* Mean wave power for austral oceanic winter, JAS, and austral oceanic summer, JFM, (brackets)
** Storm events were not classified by synoptic type due to statistical limitations.

Table 1 highlights the latitudinal gradient of wave power that exists from wave directions north to south. The most powerful types are generated in the Southern Tasman Sea and Southern Ocean, while south-easterly to easterly modes are fetch, and therefore power, limited by New Zealand to the east.

Preparation of Parametric Wave Data

Clusters of wave climate types can be conceptualized by their joint distributions of significant wave height, H_s, peak spectral wave period, T_p, and mean wave direction, θ. In the Tasman Sea, fetch limitation renders wave height largely invariable leaving the bivariate distribution of wave direction and period, $p(\theta,T_p)$, as the best descriptor of each cluster. Still, due to a mixed sea-swell environment, even the tails of these distributions overlap between adjacent clusters. Therefore only the inter-quartile range (IQR) of $p(\theta,T_p)$ for each wave climate type was used. The IQR contains the central 50% of each cluster distribution (25^{th} - 75^{th} percentile). Timeseries of each wave climate type were then de-trended for a) frequency of occurrence and b) mean wave power.

Calculation of Directional Wave Power

Directional wave power, or the wave energy flux, P_0, for each wave climate type was used to assess changes in wave climate intensity with ENSO. P_0 was calculated for each daily wave event:

$$P_0 = \frac{1}{16}\rho g {H^2}_s C_g \tag{1}$$

where ρ (kg m^{-3}) is the average density of seawater, g (m s^{-2}) is the acceleration due to gravity, H_s is the daily average significant wave height, and C_g (m s^{-1}) is the wave group velocity. P_0 describes the power density expected from a single wave event expressed in kilowatts per metre wave-crest-length (kW m^{-1}). Here we use the mean wave power of each wave climate distribution, P_W:

$$P_W = \overline{P_O} \tag{2}$$

We then integrate P_W for each wave climate for each year over the occurrence of that wave climate (n, in seconds) to express changes in terms of total seasonal wave energy, E_W, in gigajoules per metre wave-crest-length (GJ m^{-1}):

$$E_W = \int_0^n P_W \tag{3}$$

Identification of ENSO and ENSO Modoki Events

Wave climates representative of ENSO and ENSO Modoki at Sydney were identified using the Niño 3.4 index, El Niño Modoki Index (EMI) and Southern Annual Mode (SAM) index over the period of buoy operation (Figure 2).

The Niño 3.4 index measures the average SST anomaly in the Central Pacific region and is the standard measure for Canonical ENSO. Sustained positive (negative) anomalies can lead to the onset of El Niño (La Niña). ENSO events are defined as a minimum of five consecutive three-month running mean of SST anomalies in the Niño 3.4 region surpassing a threshold of +/- 0.5 °C. This is also known as the Oceanic Niño Index (ONI).

The EMI is derived from weighted SST anomalies from three regions in the central, east and west equatorial Pacific. A positive (negative) EMI indicates El Niño (La Niña) Modoki. El Niño Modoki (ENM) and La Niña Modoki (LNM) are defined as those periods +/- 0.7σ of the EMI where σ is the standard deviation of the EMI (Ashok *et al.*, 2007), for a minimum of five consecutive months. This method successfully identified all "typical" ENM events in 1994, 2002 and 2004 as described by Ashok *et al.* (2007) (with a subsequent event in 2009/2010), and LNM events in 1999/2000 and 2008 as described by Shinoda *et al.* (2011) (with a subsequent event from 2010 to 2012).

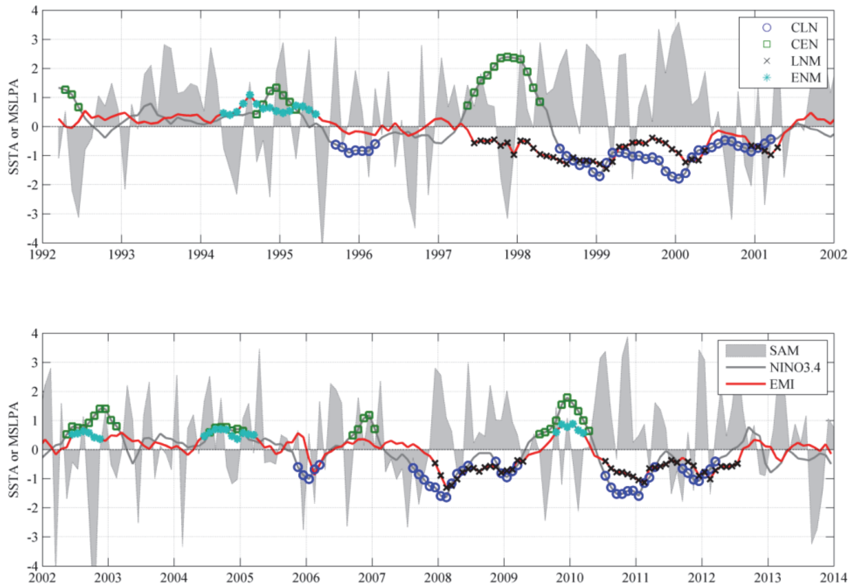

Fig. 2. Niño 3.4 (grey line), EMI (red line) and SAM indices with Canonical El Niño (CEN), La Niña (CLN), El Niño Modoki (ENM) and La Niña Modoki (LNM) events are highlighted.

We then selected seasonal composites of daily parametric wave data from the Sydney buoy record to represent ENSO phases that had a suitable coupling with the SAM. An El Niño (La Niña) wave climate in the Tasman Sea is reinforced by negative (positive) SAM. For austral summer (winter), timeslices used for wave climate composites were 1998 (1997) for CEN, 1996 (1998) for CLN, 2010 (2010) for ENM, and 2009 (2002) for LNM.

Results

Trends in Wave Climate Frequency and Power

Significant linear trends in wave climate frequency and power were found for consecutive (austral) winter and summer seasons (Table 2, Figure 3).

Table 2. Significant trends in wave climate frequency and power, P_W, at Sydney.

Mode	**Linear trend (days / season)**	***p* value**	**Linear trend (kW m^{-1} / season)**	***p* value**
Austral Summer (JFM)				
1a	+ 0.46	0.01		
2a	+ 0.34	0.07		
Austral Winter (JAS)				
2a	- 0.21	0.08	- 0.21	0.07
3a	- 0.32	0.12		
3b			- 0.24	0.05
Storms	+ 0.32	0.10	+ 0.84	0.11

Anomalous Wave Climate Associated with ENSO Modoki

Wave climates associated with Modoki-like ENSO were compared with Canonical ENSO. Figure 4 shows the significant differences ($p < 0.15$) between El Niño and La Niña Modoki, and La Niña and El Niño Modoki wave climates, for austral summer and winter. Significance levels between proportions were calculated using a Chi-Square test for summarized data. To illustrate impacts on coastal processes, we used frequency values in Figure 4 to express changes in terms of total seasonal wave energy, E_W (Figure 5).

Discussion

Wave Climate Changes with Tropical Expansion

Significant interannual trends in wave climate frequency and intensity exist between 1992 and 2013. In austral summer, easterly (Mode 1a) and south-easterly (Mode 2a) modal wave types show similar increases in frequency. In winter, south-easterly and southerly modal wave types decrease in both frequency (Mode 2a, Mode 3a) and wave power (Mode 2a, Mode 3b). The summer signal is stronger than the winter signal.

A. Significant linear trends in frequency of occurrence (days per season)

Austral Summers (JFM)

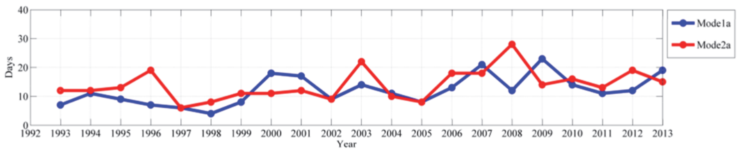

Austral Winters (JAS)

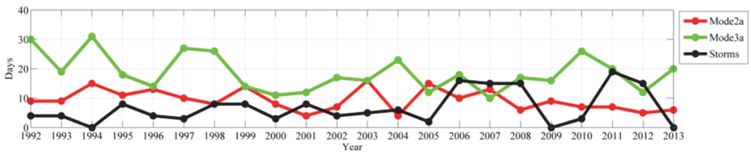

B. Significant linear trends in mean wave power (kW m^{-1} per season)

Austral Winters (JAS) – Modal Wave Climate

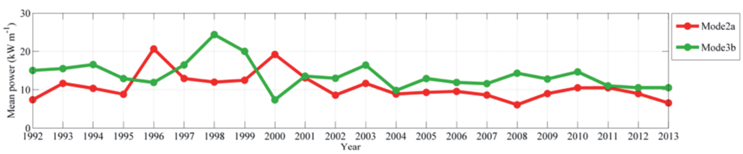

Austral Winters (JAS) – Storm Events

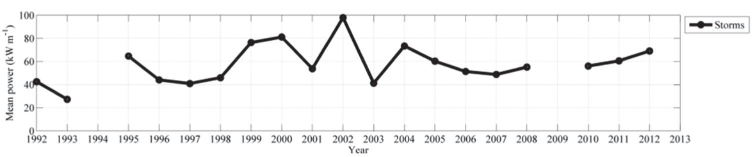

Fig. 3. Significant ($p \leq 0.15$) linear trends in (A) occurrence and (B) wave power at Sydney. Summer trends start from 1993 as buoy record begins March 1992. No significant trends in wave power exist during summer. Storm power is plotted separately for winter due to magnitude difference.

As Sydney is a sub-tropical site, the wave climate is a function of tropical (easterly) and extra-tropical (southerly) sources. The increase in trade wind easterlies and Tasman Sea south-easterlies seen in summer is consistent with a poleward shift in the Subtropical Ridge (STR) and increasing tropical influence.

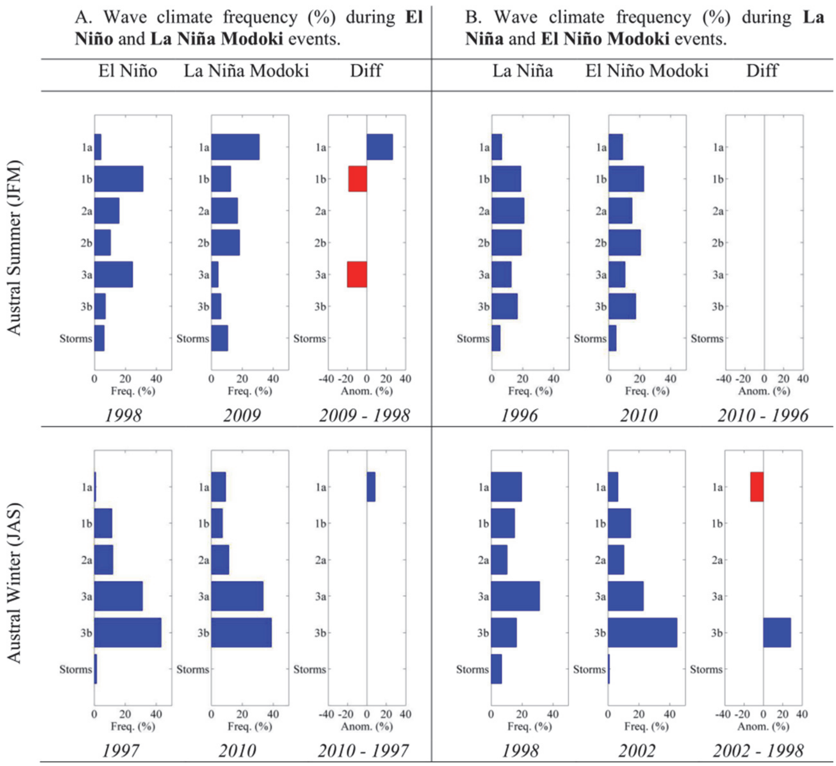

Fig. 4. Significant ($p < 0.15$) difference in wave climate frequency between (A) El Niño and La Niña Modoki, and (B) La Niña and El Niño Modoki, for austral summer and winter.

The reduction in frequency and intensity of southerly and south-easterly modal wave types in winter is also consistent with an expanding Hadley cell, teleconnected to the extra-tropics by a poleward shift in the mid-latitude westerlies because of blocking anticyclones to the north. Under such a scenario, wave generation from Southern Ocean Lows (Mode 3a) and Southern Tasman Lows (Mode 3b) is more far-field, leading to a lower-energy and less frequent contribution to the modal wave climate.

There is also an increase in winter storm frequency and intensity that co-varies with the reduction in Mode 3 modal wave types. We suggest this covariance is because the storm cluster represents the tail of the Mode 3 distribution, since the modal storm type in winter at Sydney is from Southern Tasman Lows and then Southern Secondary Lows (Shand *et al.*, 2011). An increase in storm intensity (power) is synonymous with an increase in wave height, since $P_0 \propto H_s^2$. As wave heights increase, successive wave events move out of the modal classification and exceed the storm wave threshold. This is consistent with observations (Hemer, 2010) and projections (Hemer *et al.*, 2013) of increasing wave heights in the Southern Ocean during the austral winter, associated with a strengthening of the mid-latitude westerlies.

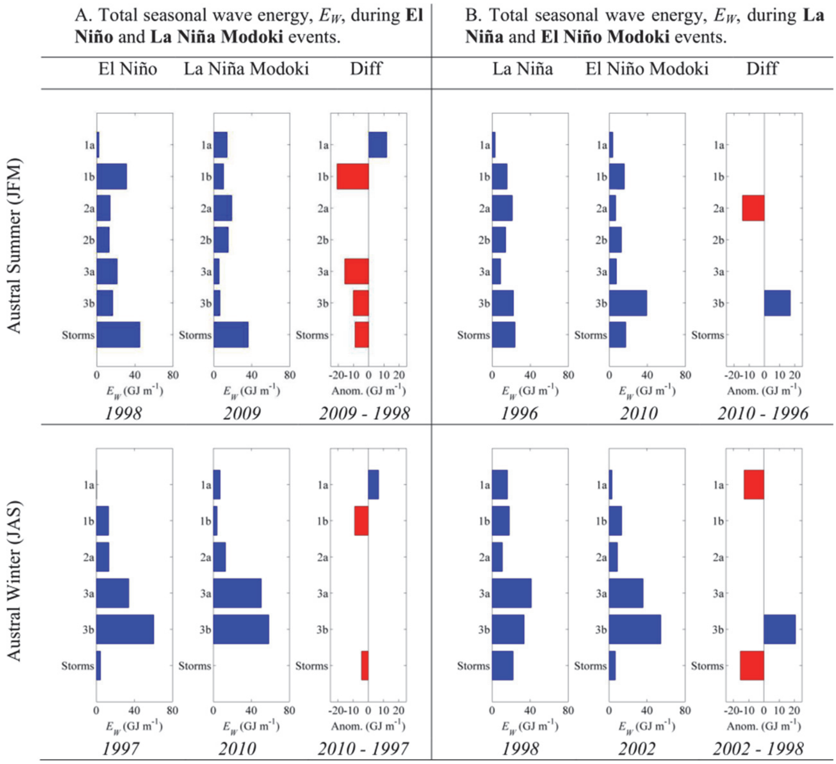

Fig. 5. Significant ($p < 0.15$) differences in total seasonal wave energy between (A) El Niño and La Niña Modoki, and (B) La Niña and El Niño Modoki, for austral summer and winter.

Wave Climate Changes with ENSO Modoki

We detect a trend towards more Modoki-like ENSO since 1992 (Figure 2), consistent with other studies since the 1970s (Ashok *et al.,* 2007; Taschetto and England, 2009). If this trend typifies future ENSO activity (Ashok *et al.*, 2007; Yeh *et al.*, 2009), then Southeast Australia may expect shifts in wave climate (and power) in cases where there are significant differences between Canonical and Modoki-like wave generation patterns.

Wave climate differences between El Niño and La Niña Modoki (La Niña and El Niño Modoki) are of most interest because patterns of anomalous SST cooling (warming) in the Tasman Sea are indistinguishable between these types, even though they are distinct in the central Pacific. As such, attribution of El Niño (La Niña) for environmental change based on regional SST anomalies may in fact be La Niña Modoki (El Niño Modoki).

The Tasman Sea sees the most significant differences between a) summer El Niño and La Niña Modoki, and b) winter La Niña and El Niño Modoki in both wave climate frequency (Figure 4) and total energy delivery (Figure 5). It follows therefore that the summer wave climate (and power) of Southeast Australia can be characterized by a preference towards either El Niño or La Niña Modoki, plus the mean of La Niña and El Niño Modoki. Similarly, the winter wave climate (and power) can be described by discriminating between either La Niña or El Niño Modoki, and the average between El Niño and La Niña Modoki.

Significantly, Figure 5 shows the only overall decrease in wave energy delivery occurs during summer La Niña Modoki. In all other cases, shifts between climate states ensure wave energy is largely conserved by a re-distribution of the frequency and intensity of wave generation. For example, the energy balance between Mode 2a and 3b in summer La Niña/El Niño Modoki is a function of a southerly shift in the STR. The balance between Mode 3b and storms in winter La Niña/El Niño Modoki reflects a decrease in wave height, reducing southerly storm (destructive) conditions to southerly modal (constructive) waves.

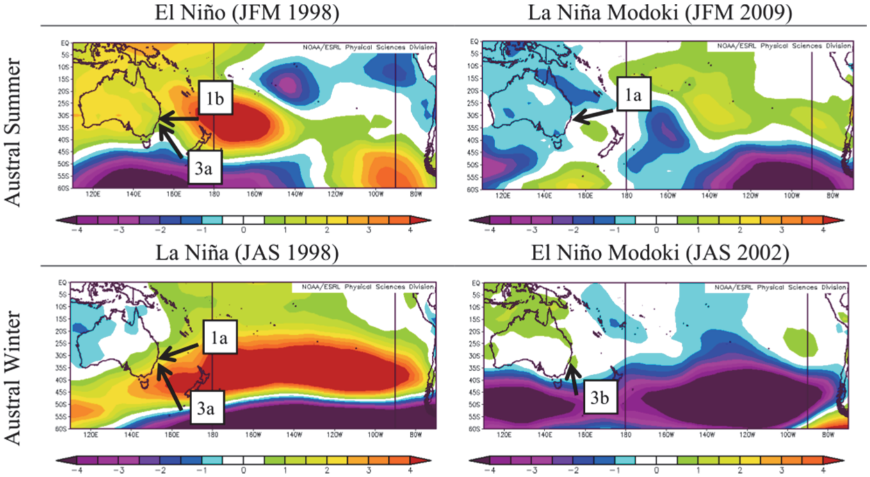

Fig. 6. Daily MSLP composite anomalies for ENSO/ENSO Modoki combinations from NNR.

Figure 6 shows MSLPAs composited for summer El Niño and La Niña Modoki and winter La Niña and El Niño Modoki using the NCEP-NCAR Reanalysis (NNR). In summer, the zonal pattern emanating from the Indian Ocean sector that produces a bi-directional 1b/3a wave climate during El Niño is replaced by a more meridional Pacific pattern that favours a north-easterly 1a wave climate during La Niña Modoki. This is produced by a subtropical anti-cyclone (STAC) in the Tasman Sea, with a shorter fetch than the zonal STAC producing Mode 1b during El Niño. The La Niña Modoki pattern also reinforces a longer-term trend towards positive SAM during summer (Abram *et al*., 2014), which has been linked to ozone depletion (Thompson and Solomon, 2002), and the combined effects of anthropogenic and natural variability (Gillet *et al*., 2013).

Implications of ENSO-Modoki and Tropical Expansion on Coastal Stability

The trends towards ENSO-Modoki and tropical expansion are coupled in the summer as both enhance the tropical Mode 1-type modal wave climate, at the expense of extra-tropical Mode 3 types, in line with a longer-term trend towards positive summer SAM. This may be the reason why positive trends in wave climate frequency are strongest in summer (Table 2).

This coupling favors intensification of the STAC in the Tasman Sea that produces Mode 1 waves. Significantly, the La Niña Modoki pattern preferences a north-easterly wave direction, and wave generation within the Tasman Sea. This could lead to a higher frequency of steeper and more destructive wave conditions as wave heights increase but periods are fetch-limited. Extreme wave events from the north-east are particularly erosive for north-east facing southern hooks of drift-aligned coastal compartments typical of the north NSW and southeast Queensland coast. It is also this section of coast that is most proximal to the northern limb of the STAC in summer La Niña Modoki.

In winter, southerly storms co-vary with a reduction in modal waves from the same direction, consistent with observations and projections of Southern Ocean storminess (Hemer, 2010; Hemer *et al*., 2013). A winter El Niño Modoki compliments this trend, promoting negative SAM and southerly waves. This is likely to be most influential in southern and central NSW, presumably promoting clockwise planform rotation of embayed compartments after the model of Ranasinghe *et al*. (2004). This extra-tropical signal is likely to be less influential on the north NSW coast, where oblique southerly waves do not undergo sufficient refraction to significantly impact nearshore processes.

Conclusions

Interannual trends at Sydney show significant changes in both austral summer and winter wave climates that are consistent with an expanding Hadley Cell and associated intensification of the STR and trade-wind zone. We also find an increase in winter storm frequency and intensity, consistent with increasing Southern Ocean wave heights.

We also see a trend towards Modoki-like ENSO since 1992, consistent with other longer-term studies. It has been suggested this trend is set to continue in the Pacific, facilitated by a weaker zonal slope of the equatorial thermocline. To evaluate associated wave climate changes, we have compared ENSO and ENSO Modoki phases that produce the same sign SSTA in the Tasman Sea. The most significant differences exist between summer La Niña Modoki and El Niño, which favours north-easterly (Mode 1a) over easterly (Mode 1b) waves, and between winter El Niño Modoki and La Niña, which preferences Southern Tasman Lows (Mode 3a) and a uni-directional southerly wave climate. Our results also indicate a broad conservation of wave energy between climate states exists, by a re-distribution of the frequency and intensity of wave generation.

We observe that wave climate changes are strongest in summer, when the trends towards ENSO-Modoki and tropical expansion are coupled. An intensification of summer La Niña Modoki may have erosive consequences for north-east facing southern hooks of drift-aligned coastal compartments, typical of the north NSW and southeast Queensland coast. High population density in these southern hooks poses a potential challenge for coastal management.

Further work includes investigating nearshore sensitivities to the changes reported, in order to highlight ‘problem’ wave climate change for coastal processes. Since those combinations of ENSO and ENSO Modoki we have investigated produce indistinguishable SSTAs in the Tasman Sea, but significantly different wave climates, past attribution of traditional ENSO for regional environmental change may also require re-assessment.

Acknowledgements

Sydney buoy data was provided by Manly Hydraulics Laboratory, NSW. The Nino 3.4 index and ONI from NOAA Climate Prediction Center; the EMI from the Japan Agency for Marine-Earth Science and Technology (JAMSTEC); the SAM index from National Environment Research Council (NERC); the NNR from NOAA Earth Systems Research Laboratory; ETOPO01 imagery from NOAA National Geophysical Data Center. This work forms PhD research by T.M. which is funded by an Australian Research Council Linkage Project (ARC LP100200348) and a Macquarie University Research Scholarship (MQiRES).

References

Abram, N. J., Mulvaney, R., Vimeux, F., *et al*. (2014). Evolution of the Southern Annular Mode during the past millennium. *Nature Climate Change*, 4(7), 564-569.

Allen, R. J., Norris, J. R., Kovilakam, M. (2014). Influence of anthropogenic aerosols and the Pacific Decadal Oscillation on tropical belt width. *Nature Geoscience*, 7(4), 270-274.

Ashok, K., Behera, S. K., Rao, S. A., *et al*. (2007). El Niño Modoki and its possible teleconnection. *Journal of Geophysical Research-Oceans*, 112(C11).

Gillett, N. P., Fyfe, J. C., Parker, D. E. (2013). Attribution of observed sea level pressure trends to greenhouse gas, aerosol, and ozone changes. *Geophysical Research Letters*, 40(10), 2302-2306.

Goodwin, I. D. (2005). A mid-shelf, mean wave direction climatology for southeastern Australia, and its relationship to the El Niño—Southern Oscillation since 1878A.D. *International Journal of Climatology*, 25(13), 1715-1729.

Goodwin, I. D., Freeman, R., Blackmore, K. (2013). An insight into headland sand bypassing and wave climate variability from shoreface bathymetric change at Byron Bay, New South Wales, Australia. *Marine Geology*, 341, 29-45.

Harley, M. D., Turner, I. L., Short, A. D., *et al*. (2010). Interannual variability and controls of the Sydney wave climate. *International Journal of Climatology*, 30, 1322-1335.

Harley, M. D., Turner, I. L., Short, A. D., *et al*. (2011). A reevaluation of coastal embayment rotation: The dominance of cross-shore versus alongshore sediment transport processes, Collaroy-Narrabeen Beach, southeast Australia. *Journal of Geophysical Research*, 116(F4).

Hemer, M. A. (2010). Historical trends in Southern Ocean storminess: Long-term variability of extreme wave heights at Cape Sorell, Tasmania. *Geophysical Research Letters*, 37(18).

Hemer, M. A., Fan, Y., Mori, N., *et al*. (2013). Projected changes in wave climate from a multi-model ensemble. *Nature Climate Change*, 3(5), 471-476.

Mortlock, T. R., Goodwin, I. D. (submitted). Directional Wave Climate and Power Variability along the Southeast Australian Shelf. Submitted to *Continental Shelf Research*.

Ranasinghe, R., McLoughlin, R., Short, A. *et al*. (2004). The Southern Oscillation Index, wave climate, and beach rotation. *Marine Geology*, 204(3-4), 273-287.

Seidel, D. J., Fu, Q., Randel, W. J., *et al*. (2008). Widening of the tropical belt in a changing climate. *Nature Geoscience*, 1(1), 21-24.

Shand, T. D., Goodwin, I. D., Mole, M. A., *et al*. (2011). NSW Coastal Inundation Hazards Study: Coastal Storms and Extreme Waves: Water Research Laboratory & Climate Futures at Macquarie University.

Shinoda, T., Hurlburt, H. E., Metzger, E. J. (2011). Anomalous tropical ocean circulation associated with La Niña Modoki. *Journal of Geophysical Research*, 116(C12).

Short A.D., Trembanis A.C., Turner I. (2000). Beach oscillation, rotation and the Southern oscillation, Narrabeen Beach, Australia. In *Proceedings of the 27th International Coastal Engineering Conference*, *Sydney;* 2439–2452.

Taschetto, A. S., England, M. H. (2009). El Niño Modoki Impacts on Australian Rainfall. *Journal of Climate*, 22(11), 3167-3174.

Thompson, D. W. J., Solomon, S. (2002). Interpretation of recent Southern Hemisphere climate change. *Science*, 296(5569), 895-899.

Timbal, B., Drosdowsky, W. (2013). The relationship between the decline of Southeastern Australian rainfall and the strengthening of the subtropical ridge. *International Journal of Climatology*, 33(4), 1021-1034.

Wang, G., Hendon, H. H. (2007). Sensitivity of Australian rainfall to inter-El Niño variations. *Journal of Climate*, 20(16), 4211-4226.

Yeh, S. W., Kug, J. S., Dewitte, B., *et al*. (2009). El Nino in a changing climate. *Nature*, 461(7263), 511-514.

You, Z. J., Lord, D. (2008). Influence of the El Nino-Southern Oscillation on NSW coastal storm severity. *Journal of Coastal Research*, 24(2B), 203-207.

APPENDIX 6

Matlab function.

Mortlock, T.R. and Suarez-Arriaga, M. (2014), Matlab implementation of Tm2Tz function. Solution of the quartic equation which describes the relationship between MIKE 21 SW modelled mean wave period (T_{m01}) and buoy-observed mean wave period (T_z) at three nearshore wave buoys in the Sydney region. Can be used to correct modelled wave period (see caveats).

```
function [ Tz ] = Tm2Tz( Tm )
%%  Tm2Tz
% ----------------------------------------------------------------------
%   T.Mortlock and M.Suarez-Arriaga Dec 2014
% ----------------------------------------------------------------------
%   Solution of the quartic equation relating MIKE 21 SW mean wave period
%   (Tm01) model output to nearshore observations of the mean wave period
%   (Tz) from three directional WaveRider buoys at Long Reef (d = 20 m),
%   Narrabeen (d = 11 m), and Wamberal (d = 12 m). The relation is only
%   valid for 4 < Tm01 < 15 s; for exposed nearshore locations in the
%   Sydney region; when MIKE 21 SW is run with wave-only boundary forcing
%   (no wind); and for the wave conditions captured during buoy
%   deployments. If these conditions are satisfied, this relation can be
%   used to adjust MIKE 21 SW Tm01 to agree with observed Tz.
%   [ Tz ] = Tm2Tz( Tm )

[Tz] = 26.524390243902438 + 0.5*sqrt(1432.0592901050961 + (-
35540.42094542018 + 1473.6125994561544*Tm)/...
    (-2.3219375e7 + 2.599875e6*Tm +
11.618950038622252*sqrt(4.241144411767e12 + Tm*(-9.25121621462e11 +
(5.1345851119e10 - 1.7643776e7*Tm)*Tm)))^...
    0.3333333333333333 + 1.1034217953637833*(-2.3219375e7 + 2.599875e6*Tm
+ ...
    11.618950038622252*sqrt(4.241144411767e12 + Tm*(-9.25121621462e11 +
(5.1345851119e10 - 1.7643776e7*Tm)*Tm)))^0.3333333333333333)...
    -  0.5*sqrt(2864.1185802101922 + (35540.42094542018 -
1473.6125994561544*Tm)/...
    (-2.3219375e7 + 2.599875e6*Tm +
11.618950038622252*sqrt(4.241144411767e12 + Tm*(-9.25121621462e11 +
(5.1345851119e10 - 1.7643776e7*Tm)*Tm)))^...
    0.3333333333333333 - 1.1034217953637833*(-2.3219375e7 + 2.599875e6*Tm
+...
    11.618950038622252*sqrt(4.241144411767e12 + Tm*(-9.25121621462e11 +
(5.1345851119e10 - 1.7643776e7*Tm)*Tm)))^0.3333333333333333 + ...
    110325.8622190624/sqrt(1432.0592901050961 + (-35540.42094542018 +
1473.6125994561544*Tm)/...
    (-2.3219375e7 + 2.599875e6*Tm +
11.618950038622252*sqrt(4.241144411767e12 + ...
    Tm*(-9.25121621462e11 + (5.1345851119e10 -
1.7643776e7*Tm)*Tm)))^0.3333333333333333 + 1.1034217953637833*(-
2.3219375e7 + 2.599875e6*Tm + ...
    11.618950038622252*sqrt(4.241144411767e12 + Tm*(-9.25121621462e11 +
(5.1345851119e10 - 1.7643776e7*Tm)*Tm)))^0.3333333333333333));
end
```